DOI: 10.5958/0976-2469.2023.00031.3

LIBRARY HERALD
Vol 61 No 4
December 2023

Altmetric Analysis of Scholarly Articles Published in DESIDOC Journal of Library and Information Technology

Sagar Khatale*
Ashish Raut**

The present study aims to examine the altmetric presence in scholarly articles and track the academic and societal utilization of research published in the DESIDOC Journal of Library and Information Technology. The population consists of the scholarly articles published in DJLIT and indexed on the Web of Science from the year 2005 to 2020. Web of Science database was used to measure the number of article citations and Altmetric Explorer was used to get the Altmetric Attention Score. Out of the 573 scholarly articles indexed on the Web of Science, 27 (4.71%) articles had an altmetric attention score. The highest number of received citations was 63, and the highest altmetric attention score was 13. The research findings demonstrated that India is the majorcontributor with 85% of the scholarly articles to DJLIT. Twitter (43.39%) followed by Wikipedia (20.75%) are the popular digital media platforms where DJLIT articles were mentioned. Librarians were the most active readers of DJLIT research on Mendeley with 242 readers (25.07%) and the Social Science discipline with 368 highest readers (38.13%) on Mendeley who reads DJLIT Publications.

Keywords: *Altmetric, Scholarly Articles, DESIDOC Journal of Library and Information Technology, DJLIT, Web of Science*

1 INTRODUCTION

Traditional citation metrics do not provide a clear understanding of the impact of research in the scholarly world, particularly in scientific communication. In recent times a new technique is developed called "Altmetric"

* Librarian, K.J. Somaiya Institute of Dharma Studies, Somaiya Vidyavihar University, Mumbai E-mail: sagar.khatale@somaiya.edu

** Librarian, Shri Shivaji College of Arts, Commerce and Science, Akola E-mail: ashish.satvik@gmail.com

which tracks and measures the scholarly impact as well as the societal impact to evaluate research published in digital forms and formats. The term altmetric, also known as alternative metrics, appeared first in the year 2010 in "Altmetrics: A manifesto" (Priem, Tarborelli, Groth, &Neylon, 2010)[1]. The manifesto did not provide a definition but gave a clear vision of what altmetrics are. Further Priem (2014)[2] defined altmetric as the "study and use of scholarly impact measures based on activity in online tools and environments." Bornmann (2014)[3] stated that "altmetric is a term to describe web-based metrics for the impact of publications and other scholarly material by using data from social media platforms." NISO (2016)[4]defined"altmetric as a broad term that encapsulates the digital collection, creation, and use of multiple forms of assessment that are derived from activity and engagement among diverse stakeholders and scholarly outputs in the research ecosystem." Altmetric works to map the scholarly impact of web-based digital tools and tracks the qualitative data complementary to citation-based, traditional metrics with the help of persistent identifiers.

2 DESIDOC JOURNAL OF LIBRARY AND INFORMATION TECHNOLOGY (DJLIT)

DESIDOC Journal of Library and Information Technology (DJLIT) is an international, open access, peer-reviewed journal which is a bi-monthly publication. It mainly publishes research articles and review papers related to library and Information Science and Information Technology applied to libraries. DJLIT covers broad subject areas like Information systems, Knowledge management, Collection building & management, Information behavior & retrieval, Librarianship/library management, Library & information services, Records management & preservation, etc. Users of DJLIT are librarians, documentation and information professionals, researchers, students etc. DJLIT is indexed in Scopus, Web of Science (Emerging Source Citation Index), UGC-CARE, Dimensions, LISA, LISTA, EBSCO, J-Gate Plus, Proquest, Library Literature and Information Science Index/Full-text, The Informed Librarian Online, Indian Science Abstracts, Indian Citation Index, WorldCat, Google Scholar, etc.[5] The periodical started in 1980 as DESIDOC Bulletin-a four-page newsletter-basically to publish the activities of the DESIDOC. In the late 1980s, a new era of information technology dawned in India. In 1992, the Bulletin was renamed as DESIDOC Bulletin of Information Technology (DBIT). In 2008, DBIT became a primary research journal and was again renamed as DESIDOC Journal of Library and Information Technology (DJLIT). Since then, only primary research work, after peer-evaluation, is accepted for publication.[6]

3 NEED AND SIGNIFICANCE OF THE STUDY:

Traditional metrics like article citation counts and journal impact factor usually take a longer time and reflect only one dimension of the impact of research but altmetric provides immediate information with broader picture of article impact.[7] Scholarly articles published in DJLIT are often practical oriented so scholarly as well as the societal impact of research may be judged more broadly by using altmetric data instead of relying on only traditional metrics. The basic purpose of this research is to examine the altmetric presence in scholarly articles and track the academic and societal utilization of research published in DJLIT.

4 REVIEW OF LITERATURE

Akers (2017)[7] conducted a study to introduce altmetric to the Journal of the Medical Library Association (JMLA) and explained how altmetrics may be better than traditional citations in reflecting the impact of JMLA articles. Erfanmasnesh (2017)[8] conducted a study to examine the altmetric presence in articles published in Scopus-indexed Library and Information Science (LIS) journals. Ezema&Ugwu (2019)[9] studied the research impact of Library and Information Science (LIS) journals using Web of Science (WoS), Scopus and Google Scholar (GS) and then examined whether there is a correlation between their citations and altmetric attention. Rangaswamy&Rajenrda Babu (2019)[10] examined which journals and articles have got the high citations as well as an altmetric attention score in the field of Library and Information Science. The objective of this study was to analyze 5 LIS journals indexed by Google Scholar Metrics 2019. Sankar and Sarangapani (2020)[11] explored the coverage of LIS literature published in 2019 with the primary objective as to know the scholarly communication of LIS Literature on social media and evaluate the altmetric attention score. Tang & Vann (2020)[12] investigated the multidimensional perspective of scholarly articles published in the top-tier Library and Information Science (LIS) journals. The relationships between the impact factors (altmetric attention score, citation count and Mendeley readership) were analyzed, and reader profiles were characterized and studied.

5 OBJECTIVES OF THE STUDY

1. To find out the country-wise count of scholarly articles published in DJLIT and indexed in Web of Science.
2. To find out the top ten highly cited scholarly articles published in DJLIT and indexed in Web of Science.
3. To track altmetric presence in scholarly articles published in DJLIT.
4. To identify mostly used digital media platforms by DJLIT readers for sharing research.

5. To find out the geographical and demographical details of Mendeley readers by professional status and readers by discipline.

6 SCOPE AND LIMITATIONS OF THE STUDY

The scope of the study was limited to the articles published in DESIDOC Journal of Library and Information Technology (DJLIT), which was indexed in the Web of Science (WoS) core collection under the Emerging Sources Citation Index (ESCI).In Web of Science, the search query was run limited to articles published between 2005 to 2020, with a Digital Object Identifier (DOI) and indexed the literature of Library and Information Science under the subject area (Category) namely 'Information Science & Library Science.' All other types of documents that are indexed in the Web of Science like Editorial Material, Review, Early Access, Letter, Correction, Biographical Item, Book Review, Proceedings Paper, News Item, Database Review, Bibliography, Software Review, Retraction, Retracted Publication, Hardware Review, Art Exhibit Review, etc. were excluded from this study.

7 MATERIALS AND METHODS

A quantitative method was adopted for this study. All statistical data of scholarly articles were collected through structured observation by reviewing the Web of Science and Altmetric Explorer databases.

7.1 Data Sources

"Web of Science (WoS) is the world's most trusted publisher-independent global citation database. Guided by the legacy of Dr. Eugene Garfield, inventor of the world's first citation index, the Web of Science is the most powerful research engine, delivering best-in-class publication and citation data for confident discovery, access and assessment".[13]

"Altmetric.com is a London-based digital science company with a vision to track and analyze the online activity around scholarly research outputs"[14]

7.2 Data Collection

Data were collected in two types i.e. primary data and secondary data.

7.2.1 Primary Data

The primary bibliographic data of the scholarly articles published in DESIDOC Journal of Library and Information Technology were retrieved from Web of Science core collection and used Emerging Sources Citation Index (ESCI) as DESIDOC Journal of Library and Information Technology is indexed in ESCI from the year 2005. Accordingly, the time span of this study was from the year 2005 to 2020.To retrieve the primary data, a structured

query was run in Web of Science with the following fields with tags:

- Publication Title (SO): DESIDOC Journal of Library and Information Technology
- DOI (DO): 10.*
- Publication Year (PY): 2005-2020
- Document Type (DT): Article

573 bibliographic records of scholarly articles were retrieved by executing the above query in the advanced search option of Web of Science.(Image 1) The above query was run on 23rd August 2021 and all the data was collected on the same date.

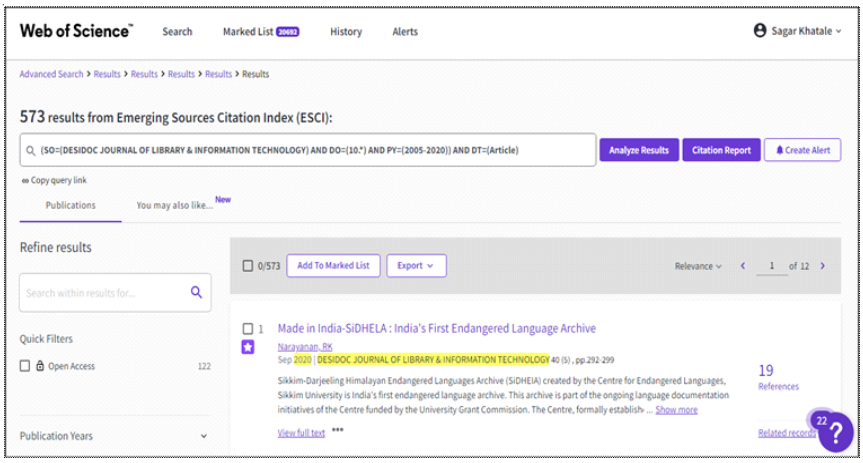

Image 1: Web of Science Search Results

7.2.2 Secondary Data

Altmetric.com provides login based free service of altmetric explorer (Research Output Tab) to librarians as a Free Librarian Account where one can search the research outputs using different scholarly identifiers like Digital Object Identifier, ArXiv ID, etc. Maximum 50 scholarly identifiers are allowed in each search.

The retrieved primary bibliographic data of 573 scholarly articles from Web of Science were checked in the altmetric database using Altmetric Explorer. 12 Search queries of 50 DOI'swere run in altmetric explorer to retrieve the secondary data. Out of 573 scholarly articles from Web of Science, 29 articles are tracked by altmetric.com out of those 27 (4.71%) scholarly articlesreceived at least 01 Altmetric Attention Score. (Image 2) All the details of the 27 articles tracked by altmetric.com were saved in excel file for further analysis.

(*Source*: Altmetric.com)

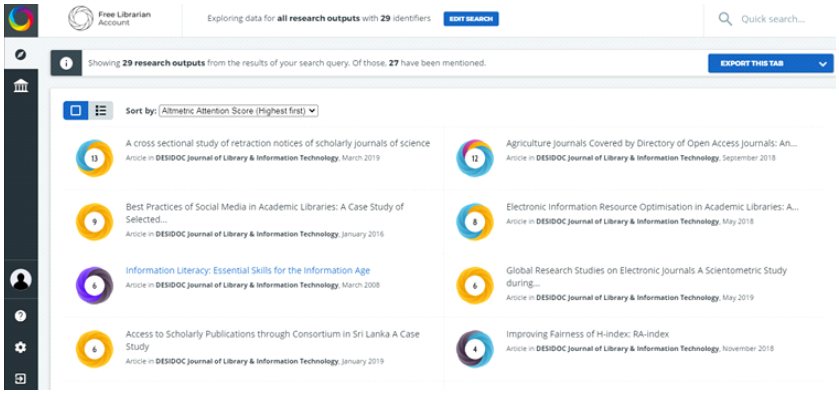

(Source: Altmetric.com)

Image 2: AltmetricExplorer Search Results

8 DATA ANALYSIS

Data retrieved from Web of Science and Altmetric Explorer is further analyzed to get the results of the research.

Article 1	A cross-sectional study of retraction notices of scholarly journals of science	Mar-2019	39 (2)
Article 2	Agriculture Journals Covered by Directory of Open Access Journals: An Analytical Study	Sep-2018	38 (5)
Article 3	Best Practices of Social Media in Academic Libraries: A Case Study of Selected Engineering College Libraries of Odisha	Sep-2016	36 (5)
Article 4	Electronic Information Resource Optimisation in Academic Libraries: A Comparative Study on Licensing Provision of Commercial Publisher	May-2018	38 (3)
Article 5	Access to Scholarly Publications through Consortium in Sri Lanka A Case Study	Jan-2019	39 (1)
Article 6	Global Research Studies on Electronic Journals A Scientometric Study during 1990 2017	May-2019	39 (3)
Article 7	Information Literacy: Essential Skills for the Information Age	Mar-2008	28 (2)

Article 7	Information Literacy: Essential Skills for the Information Age	Mar-2008	28 (2)
Article 8	Improving Fairness of H-index: RA-index	Nov-2018	38 (6)
Article 9	Finding Facets of Academic Integrity and Plagiarism through the Prism of a Citation Database	Mar-2019	39 (2)
Article 10	Secure Authenticated Key Exchange Protocol for Credential Services	Jul-2009	29 (3)
Article 11	Open Access to Electronic Theses and Dissertations	Jan-2008	28 (1)
Article 12	Retrospective Conversion of Nehru Memorial Museum and Library: Issues and Perspective	May-2008	28 (3)
Article 13	Bibliometrics to Altmetrics: Changing Trends in Assessing Research Impact	Jul-2015	35 (4)
Article 14	Research Contribution of Prof Atul H. Chokshi to Materials Science: A Scientometric Study	2013	33 (5)
Article 15	Open Access and Open J-Gate	Jan-2008	28 (1)
Article 16	Analysis of Open Access Scholarly Journals in Media & Communication	2013	33 (5)
Article 17	Development of Public Libraries through Public-private Partnership in India: Issues and Challenges	2013	33 (1)
Article 18	Building Subject Gateway in a Shifting Digital World	Mar-2009	29 (2)
Article 19	Collection Development in the E-content World: Challenges of Procurement, Access and Preservation	2013	33 (2)
Article 20	Corporate Social Responsibility: Activities in and around Visakhapatnam City	2013	33 (1)
Article 21	Indexing of Indian Journals in SCImago Citation Database: A Decadal Study (2005-2014)	Jan-2017	37 (1)
Article 22	Regulations to Prevent Plagiarism in Higher Education in India A Critical Appraisal	Mar-2019	39 (2)

Article 22	Regulations to Prevent Plagiarism in Higher Education in India A Critical Appraisal	Mar-2019	39 (2)
Article 23	Management of University Research Publication: A Case Study of JUIT Publication Database (JPubDB)	Jul-2016	36 (4)
Article 24	Journal Packing Density across Subject Disciplines among BRICS Countries: A Study	May-2018	38 (3)
Article 25	Availability of Open Access Books in DOAB: An Analytical Study	Mar-2016	36 (2)
Article 26	Tradition and Transition: The Journey of an iSchoolDeep in the Heart of Texas	Jan-2017	37 (1)
Article 27	Development of Online Legal Information System Lawyers Perceptions	Mar-2019	39 (2)

Table 1: Article Numbers with Title

Table 1 shows the list of all 27 articles with titles, published in DJLIT which were tracked by Altmetric.

8.1 Country-Wise count of Scholarly Articles Published in DJLIT

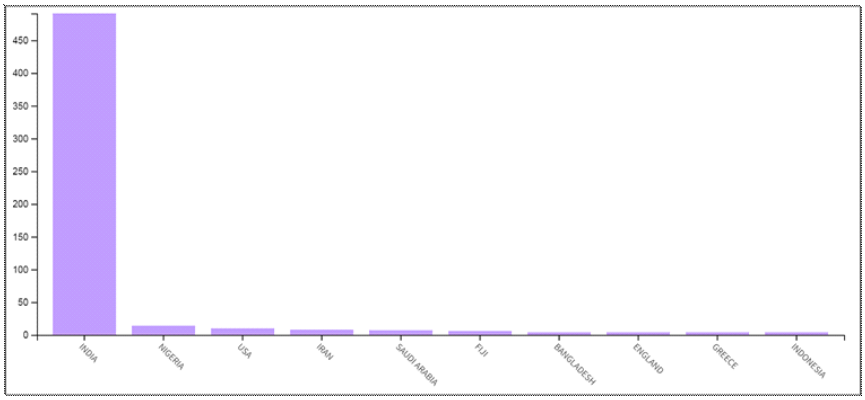

Figure 1: Country-wise count of Scholarly Articles Published in DJLIT

DJLIT has received contributions of scholarly articles from 32 countries of the world.The top10 countries in terms of the highest contribution of scholarly articles were taken for the analysis.From the 573 scholarly articles of DJLIT indexed in Web of Science, 491 (85.69 %) articles were contributed

by India, followed by Nigeria 14 (2.43 %), USA 10 (1.75 %), Iran 8 (1.40 %), Saudi Arabia 7 (1.22 %), etc. Data related to scholarly articles which are published in DJLIT showed that most articles (n=57) had been published in 2017 and 2018 and the least (n=5) in 2005.

8.2 Top Ten Highly Cited Scholarly Articles

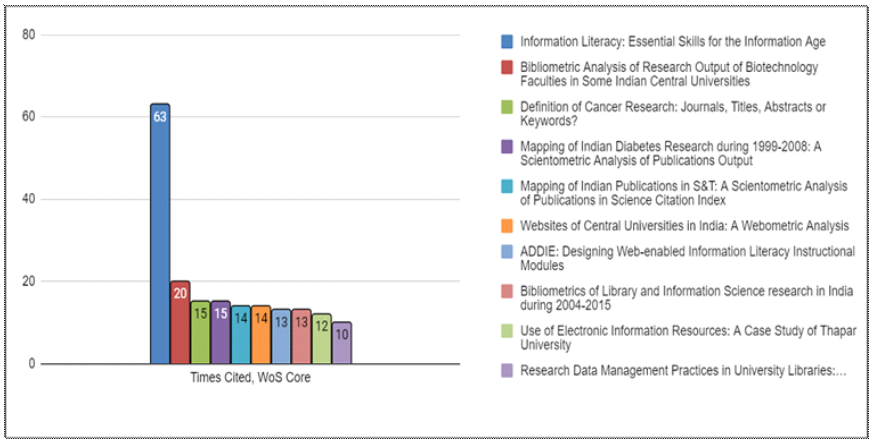

Figure 2: Top Ten Highly Cited Scholarly Articles

Figure 2 shows that the article "Information Literacy: Essential Skills for the Information Age" was the highly cited scholarly article with 63 citations and the only article from top ten highly cited articles that altmetric also tracks with an altmetric attention score of 6.

8.3 Altmetric presence in DJLIT articles:

Article Number	Altmetric Attention Score	Total Mentions																	Number of Mendeley readers
		News	Blog	Policy	Patent	Twitter	Peer review	Weibo	Facebook	Wikipedia	Google+	LinkedIn	Reddit	Pinterest	F1000	Q&A	Video	Syllabi	
Article 1	13	0	2	0	0	1	0	0	0	0	0	0	0	0	0	0	0	0	12
Article 2	12	0	2	0	0	6	0	0	0	0	1	0	0	0	0	0	0	0	13
Article 3	9	0	1	0	0	0	0	0	0	0	0	0	0	0	0	0	0	0	32
Article 4	8	0	1	0	0	1	0	0	0	0	0	0	0	0	0	0	0	0	12
Article 5	6	0	1	0	0	0	0	0	0	0	0	0	0	0	0	0	0	0	9
Article 6	6	0	1	0	0	0	0	0	0	0	0	0	0	0	0	0	0	0	13
Article 7	6	0	0	1	0	0	0	0	0	1	0	0	0	0	0	0	0	0	443

Article 8	4	0	0	0	0	1	0	0	0	1	0	0	0	0	0	0	0	0	10
Article 9	4	0	0	0	0	6	0	0	0	0	0	0	0	0	0	0	0	0	17
Article 10	3	0	0	0	3	0	0	0	0	0	0	0	0	0	0	0	0	0	0
Article 11	3	0	0	1	0	0	0	0	0	0	0	0	0	0	0	0	0	0	29
Article 12	3	0	0	0	0	0	0	0	0	1	0	0	0	0	0	0	0	0	4
Article 13	3	0	0	1	0	0	0	0	0	0	0	0	0	0	0	0	0	0	92
Article 14	3	0	0	0	0	0	0	0	0	1	0	0	0	0	0	0	0	0	21
Article 15	3	0	0	0	0	0	0	0	0	3	0	0	0	0	0	0	0	0	14
Article 16	3	0	0	1	0	0	0	0	0	0	0	0	0	0	0	0	0	0	38
Article 17	3	0	0	0	0	0	0	0	0	1	0	0	0	0	0	0	0	0	21
Article 18	3	0	0	0	0	0	0	0	0	2	0	0	0	0	0	0	0	0	8
Article 19	3	0	0	0	0	0	0	0	0	1	0	0	0	0	0	0	0	0	32
Article 20	3	0	0	1	0	0	0	0	0	0	0	0	0	0	0	0	0	0	4
Article 21	2	0	0	0	0	3	0	0	0	0	0	0	0	0	0	0	0	0	36
Article 22	1	0	0	0	0	1	0	0	0	0	0	0	0	0	0	0	0	0	22
Article 23	1	0	0	0	0	0	0	0	0	0	1	0	0	0	0	0	0	0	25
Article 24	1	0	0	0	0	2	0	0	0	0	0	0	0	0	0	0	0	0	8
Article 25	1	0	0	0	0	0	0	0	0	0	1	0	0	0	0	0	0	0	19
Article 26	1	0	0	0	0	1	0	0	0	0	0	0	0	0	0	0	0	0	15
Article 27	1	0	0	0	0	1	0	0	0	0	0	0	0	0	0	0	0	0	16

(*Source*: Altmetric.com)

Table 2: Altmetric presence in DJLIT articles

Table 2 demonstrates the Altmetric presence in DJLIT published research. Out of the total 573 scholarly articles indexed in Web of Science, Altmetric tracked 29 articles (5.06%) from which 27 (4.71%) articles received at least 01 Altmetric Attention Score. Out of 27 articles which altmetric attention score, 10 scholarly articles (37.04%) published in recent two years of data collection i.e. 2019 (n=06) and 2018 (n=04).An article titled 'A cross-sectional study of retraction notices of scholarly journals of science' receivedthe highest Altmetric Attention Score of 13.Article 07 titled 'Information Literacy: Essential Skills for the Information Age' got 443 readers on Mendeley which is highest from all scholarly articles.

8.4 Mostly Used Digital Media Platforms by DJLIT Readers

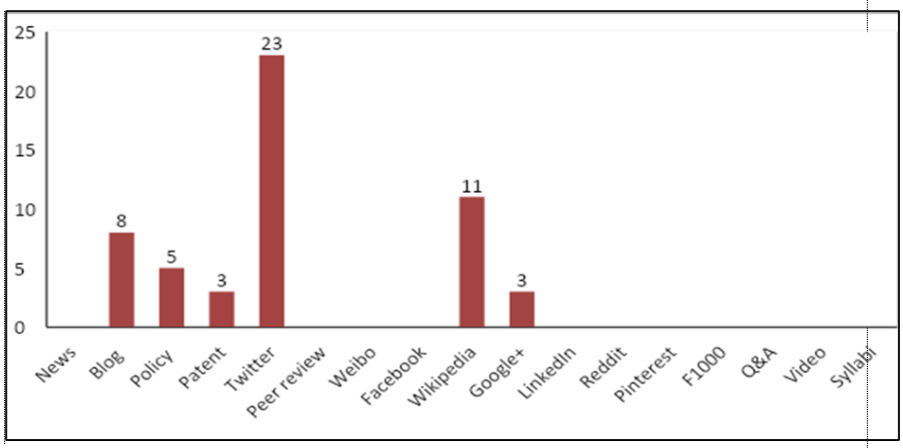

(*Source*: Altmetric.com)

Figure 3: Mostly Used Digital Media Platforms by DJLIT Readers

Figure 3 shows the mostused digital media platforms by DJLIT readers. Altmetric tracked 17 different digital media platforms to get the digital footprints of research published in DJLIT. Out of the total platforms, DJLIT users used Twitter (43.39%) to mention and share research published in DJLIT scholarly articles. The next highest number of mentions was on Wikipedia (20.75%) followed by Blog (15.09%), Policy (09.43%), Patent (05.66%) and Google+ (05.66%).

8.5 Demographic Details of Readers by Professional Status

Mendeley reader count is good evidence of the early impact of scientific output since it appears before citations.[15]

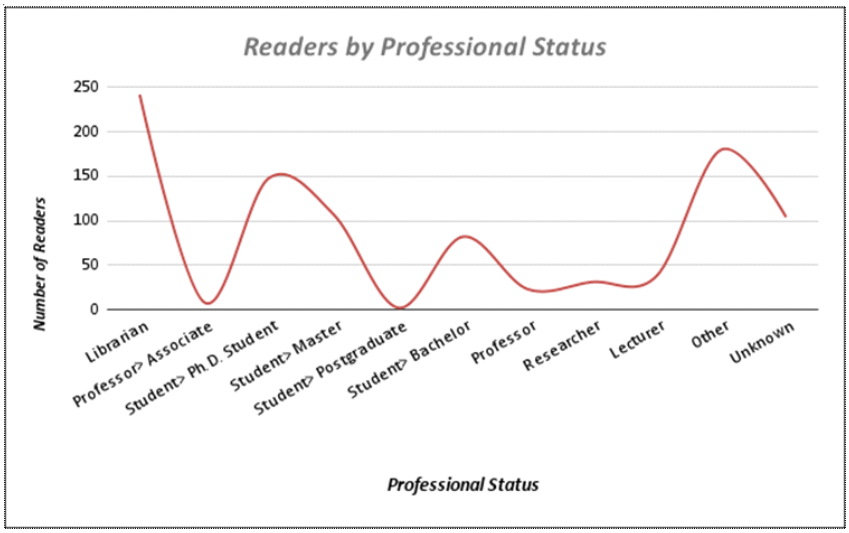

(*Source*: Altmetric.com)

Figure 4: Demographic Details of Readers by Professional Status

Figure 4 and Table 3 demonstrated the DJLIT readers on Mendeley by their professional status.There were mainly 11 categories of readers, including Librarian, Professor, Associate Professor, Lecturer, Researcher, Ph.D., Postgraduate, Master and Bachelor Students; Others and Unknown readers.Librarians were the active readers of DJLIT research on Mendeley with 242 readers (25.07%). The second highest category was the 'other'180 readers (18.65%) indicating that the non-academic community showed good interest in reading DJLIT research.The third highest number of users who reads DJLIT articleswas Ph.D. students with 148 readers (15.34%) followed by 107 Master'sstudents (11.09%).Lecturers (3.94%) were more active readers than Professors (2.38%)and Associate Professors (0.83%).

Article Number	Librarian	Associate Professor	Ph.D. Student	Master Student>	Postgraduate Student>	Bachelor Student>	Professor	Researcher	Lecturer	Other	Unknown	Total
Article 1	5	2	2	--	--	--	1	--	--	--	2	**12**
Article 2	3	--	1	--	--	2	1	--	--	4	2	**13**
Article 3	7	--	--	7	2	--	--	3	--	9	4	**32**
Article 4	3	--	2	1	--	--	--	2	--	2	2	**12**
Article 5	3	--	3		--	--	1	--	--	--	2	**9**

Article 6	3	1	2	1	--		--	2	--	--	4	**13**
Article 7	106	--	54	52	--	65	--	--	27	91	48	**443**
Article 8	1	--	6	1	--	--	--	--	--	--	2	**10**
Article 9	4	--	5	--	--	1	1	--	--	4	2	**17**
Article 10	--	--	--	--	--	--	--	--	--	--	--	**0**
Article 11	9	--	6	4	--	--	3	--	3	4	--	**29**
Article 12	--	--	2	--	--	--	1	--	--	--	1	**4**
Article 13	20	--	17	17	--	--	--	10	--	21	7	**92**
Article 14	5	--	4	3	--	--	1	--	--	3	5	**21**
Article 15	7	--	2	1	--	--	1	--	--	3	--	**14**
Article 16	14	--	3	4	--	5	--	3	--	8	1	**38**
Article 17	2	--	5	5	--	--	2	--	--	5	2	**21**
Article 18	4	--	1	--	--	--	1	2	--	--	--	**8**
Article 19	11	--	9	5	--	2	--	--	--	4	1	**32**
Article 20	--	--	1	1	--	--	1	--	1	--	--	**4**
Article 21	3	--	12	--	--	--	5	7	5	4	--	**36**
Article 22	9	--	3	--	--	--	1	--	--	4	5	**22**
Article 23	7	4	2	--	--	2	--	2	--	5	3	**25**
Article 24	1	1	2	1	--	--	1	--	--	1	1	**8**
Article 25	8	--	1	--	--	1	1	--	--	5	3	**19**
Article 26	3	--	--	3	--	1	1	--	2	3	2	**15**
Article 27	4	--	3	1	--	3	--	--	--	--	5	**16**
Total	**242**	**8**	**148**	**107**	**2**	**82**	**23**	**31**	**38**	**180**	**104**	**965**

(*Source:* Altmetric.com)

Table 3: Demographic Details of Readers by Professional Status

8.6 Readers by Discipline

Data in Figure 5 shows the discipline-wise readers of DJLIT scholarly articles on Mendeley. The top 10 disciplines were selected for analysis as per

the highest number of readers from 18 different fields. the discipline identified as 'Unknown' in Mendeley was excluded from the analysis. Readers who belong to the Social Sciences discipline were the top readers with 368 readers (38.13%). Out of the total readers, 151 (15.64%) readers were from Computer Science, which stood as the second-highest discipline in terms of readership. The next highest discipline was Arts and Humanities with 108 readers (11.19%) and on the other hand, readers from the 'other' disciplines with 102 readers (10.57%)showed a great interest in reading DJLIT publications.

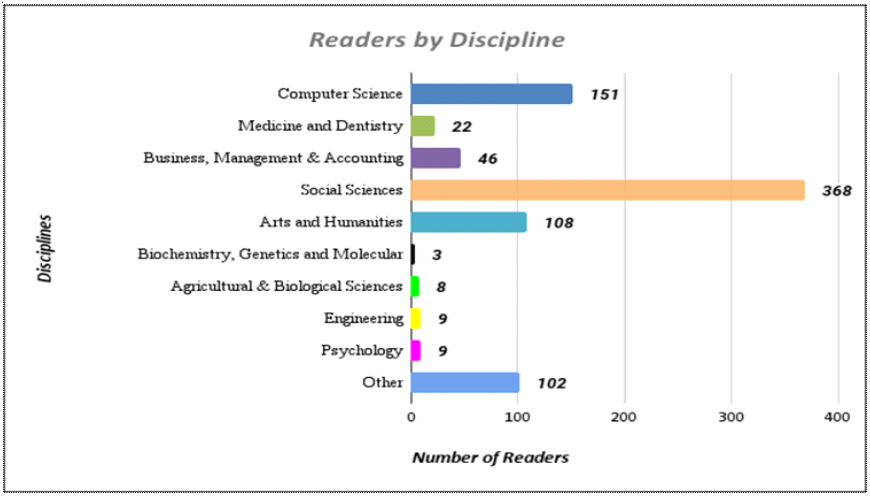

(*Source*: Altmetric.com)

Figure5: Details of Readers by Discipline

9 FINDINGS

This study investigated the altmetric presence in scholarly articles published in the DESIDOC Journal of Library and Information Technology with the highest digital media mentions. No doubt India has dominated the contribution to the journal as DJLIT is an Indian publication with 85.69 percent share amongst 32 countries who participated and published research inDJLIT. Articles published in the journal have received attention from 08 different digital media sources.27 out of the total 573 publications (with valid DOI) have received at least one attention from digital media platforms.Twitter was the platform providing the most altmetric data for DJLIT publications followed by Wikipedia mentions. Except for Twitter 43.39%,the results showed that the presence of DJLIT scholarly articles on other digital media platforms is not high, as just 15.9% of articleswere shared inBlog, 09.43%were mentioned in the Policy and 5.66% were mentionedin Patent. News, Peer Review, Weibo, Facebook,

LinkedIn, Reddit, Pinterest, F1000, Q&A, Video and Syllabi do not get even one mention for all the 27 articles tracked by Altmetric.

Mendeley is also the major source of altmetric data. This study made a profession-wise and discipline-wise comparison of the Mendeley readership of research outputs published in DJLIT.Mendeley's readership varied according to the user categories for DJLIT Publicationshowever the Librarians were reported as the highest readers. The possible reason for the highest readership by the Librarians is the subject coverage of DJLIT is Library and Information Science.Discipline-wise analysis of readership showed that 18different disciplines (including unknown) read DJLIT scholarly articles with higher readership recorded from Social Sciences, followed by Computer Science.Library and Information Technology is an interdisciplinary subject that comes under the Social Sciencesand is closely related to Computer Science.

10 CONCLUSION

DESIDOC Journal of Library and Information Technology is a well-known journal in the academic fraternity. DJLIT has set a standard to publish research related to new tools and Technologies in the field of Library and Information Science. Journal gives free online open access hence it is one of the highly preferred journalby the LIS Professionals in India. Academicians and researchers use this journal regularly to publish their research and readers to update themselves with current research performed in Library and Information Science.Findings of the research shows thatDJLIT gets very less online attention over the platforms that altmetric measure meaningthe awareness of societal impact amongst DJLIT users is less. It is suggested that the DJLIT should approach altmetric.com and enable journal-level altmetric service to track online attention more effectively and encourage the users to share and mention the research on digital media platforms as well.

Altmetric plays a vital role in measuring academic and social information and knowledge and helps to track the influence of information that is shared via various digital media platforms. Academicians have to understand the role of Altmetric in research communication and must use this new technique in the process of research evaluation.It is the need of time to study and explore the Altmetric technique to measure the research impact not only in the academic community but also in social engagements.

REFERENCES

1. PRIEM (J), TARABORELLI (D), GROTH (P)and NEYLON (C). Altmetrics: A manifesto, 26 October 2010. http://altmetrics.org/manifestoaccessed on 08.08.2022.

2. PRIEM(J).Altmetrics,*In*CRONIN (B) and SUGIMOTO(C R), Eds., Beyond bibliometrics: Harnessing multidimensional indicators of scholarly impact. 2014. MIT Press: Cambridge, MA. Pp. 263–288.
3. BORNMANN (L).Do altmetrics point to the broader impact of research? An overview of benefits and disadvantages of altmetrics. *Journal of Informetrics*, 8,4; 2014; 895–903. DOI: https://doi.org/10.1016/j.joi.2014.09.005
4. National Information Standards Organization (NISO) Outputs of the NISO Alternative Assessment Metrics Project. *NISO RP-25-2016,* 2016.
5. DESIDOC Journal of Library and Information Technology. https://publications.drdo.gov.in/ojs/index.php/djlit/about accessed on 09.08.2022
6. KUMAR (M)and MOORTHY (A). Bibliometric Analysis of DESIDOC Journal of Library and Information Technology from 2001-2010. *DESIDOC Journal of Library & Information Technology*, 31, 3; 2011.https://doi.org/10.14429/djlit.31.3.989
7. AKERS (K G).Introducing altmetrics to the Journal of the Medical Library Association. *Journal of the Medical Library Association,* 105, 3; 2017. https://doi.org/10.5195/jmla.2017.250
8. ERFANMASNESH (M). Highly-alted articles in Library and Information Science. *Webology*, 14, 2; 2017; 66-77. https://www.webology.org/data-cms/articles/20200515031407pma158.pdf
9. EZEMA (I J)and UGWU (C I). Correlating research impact of library and information science journals using citation counts and altmetrics attention. *Information Discovery and Delivery*, 47, 3; 2019; 143–153. https://doi.org/10.1108/IDD-08-2018-0029
10. RANGASWAMY and RAJENDRA (B H). An Altmetric Analysis of top journals in Library and Information Science. In: Angadi, M. & others (Eds.), *Digital Technologies and Transformation in Academic Libraries*, 2019, Vol.2., pp. 352-357. New Delhi: Shree Publishers and Distributors.
11. SANKAR (V)and SARANGAPANI (R). Scholarly Communication of Library and Information Science Literature on SocialMedia: an Altmetrics Analysis, 2020, https://digitalcommons.unl.edu/libphilprac
12. TANG (Y), TSENG (H)and VANN (C). Unwrap citation count, Altmetric Attention Score and Mendeley readership status of highly cited articles in the top-tier LIS journals. *Global Knowledge, Memory and Communication*,69, 8/9; 2020; 653–664.
13. https://clarivate.com/webofsciencegroup/solutions/web-of-science/ accessed on 08.08.2022
14. https://www.altmetric.com/about-us/ accessed on 08.08.2022
15. VYSAKH (C)and RAJENDRA (B H). Who Reads Indian and Chinese LIS Articles on Mendeley? Scoping and Comparing User Categories Through Altmetrics. *Journal of Information Science Theory & Practice (JIStaP)*,9, 4; 2021; 75–83. https://doi.org/10.1633/JISTaP.2021.9.4.6

Journal of Molecular Structure 1281 (2023) 135107

Contents lists available at ScienceDirect

Journal of Molecular Structure

journal homepage: www.elsevier.com/locate/molstr

Synthesis of new heterocyclic N'-(2–hydroxy-3-methoxybenzylidene)-4-oxopiperidine-1-carbohydrazide and its mononuclear metal (II) complexes: Spectroscopic characterization, fluorescence, DFT, thermo-kinetic, and antimicrobial studies

Gajanan Dongare[a], Anand Aswar[b,*]

[a] Department of Chemistry, Shri Shivaji College of Arts, Commerce and Science, Akola, 444001. MS, India
[b] Department of Chemistry, Sant Gadge Baba Amravati University, Amravati, 444602. MS, India

ARTICLE INFO

Article history:
Received 4 November 2022
Revised 17 January 2023
Accepted 5 February 2023
Available online 7 February 2023

Keywords:
Heterocyclic hydrazone
Metal complexes
Spectroscopic characterization
Fluorescence emission
DFT
TGA
Biological activity

ABSTRACT

New hydrazone Schiff base N'–(2–hydroxy-3-methoxybenzylidene)-4-oxopiperidine-1-carbohydrazide (H_2L), synthesized by the condensation reaction of 2–hydroxy-3-methoxybenzaldehyde (HMB) and 4-oxopiperidine-1-carbohydrazide (CPH), form mononuclear complexes, $[Mn(HL)(Cl)(H_2O)_2]$, $[Co(HL)(Cl)(H_2O)_2]$, $[Ni(HL)(Cl)(H_2O)_2]$ and $[Cu(HL)(Cl)\ (H_2O)_2]$. The formation of ligand was confirmed by elemental analysis, melting point, IR, ^1H and ^{13}C NMR, and ESI-Mass spectroscopy, Cu(II) complex was further examined by ESR spectroscopy. Other properties, like, molar conductance, IR, electronic spectra, magnetic susceptibility, DFT, powder X-ray diffractometer, fluorescence and thermal analysis have also been studied. Powder X-ray diffraction patterns inferred that compounds are nanocrystalline nature. Surface morphology further support this observation. All compounds show good absorption properties and in excited state at (λ_{334nm}), the fluorochromes of the ligand and its metal (II) complexes emitted a good fluorescence emission with the resonation of 0.2 nm in (λ_{527-}545 nm) region. The DFT B3LYP/6–311G+(d,p) calculations were carried out for the determination of the optimized structure of ligand (H_2L) and its metal complexes. The frontier MOs energies data indicated good charge transfer (*CT*) from HOMO to LUMO. Thermal study of complexes monitored under nitrogen atmosphere led us to determine the activation parameters of various decomposition steps. On the basis of activation energy evaluated by Coat-Redfern relation, thermal stability order was found to be Ni(II)<Cu(II)<Mn (II)<Co(II). The ligand and complexes have also been screened for their antibacterial and antifungal potency and metal complexes showed higher activity against multi-stranded microorganisms viz. gram -ve bacteria (*Escherichia coli* and *Salmonella. typhi)*, gram + ve bacteria (*Staphylococcus aureus, Bacillus substilis)* and fungal species (*Candida albicans, Aspergillus niger).*

© 2023 Elsevier B.V. All rights reserved.

1. Introduction

Heterocyclic moiety involving hydrazones have gained wide applications, and proven to be a very promising, versatile motif in the medicinal chemistry and drug design. Hydrazone based Schiff bases offer an adaptable series of ligands proficient to tie with different metal ions to give edifices for their various applications. Hydrazone based Schiff bases can be considered to be one of the most researched group of chemical molecules by researchers, the reasons being their versatility, selectivity, sensitivity, stability, and ease of synthesis, just to mention a few, which resulted in their wide applications. It has been reported that the azomethine functional group containing molecules contribute to their bioactivity by interacting and forming intramolecular hydrogen bonding with some responding sites within the cell structure, and thus affects the regular cell processes and signifies their biological significance. Similarly, the lone pair of electrons on the sp^2 hybridized orbital of the azomethine nitrogen is another reason for their chemical reactivity. The compounds of hydrazone Schiff base are not only synthons for the synthesis of new metal complexes but also exhibit interesting coordination mode [1–6]. The chemistry of hydrazones containing piperidine ring and their metal complexes is fascinating due to their importance in pharmacological, clinical, analytical and biological applications such as antimalarial, antibacterial, antifungal, and antiviral activities antioxidant, anti-inflammatory, anticonvulsant, analgesic, antimicrobial, anticancer, antiprotozoal,

* Corresponding author.
E-mail address: aswaranand@gmail.com (A. Aswar).

https://doi.org/10.1016/j.molstruc.2023.135107
0022-2860/© 2023 Elsevier B.V. All rights reserved.

antioxidant, antiparasitic, antiplatelet, cardioprotective, anthelmintic, antidiabetic, antitubercular, trypanocides and anti-HIV activities [7–8]. Their tautomerism, an ability to exist either in enol or keto structural forms gives them the potential to form different types of interesting coordination compounds. The architectural beauty of coordination compounds is due to the interesting ligand systems involving different donor sites say ONO, NNO, NO and NNS. Among the N–O donor ligands, hydrazones possess a special place due to their ease of synthesis, easily tunable electronic properties, denticity and formation of wide variety of complexes with chemical, structural, biological and industrial importance. Further, the remarkable biological activity of aroyl hydrazones and their mode of chelation with transition metal ions present in the living systems have been of significant interest because possessing biological and pharmaceutical properties [9–11]. The ONO triatomic donor ligand systems improve metal complexation, reactivity's, stability, physicochemical property [12–18]. Schiff base ligands like hydrazones are considered privileged ligands because they are easily prepared by a simple one-pot condensation of a carbonyl compound and primary amines in an alcoholic medium. Heterocyclic moiety of hydrazone is an important pharmacophore associated with various interesting types of biological effects which provides an extensive opportunity in exploring this moiety as an antimicrobial agent.

The literatures survey revealed that no attention has been paid to the synthesis of the N'-(2-–hydroxy-3-methoxybenzylidene)–4-oxopiperidine-1-carbohydrazide and its Mn(II), Co(II), Ni(II) and Cu(II) complexes . Furthermore, due to the resistance of antimicrobial agents, there is a continued need for developing heterocyclic compounds with good microbial activity. Hence, it was thought of interest and in view of our continuing interest in a heterocyclic hydrazone, we designed and synthesized new hydrazone Schiff base contains heterocyclic moiety derived from 2-–hydroxy-3-methoxybenzaldehyde (HMB) with 4-oxopiperidine-1-carbohydrazide (H_2L) and its Mn(II), Co(II), Ni(II) and Cu(II) complexes. The compounds were characterized by elemental, molar conductance, IR, electronic spectra, magnetic susceptibility, DFT, SEM, XRD, fluorescence and TG analysis. Also, present a DFT and the evaluation of their biological activity.

2. Experimental

2.1. Materials

All the chemicals used in this study were of analytical reagent grade and acquired from Avra synthesis, S.D. fine chemicals, and Hi-media and used without further purification. Solvents used for the reactions were purified, and dried by conventional methods. The silica granules of size 60–100 mess were used to remove the water contents from all solvents.

2.2. Analysis and physical measurements

The FT-IR spectra of the ligand and its complexes were recorded using an Advance Bruker spectrophotometer. The elemental analysis (C, H, and N) were made using Vario El III Carlo Erba 1108 elemental analyzer. The molar conductance of complexes (10^{-3} M solutions) in DMSO were measured at room temperature using a Elico conductivity meter (180). The complexes were analyzed for their metal and halide content by gravimetric method using standard procedures. The magnetic moments of the complexes were measured at room temperature on a Sherwood scientific magnetic susceptibility balance (MK-1). The NMR spectra (^{1}H, ^{13}C) ligand were carried out on Bruker model 400 MHz using *TMS* as an internal standard (d ppm) and DMSO-–d_6 as the solvent. The mass spectrum of the ligand was done on water micro-mass spectrophotometer (Q-T range 4000–20,000 a.m.u.). The micro graphical image of ligand and their metal complexes was captured by using a JEOL-6390LV SEM at high resolution (10μm-100 μm) under the magnification (X250 - X 3000) by accelerating the voltage of 10kv. The electronic spectra were recorded on a double beam Shimadzu UV–visible spectrophotometer (1800) in the range of 200-1100 nm. The ESR spectrum of Cu(II) complex was performed on JES - FA200 in X band (Std. freq.=8.75–9 to 65 GHz in LNT) at 77–78k. The optimization of molecular structure was done out using Gaussian 09 with B3LYP and Gauss View 6.0 was used for creation of a input file for the calculation of graphical interface (3D) to evaluate the data, and generate MEP. Fluorescence spectra were recorded on a Hitachi-F-7000 spectrophotometer having a scan speed of 240 nm/min. The light source 150 W xenon lamp was used with an electrical power supply at 700 V. The monochromatic stigmatic concave diffraction with power was utilized by grating at 900 lines/mm and F 2.2 for high resolution 1.00 nm, and 1 nm wavelength accuracy. The brazed wavelength was operated at excitation 300 nm and emission 400 nm, and may expandable ~900 nm accelerated drive speed-60,000 nm/min. The simultaneous TG-DTG curves were recorded on Perkin-Elmer (TGA-4000) thermal analyzer in the temperature range 40 - 800 °C with the heating rate of 20 °C per min in N_2 atmosphere. X-ray diffractograms (pattern) were recorded on a Rigaku-Miniflex (600). The melting point was determined on digital melting point apparatus.

2.3. Synthesis of (2–hydroxy-3-methoxybenzylidene)–4-oxopiperidine-1-carbohydride (H_2L)

An equimolar mixture of 4-oxo-1-carbopiperidone hydrazide (0.314 g, 2 mmol) and 3-methoxy salicylaldehyde (0.304 g, 2 mmol) dissolved in 25 mL dry ethyl alcohol and mixture was refluxed for 4 h with a catalytic amount con.H_2SO_4 (2drops). The reaction progress was monitored by TLC. The bright yellow solid obtained was separated out by vacuum filtration, washed with dry ethanol, and finally recrystallized from DMSO. The purity of ligand was checked by TLC utilizing silica gel and shown in Scheme 1. The structure of ligand was confirmed by M.p., CHN analysis, FT-IR, NMR (^{1}H and ^{13}C), and ESI-Mass spectroscopy. Color: Yellow. Yield: 0.464 g, (75.2%), M.p.:160–162 °C.

Elemental analysis of [$C_{14}H_{17}N_3O_4$] (%): Calcd.; C, 57.72; H, 5.88; N, 14.42 and found; C, 57.94; H, 5.40; N,14.85.

FT-IR ($\bar{\nu}$, cm^{-1}): 3390 (OH, broad, Ph-OH), 3268(N–H, amide), 1678(C = O, amide), 1618(C = N azomethine), 1451(C–O, -OCH_3), 1304(C–O, phenolic), 962 (N–N, azomethine).

UV/Vis (DMSO, λ_{max}, nm, ε): 331(1.67), 290(1.15), 250(2.25).

^{1H}NMR (DMSO-–d^6,500 MHz, δ ppm): 10.898(s,1H, OH, Phenolic.), 9.511 (s,1H,-C*H*=N- azomethine), 8.99 (s,1H,N*H*,amide), 6.934(d, J = 9.4 Hz, 1H,aryl-H), 7.122 (dd, J = 9.4 Hz, 1H,aryl-H), 7.303 (d, J = 9.05 Hz, 1H,aryl-H),3.839 (s, 3H, -OCH_3), and 3.358, 2.516(s, J = 4.21 Hz, 4H), 2.513,2.506 (s, J = 3.5 Hz, 4H) in the heterocyclic ring.

^{13C}NMR (DMSO–d_6, 500 MHz, δ ppm): 148.38 (C1,Ar-C, phenolic), 115.15 (C2, Ar-C), 121.92 (C3, Ar-C), 119.16 (C4, Ar-C,), 118.22 (C5, Ar-C), 147.85 (C6, Ar-C, methoxy), 162.66 (C7, C = O, amide), 55.16 (C11, -OCH_3), 147.85 (C17, HC=N, azomethine), 158.1 (C22, >NHC=O, amide), and 39.45 (C24), 39.23 (C25), 39.40 (C26), 39.56 (C28), 185.54 (C33, C = O, heterocyclic ring).

HRMS (ESI-*m/z*) calcd. for [$C_{14}H_{17}N_3O_4$], 291.30; Found $[M]^{+1}$ = 292.12.

2.4. Synthesis of Mn(II), Co(II), Ni(II), and Cu(II) complexes

Metal complexes of Mn(II), Co(II), Ni(II), and Cu(II) were synthesized by following general method. A hot ethanolic solution

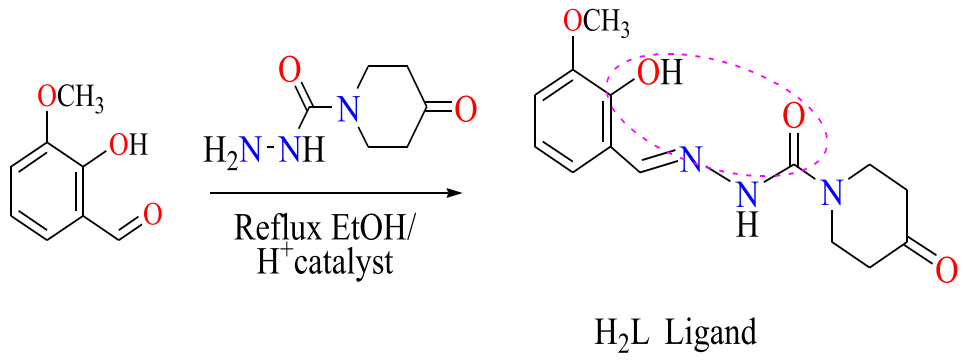

Scheme 1. Synthesis of hydrazone ligand (H_2L).

Table 1
Analytical data of ligand (H_2L) and its metal (II) complexes.

Compounds	Molecular Formula	Mol.Wt. gm/mol	Elemental analysis found, (calcd.) %				
			C	H	N	Cl	Metal
Ligand [H_2L]	$C_{14}H_{17}N_3O_4$	291.30	58.00 (57.72)	5.98 (5.88)	14.60 (14.42)	–	–-
[Mn(HL)$(H_2O)_2$Cl]	$MnC_{14}H_{20}N_3O_6Cl$	416.71	40.82 (40.34)	4.70 (4.83)	10.20 (10.08)	8.60 (8.50)	13.25 (13.18)
[Co(HL)$(H_2O)_2$Cl]	$CoC_{14}H_{20}N_3O_6Cl$	420.71	40.10 (39.99)	4.99 (4.79)	10.02 (9.98)	8.90 (8.42)	14.25 (14.00)
[Ni(HL)$(H_2O)_2$Cl]	$NiC_{14}H_{20}N_3O_6Cl$	420.47	40.00 (39.99)	4.95 (4.70)	10.00 (9.99)	8.75 (8.43)	14.00 (13.95)
[Cu(HL)$(H_2O)_2$Cl]	$CuC_{14}H_{20}N_3O_6Cl$	425.32	40.00 (39.53)	4.90 (4.73)	10.00 (9.87)	8.60 (8.33)	15.07 (14.94)

of metal salt (2.0 mmol, 20 mL) [$MnCl_2{\cdot}2H_2O$, $CoCl_2{\cdot}6H_2O$, $NiCl_2.H_2O$, $CuCl_2{\cdot}2H_2O$] was added dropwise in to a hot solution of hydrazone ligand (H_2L) (2.0 mmol, 20 mL) in DMSO. The pH of the reaction mixture was maintained at ~7–8 by the addition of alcoholic ammonia (2 ml). Further, the reaction mixture was refluxed in an oil bath for ca. 4 h. The precipitate separated out during refluxing was filtered and washed with the warm ethanol and diethyl ether, and then dried in a vacuum using anhydrous $CaCl_2$ in a desiccator [19]. The elemental data, mol. formula, mol. Wt. and molar conductance values of metal complexes are summarised in **[**Table 1**]**.

3. Results and discussion

3.1. Synthesis

The equimolar amounts of 2–hydroxy-3-methoxybenzaldehyde and 4-oxo-1-carbopiperidone hydrazide react in ethanol in the presence of H^+ catalyst yields a 2–hydroxy-3-methoxybenzylidene-4-oxopiperidine-1-carbohydrazide ligand (***H_2L***) (Scheme 1). The homogeneity of the ligand was regularly checked by TLC. The reaction of the ligand with metal salts in 1:1 molar ratio in dry ethanol-DMSO affords metal complexes, [Mn(HL)$(H_2O)_2$Cl] (**1**), [Co(HL)$(H_2O)_2$Cl] (**2**) [Ni(HL)$(H_2O)_2$Cl] (**3**) and [Cu(HL)$(H_2O)_2$Cl] (**4**). The ligand behaves as monobasic tridentate coordinating through '*ONO*' donor sequence. All these metal complexes have been obtained as colored solid, stable on prolonged exposure to air and insoluble in most common organic solvents except in DMF and DMSO. The analytical data are well agreeing with the proposed components of ligand (H_2L) and its metal (II) complexes. The analytical data of the complexes along with their molar conductance values are given in Table 1. The molar conductivity of metal complexes in DMSO ($10^{-}3$ M) has low value 6.14–26.15 Sm^2mol^{-1} in DMSO indicating non electrolytic nature.

3.2. Characterization of heterocyclic hydrazone ligand (H_2L)

The ^{1H}NMRspectrum of hydrazone ligand showed low field singlet distinctly for phenolic–O*H*, azomethine proton (-*H*C=N-), and amide proton (>*N*–-H) at high frequency resonance region at δ 10.898, 9.511 and 8.99 ppm respectively (Fig. 1). Further, another singlet was observed at δ 3.893 ppm due to the methoxy proton suggesting identical protons environment around the carbon C11. The heterocyclic ring system shows the two up-field doublets in the low frequency regions at δ 3.358 ppm corresponding to four protons of the two -C*H*$_2$- group (α-position) and another two-doublet at δ 2.513 ppm appeared of four protons in another two -C*H*$_2$- group (β-position). The three non-equivalent aryl protons exhibit three doublets in the expected region of 6.934, 7.122, 7.303 ppm with well resolution. The ^{13C}NMR spectrum of the hydrazone ligand exhibits four signals at δ 39.45, 39.23, 39.40 and 39.56 ppm respectively due to the four carbons of the heterocyclic ring. The signal observed at δ 185.54 ppm assigned for the saturated carbonyl carbon of the heterocyclic ring which appeared at low intensity whereas another signal appeared at δ158.1 ppm is assigned for amide carbonyl carbon. The azomethine carbon (-H*C*=N-) signal appeared at δ 147.85 ppm. The separate signals appeared at δ 55.16 is due to methoxy carbon, and other aromatic carbons appeared well within the region of δ148.38–118.22 ppm (**Fig.S1**).

The HR-Mass spectrum of the ligand shows M^+ = 333.34 *m/z* of its molecular ion peak, considered as to its molecular mass. Some stable fragmented molecular ion species are 260.10 *m/z* ($C_{13}H_{14}N_3O_3^+$) at 100% intensity regarded as a base peak whereas other fragmented species 206.12 *m/z* and 164.10 *m/z* indicating ($C_{11}H_{16}N_3O^+$) and ($C_{10}H_{14}NO^+$) molecular ions, respectively. The HR-mass spectrum displayed a molecular ion peak M^{+1} at 292.12 is assigned to its molecular mass. The significant stable fragmented molecular ions obtained as *m/z* ($C_{13}H_{14}N_3O_3^+$) 260.17 of 100% intensity are corresponding to a base peak. The other fragmented species assigned, *m/z* with their intensities are as; ($C_{13}H_{14}N_3O_2^+$) 244 of 48.12%, ($C_7H_{10}N_3O_2^+$)168 of 32.50%, ($C_6H_9N_2O_2^+$), 141 of 24.99%, ($C_5H_8NO^+$) 98 of 22.15% (**Fig.S2**).

3.3. IR spectral analysis of hydrazone ligand (H_2L) and its metal (II) complexes

The FTIR spectra of the ligand and its metal complexes were closely compared and the modifications in frequency vibrations due to the interaction of the metal ion with the ligand were

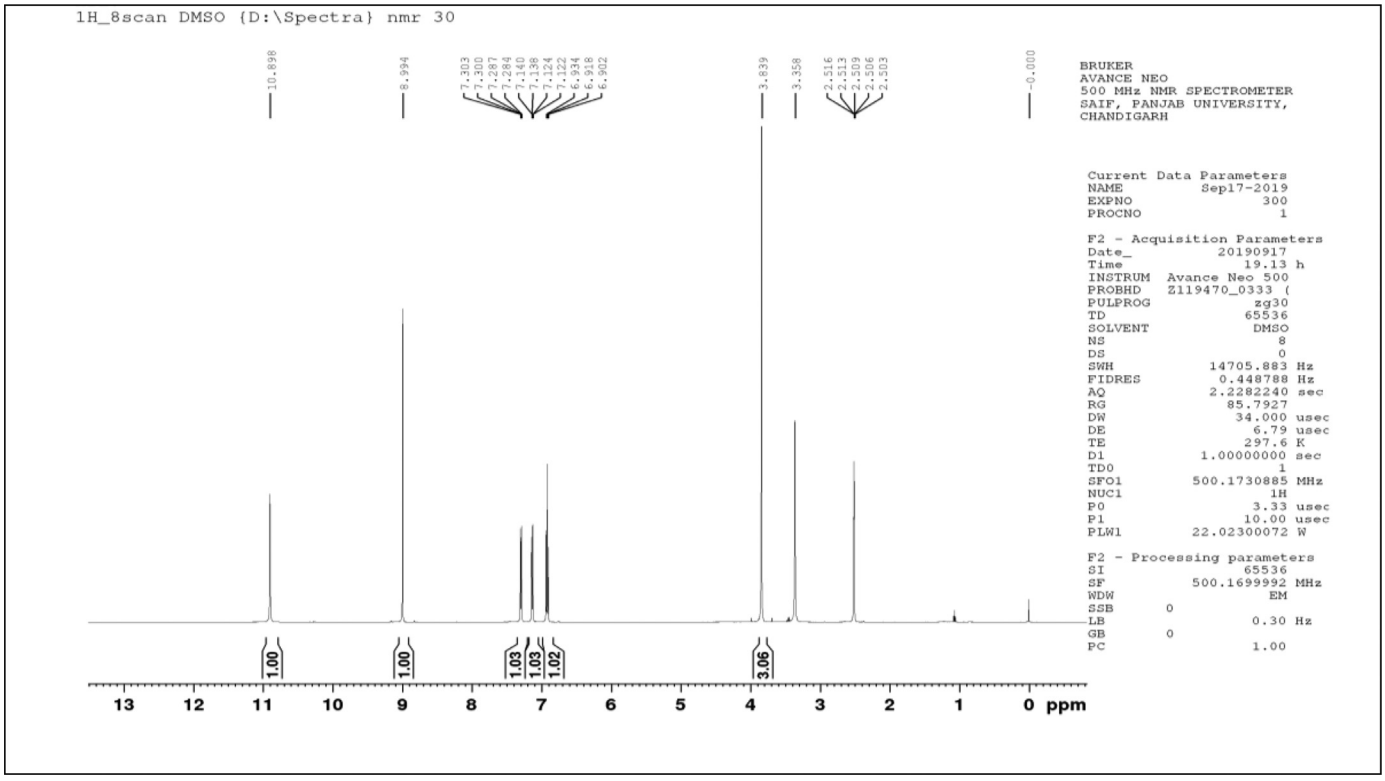

Fig. 1. ^{1H}NMR spectrum of hydrazone ligand (H_2L).

recorded. The FT-IR spectra of hydrazone ligand (H_2L) and its metal complexes are presented in (Fig. 2**)** as well as simulated spectra **(Fig.S5 a-b),** and their selected band frequencies are given in [Table 2] The ligand spectrum shows a broad band at 3390 cm^{-1} is due to phenolic ν_{O-H} group. The absence of this band in the spectra of complexes indicates the formation of coordination bond between the metal ion and phenolic oxygen *via* deprotonation. This is further confirmed by the increase in absorption frequency of ν (C–O) about 31 to 77 cm^{-1} from 1304 cm^{-1} in all the complexes indicating the participation of oxygen atom of phenolic 'OH' in

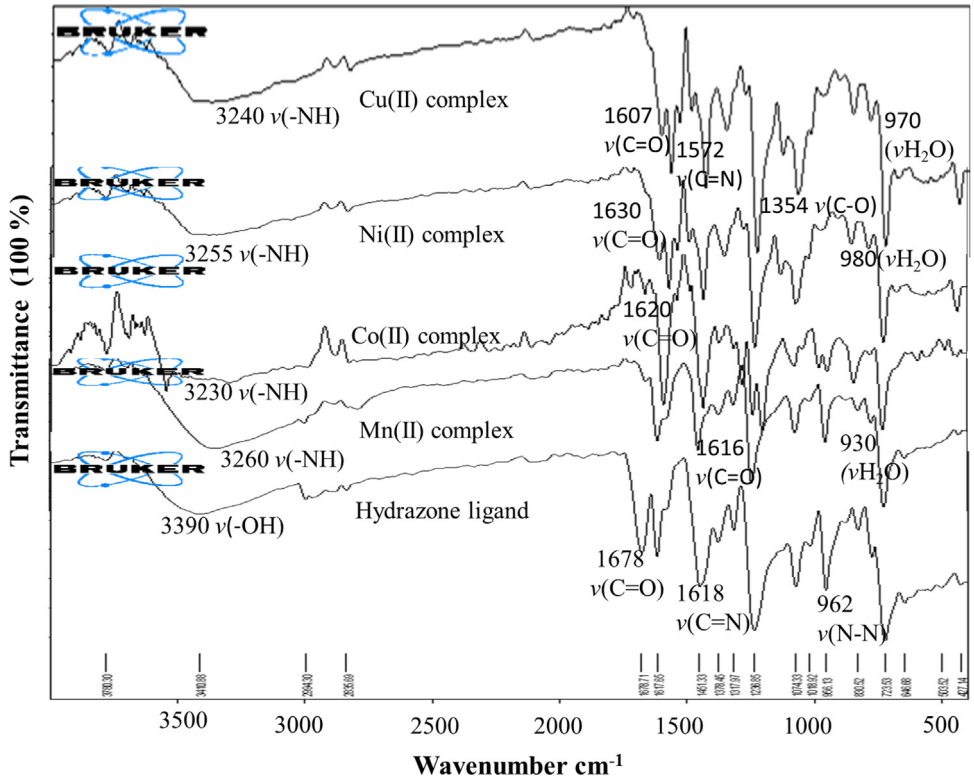

Fig. 2. FT-IR spectra of hydrazone ligand (H_2L) and its metal(II) complexes.

Table 2
Important FT-IR spectral data of ligand (H_2L) and its metal (II) complexes (cm^{-1}).

Compound	ν_{OH}	ν_{N-H}	$\nu_{C=O}$ amide	$\nu_{C=N}$ azomethine	ν_{C-O} Phenolic	ν_{N-N}	ν_{H2O} coord.	ν_{M-O}	ν_{M-N}
Hydrazone ligand	3390	3268	1678	1618	1304	962	–	–	–
$[Mn(HL)Cl(H_2O)_2]$	–	3260	1616	1605	1377	970	930	564	436
$[Co(L)Cl(H_2O)_2]$	–	3230	1620	1600	1350	975	908	591	450
$[Ni(HL)Cl(H_2O)_2]$	–	3255	1630	1614	1381	980	891	593	460
$[Cu(HL)Cl(H_2O)_2]$	–	3240	1607	1572	1354	970	890	540	439

coordination. The IR spectrum of ligand shows intense band at 1618 cm^{-1} due to azomethine $\nu_{HC==N}$ stretching frequency. This band has been shifted to the low-frequency region by 46–4 cm^{-1} in the spectra of all complexes and supported the coordination of azomethine nitrogen to metal center, this has been further strengthened by the shift of ν (N–N) band from 962 cm^{-1} in free ligand to 970–980 cm^{-1} in complexes [20,21]. The ligand shows band at 3268 cm^{-1} due to amide ν_{N-H} stretching frequency [>*N*–H of >CONH] and which appeared almost at about same position in the case of Mn(II), Co(II), Ni(II) and Cu(II) complexes, thus indicating its non-involvement in coordination and confirming the presence of ligand in its ketonic form in these complexes. Further, the shift of amide carbonyl ν (C = O) to a lower frequency side by an extent of 71–48 cm^{-1} in all these complexes supported the coordination of the oxygen atom of the amide carbonyl ν(C = O) with the metal ions as such without undergoing enolization [22,23]. The coordination of the metal ions with ligand was further confirmed by the appearance of new weak intensity, non-ligand bands in the region 540–564 cm^{-1} and 436–460 cm^{-1} in the IR spectra of the complexes are assigned to frequencies of ν(M-O) and ν(M-N) stretching vibration respectively. The IR spectra of complexes displayed the low frequencies stretching bands in the region of 891–930 cm^{-1} indicating the presence of coordinated water molecules attached to the metal center. On the basis of the IR spectral data, it is confirmed that the Schiff base ligand is coordinated in tridentate manner through the oxygen atom of the carbonyl group and the nitrogen atom of the azomethine group and phenolic-OH after deprotonation.

3.4. Magnetic moment, and UV–Visible spectroscopic studies

The electronic absorption spectrum of hydrazone ligand (H_2L) was recorded in DMSO (conc.=2 × 10^{-4}) in the UV region λ(210–432)nm and shown in Fig. (3**a**). The spectral bands observed at λ=331, 290 and 250 nm were due to the (>C = O) group, N-atom of >NH amide, (-N = C--H) in azomethine, and O-atom in phenolic-OH. The transition was due to the excitation by absorption of σ, π, and its lone pair electrons of these chromophores. The absorption band was appearing in the region of λ 405-432 nm in the azomethine –N = C--H of ($\pi \rightarrow \pi^*$) transition shifted at a higher wavelength refereed to red shift absorption. The hypsochromic shift (blue shift) also occurred due to the hydrogen bonding because of the significant impact of $n \rightarrow \pi^*$ at a shorter wavelength of 210-243 nm. The other allowed transition of $\pi \rightarrow \pi^*$ which exhibited bands in λ 210-250 nm in the substituted aromatic ring of the title ligand.

In order to obtain information concerning the stereochemistry of the metal ion, the electronic absorption spectra and magnetic moment of complexes were recorded and date are given in [Table 3] and spectra shown as (**3b**). The electronic spectrum of Mn(II) complex exhibits three weak absorption bands at 918, 755 and 328 nm which correspond to $^6A_{1g} \rightarrow {}^4E_g(^4D)$, $^6A_{1g} \rightarrow {}^4E_g$ (G) and $^6A_{1g} \rightarrow {}^4E_g$, transitions, respectively and clearly indicates the octahedral geometry of Mn (II) complex. The observed magnetic moment value 5.94 B.M. may be taken as an additional evidence for octahedral geometry. The various ligand field parameters have been calculated by known relations and values are found to be (Dq=1127 cm^{-1}, B = 700 cm^{-1}, β=0.81 and ν_2/ν_1= 1.18 and suggesting the presence of covalency in the M-L bond. The electronic spectrum of Co(II) complex displayed three absorption bands at 1085, 765, and 409 nm due to $^4T_{1g}, \rightarrow {}^4T_{2g}$, $^4T_{1g} \rightarrow {}^4A_{2g}$ and $^4T_{1g} \rightarrow {}^4T_{1g}$(P), transitions, respectively towards characteristic of high spin octahedral Co(II) complexes. The room temperature magnetic moment value was found to be 4.62 B.M. assignable of the presence of three unpaired electrons, indicating a quartet ground state, which was orbital triply degenerate and would cause an angular mo-

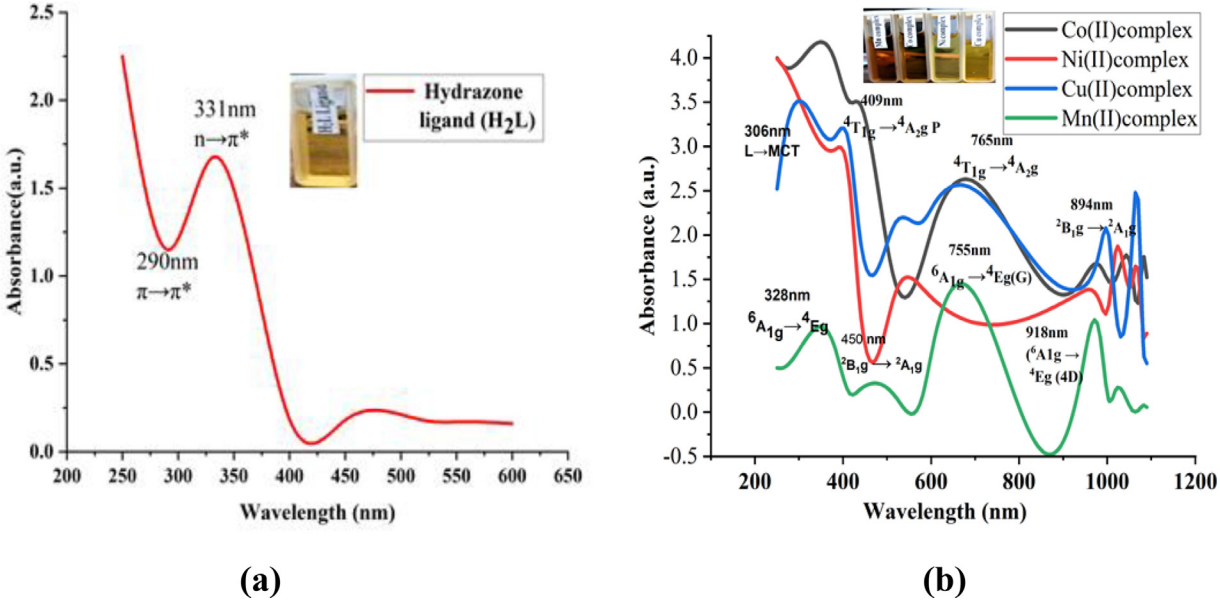

Fig. 3. (**a**) Electronic absorbance of hydrazone ligand (H_2L) and (**b**) Metal(II) complexes in DMSO (2 × 10^{-}4 mol dm^{-3}).

Table 3
Molar conductance, magnetic, electronic absorbance data of metal (II) complexes

Compounds	Molar cond.(Sm^2mol^{-1})	μ_{eff} (B.M.)	Absorption maxima (nm) cm^{-1}		Spectral transitions	Ligand Field Parameters				
			(λ_{nm})	(ν cm^{-1})		Dq (cm^{-1})	B (cm^{-1})	B_0 (cm^{-1})	β=B/B_0	ν_2/ν_1
$[Mn(HL)Cl(H_2O)_2]$	20.00	5.83	918	10,893	$^6A_{1g}\rightarrow{}^4E_g$ (^4D)	1089	737	860	0.86	1.22
			755	13,245	$^6A_{1g}\rightarrow{}^4E_g$ (G)					
			328	30,488	$^6A_{1g}\rightarrow{}^4E_g$					
$[Co(HL)Cl(H_2O)_2]$	18.40	4.62	1085	9217	$^4T_{1g}\rightarrow{}^4T_{2g}$	1152	658	971	0.68	1.42
			765	13,072	$^4T_{1g}\rightarrow{}^4A_2g$					
			409	24,450	$^4T_{1g}\rightarrow{}^4T_{1g}$(P)					
$[Ni(HL)Cl(H_2O)_2]$	15.50	2.79	1088	9191	$^3A_{2g}\rightarrow{}^3T_{2g}$	919	693	1030	0.67	1.24
			874	11,441	$^3A_{2g}\rightarrow{}^3T_{1g}$(F)					
			450	26,526	$^3A_{2g}\rightarrow{}^3T_{1g}$(P)					
$[Cu(HL)Cl(H_2O)_2]$	4.60	1.72	894	11,164	$^2B_1g\rightarrow{}^2A_1g$	––	–	––	––	–
			551	18,148	$^2B_1g\rightarrow{}^2Eg$					
			306	32,680	LMCT					

Table 4
The fluorescence emission data of hydrazone ligand (H_2L) and its metal(II) complexes excited at 334 nm.

Compounds	Wavelength (nm)	Fluorescence intensity I_F (a.u.)
Ligand (H_2L)	527	908.80
$[Mn(L)(H_2O)_2Cl]$	552	231.30
$[Co(HL)(H_2O)_2Cl]$	535	210.60
$[Ni(HL)(H_2O)_2Cl]$	545	196.90
$[Cu(HL)(H_2O)_2Cl]$	543	119.00

ment contribution to magnetic moment expected for the octahedral geometry of Co(II) complex. The different ligand field parameters have been evaluated from the spin allowed transitions and values are found to be Dq =1152 cm^{-1}, B = 658 cm^{-1}, β=0.68, and ν_2/ν_1 =1.42. The observed lower B value than free ion (971 cm^{-1}) indicated presence of covalency in the M-L bond. The Ni(II) complex exhibits three bands at 1088,874,450 nm which may be assigned to the $^3A_{2g}\rightarrow{}^3T_{2g}$, $^3A_{2g}\rightarrow{}^3T_{1g}$(F) and $^3A_{2g}\rightarrow{}^3T_{1g}$ (P) transitions, respectively in an octahedral environment around Ni(II) ion. The observed magnetic moment for Ni(II) complex is 2.89 B.M. which well within the expected for Ni(II) octahedral complexes . The observed ν_2/ν_1 ratio (1.60) is also expected for an octahedral Ni(II) complexes. The calculated B value (B = 704 cm^{-1}) for the Ni(II) complex is lower than the free Ni(II) ion value (1011cm^{-1}) due to the presence of orbital overlap and delocalization of d-orbitals. Further, β value for complex found is less than one indicating a considerable amount of covalent character in the metal–ligand bond. The Cu(II) complex showed a broad absorption band around 894 nm due to $2B_{1g}\rightarrow2A_{1g}$, transition, characteristic for a distorted octahedral geometry around the Cu(II) ion. Other two bands observed at 551, and 306 nm are assigned to $^2B_1g\rightarrow{}^2Eg$ transition and ligand to metal charge transfer (LMCT) in $\pi\rightarrow\pi^*$ and $n\rightarrow\pi^*$ state, respectively. The observed magnetic moment for Cu(II) is 1.72 B.M., which suggests the distorted octahedral geometry around Cu(II) ion [24,25].

3.5. The fluorescence emission analysis

The emission spectra of the solid hydrazone ligand (H_2L) and its Mn(II), Co(II), Ni(II), and Cu(II) complexes were recorded (the excitation and emission slit widths were 1.0 nm) in the range of (λ = 210–810) nm at room temperature and spectra are presented in (Fig. 4) as (**a**) and (**b**), and the results obtained are summarised in [Table 4]**.** The emission band measured at a rate of 240 nm/min showing excellent sensitivity at S/N 800. All the compounds exhibit excitation at $\lambda_{excitation}$334 nm, and emission intensity was measured in the solid state. The hydrazone (H_2L) ligand showed a good fluorescence intensity at 527 nm (I_F =908.80 a.u). The Mn(II), Co(II), Ni(II) and Cu(II) complexes also exhibit quick response for emission and fluorescence intensity was found to be I_F=231.30, 210.60, 196.90 and 119.00 a.u. at λ = 552, 535, 545, and 543 nm, respectively. The wavelength at which non-radiative emission was apprised in the free ligand and its complexes are as H_2L > Mn(II)> Co(II)> Ni(II) [211–213]. The emitted intensity of the hydrazone ligand and its $[Mn(HL)(Cl)(H_2O)_2]$, $[Co(HL)(Cl)(H_2O)_2]$, $[Ni(HL)(Cl)(H_2O)_2]$, and $[Cu(HL)(Cl)(H_2O)_2]$ complexes was due to the photoinduced electron transfer (PET), the combined inhibition effects of static interaction by charge transfer (*CT*) from metal ion to fluorophore groups, and active fluorochromes group viz. azomethine (-C*H*=N-) and (*C* = *O*) groups present in heterocyclic ring [26–28]. The photoemission data revealed that the ligand and its metal (II) complexes are good fluorescent candidates may be used for photochemical applications, and heavy metal ions detection in biological sciences.

3.6. ESR tensor components, and bonding parameters of Cu(II)complex

In order to obtain structural information of the Cu(II) complex from the hyperfine graphs, which elucidates the nature of the Cu-ligand bond and environment around central metal ion. The X-band spectrum (anisotropic) of Cu(II) complex is depicted in (Fig. 5) and its tensor components are given in [Table 5]. The well-defined ESR spectrum shows two peaks, $g_{||}$ are located at 2972.64 G, 2644.3 G, and another two peaks of $g_\perp$ located at 3310 G, 3339 G. The tensor components ($g_{||}$ and $g_\perp$) for complex were found to be $g_{||}$ 2.384 and $g_\perp$ 2.075 which indicate that the complex is axially symmetric. In the present study the observed measurements for Cu(II) complex is $g_{||} > g_\perp >$ ge (2.0023), suggests that copper site has a dx^2-dy^2 ground state characteristic of octahedral geometry [29]. The geometric parameter (G) is measure of extent of exchange interactions and calculated value (G = 4.27 cm^{-1}) for complex is found to be greater than 4, suggests the exchange interaction between the copper centres is negligible. The hyperfine splitting constant (HSC) also inferred that, the tensor components $A_{||}$ =287cm^{-1} and $A_{\perp}$=257cm^{-1} confirmed that electron interacted with only one copper nucleus in the distorted octahedral structure. The coordination environment of Cu^{2+} ion shows a distorted octahedral geometry an axial elongation with ligands, due to Jahn–Teller distortion. The axial bonds with the longer bond lengths which coordinated to Cu^{2+} ion.

The tensor components ($A_{||} > A_\perp$) suggested an axial symmetry with of Cu-O bond, and Cu-N bond in a distorted octahedral geometry. An inverse relation of the $A_{||}$ and $g_{||}$ was indicating the

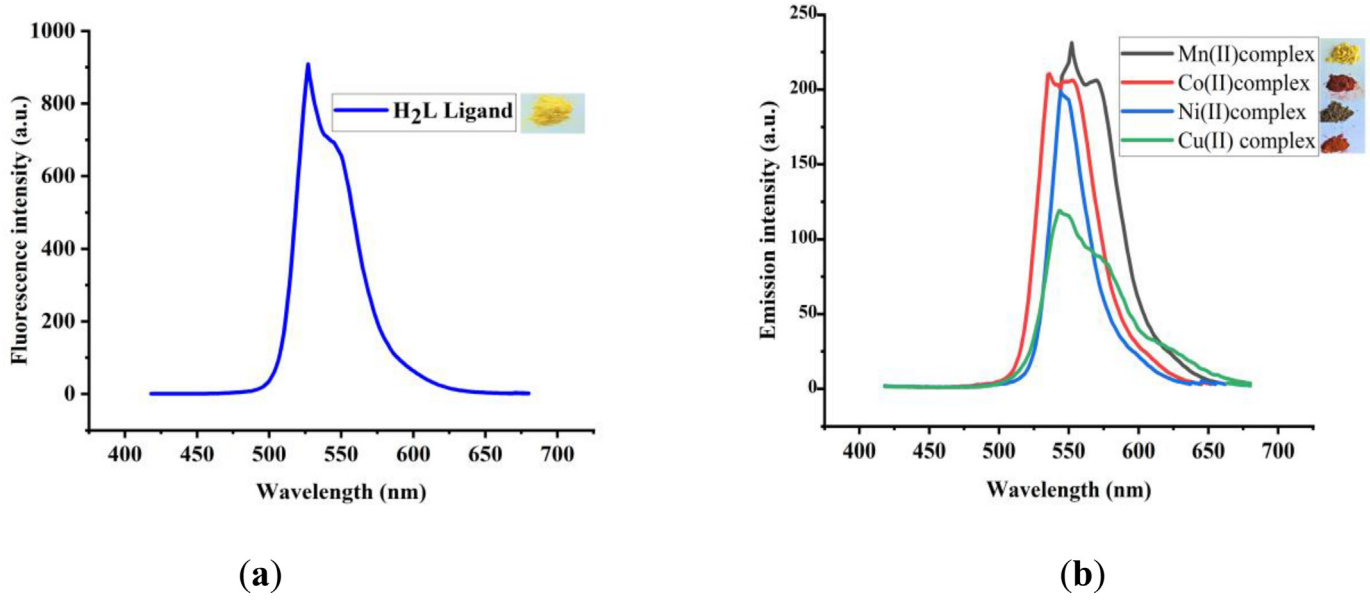

Fig. 4. Comparative fluorescence emission spectra of ligand (**a**) and (**b**) metal complexes.

Table 5
Calculation of ESR tensors and bonding parameters of Cu(II) complex.

ESR Tensors				Hyperfine splitting constant (HSC) (10^4), cm^{-1}		$A_{av.}$	$f = g_{\parallel}/A_{\parallel}$	Bonding parameter (covalency)		Orbital Reduction (overlapping)	
g	$g_{\parallel}$	$g_{\perp}$	G	$A_{\parallel}$	$A_{\perp}$	272	81.82	α^2	β^2	$K^2_{\parallel}$	$K^2_{\perp}$
2.0036	2.3485	2.075	4.27	287	257			0.44	3.02	1.19	0.95

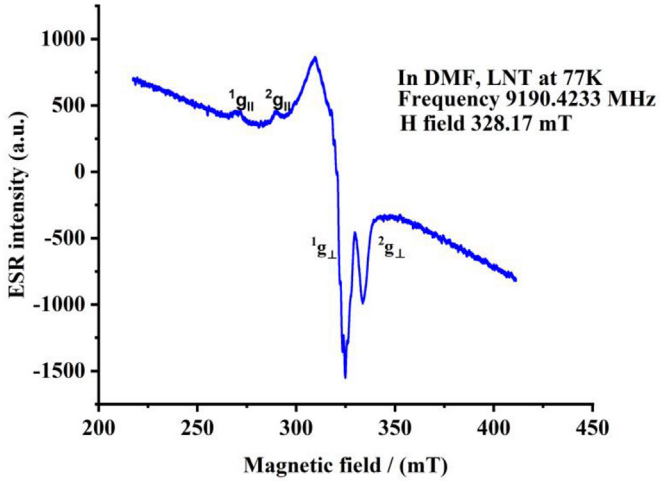

Fig. 5. ESR spectrum of Cu(II) complex.

increases in covalency of the metal−ligand bond the greater the delocalization of the electron density. As a result of this, the interaction between the electron, and nuclear spin increases with the increasing A‖ value compared while the decreasing trend of g‖ value. The values of the functioning ratio (f) =g‖/A‖ was evaluated (81.82) which clearly indicated ligand effects on the metal's unpaired electron density, and its coordination environment. Another important parameter of molecular orbital coefficients α^2= (covalency in σ bonding), and β^2 = (covalency in π bonding) were informed that (β^2=3.02)>(α^2 =1.19) that covalency in π bonding was found stronger than covalency in σ bonding. Additional confirmation of an axial distortion in the octahedral structure was validated from the evaluation of the orbital reduction parameter ($K^2_{\perp}$= 0.95) < ($K^2_{||}$=1.0) in Cu(II) complex and optimized molecular structure [30,31].

3.7. Molecular geometry optimization

The structures of hydrazone Schiff base ligand (H_2L) and its complexes $[Mn(HL)(Cl)(H_2O)_2]$, $[Co(HL)(Cl)(H_2O)_2]$, $[Ni(HL)(Cl)(H_2O)_2]$ and $[Cu(HL)(Cl)(H_2O)_2]$ were optimized by DFT and are presented along with their atom numbering in (Fig. 6) as (**a)** and (**b-e**), and the selected atomic distances, and bond angles are tabulated in [Table 6-7]. Gaussian-*09* program with a B3LYP basis sets has been used to study the molecular structure, energies, DFT calculations, and surface analysis. The quantum chemical literature inferred that the functional B3LYP basis set to yield the good results in bond lengths (Å), and bond angles (°) of connected atoms. The structural parameters of hydrazone ligand (H_2L) for selected atoms, and groups of the optimized molecule reveals that phenyl ring and a heterocyclic ring of piperidine are present in a planar form. The shorter bond length was observed for C17=N19 [1.2613(Å)] in azomethine group of free hydrazone ligand, and this information indicates a partial electron delocalization within the H18–C17–N19 fragment, while the longer bond length C18-N10 was observed from1.3440–1.4426(Å) in metal complexes. It was assigned the movement of nitrogen lone-pair electrons toward the metal's vacant orbitals which resulting the weakened C17=N19 bond [32]. The C–C bond distance was calculated of the phenyl ring of C3–C2, C4–C3, C5–C4, C6–C5 bond found well within the expected range of bond distances (1.3724–1.3935 Å), and bond angles (119.0973°–120.5788°) with sp^2 hybridised carbon atom which corresponding to delocalization of π-electrons. The heterocyclic ring of C33–C26 bond length was found 1.5162 Å, and consisting the bond angle 111.0840° of C33–C26–C24 in sp^3

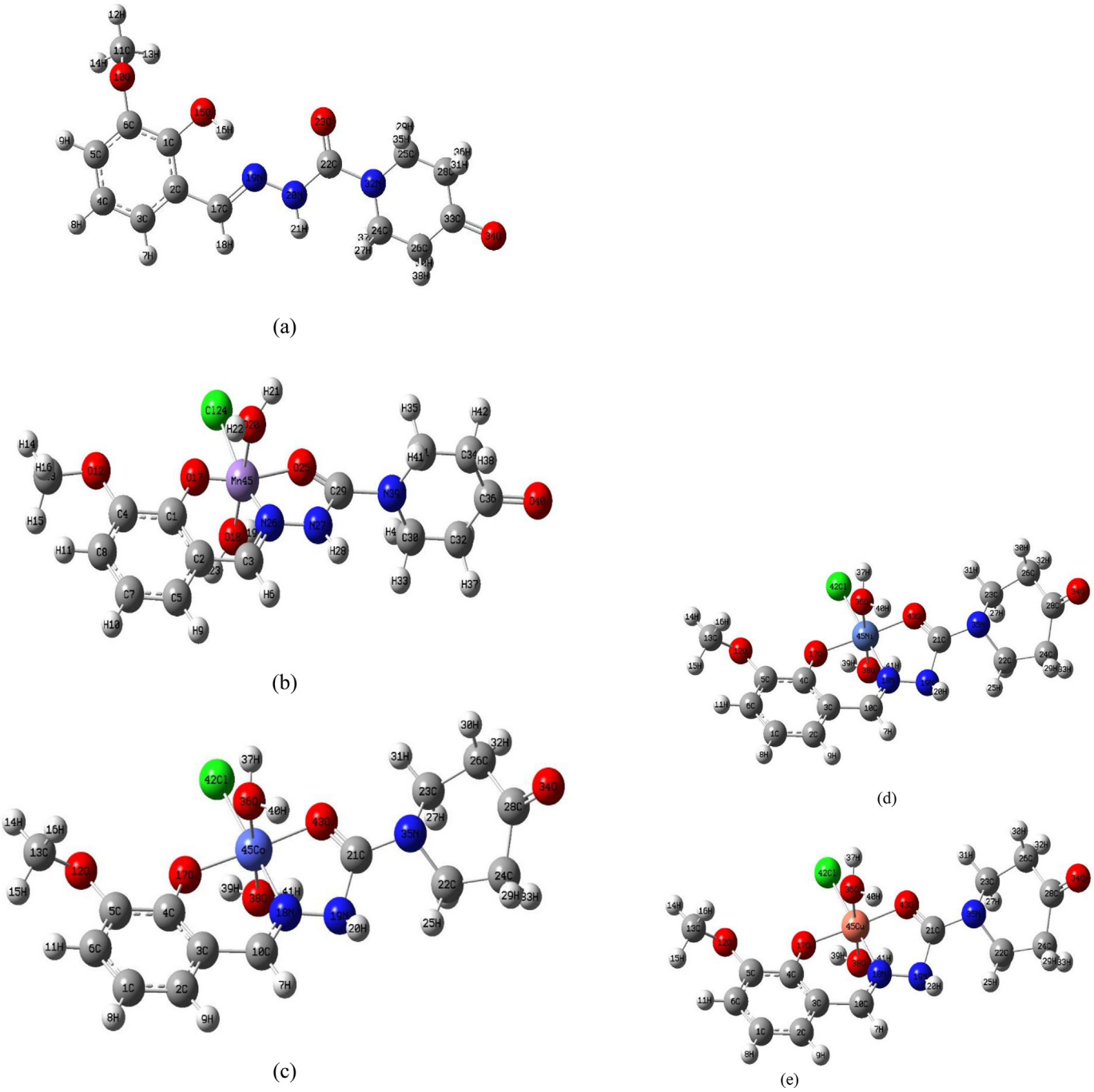

Fig. 6. Optimized molecular structure of (a) ligand, (b) Mn(II), (c) Co(II),(d) Ni(II), (e) Cu(II) complexes.

hybridized carbon atom indicating the presence of localized σ bond. The two chromophores i.e. C = O shows the nearly equal, and shorter bond length of 1.2174° (chain) and 1.2095° (heterocyclic). The shorter bond length of (H16–O15) appears (0.9792 Å) in the phenolic atoms due to the more electronegative 'O' atom bonded with the smaller H atom.

The optimized molecular structures of $[Mn(HL)(Cl)(H_2O)_2]$, $[Co(HL)(Cl)(H_2O)_2]$, $[Ni(HL)(Cl)(H_2O)_2]$ and $[Cu(HL)(Cl)(H_2O)_2]$ complexes suggested that each central metal(II) ion is bonded by six donor sites with an arrangement of the octahedral sphere. The short bond length (1.8582–1.8594) Å of the metal–O bond of deprotonated phenolic group than the metal–O bond from carbonyl group adjusted to *trans* at an angle of ~ 95° The larger bond length of M45–O36 atoms and M45–O38 atoms as well as corresponding the bond angle of O36-M45-O38 appearing at (179.774–180.101°) clearly indicating water molecules axially coordinated with the metal center at *trans* position in all metal complexes. The atomic arrangement involved two oxygen at an angle of ~ 97° informed its *trans* positions. The azomethine-N and chlorine atoms as fifth and sixth donor atom to form planar within the coordination sphere. The interatomic distances of metal–Cl (42) was calculated (2.1721–2.1861) Å inferred *trans*-directing group of azomethine nitrogen donor atom. The bond angle within the chelate cycle differs slightly from the expected values of 90°

Table 6
Selected geometrical parameters of hydrazone ligand (H_2L).

Bond connectivity	Bond lengths(Å)	Bond connectivity	Bond angles (°)
C(2)-C(1)	1.3941	–	–
C(3)-C(2)	1.3935	C(3)-C(2)-C(1)	120.2285
C(4)-C(3)	1.3724	C(4)-C(3)-C(2)	120.5788
C(5)-C(4)	1.3882	C(5)-C(4)-C(3)	119.0973
C(6)-C(5)	1.3737	C(6)-C(5)-C(4)	121.2068
O(10)-C(6)	1.3775	O(10)-C(6)-C(5)	118.1922
C(11)-C(10)	1.4548	C(11)-C(10)-C(6)	118.5076
H(16)-O(15)	0.9792	H(16)-O(15)-C(1)	113.3859
C(17)-C(2)	1.4633	C(17)-C(2)-C(1)	121.0470
C(17)-N(19)	1.2613	H(18)-C(17)-N(19) C(2)	121.1456
C(20)-N(19)	0.9960	C(20)-N(19)-C(17)	119.6748
C(22)-N(20)	1.3794	C(22)-N(20)-N(19)	119.6748
O(23)-C(22)	1.2174	O(23)-C(22)-N(20)	121.9978
H(31)-C(28)	1.0835386	H(31)-C(28)-C(25)	111.3342
C(33)-C(26)	1.5162580	C(33)-C(26)-C(24)	111.0840
O(34)-C(33)	1.2095837	O(34)-C(33)-C(26)	122.6657
H(38)-C(26)	1.0851092	H(38)-C(26)-C(24)	109.2693

Table 7
Selected geometrical parameters of metal (II) complexes.

Parameters	Mn (II) complex	Co(II) complex	Ni(II) complex	Cu(II) complex
Bond connectivity	Bond length (Å)			
M(45)-N(18)	1.8322	1.8420	1.8440	1.8426
M(45)-O(43)	1.8584	1.8594	1.8474	1.8582
M(45)-O(17)	1.8299	1.8319	1.8224	1.8339
M(45)-O(36)	1.8419	1.8319	1.8299	1.8389
M(45)-O(38)	1.8414	1.8412	1.8399	1.8487
M(45)-Cl(42)	2.1721	2.1701	2.1814	2.1861
C(10)- N(18)	1.4221	1.4420	1.3440	1.4426
Bond connectivity	Bond angles (°)			
N(18)-M(45)-O(43)	84.711	84.751	84.779	84.799
N(18)-M(45)-O(17)	97.142	97.122	97.164	97.124
N(18)-M(45)-O(36)	93.142	92.152	92.167	93.142
N(18)-M(45)-O(38)	88.209	88.123	88.150	88.130
N(18)-M(45)-O(42)	177.001	176.925	176.925	176.401
O(17)-M(45)-O(43)	179.990	179.860	179.890	179.423
O(36)-M(45)-O(43)	89.952	89.452	89.452	89.439
O(43)-M(45)-O(38)	90.221	90.152	90.152	90.159
O(43)-M(45)-Cl(42)	95.949	95.982	95.982	95.999
O(17)-M(45)-Cl(42)	95.182	95.182	95.182	95.189
O(17)-M(45)-Cl(38)	89.190	89.152	89.152	89.142
O(36)-M(45)-O(38)	180.101	179.899	179.899	179.774
O(36)-M(45)-Cl(42)	90.691	90.590	90.590	90.452
O(38)-M(45)-Cl(42)	90.887	90.691	90.691	90.571

and 180° indicating the octahedral geometry. The experimental and theoretical study show comparable values and validated for the octahedral geometry of metal complexes [33–34].

3.8. Frontier molecular orbitals (FMOs)

Frontier molecular orbitals (FMOs) calculation was performed for an optimized structure of the compounds by using the B3LYP method with 6–311G+(d,p) for the charge transfer reactions. The frontier molecular orbital (FMOs) of hydrazone ligand (H_2L) and Mn(II) complex are displayed in Fig. 7(**a-d**) as the representative case. The significant quantum chemical data of FMOs of ligand (H_2L) and Mn(II) complex viz., E(HOMO), E(LUMO), energy band gap (ΔE), properties are presented in [Table 8]. The energies of FMOs are good evidence for charge transfer (*CT*) from HOMO to LUMO. The molecules containing a small HOMO-LUMO energy gap are normally correlated with high chemical reactivity, and low kinetic stability. The energies of the ligand (H_2L) for

Table 8
Calculated energies (eV), band gaps (ΔE), properties of Frontier MOs of hydrazone ligand (H_2L) and Mn(II) complex.

Compounds	Orbitals	Energies			Chemical properties				
		Hartrees	Convertionof energy (eV)	Energy band gap (ΔE)	Chemical potential (μ)	Global hardness (η)	Softness (S)	Electrophilicity index (ω)	Nucleophilicity index (N)
Hydrazone ligand (H_2L)	HUMO	−0.21924	−5.965	4.258	−2.1295	4.2598	0.2347	0.5322	4.72
	LUMO	−0.0627	−1.706						
Mn(II) complex	HOMO	−0.1858	−5.055	3.461	−3.324	1.7305	0.5778	3.1924	3.81
	LUMO	−0.05858	−1.5940						

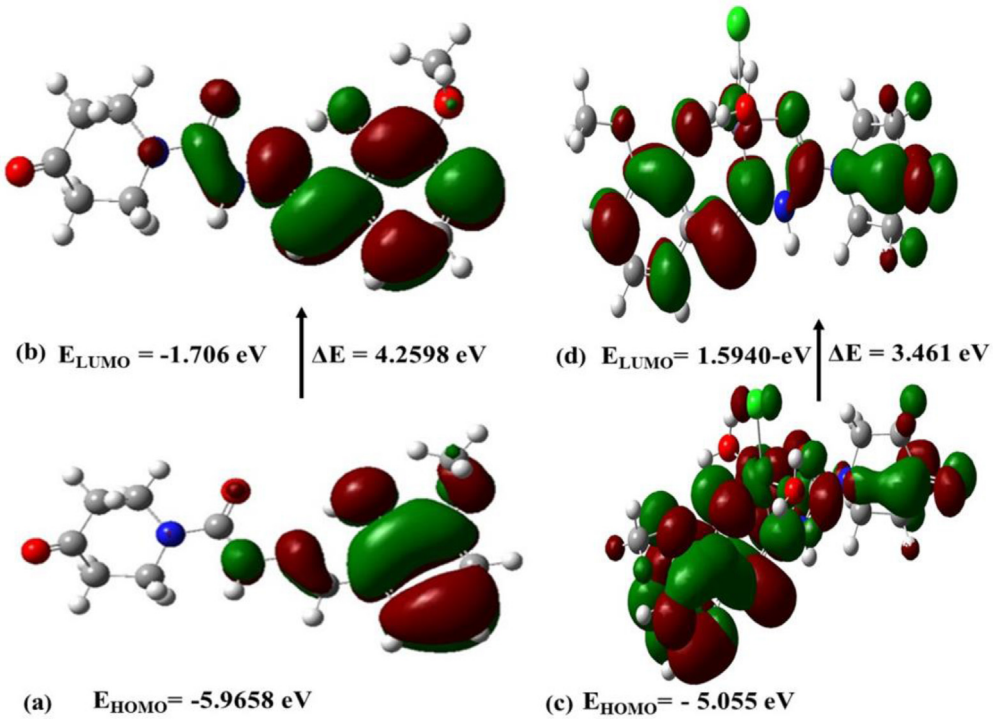

Fig. 7. Frontier molecular orbitals (a) HOMO, (b) LUMO of ligand (H_2L), and (c) HOMO and (d) LUMO of Mn(II) Complex.

HOMO consist of (−0.21924 Hartree = −5.9658 eV) due to the π-orbital in the triatomic moiety while LUMO was the π^*-orbital consist of (−0.0627 Hartree = −1.706 eV) [35] and degeneracies of Boltzmann population ratios of 6.982e+100 at 298.15 K. The very small energy gap (4.2598 eV) was observed for the ligand molecule and hence, the most probability of electron transition in ($\pi \rightarrow \pi^*$) from HOMO to LUMO. HOMO density is located at phenolic-O, azomethine-N, and carbonyl-O referred as a functional region of hydrazone ligand. The highly delocalized HOMO is specifying promptly shifted of the electrons, and hence resulting in intermolecular charge transfer (*ICT*). Furthermore, the HOMO localizes on triatomic (ONO) orbital contains the loan pairs of electrons at O-15, N-19, and O-22 indicating the presence of favorable atomic centers within hydrazone molecule for possible nucleophilic attacks. The according to the frontier orbital theory, nucleophilic attacks occur by the electron flow of a HOMO nucleophile into the LUMO of the electrophile. In the metal complexes, HOMO density is located on the metal ion, azomethine-N atom, carbonyl-O, and chlorine atom whereas LUMO region have been substantiated the charge distribution in the complete molecule. As a result of this, charge transfers occur from the electron-donor groups to electron-acceptor groups through coordination. In addition to this, the computations study of ligand and its metal complexes FMO energy (eV) shows in the order of $[Co(HL)(Cl)(H_2O)_2]$(1.7892) < $[Ni(HL)(Cl)(H_2O)_2]$ (1.9920) < $[Cu(HL)(Cl)H_2O)_2]$(−2.0101) < $[Mn(HL)(Cl)(H_2O)_2]$(3.461) < $[H_2L]$ligand (4.258) [36]. The calculated values of large stabilization occurred of the LUMO are due to the greater electron-accepting ability of the acceptor group, and causes transfers of the electron density from the triatomic active the electron-donor of azomethine-N and phenyl-O and carbonyl-O to its electron-acceptor region.

In addition to these, calculated molecular properties such as the chemical potential (μ), global hardness (η), and softness (S) are presented [37]. These molecular parameters also co-relate to each other, where

$$(\mu) = -\chi,$$

$$\text{Chemical potential}(\mu) = \frac{\text{E (HOMO)+E (LUMO)}}{2} \quad (1)$$

$$\text{Global hardness}(\eta) = \frac{\text{E (LUMO)} - \text{E (HOMO)}}{2} \quad (2)$$

The inverse relation of the global hardness (η) with the softness (S) are found as

$$\text{Softness } (S) = \frac{1}{\eta} \quad (3)$$

$$\text{Electrophilicity index } (\omega) = \frac{\mu^2}{2\eta} \quad (4)$$

$$\text{Nucleophilicity index } (N) = \text{E}(\text{HOMO}_{\text{nu}}) - \text{E}\left(\text{HOMO}_{\text{ligand}}\right) \quad (5)$$

The significant chemical properties reactivity's of molecular for ligand were calculated viz., chemical potential (μ) = –2.1295 gives stability, and global hardness (η) = 4.2598, and softness (S)= 0.2347 supported the confirmation of electron transfer. Similarly, the evaluated chemical potential (μ) of Mn(II) complex was = –3.324 which suggest a more stability of compound. Another factors of global hardness (η) = 1.7305, and softness (S)=0.5778 informed of electron transfer from HOMO to LUMO region. The evaluated nucleophilicity index are comparatively more than the electrophilicity index in ligand (N = 4.72 eV > ω= 0.5322) and in Mn(II) complex (N = 3.81 eV > ω= 3.1924) useful key indicators for in vitro biological activities. [38–39].

3.9. Molecular electrostatic potential surface analysis (MEP)

Molecular electrical potential map helped in understanding distribution of charges in ligand and also known as electrostatic potential energy maps of molecular electrical potential surfaces. This is an important tool for the study of efficient ionic binding receptors for electrophilic and nucleophilic attack in chemical reactions, hydrogen bonding interactions, and the total charge distribution in the molecule. The analysis of the electrostatic potential map from B3LYP/6–311G+(d, p) are presented in (Fig. 8) as (**a**) ligand, and (**b**) Mn(II) complex as the representative case. The different values of

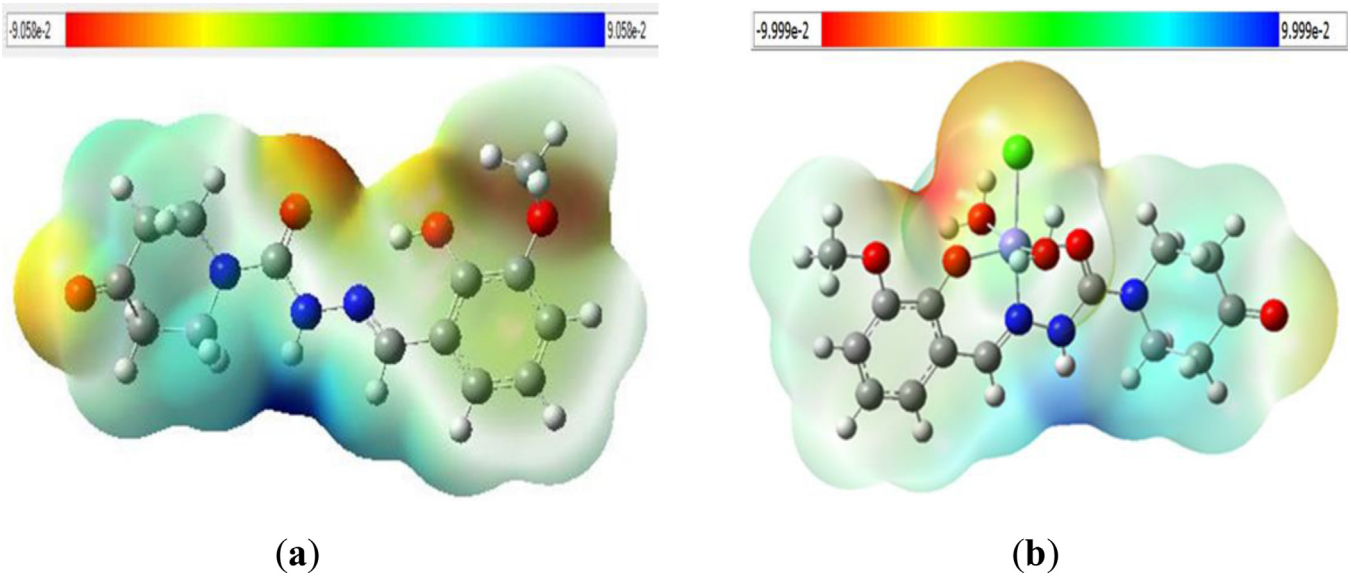

Fig. 8. Molecular electrostatic potential surface of (a) Ligand, and (b) Mn(II) complex.

the electrostatic potential are displayed by the various colors with the increase in order of yellow <green <red < blue in ligand, and these color intensities decreasing in metal complexes except the blue which are indicating a low nucleophilic or electrophilic attack after the complex formation. In ligand, the negative electrostatic potential appears at a maximum due to the presence of phenolic group, hydrazone group (>C = N − *N*<), and carbonyl group indicating a possible site for electrophilic attack. The reduction in the polarity in metal (II) complex shows a very low electrostatic potential in the structure, and followed the similar trend in the structure of Mn(II) complex.

The hydrazone ligand reveals that the electrostatic negative region belongs to the two-carbonyl oxygen (O22, O34) represented in the molecule with a magnitude in the range of −134 to 210 kJ/mol. Other the reduced magnitude of the negative electrostatic potential on the oxygen of the methoxy group (O10) was calculated and found to be in the range of −22 to 74 kJ/mol. The nitrogen atoms of the azomethine (N19), and amide N(20) displayed the negative electrostatic potential indicating an important magnitude in the range of (−50 to −85 kJ/mol). Similarly, the magnitude for the hydrogen attached to sp^2 and sp^3 carbon was in the range of ∼32 to125kJ/mol. In the heterocyclic ring, nitrogen (N32) shows a negative electrostatic potential, due to the acidic N–C of a magnitude of 92 kJ/mol [40–42].

3.10. Powder X-ray diffraction pattern

Though the newly synthesized complexes were soluble in some polar organic solvents like DMSO and DMF, crystals that are suitable for single crystal studies are not obtained. Hence powder-XRD pattern of the ligand and metal complexes have been studied in order to test the degree of crystallinity of the complexes. The powder X-ray diffraction spectra of ligand and its metal (II) complexes were scanned and shown in **Fig.3S** as (**a-e**). The unit cell and crystal lattice parameter data of compounds are summarized in [**Tables S1-S5**]. The calculated glancing angle (2Θ) and interplanar distances were compared with theoretical, and both values are comparable equal. The miller indices h, k, l which was also supported by intercepts of the faces along the crystallographic axes in unit cell dimensions. The values of unit cell parameters of hydrazone ligand areas: crystal system orthorhombic, a = 7.1200Å, b = 21.8820Å, c = 13.1561Å; and interaxial angle (α=γ=β=90) deg. The interplanar spacing from the peak position=3.343,065Å, V = 2047 Å^3 with the space group=*P*, Z = 8. The metal complex of [Mn(HL)Cl(H_2O)$_2$]: system = cubic, a = 9.4110Å, b = 9.4110Å, c = 9.4110Å, and (α=β=γ=90 deg)., V = 822.056 Å^3. Z = 1, space group = P, and interplanar spacing from the peak position=4.0828Å. [Ni(HL)Cl(H_2O)$_2$] complex: crystal system=orthorhombic, a = 7.9270Å, b = 6.1590Å, c = 22.4700Å (a≠b≠c) and α=β=γ=90 deg., V = 1086.993Å^3, Z = 2 with interplanar spacing from peak position = 3.40,008Å. The average particle size was calculated from Scherrer's equation L= [Kλ/β(2Θ)cosΘ] using (K = 0.9) constant in all cases. [CuHL)Cl(H_2O)$_2$] complex: crystal system=Ortho-rhombic, a = 8.0914 Å, b = 10.2920 Å, c = 12.8843 8843Å and α =β =γ =90 deg., volume (V) = Å^3, Z= with interplanar spacing from peak position=3.29,500Å. Upon the calculation of full width at half maximum (FWHM), the average crystallite particle size from Scherrer's equation L= [Kλ/β(2Θ)cosΘ] using (K = 0.9) constant in all cases of hydrazone ligand (H_2L), Mn(II), Ni(II), and Cu(II) complexes were found to be 18.94, 28.88, 16.98 and 25.07 nm respectively, which confirmed their nanocrystalline nature [43,44].

3.11. Scanning electron microscopic study

SEM study provides information about the comparative surface morphology and topography of ligand and metal complexes. The SEM micrographs of hydrazone ligand (H_2L) and its Co(II) complex are given in Fig. 9 as **(a)** and **(b))** as representative one**.** The ligand was magnified at X600 showed well-defined crystal free from any shadow, and appeared as scattered rod's like with sharp edges. The ligand exhibits with variable lateral dimensions as glass-smooth surface looks whereas Co(II) complex showed as small crystal of broken rods. The different characteristic shapes and size of the particles of hydrazone Schiff base and metal complexes give evidence of the metal complexation [45–46].

3.12. Thermogravimetric analysis

Thermogravimetric analysis is an important tool to evaluate the thermal stability of complexes in terms of mass loss with respect to the linear variation of temperature. The thermal behavior of the hydrazone ligand (H_2L) and its metal complexes were studied in detail under N_2 atmosphere in the temperature range of

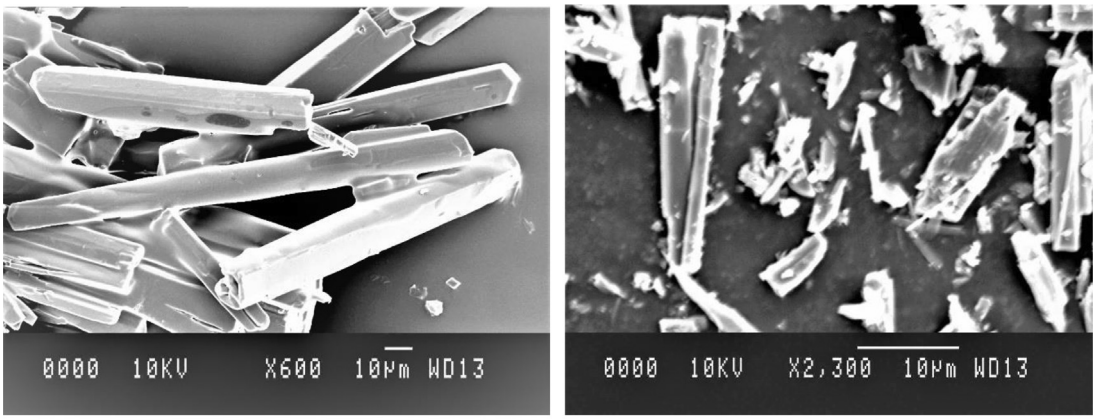

Fig. 9. SEM of (**a**) ligand (H_2L), and (**b**) Co(II) complex.

40–800 °C with a linear heating rate of 20 °C/min. The thermograms of hydrazone ligand (H_2L) and its Co(II) complex are presented as representative cases in Fig. 10(**a & b**), while thermograms of Mn(II),Ni(II),Cu(II) complexes are shown in **Fig. S4** (**c-e**). The thermogram of ligand shows a single step of decomposition with a (broad DTG_{max}) peak at ~370 °C with maximum mass loss of 88.31% (theor. 92.15 %) assignable to the fragmented loss of organic species ($-H_{17}N_3O_4$). Further, in continued heating up to 700 °C, formed the carbon residues of 11.69% (theor. 7.88%) as end product of reaction. The thermograms of Mn(II), Co(II), Ni(II), Cu(II) complexes in the range 45 °C to 800 °C indicated three steps decompositions.

The thermograms of Mn(II), Co(II), Ni(II) and Cu(II) complexes showed decomposition in three steps and thermal decompostion of Cu(II) shown in (Scheme 2) as a representative case. The proposed stepwise thermal degradation pattern of all the complexes with respect to temperature and formation of respective metal oxides are depicted in Table 9. In all complexes the first step of decomposing involving TG-DTG plateau in the temperature range of ~110–120 °C with broad DTG_{max} peak corresponding to a loss of two coordinated water molecules per mole of complex. In continued further heating, the second decomposition step in between 200–280 °c (DTG_{max}) shows a loss of one mole of chloride ions. The third degradation step observed in the range ~340–490 °c involves a mass loss of organic ligand moiety and finally, TG curve attain a horizontal level indicates the formation the stable metal oxide as residue [47–49]. A small peak appears in the thermograms was may be due to some endothermic reactions that occur simultaneously such as breaking, rearrangement of the covalent bonds, oxidative degradation, during the decomposition reaction. The vibration IR frequency data 930–908 cm^{-1} and TG 110–120 °C both indicate the presence of coordinated water molecules in the complexes, and the presence of chloride ions was confirmed by the Volhard estimation.

3.13. Kinetic studies of metal (II) complexes (Coats-Redfern relation)

The kinetic and thermodynamic energy parameters associated with various decomposition steps in the thermal process are very important for the evaluation of the nature of complexes and also a quick technique for assigning the stability of the material substances. In the present investigation significant kinetic parameters such as activation energy (Ea*), entropy (ΔS*), activation enthalpy (ΔH*), and free energy change (ΔG*) have been evaluated from the thermal decomposition by using Coats-Redfern relation and values are listed in [Table 10]. The increasing order of the activation energy (Ea*) from 9.6 to 293 kJ/mol with declining the values of entropy from −9.5 to −15.3 (J/mol/k), this confirms their more thermal stability with more ordered structure due to the more degree of structural 'complexity'. The negative values of entropy (ΔS) for the degradation process indicates more ordered activated complex than the reactants. The high value of the energy of activation of the complexes reveals the high stability of such complexes due to presence of covalency in metal-ligand bond character. It was proved in the first, second, and third steps of thermal decomposition, the lowering frequency factor (Z) are due to the decreasing trends of the entropy, and the non-spontaneous thermal decomposition reaction. When compared parameters of $E_a < \Delta G \cong \Delta H$ which informed that more thermal stability possessed by the compounds. The free energy +ΔG values (10.3 to 299 KJ/mol)

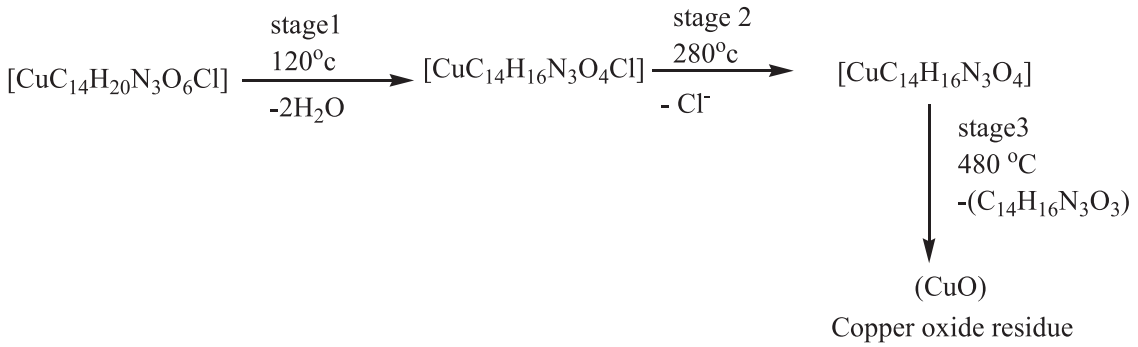

Scheme 2. Schematic representation of thermal decomposition of Cu(II) complex.

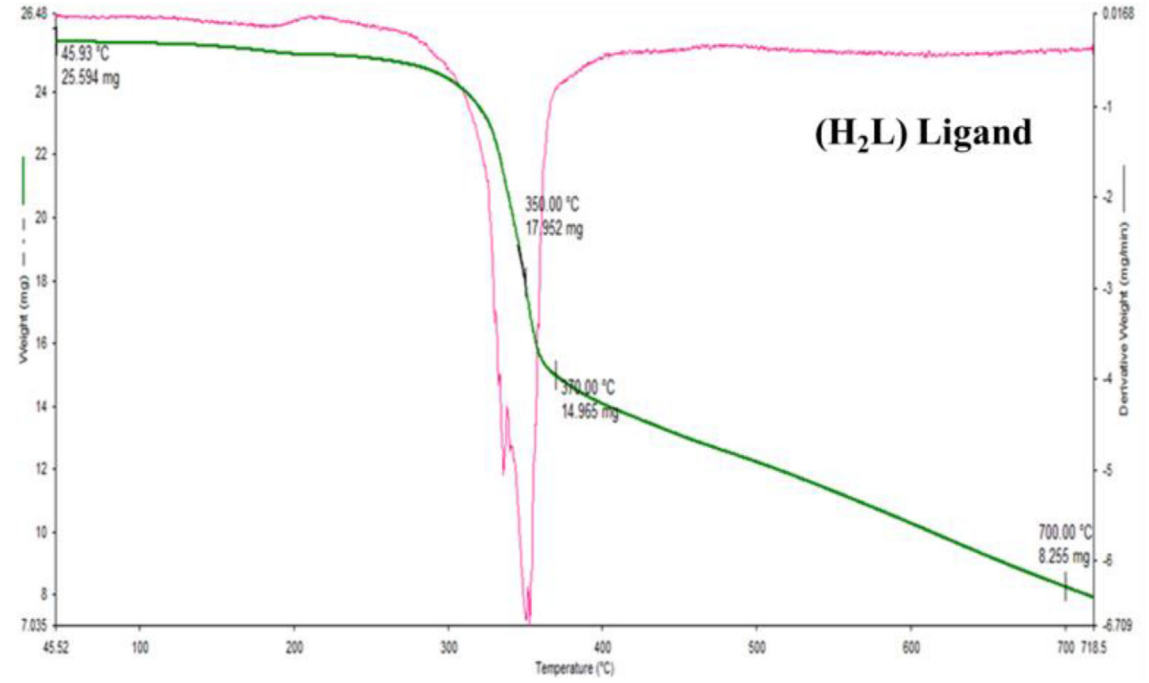

(a)

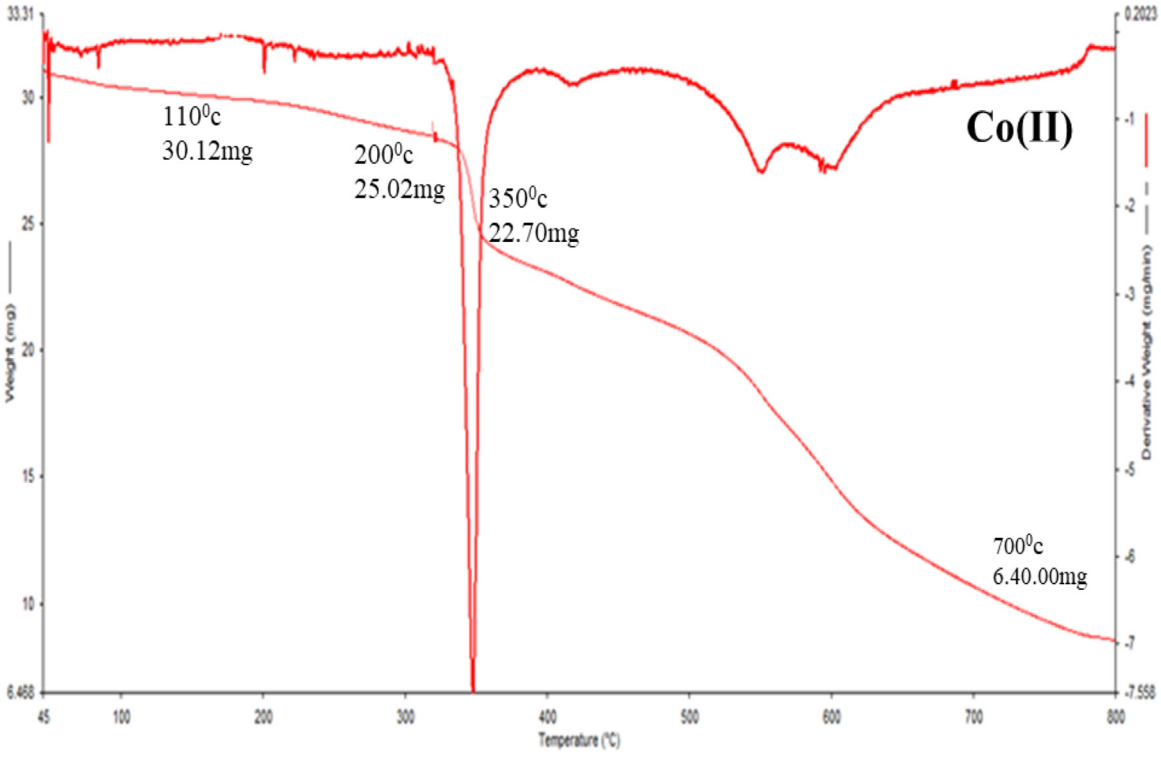

(b)

Fig. 10. Thermogravimetric curve of (a) H_2L Ligand and (b) Co(II) complex.

Table 9
Thermogravimetric data of ligand (H_2L) and its metal (II) complexes.

Compounds	Stages	Temp.range (°C)	DTG_{mx} (°C)	% Mass loss		Decomposition Assignments
				Exptl.	Calcd.	
Ligand (H_2L)	I	45–370	370	88.311	92.15	Loss of $H_{17}N_3O_4$ species
	II	375–700	–	11.69	7.88	Carbon residue
$[Mn(HL)Cl(H_2O)_2]$	I	45–110	110	9.20	8.65	Loss of two coordinated H_2O molecules
	II	110–230	130	10.81	8.51	Loss of one coordinated Cl ion
	III	230–600	340	63.12	62.23	Loss of organic moieties ($C_{14}H_{16}N_3O_3$
	IV	600–808	—	16.87	20.61	Metallic oxide residue of MnO
$[Co(HL)Cl(H_2O)_2]$	I	45–160	110	9.93	8.55	Loss of two coordinated H_2O molecules
	II	160–310	200	9.50	9.22	Loss of one coordinated Cl ion
	III	310–540	350	58.72	60.22	Loss of organic moieties ($C_{14}H_{16}N_3O_3$)
	IV	540–800	—	22.05	21.45	Metallic oxide residue of (CoO)
$[Ni(HL)Cl(H_2O)_2]$	I	45–120	120	9.90	8.56	Loss of two coordinated H_2O molecules
	II	120–250	240	10.80	9.23	Loss of one coordinated Cl ion
	III	250–490	400	60.61	60.80	Loss of organic moieties ($C_{14}H_{16}N_3O_3$)
	IV	490–800	–	19.00	21.40	Metallic oxide residue of NiO
$[Cu(HL)Cl(H_2O)_2]$	I	45–120	120	8.37	8.46	Loss of two coordinated H_2O molecules
	II	120–250	280	10.62	9.11	Loss of one coordinated Cl ion
	III	320–490	490	57.40	60.10	Loss of organic moieties ($C_{14}H_{16}N_3O_3$)
	IV	490–650	—	23.61	22.32	Metallic oxide residue of CuO

Table 10
The kinetic parameters for thermal decomposition of (H_2L) ligand and its complexes (Coat-Redfern method).

Compounds	Decomp.temp.(°C)	(Ea) (kJ mol^{-1})	Z (s^{-1})	ΔS ($Jmol^{-1}k^{-1}$)	ΔH (kJ mol^{-1})	ΔG (kJ mol^{-1})
Ligand (H_2L)	350	221.93	1.362×10^1	−14.6	216.6	225.8
$[Mn(HL)Cl(H_2O)_2]$	150	57.82	1.218×10^3	−9.8	55.2	58.3
	230	19.97	12.06×10^2	−11.2	16.9	21.2
$[Co(HL)Cl(H_2O)_2]$	180	59.62	1.224×10^3	−9.8	57.0	60.1
	250	55.44	1.212×10^2	−12.8	51.7	57.5
	347	152.71	0.1236×10^4	−13.9	148.4	155.6
$[Ni(HL)Cl(H_2O)_2]$	100	57.80	1.206×10^3	−9.8	55.2	58.3
	250	23.81	1.230×10^3	−11.2	20.7	24.9
	450	293.16	0.1230×10^4	−13.9	287	299.1
$[Cu(HL)Cl(H_2O)_2]$	120	48.31	1.218×10^3	−14.7	144.1	152.5
	350	105.30	1.230×10^3	−11.5	204.5	214.1
	490	209.72	1.239×10^3	−15.3	274.2	287.2

was investigated, it reveals that the decomposition steps are non-spontaneous processes [50,51]. On the basis of third-step of decomposition the thermo-kinetic data inferred the stability order is found to be increased as Mn (II)<Ni(II)<Co(II)<Cu(II).

3.14. Evaluation of antibacterial and antifungal activities

In recent years, the heterocyclic compounds of hydrazone and its metal complexes have gained considerable importance, especially in the repository, slow-release and long-acting drugs. A number of heterocyclic organic compounds and their metal complexes have been tested for their efficacy as antibacterial and antifungal drugs. Considering this enormous biological importance associated with hydrazone (H_2L) ligand system involving piperidine ring, inspired us to undertake synthesis and study their biological potency.

The in vitro antimicrobial activity of the ligand and its Mn(II), Co(II) Ni(II) and Cu(II) complexes were tested against the gram – ve bacterial strains of *Escherichia coli* (NCBI-0157), *Salmonella typhi* (NICM-2257); gram +ve bacterial strains *of Staphylococcus aureus* (NDCM-2257), *Bacillus substilis* (NICM-2477), and fungal species of *Candida albicans* (MTCC-1637), *Aspergillus niger* (NCIM-1005) at a conc.1.0 mg/mL using the disk diffusion method (DDM). The activity in zone of inhibition (mm) was compared with the standard drug ofloxacin, azithromycin, fluconazole and given in Table 11 and presented graphically in (Fig. 11). The ligand and its metal complexes showed different results against different bacterial strains. The newly synthesized metal complexes exhibited good results than the free ligand. This activity found to be enhanced on coordination with metal ions. This enhancement in the antimicrobial activity of the complexes over free ligand can be explained on the basis of *Tweedy's* chelation theory [52]. The chelation reduces the polarity of the metal ion mainly because of partial sharing of its positive charge with donor groups, electron delocalization over the entire ring, the effect of metals ion charges, and the geometry of the complex. Lipophilic character played an important role in the resulting liposolubility of metal (II) complex which facilitated its

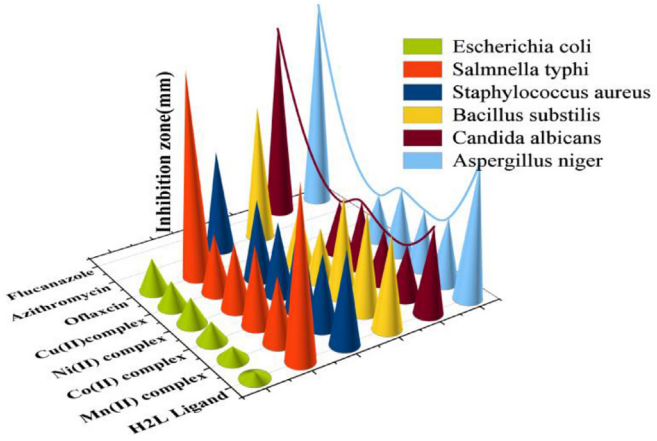

Fig. 11. Inhibition zone growth of microorganisms of tested compounds of ligand (H_2L) and its metal (II) complexes.

Table 11
Antimicrobial assay of ligand (H_2L) and its metal (II) complexes compared with std. drugs.

Compounds and standard drugs	Bacteria (Gram –ve)		Bacteria (Gram +ve)		Fungal species	
	Escherichia. coli (NCBI-0157)	*Salmonella. typhi* (NICM-2257)	*Staphylococcus aureus* (NDCM-2257)	*Bacillus substillis* (NICM-2477)	*Candida albicans* (MTCC-1637)	*Aspergillus niger* (NCIM-1005)
Ligand (H_2L)	18	25	14	14	13	20
$[Mn(HL)(H_2O)_2Cl]$	20	10	11	15	08	10
$[Co(HL)(H_2O)_2Cl]$	15	12	15	15	08	09
$[Ni(HL)(H_2O)_2Cl]$	12	10	11	08	10	10
$[Cu(HL)(H_2O)_2Cl]$	12	09	12	09	08	07
Ofloxacin*	30	30	–	–	–	–
Azithromycin*	–	–	15	20	–	–
Fluconazole*	–	–	–	–	28	30
DMSO –ve control	–	–	–	–	–	–

penetration through the lipid layer into bacterial cell walls [53]. Such enhanced intake rate of molecules, and displayed the prominent antimicrobial potency.

The experimental results showed that the complexes Mn(II) Co(II), Ni(II), Cu(II) are more active against bacterial microorganisms than the free ligand (H_2L). The ligand and its metal complexes show moderate performance against fungal species *C. albicans and A. niger and* fluconazole as standard drug because such organisms have been achieved resistance to antibiotics may through biochemical and morphological modification [54–56]. The enhancement in the antimicrobial activity may be rationalized on the basis presence of heterocyclic moiety, comprises of carbonyl group, one piperidinic ring, one azomethine (-CH=N-), ($-OCH_3$), -Cl groups. Moreover, in metal complex, the positive charge on the metal ion is partially shared with the hetero donor atoms present in the ligand and there may be π electrons delocalization over the whole chelating system. The experimental antimicrobial activity of ligand and metal complexes also validated from the theoretical study data of nucleophilicity index (N) than electrophilicity index (ω). The zone of inhibition data of the metal complexes was indicated a good biological activity as compared with free (H_2L) ligand, and may be used as a future potential antimicrobial candidate in biological science.

4. Conclusions

A comprehensive explication of synthesis, structural, electronic and biological characteristics of the new hydrazone Schiff base, N'-(2–hydroxy-3-methoxybenzyl-idene)–4-oxopiperidine-1-carbohydrazide and its Mn(II) Co(II), Ni(II), Cu(II) complexes are accomplished through this examination. The outcomes of the elemental investigation were in acceptable concurrence with theoretically determined data and affirm synthesis of complexes. The stoichiometry of the metal to ligand ratio in all complexes was observed to be 1:1. The IR, electronic absorption, and magnetic moment data confirmed that the binding of the H_2L ligand through donor (*ONO)* denticity with the metal ion and designated the octahedral structure to all complexes. The ESR tensor parameters of the Cu(II) complex indicating the presence of axial distortion in structure. The X-ray diffraction parameters viz., glancing angle (2Θ), interplanar distances, and the full width at half maximum (FWHM) indicating the hydrazone ligand (H_2L), Mn(II), Ni(II) complexes which confirmed their nano crystalline nature. Interpretations of thermal and structural data depicted that all prepared metal complexes are thermally stable and prepared successfully. The fluorescence intensity data (I_F) in excited state of emission informed concrete evidences of good fluorescent components, and may use in photochemical applications. The DFT geometrical parameters of hydrazone ligand indicating the triatomic moiety, and Mn(II), Co(II), NI(II),and Cu(II) complexes suggest the octahedral geometry. The smaller energy gap in HOMO and LUMO are more responsible for charge transfer interaction in the heterocyclic hydrazone ligand and its metal complex results in the more bioactivity. Each MEP plot of ligand and Mn(II) complex are good tools which displayed the its color scaling in the molecule as the nucleophilic reactions and electrophilic sites. The enhanced activity of metal-complexes in inhibiting the growth of specific microorganisms will be made them an effective for antibacterial and antifungal drugs.

Declaration of Competing Interest

The authors declare that they have no known competing financial interests or personal relationships that could have appeared to influence the work reported in this paper.

CRediT authorship contribution statement

Gajanan Dongare: Conceptualization, Methodology, Investigation, Writing – original draft, Formal analysis, Data curation, Investigation. **Anand Aswar:** Methodology, Validation, Supervision, Project administration, Resources, Validation, Writing – review & editing, Investigation.

Data availability

Data will be made available on request.

Acknowledgements

The authors are thankful to authorities of Sant Gadge Baba Amravati University, Amravati for providing of the laboratory facilities (Bruker-IR instrument and Perkin Elmer-TG analyser). Authors are also thankful to SAIF, Chandigarh for the analysis of elemental, NMR (^1H,^{13}C), Mass spectra, as well as analysis of SEM. Author also thankful to SAIF-IIT, Mumbai for recording ESR spectrum and Principal, Shri Shivaji Science College, Amravati (M.S.) for the recording UV–Visible, and XRD spectra respectively.

Supplementary materials

Supplementary material associated with this article can be found, in the online version, at doi:10.1016/j.molstruc.2023.135107.

References

[1] P.L. Higgs, A.J. Ruiz-Sanchez, M. Dalmina, B.R. Horrocks, A. G.Leach, D.A. Fulton, Enhancing the kinetics of hydrazone exchange processes: an experimental and computational study, Org. Biomo. Chem. 17 (2019) 3218–3224, doi:10.1039/c9ob00058e.
[2] M. Pellei, V. Gandin, C. Cimarelli, W. Quaglia, N. Mosca, L. Bagnarelli, C. Marzano, C. Santini, Syntheses and biological Studies of nitroimidazole conjugated heteroscorpionate ligands and related Cu(I) and Cu(II) complexes, J. Inorg. Chem 187 (2018) 33–40, doi:10.1016/j.jinorgbio. 2018.07.008.

[3] S. Thota, D.A. Rodrigues, P.S.M. Pinheiro, L.M. Lima, C.A.M. Fraga, E.J. Barreiro, N-Acylhydrazones Drugs. Bioorg. Med. Chem. Lett. 28 (2018) 2797–2806, doi:10.1016/j.bmcl.2018.07.015.
[4] D. Osmaniye, S. Levent, A.B. Karaduman, S. Ilgın, Y. Zkay, Z.A. Kaplancikli, Synthesis of new benzothiazole acylhydrazones as anticancer agents, Molecules 23 (2018) 1–14, doi:10.3390/molecules23051054.
[5] Q.Y. Mo, J.G. Deng, Y. Liu, G.D. Huang, Z.W. Li, P. Yu, Y. Gou, F. Yang, Mixed-ligand Cu(II) hydrazone complexes designed to enhance anticancer activity, Eur. J. of Med. Chem. 156 (2018) 368–380, doi:10.1016/j.ejmech.2018.07.022.
[6] G.L. Backes, D.M. Neumann, B.S. Jursic, Synthesis and antifungal activity of substituted salicylaldehyde hydrazones, hydrazides and sulfohydrazides, Bioorg. Med. Chem. 22 (2014) 4629–4636, doi:10.1016/j.bmc.2014.07.022.
[7] P. Goel, O.A. Naim, M.J. Nawaz, F. Iqbal, M. Alam, M. Iqbal, Recent advancement of piperidine moiety in treatment of cancer-a review, Eur. J. Med. Chem. 157 (2018) 480–502, doi:10.1016/j.ejmech.2018.08.017.
[8] N. Karaman, Y. Sicak, T. Taskın-Tok, M. Ozturk, A.K. Iyidogan, M. Dikmen, K. Kocyigit, B. Kocyigit-Kaymakcioglu, E.E. Oruc-Emre, New piperidine-hydrazone derivatives: synthesis, biological evaluations and molecular docking studies as AChE and BChE inhibitors, Eur. J. Med. Chem. 124 (2016) 29270–29283, doi:10.1016/j.ejmech.2016.08.037.
[9] N.M. El-Barasi, M.M. Miloud, M.M. El-ajaily, R.K. Sarangi, A.K. Das, D. Mahal, P.K. Parhi, L. Pintilie, S.R. Barik, M.N. Amin Bitu, M. Kudrat-E-Zahan, Z. Tabassum, S.I. Al-Resayes, M. Azam, Synthesis, structural investigations and antimicrobial studies of hydrazone based ternary complexes with Cr(III), Fe(III) and La(III) Ions, J. Saudi Chem. Soc. 24 (2020) 492–503, doi:10.1016/j.jscs.2020.04.005.
[10] E. Raczuk, B. Dmochowska, J. Samaszko-Fiertek, J. Madaj, Different schiff bases—structure, importance and classification, Molecules 27 (2022) 2–24, doi:10.3390/molecules27030787.
[11] P.C. Sharma, D. Sharma, A. Sharma, N. Saini, R. Goyal, M. Ola, R. Chawla, V.K. Thakur, Hydrazone comprising compounds as promising anti-infective agents: chemistry and structure-property relationship, Mater. Today Chem. 18 (2020) 1–21, doi:10.1016/j.mtchem.2020.100349.
[12] D. Iacopetta, J. Ceramella, A. Catalano, C. Saturnino, M.G. Bonomo, C. Franchini, M.S. Sinicropi, Schiff bases: interesting scaffolds with promising antitumoral properties, Appl. Sci. 11 (2021) 1–20, doi:10.3390/app11041877.
[13] A.A. El-asmy, W.M.A. El-maaty, M.M. Mostafa, Spectrochimica acta part A : molecular and biomolecular spectroscopy synthesis and spectroscopic studies of 2, 5-hexanedione bis (isonicotinylhydrazone) and its first raw transition metal complexes, Spectro. Acta part A: Mol. Bio. Spectr. 75 (2010) 1516–1522, doi:10.1016/j.saa.2010.02.009.
[14] S. Wu, X. Liang, F. Luo, H. Liu, L. Shen, X. Yang, Y. Huang, H. Xu, N. Wu, Q. Zhang, C. Redshaw, Synthesis, crystal structure and bioactivity of phenazine-1-carboxylic acylhydrazone derivatives, Molecules 26 (2021) 1–12, doi:10.3390/molecules26175320.
[15] P. Kumar, B. Narasimhan, P. Yogeeswari, D. Sriram, Synthesis and antitubercular activities of substituted benzoic acid N′-(substituted benzylidene/furan-2-Ylmethylene)-N-(Pyridine-3-Carbonyl)-hydrazides, Euro. J. Med. Chem. 45 (2010) 6085–6089, doi:10.1016/j.ejmech.2010.08.030.
[16] J.M.D. Filho, S.M. Pinheiro, Stereoselective, solvent free, highly efficient synthesis of aldo- and keto-: n-acylhydrazones applying grindstone chemistry, Green Chem. 19 (2017) 2212–2224, doi:10.1039/c7gc00730b.
[17] W. Al Zoubi, K. Prisla, F. Muhammad, N. Siti, N. Nisa, G.K. Young, Recent advances in hybrid organic-inorganic materials with spatial architecture for state-of-the-art applications, Prog. Mater. Sci. 112 (2020) 100663, doi:10.1016/j.pmatsci.2020.100663.
[18] W. Al Zoubi, Putri, A.K. Rosy, G.K. Young, Understanding the metal ion-ligand responsible in the plasma-assisted electrochemical reactions for optimizing chemical stability, J. Mol. Liquids 321 (2020) 114756, doi:10.1016/j.molliq.2020.114756.
[19] A.S. Aswar, G.M. Dongare, Synthesis, Spectral characterization, thermo-kinetic and biological studies of some complexes derived from tridentate hydrazone schiff base, J. Saudi Chem. Soc. 25 (2021) 1–18, doi:10.1016/j.jscs.2021.101325.
[20] N.H. Al-Shaalan, Synthesis, characterization and biological activities of Cu(II), Co(II), Mn(II), Fe(II), and UO 2(VI) complexes with a new schiff base hydrazone: o-hydroxyacetophenone-7-chloro-4-quinoline hydrazone, Molecules 16 (2011) 8629–8645, doi:10.3390/molecules16108629.
[21] M.L. Dianu, A. Kriza, N. Stanica, A.M. Musuc, Transition metal M(II) complexes with isonicotinic acid 2-(9-Anthrylmethylene)-hydrazide, J. Serbian Chem. Soc. 75 (2010) 1515–1531, doi:10.2298/JSC091113121D.
[22] R. Fouad, I.A. Shaaban, T.E. Ali, M.A. Assiri, S.S. Shenouda, Co(II), Ni(II), Cu(II) and Cd(II)-Thiocarbonohydrazone complexes: spectroscopic, DFT, thermal, and electrical conductivity studies, RSC Adv. 11 (2021) 37726–37743, doi:10.1039/d1ra06902k.
[23] Y. Bai, H. Gao, Z.Y. Qi, D.B. Dang, Synthesis, crystal structure, and luminescent properties of a helical complex [(CuL) 2.5(H 2O) 0.375] (H 2L = benzil Bis[(5-*bromo oxidobenzylidene*) *hydrazone*]), Synth. React. Inorg. Metal-Org. Nano-Metal Chem. 42 (2012) 53–58, doi:10.1080/15533174.2011.609228.
[24] S. Abou El-Enein, F.A. El-Saied, S.M. Emam, M.A. Ell-Salamony, First row transition metal complexes of salicylidene and 2- hydroxy-1-naphthylidene-Ncyanoacetohydrazone, Spectro.Acta - Part A: Mol. Biomol. Spectr. 71 (2008) 421–429, doi:10.1016/j.saa.2007.12.031.
[25] P. Jyothi, S. Koppu, V. Sumalatha, B. Ushaiah, C.G. Kumari, Synthesis, characterisation, cytotoxicity, DNA binding and antimicrobial studies of binary and ternary metal complexes of Co (II), Inorg. Chem. Commu. 110 (2019) 1–6, doi:10.1016/j.inoche.2019.107590.
[26] B. Shao, M. Baroncini, H. Qian, L. Bussotti, M. Donato, A. Credi, I. Aprahamian, Solution and solid-state emission toggling of a photochromic hydrazone, J. Am. Chem. Soc. 140 (2018) 12323–12327, doi:10.1021/jacs.8b07108.
[27] B.X. Wu, H.Y. Chang, Y.S. Liao, M.Y. Yeh, Synthesis, photochemical isomerization and photophysical properties of hydrazide-hydrazone derivatives, New J. Chem. 45 (3) (2021) 1651–1657, doi:10.1039/d0nj05172a.
[28] T. Aysha, S. Lunak, A. Lycka, R. Hrdina, Synthesis, absorption and fluorescence of hydrazone colorants based on pyrrolinone esters, Dyes Pigments 91 (2011) 170–176, doi:10.1016/j.dyepig.2011.03.013.
[29] A.P. Mishra, R.K. Mishra, S.P. Shrivastava, Structural and antimicrobial studies of coordination compounds of VO(II), Co(II), Ni(II) and Cu(II) with some Schiff bases involving 2-amino-4-chlorophenol, J. Serb. Chem. Soc. 74 (2009) 523–535, doi:10.2298/JSC0905523M.
[30] R.C. Maurya, J.M. Mir, P.K. Vishwakarma, Conjoint experimental–theoretical evaluation of pyrone-salicylic acid hydrazide copper(II) schiff base complexes: their synthesis, sod and electrochemical fronts, J. Chin. Adv. Mat. Soc. 6 (2018) 55–80, doi:10.1080/22243682.2017.1407669.
[31] R.N. Patel, Magnetic, epr and SOD studies of some CuII/CuII, CuII/NiII and Cu(II)/Zn(II) imidazolate bridged complexes, Spectrochimica Acta Part A 59 (2003) 713–721, doi:10.1016/S1386-1425(02)00217-2.
[32] S. Saouli, I. Selatnia, B. Zouchoune, A. Sid, S.M. Zendaoui, C. Bensouici, E.E. Bendeif, Synthesis, Spectroscopic characterization, crystal structure, DFT studies and biological activities of new hydrazone derivative: 1-(2,5-bis((E)-4isopropylbenzylidene) cyclopentylidene)-2-(2,4-Dinitrophenyl) hydrazine, J. Mol. Struct. 1213 (2020) 128203, doi:10.1016/j.molstruc.2020.128203.
[33] M. Toy, H. Tanak, H. Şenoz, Experimental and DFT computational studies of novel 3-(p-cyanophenyl)-5-(o,m,p-Nitrophenyl)-5-phenylformazans, J. Mol. Struct. 1213 (2020) 2–11, doi:10.1016/j.molstruc.2020.128178.
[34] R.C. Maurya, B.A. Malik, J.M. Mir, P.K. Vishwakarma, D.K. Rajak, N. Jain, Nickel(II) complexes of ONS donor schiff base ligands: synthesis, combined DFT-experimental characterization, redox, thermal, and in vitro biological investigation, J. Coord. Chem. 68 (2015) 2902–2922, doi:10.1080/00958972.2015.1064526.
[35] S.A. Rupa, R. Moni, A.M. Patwary, M. Mahmud, A. Haque, J. Uddin, S.M.T. Abedin, Biological activity, DFT, and molecular docking studies, Molecules 27 (2022) 1–20, doi:10.3390/molecules27051656.
[36] J.H. Jiang, Y.H. Lei, X. Li, Y. Pi, H. Zhu, Q.G. Li, C.H. Li, New cobalt(II) schiff base complex: synthesis, characterization, DFT calculation and antimicrobial activity, Inorg. Chem. Commun. 127 (2021) 108350, doi:10.1016/j.inoche.2020.108350.
[37] L.R. Domingo, M. Rios-Gutierrez, P. Perez, Applications of the conceptual density functional theory indices to organic chemistry reactivity, Molecules 21 (2016) 1–22, doi:10.3390/molecules21060748.
[38] M.V. Putz, Koopmans analysis of chemical hardness with spectral-like resolution, Science World J. 348415 (2013) 1–14, doi:10.1155/2013/348415.
[39] P. Jaramillo, L.R. Domingo, E. Chamorro, P.A. Perez, Further exploration of a nucleophilicity index based on the gas-phase ionization potentials, J. Mol. Struct., Theochem 865 (2008) 68–72, doi:10.1016/j.theochem.2008.06.022.
[40] R. Shukla, P. Bandopadhyay, M. Sathe, D. Chopra, Quantitative investigation on the intermolecular interactions present in 8-(4-Ethoxyphenyl)-1,3-dimethyl-3,7-dihydro-1H-purine-2,6-dione with insight from interaction energies, energy framework, electrostatic potential map and fingerprint analysis, J. Chem. Sci. 132 (2020) 1–7, doi:10.1007/s12039-019-1726-2.
[41] S. Lakshminarayanan, V. Jeyasingh, K. Murugesan, N. Selvapalam, G. Dass, Molecular electrostatic potential (mep) surface analysis of chemo sensors: an extra supporting hand for strength, selectivity and non-traditional interactions, J. Photochem. Photobio. 6 (2021) 1–3, doi:10.1016/j.jpap.2021.100022.
[42] M. Roy, D. Biswal, N.R. Pramanik, M.G.B. Drew, S. Paul, P. Kachhap, C. Haldar, S. Chakrabarti, Structural elucidation, DFT calculations and catalytic activity of dioxomolybdenum(VI) complexes with N–N donor ligand: role of halogen Atom coordinated to the molybdenum centre, Polyhedron 200 (2021) 1–13, doi:10.1016/j.poly.2021.115144.
[43] T.M. Seck, A. Sy, D. Lo, P.A. Gaye, M.L. Sall, O. Diouf, M. Diaw, M. Gaye, Synthesis, spectroscopic studies and X-ray diffraction of heptacoordinated Mn(II) and Co(II) complexes with ligands derived from carbonohydrazide, Open J. Inorg. Chem. 09 (2019) 35–52, doi:10.4236/ojic.2019.94004.
[44] M. Rafiq, M. Khalid, M.N. Tahir, M.U. Ahmad, M.U. Khan, M.M. Naseer, A.A.C. Braga, S. Muhammad, Z. Shafiq, Synthesis, XRD, spectral (IR, UV–Vis, NMR) characterization and quantum chemical exploration of benzoimidazole-based hydrazones: a synergistic experimental-computational analysis, Appl. Org. Chem. 33 (2019) 1–17, doi:10.1002/aoc.5182.
[45] M.I. Khan, A. Khan, I. Hussain, M.A. Khan, S. Gul, M. Iqbal, F. Khuda, Spectral, XRD, SEM and biological properties of new mononuclear schiff base transition metal complexes, Inorg. Chem. Commun. 35 (2013) 104–109, doi:10.1016/j.inoche.2013.06.014.
[46] M. Shakir, S. Hanif, M.A. Sherwani, O. Mohammad, S.I. Al-Resayes, Pharmacologically significant complexes of Mn(II), Co(II), Ni(II), Cu(II) and Zn(II) of novel schiff base ligand, (E)-N-(furan-2-yl methylene) quinolin-8-amine: synthesis, spectral, XRD, SEM, antimicrobial, antioxidant and in vitro cytotoxic studies, J. Mol. Struct. 1092 (2015) 143–159, doi:10.1016/j.molstruc.2015.03.012.
[47] B. S.Kusmariya, A.P. Mishra, Co(II), Ni(II), Cu(II) and Zn(II) complexes of tridentate ONO donor schiff base ligand: synthesis, characterization, thermal, non-isothermal kinetics and DFT calculations, J. Mol. Struct. 1130 (2017) 727–738, doi:10.1016/j.molstruc.2016.11.009.
[48] M.A. Ayoub, E.H. Abd-Elnasser, M.A.-A Ahmed, M.G. Rizk, Synthesis, physicochemical, thermal, fluorescence and catalytic activity studies of novel

Mn(II), Co(II), Ni(II) and Cu(II) complexes with tridentate (ONS) schiff base ligand, Euro. J. Chem. 8 (2017) 85–95, doi:10.5155/eurjchem.8.1.85-95.1513.

[49] G. Swiderski, R. Swisłocka, R. Lyszczek, S. Wojtulewski, M. Samsonowicz, W. Lewandowski, Thermal, spectroscopic, X-ray and theoretical studies of metal complexes (sodium, manganese, copper, nickel, cobalt and zinc) with pyrimidine-5-Ccarboxylic and pyrimidine-2-carboxylic acids, J. Thermal Anal. Calor. 138 (2019) 2813–2837, doi:10.1007/s10973-019-08594-x.

[50] S.M. Abdallah, G.G. Mohamed, M.A. Zayed, M.S.A. El-Ela, Spectroscopic study of molecular structures of novel schiff base derived from O-phthaldehyde and 2-aminophenol and its coordination compounds together with their biological activity, Spectro. Acta - Part A: Mol. Biomol. Spectr. 73 (2009) 833–840, doi:10.1016/j.saa.2009.04.005.

[51] B.K. Singh, U.K. Jetley, R.K. Sharma, B.S. Garg, Synthesis, characterization and biological activity of complexes of 2-hydroxy-3,5-dimethylacetophenoneoxime (HDMAOX) with copper(II), cobalt(II), nickel(II) and palladium(II), Spectro, Acta Part A 68 (2007) 63–73, doi:10.1016/j.saa.2006.11.001.

[52] V.K. Srivastava, Synthesis, characterization, and biological studies of some biometal complexes, Future J. Pharma. Sci. 7 (2021), doi:10.1186/s43094-021-00191-w.

[53] E. MacKova, K. Hruskova, P. Bendova, A. Vavrova, H. Jansova, P. Haskova, P. Kovarikova, K. Vavrova, T. Simunek, Methyl and ethyl ketone analogs of salicylaldehyde isonicotinoyl hydrazone: novel iron chelators with selective antiproliferative action, Chem. Biol. Interact. 197 (2012) 69–79, doi:10.1016/j.cbi.2012.03.010.

[54] R.N. Patel, S.P. Rawat, M. Choudhary, V.P. Sondhiya, D.K. Patel, K.K. Shukla, D.K. Patel, Y. Singh, R. Pandey, Synthesis, structure and biological activities of mixed ligand copper(II) and nickel(II) complexes of N′-(1E)-[(5-bromo-2-hydroxyphenyl)methylidene] benzoylhydrazone, Inorg. Chimica Acta 392 (2012) 283–291, doi:10.1016/j.ica.2012.03.040.

[55] S. Sharma, F. Athar, M.R. Maurya, F. Naqvi, A. Azam, Novel bidentate complexes of Cu(II) derived from 5-nitrofuran-2- carboxaldehyde thiosemicarbazones with antiamoebic activity against E. histolytica, Euro. J. Med. Chem. 40 (2005) 557–562, doi:10.1016/j.ejmech.2005.01.003.

[56] G. Sridhar, B.I. Mohammed, D. Easwaramoorthy, R.S. Kutti, S. B.Kumar, C.S. Manohar, Synthesis, characterization and antimicrobial activities of copper, nickel, cobalt, chromium complexes derived from (Z)-4-fluoro-N-(2,7-dimethylhept-6-enylidene) benzenamine, J. Braz. Chem. Soc. 28 (2017) 756–767, doi:10.21577/0103-5053.20160224.

Clinical Interventions and Clinical Trials
2023 Volume 1, Issue 1
DOI: 10.59657/cict.brs.23.002

BioRes Scientia
Value your Research

Research Article

Open Access

Synthesis, Characterization and Antimicrobial Activity of Copper Oxide Nanoparticles Using Sol-Gel Method

Jagannath S. Godse[1], Kishore Puri[2], Santosh B. Gaikwad[3], Sanjay B. Ubale[1]*, Savita A. Kate[4] and Rajendra P. Pawar[4]*

[1]*Department of Chemistry, Deogiri College, Aurangabad, India.*
[2]*Department of Chemistry, Shri Shivaji College of Arts, Commerce and Science, Akola, India.*
[3]*Department of Chemistry, L P G Arts and Science College, Shirpur (Jain), Washim, India.*
[4]*Department of Chemistry, Shi Chhatrapati College, Aurangabad, India.*
Corresponding Author: Sanjay B. Ubale & Rajendra P. Pawar.

Abstract

This study investigates a novel way for producing copper oxide (CuO) nanoparticles using the sol-gel process and citric acid as a surfactant. In this technique, water is used as a potent solvent. Because of its low cost, ease of preparation, and commercial practicality, the synthetic approach is environmentally beneficial. X-ray diffraction (XRD), Field Emission Scanning Electron Microscopy (FE-SEM), Energy-Dispersive X-ray spectroscopy (EDX), Fourier Transform Infra-Red spectroscopy (FTIR), and Ultra-Violet visible spectroscopy (UV-Vis) were used to examine the antimicrobial activity of bacterial, fungal, as well as Pneumonia activity. Copper oxide NPs synthesized demonstrates highly scattered characterization and application findings. The green method is a practical, eco-friendly, simple, and valuable method for producing copper oxide nanoparticles.

Keywords: Copper oxide; sol-gel method; nanomaterial; antimicrobial; antifungal

Introduction

The unique properties of nanomaterials, as well as their high surface-to-volume ratio, have made them a viable and new tool in many scientific disciplines. This flexible material has numerous applications, including antimicrobial activities, photovoltaics, sensors, storage devices, medicine administration, photocatalytic training, and so on. Copper oxide nanoparticles most used because they are cheap, common, have low toxicity, and are easy to manufacture. Because of their high catalytic activity and durability, photo-catalysts constructed of single metal oxides are becoming increasingly popular [1-2].

A multitude of procedures can be used to create single metal oxide nanoparticles. Solid-state synthesis, the hydrothermal method, the electrochemical approach, the sol-gel technique, co-precipitation, microwave-assisted synthesis, the thermal decomposition method, and others are examples[3-4]. We choose the sol-gel process due to worries about overheating and hazardous solvents in other procedures. The sol-gel method is the most environmentally friendly and cutting-edge of these techniques because it does not require high pressure or high temperature, is inexpensive, and allows for easy monitoring of the crystalline size and structure of the nanomaterial through pH modification of the medium while preparing a large amount of sample. This paper describes a simple sol-gel method for producing copper oxide (CuO) nanoparticles with citric acid as a suitable surfactant. Synthesized Copper oxide nanoparticles were screened for biological activity of antibacterial, antifungal, and antimalarial activity which showed better to excellent results.

Experimental

Characterization

Copper chloride, citric acid, hydrochloric acid, and ammonium hydroxide were purchased from SD-Fine Chemical Company and used without further purification. The X-ray diffraction (XRD) pattern was recorded by the Rigaku X-ray Diffractometer with a Cu

© 2023 Rajendra P. Pawar & Sanjay B. Ubale, et al.

K-α radiation source (λ=1.5406 A°) operated at 40 kV. Field emission scanning electron microscopy (FE-SEM) images were obtained on JEOL 6390LA, Japanand the energy dispersive spectrometry (EDS) analysis was studied by JEOL/JEM 2100, Japan, with an acceleration voltage of 200 kV. Fourier transform infrared (FT-IR) spectra were recorded on Shimadzu IR spectrophotometer. Ultraviolet visible (UV-Vis) spectra were recorded on Thermo Scientific UV-Vis's spectrophotometer.

Synthesis of CuMn2O4 nanoparticles

Synthesis of Copper oxide (CuO) nanoparticles was carried out by the sol-gel method. Initially, 0.25 M of copper chloride were dissolved in 100 ml of distilled water. 0.1 N hydrochloric acid improves the solubility of copper chloride in water. Both the solutions were mixed with constant stirring. After mixingthe solutions, 1 gm of the citric acid solution was added as a surfactant. The pH of the above solution was adjusted at 8-8.5 (basic) using 3 to 3.5 ml NH_4OH solution. Precipitation was formed, which stirred with constant stirring for an hour at room temperature. The mixture was filtered using Whatman filter paper No. 42 and washed with deionized water 2-3 times. The obtained product was dried in an oven at 100°C for 2 hours. Finally, the dried material was calcinated for 3 hours at 500°C in the furnace. The black-colored precipitate was obtained as a final product and was stored for further study **(Figure 1).**

Figure 1: Flow Chart for Synthesis Method of CuO NPs

Result and Discussion

UV-Visible Analysis of CuO oxide Nanoparticle

The UV-Visible diffused reflectance spectra of nanostructured equimolar concentration of copper oxide NPs are shown in Figure. It has a wide range of absorption at 260 to 300 nm [5]. This proves that equimolar concentrations of copper oxide NPs result in lower reflectance. These findings suggest that synthesized copper oxide NPs metal to shift the absorption of the resulting nanoparticles from the infrared to the visible. This indicates that transition metal oxides that have been optically active. The copper oxide NPs effect on the band gaps of CuO semiconductors is the more immediate cause of the change in reflectance. The increased photogeneration rate of charge-transfer between Cu^{2+} electrons valence band greatly improves the photo reactivity, catalytic activity of copper oxide NPs **(Figure 2)**.

© 2023 Rajendra P. Pawar & Sanjay B. Ubale, et al.

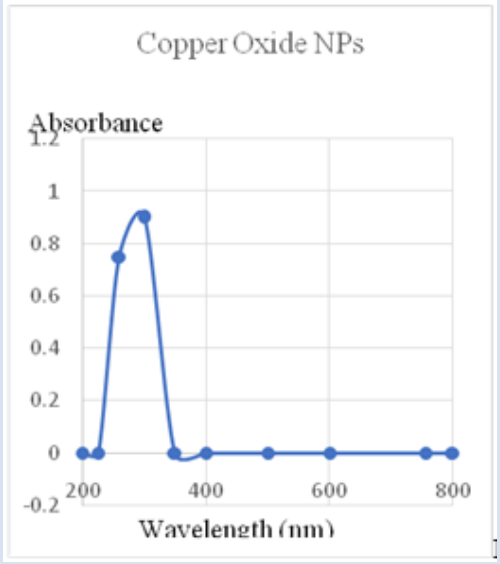

Figure 2: Uv-Vis's data of CuO NPs

FTIR analysis of CuO oxide nanomaterial

Fourier transform infrared spectrometer confirms the formation of metal oxide bonds in the CuO nanoparticles as shown in Figure 2. Investigation of nanomaterial is observed at the wavelength range from 397 cm^{-1} to 3980 cm^{-1}. The low-frequency vibrations of the M-O bond appear below 1000 cm^{-1}. In Figure 1the firm peaks at position 403.12cm^{-1} and 462.92 cm^{-1} represent Cu–O stretching of CuO stretching vibrational modes, respectively and the band that appeared in the range of 800–1300 cm^{-1} is recognized as the stretching vibration of –OH (**Figure 3**). These results as approximately match with another study [6-7].

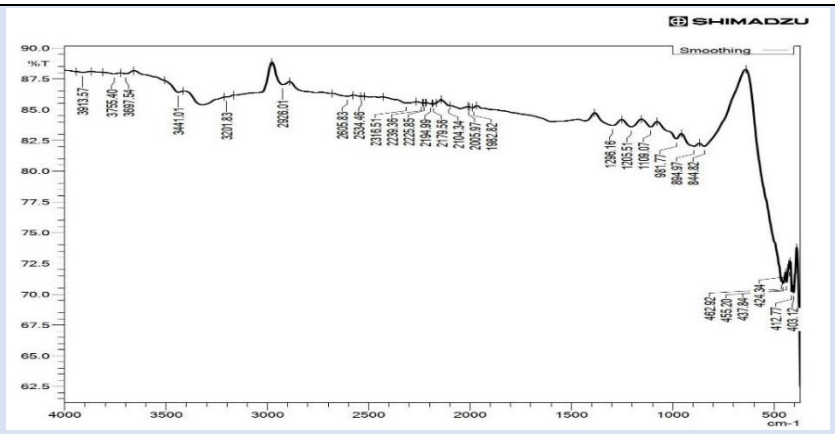

Figure 3: FTIR data of CuO NPs

XRD characterization of CuMn2O4 oxide nanomaterial

The X-ray diffraction technique investigated the chemical, structural, and spectroscopic properties of CuO nanomaterial. All X-ray diffraction peaks were indexed according to the standard data for CuO as shown in Figure 2. The significant peaks are obtained for 2θ at 32.5°,35.49°, 38.71°, 47.42°, 56.29°, 61.59°, 66.32°68.11°and 75.17°, corresponding to the planes (110), (111), (111), (220), (020), (113), (022) (220) and (004) respectively (**Figure 4**). In addition, the Fd-3m space group and Monoclinic Crystal system of CuO nanomaterial are recognized in the X-ray diffraction pattern and correctly matched with the standard JCPDs card no. 05-0661[8-9]. The average crystallite size (D) of CuO nanomaterial was calculated by using the Scherer formula [5, 10].

$$D = \frac{K\lambda}{\beta Cos\theta} \qquad (1)$$

Where, K is a shape factor, D is the size of the nanomaterial, λ is the incident X-ray beam's wave length, θ is Bragg's diffraction angle, and β is the Full width half maximum. The average particle size of the investigating nanomaterial was 15.5 nm.

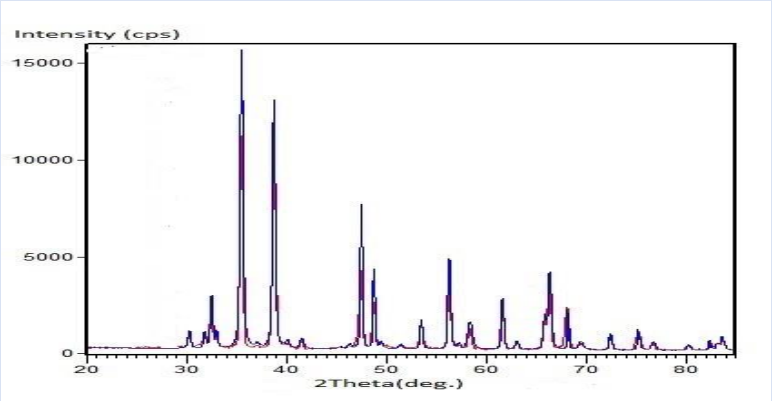

Figure 4: XRD data of CuO NPs

SEM and EDX studies of CuO oxide nanomaterial

The morphology and complete structures of CuO nanomaterial were contributed by scanning electron microscope (SEM) and energy-dispersive X-ray (EDX) spectroscopy. SEM images of CuO nanomaterial synthesized by sol-gel method from chloride precursors strengthening the precursors at 500°C are shown in as shown in (Figure 6 and Figure 7). Scanning electron microscope (SEM) instrument in the range of scale taken between 500 nm and 1µm.

The elemental compositional investigation of CuO nanomaterial is shown in as shown in (Figure 8 and Table 1). The presence of Cu and O and the Cu/O ratio were determined by EDX investigation, which matches perfectly with CuO. This confirms the availability of copper and oxygen with a weight percentage of 94 %, 6 %, and atomic percentages of 79.9% and 20.1% respectively.

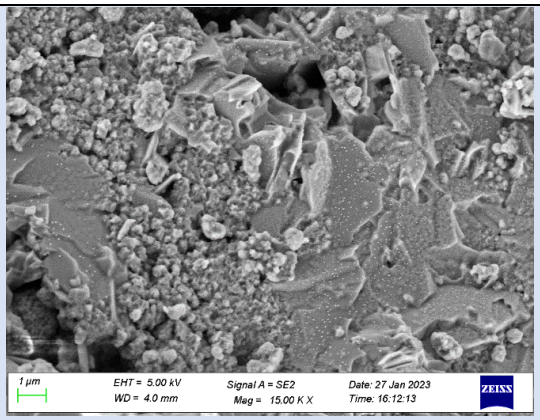

Figure 5: FESEM data of CuO NPs

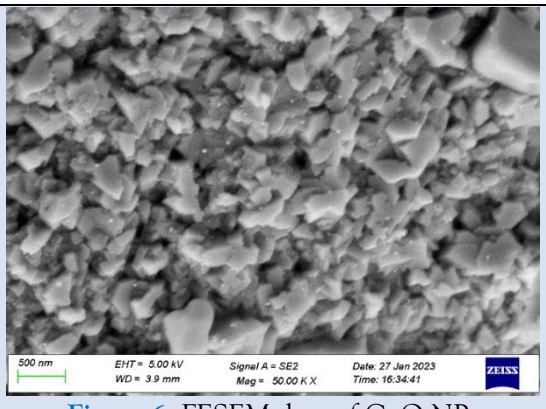

Figure 6: FESEM data of CuO NPs

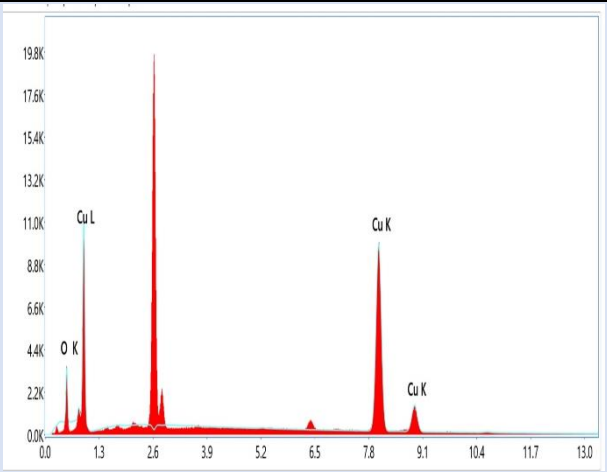

Figure 7: EDX data of CuO NPs

Table 1: EDX data of CuO NPs

Element	Line Type	Wt.%	Atomic %
O	K series	6	20.1
Cu	K series	94	79.9
Total:		100	100

In recent years, nanomaterial has a broader range of applications and uses in various fields. Some researchers have studied the use of nanomaterials for catalytic activity for oxidation [11], photo-catalytic activity [12], a high-performance electrode for supercapacitors [13], solid oxide fuel cells [14]and catalytic ozonation membrane reactor [15]. These example sconfirm that CuO oxide nanomaterial is environmentally supportive for living organisms and extremely useful in different fields.

Biological Activity

Synthesized copper oxide nanoparticles were tested for their antimicrobial efficacy against four different bacteria. - S. *aureus* (MTCC 96), *E. coli* (MTCC 443), *P. aeruginosa* (MTCC 1688), S. *pyogenus* (MTCC442), and three fungi-C. *Albicans* (MTCC 227), A. *clavatus* (MTCC1323)and A. *niger* (MTCC282)using broth dilution method[16-17]. Gentamycin, Ampicillin chloramphenicol, ciprofloxacin and norfloxacin were used as the standards for antibacterial activity, whereas griseofulvin and nystatin were used as the standards for antifungal activity. Minimum Inhibitory Concentration (MIC) values were used to describe the outcomes. The MIC of a drug is the smallest concentration of the sample that clearly stunts the growth of the microbe. Minimum Inhibitory Concentration (MIC) values were used to describe the outcomes. The MIC of a drug is the smallest concentration of the sample that clearly stunts the growth of the microbe[18-19].

The efficiency of synthesized copper oxide nanoparticles to act as antimalarial hits was studied in-*vitro* against *Plasmodium falciparum* in 96-well microtitre plate according to the different reported method [20-21].chloroquine was used as the standard, and the results were reported in terms of IC50 values. All the screening was performed at Microcare Laboratory, Surat, Gujarat, India.

Antibacterial activity

Antibacterial activity was tested on the synthesized copper oxide nanoparticles compounds[22-23]. The broth dilution technique was used to demonstrate antibacterial activity against *E. coli* (MTCC443), P. *aeruginosa* (MTCC1688), *S. aureus* (MTCC96), S. *pyogenus* (MTCC442) bacterial strains using *Gentamycin, Ampicillin, chloramphenicol, ciprofloxacin* and *norfloxacin* as the standard drugs. Copper oxide nanoparticles showing a strong and excellent antibacterial activity against *S. aureus*. The standard *chloramphenicol* (50µg/mL) other had weaker antibacterial activity against *E. coli*, P. *aeruginosa* and S. *pyogenus* as compared to the standard chloramphenicol show in (Table1). copper oxide nanoparticles showing a weak antibacterial activity against *E. coli*, P. *aeruginosa*, *S. aureus* and S. *pyogenus* the standard *Gentamycin, Ampicillin, ciprofloxacin* and *norfloxacin* show in **(Table 2)**.

Table 2: Antibacterial activity data of CuO NPs

Antibacterial Activity Table					
Minimum Inhibition Concentration (Microgram /ML)					
SR.	Code	E. Coli	P. Aeruginosa	S. Aureus	S. Pyogenus
NO	NO	MTCC 443	MTCC 1688	MTCC 96	MTCC 442
1	**Sample CuO NPs**	**250**	**50**	**100**	**100**
2	*Gentamycin	0.05	1	0.25	0.5
3	*Ampicillin	30	-	40	25
4	*Chloramphenicol	50	50	50	50
5	*Ciprofloxacin	25	25	50	50
6	*Norfloxacin	10	10	10	10

Antifungal Activity

Antifungal Activity was studied against *C. albicans* (MTCC227), *A. niger* (MTCC282), *A. clavatus* (MTCC1323) fungal strains. The results of antifungal activity reveal that the copper oxide nanoparticles synthesized compounds showed lower antifungal activity as compared to the standard *Nystatin* and *Greseofulvin*. The compounds were less active against the *C. albicans*, *A. niger* and *A. clavatus* fungal strains in comparison with both the standards **(Table 3)**.

Table 3: Antifungal activity data of CuO NPs

Antifungal Activity Table				
Minimum Inhibition Concentration (Microgram /ML)				
SR.	Code	C. Albicans	A. Niger	A. Clavatus
NO	NO	MTCC 227	MTCC 282	MTCC 1323
1	**Sample CuO NPs**	**>1000**	**500**	**500**
2	*Nystatin	100	100	100
3	*Greseofulvin	500	100	100
***Standard Drug**				

Antimalarial Activity

Copper oxide nanoparticles synthesized compounds showed the antimalarial activity was carried against Plasmodium falciparum. The compound copper oxide nanoparticles showed less antimalarial activity. The results of antimalarial activity revealed that copper oxide nano particles compounds were moderately active but less potent than the standard chloroquine, which is show in (Table 4).

Table 4: Antimalarial activity data of CuO NPs

Antimalarial Activity (Plasmodium Falciparum)		
Minimum Inhibition Concentration (Microgram /ML)		
SR.	Code	Mean IC50 Values a
NO	NO	MTCC 227
1	**Sample CuO NPs**	**0.88**µg /ml
2	*Chloroquine IC50	0.020 µg /ml
***Standard Drug, a: mean values in representative assay.**		

Conclusions

In summary, we report the synthesis, characterization, antibacterial, antifungal and antimalarial activity of copper oxide nano particles antibacterial activity against *E. coli* as they had lower MIC values in comparison with the standard ampicillin. Copper oxide nanoparticles compounds the compounds were less active against the *C. albicans*, *A. niger* and *A. clavatus* fungal strains in comparison with both the standards. The compounds exhibited moderate antimalarial activity but less than the standard chloroquine. Antibacterial and antimalarial entities are thus revealed by the current studies, highlighting their potential future significance in medicinal chemistry. A CuO oxide nanomaterial was successfully prepared using a sol-gel, an environmentally supportive method. In the

© 2023 Rajendra P. Pawar & Sanjay B. Ubale, et al.

synthesis of CuO nanomaterial, copper chloride with using citric acid as a surfactant. This method is eco-friendly, cheap, easy handling, non-hazardous, and harmless aqueous solvent systems.

Declarations

Funding

This research received no external funding.

Acknowledgments

This research has no acknowledgment.

Conflicts of Interest

The authors declare no conflict of interest.

References

1. Ananda Murthy, H. Abebe, B. CH, P. Shantaveerayya, K. (2018). A review on green synthesis and applications of Cu and CuO nanoparticles. *Material Science Research India*. 15 (3):279-295.
2. Ren, G. Hu, D. Cheng, E. W. Vargas-Reus, M. A. Reip. et.al. (2009). Characterization of copper oxide nanoparticles for antimicrobial applications. *International journal of antimicrobial agents*. 33(6):587-590.
3. Singh, J. Kaur, G. Rawat, M. (2016). A brief review on synthesis and characterization of copper oxide nanoparticles and its applications. *J. Bio electron. Nano technol*.
4. Dörner, L. Cancellieri, C. Rheingans, B. Walter, M. Kägi, et.al. (2019). Cost-effective sol-gel synthesis of porous CuO nanoparticle aggregates with tunable specific surface area. *Scientific reports*. 9(1):1-13.
5. Sahooli, M. Sabbaghi, S. Saboori, R. (2012). Synthesis and characterization of mono sized CuO nanoparticles. *Materials Letters*. 81:169-172.
6. Sahai, A. Goswami, N. Kaushik, S. Tripathi, S. (2016). Cu/Cu2O/CuO nanoparticles: Novel synthesis by exploding wire technique and extensive characterization. *Applied Surface Science*. 390:974-983.
7. Nabila, M. I. Kannabiran, K. Biosynthesis, (2018). characterization and antibacterial activity of copper oxide nanoparticles (CuO NPs) from actinomycetes. *Bio catalysis and agricultural biotechnology*. 15:56-62.
8. Mohammed, W. M. Mubark, T. H. Al-Haddad, R. M. (2018). Effect of CuO nanoparticles on antimicrobial activity prepared by sol-gel method. Int. J. Appl. Eng. Res. Dev. 13:10559-10562.
9. Dhineshbabu, N. Rajendran, V. Nithyavathy, N. Vetumperumal, R. (2016). Study of structural and optical properties of cupric oxide nanoparticles. *Applied Nanoscience* 6:933-939.
10. Manimaran, R. Palaniradja, K. Alagumurthi, N. Sendhilnathan, S. Hussain, J. (2014). Preparation and characterization of copper oxide nanofluid for heat transfer applications. *Applied Nanoscience*. 4:163-167.
11. Zedan, A. F. Mohamed, A. T. El-Shall, M. S. AlQaradawi, S. Y. AlJaber, A. S. (2019). Tailoring the reducibility and catalytic activity of CuO nanoparticles for low temperature CO oxidation. *RSC advances*. 8(35):19499-19511.
12. Siddique, S. Waseem, M. Naseem, T. Bibi, A. (2021). Hafeez, et.al. S. Photo-Catalytic and Anti-microbial Activities of r GO/CuO Nanocomposite. *Journal of Inorganic and Organometallic Polymers and Materials*. 31:1359-1372.
13. Zhan, Y. Bai, J. Guo, F. Zhou, H. Shu, R. Yu, Y. Qian, L. (2021). Facile synthesis of biomass-derived porous carbons incorporated with CuO nanoparticles as promising electrode materials for high-performance supercapacitor applications. *Journal of Alloys and Compounds*. 885:161014.
14. Beigzadeh, M. Pourfayaz, F. Ahmadi, M. H. (2020). Modeling and improvement of solid oxide fuel cell-single effect absorption chiller hybrid system by using nanofluids as heat transporters. *Applied Thermal Engineering*. 166:114707.
15. Coelho, L. L. Scaratti, G. Hissanaga, A. M. Oechsler, B. F. José, et.al. (2021). Modeling and fouling control in a hybrid membrane process using CuO-catalytic membrane coupled to ozone. *Journal of Environmental Chemical Engineering*. 9(5):106138.
16. Padil, V. V. T. Černík, M. (2013). Green synthesis of copper oxide nanoparticles using gum karaya as a biotemplate and their antibacterial application. *International journal of nanomedicine*. 889-898.
17. Ahamed, M. Alhadlaq, H. A. Khan, M. M. Karuppiah, P. Al-Dhabi, N. A. Synthesis, (2014). characterization, and antimicrobial activity of copper oxide nanoparticles. *Journal of Nanomaterials*. 17-17.
18. Fouda, A. Hassan, S. E.-D. Eid, A. M. Awad, M. A. Althumayri, et.al. (2022). Endophytic bacterial strain, Brevibacillus brevis-mediated green synthesis of copper oxide nanoparticles, characterization,

© 2023 Rajendra P. Pawar & Sanjay B. Ubale, et al.

antifungal, in vitro cytotoxicity, and larvicidal activity. *Green Processing and Synthesis*. 11(1):931-950.

19. Chaerun, S. K. Prabowo, B. A. Winarko, R. (2022). Bio nano technology the formation of copper nanoparticles assisted by biological agents and their applications as antimicrobial and antiviral agents. *Environmental Nanotechnology, Monitoring & Management*. 18:100703.
20. Hang, X. Peng, H. Song, H. Qi, Z. Miao, X. Xu, W. (2015). Antiviral activity of cuprous oxide nanoparticles against Hepatitis C Virus in vitro. *Journal of virological methods*. 222:150-157.
21. Jayaseelan, C. Abdulhaq, A. Ragavendran, C. Mohan, S. (2022). Phytoconstituents Assisted Biofabrication of Copper Oxide Nanoparticles and Their Antiplasmodial, and Antilarval Efficacy: A Novel Approach for the Control of Parasites. Molecules 27(23):8269.
22. Meghana, S. Kabra, P. Chakraborty, S. Padmavathy, N. (2015). Understanding the pathway of antibacterial activity of copper oxide nanoparticles. *RSC advances*. 5(16):12293-12299.
23. Khatami, M. Heli, H. Mohammadzadeh Jahani, P. Azizi, H. Lima Nobre, M. A. (2017). Copper/copper oxide nanoparticles synthesis using Stachys lavandulifolia and its antibacterial activity. *Iet Nanobiotechnology*.11(6)709-713.

Cite this article: Rajendra P. Pawar, Kishore Puri, Santosh B. Gaikwad, Sanjay B. Ubale, Savita A. (2023). Synthesis, Characterization and Antimicrobial Activity of Copper Oxide Nanoparticles Using Sol-Gel Method, *Clinical Interventions and Clinical Trials*, BRS Publishers. 1(1); DOI: 10.59657/cict.brs.23.002

Copyright: © 2023 Rajendra P. Pawar and Sanjay B. Ubale, this is an open-access article distributed under the terms of the Creative Commons Attribution License, which permits unrestricted use, distribution, and reproduction in any medium, provided the original author and source are credited.

Article History: **Received:** April 10, 2023 | **Accepted:** April 28, 2023 | **Published:** May 05, 2023

Check for updates

Received: 5 December 2023 | Revised: 30 January 2024 | Accepted: 2 February 2024

DOI: 10.1002/aoc.7405

FULL PAPER

Applied Organometallic Chemistry WILEY

Solvothermal single-pot synthesis of Pd-Fe_3O_4@GO catalyst: Enhanced catalytic performance in Sonogashira coupling reactions

Mahesh A. Pawar[1] | **Akhil V. Nakhate**[2] | **Samidha S. Kadu**[1] | **Pradip V. Tekade**[2]

[1]Shri Shivaji College of Arts, Commerce and Science, Akola, India

[2]Bajaj College of Science, Wardha, India

Correspondence
Akhil V. Nakhate, Bajaj College of Science, Wardha 442001, India.
Email: akhiln30@gmail.com

In this study, we present a new approach to synthesizing a magnetically separable Pd-Fe_3O_4@GO catalyst using a simple single-pot method. The catalyst was employed in Sonogashira coupling reactions, demonstrating excellent results. The catalyst was studied using a various characterization method, including X-ray photoelectron spectroscopy (XPS), scanning electron microscope–energy-dispersive X-ray spectroscopy (SEM-EDS) mapping, TEM, X-ray diffraction (XRD), FTIR, and inductively coupled plasma mass spectrometry (ICP-MS). Pd-Fe_3O_4@GO exhibited superior catalytic activity compared with its conventional counterparts in phenylacetylene-iodobenzene coupling reactions under copper co-catalyzed-free and ligand-free conditions, with a higher turnover frequency (TOF) of 118.3 h^{-1}. Optimized conditions yielded high yields for various substrates, including inactive aryl chloride and bromide substrates, emphasizing its versatility. Also, a reaction mechanism was proposed and a kinetic model was developed. The catalyst's green chemistry potential was highlighted because of its high efficiency, purity of products, recoverability, and ease of preparation. Moreover, Pd-Fe_3O_4@GO demonstrated impressive stability through multiple recycling rounds without loss of functionality, making it a promising tool for sustainable chemical processes.

KEYWORDS

graphene oxide, magnetic separable catalyst, palladium, Sonogashira coupling reactions

1 | INTRODUCTION

Catalysis plays a crucial role in the production of pharmaceuticals, agrochemicals, and essential molecules through diverse chemical transformations.[1–6] The use of catalysts to facilitate coupling reactions holds tremendous potential for advancing sustainable organic syntheses, thereby overcoming significant drawbacks linked to conventional approaches. Catalysts contribute to heightened selectivity, significantly accelerated reaction rates, and a reduction in by-product generation. Various catalytic methods have been developed to address diverse coupling reactions.[7] Cross-coupling reactions, particularly in the synthesis of medicinal, natural, and agricultural products, have garnered considerable attention.

The Sonogashira coupling process stands out as a highly effective synthetic technique for establishing carbon–carbon bonds.[8,9] Palladium metal salts have typically been utilized as catalysts in Sonogashira coupling procedures involving aryl halides and alkynes, in combination with co-catalytic like copper, toxic phosphine, N-based ligands, and significant volumes of solvents. Although the presence of Cu(I) salt improves the reaction by generating Cu acetylide, it has the disadvantage of

 © 2024 John Wiley & Sons Ltd.

forming an unwanted alkyne homocoupled product alongside the intended product by Glaser-type oxidative dimerization, which reduces the efficiency of the cross-coupling reaction.[10,11]

Noble metals have lately gained attraction because of their applications in catalysis, biomedicine, solar energy conversion, photocatalysis, gas sensors, fuel cells, and drug delivery.[12–15] Metal nanoparticles (NPs) have attracted the interest of researchers because of their high catalytic activity and huge surface area, allowing effective interaction between the reactant and the catalyst surface. However, metal NPs have two fundamental drawbacks, that is, rapid agglomerate during chemical transformation due to their high surface energy, and their tiny size making their separation from the reaction mixture extremely challenging.[16] However, immobilizing NPs on a structurally suitable support can solve these problems.[17]

Throughout the last decade, researchers have explored NPs anchored on various materials as catalysts, including activated carbon nanotubes, metal oxides, graphene, graphene oxide (GO), polymers, zeolite, alumina, magnetic materials, and metal–organic frameworks. A variety of nanocatalysts for carbon–carbon bond formation have been discovered, with Pd NP-supported catalysts showing exceptional catalytic activity.[18] Graphene, along with its equivalents, has recently piqued the interest of scientists globally because of its two-dimensional structure, large surface area, great tensile strength, outstanding thermal conductivity, tremendous dispersibility, and other exceptional features.[19,20] It finds various applications in the fields of sensors, the biomedical sector, storage and conversion, and catalytic support.[21,22] Because of the oxygen functionality on the surface, GO gets readily dispersed in water as well as different organic solvents, making it easier to handle. Metal anchoring is also conceivable, resulting in increased catalytic activity. Chemically produced graphenes like GO and reduced graphene oxide (rGO) are promising candidates for catalytic support due to their inertness, wide surface area, accessibility, and stability.[23] Various investigations on catalysis with GO as support have been reported including Pd/graphene (Pd/G),[24] Ag-Pd@rGO,[25] Pd-Co/G,[26] Pd@g-C_3N_4-Fe-GO,[27] (Pd@APGO),[28] Pd/PRGO,[29] and Pd/Cu@GO.[30]

However, the use of traditional catalyst isolation techniques, such as centrifugation or filtering, is required, limiting the economic viability of nanocatalysts. Consequently, magnetically separable catalysts, known for their exceptional stability, present an attractive alternative, especially when compared with commercial palladium catalysts used in coupling reactions. These catalysts can be easily separated from the reaction media by utilizing a magnet.[31] Various magnetically separable heterogeneous catalysts have been reported for Sonogashira reactions as well as other coupling reactions, such as Nano-Fe_3O_4@CA-Pd,[32] Pd-GO-Fe_3O_4-Cellulose,[33] Pd-$CuFe_2O_4$@SiO_2,[31] Pd–Fe_3O_4 heterodimeric nanocrystal catalyst,[34] γ-Fe_2O_3@SiO_2–$(CH_2)_3$–PDTC–Pd,[35] Pd NPs on magnetic nanoparticle starch substrate (MNPSS),[36] CPS-MNPs-NNN-Pd,[37] MNP-CD-Pd,[38] Palladium anchored PEI grafted Fe_3O_4/SiO_2/P (GMA-co-EGDMA) NP nanocatalyst,[39] Pd-Fe_3O_4, a rose-shaped nanocatalyst,[40] bis-salophen palladium complex immobilized on Fe_3O_4@SiO_2,[41] Pd@GO/Fe_3O_4/PAA/DCA catalyst,[42] palladium supported magnetically separable moisture- and air-stable catalyst,[43] Pd NPs immobilized on metal NPs with dendritic "click" PEGylated ligands ("Click" PEGylated γ-Fe_2O_3–Pd),[44] and palladium supported on guanidine-terminated magnetic dendrimer (G3-Gu-Pd).[45] Notably, Pd/Fe_3O_4@SiO_2/Schiff base,[46,47] Cu/Fe_3O_4@SiO_2/Schiff base,[48] and Ni(II) EDTA-Fe_3O_4@SiO_2/Schiff base[49] have been developed as magnetically separable catalysts for constructing C-N bonds. The Sonogashira coupling as well as other coupling processes like C-N bond formation and heck reactions was carried out with the aforementioned catalysts, resulting in satisfactory yields of the desired products. It overcomes catalyst separation using a simple magnet. However, it has been observed that Pd catalyst synthesis involves multistep synthesis use of excessive non-green solvents, a long reaction time, and expensive ligands and reagents.

To address these challenges, the current study introduces a single-pot synthesis method for ligand-free Pd NPs supported on Fe_3O_4@GO a heterogeneous catalyst that is magnetically separable, reusable, effective, and environmentally friendly. This catalyst has been successfully employed in the Sonogashira cross-coupling reaction (Scheme 1). The kinetics of the reaction were studied systematically and validated against experimental data.

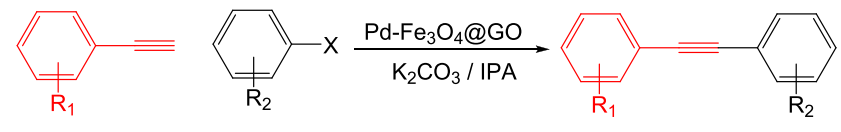

R_1 - H, $-C_2H_5$

R_2 - H, -F, $-CF_3$, -OMe, -Me, $-NO_2$, -Cl, -Br

X- I, Br[a] & Cl[b]

SCHEME 1 Sonogashira cross-coupling reaction.

10990739, 0, Downloaded from https://onlinelibrary.wiley.com/doi/10.1002/aoc.7405 by Institute Of Chemical Technology, Mumbai, Wiley Online Library on [26/02/2024]. See the Terms and Conditions (https://onlinelibrary.wiley.com/terms-and-conditions) on Wiley Online Library for rules of use; OA articles are governed by the applicable Creative Commons License

2 | EXPERIMENTAL

The Electronic Supporting Information (ESI) contains information about the chemicals, testing technique, compounds, and characterizations.

2.1 | Synthesis of GO

The modified Hummer's method was used to synthesize GO from natural graphite powder, synthesis process mentioned in supporting information.[50]

2.2 | Preparation of Pd-Fe_3O_4@GO

In a typical synthesis, previously synthesized GO (0.3 g) was disseminated for 60 min under sonication in a beaker of 100 mL containing 50 mL of ethylene glycol. Simultaneously, $FeCl_3{\cdot}6H_2O$ (5 mmol) in 50 mL of ethylene glycol was sonicated for 3 min. Both solutions were then agitated for 1 h at room temperature. The well-dispersed GO solution was combined with the $FeCl_3{\cdot}6H_2O$ solution, and the reaction mass was sonicated and agitated for an hour. Then, a $PdCl_2$ solution was prepared by dissolving 15 mg in a small amount of saline water. The palladium solution was gradually introduced into the previously described solution while continuously stirring. While stirring, 7 g of sodium acetate was added to the solution. The entire suspension was then transferred in an autoclave with internal Teflon-coated stainless-steel lining and heated for 24 h in a hot air oven at 180°C. Following solvothermal synthesis, the autoclave was allowed to cool to ambient temperature. The Pd-Fe_3O_4@GO nanomaterial was rinsed many times with distilled water and IPA before being centrifuged for 25 min at 6000 rpm. The produced Pd-Fe_3O_4@GO nanocatalyst was vacuum-dried for 24 h at 60°C. The palladium concentration of Pd-Fe_3O_4@GO was determined by inductively coupled plasma mass spectrometry (ICP-MS) and was found to be 1.92% wt. Pd.

2.3 | General procedure for Sonogashira cross-coupling reaction using Pd-Fe_3O_4@GO catalyst

A mixture of aryl halide (1 mmol), alkyne (1.1 mmol), K_2CO_3 (1.5 mmol), isopropyl alcohol (IPA) (5 mL), and 9 mg of the catalyst (1.92 wt.% Pd) was placed in a 20 mL sealed glass tube. The reaction mixture was vigorously stirred for 3 h at 90°C. The progress of the reaction was checked by TLC. Once the reaction was completed, the catalyst was separated using an external magnet, and the reaction mixture was washed successively with water-ethyl acetate, followed by brine. The mixture was then dehydrated using anhydrous Na_2SO_4. The resulting residue was purified through column chromatography to obtain the desired product.

3 | RESULT AND DISCUSSION

The prepared materials were characterized by scanning electron microscope (SEM), energy dispersive X-ray (EDX)-mapping, TEM, X-ray photoelectron spectroscopy (XPS), FTIR, single crystal X-ray diffraction (XRD), and XRD.

3.1 | SEM

The surface morphology of the synthesized Pd-Fe_3O_4@GO was examined using SEM at various magnifications (Figure 1). The structure of Pd-Fe_3O_4@GO was found to be uneven, displaying some Pd-Fe_3O_4 NPs agglomerated on the surface along with some semi-spherical-shaped particles. Furthermore, the SEM results for the Pd-Fe_3O_4@GO catalyst are consistent with the EDX and elemental mapping data. The chemical composition of Pd-Fe_3O_4@GO, as well as the dispersion of palladium and iron atoms on the GO surface, were determined using energy-dispersive X-ray spectroscopy (EDS) and mapping analysis. The SEM revealed that only palladium (yellow), iron (orange), oxygen (red), and carbon (green), were evenly dispersed across the surface of GO, confirming the excellent purity of Pd-Fe_3O_4@GO NPs.

3.2 | HR-TEM

The morphology and metal distribution of Pd-Fe_3O_4@GO were investigated using high-resolution transmission electron microscopy (HR-TEM), as shown in Figure 2a–d. Figure 2a,b displays a typical TEM image of the GO sheet, illustrating the structure and arrangement of Pd-Fe_3O_4 NPs on the surface of the GO sheet. In the cross-sectional view of the HR-TEM image of Pd-Fe_3O_4@GO, the intersecting crystal fringes indicate the coexistence of Pd and Fe_3O_4 as a mixture, rather than individual metal entities (Figure 2a). The combination of palladium NPs with iron oxide NPs has a synergistic impact in the form of palladium NP stability and dispersion, reducing agglomeration during the reaction and therefore increasing catalytic activity. From the particle size distribution, it was observed that the size of particles falls within the

10990739, 0, Downloaded from https://onlinelibrary.wiley.com/doi/10.1002/aoc.7405 by Institute Of Chemical Technology, Mumbai, Wiley Online Library on [26/02/2024]. See the Terms and Conditions (https://onlinelibrary.wiley.com/terms-and-conditions) on Wiley Online Library for rules of use; OA articles are governed by the applicable Creative Commons License

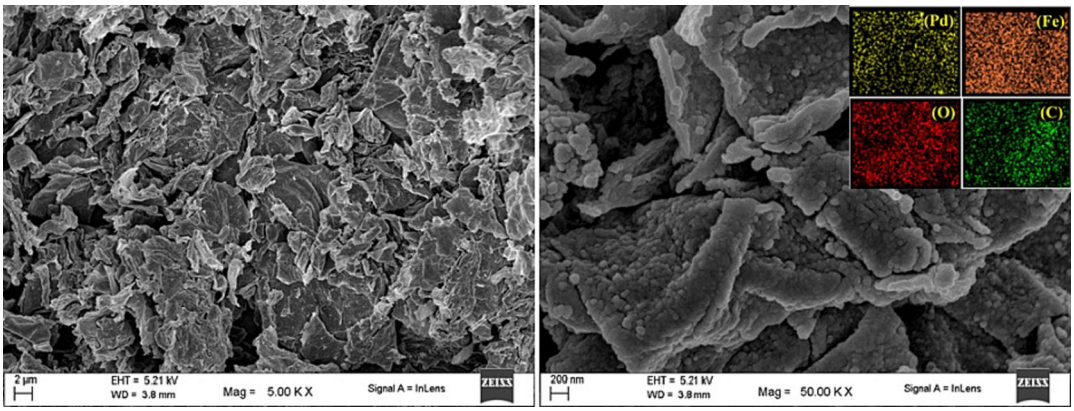

FIGURE 1 SEM image and elemental mapping of Pd-Fe_3O_4@GO.

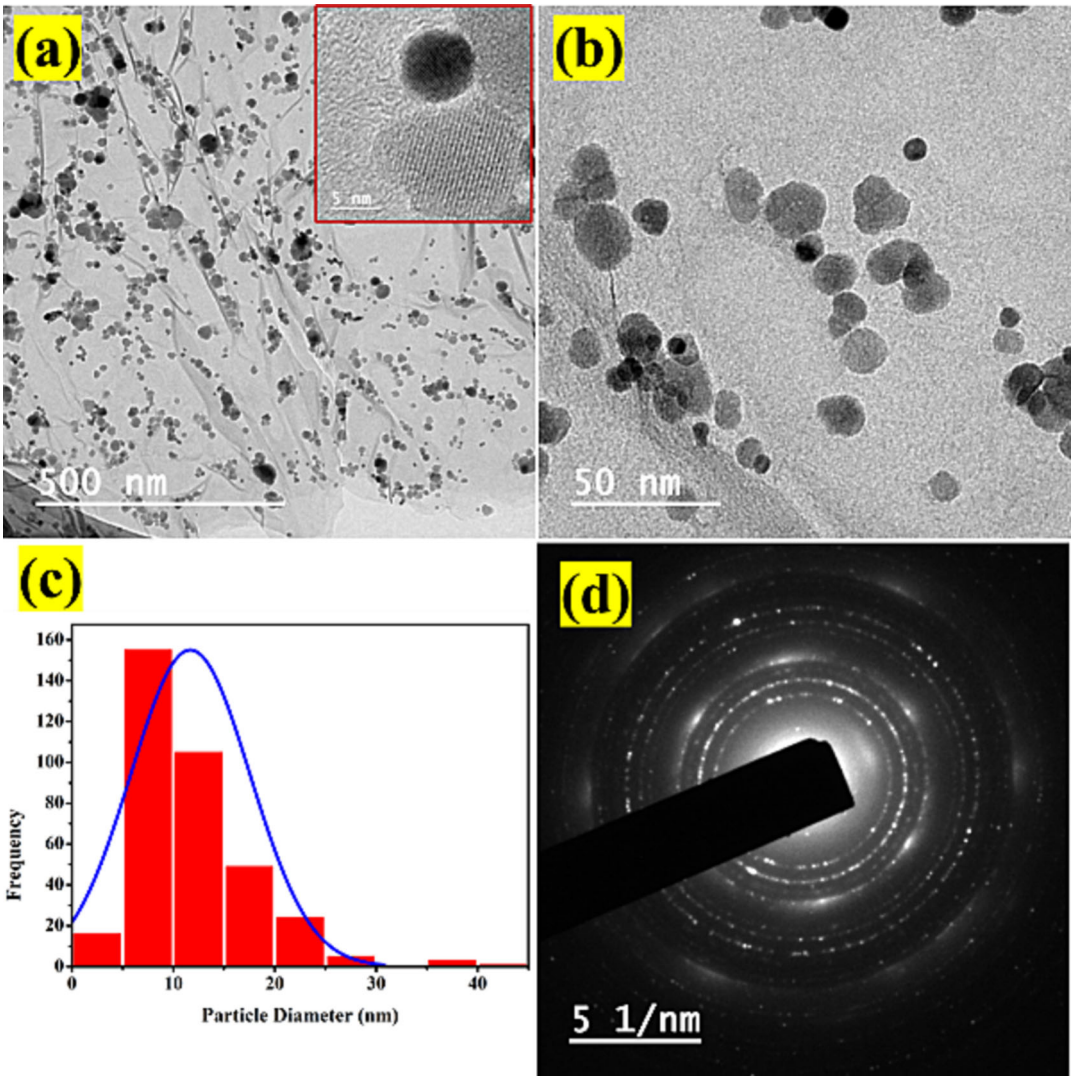

FIGURE 2 TEM image of (a, b) Pd-Fe_3O_4@GO low and high magnifications (c) particle size distribution (d) selected area electron diffraction (SAED) pattern.

range of 5–20 nm. Palladium exhibits a smaller particle size, while Fe_3O_4 has a larger size (Figures 2c and S1). The selected area electron diffraction (SAED) patterns confirm their crystallinity (Figure 2d). According to TEM analysis, Pd-Fe_3O_4 NPs are distributed on the GO surface, with a higher percentage of Fe than Pd.

10990739, 0, Downloaded from https://onlinelibrary.wiley.com/doi/10.1002/aoc.7405 by Institute Of Chemical Technology, Mumbai, Wiley Online Library on [26/02/2024]. See the Terms and Conditions (https://onlinelibrary.wiley.com/terms-and-conditions) on Wiley Online Library for rules of use; OA articles are governed by the applicable Creative Commons License

3.3 | XPS

Pd-Fe_3O_4@GO was subjected to XPS studies to explore the chemical states of Pd3d, Fe2p, O1s, and C1s on the catalyst's surface (Figure 3). The Pd3d high-resolution XPS splitting pattern revealed two doublet peaks of Pd $3d_{5/2}$ and Pd $3d_{3/2}$ spin-orbit components at 335.5 and 340.8 eV, which are related to metallic Pd, whereas the other doublet peaks at 337.9 and 343.3 eV are connected with Pd's + 2-oxidation state. The Pd3d high-resolution XPS splitting pattern showed two doublet peaks of Pd $3d_{3/2}$ and Pd $3d_{5/2}$ spin-orbit components at 340.8 and 335.5 eV are attributed to metallic Pd, whereas the additional doublet peaks at 343.3 and 337.9 eV are associated with the Pd + 2-oxidation.[16] The existence of Pd in metallic form in the catalyst could be due to the solvothermal process's reduction of Pd ions by ethylene glycol and sodium acetate, as well as the occurrence of PdO from the oxidation of bare metal Pd atoms under atmospheric circumstances. Peaks in the Fe2p high-resolution XPS had binding energies of 710.9 and 724.3 eV are associated with $Fe2p_{3/2}$ and Fe $2p_{1/2}$, showing the development of composite oxides of Fe(III) and Fe(II). Three peaks at 284.5 eV in the C1s high-resolution XPS relate to GO carbon, which corresponds to the non-oxygenated ring C=C: the C atom in the C-O bond at 285.6 eV, and carbonyl C (C=O) at 288.3 eV. In addition, an O1s signal was found at 530.2 eV, showing that the oxygen groups on GO were effectively incorporated. Furthermore, the O1s XPS spectrum showed peaks at 530.2, 531.4, and 532.9 eV, which are ascribed to O-C=O, C=O, and C-OH moieties, respectively.[51] The nanoscale interactions among palladium, iron oxide, and GO resulted in electronic modifications in the catalyst. These modifications optimized the binding energies of reactants and intermediates, enhancing the catalyst's catalytic activity in promoting Sonogashira coupling reactions.

3.4 | XRD

Further insight into the structural properties of GO, Fe_3O_4, and Pd-Fe_3O_4@GO was gained through XRD characterization, as depicted in Figure 4a–c. In the XRD pattern of GO, a prominent peak at 2θ 10.7 arises from its (001) planes, confirming the complete oxidation of graphite to GO due to the successful incorporation of epoxy and hydroxyl groups into the graphite sheets (Figure 4a).[50] Moving to the XRD pattern of Fe_3O_4 (Figure 4b), significant peaks at 2θ values of 30.2 (220), 35.8 (311), 43.3 (400), 53.8 (422), 57.1 (511), and 62.7 (440) are observed.[52] These peaks correspond to the face-centered cubic (FCC) structure of Fe_3O_4, consistent with the reference pattern from JCPDS 75-0033. In the XRD pattern of Pd-Fe_3O_4@GO, distinct peaks at 2θ = 40.1 and 47.1 are observed, corresponding to the 111 and 200 planes of the FCC structure of Pd (Figure 2c).[52] The SAED image of Pd-Fe_3O_4@GO aligns with the XRD

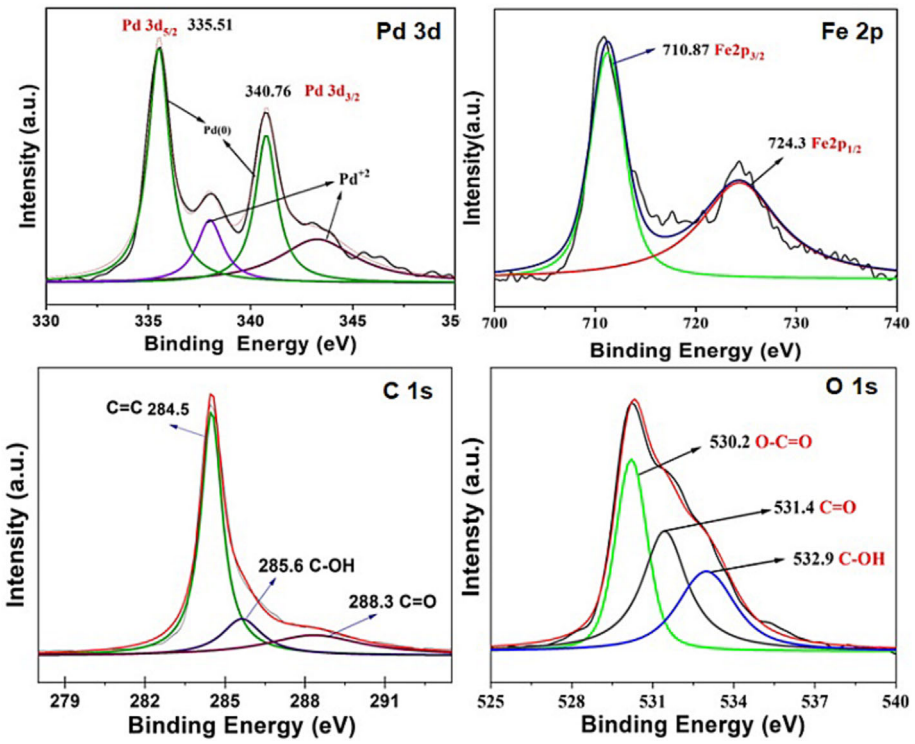

FIGURE 3 XPS of Pd-Fe_3O_4@GO, Pd3d, Fe2p, C1s, and O1s.

10990739, 0, Downloaded from https://onlinelibrary.wiley.com/doi/10.1002/aoc.7405 by Institute Of Chemical Technology, Mumbai, Wiley Online Library on [26/02/2024]. See the Terms and Conditions (https://onlinelibrary.wiley.com/terms-and-conditions) on Wiley Online Library for rules of use; OA articles are governed by the applicable Creative Commons License

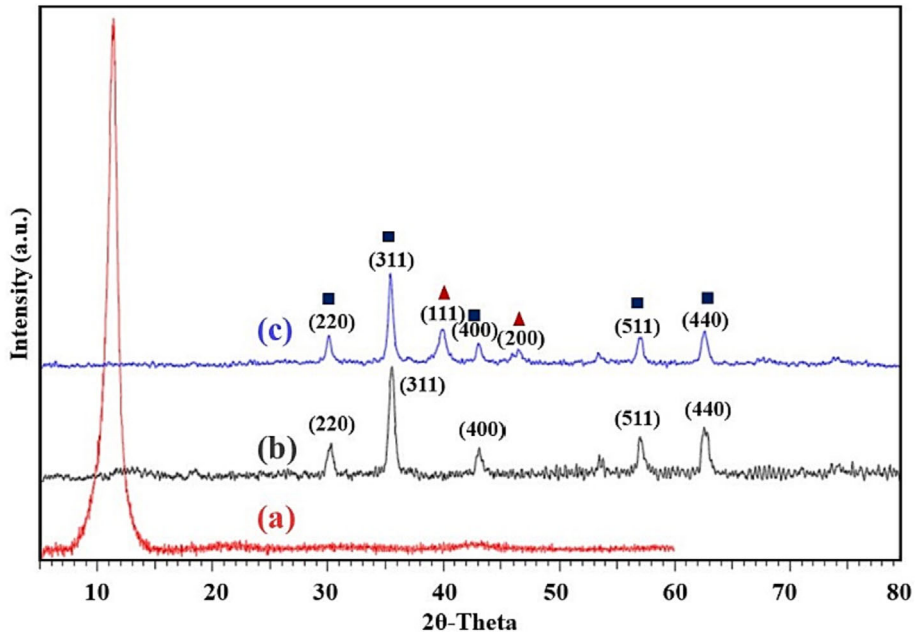

FIGURE 4 XRD of (a) graphene oxide (GO) (b) Fe_3O_4 (c) Pd-Fe_3O_4@GO.

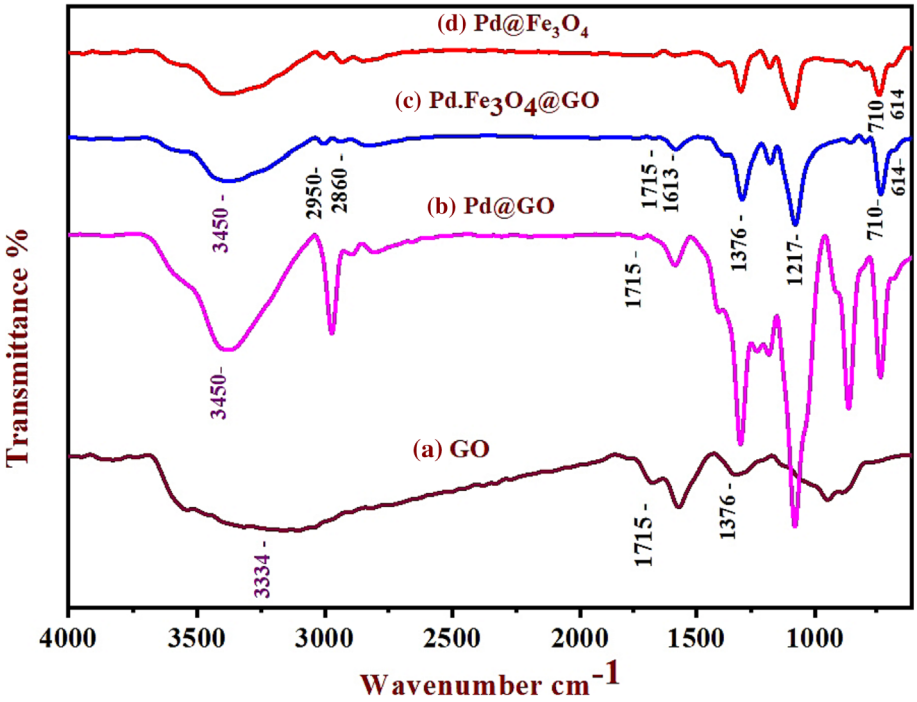

FIGURE 5 FTIR of (a) graphene oxide (GO) (b) Pd@GO (c) Pd-GO@Fe_3O_4 (d) Pd@Fe_3O_4.

results, confirming the face-centered crystalline structure of Pd and Fe_3O_4. The XRD pattern of Pd-Fe_3O_4@GO further validates the presence of Fe_3O_4 with an FCC structure, as evidenced by peaks at the same 2θ positions as those of pure Fe_3O_4. This confirmation indicates the successful incorporation of Pd and GO into the Fe_3O_4 structure without inducing a phase transformation, resulting in the formation of a composite material with the desired crystal structure.

3.5 | FTIR

Figure 5a–d illustrates the infrared (IR) spectra of diverse materials, namely, GO, Pd@GO, Pd-Fe_3O_4@GO, and Pd-@Fe_3O_4. In the spectra of GO, Pd@GO, and Pd-Fe_3O_4@GO, a noticeable peak at 1715 cm^{-1} and broad absorption band ranging from 3100 to 3700 cm^{-1}, attributed to the stretching vibration of the O-H functional group.[50] Comparative analysis of the spectra of GO,

10990739, 0, Downloaded from https://onlinelibrary.wiley.com/doi/10.1002/aoc.7405 by Institute Of Chemical Technology, Mumbai, Wiley Online Library on [26/02/2024]. See the Terms and Conditions (https://onlinelibrary.wiley.com/terms-and-conditions) on Wiley Online Library for rules of use; OA articles are governed by the applicable Creative Commons License

Pd@GO, and Pd-Fe_3O_4@GO reveals a noteworthy reduction in the intensity of the stretching vibration peak of the -C=O (carbonyl) functional group in Pd@GO and Pd-Fe_3O_4@GO. This decline may be attributed to the interaction between the carbonyl group and Pd and $PdFe_3O_4$ NPs. Furthermore, Figure 5a–c exhibits distinct bands at 1376, 1092, 1613, and 1217 cm^{-1} corresponding to the stretching frequencies of various functional groups, namely, C-O-C, -C-OH, C=C (aromatic), and epoxy C-O functionality.[51] Additionally, absorption bands at 2950 and 2860 cm^{-1} are assigned to the symmetric and asymmetric stretching vibrations of -CH_2 groups. In the spectrum of Figure 5c, corresponding to Pd-Fe_3O_4@GO, and Figure 5d, representing Pd@Fe_3O_4, two prominent peaks cantered at 710 and 614 cm^{-1} are observed. These peaks are indicative of the Fe-O stretching vibration of Fe_3O_4 NPs, suggesting the successful adsorption of Pd-Fe_3O_4 on GO.

3.6 | Refining reaction conditions for optimal performance

In order to determine the best reaction conditions, we selected iodobenzene and phenylacetylene as the model substrates and conducted a series of reactions under different conditions, as presented in Table 1. The model reaction began at room temperature using phenylacetylene (1.1 mmol) and iodobenzene (1 mmol) as coupling partners. We employed 6 mg of Pd-Fe_3O_4@GO as a catalyst, IPA as a solvent, and Et_3N as the base. Initially, the reaction progressed slowly, and as it continued, the temperature of the reaction rose. Fortunately, the desired product was obtained in 5 h with an impressive yield of 85%. This finding prompted us to focus on optimizing reaction parameters, including the catalyst, catalyst loading, base, and temperature. Our initial investigation involved testing various catalysts, namely, Pd@Fe_3O_4, Pd@GO, Pd/C (commercial catalyst), and Pd-Fe_3O_4@GO (Table 1 entries 1–4). We utilized iodobenzene and phenylacetylene as coupling partners, with K_2CO_3 as the base and IPA as the solvent, at 90°C. Additionally, we tested the same conditions without a catalyst and did not get any product formation (Table 1 entry 5). Pd-Fe_3O_4@GO emerged as the superior catalyst, providing 85% conversion and producing excellent products (Table 1 entry 4). Consequently, Pd-Fe_3O_4@GO was selected for further study. Following catalyst screening, we explored various bases, including NaOH, pyridine, Et_3N, and K_2CO_3, to achieve a high yield in the desired

TABLE 1 Optimizing the experimental conditions for the coupling of phenylacetylene and iodobenzene.[a]

Entry	Catalyst	Solvent	Base	Catalyst loading	Temperature (°C)	Yield %
1	Pd@Fe_3O_4	IPA	K_2CO_3	6 mg	90	34
2	Pd@GO	IPA	K_2CO_3	6 mg	90	55
3	Pd/C (commercial)	IPA	K_2CO_3	6 mg	90	68
4	Pd-Fe_3O_4@GO	IPA	K_2CO_3	6 mg	90	85
5	-	IPA	K_2CO_3	6 mg	90	0
6	Pd-Fe_3O_4@GO	IPA	NaOH	6 mg	90	23
7	Pd-Fe_3O_4@GO	IPA	Pyridine	6 mg	90	45
8	Pd-Fe_3O_4@GO	IPA	Et_3N	6 mg	90	59
9	Pd-Fe_3O_4@GO	DCM	K_2CO_3	6 mg	90	65
10	Pd-Fe_3O_4@GO	DMF	K_2CO_3	6 mg	90	73
11	Pd-Fe_3O_4@GO	Toluene	K_2CO_3	6 mg	90	23
12	Pd-Fe_3O_4@GO	Acetonitrile	K_2CO_3	6 mg	90	55
13	Pd-Fe_3O_4@GO	IPA	K_2CO_3	3 mg	90	65
14	Pd-Fe_3O_4@GO	IPA	K_2CO_3	6 mg	90	85
15	Pd-Fe_3O_4@GO	IPA	K_2CO_3	9 mg	90	96
16	Pd-Fe_3O_4@GO	IPA	K_2CO_3	12 mg	90	97
17	Pd-Fe_3O_4@GO	IPA	K_2CO_3	9 mg	70	33
18	Pd-Fe_3O_4@GO	IPA	K_2CO_3	9 mg	80	65
19	Pd-Fe_3O_4@GO	IPA	K_2CO_3	9 mg	100	97

Abbreviations: GO, graphene oxide; IPA, isopropyl alcohol.

[a]All reactions were conducted using 1 mmol of aryl halide, 1.1 mmol of alkyne, 1.5 mmol of the base, and 5 mL of solvent.

10990739, 0, Downloaded from https://onlinelibrary.wiley.com/doi/10.1002/aoc.7405 by Institute Of Chemical Technology, Mumbai, Wiley Online Library on [26/02/2024]. See the Terms and Conditions (https://onlinelibrary.wiley.com/terms-and-conditions) on Wiley Online Library for rules of use; OA articles are governed by the applicable Creative Commons License

product (Table 1 entries 6–8). Among these, K_2CO_3 exhibited outstanding results, as depicted in Table 1 entry 4. The superiority of K_2CO_3 can be attributed to factors such as its suitable basicity, solubility, and stability under the given reaction conditions. K_2CO_3 efficiently deprotonated specific alkyne, enhancing the interaction between the catalyst and reactants, leading to higher yields. After base screening, we tested various solvents such as toluene, acetonitrile (CH_3CN), dichloromethane (DCM), and N,N-dimethylformamide (DMF) for the model reaction, comparing them to IPA. However, alternative solvents did not result in a higher yield (Table 1 entries 9–12), so IPA was chosen for further research (Table 1 entry 4). IPA, recognized as a polar protic solvent, shows an intermediate coordinating polarity in relation to other solvents like DMF, DCM, CH_3CN, and toluene. This intermediate coordinating polarity of IPA proves to be advantageous in Sonogashira coupling reactions by facilitating a balanced interplay between the formation and desorption of palladium intermediates without excessively stabilizing them.[53,54] This equilibrium prevents the undue stabilization of palladium intermediates, leading to exceptional conversion selectivity towards the desired product. Following the solvent screening, we explored the catalyst loading, as shown in Table 1 entries 13–16, revealing that the quantity of palladium is a critical parameter influencing catalyst activity during coupling processes. The reaction yield increased from 65% to 96%

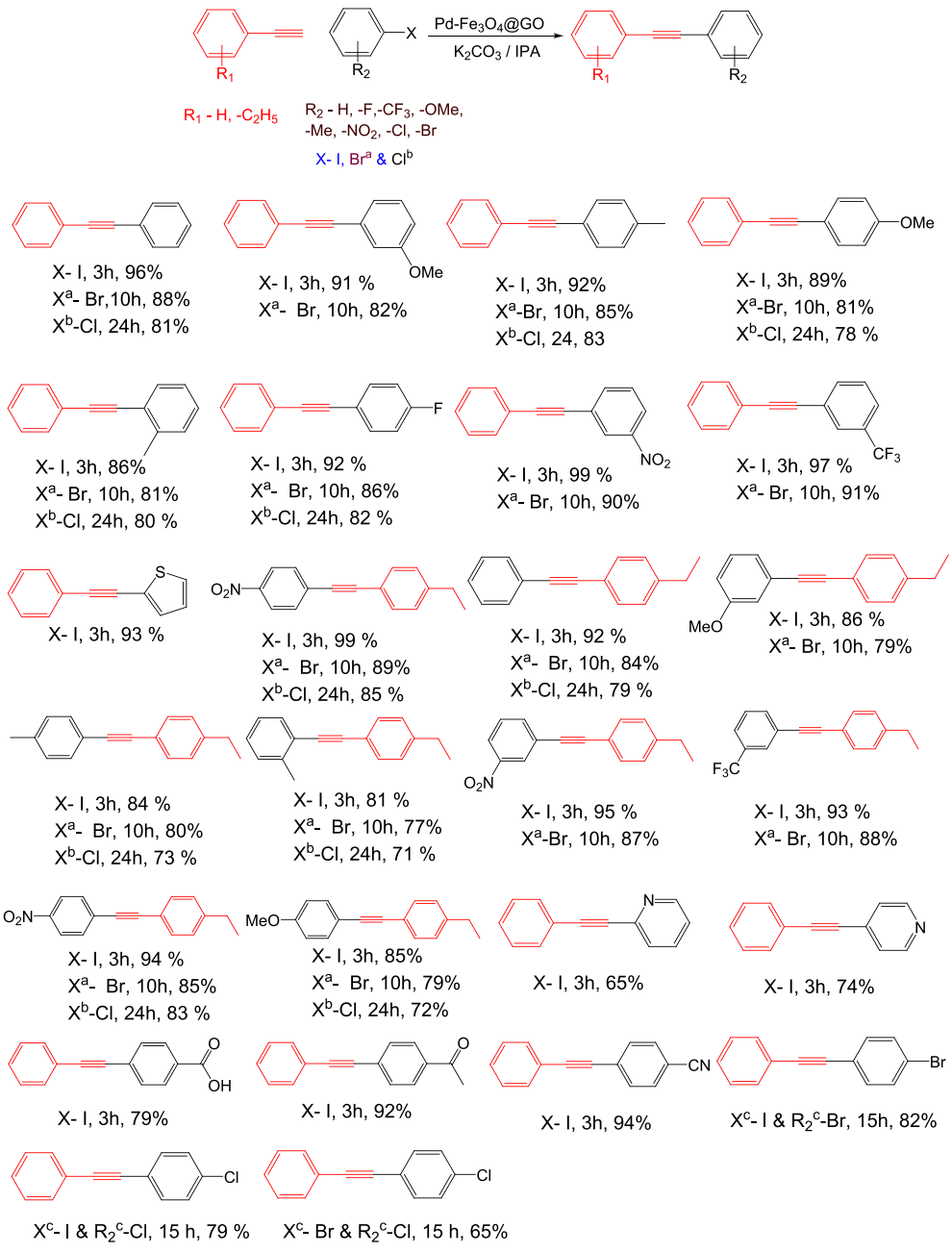

SCHEME 2 Sonogashira coupling, reaction condition: aryl halide (1 mmol), substituted phenylacetylene (1.1 mmol), K_2CO_3 (1.5 mmol), Pd-Fe_3O_4@GO (9 mg), solvent isopropyl alcohol (IPA) (5 mL), temperature (90°C), (110°C)[a], (130°C)[b] and (2 mmol phenylacetylene, 110°C)[c].

10990739, 0, Downloaded from https://onlinelibrary.wiley.com/doi/10.1002/aoc.7405 by Institute Of Chemical Technology, Mumbai, Wiley Online Library on [26/02/2024]. See the Terms and Conditions (https://onlinelibrary.wiley.com/terms-and-conditions) on Wiley Online Library for rules of use; OA articles are governed by the applicable Creative Commons License

when the quantity of Pd-Fe_3O_4@GO was increased from 3 to 12 mg. Notably, increasing the catalyst concentration to 12 mg had no impact on performance. Thus, 9 mg of Pd-Fe_3O_4@GO in an IPA solvent at 90°C was confirmed as the optimal condition for the coupling reaction (Table 1 entry 14). Finally, we conducted the reaction at various temperatures such as 70, 80, 90, and 100°C to identify the ideal reaction temperature (Table 1 entry 16–19). The reaction successfully progressed at 90°C within 3 h, yielding 96%. The yield remained stable above 90°C; however, below this temperature, the product yield significantly declined.

3.7 | Substrate scope

The catalytic efficiency of Pd-Fe_3O_4@GO was investigated across a diverse range of functionalized phenylacetylene compounds with aryl halide substrates, as outlined in Scheme 2. Notably, iodobenzene exhibited strong interaction with phenylacetylene over Pd-Fe_3O_4@GO, leading to an impressive 96% conversion of the desired product within 3 h. This desired product, substituted diphenylethyne, was consistently generated in exceptionally high yields. This was achieved through the Sonogashira coupling reaction involving iodobenzene and electron-withdrawing substituents like -NO_2, -F, -COOH, -$COCH_3$, CN, and -CF_3 at the o, p, and m positions. Furthermore, aryl iodides featuring electron-releasing substitutions such as -CH_3 and -OCH_3 at the p- and o-positions, when combined with phenylacetylene, yielded the anticipated products with consistently high to exceptional yields. It was noted that iodobenzene with electron-withdrawing groups displayed superior yields compared with those with electron-donating groups. In addition to iodobenzene, other compounds including bromobenzene, chlorobenzene, substituted bromobenzene, substituted chlorobenzene, and heterocyclic derivatives such as 2-iodothiophene, 4-iodopyridine, and 2-iodopyridine when reacted with phenylacetylene, all resulted in a high yield of the desired product. Moreover, 1-ethyl-4-ethynylbenzene, when subjected to reactions with substituted iodobenzene, bromobenzene, and chlorobenzene, demonstrated a favorable yield of the desired products. We conducted screening tests using 1-Bromo-4-iodobenzene, 1-Chloro-4-iodobenzene, and 1-Bromo-4-chlorobenzene to understand the competitive preferences for breakage of C-I, C-Br, and C-Cl bonds. In the screening of 1-Bromo-4-iodobenzene with phenylacetylene, we observed that the C-I bond broke preferentially, leading to the formation of 1-bromo-4-(phenylethynyl)benzene as the major product, along with the small quantity of bisphenyl product, 1,4-bis (phenylethynyl)benzene, with a less than 15% conversion. Then, we conducted screenings on 1-Chloro-4-iodobenzene and 1-Bromo-4-chlorobenzene, revealing a preference for C-I and C-Br bond cleavage, respectively. The results showed the predominant formation of 1-chloro-4-(phenylethynyl)benzene in both reactions, with no bis-product formation. From the above experiments, it was observed that the C-I bond

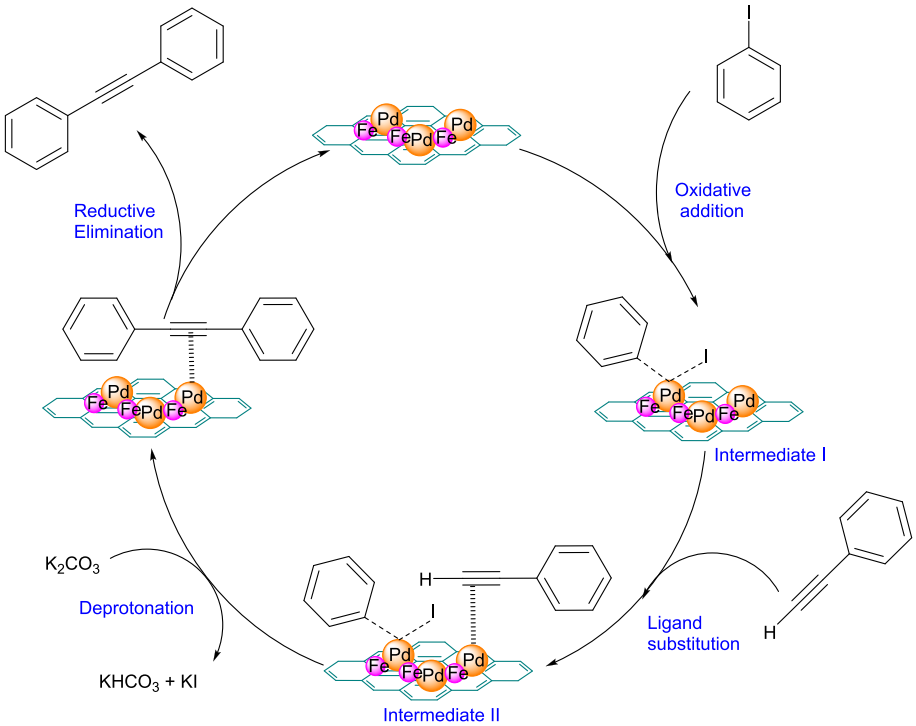

SCHEME 3 Sonogashira coupling reaction mechanism.

10990739, 0, Downloaded from https://onlinelibrary.wiley.com/doi/10.1002/aoc.7405 by Institute Of Chemical Technology, Mumbai, Wiley Online Library on [26/02/2024]. See the Terms and Conditions (https://onlinelibrary.wiley.com/terms-and-conditions) on Wiley Online Library for rules of use; OA articles are governed by the applicable Creative Commons License

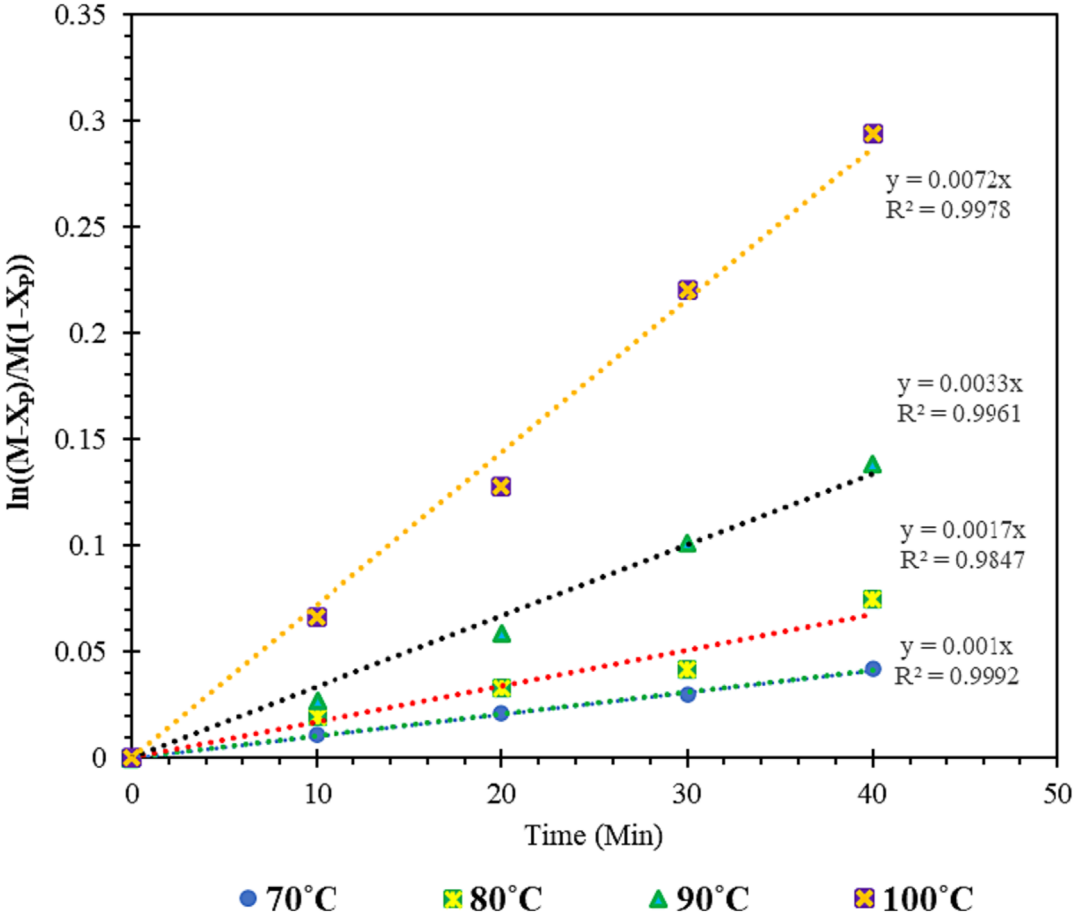

FIGURE 6 Plot of [ln ((M − X_P)/M(1 − X_P))] versus time at different temperatures.

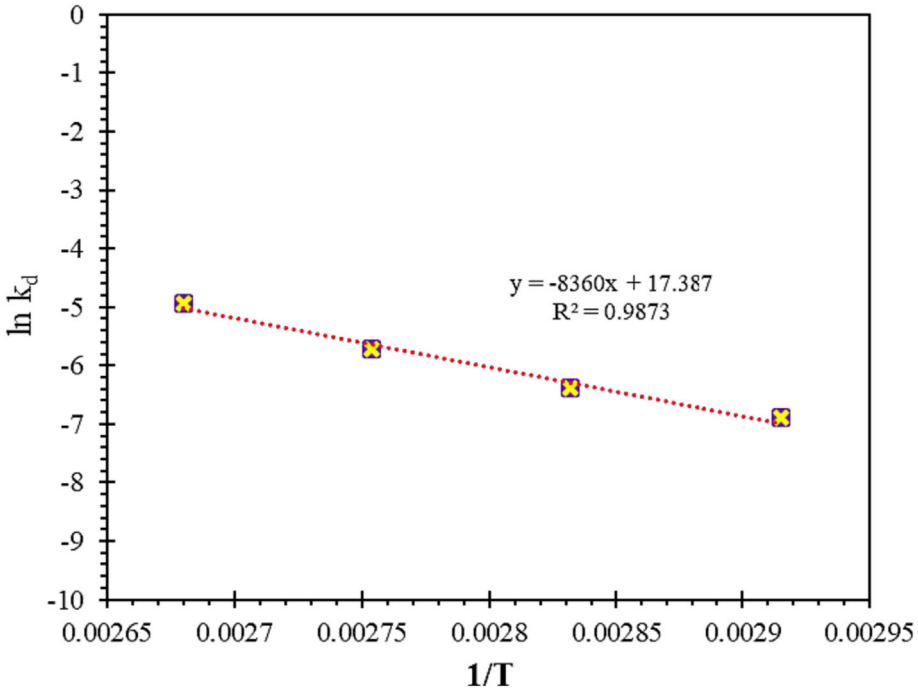

FIGURE 7 Arrhenius plot lnkp versus 1/T.

10990739, 0, Downloaded from https://onlinelibrary.wiley.com/doi/10.1002/aoc.7405 by Institute Of Chemical Technology, Mumbai, Wiley Online Library on [26/02/2024]. See the Terms and Conditions (https://onlinelibrary.wiley.com/terms-and-conditions) on Wiley Online Library for rules of use; OA articles are governed by the applicable Creative Commons License

easily breaks down compared with C-Br and C-Cl. This indicates a cascade reaction in which weaker bonds, such as C-I, break down preferentially before stronger bonds like C-Br and C-Cl. This comprehensive study showcases the versatility of Pd-Fe_3O_4@GO in facilitating these reactions, providing valuable insights into the reactivity of various substrates and their yields in the presence of different aryl halides.

3.8 | Reaction mechanism and kinetic modeling

The mechanism of Sonogashira cross-coupling reactions is well-documented in the literature.[55,56] Scheme 3 illustrates the potential reaction mechanism involved in the Sonogashira coupling between phenylacetylene and iodobenzene. In heterogeneous catalyst adsorption, surface reaction and desorption pathways follow. The deprotonation mechanisms involve the initial oxidative addition of iodobenzene to Pd(0), resulting in the formation of a benzene-catalyst-iodide complex (intermediate 1). Subsequently, phenylacetylene coordinates with palladium, leading to the formation of intermediate 2. At this stage, deprotonation of phenylacetylene occurs via the base K_2CO_3, resulting in a Pd complex with the two organic groups in a cis disposition. Finally, the coupled product 1,2-diphenylethyne is expelled through reductive elimination. This depicted mechanism serves as the foundation for formulating a mathematical model. Building upon the Langmuir–Hinshelwood–Hougen–Watson (LHHW) type of mechanism, a model was developed to describe the reaction kinetics, revealing a second-order reaction. The kinetic model derivation is given in the supplementary information. To assess the validity of the model, a plot of $\ln(M - X_P)/M(1 - X_P)$ against time was generated at various temperatures, demonstrating a linear correlation (Figure 6) and confirming the model's appropriateness. Subsequently, an Arrhenius plot, employing the slopes obtained from the aforementioned linear relationships, was constructed to determine the apparent activation energy, yielding a value of 16.61 kcal/mol (Figure 7). This outcome suggests that the reaction is under kinetic control.

3.9 | Comparison of Pd-Fe_3O_4@GO with other reported catalysts systems

The catalytic efficiency of the Pd-Fe_3O_4@GO catalyst has been systematically evaluated through a comparative analysis with previously reported catalysts, as outlined in Table 2. Noteworthy among these are the Fe_3O_4/GO-

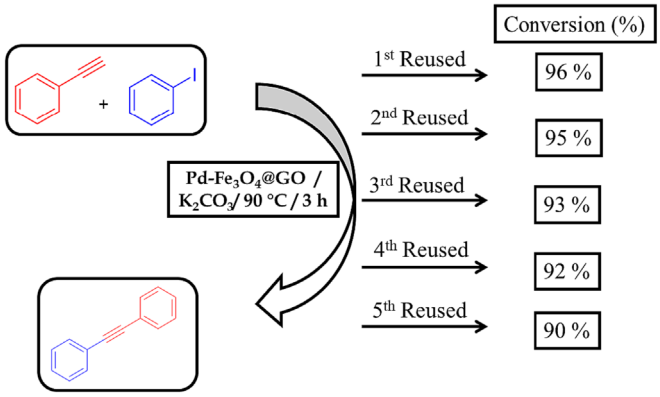

FIGURE 8 Reusability of Pd-Fe_3O_4@GO catalyst.

TABLE 2 Comparison of Pd-Fe_3O_4@GO system and other reported catalysts systems.

Sr. no	Catalyst[a]	Base/solvent/catalyst	Temp. (°C)	Time (h)	Yield[b] (%)	Ref.
1	Fe_3O_4/GO-Cellulose-Pd	K_2CO_3/DMAC:Gly/0.024 g	120	8	91	33
2	Pd@Fe_3O_4 NPs	Piperidine/DMF/0.024 g	110	24	83	34
3	CS/MMT/Pd	CH_3COOK/DMSO + ethylene glycol/0.026 g	110	5	94	57
4	CPS-MNPs-NNN-Pd	K_2CO_3/H2O DMF/ (0.020 mmol Pd), PPh_3, CuI	90	7	91	37
5	Pd-Co/G	Et_3N/THF-H_2O/ (0.020 mmol Pd), PPh_3, CuI	80	12	98	26
6	G3-Gu-Pd	K_2CO_3/H_2O/0.012 g	100	8	85	45
7	MNPs–PdNPs	Et_3N/THF/0.012 g	65	24	85	44
8	Pd/$CuFe_2O_4$	K_2CO_3/DMSO/4 mol%	120	12	78	58
9	Pd-Fe_3O_4@GO	K_2CO_3/IPA/0.009 g	90	3	96	This Work

Abbreviations: GO, graphene oxide; IPA, isopropyl alcohol; NPs, nanoparticles.
[a]All reactions were carried out with phenylacetylene and iodobenzene.
[b]Yield refers to isolated pure products.

10990739, 0, Downloaded from https://onlinelibrary.wiley.com/doi/10.1002/aoc.7405 by Institute Of Chemical Technology, Mumbai, Wiley Online Library on [26/02/2024]. See the Terms and Conditions (https://onlinelibrary.wiley.com/terms-and-conditions) on Wiley Online Library for rules of use; OA articles are governed by the applicable Creative Commons License

Cellulose-Pd,[25] CS/MMT/Pd,[40] G3-Gu-Pd,[37] and MNPs–PdNPs[36] catalysts, which exhibited higher yields. However, these catalysts are associated with the use of harsh reaction conditions, prolonged reaction times, and higher catalytic loadings. On the other hand, the catalysts $Pd/CuFe_2O_4$[41] and $Pd@Fe_3O_4$ NPs[26] demonstrated lower yields, attributed to their reliance on harsh reaction conditions and extended reaction times. Catalysts like CPS-MNPs-NNN-Pd[29] and Pd-Co/G[18] have shown improved yields in Sonogashira coupling reactions. However, these catalysts utilize copper as a co-catalyst, toxic phosphine ligands, and also higher catalytic loadings. However, the $Pd\text{-}Fe_3O_4$@GO catalyst offers several advantages over these methods: (i) it functions under mild reaction conditions, devoid of ligands and additional co-catalysts; (ii) it proves cost-effective; and (iii) the catalyst exhibits recyclability without apparent leaching. The preparation of the catalyst via the solvothermal process presents further benefits: (i) It allows for a single-pot synthesis of the catalyst rather than a multi-step catalyst synthesis. (ii) Utilizes simple ethylene glycol as both solvent and reducing agent, replacing the need for toxic chemicals. (iii) Solvothermal conditions provide precise control over temperature and pressure, enhancing control over particle size, morphology, and crystallinity. (iv) Elevated temperature and pressure enable unique catalyst properties

TABLE 3 Reusability of catalyst data.

Reusability run	Catalyst loading (mg)	Recovered catalyst (mg)	Top-up catalyst (mg)	Top-up (%)
1st reused	9	8.4	0.6	7
2nd reused	9	8.3	0.7	8
3rd reused	9	8.6	0.4	4
4th reused	9	8.5	0.5	6
5th reused	9	8.3	0.7	8

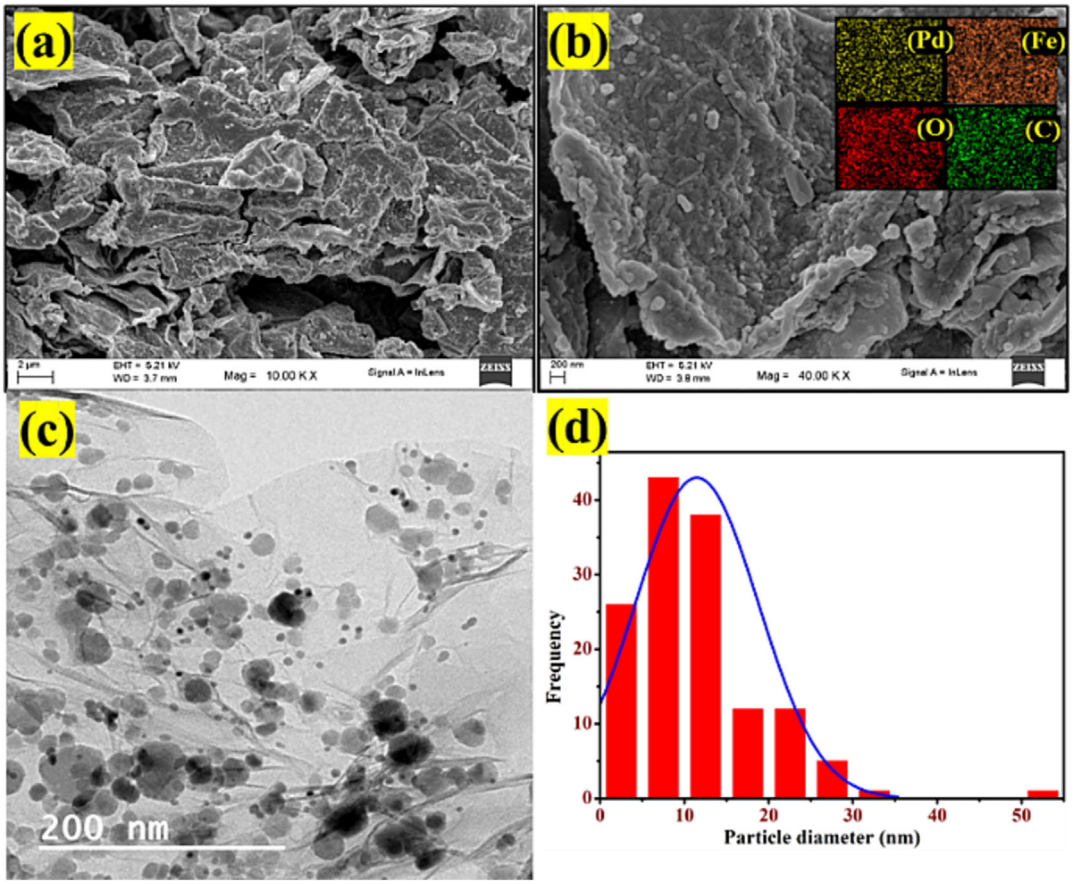

FIGURE 9 Reused $Pd\text{-}Fe_3O_4$@GO catalyst (a, b) SEM image and mapping (c) TEM (d) particle size distribution.

10990739, 0, Downloaded from https://onlinelibrary.wiley.com/doi/10.1002/aoc.7405 by Institute Of Chemical Technology, Mumbai, Wiley Online Library on [26/02/2024]. See the Terms and Conditions (https://onlinelibrary.wiley.com/terms-and-conditions) on Wiley Online Library for rules of use; OA articles are governed by the applicable Creative Commons License

that may not be achievable with other methods. (v) While controlled nucleation and growth lead to well-defined structures and improved catalytic activity.

3.10 | Reusability of catalyst

Five tests were conducted to assess the recyclability of the Pd-Fe_3O_4@GO catalyst, as illustrated in Figure 8. The catalyst was recovered by a magnet, washed with water, dried, and then refluxed in 5 mL of IPA for 4 h. Subsequently, it underwent another wash with IPA before being vacuum-dried for 5 h at 50°C. Despite a slight decrease in conversion, indicating changes in the catalyst's selectivity, activity, and reusability, it remained effective. The reduction in the quantity of the catalyst obtained after separation and drying (approximately 4%–8%) was compensated by the addition of virgin catalyst (Table 3). The catalyst's activity remained practically consistent in all experiments. Moreover, when the reused catalyst was utilized without additional supplementation, but the volume of the reaction mass was decreased to maintain the same catalyst loading, comparable rates and conversions were achieved. Consequently, the catalyst exhibited robustness, sustained activity, and reusability.

3.11 | Hot filtration test

To further assess the catalyst's reusability, a hot filtration test was conducted using iodobenzene and phenylacetylene as model substrates under optimized reaction conditions. Stirring was halted after 1 h, and the reaction mixture was filtered to separate the catalyst. The

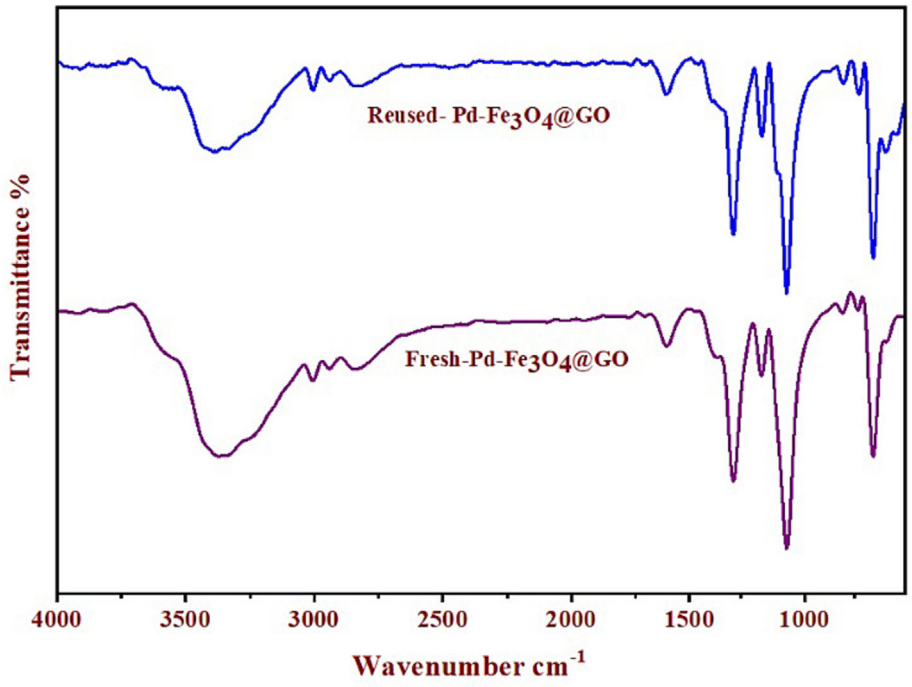

FIGURE 10 FTIR of Fresh and Reused Pd-Fe_3O_4@GO catalyst.

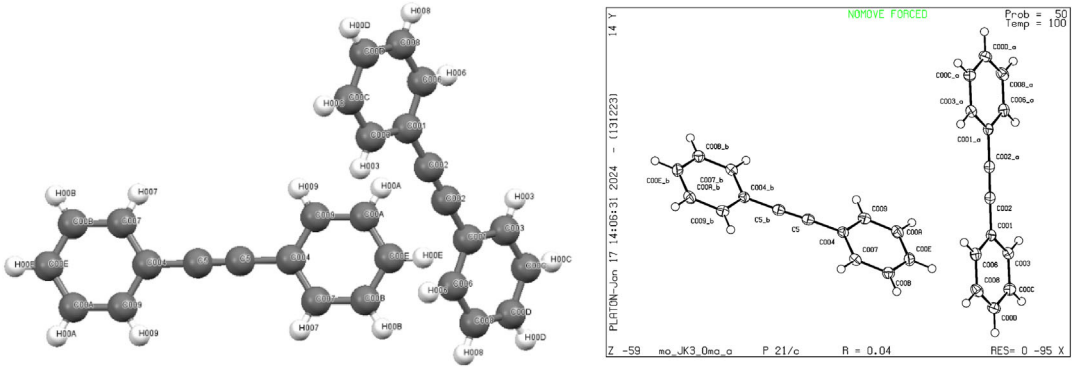

FIGURE 11 Single crystal XRD structure of 1,2-diphenylethyne (mo_JK3_0ma_a).

10990739, 0, Downloaded from https://onlinelibrary.wiley.com/doi/10.1002/aoc.7405 by Institute Of Chemical Technology, Mumbai, Wiley Online Library on [26/02/2024]. See the Terms and Conditions (https://onlinelibrary.wiley.com/terms-and-conditions) on Wiley Online Library for rules of use; OA articles are governed by the applicable Creative Commons License

percentage of product formation was analyzed using GC (61%). The clear filtrate was continuously stirred for the next 2 h at 90°C, revealing no change in conversion. This lack of alteration confirmed the absence of catalyst leaching into the reaction mass filtrate, demonstrating the retention of active Pd sites. Furthermore, ICP-MS measurements of the reaction mass indicated that palladium leaching was below the detection limit. This comprehensive analysis validates the catalyst's stability and suitability for repeated use.

3.12 | Reused catalyst characterization

The fifth reused catalyst was thoroughly characterized using SEM, EDS, TEM, and IR. From the SEM images, we observed that the morphology of the reused catalyst closely resembles that of the fresh catalyst, with Pd-Fe_3O_4 NPs agglomerated on the surface. The majority of the particles exhibit a spherical or semi-spherical shape with a smooth surface. EDS mapping revealed that the concentrations of Pd and Fe are the same as those in the fresh catalyst (Figure 9a,b). TEM analysis showed that the Pd-Fe_3O_4 particles are distributed on GO, along with some agglomeration of larger particles. The particle size distribution indicated a slight increase in size, ranging from 2 to 30 nm in diameter (Figures 9c,d and S2). The IR spectra of both the synthesized catalyst and the catalyst recovered from the reaction mass after five runs were analyzed. No significant changes in functional groups were observed (Figure 10).

3.13 | Single crystal XRD parameters of 1,2-diphenylethyne (mo_JK3_0ma_a)

Examine the crystal structure analysis of 1,2-diphenylethyne, including insights into bond lengths, angles, and packing arrangement (Figures 11 and S3). Table S1 provides a summary of the crystallographic data and refinement parameters.

4 | CONCLUSION

The main findings of this study can be summed up as follows:

Single-pot synthesis of Pd-Fe_3O_4@GO: In this study, we successfully synthesized a magnetically separable catalyst using the single-pot solvothermal method for the first time, showcasing its efficacy in Sonogashira coupling reactions.

Advanced catalyst characterization: The catalyst was comprehensively characterized using sophisticated techniques, ensuring a thorough understanding of its properties and structure.

Outstanding performance in Sonogashira coupling: Among the reported palladium-based catalysts, Pd-Fe_3O_4@GO demonstrated exceptional performance in the Sonogashira coupling process (iodobenzene [1 mmol], phenylacetylene [1.1 mmol], K_2CO_3 [1.5 mmol], Pd-Fe_3O_4@GO [9 mg]) at 90°C in IPA solvent with high turnover frequency (TOF, 118.3 h^{-1})1.

Sustained activity and stability: Remarkably, even after the fifth cycle, Pd-Fe_3O_4@GO maintained outstanding conversion rates in the Sonogashira coupling reaction. This enduring activity and stability can be attributed to the redox behavior of Fe_3O_4 and the GO support, enhancing electron transfer between the metal and the support.

Efficient conversion without co-catalysts: The catalyst achieved remarkable conversion rates to the desired product without requiring co-catalysts like copper or any other expensive ligands. Additionally, it exhibited excellent conversion rates for inactive substituted aryl chlorides and bromides.

Reaction mechanism and kinetic modeling: A reaction mechanism was suggested, and a kinetic equation was formulated for the Sonogashira reaction, which is under kinetic control. It adheres to a second-order kinetic equation, with an apparent activation energy of 16.61 kcal/mol.

Versatile applications in industrial processes: Pd-Fe_3O_4@GO demonstrates significant potential as a catalyst in a wide array of industrial manufacturing processes. Its versatility positions it as a valuable asset in diverse industrial applications.

AUTHOR CONTRIBUTIONS

Mahesh A. Pawar: Data curation; formal analysis; writing original draft. **Akhil V. Nakhate**: Supervision; correcting draft; writing original draft. **Samidha S. Kadu**: Supervision; correcting draft; final writing. **Pradip V. Tekade**: Supervision; writing original draft.

ACKNOWLEDGMENTS

SSK and MAP gratefully acknowledge the support provided by Shri Shivaji College of Arts, Commerce, and Science in Akola, while AVN and PVT gratefully acknowledge the support provided by Bajaj College of Science, Wardha.

CONFLICT OF INTEREST STATEMENT

The authors declare no competing financial interest.

10990739, 0, Downloaded from https://onlinelibrary.wiley.com/doi/10.1002/aoc.7405 by Institute Of Chemical Technology, Mumbai, Wiley Online Library on [26/02/2024]. See the Terms and Conditions (https://onlinelibrary.wiley.com/terms-and-conditions) on Wiley Online Library for rules of use; OA articles are governed by the applicable Creative Commons License

DATA AVAILABILITY STATEMENT

The authors confirm that the data supporting the findings of the study are available within the article and its supplementary material. Raw data that supports the findings of this study are available from the corresponding author upon reasonable request.

REFERENCES

[1] M. Khoobi, A. Foroumadi, S. Emami, M. Safavi, G. Dehghan, B. H. Alizadeh, A. Ramazani, S. K. Ardestani, A. Shafiee, *Chem. Biol. Drug Des.* **2011**, *78*, 580. https://doi.org/10.1111/j.1747-0285.2011.01175.x

[2] A. Ramazani, A. Reza Kazemizadeh, *Curr. Org. Chem.* **2011**, *15*, 3986. https://doi.org/10.2174/138527211798072412

[3] I. Yavari, A. Ramazani, *Synth. Commun.* **1997**, *27*, 1449. https://doi.org/10.1080/00397919708006076

[4] M. Khoobi, S. Emami, G. Dehghan, A. Foroumadi, A. Ramazani, A. Shafiee, *Arch. Pharm. (Weinheim).* **2011**, *344*, 588. https://doi.org/10.1002/ardp.201000271

[5] F. Kalantari, S. Rezayati, A. Ramazani, M. Poor Heravi, *Appl. Organomet. Chem.* **2023**, *37*. https://doi.org/10.1002/aoc.7064

[6] H. Aghahosseini, A. Ramazani, N. S. Jalayer, Z. Ranjdoost, A. Souldozi, K. Ślepokura, T. Lis, *Org. Lett.* **2019**, *21*, 22. https://doi.org/10.1021/acs.orglett.8b03388

[7] M. Dodangeh, A. Ramazani, M.-T. Maghsoodlou, A. Zarei, S. Rezayati, *Curr. Org. Chem.* **2020**, *24*, 1582. https://doi.org/10.2174/1385272824999200616114037

[8] J. Rayadurgam, S. Sana, M. Sasikumar, Q. Gu, *Org. Chem. Front.* **2021**, *8*, 384. https://doi.org/10.1039/D0QO01146K

[9] P. Devendar, R.-Y. Qu, W.-M. Kang, B. He, G.-F. Yang, *J. Agric. Food Chem.* **2018**, *66*, 8914. https://doi.org/10.1021/acs.jafc.8b03792

[10] K. Karami, S. Abedanzadeh, P. Hervés, *RSC Adv.* **2016**, *6*, 93660. https://doi.org/10.1039/C6RA17914B

[11] Y. Liang, Y.-X. Xie, J.-H. Li, *J. Org. Chem.* **2006**, *71*, 379. https://doi.org/10.1021/jo051882t

[12] G. Li, Z. Tang, *Nanoscale.* **2014**, *6*, 3995. https://doi.org/10.1039/C3NR06787D

[13] M. Azharuddin, G. H. Zhu, D. Das, E. Ozgur, L. Uzun, A. P. F. Turner, H. K. Patra, *Chem. Commun.* **2019**, *55*, 6964. https://doi.org/10.1039/C9CC01741K

[14] S. Yang, X. Luo, *Nanoscale.* **2014**, *6*, 4438. https://doi.org/10.1039/C3NR06858G

[15] S. F. Motevalizadeh, M. Alipour, F. Ashori, A. Samzadeh-Kermani, H. Hamadi, M. R. Ganjali, H. Aghahosseini, A. Ramazani, M. Khoobi, E. Gholibegloo, *Appl. Organomet. Chem.* **2018**, *32*. https://doi.org/10.1002/aoc.4123

[16] A. V. Nakhate, G. D. Yadav, *ChemistrySelect* **2016**, *1*, 3954. https://doi.org/10.1002/slct.201600819

[17] C. Gao, F. Lyu, Y. Yin, *Chem. Rev.* **2021**, *121*, 834. https://doi.org/10.1021/acs.chemrev.0c00237

[18] M. Aksoy, H. Kilic, B. Nişancı, Ö. Metin, *Inorg. Chem. Front.* **2021**, *8*, 499. https://doi.org/10.1039/D0QI01283A

[19] A. Chouhan, H. P. Mungse, O. P. Khatri, *Adv. Colloid Interface Sci.* **2020**, *283*, 102215. https://doi.org/10.1016/j.cis.2020.102215

[20] M. Terrones, A. R. Botello-Méndez, J. Campos-Delgado, F. López-Urías, Y. I. Vega-Cantú, F. J. Rodríguez-Macías, A. L. Elías, E. Muñoz-Sandoval, A. G. Cano-Márquez, J.-C. Charlier, *Nano Today* **2010**, *5*, 351. https://doi.org/10.1016/j.nantod.2010.06.010

[21] A. T. Lawal, *Biosens. Bioelectron.* **2019**, *141*, 111384. https://doi.org/10.1016/j.bios.2019.111384

[22] J. Martínez-Laguna, A. Caballero, P. J. Pérez, *Adv. Synth. Catal.* **2021**, *363*, 1740. https://doi.org/10.1002/adsc.202001325

[23] X. Fan, G. Zhang, F. Zhang, *Chem. Soc. Rev.* **2015**, *44*, 3023. https://doi.org/10.1039/C5CS00094G

[24] K. H. Lee, S.-W. Han, K.-Y. Kwon, J. B. Park, *J. Colloid Interface Sci.* **2013**, *403*, 127. https://doi.org/10.1016/j.jcis.2013.04.006

[25] M. Chen, Z. Zhang, L. Li, Y. Liu, W. Wang, J. Gao, *RSC Adv.* **2014**, *4*, 30914. https://doi.org/10.1039/C4RA05186F

[26] Y.-S. Feng, X.-Y. Lin, J. Hao, H.-J. Xu, *Tetrahedron.* **2014**, *70*, 5249. https://doi.org/10.1016/j.tet.2014.05.083

[27] S. Sadjadi, M. Malmir, M. M. Heravi, F. Ghoreyshi Kahangi, *Inorganica Chim. Acta.* **2019**, *488*, 62. https://doi.org/10.1016/j.ica.2018.12.048

[28] V. B. Saptal, M. V. Saptal, R. S. Mane, T. Sasaki, B. M. Bhanage, *ACS Omega.* **2019**, *4*, 643. https://doi.org/10.1021/acsomega.8b03023

[29] S. Moussa, A. R. Siamaki, B. F. Gupton, M. S. El-Shall, *ACS Catal.* **2012**, *2*, 145. https://doi.org/10.1021/cs200497e

[30] S. Sultana, S. D. Mech, F. L. Hussain, P. Pahari, G. Borah, P. K. Gogoi, *RSC Adv.* **2020**, *10*, 23108. https://doi.org/10.1039/D0RA01189D

[31] M. Gholinejad, J. Ahmadi, *Chempluschem.* **2015**, *80*, 973. https://doi.org/10.1002/cplu.201500015

[32] E. Ghonchepour, M. R. Islami, A. M. Tikdari, *J. Organomet. Chem.* **2019**, *883*, 1. https://doi.org/10.1016/j.jorganchem.2019.01.008

[33] M. Niakan, M. Masteri-Farahani, H. Shekaari, S. Karimi, *Carbohydr. Polym.* **2021**, *251*, 117109. https://doi.org/10.1016/j.carbpol.2020.117109

[34] J. Chung, J. Kim, Y. Jang, S. Byun, T. Hyeon, B. M. Kim, *Tetrahedron Lett.* **2013**, *54*, 5192. https://doi.org/10.1016/j.tetlet.2013.07.057

[35] Z. Tashrifi, S. Bahadorikhalili, H. Lijan, S. Ansari, H. Hamedifar, M. Mahdavi, *New J. Chem.* **2019**, *43*, 8930. https://doi.org/10.1039/C9NJ01562K

[36] M. Tukhani, F. Panahi, A. Khalafi-Nezhad, *ACS Sustain. Chem. Eng.* **2018**, *6*, 1456. https://doi.org/10.1021/acssuschemeng.7b03923

[37] F. Dehghani Firuzabadi, Z. Asadi, F. Panahi, *RSC Adv.* **2016**, *6*, 101061. https://doi.org/10.1039/C6RA22535G

[38] H. Salemi, B. Kaboudin, F. Kazemi, T. Yokomatsu, *RSC Adv.* **2016**, *6*, 52656. https://doi.org/10.1039/C6RA04575H

[39] W. Li, X. Jia, B. Zhang, L. Tian, X. Li, H. Zhang, Q. Zhang, *New J. Chem.* **2015**, *39*, 2925. https://doi.org/10.1039/C4NJ02117G

[40] H. Woo, K. Lee, J. C. Park, K. H. Park, *Solid State Sci.* **2016**, *53*, 78. https://doi.org/10.1016/j.solidstatesciences.2016.01.010

[41] A. R. Sardarian, M. Kazemnejadi, M. Esmaeilpour, *Dalt. Trans.* **2019**, *48*, 3132. https://doi.org/10.1039/C9DT00060G

[42] M. Daraie, M. M. Heravi, S. S. Kazemi, *J. Coord. Chem.* **2019**, *72*, 2279. https://doi.org/10.1080/00958972.2019.1640360

[43] P. Li, L. Wang, L. Zhang, G.-W. Wang, *Adv. Synth. Catal.* **2012**, *354*, 1307. https://doi.org/10.1002/adsc.201100725

10990739, 0, Downloaded from https://onlinelibrary.wiley.com/doi/10.1002/aoc.7405 by Institute Of Chemical Technology, Mumbai, Wiley Online Library on [26/02/2024]. See the Terms and Conditions (https://onlinelibrary.wiley.com/terms-and-conditions) on Wiley Online Library for rules of use; OA articles are governed by the applicable Creative Commons License

[44] D. Wang, C. Deraedt, L. Salmon, C. Labrugère, L. Etienne, J. Ruiz, D. Astruc, *Chem. - A Eur. J.* **2015**, *21*, 1508. https://doi.org/10.1002/chem.201404590
[45] E. Niknam, A. Moaddeli, A. Khalafi-Nezhad, *J. Organomet. Chem.* **2020**, *923*, 121369. https://doi.org/10.1016/j.jorganchem.2020.121369
[46] A. R. Sardarian, M. Zangiabadi, I. D. Inaloo, *RSC Adv.* **2016**, *6*, 92057. https://doi.org/10.1039/C6RA17268G
[47] I. D. Inaloo, S. Majnooni, *European J. Org. Chem.* **2019**, *2019*, 6359. https://doi.org/10.1002/ejoc.201901140
[48] A. R. Sardarian, I. Dindarloo Inaloo, M. Zangiabadi, *New J. Chem.* **2019**, *43*, 8557. https://doi.org/10.1039/C9NJ00028C
[49] I. Dindarloo Inaloo, S. Majnooni, H. Eslahi, M. Esmaeilpour, *Mol. Catal.* **2020**, *492*, 110915. https://doi.org/10.1016/j.mcat.2020.110915
[50] A. V. Nakhate, G. D. Yadav, *ACS Sustain. Chem. Eng.* **2016**, *4*, 1963. https://doi.org/10.1021/acssuschemeng.5b01205
[51] A. V. Nakhate, G. D. Yadav, *ChemistrySelect.* **2017**, *2*, 7150. https://doi.org/10.1002/slct.201700556
[52] M. Kim, H. Kang, K. H. Park, *Catal. Commun.* **2015**, *72*, 150. https://doi.org/10.1016/j.catcom.2015.09.032
[53] J. Sherwood, J. H. Clark, I. J. S. Fairlamb, J. M. Slattery, *Green Chem.* **2019**, *21*, 2164. https://doi.org/10.1039/C9GC00617F
[54] C. Reichardt, T. Welton, *Solvents and Solvent Effects in Organic Chemistry*, Wiley **2010**.
[55] M. García-Melchor, M. C. Pacheco, C. Nájera, A. Lledós, G. Ujaque, *ACS Catal.* **2012**, *2*, 135. https://doi.org/10.1021/cs200526x
[56] P. Veerakumar, P. Thanasekaran, K.-L. Lu, K.-C. Lin, S. Rajagopal, *ACS Sustain. Chem. Eng.* **2017**, *5*, 8475. https://doi.org/10.1021/acssuschemeng.7b00922
[57] M. Zeng, X. Yuan, S. Zuo, C. Qi, *RSC Adv.* **2015**, *5*, 37995. https://doi.org/10.1039/C5RA01902H
[58] B. Lakshminarayana, J. Chakraborty, G. Satyanarayana, C. Subrahmanyam, *RSC Adv.* **2018**, *8*, 21030. https://doi.org/10.1039/C8RA03697G

SUPPORTING INFORMATION

Additional supporting information can be found online in the Supporting Information section at the end of this article.

How to cite this article: M. A. Pawar, A. V. Nakhate, S. S. Kadu, P. V. Tekade, *Appl Organomet Chem* **2024**, e7405. https://doi.org/10.1002/aoc.7405

10990739, 0, Downloaded from https://onlinelibrary.wiley.com/doi/10.1002/aoc.7405 by Institute Of Chemical Technology, Mumbai, Wiley Online Library on [26/02/2024]. See the Terms and Conditions (https://onlinelibrary.wiley.com/terms-and-conditions) on Wiley Online Library for rules of use; OA articles are governed by the applicable Creative Commons License

Indian Journal of Heterocyclic Chemistry
Vol. 33 - Number XX (xxx-xxx 2023) 1-5
https://connectjournals.com/01951.2023.33.X
https://doi.org/10.59467/IJHC.2023.33.x

ISSN (Print) : 0971-1627
ISSN (Online) : 2456-4311

Synthesis and Antimicrobial Evaluation of 3-Carbonyl-(pyrid-4-yl)-5-hepta-*O*-benzoyl-β-D-lactosylimino-2-arylimino-1,3,4-thiadiazolidines

Dipali S. Mankar[1]*, Mamata T. Sangole[1] and Sham H. Mankar[2]

[1]Department of Chemistry, Shri Shivaji College of Arts, Commerce and Science, Akola, Maharashtra, India
[2]Department of Mechanical Engineering, Pimpri Chinchwad College of Engineering and Research, Pune, Maharashtra, India

ABSTRACT A new series of 3-carbonyl-(pyrid-4-yl)-5-hepta-*O*-benzoyl-β-D-lactosylimino-2-arylimino-1,3,4-thiadiazolidines was synthesized by the interaction of 1-carbonyl-(pyrid-4-yl)-4-hepta-*O*-benzoyl-β-D-lactosyl-3-thiosemicarbazide with aryl isocyanodichlorides. The required 1-carbonyl-(pyrid-4-yl)-4-hepta-*O*-benzoyl-β-D-lactosyl-3-thiosemicarbazide was synthesized by the interaction of 1-hepta-*O*-benzoyl-β-D-lactosyl isothiocyanates and isoniazid. These compounds were screened for their antibacterial and antifungal activity against some pathogenic organisms to get potent bioactive molecule.

KEYWORDS 1-hepta-*O*-benzoyl-β-D-lactosyl isothiocyanate, Thiosemicarbazide, Thiadiazolidines, Antimicrobial activity.

How to cite this article: Mankar, D.S., Sangole, M.T. and Mankar, S.H. Synthesis and Antimicrobial Evaluation of 3-Carbonyl-(pyrid-4-yl)-5-hepta-*O*-benzoyl-β-D-lactosylimino-2-arylimino-1,3,4-thiadiazolidines, *Indian J. Heterocycl. Chem.*, **2023**, *33*, 1–5. *https://doi.org/10.59467/IJHC.2023.33.X*

INTRODUCTION

Carbohydrates mediate a variety of important, medicinally relevant biological processes, playing a key role in numerous diseases.[1] The ability to understand their functions is of paramount importance for the development of new drugs and therapeutics to treat human diseases.

Heterocyclic compounds[2] play a vital role among organic compounds with biological activities that are used as medicines in human and veterinary drugs or as insecticides and pesticides in agricultural applications. Chemical rings, available in various medicines, may have pharmacological characteristics or may provide a platform for the pharmacophoric sets, which will work to gather with the receptors. Thiadiazoles belong to the group of nitrogen–sulfur-containing heterocycles with wide application as structural parts of biologically active molecules and as useful intermediates in medicinal chemistry. Since the past few years, substituted 1,3,4-thiadiazole derivatives have received important consideration and have been increasingly investigated due to their large spectrum of pharmacological characteristics. It is assumed that 1,3,4-thiadiazole derivatives show different biological activities due to the occurrence of =N-C-S- moiety. Other authors assume that the biological activities of 1,3,4-thiadiazole derivatives are due to strong aromaticity of the ring, which also gives great *in vivo* stability to this five-membered ring system and low toxicity for higher vertebrates, including humans.

1,3,4-Thiadiazoles are significant heterocyclic compounds with a wide range of applications in medicinal, agricultural, and materials chemistry.[3] Their derivatives bearing an amino or imino group display a broad spectrum of pharmaceutical and biological properties[4] including antimicrobial,[5] antitubercular,[6] anticancer,[7] anti-inflammatory/analgesic,[8] antidepressant,[9] and antioxidant activities.[10] In view of these observations, we report herein synthesis and antimicrobial evaluation of some new 3-carbonyl-(pyrid-4-yl)-5-hepta-*O*-benzoyl-β-D-lactosylimino-2-arylimino-1,3,4-thiadiazolidines.

*Corresponding author: Email: dipalimhaisne@rediffmail.com

Published & Hosted by :
Journal Homepage :
www.connectjournals.com/ijhc
www.connectjournals.com

©2023 Connect Journals

RESULTS AND DISCUSSION

The synthetic routes for the preparation of new thiosemicarbazide **(3)** and thiadiazolidines **(5a-g)** are shown in **Scheme 1**. In the first step, 1-carbonyl-(pyrid-4-yl)-4-hepta-*O*-benzoyl-β-D-lactosyl-3-thiosemicarbazide **(3)** was prepared by reacting hepta-*O*-benzoyl-β-D-lactosyl isothiocyanate **(1)** with isoniazid **(2)** in acetone as a solvent. In the second step, 3-carbonyl-(pyrid-4-yl)-5-hepta-*O*-benzoyl-β-D-lactosylimino-2-arylimino-1,3,4-thiadiazolidines **(5a-g)** was prepared by interaction of 1-carbonyl-(pyrid-4-yl)-4- hepta-*O*-benzoyl-β-D-lactosyl-3-thiosemicarbazide **(3)** with various aryl isocyanodichlorides **(4a-g)** using acetone as a solvent. The products were found to be optically active. The chemical structures of the title compounds were deduced by infrared (IR),[13,14] ^{1}H NMR,[15] mass spectra,[16] and elemental analysis [**Table 1**].

EXPERIMENTAL SECTION

Chemicals, reagents, and solvent were obtained from chemical sources and purified by either distillation or crystallization before use. Thin-layer chromatography (TLC), performed on E. Merck pre-coated silica gel plates, was used to test the compound purity. Melting points were determined in open capillary tubes on Mac digital melting point apparatus and are uncorrected. IR spectra were recorded in solid phases KBr pellets on Shimadzu IRAffinity-1 Fourier-transform infrared spectroscopy spectrometer. ^{1}H NMR spectra were recorded in $CHCl_3$ on Bruker of NMR spectrometer 500 MHz. The mass of the synthesized compounds was also obtained from CIF, SPPU, Pune, using mass spectrometer (Bruker Compass). Equiptronics Digital Polarimeter EQ-801 at 31°C in $CHCl_3$ was used to determine optical rotations $[\alpha]_D^{31}$.

Synthesis of 1-carbonyl-(pyrid-4-yl)-4-hepta-O-benzoyl-β-D-lactosyl-3-thiosemicarbazide (3)

Lactosyl isothiocyanate (0.009 M, 10 g) and isoniazid (0.009 M, 1.23 g) were mixed together in acetone solution (60 mL). The reaction mixture was shaken for some time to form clear solution and refluxed for 12 h. This reaction was monitored by TLC. After completion of reaction, reaction mixture was brought to the room temperature and solvent was distilled off to obtain a sticky residue. This residue was triturated by means of petroleum ether (60–80°C) to afford a pale-yellow solid product **(3)**.

3) Yield-11.1 g, m.p. 107–109°, $[\alpha]^{D3}1$ = +37 (c, 0.1 in chloroform)

IR (KBr, cm^{-1}): υ3495 (N-H stretch), 3070 (Aromatic C-H stretch), 2970 (Aliphatic C-H stretch), 1720 (C=O

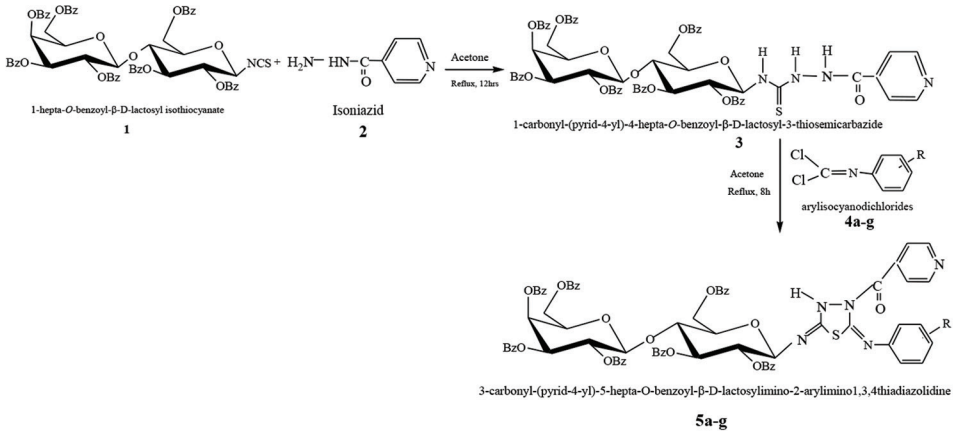

(Bz =COC_6H_5, **4a/5a**: R = phenyl; **4b/5b**: R = *o*-tolyl; **4c/5c**: R = *m*-tolyl; **4d/5d**: R = *p*-tolyl; **4e/5e**: R = *o*-Cl-phenyl; **4f/5f**: R = *m*-Cl-phenyl; **4g/5g**: R = *p*-Cl-phenyl)

Scheme 1: Synthesis of 3-carbonyl-(pyrid-4-yl)-5-hepta-*O*-benzoyl-β-D-lactosylimino-2-arylimino1,3,4-thiadiazolidines (5a-g)

Table 1: Physical and analytical data of compounds (5a-g)

Products	Yield (%)	M.P. (°C)	$[\alpha]_D^{31}$ (c, in$CHCl_3$)	Elemental analysis (%) found (required)	
				N	S
5a	96.30	143–145	+154.50	5.17 (5.19)	2.38 (2.37)
5b	75.91	132–133	−300	5.12 (5.14)	2.36 (2.35)
5c	75.09	124–125	+262	5.13 (5.14)	2.37 (2.35)
5d	81.75	142–143	+229	5.13 (5.14)	2.39 (2.35)
5e	92.80	121–123	+145.40	5.04 (5.06)	2.33 (2.31)
5f	87.05	136–137	+71.40	5.03 (5.06)	2.34 (2.31)
5g	81.29	121–122	−88.23	5.03 (5.06)	2.32 (2.31)

stretch), 1265 (C-O stretch), 1172 (C-N stretch), 1095, 1064 and 1026 (characteristics of lactose unit), 709 (C-S stretch). ^{1}H NMR ($CDCl_3$, ppm): δ 8.75 (1H, *s*, NH), δ 8.02–7.20 (39 H, *m*, aromatic protons), δ6.15 (1H, *s*, NH), δ 5.75–3.73 (14 H, *m*, lactosyl ring protons), δ1.94 (1H, *s*, NH). Mass (m/z): (M^+) 1248, (M+1) 1249 (100%), 1053, 949, 579. Found: C: 65. 25; H: 4.37; N: 4.36; S: 2.48, $C_{68}H_{56}O_{18}N_4S$: Required C: 65.38; H: 4.49; N: 4.49; S: 2.56%.

5a) Synthesis of 3-carbonyl-(pyrid-4-yl)-5-hepta-O-benzoyl-β-D-lactosylimino-2-phenylimino-1,3,4-thiadiazolidines

The 1-carbonyl-(pyrid-4-yl)-4-hepta-*O*-benzoyl-β-D-lactosyl-3-thiosemicarbazide (0.001 M, 1.25 g) **(3)** was mixed with phenyl isocyanodichloride (0.001 M, 0.174 g) **(4a)** in acetone (30 mL). This reaction mixture was refluxed for 3. This reaction was monitored by TLC. After completion of reaction, the reaction mixture was brought to room temperature and solvent was distilled off to give a sticky residue. The sticky residue was triturated several times with petroleum ether (60–80°C) and the product was obtained as yellow solid **(5a)**.

IR (KBr, cm^{-1}): υ3425 (N-H stretch), 3062 (Aromatic C-H stretch), 2970 (Aliphatic C-H stretch), 1728 (C=O stretch), 1597 (C=N stretch), 1265 (C-O stretch), 1172 (C-N stretch), 1095, 1064 and 1026 (characteristics of lactose), 709 (C-S stretch). ^{1}H NMR ($CDCl_3$, ppm): δ 8.02–7.21 (44H, *m*, aromatic protons), 5.75 (1H, *s*, NH), δ 5.75–3.74 (14H, *m,* lactosyl ring protons). Mass (*m/z*): (M^+) 1349, 1249 (100%), 1053, 579. Found: C: 66.71; H: 4.35; N: 5.17; S: 2.38, $C_{75}H_{59}O_{18}N_5S$: Required: C: 66.72; H: 4.37; N: 5.19; S: 2.37%.

Similar method was used to prepare remaining compounds **(5b-g)**. The physical characterization data of thus obtained compounds are summarized in **Table 1: (5a-g).**

5b) Synthesis of 3-carbonyl-(pyrid-4-yl)-5-hepta-O-benzoyl-β-D-lactosylimino-2-o-tolyl imino-1,3,4-thiadiazolidines

IR (KBr, cm^{-1}): υ3433 (N-H stretch), 3062 (Aromatic C-H stretch), 2970 (Aliphatic C-H stretch), 1720 (C=O stretch), 1604 (C=N stretch), 1257 (C-O stretch), 1172 (C-N stretch), 1095, 1064 and 1026 (characteristics of lactose), 709 (C-S stretch). ^{1}H NMR ($CDCl_3$, ppm): δ 8.06–7.18 (43H, *m*, aromatic protons), δ 5.77–3.74 (14H, *m*, lactosyl ring protons) δ 5.77 (1H, *s*, NH), δ 2.56 (3H, *s*, CH_3). Mass (m/z): M^+ 1363, 1053, 579 (100%). Found: C: 66.89; H: 4.45; N: 5.12; S: 2.36, $C_{76}H_{61}O_{18}N_5S$: Required: C:66.91; H:4.48; N:5.14; S:2.35.

5c) Synthesis of 3-carbonyl-(pyrid-4-yl)-5-hepta-O-benzoyl-β-D-lactosylimino-2-m-tolyl imino-1,3,4-thiadiazolidines

IR (KBr,cm^{-1}): υ3433 (N-H stretch), 3070 (Aromatic C-H stretch), 2970 (Aliphatic C-H stretch), 1728 (C=O stretch), 1604 (C=N stretch), 1265 (C-O stretch), 1172 (C-N stretch), 1095, 1064 and 1026 (characteristics of lactose), 709 (C-S stretch). ^{1}H NMR ($CDCl_3$, ppm): δ 8.02–7.18 (43H, *m*, aromatic protons), δ 5.62 (1H, *s*, NH), δ5.77–3.88 (14H, *m*, lactosyl ring protons) δ 2.16 (3H, *s*, CH_3). Mass (m/z): (M+) 1363, 1215 (100%), 1053, 949, 579. Found: C: 66.88; H: 4.46; N: 5.13; S: 2.37, $C_{76}H_{61}O_{18}N_5S$: Required: C: 66.91; H: 4.48; N:5.14; S:2.35%.

5d) Synthesis of 3-carbonyl-(pyrid-4-yl)-5-hepta-O-benzoyl-β-D-lactosylimino-2-p-tolyl imino-1,3,4-thiadiazolidines

IR(KBr,cm^{-1}): υ3425 (N-H stretch), 3070 (Aromatic C-H stretch), 2970 (Aliphatic C-H stretch), 1720 (C=O stretch), 1604 (C=N stretch), 1265 (C-O stretch), 1172 (C-N stretch), 1095, 1064 &1026 (characteristics of lactose), 709 (C-S stretch). ^{1}H NMR ($CDCl_3$,ppm): δ 8.00-7.12 (43H,*m*, aromatic protons), δ 6.81 (1H,*s*,NH), δ5.90-3.88 (14H,*m*, lactosyl ring protons) δ 2.34 (3H,*s*,CH_3).Mass (m/z): (M+)1363, 1053, 949, 579 (100%). Found: C: 66.89; H:4.44; N:5.13; S:2.36, $C_{76}H_{61}O_{18}N_5S$: Required: C:66.91; H:4.48; N:5.14; S:2.35%.

5e) Synthesis of 3-carbonyl-(pyrid-4-yl)-5-hepta-O-benzoyl-β-D-lactosylimino-2-o-chloro phenylimino-1,3,4-thiadiazolidines

IR (KBr, cm^{-1}): υ3433 (N-H stretch), 3062 (Aromatic C-H stretch), 2978 (Aliphatic C-H stretch), 1728 (C=O stretch), 1604 (C=N stretch), 1265 (C-O stretch), 1172 (C-N stretch), 1095, 1064 and 1026 (characteristics of lactose), 709 (C-S stretch). ^{1}H NMR ($CDCl_3$, ppm): δ 8.02–7.21 (43H,*m*, aromatic protons), δ 7.20 (1H, *s*, NH), δ 5.77–3.89 (14H, *m*, lactosyl ring protons). Mass (m/z): (M+) 1383, 1053, 949, 579 (100%). Found: C: 65.01; H: 4.17; N: 5.04; S: 2.33% $C_{75}H_{58}O_{18}N_5SCl$: Required: C: 65.05; H: 4.19; N: 5.06; S: 2.31%.

5f) Synthesis of 3-carbonyl-(pyrid-4-yl)-5-hepta-O-benzoyl-β-D-lactosylimino-2-m-chloro phenyl imino-1,3,4-thiadiazolidines

IR (KBr, cm^{-1}): υ3417 (N-H stretch), 3062 (Aromatic C-H stretch), 2970 (Aliphatic C-H stretch), 1720 (C=O stretch), 1597 (C=N stretch), 1257 (C-O stretch), 1172 (C-N stretch), 1095, 1064 and 1026 (characteristics of lactose), 709 (C-S stretch). ^{1}H NMR ($CDCl_3$, ppm): δ 8.02–7.26 (43H, *m*, aromatic protons), δ 5.74 (1H, *s*, NH), δ 5.39–3.72 (14H, *m*, lactosyl ring protons). Mass (m/z): M^+1383, (M+2) 1385, 1053, 579 (100%). Found: C: 65.04; H: 4.17; N: 5.03; S: 2.33%. $C_{75}H_{58}O_{18}N_5SCl$: Required: C: 65.05; H: 4.19; N: 5.06; S: 2.31.

5g) Synthesis of 3-carbonyl-(pyrid-4-yl)-5-hepta-O-benzoyl-β-D-lactosylimino-2-p-chloro phenylimino-1,3,4-thiadiazolidines

IR (KBr, cm^{-1}): υ3425 (N-H stretch), 3070 (Aromatic C-H stretch), 2962 (Aliphatic C-H stretch), 1720 (C=O stretch), 1604 (C=N stretch), 1265 (C-O stretch), 1172 (C-N stretch), 1095, 1064 and 1026 (characteristics of lactose), 709 (C-S stretch). ^{1}H NMR ($CDCl_3$, ppm): δ 8.02–7.19 (43H, *m*, aromatic protons), δ 6.04 (1H, *s*, NH), δ5.77–3.72 (14H, *m*, lactosyl ring protons). Mass (m/z): (M+) 1383, (M+2)

1385, 1053, 949, 579 (100%). Found: C: 65.02; H: 4.16; N: 5.03; S: 2.32 $C_{75}H_{58}O_{18}N_5SCl$: Required: C: 65.05; H: 4.19; N: 5.06; S: 2.31.

Antimicrobial Activity

All the synthesized compounds were evaluated for their minimum inhibitory activity against bacteria (*Salmonella typhi*) and fungal strain (*Aspergillus Niger*) using cup plate agar diffusion method[17-19] by measuring the inhibition zone in mm. The compounds were taken at a concentration of 1 mg/mL using dimethyl sulfoxide as a solvent. The minimum inhibition concentration of all the synthesized compounds was obtained. Similarly, study was also conducted for the reference standard amikacin for antibacterial activity and fluconazole for antifungal activity. The zone of incubation observed around the cup after incubation was measured. The results are presented in **Table 2.** The results of this preliminary screening study are also shown in the graphical method. From the data, it is clear that novel compounds 5a, 5b, 5d, 5e, 5f possess good activity, while compounds 5c possess moderate activity against bacteria (*S. typhi)* and fungi (*A. Niger*).

Table 2: Antimicrobial activities of newly synthesized 3-carbonyl-(pyrid-4-yl)-5-hepta-*O*-benzoyl-β-D-lactosylimino-2-arylimino-1,3,4-thiadiazolidines (5a-g)

Compound	Antibacterial	Antifungal
	Salmonella typhi	*Aspergillus niger*
5a	21	21
5b	19	22
5c	15	19
5d	18	22
5e	22	23
5f	20	22
5g	19	21
Amikacin	26	-
Fluconazole	-	28

**Zone of inhibition measured in mm, (15 or less) resistance, (16–20 mm) moderate and (more than 20 mm) sensitive

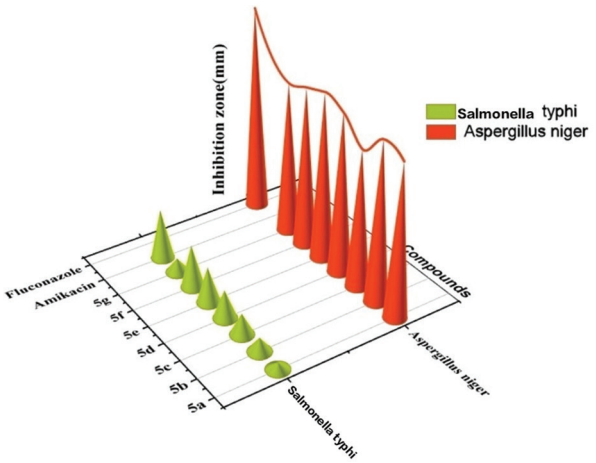

CONCLUSION

Novel compounds were prepared with good yields through a facile synthetic pathway, and their chemical structures were characterized by detecting their physicochemical properties and analyzing their IR, ^{1}H NMR and mass spectra. These compounds also were screened for their antimicrobial activity against bacteria (*S. typhi*) and fungi (*A. niger*) using a solution of amikacin and fluconazole as a positive control, respectively. Some of these compounds possess a high response against bacteria as well as fungi. Therefore, these novel compounds can be considered as an encouraging wide spectrum antibacterial agent and antifungal agent.

ACKNOWLEDGMENT

Authors are grateful to CIF, SPPU, Pune, for providing the spectral data and also to Dr. A. L. Kulat Principal, Shri Shivaji College of Art's Commerce and science Akola, for encouragement and providing necessary facilities.

REFERENCES

[1] Fernandez-Tejada, F., Canada, F.J. and Jimenez-Barbero, J. Recent developments in synthetic carbohydrate-based diagnostics, vaccines, and therapeutics, *Chem. Eur. J*., **2015,** *21*, 10616–10628.

[2] Serban, G., Stanasel, O., Serban, E. and Bota, S. 2-Amino-1,3,4-thiadiazole as a potential scaffold for promising antimicrobial agents, *Drug Des. Devel. Ther*., **2018,** *12*, 1545–1566.

[3] Huang, Z., Zhang, Q., Zhao, Q., Yu, W. and Chang. ???, J. *Am. Chem. Soc. Org. Lett*., **2022**, ???, ???.

[4] (a) Supuran, C.T., Briganti, F., Tilli, S., Chegwidden, W.R. and Scozzafava, A. Carbonic anhydrase inhibitors: Sulfonamides as antitumor agents?, *Bioorg. Med. Chem*., **2001,** *9*, 703−704. (b) Serban, G., Stanasel, O., Serban, E. and Bota, S. 2-Amino-1,3,4-thiadiazole as a potential scaffold for promising antimicrobial agents, *Drug Des. Devl. Ther*., **2018,** *12*, 1545−1566.

[5] (a) Chandrakantha, B., Isloor, A.M., Shetty, P., Fun, H.K. and Hegde, G. Synthesis and biological evaluation of novel substituted 1,3,4-thiadiazole and 2,6-di aryl substituted imidazo [2,1-b] [1,3,4] thiadiazole derivatives, *Eur. J. Med. Chem*., **2014,** *71*, 316−323. (b) Farghaly, T.A., Abdallah, M.A., Masaret, G.S. and Muhammad, Z.A. New and efficient approach for synthesis of novel bioactive [1,3,4] thiadiazoles incorporated with 1,3-thiazole moiety, *Eur. J. Med. Chem*., **2015**, *97*, 320−333. (c) Kumar, G.S., Poornachandra, Y., Reddy, K.R., Kumar, C.G. and Narsaiah, B. Synthesis of novel triazolothione, thiadiazole, triazole-functionalized furo/thieno[2,3-b] pyridine derivatives and their antimicrobial activity, *Synth. Commun*., **2017,** *47*, 1864−1873.

[6] (a) Alegaon, S.G., Alagawadi, K.R., Sonkusare, P.V., Chaudhary, S.M., Dadwe, D.H. and Shah, A.S. Novel imidazo[2,1-b][1,3,4]thiadiazole carrying rhodanine-3-acetic acid as potential antitubercular agents, *Bioorg. Med. Chem. Lett*., **2012,** *22*, 1917−1921. (b) Patel, H.M., Noolvi, M.N., Sethi, N.S., Gadad, A.K. and

Cameotra, S.S. Synthesis and antitubercular evaluation of imidazo[2,1-b][1,3,4]thiadiazole derivatives, *Arabian J. Chem*., **2017,** *10*, S996−S1002.

[7] (a) Andreani, A., Burnelli, S., Granaiola, M., Leoni, A., Locatelli, A., Morigi, R., Rambaldi, M., Varoli, L., Calonghi, N., Cappadone, C., Voltattorni, M., Zini, M., Stefanelli, C., Masotti, L. and Shoemaker, R.H. Antitumor activity of bis-indole derivatives (1), *J. Med. Chem*., **2008,** *51*, 7508−7513. (b) Noolvi, M.N., Patel, H.M., Singh, N., Gadad, A.K., Cameotra, S.S. and Badiger, A. Synthesis and *in vitro* antitumor activity of substituted quinazoline and quinoxaline derivatives: Search for anticancer agent, *Eur. J. Med. Chem*., **2011,** *46*, 4411−4418. (c) Yang, X.H., Xiang, L., Li, X., Zhao, T.T., Zhang, H., Zhou, W.P., Wang, X.M., Gong, H.B., Zhu, H.L. Synthesis, biological evaluation, and molecular docking studies of 1,3,4-thiadiazol-2-amide derivatives as novel anticancer agents, *Bioorg. Med. Chem*., **2012,** *20*, 2789−2795. (d) Li, Y.J., Qin, Y.J., Makawana, J.A., Wang, Y.T., Zhang, Y.Q., Zhang, Y.L., Yang, M.R., Jiang, A.Q. and Zhu, H.L. Synthesis, biological evaluation and molecular modeling of 1,3,4-thiadiazol-2-amide derivatives as novel antitubulin agents, *Bioorg. Med. Chem*., **2014,** *22*, 4312−4322. (e) Dawood, K.M. and Gomha, S.M. Synthesis and anti-cancer activity of 1, 3, 4-thiadiazole and 1, 3-thiazole derivatives having 1, 3, 4-oxadiazole moiety, *J. Heterocyclic Chem*., **2015,** *52*, 1400−1405. (f) Gomha, S.M., Abdulla, M.M. and Abou-Seri, S.M. Identification of novel aminothiazole and aminothiadiazole conjugated cyanopyridines as selective CHK1 inhibitors, *Eur. J. Med. Chem*., **2015,** *92*, 459−470.

[8] (a) Gadad, A.K., Palkar, M.B., Anand, K., Noolvi, M.N., Boreddy, T.S. and Wagwade, J. Synthesis and biological evaluation of 2-trifluoromethyl/sulfonamido-5,6-diaryl substituted imidazo[2,1-b]-1,3,4-thiadiazoles: A novel class of cyclooxygenase-2 inhibitors, *Bioorg. Med. Chem*., **2008**, *16*, 276−283. (b) Gilani, S.J., Khan, S.A. and Siddiqui, N. Synthesis and pharmacological evaluation of condensed heterocyclic 6-substituted 1,2,4-triazolo-[3,4-b]-1,3,4-thiadiazole and 1,3,4-oxadiazole derivatives of isoniazid, *Bioorg. Med. Chem. Lett*., **2010,** *20*, 4762−4765.

[9] Jubie, S., Ramesh, P.N., Dhanabal, P., Kalirajan, R., Murugananthan, N. and Antony, A.S. Synthesis, antidepressant and antimicrobial activities of some novel stearic acid analogues, *Eur. J. Med. Chem*., **2012,** *54*, 931−935.

[10] (a) Al-Omair, M.A., Sayed, A.R. and Youssef, M.M. Synthesis of novel triazoles, tetrazine, thiadiazoles and their biological activities, *Molecules*, **2015**, *20*, 2591−2610. (b) Badrey, M.G., Gomha, S.M., Arafa, W.A.A. and Abdulla, M.M. An approach to polysubstituted triazipines, thiadiazoles and thiazoles based on benzopyran moiety through the utility of versatile hydrazonoyl halides as *in vitro* monoamine oxidase inhibitors, *J. Heterocyclic Chem*., **2017**, *54*, 1215−1227.

[11] Tale, P.V. and Deshmukh, S.P. Synthesis of 2-phenylimino-3-aryl-4-S-benzyl-6-hepta-O-acetyl- β -Dlacosylimino-2,3-dihydro-1,3,5-thiadiazine hydrochlorides, *Indian J. Chem*., **2006**, *45B*, 558–560.

[12] Yadgire, A.V., Barate, D.L. and Deshmukh, S.P. Dithiazolidines: Synthesis and anti-microbial activity of some novel n-maltosides, *Rasayan J. Chem*., **2011**, *4*, 780–783.

[13] Silverstein, R.M. and Webster, F.X. S*pectrometric Identification of Organic Compounds*, 6th ed. John Wiley and Sons, Inc., New York, **2011**.

[14] Dyer, J.R. *Applications of Absorption Spectroscopy of Organic Compounds, PHI Learning Private Limited*, New Delhi, **2010.**

[15] Williams, D.H. and Fleming, L. *Spectroscopic Methods in Organic Chemistry*. 6th ed. United States: Tata McGraw-Hill Education, **2011.**

[16] Budzikiewicz, H., Djerassiand, C. and Williams, H. *Structural Elucidation of Natural products by mass Spectrometry*, Vol. 2. Holden-Day 207, San Francisco, **1964.**

[17] Kawangh, F. *Analytical Microbiology*, Academic Press, NewYork, **1963.**

[18] British Pharmacopeia-II. *Biological Assay and Tests*, The Stationary Office Ltd., London, **1998**, pA205.

[19] Kumar, V.M.M.J., Jayadevaiah, K.V., Nagaraj, T.S., Jayachandran, E., Bharathi, D.R. Sreenivasa, G.M., Synthesis, characterization and antimicrobial activity of new N-substituted-3-chloro-2-azetidinones, *Arch. Pharm. Sci. Res*., **2009,** *1*, 31–29.

Received: 31 Jan 2023; Accepted: 24 May 2023

Author Queries???
AQ1: Kindly check and confirm the heading level
AQ2: Kindly cite references 11 and 12 in the text part
AQ3: Kindly provide article title
AQ4: Kindly provide volume number and page number

ResearchGate

See discussions, stats, and author profiles for this publication at: https://www.researchgate.net/publication/371033080

Current Scenario of Wild Edible Plants (WEPs), their Importance, Possible Threats, and Conservation: A Mini Review

Article *in* Journal of Agriculture and Ecology Research International · May 2023

DOI: 10.9734/jaeri/2023/v24i5538

CITATIONS
0

READS
196

5 authors, including:

R. Shirsat
Shri Dr R. G. Rathod Arts and Science college Murtizapur Dist-Akola
23 PUBLICATIONS **356** CITATIONS
SEE PROFILE

Dipak Koche
Shri Shivaji College of Arts, Commerce and Science
51 PUBLICATIONS **443** CITATIONS
SEE PROFILE

All content following this page was uploaded by Dipak Koche on 02 June 2023.

The user has requested enhancement of the downloaded file.

Journal of Agriculture and Ecology Research International

Volume 24, Issue 5, Page 18-27, 2023; Article no.JAERI.100019
ISSN: 2394-1073

Current Scenario of Wild Edible Plants (WEPs), their Importance, Possible Threats, and Conservation: A Mini Review

Rupali Shirsat [a], Tripty Jagtap [b], Ashwini Sirsat [b], Shubham Rathod [b] and Dipak Koche [b*]

[a] Department of Botany, Shri Dr. R. G. Rathod College of Arts and Science, Murtizapur, District- Akola, M.S.-444107, India.
[b] Department of Botany, Shri Shivaji College of Arts, Commerce and Science, Akola, District- Akola, M.S.-444003, India.

Authors' contributions

This work was carried out in collaboration among all authors. Author DK conceptualize the review, RS prepare a primary manuscript. Authors AS, TJ and SR improvise the manuscript section-wise and all authors finalized the review. All authors read and approved the final manuscript.

Article Information

DOI: 10.9734/JAERI/2023/v24i5538

Open Peer Review History:
This journal follows the Advanced Open Peer Review policy. Identity of the Reviewers, Editor(s) and additional Reviewers, peer review comments, different versions of the manuscript, comments of the editors, etc are available here: https://www.sdiarticle5.com/review-history/100019

Mini-review Article

Received: 11/03/2023
Accepted: 15/05/2023
Published: 24/05/2023

ABSTRACT

The knowledge of Wild Edible Plants (WEPs) is as old as human civilization and still, they are playing a supplementary role in global food security. WEPs are an integral part of their traditional food systems and have nutritional and cultural values in their routine livelihood. WEPs are increasingly considered a potential source of a naturally healthy diet. But in many cases, the available WEPs resources are under threat of various kinds like overexploitation, overgrazing, forest fires, agricultural encroachment, etc.; the changing climate also negatively impacts on WEPs. Therefore, there is an urgent need for the conservation of the diversity of WEPs and their

**Corresponding author: E-mail: kochedeepak77@gmail.com;*

sustainable management. The present mini-review is an attempt to present the current scenario of WEPs, their importance, and a potential source of nutrients for future food security, ethnic knowledge associated with them, threats encountered by WEPs, and their possible sustainable management scheme.

Keywords: Traditional food system; food security; sustainable management; ethnic knowledge.

1. INTRODUCTION

Since early civilization, humans use to consume wild edible plants (WEPs) which later became an integral part of their routine food. During their early evolutionary period, humans use to obtain their food by gathering eatable items from plants or plant parts (like roots, stems, leaves, flowers, seeds, etc.) and hunting animals. When the humans started settling by making huts and shades, they also started the domestication of some plants and animals [1]. Still, such types of traditions could be observed in different tribal communities across the globe [2].

It is now a clear fact that all the cultivated crop plants of today's era were ones known as wild edible plants (WEPs). After thousands of years of regular practice of cultivation by humans following the strategy of selecting more favorable traits of plants, some of them have reached the status of domesticated crop plants. With the emergence of domesticated crops, another term 'weed' comes into the picture. Weeds are the undesired plants growing along with crop plants. It was noted that most of the weed species are found to be the relatives of domesticated crop plants.

As per literature, the term "Wild", commonly indicates those species that grow spontaneously in self-sustaining populations outside cultivated areas, along the field margins, hedges, grasslands, and forest woodlands [3]. However, the distinction between "wild" and "domesticated" or "cultivated" is not so clear, and many WFPs fall somewhere in between these extremes depending on the degree of human intervention [4]. There are several plant species that are not domesticated to that extent but play prominent roles as good sources of food and nutrition by various local as well as tribal communities globally. There are a few examples that farmers use to grow a few wild species to meet their food and nutrition needs [5,6]. Under the WEPs, various communities across the globe consume leaves, flowers, fruits, nuts, legumes, pods, fruiting bodies of mushrooms, and other non-timber forest products [7].

The knowledge of WEPs is as old as human civilization and still, they are playing a supplementary role in global food security. But in many cases, the available WEPs resources are under threat of various kinds like overexploitation, overgrazing, forest fires, agricultural encroachment etc. Recent studies suggest that there are more than 7000 wild edible plant species that are being used for their multiple uses as food, nutrition, medicine, or environmental cause [8] and about 11% of them are under the threatened category of IUCN.

In this review, the authors tried to explain the term wild edible plants (WEPs) considering all possible dimensions [9] and elaborate on their importance to human beings and will also focus on the possible threats.

2. MATERIALS AND METHODS

For the present work, all the work related to wild edible plants (WEPs), their food values and nutrition, traditional knowledge associated with WEPs, and probable threats to the existing biodiversity of WEPs was collected from different online and offline journals included in various reputed databases like Scopus, WOS, Springer, Elsevier, etc. Later, the collected resource material was analyzed and interpreted critically and thematically presented in this mini-review. The related articles published in different databases were selected on the basis of their titles, abstracts, and text focusing on the reasons to include the reference in the present article and later screened by reading the full text and removing the references or part of it which do not meet the criteria of inclusion.

3. RESULTS AND DISCUSSION

3.1 The Importance of WEPs as a Source of Food and Nutrition

Since ancient days, wild edible plants (WEPs) continue to play a vital role as the principal provider of food and nutrition to sizable human populations particularly under the scarcity and

unavailability of main food crops. Further, many tribals and poor villagers residing in the vicinity of the forest depend on WEPs for their food, nutrition, and medicine [8–13].

The studies on various indigenous communities confirm the fact that wild edible plants (WEPs) are an integral part of their traditional food systems and have nutritional and cultural values in their routine livelihood [14]. Indigenous community peoples about 5% of the global population, are deeply connected to their land. Today these indigenous peoples are considered the sole custodians of rich and diverse traditional knowledge about how to use different plants, traditional food systems, and local biodiversity within the ecosystem range [15].

Indigenous communities also have a better ecological understanding of local environments and thus they could use the available food resources as per their requirement [16]. However, it was noted that the caloric contribution of WEPs is a little low compared to conventional staple foods [17]. But, these wild species contribute to diet diversification in many geographical regions which usually have different types of monotonous food systems, unique to that region [18-19].

The foods obtained from wild edible plants and plant parts usually contain a significant amount of mineral nutrients (Calcium, copper, iron, manganese, potash, sulfur, zinc, etc.) and different vitamins [17] required to support proper growth and development. These wild edible plants are otherwise neglected biological resources as the work in this field is comparatively less, but available reports indicate that these contain a significant amount of nutrients compared to available regional commercial crops [20,21]. If the nutritional potential of wild edible plants is properly assessed and managed, could be introduced as one of the main-stream foods; it might be a step towards food and nutrition security with nutrient adequacy. WEPs are increasingly considered a potential source of natural health products, therefore it is necessary to foster biochemical research on them and document their nutritional properties and main bioactive products [22,23].

If managed properly, Wild edible plants (WEPs) could also boost to empower the local market in turn local communities as it will reduce the distance between the producers and consumers. Further, it will also reduce the complete reliance of the local market on the global market. Some major pieces of evidence indicate that the local trade and markets where the local minor crops, traditional varieties, and wild edible plants are traded, have the potential to empower communities and increase livelihoods in rural areas, particularly of women and youth [24-26].

The current global crisis of the Covid-19 pandemic reveals the importance of local markets and locally available wild edible plants as most of the global food systems and supply chains were affected adversely due to pandemic lockdowns [27-29]. Several workers reported that such a situation opens up opportunities for a new type of food system that supports the local traditional market [30,31]. If such situations create food shortages, peoples turn towards traditional foods and wild edible plants as an important available source of minerals and vitamins, and herbal ingredients [7-8,32,33].

3.2 Traditional Knowledge Associated with WEPs

If we knew and understand the nutritional importance of WEPs and the traditional knowledge associated with them, it might be useful that assist in the prioritization process. The availability of nutrient content and health-promoting properties of WEPs could help in developing local guidelines in different geographical patches. The collection of nutritional data from earlier references is daunting work [34]. The documentation and protection of traditional knowledge related to consumption and recipe preparation of WFPs are available largely to the local users, i.e., rural, indigenous, and forest-dependent communities, including local farmers and elder peoples. The national floras, herbaria, and ethnological studies of local ethnic groups also provide additional botanical, culinary, nutritional, and cultural information needed for research requirements to fill this knowledge gap.

Biological knowledge of individual species is also frequently lacking but particularly essential for conservation. One of the most recent and comprehensive attempts to fill the evidence gap in food composition data is provided by the GEF-supported Biodiversity for Food and Nutrition Project (BFN). Led by Brazil, Kenya, Sri Lanka, and Turkey, and implemented by Biodiversity International with support from the UN Environment Programme (UNEP) and the Food and Agriculture Organization of the United

Nations (FAO), the project has generated food composition data for 185 plant species, many of them wild, particularly in Brazil and Turkey [34,35]. Considering the significance and role of WEPs, they are considered as food for the future [36].

In a case study of Central India, authors have demonstrated that WEPs supplements significantly higher quantities of nutrients in the core zone compared to other zones. These are currently underutilized especially in buffer and transition zones and complement the local staple foods and partially supplement the essential macro- and micro-nutrients [7]. However, most of these WEPs have the potential to fulfill dietary needs and ensure balanced nutrition. Peduruhewa et. al. explained the potential of underutilized WEPs to cope with malnutrition and food insecurity, which are burning issues that need immediate attention [36]. About 71 wild edible plants (WEPs) belonging to 57 genera and 27 families from the semi-arid zone of Punjab, Pakistan were reported by Waheed et al. [35]. They further stated that most of these WEPs are also being used as ethnomedicinal plants for long and as seasonal wild vegetables that have high amounts of nutrition.

3.3 Threats to Wild Edible Plants (WEPs)

The researchers in recent past indicate that Wild edible plants (WEPs) are an integral part of local biodiversity and play a vital role in food security at the local level. Despite its importance, it was found that the diversity of WEPs is declining rapidly. To combat this issue, in 2019, the Food and Agricultural Organization (FAO) constituted “The State of World Biodiversity for Food and Agriculture (SOWBFA), an independent body to take care of and assess the diversity of food and agriculture [37].

According to the reports of FAO [37] and Royal Botanical Garden [38] changes in land use and management like conversion of forest-covered land area to agriculture, for industry and infrastructure development, habitat destruction due to grazing, forest fires, and overharvesting of forest products are some of the major causes of depletion in plant diversity including WEPs. These reasons account for about 62% of threats to WEPs which are growing beyond the range of protected forests [7]. Some workers also reported a decline in the abundance and diversity of WEPs from different areas [39,40]. Many WEPs found to grow in agricultural lands as weeds, in hedges, as wild trees in agroforestry systems, and in some small forest patches [17]. The change in agricultural practices, including intensification, use of more pesticides, and removal of existing flora can negatively impact the existence of these biological resources [41,42].

The SOWBFA used the Sampled Red List Index for Plants prepared by the International Union for Conservation on Nature (IUCN) [41]. Under this project, a total of 822 WEPs species were considered across 7 different classes of which 73% are currently at low risk of extinction but some classes are highly threatened in the wild. However, the IUCN Red List Index for Plants includes global conservation assessments for only one-third (31%) of known WFPs. Furthermore, International Center for Tropical Agriculture (CIAT) as part of a larger study to identify conservation gaps for useful plants, an assessment of the comprehensiveness of conservation of 1587 WFP taxa was carried that showed only 3.3% of WFPs are sufficiently conserved ex-situ, while 89.1% require urgent off-site conservation measures [42]. Of the WFP taxa analyzed 42.1% are sufficiently conserved, 46.7% deserve medium priority and 11.1% require stepping up conservation measures [42]. Rapidly increasing temperatures and habitat destruction can alter the species’ geographic distribution, driving them across the artificially designated boundaries of many protected areas in pursuit of favorable growing conditions.

3.4 Priorities and Integrated Approach for Conservation of WEPs

The conservation and sustainable management strategies of WFPs must include close collaboration with indigenous and local communities and tribes who are the main users and custodians of WEPs local diversity. It must have participatory research approaches that integrate traditional and scientific knowledge about WEPs; it will be most appropriate to maximize benefits for those communities or community peoples who are involved in the process. Before starting such work, the local community people should be made aware and they should agree on every aspect of the research process including methodology, analysis, and purpose of research or data collection [43].

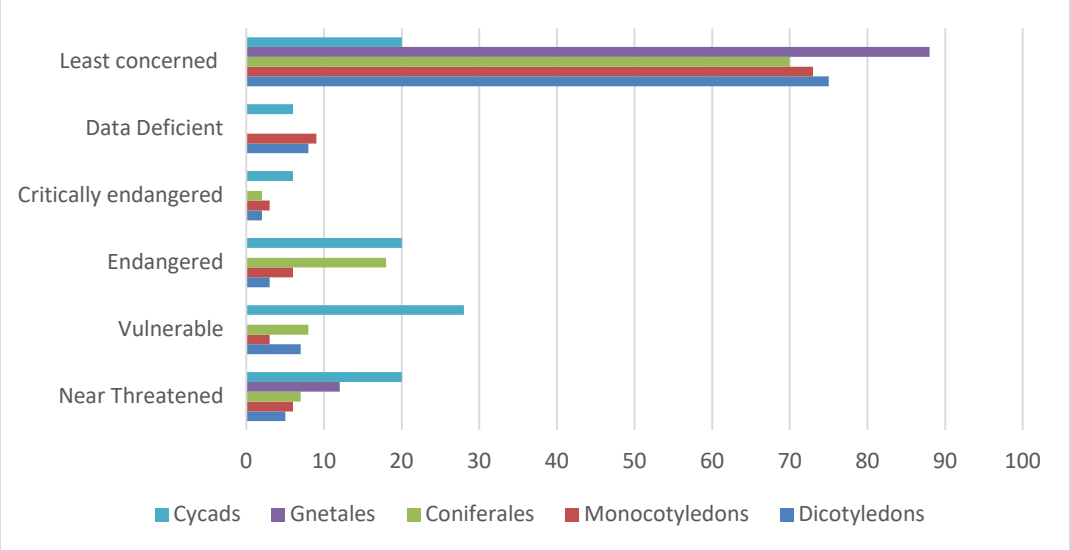

Fig. 1. Major plant groups and their IUCN status (2019)
(Note: All values are in percentage. Adopted from FAO (2019))

There are several reports on declining of WEPs from their habitats, local markets, and even from regular diets of different local communities. Therefore, their conservation and sustainable management for future food security is one of the very difficult tasks for the entire human community. For the sustainable management of WEPs, Borelli [35] proposed a highly appreciable scheme. It includes the challenges in environmental conditions, information, and infrastructure, and the practices to be conducted for sustainable management of WEPs. Reportedly there are over 20,000 species of WEPs across the globe; some of which are enlisted in the form of their respective references in Table 1 as per the literature available [51]. Currently, we are utilizing less than 10% of these WEPs, others are declining due to mere negligence and less awareness of these species worldwide. For future food security, and to maintain the ecological balance these species must have to conserved. It is very urgent to conserve the diversity of WEPs using both in-situ and ex-situ conservation methods. For maximum utilization, we need to develop a specific knowledge system for WEPs and provide the required infrastructure and support (Fig. 2) to strengthen the developing system for the conservation and management of WEPs across the globe.

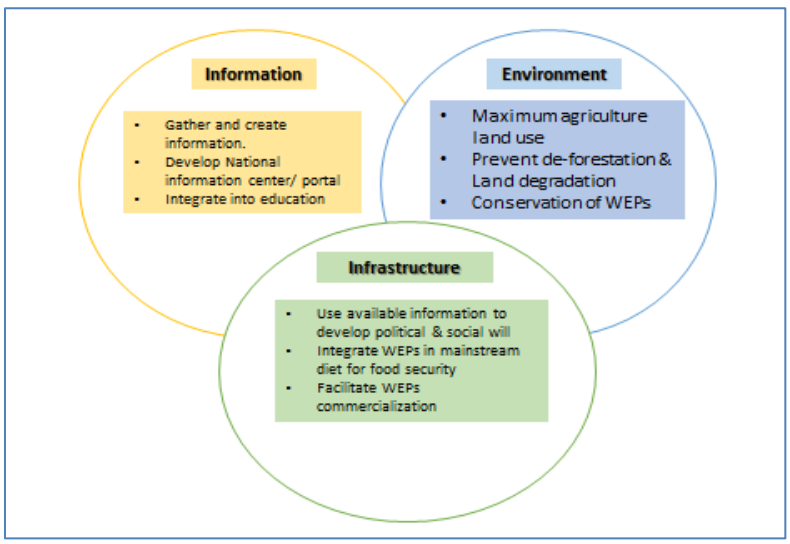

Fig. 2. Integrated approach to conserving WEPs

Table 1. Literature available on wild edible plants (WEPs) from different countries

Sr. No.	Country	Work done by
1	African countries (South Africa, Ethiopia, Kenya, Tanzania, Zambia)	[44,45,46,47,48,49,50,52]
2	America (USA)	[5,80]
3	China	[56,57,58,59,60]
4	European Countries	[61,62,63,64,65]
5	Asian Countries excluding China (India, Pakistan, Bhutan, Nepal, Srilanka, Thailand, etc.)	[53,54,55,66,67,68,69,70,71,72,73,74,75, 76,77,78,79]
6	Australia	[81,82]

4. CONCLUSION

At the local level, Wild edible plants (WFPs) contribute significantly to the diets and livelihoods of millions of people worldwide. Several workers reported the importance of WEPs at the local level, but their national scenario and conservation assessment are not recorded, and thus it fails to convey the full utility of WEPs in food security and as a bioresource. As we do not explore the WEPs fully, their role in mankind is not fully appreciated and they remain neglected. There are limited cases that clearly demonstrate that the contribution of WFPs to food security, nutrition, and livelihoods is significant. Now it becomes a challenge to apply useful strategies for the conservation and sustainable management of WEPs. Further, we are unaware of how the changing climate impacts the WEPs now and in the future. For sustainable management of WEPs, we have to follow the integrated conservation approach. For the same, apart from their nutritional potential, medicinal values, and pharmacological importance must have to be considered to bridge the knowledge gap while strategic planning WEP's sustainable management. Further, it is essential to involve local communities in the conservation process of WEPs so that they could cooperate and will get the maximum benefit out of it.

COMPETING INTERESTS

Authors have declared that no competing interests exist.

REFERENCES

1. Sowunmi MA. The beginnings of agriculture in West Africa: botanical evidence. Curr Anthropol. 1985;26(1):127-9.
2. Johnson A, Behrens CA. Nutritional criteria in Machiguenga food production decisions: A linear- programming analysis. Hum Ecol. 1982;10(2):167-89.
3. Heywood VH. Use and potential of wild plants in farm households; FAO farm system management series. Rome, Italy: Food and Agriculture Organization. 2010;1999. Bharucha Z, Pretty J. The roles and values of wild foods in agricultural systems. Philos Trans R Soc Lond B Biol Sci. 2010;365(1554):2913-26.
4. Bharucha Z, Pretty J. The role and importance of wild foods in agricultural systems. Phil Trans R Soc B. 2010;365 (1554):2913-26.
5. Casas A, Otero-Arnaiz A, Pérez-Negrón E, Valiente-Banuet A. In situ management and domestication of plants in Mesoamerica. Ann Bot. 2007;100(5): 1101-15.
6. Cruz-Garcia GS. Management and motivations to manage "wild" food plants. A case study in a mestizo village in the amazon deforestation frontier. Front Ecol Evol. 2017;5:127.
7. Mishra A, Swamy SL, Thakur TK, Bhat R, Bijalwan A, Kumar A. Use of wild edible plants: can they meet the dietary and nutritional needs of indigenous communities in central India. Foods. 2021; 10(7):1453.
8. Ulian T, Diazgranados M, Pironon S, Padulosi S, Liu U, Davies L, et al. Unlocking plant resources to support food security and promote sustainable agriculture. Plants People Planet. 2020; 2(5):421-45.
9. Asprilla-Perea J, Díaz-Puente JM. Importance of wild foods to household food security in tropical forest areas. Food Sec. 2019;11(1):15-22.
10. Broegaard RB, Rasmussen LV, Dawson N, Mertz O, Vongvisouk T, Grogan K. Wild food collection and nutrition under commercial agriculture expansion in

agriculture-forest landscapes. For Policy Econ. 2017;84:92-101.
11. Ickowitz A, Powell B, Rowland D, Jones A, Sunderland T. Agricultural intensification, dietary diversity, and markets in the global food security narrative. Glob Food Sec. 2019;20:9-16.
12. Ojelel S, Mucunguzi P, Katuura E, Kakudidi EK, Namaganda M, Kalema J. Wild edible plants used by communities in and around selected forest reserves of Teso-Karamoja Region, Uganda. J Ethnobiol Ethnomed. 2019;15(1):3.
13. Rowland D, Ickowitz A, Powell B, Nasi R, Sunderland T. Forest foods and healthy diets: Quantifying the contributions. Environ Conserv. 2017;44(2):102-14.
14. Kuhnlein HV, Erasmus B, Spigelski D. Indigenous peoples' food systems: the many dimensions of culture, diversity and environment for nutrition and health. Rome, Italy: food and agriculture organization of the United Nations; 2009.
15. Kuhnlein HV. Holding on to agrobiodiversity: human nutrition and health of indigenous peoples. In: Hunter D, Guarino L, Spillane C, McKeown PC, editors. Routledge handbook of agricultural biodiversity. London, UK: Routledge. 2017;692.
16. Angelsen A. Policies for reduced deforestation and their impact on agricultural production. Proc Natl Acad Sci U S A. 2010;107(46):19639-44.
17. Powell B, Thilsted SH, Ickowitz A, Termote C, Sunderland T, Herforth A. Improving diets with wild and cultivated biodiversity from across the landscape. Food Sec. 2015;7(3):535-54. .
18. Aryal KP, Poudel S, Chaudhary RP, Chettri N, Chaudhary P, Ning W et al. Diversity and use of wild and non-cultivated edible plants in the western Himalayas. J Ethnobiol Ethnomed. 2018;14(1):10.
19. Smith E, Ahmed S, Dupuis V, Running Crane M, Eggers M, Pierre M et al. Contribution of wild foods to diet, food security, and cultural values amidst climate change. J Agric Food Syst Community Dev. 2019;9;Suppl 2:1-24.
20. Fernández-Ruiz V, Morales P, Ruiz-Rodríguez BM, Isasa ET. Nutrients and bioactive compounds in wild fruits through different continents. In: Wild plants, mushrooms and nuts. Chichester, UK: John Wiley & Sons, Ltd. 2016; 263-314.
21. Hunter D, Borelli T, Beltrame DMO, Oliveira CNS, Coradin L, Wasike VW, et al. The potential of neglected and underutilized species for improving diets and nutrition. Planta. 2019;250(3):709-29.
22. Alwafa RA, Mudalal S, Mauriello G. *Origanum syriacum* L. (Za'atar), from raw to go: A review. Plants (Basel). 2021;10(5):1001.
23. Sibiya NP, Kayitesi E, Moteetee AN. Proximate analyses and amino acid composition of selected wild indigenous fruits of Southern Africa. Plants (Basel). 2021;10(4):721.
24. Kinnunen P, Guillaume JHA, Taka M, D'Odorico P, Siebert S, Puma MJ et al. Local food crop production can fulfill the demand for less than one-third of the population. Nat Food. 2020;1:229-37.
25. Padulosi S, Mal B, King O, Gotor E. Minor millets as a central element for sustainably enhanced incomes, empowerment, and nutrition in rural India. Sustainability. 2015;7(7):8904-33.
26. Shackleton S, Paumgarten F, Kassa H, Husselman M, Zida M. Opportunities for enhancing poor women's socioeconomic empowerment in the value chains of three African Non-Timber Forest Products (NTFPs). Int For Rev. 2011;13(2):136-51.
27. Béné C. Resilience of local food systems and links to food security—A review of some important concepts in the context of COVID-19 and other shocks. Food Secur. 2020;12(4):805-22.
28. Fernandes N. Economic effects of coronavirus outbreak (COVID-19) on the world economy. SSRN Electron J; 2020.
29. Torero M. Without food, there can be no exit from the pandemic. Nature. 2020;580(7805):588-9.
30. Cappelli A, Cini E. Will the COVID-19 pandemic make us reconsider the relevance of short food supply chains and local productions? Trends Food Sci Technol. 2020;99:566-7.
31. Vandebroek I, Pieroni A, Stepp JR, Hanazaki N, Ladio A, Alves RRN, et al. Reshaping the future of ethnobiology research after the COVID-19 pandemic. Nat Plants. 2020;6(7):723-30..
32. Kitessa GB, Tokuma UG. Edible woody plants diversity and potential contribution to food security in Ethiopia. Int J Ecotoxicol Ecobiol. 2022;7(3):37-48.
33. Waheed M, Haq SM, Arshad F, Bussmann RW, Pieroni A, Mahmoud EA et al.

Traditional wild food plants gathered by ethnic groups living in semi-arid region of Punjab, Pakistan. Biology. 2023;12(2):269.
34. Gee E, Borelli T, Beltrame DMO, Oliveira CNS, Coradin L, Wasike V, et al. The ABC of mainstreaming biodiversity for food and nutrition. Concepts, theory and practice. In: Hunter D, Borelli T, Gee E, editors. Biodiversity food and nutrition. A new agenda for sustainable food systems. Abingdon, UK: Routledge; 2020.
35. Borrelli P, Robinson DA, Panagos P, Lugato E, Yang JE, Alewell C et al. Land use and climate change impacts on global soil erosion by water (2015-2070). Proc Natl Acad Sci U S A. 2020;117(36): 21994-2001.
36. Peduruhewa PS, Jayathunge KGLR, Liyanage R. Potential of Underutilized Wild Edible Plants as the Food for the Future – a review. J Food Sec. 2021;9(4):136-47.
37. FAO. The state of the World's biodiversity for food and agriculture. Rome, Italy: Food and Agriculture Organization; 2019.
38. Royal Botanic Gardens, Kew. State of the World's plants. London, UK: Royal Botanic Gardens, Kew; 2016.
39. Díaz S, Settele J, Eduardo B, Ngo HT, Guèze M, Agard J, et al. The global assessment report on biodiversity and ecosystem services. Summary for policymakers. Bonn, Germany: IPBES; 2019.
40. Masson-Delmotte V, Zhai P, Pörtner H-O, Roberts D, Skea J, Calvo E, et al. Climate change and land [IPCC report]. Geneva, Switzerland: IPCC; 2019.
41. Kew. Plants under pressure—A global assessment. London, UK: Royal Botanic Gardens, Kew, UK and Natural History Museum; 2016.
42. Khoury CK, Amariles D, Soto JS, Diaz MV, Sotelo S, Sosa CC, et al. Comprehensiveness of conservation of useful wild plants: an operational indicator for biodiversity and sustainable development targets. Ecol Indic. 2019; 98:420-9.
43. SCBD. Report of the AHTEG on indicators for the Strategic Plan for biodiversity 2011-2020. Montreal: Secretariat of the Convention on Biological Diversity; 2011.
44. Boedecker J, Termote C, Assogbadjo AE, Van Damme P, Lachat C. Dietary contribution of Wild Edible Plants to women's diets in the buffer zone around the Lama forest, Benin-an underutilized potential. Food Sec. 2014;6(6):833-49.
45. Shackleton C, Shackleton S. The importance of non-timber forest products in rural livelihood security and as safety nets: A review of evidence from South Africa. S Afr J Chem. 2004;100:658-64.
46. Ogoye-Ndegwa C. Traditional gathering of wild vegetables among the luo of Western Kenya-a nutritional anthropology project1. Ecol Food Nutr. 2003;42(1):69-89.
47. Shumsky SA, Hickey GM, Pelletier B, Johns T. Understanding the contribution of wild edible plants to rural social-ecological resilience in semi-arid Kenya. Ecol Soc. 2014;19(4).
48. Mulenga BP, Richardson RB, Tembo G. Non-timber forest products and rural poverty alleviation in Zambia. Zambia: Indaba Agricultural Policy Research Institute; 2012.
49. Maundu P. Utilization and conservation status of wild food plants in Kenya. In: The biodiversity of African plants. Springer. 1996; 678-83.
50. Keller GB, Mndiga H, Maass BL. Diversity and genetic erosion of traditional vegetables in Tanzania from the farmer's point of view. Plant Genet Resour. 2005; 3(3):400-13.
51. Tinsae Bahru ZA, Sebsebe D. Wild edible plants: sustainable use and management by in and the buffer area of awash national park, Ethiopia. Ethiopian J Sci. 2013;3:93-108.
52. Tahir M, Abrahim A, Beyene T, Dinsa G, Guluma T, Alemneh Y et al. The traditional use of wild edible plants in pastoral and agro-pastoral communities of Mieso District, eastern Ethiopia. Trop Med Health. 2023;51(1):10.
53. Ugyen J, Gurung T. Assessment of yam (*Dioscorea spp.*) diversity at community level in Nangkor gewog under Zhemgang dzongkhag. J Bhutan Stud. 2015;33.
54. Chhoeda Yangchen U. Wild vegetable diversity and their contribution to household income at Patshaling gewog, Tsirang. Bhutan J Nat Resour Dev. 2017;4(1):30-8.
55. FAO, editor. Non-wood forest products of Bhutan Bangkok, Thailand RAP publication; 1996.
56. Ju Y, Zhuo J, Liu B, Long C. Eating from the wild: diversity of wild edible plants used by Tibetans in Shangri-la region, Yunnan,

China. J Ethnobiol Ethnomed. 2013;9 (1):28.
57. Kang Y, Łuczaj Ł, Kang J, Zhang S. Wild food plants and wild edible fungi in two valleys of the Qinling Mountains (Shaanxi, central China). J Ethnobiol Ethnomed. 2013;9(1):26.
58. Baranov AI. Wild vegetables of the Chinese in Manchuria. Econ Bot. 1967;21(2):140-55.
59. Cheng Z, Lu X, Lin F, Naeem A, Long C. Ethnobotanical study on wild edible plants used by Dulong people in northwestern Yunnan, China. J Ethnobiol Ethnomed. 2022;18(1):3.
60. Sachula G, Zhang, Zhang YY, Zhao H, Khasbagan. *et al*. Wild edible plants collected and consumed by the locals in Daqinggou, Inner Mongolia, China. J Ethnobiol Ethnomed. 2020;16(1):60.
61. Radina K, editor. Booklet. Common useful wild plants in Central Europe. Promoting traditional collection and use of wild plants to reduce social and economic disparities in Central Europe. Budapest, Hungary: TRAFFIC and WWF Verlagsgesellschaft; 2013.
62. Pardo De Santayana M, Pieroni A, Puri RK. Ethnobotany in the new Europe: people, health, and wild plant resources. New York: Berghahn Books; 2010.
63. Tardío J, Pascual H, Morales R. Wild food plants traditionally used in the province of Madrid, Central Spain. Econ Bot. 2005;59(2):122-36.
64. Benítez G, Molero-Mesa J, González-Tejero MR. Wild edible plants of Andalusia: Traditional uses and potential of eating wild in a highly diverse region. Plants (Basel). 2023;12(6):12-8.
65. Łuczaj Ł, Pieroni A, Tardío J, Pardo-de-Santayana M, Sõukand R, Svanberg I et al. Wild food plant use in 21st century Europe: the disappearance of old traditions and the search for new cuisines involving wild edibles. Acta Soc Bot Pol. 2012;81(4):359-70.
66. Barua U, Hore D, Sarma R. Wild edible plants of Majuli island and Darrang districts of Assam. Indian J Trad Knowl. 2007;6(1):191-4.
67. Yesodharan Y, Sujana KA. Wild edible plants traditionally used by the tribes in the Parambikulam wildlife sanctuary, Kerala, India. Nat Prod Radiance. 2007;6(1):7.
68. Tiwari J, Ballabha R, Tiwari P. Some promising wild edible plants of Srinagar and its adjacent area in Alaknanda valley of Garhwal Himalaya, India. J Am Sci. 2010;6(4):167-74.
69. Sundriyal M, Sundriyal RC, Sharma E. Dietary use of wild plant resources in the Sikkim Himalaya, India. Econ Bot. 2004;58(4):626-38.
70. Arora RK, Pandey A. Indian Council of Agricultural Research. National Bureau of Plant Genetic Resources: wild edible plants of India: diversity, conservation, and use. New Delhi: Indian Council of Agricultural Research. National Bureau of Plant Genetic Resources; 1996.
71. Ray A, Ray R, Sreevidya EA. How many wild edible plants do we eat—their diversity, use, and implications for sustainable food system: an exploratory analysis in India. Front Sustain Food Syst. 2020;4:56.
72. Abbasi AM, Khan MA, Shah MH, Shah MM, Pervez A, Ahmad M. Ethnobotanical appraisal and cultural values of medicinally important wild edible vegetables of Lesser Himalayas-Pakistan. J Ethnobiol Ethnomed. 2013;9(1):66.
73. Shaheen S, Ahmad M, Haroon N. Status of edible wild plants in Pakistan: Case studies. In: Edible Wild Plants: An alternative approach to food security. Springer. 2017;65-125.
74. Gajurel PR, Singh B, Kashung S, Adhikary P, Nopi S, Barman R et al. Foods from the wild: a review on the diversity and use pattern of wild edible plants of Arunachal Himalaya for sustainable management. Plant Sci. Today. 2023;10(1):80-9.
75. Talang H, Yanthan A, Rathi RS, Pradheep K, Longkumer S, Imsong B et al. Nutritional evaluation of some potential wild edible plantsof North Eastern region of India. Front Nutr. 2023;10: 1052086.
76. Aryal K, Berg Å, Ogle BM. Uncultivated plants and livelihood support: A case study from the Chepang people of Nepal. Ethnobot Res Appl. 2009;7:409-22.
77. Nirmala J, Siwakoti M, Kehlenbeck K. Developing a Domestication Priority Setting Approach for Wild Vegetable to improve food security in Makanwar District, Central Nepal. Stuttgart-Hohenheim Tropentag. 2013;3.
78. Bhattarai S, Chaudhary RP, Taylor RS. Wild edible plants used by the people of Manang district, Central Nepal. Ecol Food Nutr. 2009;48(1):1-20.

79. Panyadee P, Wangpakapattanawong P, Inta A, Balslev H. Very high food plant diversity among ethnic groups in Northern Thailand. Diversity. 2023;15(1):120.
80. Available:https://www.kuhl.com/borninthemountains/edible-plants-on-the-trails-in-usa.
81. Canning AD. Rediscovering wild food to diversify production across Australia's agricultural landscapes. Front Sustain Food Syst. 2022;6:865580.
82. Fyfe S, Smyth HE, Schirra HJ, Rychlik M, Sultanbawa Y. The framework for responsible research with Australian native plant foods: A food chemist's perspective. Front Nutr. 2021;8: 738627.

© 2023 Shirsat et al.; This is an Open Access article distributed under the terms of the Creative Commons Attribution License (http://creativecommons.org/licenses/by/4.0), which permits unrestricted use, distribution, and reproduction in any medium, provided the original work is properly cited.

Peer-review history:
The peer review history for this paper can be accessed here:
https://www.sdiarticle5.com/review-history/100019

View publication stats

Nanotechnology Perceptions
ISSN 1660-6795
www.nano-ntp.com

Machine Learning for Fraud Detection: Comparative Analysis of Algorithms and Performance Evaluation

Dr. Swapnil G. Deshpande[1], Gopal P. Gawali[2], Ram B Ghayalkar[3], Dr. Santosh Madhusing Chavan[4], Jaykumar H. Meshram[5], Dr. Diwakar Ramanuj Tripathi[6]

[1]Assistant Professor, S.S. Maniar College of Computer and Management, India, swapnildeshpande33@gmail.com
[2]Head, Department of Computer Science, R.A.Arts, Shri M.K.Commerce and Shri S.R.Rathi Science College, India, gawali.gopal@rediffmail.com
[3]Assistant Professor, Sri R. L. T. College of Science, Akola, India, rambg29@gmail.com
[4]Assistant Professor, Shri Shivaji Art's Commerce and Science College, Akola, India, santoshchavan9881@gmail.com
[5]Research Scholar, smt Narsamma Arts commerce and Science College, Amravati, India, jaykumarmeshram1996@gmail.com
[6]HOD/Assistant Professor, PGTD Computer Science, S.S. Maniar College of Computer and Management, India, drtcomptech@live.com

One type of fraud involves using another customer's credit card account to secure or get loans. By creating credit card exchanges with the knowledge of those that have been fraudulent, the Credit Card fraud detection project recognizes the fraudulent notion of the new exchange. Such unethical actions can have an impact on a large number of people worldwide due to the data fraud and financial shortage. The financial sector is more at risk from crime, which is arriving at recommendations. Data extraction appeared to have been anticipated to be a crucial task in the recognition of online instalment fraud because the effectiveness of fraud detection in credit card purchases is significantly influenced by the informational collection estimating methodology, the choice of variable, and the detection procedures used. This distribution assesses the performance of Backing Vector Machine, Guileless Bayes, Strategic Relapse, and K-Closest Neighbour on highly distorted data on credit card fraud. These techniques must be carried out with precision, awareness, accuracy, and explicitness. The overall results demonstrate that strategic relapse outperforms other algorithms.

Keywords: Machine Learning, Fraud Detection, Comparative Analysis, Performance Evaluation, Algorithms, Credit Card fraud.

1. Introduction

Theft of credit cards is a growing, serious problem that costs banks and card issuer cooperatives a tremendous amount of money. Banking institutions combine a variety of security measures in an effort to prevent account abuse. As security measures get significantly more complex, fraudsters become more skilled; for instance, they gradually alter their tactics. Therefore, improving fraud detection and counteraction techniques It is crucial to use security modules that aim to prevent fraud. Fraud detection has evolved into a crucial step toward reducing the negative impact on the provision of services, prices, and the reputation of the organization of fraudulent trades. With the aim of maintaining excellent administration, there are numerous methods for spotting fraud. great assistance performance while reducing to a minimum the number of passings. Fraud is expensive, and before the data is discovered, fraud detection can cost a fortune. The structure is incredibly exact and doesn't emphasize many unfounded warnings. Genuine proactive handling, according to Edge and Falcone Pre-decisional, significantly reduces the amount of time available for PC processing and the precise decision made in light of new exchanges. The proactive techniques also increase the likelihood of early fraud warnings.

A framework for detecting fraud should be as quick as possible. Frameworks for detecting fraud are developed using historical exchange data to select new ones. This preparation method is typically compared to. Processing time can be reduced by reducing the number of previous exchanges handled by avoiding a time period with less complicated techniques.

Any attempt to use the cardholder's information without their knowledge or consent is considered credit card fraud and is considered illegal behaviour. Credit cards can be used in two different ways: online fraud, which can be discovered through mobile devices, the internet, and online purchasing, and offline fraud, which can identify a card that has been stolen by using the perpetrator's personal details. Credit card fraud is one of the vindictive acts that happen in a web-based commerce. Unauthorized use of a credit or charge card to make instalment payments is referred to as credit card fraud frequently. In essence, these are the fictitious sources of assets that are employed in various exchanges. With the growth of online commerce, credit card use and acceptance for online purchases as well as other payments have increased. Customers are increasingly relying on the well-known credit card instalment plan today to pay their payments and conduct beneficial online purchasing. Credit card fraud is growing daily in tandem with their increased use, causing a global catastrophe as a single fraud can result in a significant number of catastrophes. Fraud is happening at an alarming pace as a result of innovations on the increase and the ensuing significant financial loss. A person's credit or charge card may really be confiscated, or credit card details, like the cardholder's name, card number, expiration date, GOT code, etc., may have been compromised. are directly taken from an actual credit card. From the many datasets, fraud detection predicts if something is fraudulent or not. The deluge of information is recognized by several fraud detection systems, which then study fraud schemes. To distinguish these workouts, numerous machine learning models have been developed. There are a number of reasons why machine learning algorithms can't resolve the problem completely.

2. Literature Review

Sonal Mehndiratta and others In this study, various techniques for detecting credit card fraud are examined and held to particular standards. Here, predictive analysis techniques can be applied to acquire verified data in order to spot fraud. Here, a variety of techniques are used, including Counterfeit Brain Organization, Stowed away Markov Model, Hereditary Calculation, Innocent Bayes, and KNN classifier. In this study, credit card fraud detection is mostly accomplished using the two steps of highlight extraction and grouping, and a half-breed strategy is chosen to be used in the future.

Zarrabi and co. The developer suggests Profound Auto encoder, which performs as the best extraction of the finer points of the credit card fraud exchange's highlights. The author used softmax devices in this case to address class mark concerns. Here, an AutoEncoder is used to map the data into a highly layered space for the purpose of sorting a specific type of fraud. Deep learning is one of the greatest methods for identifying credit card fraud, it may be mentioned. Understanding the distinctive way that information is distributed among the various organizational kinds becomes challenging. Organizations used Profound Auto encoder to extract the greatest informational components with a high degree of precision and little variation.

Al-Khatib, Adnan M. The separation of honest transactions from dishonest transactions frequently has the downside of making fraud detection more difficult. Fraud detection includes observing the dishonest behavior of customers and clients in order to identify, separate, or get away from annoying behavior. In today's world, using credit cards is commonplace. The engineer is also investigating a few issues related to credit card fraud detection. Brain Organizations, Hereditary Algorithms (GAs), Rule acceptance, Master frameworks, Case-based thinking (CBR), Inductive rationale programming (ILP), Relapse, Man-made consciousness, and other cutting-edge fraud detection techniques have all been used by the research laborer to identify shady transactions. Comparative focus on information mining techniques are used to spot dishonest inclusion and obtain a low fake problem rate. This study demonstrates the use of several computational procedures to obtain bigger expense reserve funds.

To create a three layer backpropagation ANN, RaghavendraPatidar et al. used a dataset with hereditary algorithms (GA) for the identification of credit card fraud. In this analysis, the organization design, location, number of secret layers, and number of hubs inside each layer were managed by hereditary algorithms.

The research of the outcomes of a few classifier-examining procedures when applied to the informative collection on credit card fraud, when classes are imbalanced, was done by Dilip Singh Sisodia et al. 28 essential parts were found in the information using head part analysis (PCA) for real data with the factors time, amount, and class. From the three datasets we used, we were able to access 10,000, 15,000, and 20,000 times. The researchers looked into five over-testing procedures and four under-inspecting strategies independently. Few expensive delicate and gathering classifiers are used.

Guanjun Liu and others. Here, the author used two different types of erratic woodlands to instruct how to conduct honest and dishonest transactions in order to examine each separately

for the purpose of a classifier and perform on the identification of credit card fraud. The data used to examine the performance of those 2 types of irregular wood models is in partnership with a web-based commercial organization in China. To identify duplicitous B2C datasets used by the authors in this paper. The use of an arbitrary Woodland classifier, which improved results only on small datasets and cannot handle imbalanced datasets, is inefficient because fraud datasets are typically uneven.

A. Roy et al. suggested a sophisticated learning method for identifying fraud swaps. Exchanges of 80 million have been reported as fraudulent. To achieve outstanding performance, they made use of cloud-based climate. A dep learning technique with adjusting boundary for shady trades identification has been completed by the scientists, helping to build the financial foundation for the enforcement of legal procedures.

A cutting-edge procedure that includes installment of solicitations or invoices was proposed by Dastgir Pojee and colleagues. The "No Money" cell phone program is the name of this tactic, which is primarily used by merchants who may enable customer installment services. The NFC-Enabled Retail location (PoS) Machines Approach is not necessary in the current situation; only phones are needed. This architecture was designed to limit the clients' need to bring their cards and to provide a straightforward approach for making payments. Due to the growth in the number of NFC-enabled cell phones, the program No Cash, which has a few highlights, is utilized, which enhances the customer's buying experience. Clients of the application can make references to the historical context of the cost, and exorbitant charges will be reduced.

3. Experimental Methodology

The techniques and methods utilized to analyze the dataset that was used to develop the model, as well as the four machine learning review procedures—Backing Vector Machine, Credulous Bayes, K-Closest Neighbor, and Calculated Relapse—are explained in this section. Data collection, management, evaluation, classifier calculation, and evaluation—division of the data into train set and test set—were among the numerous stages of the trial.

After receiving the separated data, the classifier's framework is formed, and the test is then assessed using disarray lattice estimation rates.

3.1 Dataset

Out of the Kaggle Machine Learning stage, the dataset appears [24]. The 3075 interactions in this dataset are presented as 12 exchange items in a CSV record. The key nuances and foundational information cannot be introduced because of privacy concerns. The components include the daily average of exchange, exchange amount, whether it has dropped or not, whether it is an unknown exchange or not, if it is high-risk, and the half-year normal equilibrium in the dataset. The "is fraudulent" highlight, which has priority Y for illegal activity (fraud) and N for legal activity (not fraud), may be the mark for the Boolean evaluation.

3.2 Logistic Regression:

The computed relapse computation makes use of the sigmoid and strategic relapse capabilities

to perform paired grouping in light of the various dataset components. The following is a presentation of the sigmoid capability:

$$y^i = \frac{1}{1 + e^{-(Z)}} \qquad (1)$$

To find a paired order likelihood, the Sigmoid capability is used. In this instance, z represents the log-chances of the model, and y is the likelihood of the output.

$$z = b + m_1x_1 + m_2x_2 + m_3x_3 + \ldots\ldots\ldots\ldots m_{\cap}x_{th} \qquad (2)$$

Where m stands for the weighted traits and predisposition, x stands for the highlighted qualities, and b is the direct relapse capture. The sigmoid capacity predicts the likelihood of a given outcome.

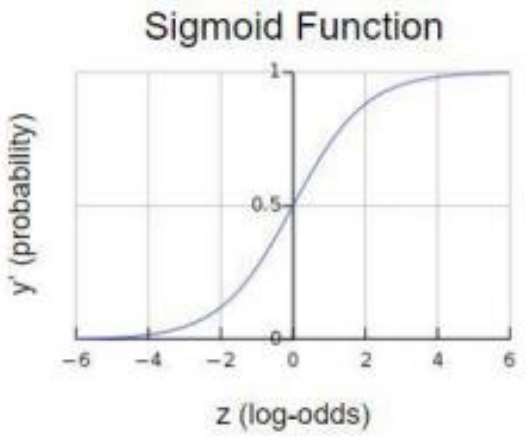

Figure 1: graph of the logistic regression's sigmoid function

Any number greater than this edge is seen as 1, and any value less than this edge is obviously regarded as 0. There is a maximum of 0.5. Strategic relapse is used to characterize paired events as either 1 or 0.

3.3 K-Nearest Neighbor (KNN):

The K-closest neighbour computation is an order calculation that predicts the properties of various educational highlights based on its relative position. Based on estimations of comparability such the Manhattan distance and Euclidean distance, it is categorized. It is expected that the pertinent preparation set data that is closest to the test point in Euclidean space would have the same cryptic property as the test point. Using the Euclidean distance metric, the KNN classifier is employed in this review. The distance between the two-point vectors of Euclidean (EC's) geometry (x1) is not fixed by:

$$EC = \sqrt{\sum (X_1 - X_2)^2} \qquad k = 1,2,\ldots\ldots,n \qquad (3)$$

Manhattan distance measure is a measurement where the distance between two focuses (xi, yi) and (xn, yn) is the outright contrast of their Cartesian direction.

$$M = (x_i - x_n) + (y_i - y_n) \quad (4)$$

3.4 Naïve Bayes:

Trustworthy Bayes classifiers rely on the Bayes hypothesis, which selects the most notable likelihood-based option. Bayesian likelihood measurements are based on known probabilities and values.

The calculation is a directed machine learning calculation, and

$$P(A|B) = \frac{p(B|A).\,p(A)}{P(B)} \quad (5)$$

The Bayes hypothesis provides a method for calculating the likelihood of a result (A) given specified circumstances (B), or the back-probability P (A|B).

With almost no knowledge of compelling circumstances, the hypothesis calculates the later likelihood by relating it to the past likelihood of the result using the likelihood proportion P (B|A) = P (B).

The guileless bayes hypothesis is predicated on the knowledge that each element effects the outcome independently and is thus gullible. A technique for identifying fraudulent credit card exchange is the guileless bayes classifier.

3.5 Support Vector Machine

Examples of directed learning techniques that can be applied to grouping and relapsing issues include support vector machines. A helper vector machine will choose the most precise data grouping technique.

A distinct hyper-plane legally classifies a help machine (SVM) as a biased classifier. As a result, the calculation that categorizes fresh models delivers an optimum hyper-plane given the marked preparation. A plane that lies on one side or the other in each class of a two-dimensional space is divided into two portions by a line known as a hyperplane.

Information concentrations on one side of the hyper-planes are said to be non-fraudulent, whilst information concentrations on the other side are said to be fraudulent. In the figure above, both hyper-plane successfully segregate the data that fraudsters are interested in, but the better hyper-plane will achieve a comparable degree of accuracy when it is necessary to group unrelated data.

This decides on the ideal hyper-plane based on the line distance as depicted in picture 2. Support vector machines split the class at the points on either side that are closest to them. Help vectors relate to the edge at this distance and the edge point.

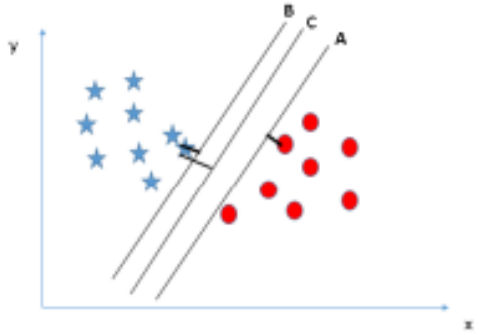

Figure 2: Static Vector Machine

4. Evaluation and Result

We concentrated on two different methods to assess these machine learning models:

(1) Classification accuracy, as determined by condition 6, is the proportion of accurate predictions to all information examined. However, if each class has an equal amount of assessments, this is quite effective.

$$\text{Accuracy} = \frac{\text{number of correct prediction}}{\text{total number of predicted made}} \qquad (6)$$

(2) Confusion Matrix: This produces a network as a consequence and illustrates how well the model performed overall. Genuine Positive Proportion (TPR), Genuine Negative Proportion (TNR), Bogus Positive Proportion (FPR), and Misleading Negative Proportion (FNR) rates metrics independently are the four primary estimations that are utilized to evaluate the tests.

P and n are the unmistakable benefits of the positive and negative class cases that are being decided because the amounts described by obvious positive, bogus positive, genuine negative, and misleading negative analyses are genuine positive, genuine negative, misleading positive, and bogus positive, respectively.

Genuine positive classes are those that are both supposed to be and actually are positive, whereas genuine negative classes are those that are both expected to be and actually are negatively. Classes that should be negative but are positive instead are known as false positives, while classes that should be certain but are assumed to be negative are known as misleading positives.

In terms of exactness, responsiveness (review), particularity, and accuracy, the efficacy of the assist vector machine, credulous bayes, k-nearest neighbor, and calculated relapse classifier is assessed.

Table 1: Confusion Matrix Table

Actual no of sample	Predicted No	Predicted Yes
Actual No	True Negative	False Positive
Actual Yes	False Negative	True Positive

Equation 7 states that exactness is defined as the ratio of the number of genuine occurrences of the positive and negative to the number of many expected examples.

$$\text{Accuracy} = \frac{\text{TP} + \text{TN}}{\text{TP} + \text{TN} + \text{FP} + \text{FN}} \qquad (7)$$

Awareness, also called examine, is the proportion of accurate positive forecasts to the total of inaccurate negative and accurate positive forecasts. The review evaluates the program's success by counting the number of really good outcomes that were noted. According to equation 8.

$$\text{Sensitivity (recall)} = \frac{\text{TP}}{\text{TP} + \text{FN}} \qquad (8)$$

What jumps out is the ratio of actual negative to the total of actual negative and fictional positive.

$$\text{Specificity} = \frac{\text{TN}}{\text{TN} + \text{FP}} \qquad (9)$$

Accuracy is defined as the ratio of the total number of real positive results to the total number of real positive results and fake positive results. It is possible to say that being the fraction of the nature of positive input data can be said. Equation 10 is where you should be looking to find the equation for accuracy.

$$\text{Precision} = \frac{\text{TP}}{\text{TP} + \text{FP}} \qquad (10)$$

In the course of this investigation, four distinct calculation frameworks are developed. These frameworks are dependent on the following: strategic relapse, svm, guileless bayes, and kclosest neighbor. While 80% of that analogous example is put toward planning and evaluating the strategy, the remaining 20% is set aside for testing and learning from mistakes. The concepts of particularity, precision, exactness, and responsiveness are brought into play when evaluating the performance of the classifiers.

Table 2: Table of comparisons for the four different classifiers

Metrics	Classifiers (%)			
	Support Vector Machine	K-nearest Neighbour	Naïve Bayes	Logistic Regression
Accuracy	86.42%	85.82%	84.88%	88.163%
Sensitivity	86.65%	98.25%	1%	200%
Specificity	86.42%	89.28%	200%	89.83%
Precision	94.2%	98.25%	200%	82.53%

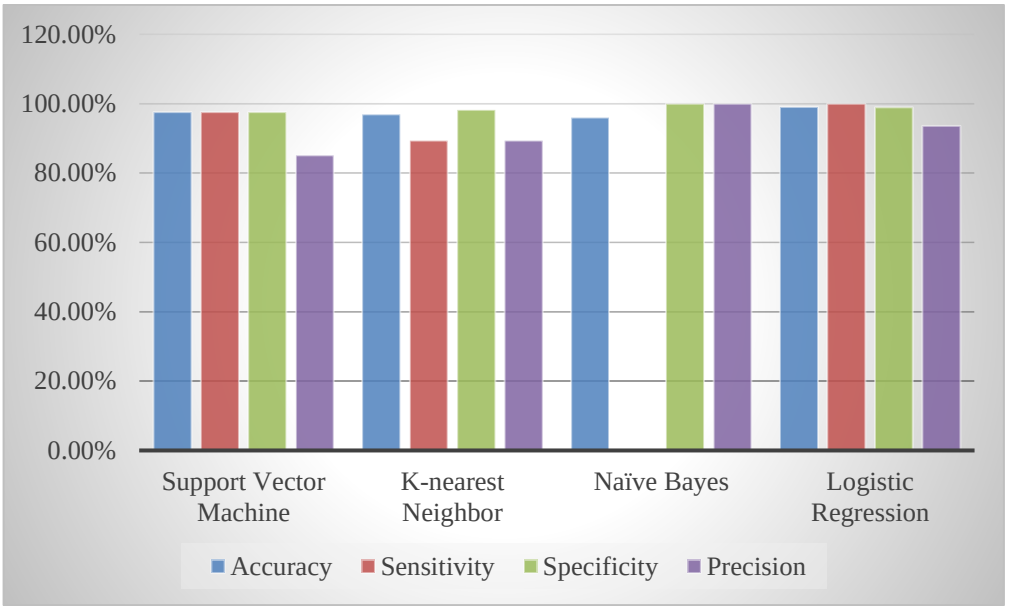

Figure 3: Graph showing the differences between the four classifiers

The efficiency of each of the four models for data designation is compared and contrasted in Table 2, which can be found above. This data assignment demonstrated the effectiveness that is better founded in reality. The method of calculated relapse had the highest degree of accuracy in terms of results across all of the evaluation measurements that were used.

5. Conclusion

In the past ten years, the strategies for detecting fraudulent use of credit cards have come into prominence thanks to the development of factual models, machine learning algorithms, and information mining technologies. The comparative examination of machine learning algorithms for the detection of fraud provides crucial experiences into the performance and viability of the algorithms. The investigation demonstrates that different algorithms exhibit varying degrees of exactness, responsiveness, explicitness, and accuracy when it comes to spotting fraudulent activities. The Help Vector Machine demonstrates a high level of exactness and explicitness, but the K-closest Neighbour algorithm achieves a respectable harmony between preciseness and responsiveness. Calculated Relapse performs astonishingly well across all measurements, while Gullible Bayes is successful in explicitness but has lesser awareness. These discoveries highlight how important it is to evaluate fraud detection systems while taking a variety of measurements into consideration. The article discusses the significance of machine learning in the detection of fraud and draws attention to the importance of selecting the appropriate computation in consideration of specific requirements. In order to increase the accuracy and productivity of fraud detection systems, further research in this area can concentrate on honing algorithms, looking into different techniques, and compiling new information sources.

References

1. Adnan M. Al-Khatib "Electronic Payment Fraud Detection Techniques", World of Computer Science and Information Technology Journal (WCSIT) ISSN: 2221-0741 Vol. 2, No. 4, 137-141, 2012.
2. Bahnsen, A. C., Stojanovic, A., Aouada, D., & Ottersten, B. (2014). Improving credit card fraud detection with calibrated probabilities. In Proceedings of the 2014 SIAM International Conference on Data Mining (pp. 677-685).
3. Data Analytics vs Data Science: Two Separate, but Interconnected Disciplines, Data Scientist Insights, 28-Apr-2018.
4. J. Steele and J. Gonzalez, Credit card fraud and ID theft statistics, CreditCards.com.
5. K. Ratna Sree Valli, P. Jyothi, G.Varun Sai, R. Rohith Sai Subash (2020), "Credit card fraud detection using Machine learning algorithms, Quest Journals Journal of Research in Humanities and Social Science Volumn 8, Issue 2 (2020) pp: 04-11 ISSN(Online): 2321-9467
6. Khyati Chaudhary, Jyoti Yadav, Bhawna Mallick, "A review of Fraud Detection Techniques: Credit Card", International Journal of Computer Application, Volume 45- No.1 2012.
7. Maes, S., Tuyls, K., Vanschoenwinkel, B. and Manderick, B., (2002). Credit card fraud detection using Bayesian and neural networks. Proceeding International NAISO Congress on Neuro Fuzzy Technologies.
8. Ogwueleka, F. N., (2011). Data Mining Application in Credit Card Fraud Detection System, Journal of Engineering Science and Technology, Vol. 6, No. 3, pp. 311 – 322
9. Patil, S., Somavanshi, H., Gaikwad, J., Deshmane, A., and Badgujar, R., (2015). Credit Card Fraud Detection Using Decision Tree Induction Algorithm, International Journal of Computer Science and Mobile Computing (IJCSMC), Vol.4, Issue 4, pp. 92-95, ISSN: 2320-088X
10. R. Harrow, Is Your Credit Card Less Secure Than Ever Before? Forbes, 20-Apr-2018.
11. RamaKalyani, K. and UmaDevi, D., (2012). Fraud Detection of Credit Card Payment System by Genetic Algorithm, International Journal of Scientific & Engineering Research, Vol. 3, Issue 7, pp. 1 – 6, ISSN 2229-5518
12. Seeja, K. R., and Zareapoor, M., (2014). FraudMiner: A Novel Credit Card Fraud Detection Model Based on Frequent Itemset Mining, The Scientific World Journal, Hindawi Publishing Corporation, Volume 2014, Article ID 252797, pp. 1 – 10.
13. Singh, G., Gupta, R., Rastogi, A., Chandel, M. D. S., and Riyaz, A., (2012). A Machine Learning Approach for Detection of Fraud based on SVM, International Journal of Scientific Engineering and Technology, Volume No.1, Issue No.3, pp. 194-198, ISSN: 2277-1581
14. Sonal Mehndiratta and K. Gupta (2018), "Credit Card Fraud Detection Techniques: A Review, :IJCSMC, Vol 8, Issue 8, August 2019.
15. Zarrabi, H. Kazemi, "Using deep networks for fraud detection in the credit card transactions, "IEEE 4th International Conference In Knowledge-Based Engineering and Innovation (KBEI), pp. 0630-0633, 2017

Research on Chemical Intermediates
https://doi.org/10.1007/s11164-023-05169-2

New aroyl heterocyclic (*E*)-*N*′-((2-hydroxynaphthalen-1-yl)methylene)-4-oxopiperidine-1-carbohydrazide and its metal complexes: synthesis, spectroscopic, thermal, DFT, molecular docking and antimicrobial studies

Gajanan Dongare[1] · **Anand Aswar**[2]

Received: 11 September 2023 / Accepted: 16 October 2023
© The Author(s), under exclusive licence to Springer Nature B.V. 2023

Abstract

In order to resist the growth of human pathogenic microorganisms, a new N-heterocyclic ligand of (*E*)-*N*′-((2-hydroxynaphthalen-1-yl)methylene)-4-oxopiperidine-1-carbohydrazide was synthesised from the condensation reaction of 4-oxopiperidine-1-carbohydrazide and 2-hydroxynaphthalene-1-carbaldehyde in ethanol. Reaction of metal salt of $(M(II/III)\cdot Cl_2)\cdot nH_2O$ M = Cr(III), Fe(III), Mn(II), Co(II), Ni(II) and Cu(II) with ligand resulted in the formation the two types of complexes $[M(III)C_{17}H_{19}N_3O_5Cl]$ and $[M(II)C_{17}H_{20}N_3O_5Cl]$ which adopted octahedral geometry. The ligand was thoroughly characterized by elemental analysis, FT-IR, UV–Vis, NMR (^1H, ^{13}C) and HR-mass spectroscopy while the structure of metal complexes was confirmed on the basis of elemental analysis, UV–Vis spectra, molar conductivity, magnetic susceptibility, and TGA-DTA analysis. The ligand behaves as dibasic tridentate, linkages via phenolic-O, azomethine-N, enolic-O atoms in metal (III) complexes and as monobasic tridentate in metal (II) complexes. The decomposition pattern were ascertained by TG analysis, and kinetics accountability from Coats–Redfern relation. The compounds were excited at $\lambda_{ex} = 380$ nm and observed intense emission intensity at $\lambda_{em} = \lambda 527–533$ nm. SEM analysis was performed to observe their surface analysis. The molecular geometry optimization and quantum chemical properties have been retrieved from DFT. ADMET score have been predicted as a drug-likeness prospect from admetSAR. The molecular docking outcomes revealed the good binding score of ligand with Adenylate kinase, Peptide deformylase (bacterial enzymes) and DNA polymerase (fungal enzyme). The in vitro antimicrobial

✉ Anand Aswar
aswaranand@gmail.com

Gajanan Dongare
infogmdongare@gmail.com

[1] Department of Chemistry, Shri Shivaji College of Arts, Commerce & Science, Akola 444001, MS, India

[2] Department of Chemistry, Sant Gadge Baba Amravati University, Amravati 444602, MS, India

Published online: 09 November 2023

potency of ligand and its metal complexes were carried against the bacterial species (*Escherichia coli*, *Salmonella typhi*, *Staphylococcus aureus, Bacillus substilis*), and fungal species (*Candida albicans*, *Aspergillus niger*) and showed their promising activity.

Graphical abstract

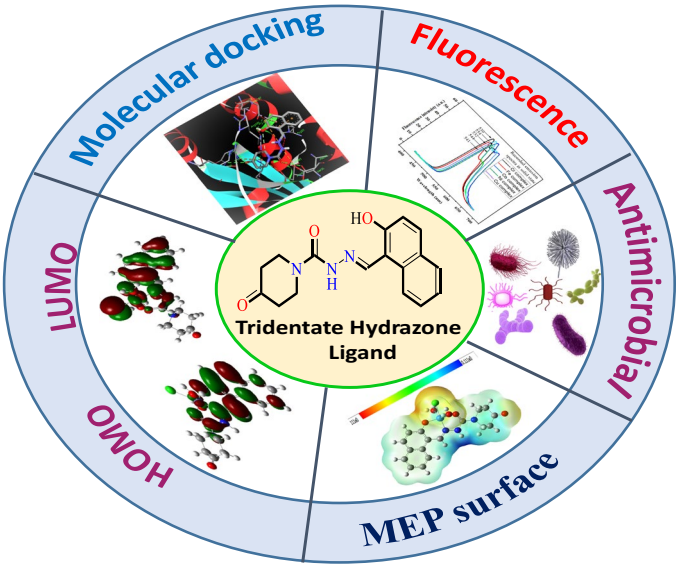

Keywords Aroyl hydrazone · Density functional theory · Fluorescence · Molecular docking · Thermo-kinetics · Antimicrobial evaluation

Introduction

The aroyl tridentate hydrazones are a distinctive class of ligands (triatomic moiety (>C=N–N–C<) possesses flexible donor azomethine (>HC=N–) group that are effective metal ion chelators. They are perfect pioneers in biological, catalytic potential, increasing efficacy and decreasing toxicity. The structural motifs of aroyl hydrazone have been verified by their multifunctional potential in drug-design, favourable catalytic and ultra-trace detection of elements in biological samples [1–3]. In recent years, there is an enhanced interest in the chemistry of hydrazones and their complexes due to their wide range of antidepressant [4], antibacterial, antiviral, antifungal, analgesic, anti-inflammatory, anticonvulsant and antimalarial activities [5, 6]. The core structure of hydrazone ligand contains the nucleophilic imine, amino nitrogen, imine carbon (electrophilic and nucleophilic nature), and intrinsic character of (>C=N–) bond are played the distinctive role in various potential activities [7]. The functional diversity of aroyl hydrazone ligands are responsible for their

pharmacological as well as biological potentials, viz., tuberculosis, antitumoral [4, 8] anticoagulant, antiplatelet [9], and enzymatic inhibitors [10]. The structural tautomerism of hydrazone ligand is also responsible for enhancing their flexibility in donation (ONO) and capable to stable metal complex synthesis. A ligand system having electronegative atoms like nitrogen, oxygen, sulphur and halide atoms also enhances the coordination possibilities [11, 12]. Further, the hydrazone Schiff bases also exhibit numerous biological applications, such as insecticides, herbicides, rodenticides, nematicides and plant growth regulators [13]. Compared with simple hydrazone Schiff bases, aroyl or heteroaroyl Schiff base ligands have additional donor sites which introduces a wider range of properties for these molecules [14]. To the best of our knowledge, there is no such report was found in the literature on synthesis of aroyl hydrazone bearing 4-oxopiperidone moiety and therefore our interest has been grown up to synthesis of importance associated hydrazone ligand and its metal complexes. Such tridentate ligand displayed their better coordinating properties with metal ions showing the pharmacological potential, fluorescence, thermo-kinetic stability. Furthermore, the aroyl hydrazones ligands demonstrated a paramount role in the field of medicinal chemistry as the iron chelators in vivo as well as in vitro for the iron overload treatment. The excellent biological sensitivities of aroyl hydrazones and their mode of chelation with transition metal ions present in living systems have been of significant interest. Additionally, aroyl carbohydrazone are known to have strong chelating properties resulting in the several geometries, e.g. bidentate to multidentate linkages via ONO and N_2O_4, NO donor system. The metal complexes of Mn(II)L, Co(II)L, Ni(II)L, Cu(II)L and Cr(III) L and Fe(III)L have been displayed role in the various diseases belonging to the antioxidant, DNA and cytotoxicity [15]. Therefore, it is envisaged that the 4-oxopiperidone moiety involving in the hydrazide, (*E*)-*N*′-((2-hydroxynaphthalen-1-yl) methylene)-4-oxopiperidine-1-carbohydrazide ligand (H_2L,C) (Scheme 1) and its metal complexes would result in compounds of interesting biological activities. Consequently, in the light of the foregoing details and as a continual of our work on the synthesis of Schiff base complexes, here we report synthesis, spectroscopic characterization, thermal behaviours and the antimicrobial susceptibility of Cr(III) L, Fe(II/III)L Mn(II)L, Co(II)L, Ni(II)L and Cu(II)L complexes with above ligand. DFT calculation has made to confirm the molecular structures and to determine the quantum chemical parameters. Moreover, in silico molecular docking has been used to determine possible binding interaction of the ligand with gram-positive bacteria (*E. coli*) and fungal protein. In addition to above, an in silico-ADMET prediction has also been presented for the development of future potential research, pharmacological applications and drug developments.

Experimental

Materials

The analytical grade reagents of 1-methylpiperidin-4-one (≥98%), 1-Chloroethyl carbonochloridate (≥95%) from, 2-hydroxynaphthalene-1-carbaldehyde (≥98%)

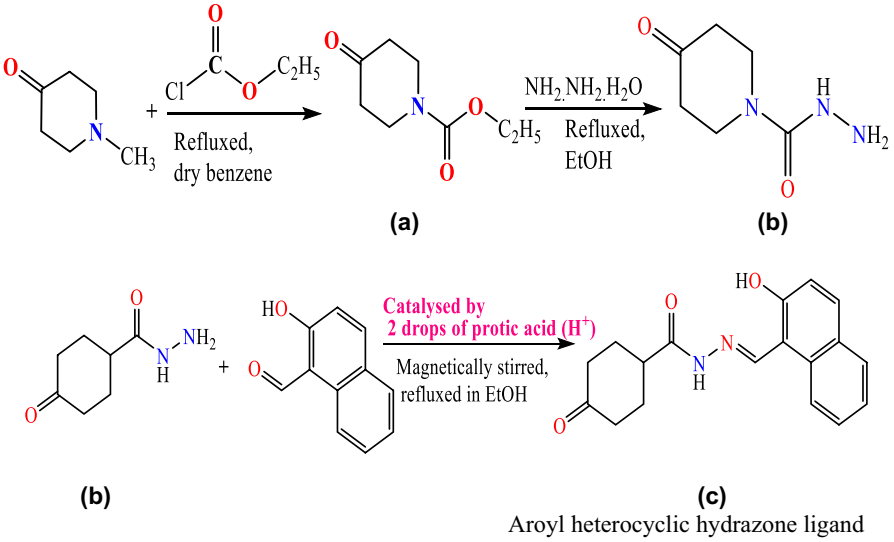

Scheme 1 Synthesis of ethyl 4-oxopiperidine-1-carboxylate (**a**), 4-oxopiperidine-1-carbohydrazide (**b**) and (*E*)-*N*′-((2-hydroxynaphthalen-1-yl)methylene)-4-oxopiperidine-1-carbohydrazide ligand (H_2L, **c**)

were purchased from Fischer Scientific Ltd India, TCI Chemicals Ltd. India, Alpha Aesar (Great Britain) respectively. The metal salts of chromium chloride hexahydrate, manganous chloride tetrahydrate, ferric chloride hexahydrate, cobalt chloride hexahydrate, nickel chloride hexahydrate, copper chloride dihydrate (≥ 95%) and hydrazine monohydrate (≥ 98%) purity were purchased from SD fine Chem (India). The doubly distilled solvent were used for the present works. The pre-coated silica gel (Merck's silica plates 60 F254) of aluminum plates TLC plate was used for completion of reaction and visualized under the UV (255 nm) radiation.

Instrumentation

The elemental analysis of (C, H, N) of ligand and metal complexes were performed on an elemental analyzer (Carlo Erba-1108). The metal contents of the complexes were estimated by gravimetric method by decomposing the organic matter by $HClO_4$: H_2SO_4: HNO_3 (1:1.5:2.5) and later to ignite until they form their respective metal oxide. The molar conductance of complexes was measured in DMSO (10^{-3} M) from the Elico conductivity meter (180). IR spectra were recorded on a Bruker advance FT-IR spectrometer. The magnetic susceptibilities were measured on Sherwood magnetic susceptibility balance (MK-1) of complexes in the solid phase at RT. (^{1}H NMR, ^{13}C NMR) spectra were recorded on the Bruker advance-II Neo NMR spectrophotometer of 500 MHz in DMSO-d_6 solvent and TMS as an internal standard. Mass spectrum was recorded on water micromass (Q-T) spectrophotometer. The UV–visible electronic absorption spectra were recorded on a Shimadzu Spectrophotometer (1800). The ESR spectrum of Cu(II) complex was measured on JES-FA200

in 77 K (− 196 °C) in liquid N_2 atmosphere having an X band at std. freq. of (8.75–9.65 GHz) for precise tensor values. The simultaneous thermogravimetric (TGA-DTA) analysis were carried out on Perkin-Elmer TGA-4000 analyzer in (N_2) atmosphere in the temperature range of 40–750 °C maintaining of a heating rate 20 °C/min (precision of ± 0.8–0.9 °C), digitally uploaded 0.21–22 µg. The powder X-ray diffraction was performed on a Rigaku Miniflex (600) X-ray diffractometer using a target source of CuK_α radiation = 1.5405 Å, scan capacity (10°–80°) pertaining the scan-axis $2\theta/\theta$. The surface morphology of ligand and its complex was captured using a JEOL-6390LV scanning electron microscope. The fluorescence emission spectra were recorded on Fluorescent spectrophotometer (FS) Hitachi F-7000.

Density functional theory calculations

All DFT calculations were retrieved by using Gaussian *09* program with a basis set of functional B3LYP/6–311G++d, p (organic ligand) and LanL2DZ method (metal complex). Gauss View 6.0.16 was utilized for preparative input files towards significant data, and (3D) graphical interface for MEP surface.

ADMET parameters

The ADMET properties, including five parameters such as absorption, distribution, metabolism, excretion, and toxicity were predicted from admetSAR a user-friendly interface tools and bioavailability were predicted by subjecting to computations over Molinspiration cheminformatics tool.

Molecular Docking analysis

The 3D crystallographic structures of *Escherichia coli* protein of peptide deformylase, adenylate kinase and fungal protein of DNA polymerase have been retrieved from the database of RCSB protein data bank (PDB). The preparation of proteins was performed on CHARMM force fields generator. Autodock 4.2.6 was used for molecular docking experiments. Discovery Studio 2.0 (Accelrys, USA) was employed in silico and post docking visualization.

Synthesis of ethyl 4-oxopiperidine-1-carboxylate

To the round flask, 1-methylpiperidin-4-one (2.067 g, 0.02 mol) was added drop wise to a boiling solution of 1-chloroethyl carbonochloridate (2.485 g, 0.02 mol) in 50 ml dry benzene in the course of 50 min with continuous stirring. The reaction mixture was continuously stirred for a ~ 1 h and then refluxed further for 6 h. The progress of reaction was routinely monitored by TLC (70:30 mixtures of n-hexane and ethyl acetate). The benzene was evaporated in rota vapour. The yellow product of ethyl 4-oxopiperidine-1-carboxylate (**a**) was collected with yield: 4.146 ml (85.50%), and boiling point was ~ 138–139 ^{0}C according to reported

literature [16]. The miscibility in common organic solvent, pH recorded ~ 4.6, density 1.4716 /ml at 25 °C and slightly miscible in water (Scheme 1a).

Synthesis of 4-oxopiperidine-1-carbohydrazide (OPCH)

To a hot stirred ethanolic solution (25 mL) of ethyl 4-oxopiperidine-1-carboxylate (a) (3.88 g, 0.020 mol) was add to hydrazine monohydrate solution (1.0302 g, 0.020 mol). The reaction mixture was refluxed for 24 h. The progress reaction was continuously monitored by TLC in (70:30) n-hexane and ethyl ethanoate. The product of 4-oxopiperidine-1-carbohydrazide (Scheme 1b) was isolated filtration by vacuum suction and recrystallized by aprotic solvent DMSO. The solubility was observed in the solvents of ethanol, DMF and DMSO. The off white solid product obtained was dried under vacuum over $CaCl_2$ in desiccator. Yield: (4.143 g), 84.35%. M.P.:78–80 °C. The structure of hydrazide was confirmed by C-H-N-S analyser, FT-IR and NMR (^{1}H and ^{13}C) spectroscopy.

Micro-analytical data of 4-oxopiperidine-1-carbohydrazide

Color: Off white, mol.wt. = 311.34 (g/mol), yield: 0.4935 g (75%). M.P.: 240–242 °C. Elemental Analysis for $C_6H_{11}N_3O_2$ (%): Calc. C, (45.85); H, (7.05); N, (26.73); Found C, (45.90); H, (7.15), N, (26.85). FT-IR (cm^{-1}): 3401 *ν*(–NH pri.), 2976 *ν*(NH sec.), 1696*ν*(C=O keto), 1641 *ν*(C=O amide), 1228 *ν*(C-N aliphatic) (Fig. S1). ^{1}H-NMR (DMSO-d_6, 500 MHz)ppm: $\delta = 2.5$ (s,4H, $J = 3.0$ Hz, α position of the ring,–C(C=O)–CH_2–), δ3.4 (s,4H, $J = 2.9$ Hz, β position of the ring, –NC(=O)–CH_2), δ8 (s, 1H, –NH), δ4 (d, 2H, –NH_2) (Fig. S2). ^{13}C-NMR (DMSO-d_6, 500 MHz, ppm): 39.66(C2), 43.57(C3), 154.75(C4, C=O), C5(43.76), C6 (39.75,C7 (162.75, O=C–NH, Amide) (Fig. S3).

Synthesis of heterocyclic (*E*)-*N*′-((2-hydroxynaphthalen-1-yl) methylene)-4-oxopiperidine-1-carbohydrazide ligand (H_2L)

A hot ethanolic solution in total (20 mL) of precursor 4-oxopiperidine-1-carbohydrazide (b) (0.315 g, 2 mmol) was added slowly to a 20 mL solution of 2-hydroxynaphthalene-1-carbaldehyde (0.344 g, 2 mmol) by magnetically stirring. The reaction mixture was refluxed in acidic condition for ~ 3–4 h with the addition of two drops of conc. H_2SO_4 as a catalyst. [17]. The success of reaction was routinely monitored by TLC. The resulting solution was concentrated to *ca.* 10 mL and then allowed to cool at room temperature where a bright yellow product was obtained (c). The solid product was separated by filtration, washed with warm petroleum ether (boiling range 40–60 °C) (2 × 5 mL) and dried in vacuum over $CaCl_2$ in a desiccator. The ligand (H_2L) was found to be soluble in DMF, and DMSO (Scheme1 **c**).

Micro-analytical data of H_2L Ligand ($C_{17}H_{17}N_3O_3$)

Color: yellow, mol.wt. = 311.34 (g/mol), yield: 0.4935 g (75%). M.P.: 240–242 °C. Elemental analysis: Calc. for: C, 65.58; H, 5.50; N 13.50%. Obs.: C, 65.60; H, 5.59; N, 13.55%. FT-IR: 3347 ν(OH, broad), 3262 ν(N–H), 1670 ν(C=O_{amide}), 1615 ν(C=$N_{azomethine}$), 1230 ν(C–$O_{phenolic}$), 953 ν(N–N) cm^{-1}. UV-Visible: (DMSO, conc. 2×10^{-4} mol dm^{-3}): λ max: 267, 331 and 405 nm. ^{1}H-NMR (DMSO-d^6, 500 MHz, δ ppm): 10.59 (s, 1H, J = 7.90 Hz –OH phenyl), 9.01 (s, 1H, J = 5.30 Hz –(HC=N–) azomethine), 7.95 (d, J = 2.15 Hz aryl, 1H), 7.52 (d, aryl, 1H), 6.80 (t, 1H, aryl), 6.72 (t, aryl, 1H), 6.20 (d, aryl, 2H), and 3.4, 2.5 (s, J = 4.70 Hz, 4H), 2.513, 2.506 (s, J = 3.5 Hz, 4H) of the heterocyclic ring in both α, and β position. ^{13}C-NMR (DMSO-d^6, 500 MHz, δ ppm): 207.78(carbon C=O), 160 (phenyl-C), amide group), 145(azomethine—C), 119 (C11), 131(C12), 118(C13), 126.8 (C14), 127(C15), 128 (C16), 130(C17), 135 (C18). HRMS (ESI-Mass *m/z*): Calc. for [$C_{17}H_{17}N_3O_3$], 311.34; found 312.22.

Synthesis of metal complexes-a general method

An equimolar quantities 1:1 (L:M) of hydrazone ligand (H_2L) (0.623 g, 2.0 mmol) and each metal chloride salts, viz., chromium chloride hexahydrate (0.532 g, 2.0 mmol), manganous chloride tetrahydrate (0.394 g, 2.0 mmol), ferric chloride hexahydrate (0.541 g, 2.0 mmol), cobalt chloride hexahydrate (0.475 g, 2.0 mmol), nickel chloride hexahydrate (0.475 g, 2.0 mmol), copper chloride dihydrate (0.341 g, 2.0 mmol) were dissolved separately in 20.00 mL of warm (DMSO and dry ethanol) solvents. The each reaction mixture was turned to alkaline condition at ~ 8 pH by the addition of 2 ml of ethanol-ammonia in ratio of (7:3). The reaction mixture was refluxed at *ca*. 80 °C with constant stirring for *ca*. 5 h in an oil bath [18]. The colored solid product was cooled at room temperature, filtered, washed several times by the addition of warm ethanol and dried vacuum over $CaCl_2$ in a desiccator. The molar conductivity was found low (4.12–39.20 Sm^2 mol^{-1}) using aprotic/polar solvent of DMSO (10^{-3} M) which indicates the non-electrolyte nature. However, the higher values in some cases may possibly due to the exchange of chloride ion with DMSO. The metal complexes do not melt they undergo decomposition at higher temperature above 300 °C. The physicochemical data of ligand, and metal complexes in terms of molecular formula, elemental analysis, and molar conductance are presented in Table 1.

Micro-analytical data of ($CrC_{17}H_{19}N_3O_5Cl$) complex: Color: Sand stone, Yield (0.99 g, 85%), Mol.Wt = 432.80 (g/mol). Elemental (%): found; C, (47.25); H, (4.50); N (9.85); Cl (8.35); Cr (12.34). Obs.: C (65.60); (H), 5.59; (N), 13.55.Cl (8.19); Cr (12.34). Calcd; C, (47.17); H, (4.42); N (9.70); Cl (8.19); Cr (12.01). $\Lambda_m = 39.20 Sm^2 mol^{-1}$, M.P.: < 300 °C. FT-IR (cm^{-1}): 1573 ν(C=O),1610 ν(C=N) azomethine, 1310 ν(C–O) of phenolic, 1231 ν(C-O)in enolic state, 958 ν(N–N), 850 coordinated ν(H_2O), 520ν(Cr–O), 430ν(Cr–N).

Table 1 Physical and analytical data of ligand (H_2L), and its metal (II/III) complexes

Compounds	M.F. and Mol.Wt. (g/mol)	Color (yield %)	% Found (Calcd.)					Λ_m ($Sm^2\ mol^{-1}$)
			C	H	N	Cl	Metal	
OPCH	$C_6H_{11}N_3O_2$ 157.17	Off white (84)	45.90 (45.85)	7.15 (7.05)	26.85 (26.73)	–	–	–
Hydrazone ligand [H_2L]	$C_{17}H_{17}N_3O_3$ 311.34	Yellow (75)	65.60 (65.58)	5.59 (5.50)	13.55 (13.50)	–	–	–
[Cr(L)$(H_2O)_2$Cl]	$CrC_{17}H_{19}N_3O_5Cl$ 432.80	Sand stone (85)	47.25 (47.17)	4.50 (4.42)	9.85 (9.70)	8.35 (8.19)	12.34 (12.01)	39.20
[Mn(HL)$(H_2O)_2$Cl]	$MnC_{17}H_{20}N_3O_5Cl$ 436.75	Buff yellow (88)	46.80 (46.75)	4.70 (4.61)	9.80 (9.62)	8.34 (8.11)	12.57 12.50	12.35
[Fe(L)$(H_2O)_2$Cl]	$FeC_{17}H_{19}N_3O_5Cl$ 436.64	Desert sand (92)	46.76 (43.60)	4.40 (4.38)	9.60 (9.40)	8.20 (8.11)	12.90 (12.78)	24.80
[Co(HL)$(H_2O)_2$Cl]	$CoC_{17}H_{20}N_3O_5Cl$ 440.74	Timber brown (91)	46.60 (46.32)	4.60 (4.57)	9.64 (9.53)	8.10 (8.04)	13.45 (13.37)	14.40
[Ni(HL)$(H_2O)_2$Cl]	$NiC_{17}H_{20}N_3O_5Cl$ 440.50	Glorious sunset (87)	46.55 (46.35)	4.65 (4.57)	9.60 (9.53)	8.12 (8.04)	13.35 (13.32)	19.90
[Cu(HL)$(H_2O)_2$Cl]	$CuC_{17}H_{20}N_3O_5Cl$ 445.35	Golden brown (89)	45.75 (45.84)	4.58 (4.52)	9.55 (9.43)	8.05 (7.96)	14.30 (14.26)	4.12

($MnC_{17}H_{20}N_3O_5Cl$) complex: Color: Buff yellow, Yield (0.903 g, 88%), Mol. Wt = 436.75 (g/mol). Elemental (%): found; C, (46.80); H, (4.70); N (9.80); Cl (8.34); Cr (12.57). Obs.: C, (46.75); H, (4.61); N, (9.62); Cl (8.11); Mn (12.50). $\Lambda_m = 12.35$ Sm^2mol^{-1}, M.P.: < 300 °C. FT-IR (cm^{-1}): 3245 ν(N–H) amide,1625 ν(C=O), 1612 ν(C=N) azomethine, 1319 ν(C-O) of phen., 973 ν(N–N), 887 coordinated $\nu(H_2O)$, 592 ν(Mn–O), 432 ν(Mn-N).

($FeC_{17}H_{19}N_3O_5Cl$) complex: Color: Desert sand, Yield (1.172 g, 92%), Mol. Wt = 436.64 (g/mol). Elemental (%): found; C, (46.76); H, (4.40); N (9.60); Cl (8.20); Cr (12.90). Obs.: C, (43.60); H, (4.38); N, (9.40); Cl (8.11); Fe (12.78). $\Lambda_m = 24.80$ Sm^2mol^{-1},M.P.: < 300 °C. FT-IR (cm^{-1}): 1609 ν(C=O), 1573 ν(C=N) azomethine, 1314 ν(C-O) of phen, 1239 ν(C-O)in enolic state, 960 ν(N–N), 863 coord. $\nu(H_2O)$, 573 ν(Fe–O) 435 ν(Cr–N).

($CoC_{17}H_{20}N_3O_5Cl$) complex: Color: Timber brown, Yield (0.997 g, 91%), Mol. Wt = 440.74 (g/mol). Elemental (%): found; C, (46.60); H, (4.60); N (9.64); Cl (8.10); Co (13.45). Obs.: C, (46.72); H, (4.53); N, (9.53); Cl (8.04); Mn (13.37). $\Lambda_m = 14.40$ Sm^2mol^{-1}, M.P.: < 300 °C. FT-IR (cm^{-1}): 3252 ν(N–H) amide,1652 ν(C=O), 1592 ν(C=N) azomethine, 1331 ν(C-O) of phen., 968 ν(N–N), 827 coordinated $\nu(H_2O)$, 528 ν(Co–O), 460 ν(Co–N).

($NiC_{17}H_{20}N_3O_5Cl$) complex: Color: Glorious sunset, Yield (0.963 g, 87%), Mol. Wt = 440.74(g/mol). Elemental (%): found; C, (46.55); H, (4.65); N (9.60); Cl (8.12); Co (13.35). Obs.: C, (46.35); H, (4.57); N, (9.53); Cl (8.04); Ni(13.32). $\Lambda_m = 19.90$ Sm^2mol^{-1}, M.P.: < 300 °C. FT-IR (cm^{-1}): 3235 ν(N–H) amide,1610 ν(C=O), 1598 ν(C=N) azomethine, 1340 ν(C-O) of phen., 960 ν(N–N), 941 coordinated $\nu(H_2O)$, 540 ν(Ni–O), 492 ν(Ni–N).

($CuC_{17}H_{20}N_3O_5Cl$) complex: Color: Golden brown, Yield (0.866 g, 89%), Mol. Wt = 445.35 (g/mol). Elemental (%): found; C, (45.75); H, (4.58); N (9.55); Cl (8.05); Cu(14.30). Obs.: C, (45.84); H, (4.52); N, (9.43); Cl (7.96); Cu (14.26). $\Lambda_m = 4.12$ Sm^2mol^{-1}, M.P.: < 300 °C. FT-IR (cm^{-1}): 3254 ν(N–H) amide,1600 ν(C=O), 1597 ν(C=N) azomethine, 1318 ν(C-O) of phen., 965 ν(N–N), 859 coordinated $\nu(H_2O)$, 549 ν(Cu–O), 460 ν(Cu–N).

Results and discussion

Synthesis of heterocyclic hydrazone ligand (H_2L) and complexes

The structural skeleton of newly synthesized (*E*)-*N*′-((2-hydroxynaphthalen-1-yl) methylene)-4-oxopiperidine-1-carbohydrazide (H_2L) (Fig. S8 was thoroughly confirmed from C-H-N-S micro-analyzer and (IR, ^1H, ^{13}C NMR and HR-Mass) spectroscopic tools. The ligand reacted with the corresponding metal salts in DMSO: EtOH and yielded two types of complexes: (I) $[Cr(L)(H_2O)_2Cl]$ (1) and $[Fe(L)(H_2O)_2Cl]$, (II) $[Mn(HL)(H_2O)_2Cl]$ (3), $[Co(HL)(H_2O)_2Cl]$ (4), $[Ni(HL)(H_2O)_2Cl]$ (5) and $[Cu(HL)(H_2O)_2Cl]$ (6). These metal complexes were found non-hygroscopic, colored solid, thermally stable, insoluble in water and common organic solvent except in highly polar solvent like DMF and DMSO. The physico-analytical

data of the metal complexes are in good agreement with the calculated values and well support to the proposed formula as presented in Table 1.

Characterization of heterocyclic hydrazone ligand (H_2L)

The proton-NMR spectrum of ligand exhibits one doublet observed at δ (2.5) ppm due to four H-atoms of the (-CH_2-) group present at both side of α-position in the piperidinic ring. Another doublet appeared at δ(3.4) ppm are due to the (–CH_2–) group of four hydrogen's present at both at β-position in the piperidinic ring. The two separate singlets appeared at δ (10.52, 9.01) ppm due to the phenyl ring (–OH) and azomethine protons (–HC=N–) respectively. The signals due to aromatic protons of the naphthyl ring that appeared in the expected range of δ(6.20–7.95)ppm (Fig. S4). ^{13}C-NMR spectrum of ligand which is shown in (Fig. S5) presented two signals that appeared at δ (39.48, 40.00) ppm due to the (C3, C5; α position) of the carbon atom of the (–CH_2–) group of piperidinic ring, respectively. Another two signals appeared at δ (42.00, 42.36) ppm due to the (C2, C6; β position) of the carbon atoms of (–CH_2–) group of piperidinic ring, respectively. The carbonyl carbon (C–O) (C4) signal appeared at δ (207) in piperidinic ring and another carbon of the amide group (C7) shifted to a higher field δ (154) ppm. Another expected signal appeared at δ(160) due to the phenyl ring (O–H) of C10 position. The azomethine (HC=N–) carbon atom (C8) position signal appeared at δ (145). The signals due to the aromatic carbon of naphthoyl ring have appeared as δ 119 (C11), 131(C12), 118(C13), 126.8 (C14), 127(C15), 128 (C16),130 (C17), 135(C18) ppm. The mass spectrum of the hydrazone (H_2L) ligand with its fragmented species are represented in. The mass spectrum shows a molecular ion peak appeared in [M^{+1}] = 312.22 (Fig. S6) equal to its mol.wt. The molecular ions peaks of fragmented species are observed at 294.11 due to ($C_{17}H_{16}N_3O_2^+$) ion showed 100% intensity and other fragmented masses were found as 168 ($C_7H_{10}N_3O_2^+$), 141 ($C_6H_9N_2O_2^+$), 126 ($C_6H_8NO_2^+$) and 98 ($C_5H_8NO^+$) ion species.

FT-IR Spectroscopy and metal–ligand bonding mode

The FT-IR spectra of ligand (H_2L) and its metal (II/III) complexes are closely correlating, and modifications observed in the vibrational frequency are due to the interaction of metal ions with the ligand molecule. The spectra of ligand and its metal complexes are depicted in Fig. 1), along with simulated spectra presented in Fig. S7(a–e). The important FT-IR spectral bands data are summarized in Table 2. The ligand spectrum showed a medium broad absorption band at 3347 cm^{-1} due to stretching vibrations of the phenolic ν(O–H) group [19]. Further, the disappearance of this band in the spectra of complexes indicated the deprotonation of the phenolic proton, followed by the coordination of the phenolate O-atom to the metal ions and sustained by shifting of ν(C–O) phenolic frequency by 5–35 cm^{-1} from 1305 cm^{-1} indicated the deprotonation and participating in coordination of (C–O–M) bond formation. A sharp band appeared at 1630 cm^{-1} due to the azomethine ν(C=N) group and moved this band to a lower frequency by 57–18 cm^{-1} in the complex

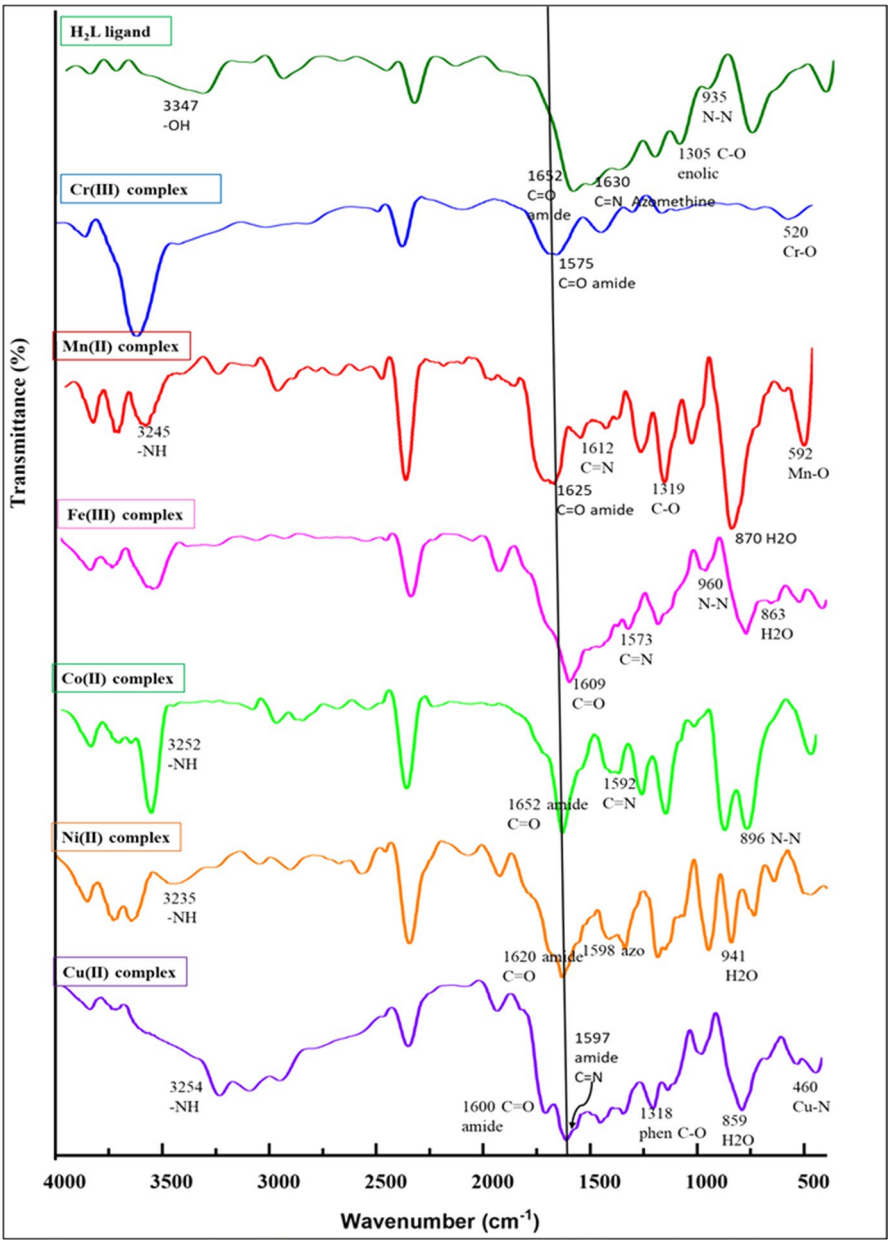

Fig. 1 FT-IR spectra of hydrazone ligand (H_2L), and its metal complexes

spectra which suggested the coordination of the azomethine nitrogen atom to the metal center. The upward shift of ν(N–N) band from 953 cm^{-1} to 958–973 cm^{-1} was found in IR spectra of all complexes [20]. In the spectra of Mn(II), Co(II), Ni(II), and Cu(II) complexes a medium intensity band was observed at ~ 3262 cm^{-1} due to

Table 2 Selected FT-IR spectroscopic data (cm^{-1}) of free hydrazone ligand (H_2L), and its metal (II/III) complexes

Compounds	ν (OH)	ν (N–H) amide	ν (C=O)	ν (C=N) azomethine	ν (C–O)phenolic	ν (C–O)in enolic	ν (N–N)	Coordν (H_2O)	ν (M–O)	ν (M–N)
Ligand (H_2L)	3347	3262	1670	1630	1305	–	953	–	–	–
[Cr(III) complex]	–	–	1573	1610	1310	1231	958	850	520	430
[Mn(II) complex]	–	3245	1625	1612	1319	–	973	887	592	432
[Fe(III) complex]	–	–	1609	1573	1314	1239	960	863	573	435
[Co(II) complex]	–	3252	1652	1592	1331	–	968	827	528	460
[Ni(II) complex]	–	3235	1610	1598	1340	–	960	941	540	492
[Cu(II) complex]	–	3254	1600	1597	1318	–	965	859	589	460

amide (N–H) group which appeared almost as in the case of ligand, thus confirming ligand in its ketonic form in these complexes. Further, the shift of the amide carbonyl (C=O) moiety to lower frequency by 18–97 cm^{-1} in all these complexes confirms the coordination of the amido-O atoms to the metal ions without undergoing enolization. However, the absence of these bands at 3262 and 1670 cm^{-1} due to ν(N–H) and ν(C=O), respectively, in the spectra of Cr(III) and Fe(III) complexes and appearance of a new bands in the range 1231–1239 cm^{-1} due to ν(C–O) (enolate) indicates the destruction of the carbonyl group and coordination of enolic.

Oxygen to these metal ions after deprotonation. The non-ligand bands observed at about 827–950 cm^{-1} in all complexes possibly due to the presence of water molecule was further confirmed by dehydration in thermal study. The appearance of weak intensity of non-ligand band at 592–520 and 492–430 cm^{-1} in the spectra of complexes are characteristics of ν(M–O) and ν(M–N) stretching vibration, respectively [21].

Magnetic susceptibility and UV–Visible spectroscopy

The room temperature magnetic moments and UV–visible absorption spectral data of metal complexes are summarised in Table 3 and spectra are represented in (Fig. S9a–b). The electronic spectrum of ligand displayed an absorption band at shorter (λ_{max} = 267 nm, 331) nm may be significant impact of π–π*, n–π* transition which are the characteristic of (C=O), (C=N) group respectively. The shift of absorption band at to higher wavelength in the spectra of metal complexes indicates the complexation of ligand to the metal ions. The Cr(III) complex displayed three absorption bands at (λ_{max} = 1020, 936 and 500) nm was due to $^4A_{2g} \rightarrow {}^4T_{2g}$, $^4A_{2g} \rightarrow {}^4T_{1g}$(F), and $^4A_{2g} \rightarrow {}^4T_{1g}$(P) transitions, respectively indicating octahedral geometry which was supported by its observed magnetic moment of 3.82 B.M. and its (d^3) configuration [22]. The important ligand field parameters were calculated and values are found to be: Dq = 980 cm^{-1}, B = 680 cm^{-1}, β = 0.74 and v_2/v_1 = 1.09. The low value of B was observed in the metal complex compared to its free metal ion (918 cm^{-1}), which signified the covalent character of the metal-ligand bond. The Mn(II) complex exhibits three weak bands at λ_{max} = 950, 884 and 320 nm was due to $^6A_{1g} \rightarrow {}^4E_g$ (^{4}D)$^6A_{1g} \rightarrow {}^4E_g$ (G) and $^6A_{1g} \rightarrow {}^4E_g$, transitions, respectively, in octahedral complex [23].The observed magnetic moment for the Mn(II) complex is 5.89 B.M. which confirms octahedral geometry having (d^5) configuration. The Fe(III) complex shows three weak absorption bands at 982, 884 and 528 nm assignable to $^6A_{1g} \rightarrow {}^4T_{1g}$(G), $^6A_{1g} \rightarrow {}^4T_{2g}$(D), and $^6A_{1g} \rightarrow {}^4$Eg(D), transitions, respectively, and are consistent with octahedral (O_h) geometry. The observed magnetic moment of this complex was found to be 5.97 B.M., which informs d^5 degeneracy supporting to octahedral field around metal ion [24]. The electronic spectrum of Co(II) complex exhibits three bands at λ_{max} = 1075, 930, and 560 nm due to $^4T_{1g} \rightarrow {}^4T_{2g}$, $^4T_{1g} \rightarrow {}^4A_2$g and $^4T_{1g} \rightarrow {}^4T_{1g}$(P), transitions, respectively for octahedral geometry of Co(II) complex [25]. The observed magnetic moment value 4.30 B.M., for the complex is in accordance with its octahedral geometry. The various ligand field parameters [Dq, B, β and v_2/v_1] have been evaluated from the spin-allowed transitions and their values are

Table 3 Magnetic susceptibility and electronic absorption spectral parameters of metal complexes

Metal complexes	μ_{eff} (B.M)	Absorption maxima (nm)	Band assignments	Ligand field data				
				Dq (cm^{-1})	B (cm^{-1})	B_0 (cm^{-1})	$\beta = B/B_0$	v_2/v_1
[Cr(III) complex]	3.82	1020(v_1) 936(v_2) 500(v_3)	$^4A_{2g} \rightarrow {}^4T_{2g}$ $^4A_{2g} \rightarrow {}^4T_{1g}(F)$ $^4A_{2g} \rightarrow {}^4T_{1g}(P)$	980	680	918	0.74	1.09
[Mn(II) complex]	5.89	950(v_1) 884(v_2) 480(v_3)	$^6A_{1g} \rightarrow {}^4E_g({}^4D)$ $^6A_{1g} \rightarrow {}^4E_g(G)$ $^6A_{1g} \rightarrow {}^4T_2(G)$	1053	687	860	0.80	1.07
[Fe(III) complex]	5.97	982(v_1) 864(v_2) 528(v_3)	$^6A_{1g} \rightarrow {}^4T_{2g}(G)$ $^6A_{1g} \rightarrow {}^4T_{2g}(G)$ $^6A_{1g} \rightarrow {}^4E_g(D)$	–	–	–	–	–
[Co(II) complex]	4.30	1075(v_1) 930(v_2) 780(sh) 560(v_3)	$^4T_{1g} \rightarrow {}^4T_{2g}$ $^4T_{1g} \rightarrow {}^4A_{2g}$ – $^4T_{1g} \rightarrow {}^4A_{2g}(F)$	1163	725	971	0.75	1.16
[Ni(II) complex]	2.92	970 (v_1) 880 (v_2) 729(sh) 460 (v_3)	$^3A_{2g} \rightarrow {}^3T_{2g}(F)$ $^3A_{2g} \rightarrow {}^3T_{1g}(F)$ – $^3A_{2g} \rightarrow {}^3T_{1g}(P)$ $^3A_{2g} \rightarrow {}^3T_{1g}$	1031	762	1030	0.74	1.10
[Cu(II) complex]	1.72	908(v_1) 832(sh) 682(v_2) 565	$^2B_1g \rightarrow {}^2A_1g(v_1)$ – $^2B_1g \rightarrow {}^2B_2g$ (v_2) *Charge transfer(CT)*	–	–	–	–	–

found to be Dq = 1163 cm^{-1} and $B = 725$ cm^{-1}, $\beta = 0.75$ and $v_2/v_1 = 1.16$. The calculated electronic lower value of B for the complex suggests the orbital overlap and delocalization of d-orbitals. The electronic spectrum of Ni(II) complex shows three bands at 970, 880 and 460 nm which are assigned to $^3A_{2g} \rightarrow {}^3T_{2g}$, $^3A_{2g} \rightarrow {}^3T_{1g}(F)$ and $^3A_{2g} \rightarrow {}^3T_{1g}(P)$, transitions, respectively, suggested an octahedral environment around Ni(II) ion [26]. The observed magnetic moment value for the complex is 2.92 B.M., which is well within the expected range (2.83–3.50 B.M.) for the Ni(II) octahedral complexes. The various ligand field parameters have been calculated from the spin-allowed transitions. The ligand field parameter calculated as Dq = 1031 cm^{-1} and $B = 762$ cm^{-1}, $\beta = 0.74$, and $v_2/v_1 = 1.10$ and these values are also in compatible with those reported for Ni(II) octahedral complexes. The electronic spectrum of Cu(II) complex shows broad band around at 908 nm due to $^2B_1g \rightarrow {}^2A_1g$, transition, is characteristic for a elongation due to distortion in Cu(II) of an octahedral field and well supported by ESR spectra [27]. The other bands observed at $\lambda_{max} = 682$ and 565 nm are assigned for $^2B_1g \rightarrow {}^2Eg$ and ligand → metal charge transfer (LMCT) $\pi \rightarrow \pi^*$ transitions, respectively, while observed value of magnetic moment $\mu = 1.72$ B.M. for complex is consistent for single unpaired electron [28].

Evaluation of ESR tensor parameters for copper (II) complex

The well resolved isotropic X band spectrum of Cu(II) complex is shown in Fig. 2 and its expressing significant tensor data are presented in Table S1. The spectrum shows a $g_{||}$ peak at 2933.9 Gand another single peak $g_{\perp}$ peak at 3214.37G. The observed values 2.249 and 2.053 of $g_{||}$ and $g_{\perp}$ components clearly suggest the

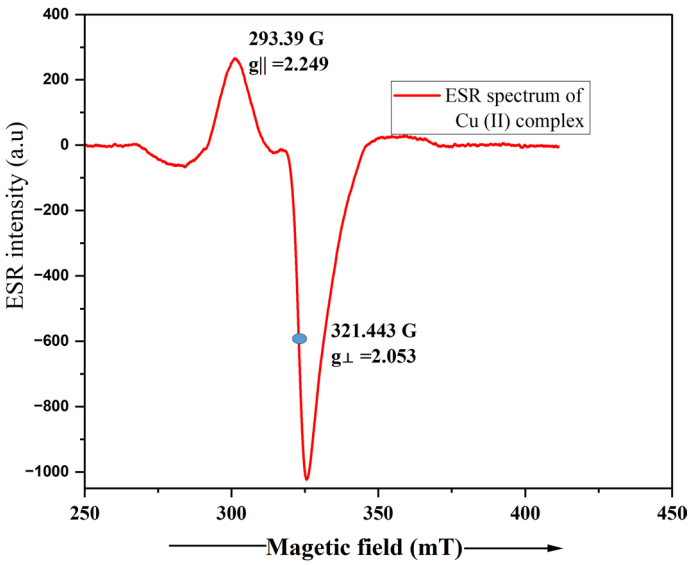

Fig. 2 ESR spectrum of Cu(II) complex

presence of axial symmetry in the complex. The $g_{\parallel} > g_{\perp}$ and with trend g‖> $g_{\perp}$ > ge (2.0023) suggests the presence of one unpaired electron in (dx^2-dy^2) orbital in the ground state of Cu(II) metal ion. The $g_{\parallel}$ value is sensitive towards the covalent nature of the Cu-ligand bond as well as the deviation of 'g' avg.value from free electron values (2.0023) also confirms the presence of covalency in the M-L bond. The 'G' parameter was calculated by Hathway's equation $G = (g_{\parallel} - 2.0023)/(g_{\perp} - 2.002$ 3) which indicates the exchange occurred at the copper center in the structure of the compound. The G value was found to be 5.52 which is greater than four suggesting the negligible interactions between the metal center [29]. The calculated value of component $A_{\parallel}$ (168 cm^{-1}) and $A_{\perp}$ (55.54 cm^{-1}) with ($A_{\parallel} > A_{\perp}$) is in agreement with that electron interacts with only one copper nucleus and the complex has distorted octahedral geometry due to axial elongation. Other supporting parameter $A_{\parallel}$ value was also dependent on the directly coordinated ligand. Due to this effect, the interaction between the electrons with nuclear spin increases with increasing the $A_{\parallel}$ compared with naturally decreased $g_{\parallel}$ value. The values $g_{\parallel}$ and $A_{\parallel}$ of the coefficient value fv = 133 confirmed that ligand influence on the density of metal's unpaired electron and coordination fields. The molecular orbital coefficients α^2 (covalency of in σ-bond) and β^2 (covalency of in π-bond) were found β^2 (2.45) > α^2 (0.35) which indicates that covalency in π-bonding was much stronger than expected covalency in σ-bonding. The orbital reduction parameter found of the component $K^2_{\perp}$ (0.78) > $K^2_{\parallel}$ (0.53) indicates the plane bonding of ligand with metal in the octahedral field [30].

SEM analysis

In the present investigation, we just compared the surface morphology of the hydrazone (H_2L) ligand and its [Fe(L)(H_2O)$_2$Cl] complex are as a representative cases that provides empirical information regarding the molecular aggregation pattern in bulk form. The SEM micrographs of the ligand and its [Fe(L)(H_2O)$_2$Cl] complex are shown in (Fig. 3a, b). The microscopic image of ligand was magnified at 200X, 100 µm, WD13 which clearly indicated that the unit cell with a regular surface area

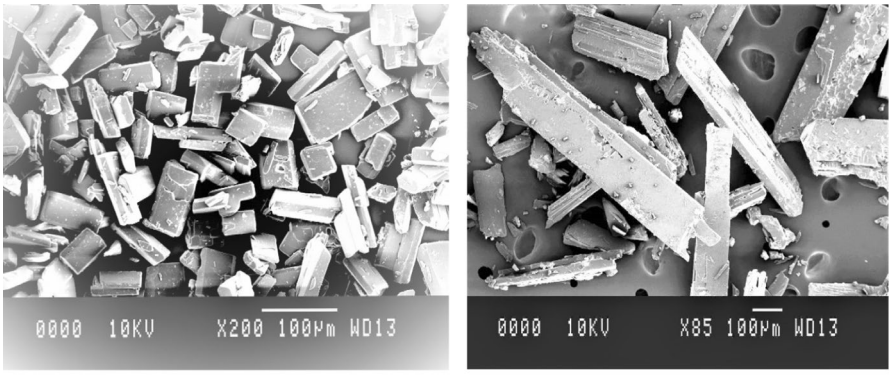

Fig. 3 Scanning electron microscopic EM images of **a** hydrazone ligand (H_2L), and **b** Fe(III) complex

without any shadows possessed the cuboidal in shape. The metal complex magnifies at 85X, 100 µm, WD13 revealed that aggregation appeared in that as broken bricks in a non-uniform irregular shape. The image of surface morphology of two compounds particle were identified differently in shapes and size give evidence for the involvement of metal complexation reaction [31].

X-ray diffraction studies

The nature of ligand (H_2L) and its Cr(III), Mn(II), Fe(III) and Cu(II) complexes were also ascertained by powder X-ray diffraction studies. The XRD pattern compounds are depicted in Fig. S10a–e and data listed in Tables S2–S6. The angle (2θ) and interplanar distance (d) were evaluated by Bragg's equation ($n\lambda = 2d\sin\theta$). The miller indices were found in specified directions along with the lattice plane (*h*, *k*, and *l*). The unit cell parameters for ligand, and its metal complexes are as follows; H_2L ligand: crystal system = rhombohedral, $a = 8.5680$ Å, $b = 6.1020$ Å, $c = 15.9870$ Å and $\alpha = \beta = \gamma = 90°$, V = 835.65 Å^3 [32]. [Cr(L)Cl(H_2O)$_2$] complex: crystal system = orthorhombic, $a = 9.8045$ Å, $b = 7.1020$ Å, $c = 16.701$ Å, and $\alpha = \beta = \gamma = 90°$, V = 1000.55 Å^3; [Mn(HL)Cl(H_2O)$_2$]: Crystal system = orthorhombic, $a = 8.7080$ Å, $b = 7.1312$ Å, $c = 16.2070$ Å and $\alpha = \beta = \gamma$ (90°), V = 1200.221 Å; [Fe(L)Cl(H_2O)$_2$] complex: crystal system = orthorhombic, $a = 18.5680$ Å, $b = 16.1020$ Å, $c = 15.9870$ Å and $\alpha = \beta = \gamma = (90°)$,V = 1600.178 Å^3; [Cu(HL)Cl(H_2O)$_2$] complex: crystal system = monoclinic, $a = 9.9540$ Å, $b = 16.1700$ Å, $c = 17.8373$ Å and $\alpha = \gamma = 90$, $\beta \neq 120°$,V = 2808.992 Å^3. The avg. crystalline size of the H_2L ligand, Cr(III), Mn(II), Fe(III), and Cu(II) complexes were evaluated from Scherer's equation. Upon the full width half maximum intensity (FWHM) calculation, the average crystallite size was 19.98, 33.28, 25.11, 31.46, and 26.28 nm, respectively. All these indicate their nanocrystalline nature [33].

Simultaneous thermal (TGA-DTA) analysis

The simultaneous thermogravimetric analysis of complexes consists of the three decomposition steps: temperature scale (40–750 °C), decomposed species in addition to mass loss (%) of ligand and metal complexes are presented in Table 4. The thermograms of hydrazone ligand and its metal complexes are shown in Fig. 4a–g. The thermal reaction data are the good agreements with the proposed formula weight as expected from an analytical and the spectral data. TGA analysis, an important technique, was performed with a thermal rate 20 °C min^{-1} under N_2 atmosphere for the analysis of decomposition pattern, thermal stability, and information regarding about the ligation of different groups associated with metal ions. The ligand (H_2L) shows a single broad (DTG_{max}) peak in the temperature range 365–370 ^{0}C with a maximum mass loss which occurred of 67.27% (theor. 65.55%) due to the complete removal of ligand moiety. Upon continued heating up to 700 ^{0}C, the thermal curve was turned to horizontal state, which signify the formation of stable carbon residue [found: 32.73%, (theor: 34.45%)]. The general thermal decomposition pattern for

Table 4 Stepwise thermal decomposition data of hydrazone ligand and its metal (II/III) complexes

Compounds	Steps	Temp range (°C)	DTG_{max} (°C)	Wt. losses %		Decomposed species
				Expt	Calcd	
Ligand (H_2L)	I	45–370	370	89.50	89.00	Loss of $H_{17}N_3O_3$ species
	II	370–660	–	11.25	11.00	Carbonic residue
$[Cr(L)(H_2O)_2Cl]$	I	45–150	100	08.78	08.31	Elimination of two coord-H_2O molecules
	II	150–360	250	09.10	08.94	Loss of one coord-Cl^- ion
	III	360–500	360	60.12	61.72	Loss of organic moieties ($C_{17}H_{15}N_3O_2$)
	IV	500–700	–	22.00	21.03	metallic oxide residue
$[Mn(HL)(H_2O)_2Cl]$	I	45–150	150	08.50	08.24	Elimination of two coord-H_2O molecules Loss of one coord-Cl^- ion
	II	150–360	260	09.10	08.85	
	III	360–500	500	62.90	63.49	Loss of organic moieties ($C_{17}H_{16}N_3O_2$)
	IV	500–700	–	19.50	19.41	Metallic oxide residue
$[Fe(L)(H_2O)_2Cl]$	I	45–140	140	8.90	08.64	Elimination of two coord-H_2O molecules
	II	140–290	260	9.10	08.86	Loss of one coord-Cl^- ion
	III	290–360	360	61.00	60.72	Loss of organic moieties ($C_{17}H_{15}N_3O_2$)
	IV	360–700	–	22.00	21.77	metallic oxide residue
$[Co(HL)(H_2O)_2Cl]$	I	45–150	150	08.20	08.18	Elimination of two coord-H_2O molecules
	II	150–390	200	08.80	08.77	Loss of one coord-Cl^- ion
	III	390–500	410	63.05	63.01	Loss of organic moieties ($C_{17}H_{16}N_3O_2$)
	IV	500–800	–	20.05	20.03	metallic oxide residue
$[Ni(HL)(H_2O)_2Cl]$	I	45–150	150	08.25	08.18	Elimination of two coord-H_2O molecules
	II	150–380	280	8.87	08.77	Loss of one coord-Cl^- ion
	III	380–600	600	63.25	63.01	Loss of organic moieties ($C_{17}H_{16}N_3O_2$)
	IV	600–709	–	20.07	20.04	metallic oxide residue
$[Cu(HL)(H_2O)_2Cl]$	I	45–110	110	08.92	08.08	Loss of two coord-H_2O molecules
	II	110–245	245	08.70	08.67	Loss of one coord-Cl^- ion
	III	245–345	345	62.30	62.23	Loss of organic moieties ($C_{17}H_{16}N_3O_2$)
	IV	500–703	–	21.08	21.02	Metal oxide residue

$[CoC_{17}H_{20}N_3O_5Cl]$ complex is shown in **Scheme S2**. The following comments were suggested from the simultaneous TG–DTA analysis.

i. Cr(III), Mn(II), Fe(III), Co(II) and Cu(II) complex show thermal decomposition at ca.100–150 °C (broad DTG_{max}) indicated removal of two coordinated water

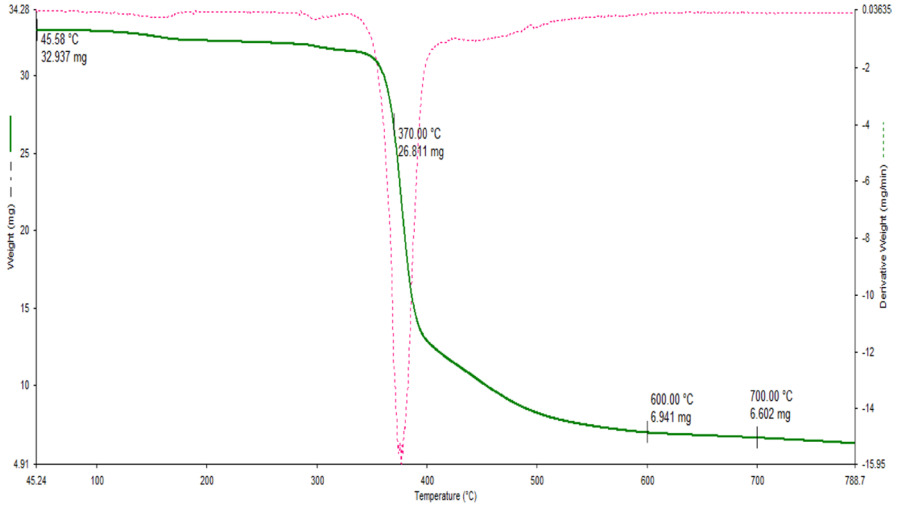

(a)

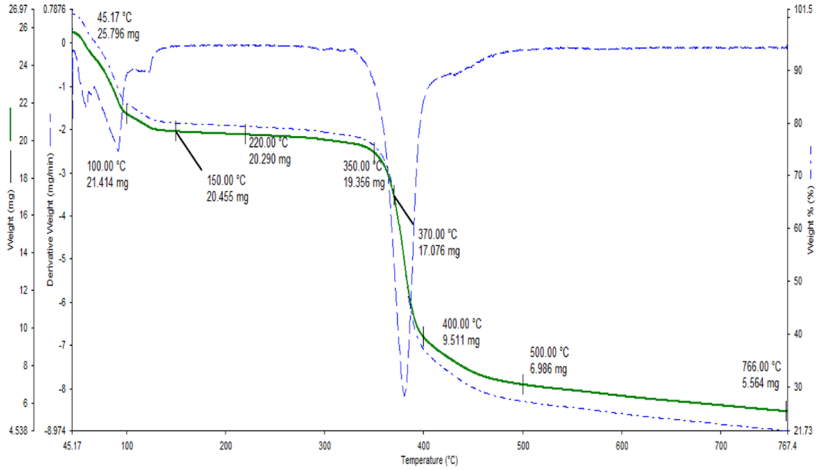

(b)

Fig. 4 TGA—, DTA --- curves of **a** hydrazone ligand, **b** Cr (III), **c** Mn(II), **d**)Fe(III), **e** Co(II), **f** Ni(II), and **g** Cu(II) complexes

molecules and as expected nearly same loss of mass ~ 8.25–8.90% equivalent to theoretical loss of (~ 8.30–8.64%) [34].

ii. The second step exhibits loss of mass (8.70–9.10%) which coincides with theoretical loss of (8.67–8.94%) in the range of 200–245 °C (DTG_{max}) and these may specify to the loss of chloride ions.

iii. At the end of thermal reaction, the non-coordinated organic moieties mass loss was observed (60.12–63.25%) equivalent to loss of mass (calc.60.72–63.72%)

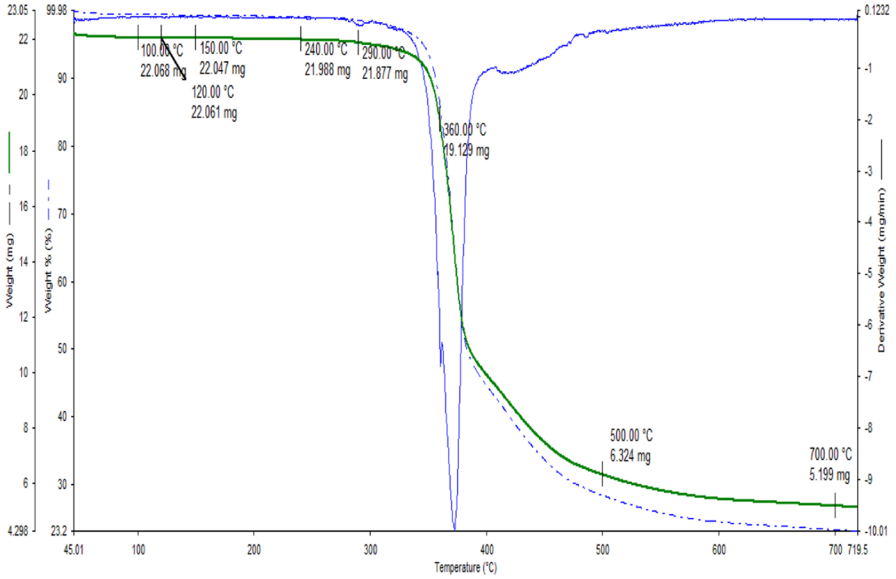

(c)

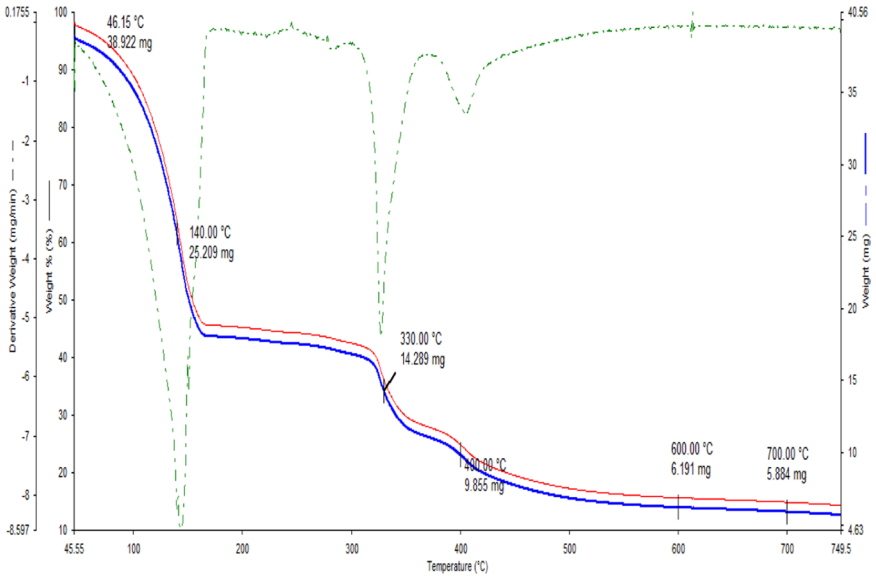

(d)

Fig. 4 (continued)

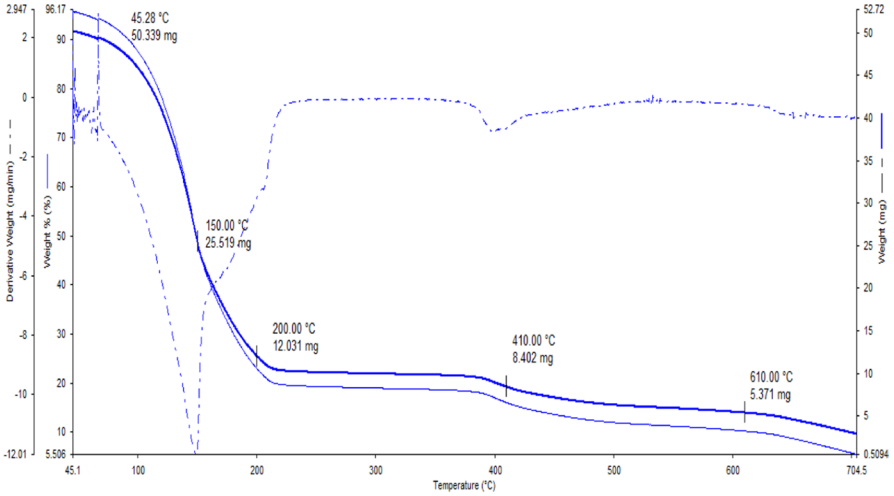

(e)

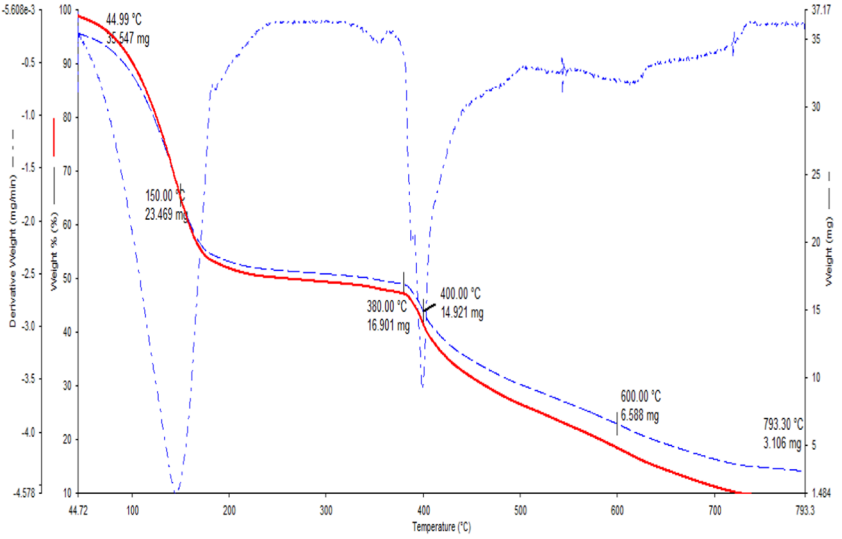

(f)

Fig. 4 (continued)

when the temperature increased more than 360 oC, the thermal curve became horizontal which possibly notifies the formation of respective stable metal oxide (60.12–63.25%) (Calc. 63.25–63.72%). The presence of water molecule (coordinated) are well supported to IR vibrational frequency data. The thermal stability

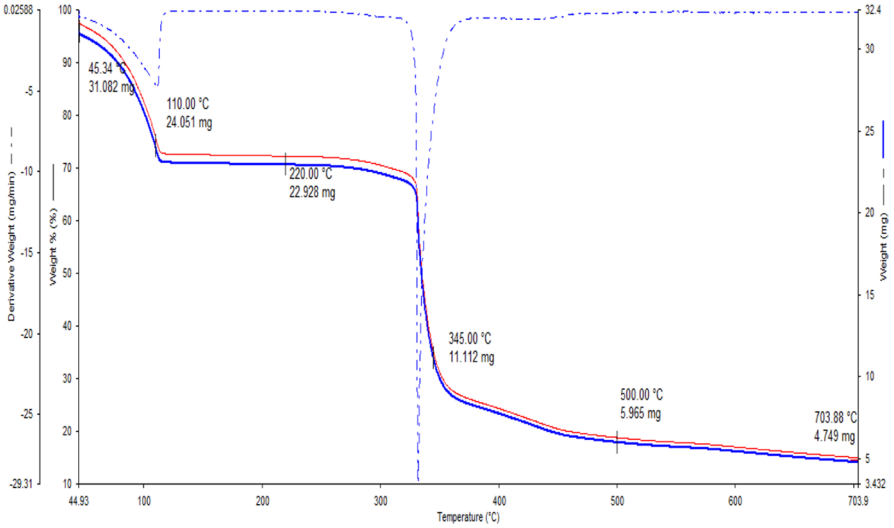

(g)

Fig. 4 (continued)

order of metal complexes was found to be in the order of Cu(II) < Fe(III) ≅ Cr (III) < Co(II) ≅ Mn (II) < Ni (II) [35].

Kinetic parameters evaluation-(Coat-Redfern method)

The thermo-kinetic parameters for the non-isothermal degradation of complexes viz., (Ea), (ΔS), (ΔH) and free energy change (ΔG) were evaluated by using the integral method of Coats-Redfern equation [43] and the calculated values are presented in Table 5. From the kinetic data, increasing trends of activation energy (Ea) from (5.15 to 324 kJ/mol) comparing with the decreasing order of entropy (ΔS) was found to be −21.79 to −11.50 $Jmol^{-1}$ k^{-1} [36]. The negative values of (ΔS) in the overall first, second and third steps of decomposition reaction of complexes indicate slow decomposition reactions, the non-spontaneous nature, degree of structural 'complexity' with the low-frequency factor (Z) values and which is further supported by positive values of (ΔG). The activation energy was compared with free energy and heat of the reaction displaying its significance as (Ea) < (ΔG) ≅ (ΔH). The enthalpy parameter (ΔH) and change in the free energy (ΔG) of reaction were found positive term in the range (10.15–521.00) kJ mol^{-1} and (10.22–329.00) kJ mol^{-1}, respectively suggesting that the decomposition of complexes undergo to endothermicity and more stability [37].

Fluorescence emission spectra

The solid state compounds of hydrazone ligand (H_2L) and its metal complexes were excited at room temperature ($\lambda_{ex} = 335$ nm) and recorded

Table 5 Kinetic parameters for decomposition of hydrazone ligand (H_2L), and its metal (II/III) complexes (Coats-Redfern method)

Compounds	Steps	Decomp temp (^{0}C)	(Ea) kJ/mol	(Z) s^{-1}	ΔS (J/mol/k)	ΔH (kJ/mol)	ΔG (kJ/mol)
Ligand (H_2L)	I	370	211.02	1.362×10^{1}	− 14.50	205.80	214.90
Cr(III) complex	I	100	15.84	1.121×10^{1}	− 15.84	12.70	16.90
	II	150	21.79	1.2×10^{3}	− 21.79	18.30	23.50
	III	350	167.01	1.126×10^{3}	− 15.30	161.80	171.40
Mn(II) complex	I	150	111.69	1.106×10^{3}	− 12.11	108.20	113.30
	II	360	309.86	1.230×10^{3}	− 15.30	304.60	314.30
	III	500	175.72	1.121×10^{3}	− 17.30	166.30	179.60
Fe(III) complex	I	140	06.65	1.106×10^{3}	− 12.10	10.15	11.22
	II	330	117.69	1.121×10^{3}	− 15.10	112.70	212.80
	III	400	221.47	1.236×10^{3}	− 16.90	215.90	226.60
Co(II) complex	I	150	05.15	1.224×10^{3}	− 12.30	10.60	10.22
	II	410	112.85	1.236×10^{3}	− 16.00	107.30	117.90
Ni(II) complex	I	150	13.42	1.230×10^{3}	− 12.70	10.00	15.10
	II	380	165.37	1.230×10^{3}	− 15.70	159.90	170.20
	III	600	258.00	1.236×10^{3}	− 18.10	12.17	267.20
Cu(II) complex	I	110	12.02	1.368×10^{3}	− 11.50	10.00	13.20
	II	220	101.08	1.106×10^{3}	− 13.40	97.70	104.30
	III	500	324.84	1.230×10^{3}	− 15.10	521.90	329.00

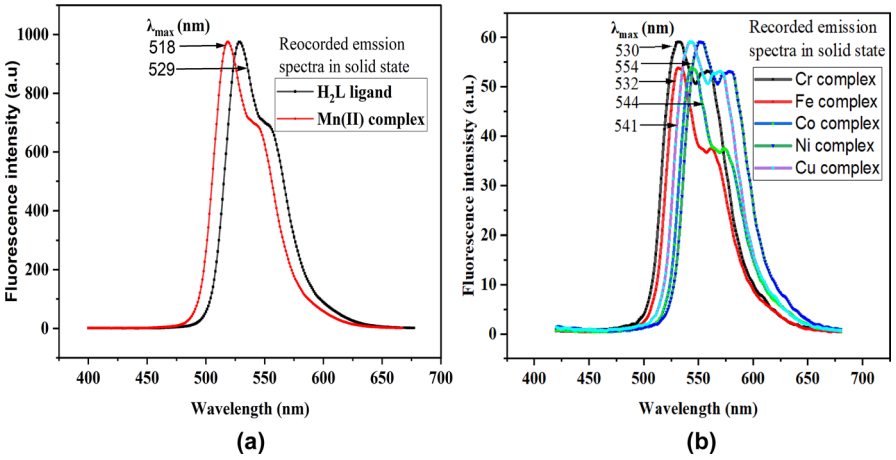

Fig. 5 Emission spectra of **a** hydrazone ligand (H_2L), and Mn (II) complex and **b** its metal (II/III) complexes

Table 6 The fluorescence emission spectral data of ligand, and its metal complexes (solid state)

Compounds	Wavelength (nm)	Emission intensity I_F (a.u.)
Ligand (H_2L)	529	974.60
Mn(II) complex	518	974.20
Cr(III) complex	530	59.11
Fe(III) complex	532	53.58
Co(II) complex	546	59.08
Ni(II) complex	546	54.66
Cu(II) complex	541	59.04

emission spectra (λ_{em} = 480–650)nm through the emission slit widths 1.0 nm, scan rate ~ 240 nm min^{-1}. The fluorescence spectra are depicted in Fig. 5a, b and, data are presented in Table 6. The compounds emitted broad emissions due to the combined effects of inhibition photo-induced electron transfer (PET), magnetic perturbation, redox activity, static interaction of metal ion and causing the hyperchromic to bathochromic shift. [38, 39]. The hydrazone ligand (H_2L), Mn(II) and Cr(III) complexes emitted the radiation in higher intensity (λ_{em} = 518–529)nm whereas other Fe(III), Co(II), Ni(II), and Cu(II) complexes demonstrated lower emission intensity (λ_{em} = 530–546)nm. The free ligand (2-hydroxynaphthalen-1-yl) methylene-4-oxopiperidine-1-carbohydrazide) contains two free (>C=O) chromophores present at two different position characteristics for quenching fluorescence and supported by azomethine group (–HC=N–) which is capable in exchanging the proton of redox reaction as well as extra aryl-π electrons. The emission intensity (I_E) of hydrazone ligand (H_2L) decreases upon complexation with metal ion in the order of; ligand (H_2L) > Mn (II) > Cr (III) > Co(II) > Ni(II) > Cu(II) > Fe (III) complexes. Upon examination of spectral data, the hydrazone and its metal complexes are considered to be a marks of the good fluorescent components, applicable in the photochemical reaction and in detection heavy metal ions in biological samples [40].

Computational study

Optimization of molecular geometry

The DFT calculation have been carried out by using the B3LYP function with 6-311++G (d, p) for hydrazone ligand (H_2L) and LanL2DZ basis set for metal complexes for an account of relativistic effect from Gaussian 09 tool and Gauss view 6.0.16. The optimized structure of ligand (H_2L) and its Cr(III), Mn(II) and Fe(III) complexes with their atoms numbering presented in Fig. 6a–d are as representative cases and others, i.e. Co(II), Ni(II) and Cu(II) complexes are in Fig. S11e–g, and supporting geometrical data are listed in Table 7a–c. The optimized hydrazone ligand consists of two fused aryl rings in a planar and another side of heterocyclic (piperidinic) ring were in the angular strain at C9 atom making an angle of 112.176 (°) of the fragment of C(12)-(C9)-(N16) and similarly at C10

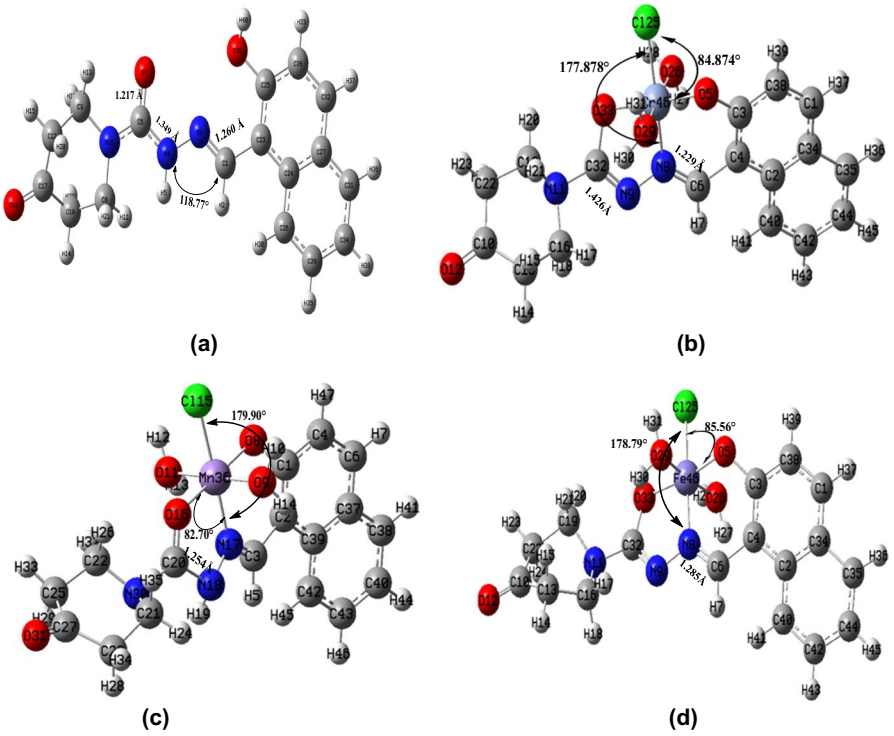

Fig. 6 Optimized molecular structures of **a** hydrazone ligand (H_2L), an octahedral geometry of **b** Cr(III), **c** Mn(II). **d**)Fe(III) complexes

atom making an angle of 111.16 (°) of the fragment of C(17)-(C10)-(C8) with sp^3 (C-atom). The decreased bond lengths of C(12)-C(9) and C17-C10 bonds were found as 1.529 (Å) and 1.5160 (Å), respectively. The bond angle was also decreased and this may be due to the electronegative N(16) hetero atom and O(18) of carbonyl group presence in the ring. The validated torsion angle were found as of C(12)-(C9)-(N10)-(C6) of 55.966 (°) and C (17)-(C10)-(C8)-(C6) of 57.915(°). The atoms of the azomethine group consists of a bond C(1) = N(3) shows the shorter bond length of 1.260 Å which indicates the partial electron delocalization in the fragments of H(2)-C(1) = N(3) with bond angle of 122.032 Å. The phenolic group of atom shows O(39)-H(40) which indicates a short bond length of 0.963 Å with an angle of 113.05(°) of terminal atoms of C(25)-O(39)-H(40) and torsion angle of connected atoms of C(25)-O(39)-H(40)-C(1) was 0.0443(°). The naphthoyl rings displayed torsion angle of C(29)-C(26)-C(24)-C23) and C(32)-C(28)-C(25) = C(23) of two fused aryl ring atoms was found to be 179.93(°) and 0.02514 (°) respectively which indicates the resonance by the delocalization of π-electrons in the ring with sp^2 hybridized carbon atom in the orbitals by extending the above and below the plane of the ring [41, 42]. The metal complexes have coordination number six and revealed slightly distorted octahedral

Table 7 (a) Selected geometrical parameters of (H_2L) ligand, (b) Selected geometrical parameters of Cr(III), and Fe(III) complexes, (c) Selected geometrical parameters of Mn(II), Co(II), Ni(II), and Cu(II) complexes

Bond connectivity	Bond lengths (Å)	Bond connectivity	Bond angles (°)	Bond connectivity	Torsion angle (°)
C(1) = N(3)	1.260	H(2)–C(1) = N(3)	122.034	–	–
N(3)–N(4)	1.387	N(4)–N(3)–C(1)	118.77	N(4)–N(3)–C(1)–H(2)	0.0257
N(4)–C(6)	1.349	N(3)–N(4)–C(6)	116.70	–	–
C(1)–C(23)	1.347	N(3)–C(1)–C(23)	123.52	–	–
C(6)–O(7)	1.217	N(4)–C(6)–O(7)	122.89	N(4)–C(6)–O(7)–N(3)	−1.638
C(6)–N(16)	1.371	N(4)–C(6)–O(16)	114.38	N(3)–N(4)–C(6)–O(16)	178.63
C(12)–(C9)	1.529	C(12)–(C9)–(N16)	112.176	C(12)–(C9)–(N16)–C6	55.966
C(17)–(C10)	1.560	C(17)–(C10)–(C8)	111.166	C(17)–(C10)–(C8)–C6	−57.915
C(17)–O(18)	1.209	O(18)–C(17)–C(10)	122.67	O(18)–C(17)–C(10)–C(8)	−136.49
H(15)–C(12)	1.083	C(15)–C(12)–C(9)	111.45	–	–
O(39)–H(40)	0.963	C(25)–O(39)–H(40)	113.05	C(25)–O(39)–H(40)–C(1)	0.0443
C(23)–C(25)	1.368	C(25)–C(23)–C(1)	115.83	–	–
C(24)–C(27)	1.415	C(23)–C(24)–C(27)	118.65	–	–
C(24)–C(26)	1.413	C(24)–C(26)–C(29)	120.47	C(29)–C(26)–C(24)–C23)	179.93
C(28)–C(32)	1.352	C(32)–C(28)–C(25)	120.040	C(32)–C(28)–C(25)–C23)	0.02514
(b)					
Cr(46)–O(5)	1.855	O(5)–Cr(46)–O(29)	88.829	O(26)–Cr(46)–Cl(25)	87.881
Cr(46)–O(29)	1.887	O(5)–Cr(46)–O(26)	91.242	O(26)–Cr(46)–O(33)	89.048
Cr(46)–O(26)	1.887	O(5)–Cr(46)–Cl(25)	84.874	O(26)–Cr(46)–N(8)	90.226
Cr(46)–Cl(25)	2.219	O(5)–Cr(46)–O(33)	177.640	Cl(25)–Cr(46)–O(33)	97.477
Cr(46)–O(33)	1.866	O(5)–Cr(46)–N(8)	96.130	Cl(25)–Cr(46)–N(8)	177.878
Cr(46)–N(8)	1.914	O(29)–Cr(46)–O(26)	179.132	O(33)–Cr(46)–N(8)	81.526
C(6) = N(8)	1.299	O(26)–Cr(46)–Cl(25)	91.264	O(26)–Cr(46)–N(8)	90.625

Table 7 (continued)

Bond connectivity	Bond lengths (Å)	Bond connectivity	Bond angles (°)	Bond connectivity	Torsion angle (°)
N(9) = C(32)	1.426	O(26)–Cr(46)–O(33)	90.916	O(33)–C(32)–N(9)	117.030
Fe(46)–O(5)	1.850	O(5)–Fe(46)–O(29)	89.721	O(26)–Fe(46)–Cl(25)	88.720
Fe(46)–O(29)	1.889	O(5)–Fe(46)–O(26)	91.310	O(26)–Fe(46)–O(33)	89.152
Fe(46)–O(26)	1.890	O(5)–Fe(46)–Cl(25)	85.567	O(26)– Fe(46)–N(8)	89.887
Fe(46)–Cl(25)	2.224	O(5)–Fe(46)–O(33)	178.532	Cl(25)–Fe(46)–O(33)	96.421
Fe(46)–O(33)	1.870	O(5)–Fe–(46)–N(8)	95.310	Cl(25)–Fe(46)–N(8)	178.789
Fe(46)–N(8)	1.910	O(29)–Fe(46)–O(26)	178.231	O(33)–Fe(46)–N(8)	84.612
C(6) = N(8)	1.285	O(29)–Fe(46)–Cl(26)	91.142	O(26)–Fe(46)–N(8)	89.981
N(9) = C(32)	1.288	O(26)–Fe(46)–O(33)	90.820	O(33)–C(32)–N(9)	119.195
(c)					
Mn(36)–N(17)	1.789	N(17)–Mn(36)–O(16)	82.699	O(16)–Mn(36)–Cl(15)	96.913
Mn(36)–O(16)	1.799	N(17)–Mn(36)–O(8)	97.821	O(16)–Mn(36)–O(9)	89.981
Mn(36)–O–(8)	1.831	N(17)–Mn(36)–O(9)	91.012	O(8)–Mn(36)–(11)	89.182
Mn(36)–O–(9)	1.832	N(17)–Mn(36)–O(11)	88.802	O(8)–Mn(36)–Cl(15)	85.399
Mn(36)–O(11)	1.829	N(17)–Mn(36)–Cl(15)	179.901	O(9)–Mn(36)–O(11)	178.986
Mn(36)–Cl(15)	2.170	O(16)–Mn(36)–O(8)	178.125	O(9)–Mn(36)–Cl(15)	89.799
Co(47)–N(17)	1.841	N(17)–Co(47)–O(16)	82.755	O(16)–Co(47)–Cl(15)	95.106
C(3) = N(17)	1.128	O(16)–Mn(36)–O(9)	89.803	O(11)–Mn(36)–Cl(15)	88.971
Co(47)–O(8)	1.830	N(17)–Co(47)–O(9)	91.053	O(8)–Co(47)–O(11)	90.170
Co(47)–O(9)	1.831	N(17)–Co(47)–O(11)	88.913	O(8)–Co(47)–Cl(15)	85.125
Co(47)–O(11)	1.824	N(17)–Co(47)–Cl(15)	177.991	O(9)–Co(47)–O(11)	179.012
Co(47)–Cl(15)	2.170	O(16)–Co(47)–O(8)	180.152	O(9)–Co(47)–Cl(15)	89.901
Ni(47)–N(17)	1.839	N(17)– Ni(47)–O(16)	82.800	O(16)– Ni(47)–Cl(15)	95.122
Ni (47)–O(16)	1.802	N(17)– Ni(47)–O(8)	97.127	O(16)– Ni(47)–O(9)	91.788

Table 7 (continued)

Bond connectivity	Bond lengths (Å)	Bond connectivity	Bond angles (°)	Bond connectivity	Torsion angle (°)
Ni (47)–O(8)	1.832	N(17)– Ni(47)–O(9)	90.088	O(8)– Ni(47)–O(11)	91.165
Ni(47)–O(9)	1.841	N(17)– Ni(47)–O(11)	89.813	O(8)– Ni(47)–Cl(15)	86.130
Ni(47)–O(11)	1.820	N(17)– Ni(47)–Cl(15)	178.012	O(9)– Ni(47)–O(11)	179.125
Ni(47)–Cl(15)	2.172	O(16)– Ni(47)–O(8)	179.195	O(9)– Ni(47)–Cl(15)	89.813
N(18)–C(20)	1.399	O(16)– Ni(47)–O(11)	89.813	O(16)–C(20)–N(18)	104.231
Cu(47)–N(3)	1.859	N(3)–Cu(47)–O(6)	82.739	O(6)–Cu(47)–Cl(30)	95.996
Cu(47)–O(6)	1.834	N(3)–Cu(47)–O(23)	96.810	O(6)–Cu(47)–O(26)	90.834
Cu(47)–O(23)	1.834	N(3)–Cu(47)–O(26)	92.050	O(23)–Cu(47)–O(24)	89.172
Cu(47)–O(26)	1.830	N(3)–Cu(47)–O(24)	87.926	O(23)–Cu(47)–Cl(30)	84.427
Cu(47)–O(24)	1.830	N(3)–Cu(47)–Cl(30)	176.975	O(26)–Cu(47)–O(24)	179.976
Cu(47)–Cl(30)	2.160	O(6)–Cu(47)–O(23)	179.260	O(26)–Cu(47)–Cl(30)	90.690

(O_h) geometry around the metal ion. The molecular geometry is connected with an ONO donor Schiff base and a monodentate coordination of Cl^- ion to Cr(III) and Fe(III), while Mn(II), Co(II), Ni(II) and Cu(II) center as monomeric species with a basal plane. The four basal positions are occupied by the tridentate, diprotic hydrazone ligand, which furnishes an ONO donor set with interatomic distance (Å) in (Cr/Fe); M(46)-O(5); 1.855–1.850, M(46)-O(33);1.866–1.870, M(46)-N(8);1.914–1.910. The fourth position in the case of Cr(III) and Fe(III) complexes was occupied by a Cl of M(46)-Cl(25); 2.219, 2.224 (Å). The four angles are O(5)-Cr(46)-Cl(25); 84.874, O(5)-Cr(M)-N(8); 96.130, Cl(25)-M(46)-O(33); 97.477, O(33)-M(46)-N(8), 81.526 close to 90 (°) and two angles are O(5)-M(46)-O(33); 177.640 and Cl(25)-M(46)-N(8); 177.878 are close to 180(°) which suggests the presence of the basal plane in the complex. The fifth and sixth coordination positions in the complexes were occupied by two water molecules equatorially as trans to each other with O(29)-M(46)-O(26) 179.132 which suggests an irregular geometry of the studied compounds with a distorted octahedral geometry. The optimized structure of other complexes contains a central metal ion with their atoms numbering represented as Mn(36),Co(47),Ni(47) and Cu(47) were bonded by six donor atoms of the octahedral sphere. The complex exhibits shorter bond length (1.831–1.834) Å for the deprotonated M–O bond of the phenyl-OH group. The triatomic in the range of 1.789–1.831(Å), 1.799–1.834(Å) and 1.830–1.834(Å) indicates a shorter bond of phenolic-O, azomethine-N and carbonyl-O respectively. The atomic arrangement involves two oxygen (*trans* positions), one nitrogen of azomethine (ONO) donor monobasic tridentate Schiff base ligand and chlorine as fourth donor atom to form a planar structure. The fifth and sixth *trans*-coordination sites in the complexes were occupied by H_2O molecules inside the coordination field. The interatomic M-Cl bond distances was found in the range 2.160–2.172 (Å) destine of group to azomethine N-donor atom. The triatomic moieties of the chelate cycle approaches to 89–90 (°) equatorial and the axial bond of the M–O bond of H_2O molecule to the plane by an angle of 178.986–178.976 (°) indicates *trans* directing group. The bond lengths, bond angles within the chelate cycle, equatorial and axial plane approaches to the expected values which confirms the structure of octahedral geometry of metal (II, III) complexes [43, 44].

Frontier MO's: HOMO–LUMO analysis

The frontier molecular orbitals (HOMO–LUMO) of ligand and its metal complexes were analyzed in the ground state to demonstrate the quantum chemical properties evaluated from DFT study. The charge transfer from (HOMO → LUMO) of hydrazone ligand (H_2L) and its metal (II/III) complexes are displayed in Fig. 7a–g. The significant FMO's energies and quantum chemical parameters have been charted in Table 8. The charge transfer was occurred from HOMO → LUMO due the small energy band gap favorable of the polarization to the soft molecules. The analysis of HOMO and LUMO signifies the properties of hardness, softness, chemical stability and reactivity. The implication of the small energy band gap between FMO's of ligand at 5.412 eV clearly

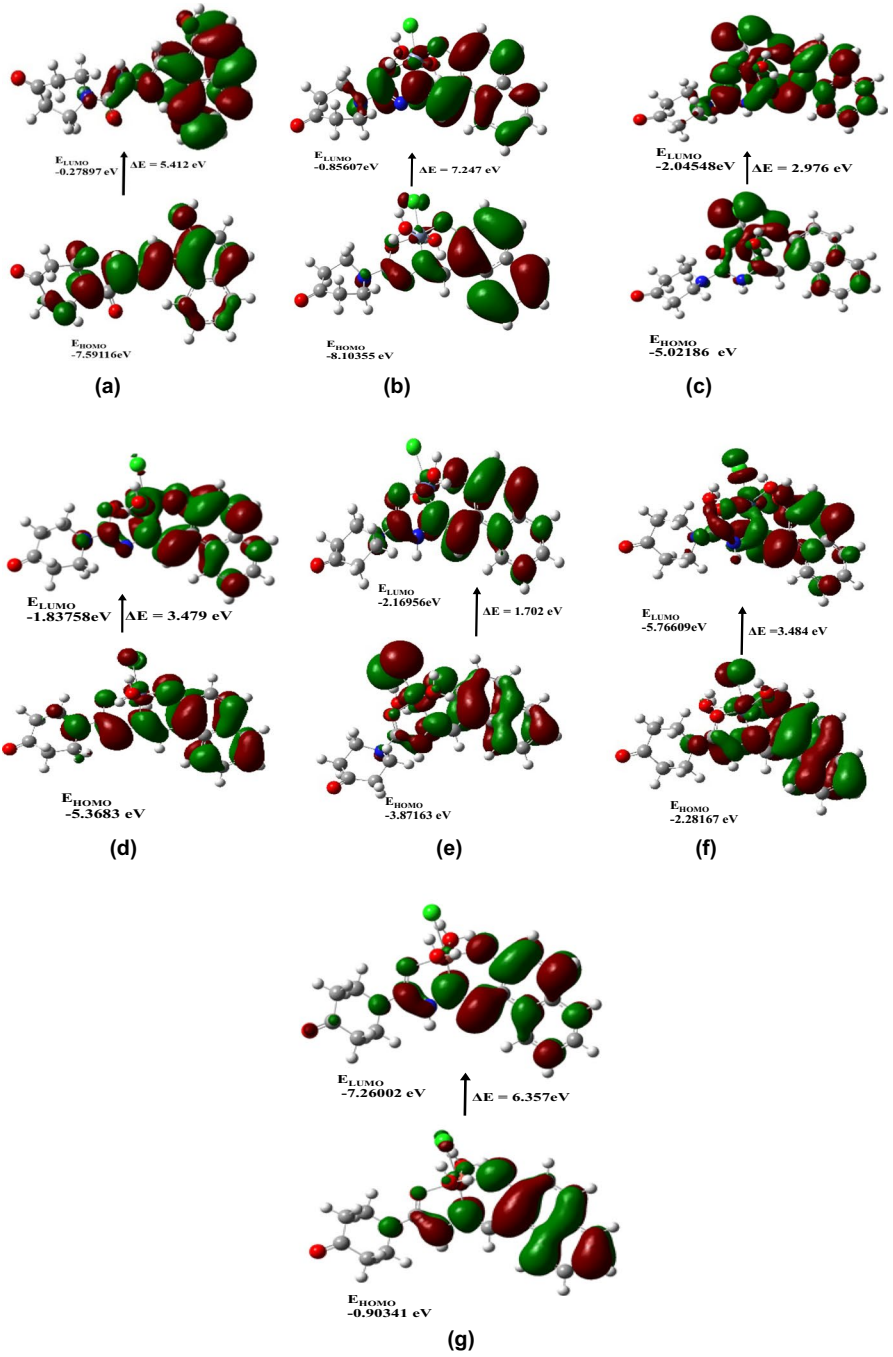

Fig. 7 Plot of frontier MO's HOMO→LUMO **a** Ligand (H_2L), **b** Cr(III), **c** Mn(II), **d** Fe(III), **e** Co(II), **f** Ni(II), and **g** Cu(II) complexes

Table 8 Calculated quantum chemical parameters of hydrazone ligand (H_2L), and its metal complexes

Compounds	FMO's	Energies (eV)	(ΔE)	Quantum chemical parameters								
				(μ)	(η)	(S)	(ω)	(N)	(ΔN_{max})	T. energy (Kcal/mol)	Dipole (debye)	(α)	($\Delta\chi$)
Ligand (H_2L)	E_{HOMO}	−7.5911	5.412	−4.8849	2.7061	0.3695	4.4090	6.346	1.805	−175.19	4.6942	227.86	−8.681
	E_{LUMO}	−2.1788											
Cr(III) complex	E_{HOMO}	−8.1035	7.247	−4.4798	3.6237	0.2759	2.7690	6.859	1.236	−187.01	6.9698	250.97	−8.532
	E_{LUMO}	−0.8560											
Mn(II) complex	E_{HOMO}	−5.0219	2.976	−3.5337	1.4882	0.6720	4.1953	3.777	2.374	−115.89	12.125	237.60	−6.045
	E_{LUMO}	−2.0455											
Fe(III) complex	E_{HOMO}	−5.3168	3.479	−3.5772	1.7396	0.5748	3.6779	4.072	2.056	−122.70	5.2894	240.63	−6.236
	E_{LUMO}	−1.8376											
Co(II) complex	E_{HOMO}	−3.8716	1.702	−3.0206	0.8510	1.1750	5.3605	2.627	3.549	−89.35	9.1312	329.03	−4.956
	E_{LUMO}	−2.1696											
Ni(II) complex	E_{HOMO}	−5.7661	3.484	−4.0239	1.7422	0.5740	4.4912	4.521	2.310	−133.07	8.8182	242.17	−6.907
	E_{LUMO}	−2.2817											
Cu(II) complex	E_{HOMO}	−7.2600	6.357	−4.0817	3.1783	0.3146	2.6210	6.015	1.284	−167.55	8.6190	241.12	−7.712
	E_{LUMO}	−0.9034											

indicates the charge transfer effects at a qualitatively level. The electronic transition ($\pi \rightarrow \pi^*$) occurred from HOMO to LUMO in atoms of phenolic (O-39), carbonyl (O7) and azomethine (N4) group. The metal complexes contain the greater electron density found on 'd' orbital, azomethine-N atom, carbonyl-O atom and Cl^- ion. The FMO's energies indicate the clear evidence in support of charge transfer within metal complex structure. The hydrazone ligand and its metal (II/III) complexes, i.e. energy band gap (ΔE) found decreasing in the order of Cr(III) (7.247) > (Cu (II) (6.357) > (H_2L) ligand (5.412) > Ni(II) (3.484) > Fe(III) (3.479) > Mn (II) (2.976) > Co (II) (1.702) eV which was well supported towards charge transfer within molecule. The other important quantum chemical parameters, i.e. Chemical potential (μ), Global hardness (η), and Softness (S), Electrophilicity index (ω), Nucleophilicity index (N) were calculated [45]. The calculated chemical reactivity's parameters of ligand viz., chemical potential of ligand (μ) = – 4.48849 eV indicating the structural stability and its global hardness (η) = 2.7061, and softness (S) = 0.3695 imply of electron transfer effects. The inverse correlation observed of the global hardness (η) = 1.7305 with the softness (S) = 0.5778 was confirmed the electron transfer from HOMO to LUMO region. This helps in the participating as strong nucleophile which favored to more reactive in the nucleophilic substitution reaction (S_N). The chemical potential of the metal complexes were calculated as (μ) = (–3.0203) to (–4.8849) reflecting their higher stability of molecules. Other factors of global hardness (η) = (0.8510 to 3.6178), compared to softness (S) = (0.2759 to 1.1750) evidence of the complete transfer of electrons occurred from HOMO → LUMO. The calculated nucleophilicity index (N) was more than the electrophilicity index (ω) in ligand (H_2L); ($N = 6.346$ eV > ω = 4.409) and where as in metal complexes of Cr(III); ($N = 6.859 > \omega = 2.769$), Mn(II); ($N = 4.1953 > \omega = 3.777$), Fe(III); ($N = 4.072 > \omega = 3.6779$), Co(II); ($N = 5.3605 > \omega = 2.627$), Ni(II); ($N = 4.521 > \omega = 4.491$), Cu(II); ($N = 6.015 > \omega = 2.621$) as expected. The ($N$) and ($\omega$) are useful key indicators for the concrete information towards in *vitro* anti-microbial potency and well supported by molecular docking [46, 47]. The electrophilic index (ω) was calculated for stabilization purpose after received an additional electron density (ΔN_{max}) from the environment [48, 49].

$$\Delta N_{\max} = -\frac{\mu}{\eta} \tag{6}$$

The overall changes in the total negative energy were calculated (−89.35 to −175.190) kcal mol^{-1} of ligand (H_2L), and its complexes indicate the stabilization of molecular structure at the B3LYP level [59, 60]. The dipole moment of the ligand and metal complexes was evaluated (4.694212.125)D designatory of polarity of molecules in the ground state. The greater the electronegativity difference ($\Delta\chi$) = (−4.956 to −8.681) between two atoms implying the larger the bond's dipole moment and its polarization (α) = (227.89 to 329.031) D. The bonding properties of ligand and its metal complexes show polarity and covalency nature of the molecules were predicted due to the greater electronegativity character ($\boldsymbol{\Delta}\chi$) [50, 51].

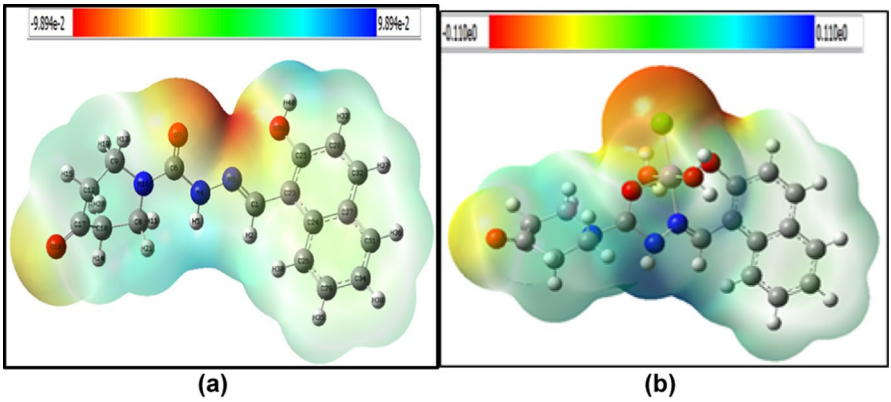

Fig. 8 Molecular electrostatic potential map surface of **a** ligand (H_2L), **b** Mn(II) complex

Molecular electrostatic potential map (MEP)

Molecular electrostatic potential (MEP) map are three-dimensional isocounter surface and are useful descriptor in the understanding of electrophilic and nucleophilic attack to centre and hydrogen bonding interactions on the basis of its electronic charge distribution. The well resolved MEP map were generated from Gaussian *09* of optimized structure of ligand and its Mn(II) complex showed in Fig. 8a, b are as representative cases and other four complexes of Cr(III), Co(II), Ni(II), Cu(II) shown in Fig. S6a–d imaged. The MEP of ligand and its metal complexes correlates the electrophilic and nucleophilic properties which authenticate to negative (red color) and positive (blue) region respectively. The electrostatic potential distinctly increases in the sequence order of yellow < green < red < blue in ligand which informed the exhibiting the nucleophilic active center. In ligand, the –ve electrostatic potential appeared in the maximum region due to the presence of phenyl O(39)-H(40) group, hydrazone group C(1) = N(3)–N(4) and C(6) = O(7) group favorable to electrophilic attack. The MEP of the ligand consists of the negative region of electrostatic belonging to the two–carbonyl-O i.e. (O7, O18), hydrazone group C(1) = N(3)-N(4) and phenolic O(39)-H(40) group showing the magnitude level at − 732.435 kJ/mol. On the other hand, the magnitude for the H-atoms linked to sp^2, sp^3 carbon atom was found in the range of ~ 40 to 150 kJ/mol. The color scale ranges from deep red (− 9.844e−2 a.u.) to deep blue (9.894 e−2 a.u.) in ligand. The deep blue indicates the strong attraction of electrons and red color indicates the repulsion of electrons in ligand, and metal complexes. The region of color in the metal complexes is varied from the ligand after the complex formation. The variation in colored map region of the compounds depends upon the charge distribution, polarity and hydrazone bonding interaction in the complex structures [52, 53].

Absorption, distribution, metabolism, excretion, and toxicity parameters (ADMET)

Experimental

In silico bioactivity prediction of drug-likeness properties was assumed by subjecting them to the calculations from Molinspiration cheminformatics tool. The ADMET properties, including five parameters such as absorption, distribution, metabolism, excretion and toxicity were predicted from a user-friendly interface tools, i.e. admetSAR which is supportive methodology [54]. The pharmacological activity of drugs is defined by the interaction of highly applicable biological targets including enzymes, ion channels and receptors in living things. The bioavailability of the studied compounds were predicted by subjecting them to computations over Molinspiration cheminformatics tool and the results are cited in Table S7. The bioactivity scores of the studied compounds were observed based on six important parameters viz., (i) G-protein coupled receptor ligand (GPCRL), (ii) kinase inhibitor (KI), (iii) ion channel modulation (ICM), (iv) nuclear receptor ligand (NRL), (v) protease inhibition (PI) and (vi) enzyme inhibition (EI). According to earlier researchers, bioactivity scores of 0.0 or higher, then the compounds are promisingly bioactive, while those with scores between 0.50 to 0 have considered moderate activity, and those with a score of −0.50 are inactive [55]. In the present study the compounds exhibit values −0.46 to 0.18 and hence they are expected to show moderate activity. These are predictable to retain such properties as demand for them to behave as possible drugs with some alterations in their molecular structure [56].

Lipinski's rule

In the field of drug design and its development, Lipinski's five (RO5) rule was supported to drugs molecular characteristics. This gives various pharmacokinetic parameters, viz., absorption, distribution, metabolism and excretion (ADME) for predicting the success of an orally administered drug's journey over the body to the site of actions. Some certain molecular characteristics are as follows: (i) The logP (partition coefficient), (ii) Molecular weight (MW) (iii) Number of hydrogen bond acceptors (nON) (iv) Number of Hydrogen bond donors (nOHNH), (iv) Topological polar surface area (TPSA). A drug for an orally active medication should contain logP (≤ 5), hydrogen bond acceptors (≤ 10), hydrogen bond donors (≤ 5) and a molecular weight of (≤ 500), according to RO5 [57]. An orally active medicine should not typically exhibit any rule of violations. Here, the data of the studied compounds based on said parameters are computed and charted in Table S8. Under this rule, milLogP values of ligand (H_2L) (2.63) and its complexes (−5.04 to −5.33) are within the acceptable range for a drug to pass through the bio-membranes and exhibits a good bioavailability. So, the studied compounds can be considered to be oral therapeutic uses of molecules as per RO5.

ADMET Prediction

The theoretical approach has been used for the evaluation in silico ADMET properties. These are pre-indicative whether the studied compounds show toxicity after administration in the body or show any pharmacokinetics. The proceeding for this purpose, the admetSAR methodology was used in the present investigation. The compound was studied on the basis of their molecular structure and the desired compounds were analyzed for the prediction of their pharmacokinetics viz., absorption, distribution, metabolism and elimination (ADMET) as well as their toxicity nature to avoid further potential interactions of drugs with anti-targets causing some side effects. The various absorption as well as excretion models namely (i) aqueous solubility (LogS) (ii) Caco-2 cell permeability, (iii) Blood–Brain Barrier (BBB) penetration, (iv) Human Intestinal Absorption (HIA) and toxicity parameters like (i) carcinogenetic, (ii) LD50 dosage have been used. The predicted ADMET data of the studied ligand (H_2L) and its metal (II, III) complexes are tabulated in Table 9. It was observed that the studied compounds showed absorption and distribution properties indicated by the value of HIA, BBB and Caco2 permeability values which suggests their more auspicious pharmacokinetics. The carcinogenic profile of ligand and its metal (II, III) complexes was also exhibited a non-carcinogenic nature. One of the more applicable information collected from admetSAR is the computed median lethal dose (LD50) in the rat model (acute rat toxicity) which aids in deciding the lethalness of the compounds. Thus, the lower the LD50 value, was more lethal as compared to those with higher LD50 values of the compounds. The LD50 values of studied compounds were mostly more than commonly used as a drug streptomycin (LD50 = 1.841 mol/kg) [58].

Molecular docking

Protein preparation

The three-dimensional crystallographic structures of peptide deformylase, adenylate kinase and DNA polymerase were retrieved from the RCSB protein data bank and used for further processing. Initially, in protein structure modification requires

Table 9 ADMET activity score of hydrazone ligand (H_2L), and its metal complexes

Compounds	BBB	HIA	Caco2	ROCT	Carcinogenicity	LogS	LD50 (mol/kg)
H_2L ligand	0.766	0.974	0.636	Non-inhibitor	Non-carcinogens	− 3.352	2.351
Cr(III) complex	0.578	0.573	0.594	Non-inhibitor	Non-carcinogens	− 3.510	2.635
Fe(III) complex	0.574	0.894	0.596	Non-inhibitor	Non-carcinogens	− 3.518	2.636
Mn(II) complex	0.647	0.510	0.628	Non-inhibitor	Non-carcinogens	− 3.535	2.622
Co(II) complex	0.641	0.921	0.622	Non-inhibitor	Non-carcinogens	− 3.452	2.623
Ni(II) complex	0.641	0.921	0.622	Non-inhibitor	Non-carcinogens	− 3.542	2.623
Cu(II) complex	0.641	0.921	0.622	Non-inhibitor	Non-carcinogens	− 3.542	2.623

various tasks such as insertion of atoms missing in incomplete residues, deletion of alternate confirmations, missing loop region modelling and protonation of titrable residues. The preparation of proteins was performed with the aid of CHARMM force fields generator. For the molecular docking, analysis was performed on the crystal structure of Adenylate kinase (PDB ID-3BE4), peptide deformylase (1LQY) of *Escherichia coli* and fungal enzymes of DNA polymerase (PDB ID-4M8O).

Protein–ligand docking

Discovery studio 2.0 (Accelrys, USA) was employed in silico and post docking visualization. The molecular docking study was completed by a LibDock program of Discovery studio which revealed that the bioactive binding sites of receptor. In LibDock, two protein site features of polar and a polar are available called as hotspots. Further, test compounds were interacted with the polar and a polar sites of receptors. Additionally, the identification to specific interacting residues of the receptor with a bound ligand, a 2D diagram of the docking study was carried out. The molecular docking have been provided the insight of receptor bioactive ligand with specific interactions. Molecular docking structure are presented in Fig. 9a, c, e in 3D view image contains the tube form structure in which hydrogen bond and its bond distance are showed by red color line Fig. 9b, d, f 2D view image contains hydrogen bonding interactions of tridentate hydrazone ligand with enzymes of adenylate kinase, peptide deformylase and DNA polymerase. The molecular docking revealed that the compound have been showed the good binding score with adenylate kinase, peptide deformylase (*E. coli* enzymes) and DNA polymerase (fungal enzyme) as shown in Table 10. Autodock 4.2.6 molecular docking software was operated for the docking analysis in the detection of intramolecular binding of the corresponding linkage of hydrazone ligand with the targeted receptor protein. Before the operation of the docking, the proteins were refined by the removal of water molecules and co-crystallized by adding Kollmann charges and polar hydrogen. The binding affinity of tridentate ligands with the receptors Adenylate kinase and DNA polymerase have signified the dock score of amino acid residues. The greater negative binding energy (-7.42 kcal mol^{-1}) was found in negative terms which displaying the significant binding affinity of ligand with receptor proteins. The binding interactions such as H-bond, van der Wall and hydrophobic interactions distinctly indicate the possible binding ligands with receptor protein [59]. In order to obtain optimum interaction between the protein with the hydrazone ligand, a grid box axis of X, Y and Z with 39, 41 and 41 points was giving rise using Autodock 4.2.6 respectively. The hydrazone ligand have been found pursue in the vicinity of interaction within the active site of the receptor through H-bonding interaction with ASP 167, OSer16, Gly15, Lys18, Ser35, Asp167 residues. The amino acid residue corresponds to binding and holding of the ligand molecule in the active site of Adenylate kinase protein. The molecular docking result indicates that ligand has also Adenylate kinase inhibitory potential. Similarly, the hydrazone ligand when docked with the peptide deformylase showed score with low binding energy (-7.12) kcal mol^{-1} of Gly58, Gly109 which suggested the good inhibitory potential. The molecular docking and its binding data of tested hydrazone ligand showed considerable docking output score of

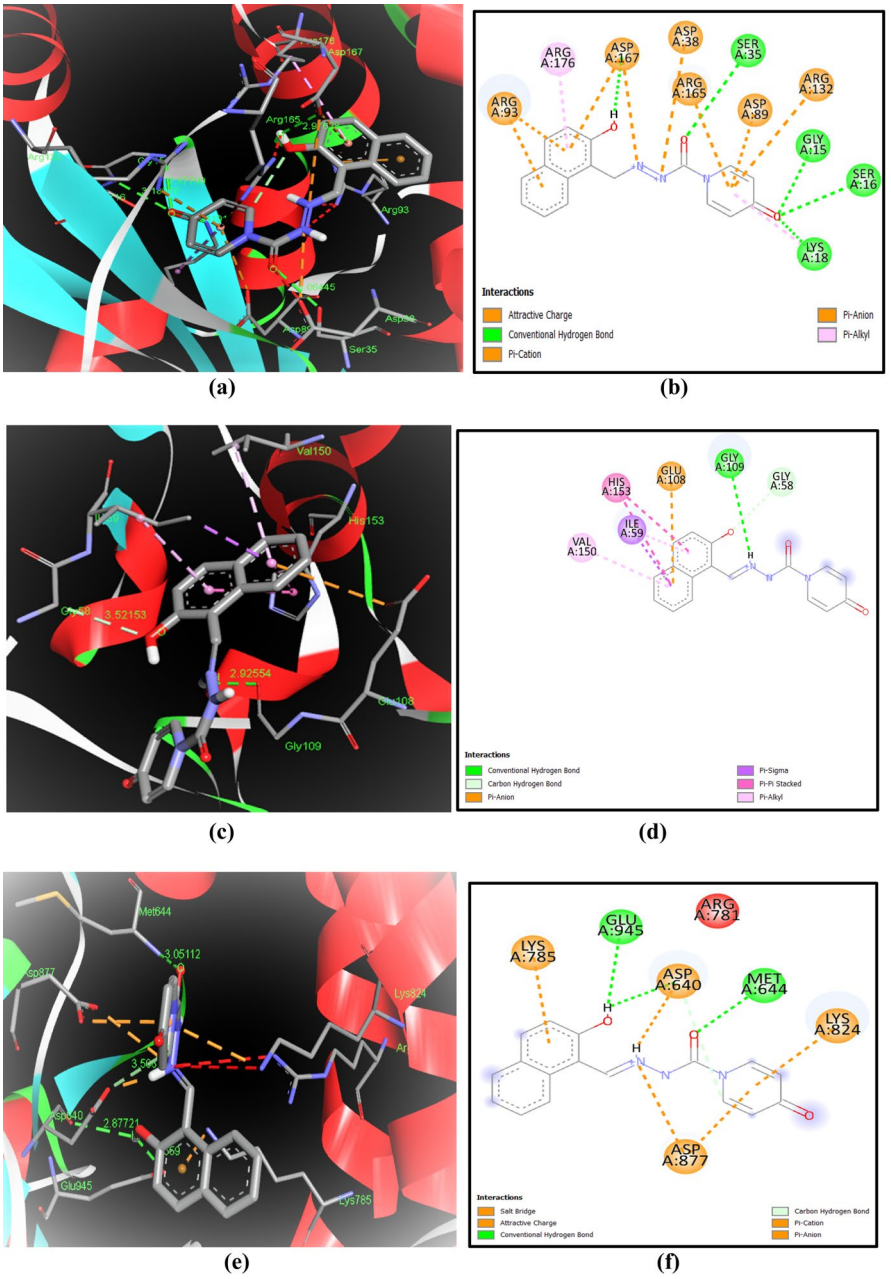

Fig. 9 Molecular docked 3D view image **a**, **c**, **e** in tube form displayed hydrogen bond by red color line and bond distance, and 2D view image of H-bonding interactions of hydrazone ligand (H_2L) with enzymes of **b** adenylate kinase, **d** peptide deformylase, **f** DNA polymerase

Table 10 Molecular docking analysis of bacterial enzyme and fungal enzymes

Compounds	Protein ID	Atom–amino acid residues receptor involved in hydrogen bonding	H-bond distance (Å)	ΔG (kcal/mol)
Adenylate kinase	(3BE4)	O-Ser16	3.18078	−7.42
		O-Gly15	2.87709	
		O-Lys18	2.91191	
		O-Ser35	3.06445	
		H-Asp167	2.97628	
Peptide deformylase	(1LQY)	O-Gly58	3.52153	−7.12
		H-Gly109	2.92554	
DNA polymerase	(4M8O)	H-Glu945	2.55901	−7.20
		H-Asp640	2.87721	
		O-Met644	3.05112	

binding energy (−7.20) kcal mol^{-1}. The 2D docking image well informed the DNA polymerase amino residue has involved in hydrogen bonding of Glu945, Asp640, Met644. The targeted DNA polymerase interacted with ligand through active binding which is capable of damaging the membrane of fungal protein [60, 61].

Antibacterial and antifungal evaluations

The in vitro antibacterial susceptibility of ligand (*E*)-*N*′-((2-hydroxynaphthalen-1-yl)methylene)-4-oxopiperidine-1-carbohydrazide ligand (H_2L) and its metal (II/III) complexes were screened by standard procedure recommended by WHO expert committee on biological standardization; European Committee on antimicrobial susceptibility testing (EUCAST). The disk-diffusion method was employed for the antimicrobial screening against human pathogens of gram-positive bacteria viz., *Staphylococcus aureus* (NDCM-2257), *Bacillus subtilis* (NICM-2477), (gram-negative); *Escherichia coli* (NCBI-0157), *Salmonella typhi* (NICM-2257) and fungi *Candida albicans;* (MTCC-1637) and *Aspergillus niger* (NCIM-1005) at a concentration of 1.0 mg/mL. The microbiological assay was performed in the diagnostic laboratory using fine culture base medium. The mono microbial sensitivity disk was used for the semi-qualitative to evaluate in vitro susceptibility of antimicrobial agents of fast growing human threatening pathogenic species, and several difficult species using an agar disk diffusion techniques. The plates were incubated at temperatures $+35^0$c to $+37^0$c for 24 h. The sensitivity was evaluated by estimating the inhibition zone growth around the loaded disk [62]. The size of the inhibition zone was considered as a basis of resistivity, intermediate or sensitivity and its result were interpreted in (mm). The inhibition activities were presented as a percentage and calculated by the formula ($I = C - TC \times 100$) where I denotes inhibition rate (%); C denotes radial growth of pathogenic microorganism (mm) with solvent DMSO (-ve control); T denotes the radial growth (mm). The commonly useful antibiotic drugs viz., ofloxacin,

Table 11 In vitro antimicrobial result (MICs 1.0 mg/mL) of the tested compounds

Ligand/complexes/ standard drugs	Bacteria (gram negative)		Bacteria (gram positive)		Fungus species	
	Escherichia coli (NCBI-0157)	*Salmonella typhi* (NICM-2257)	*Staphylococcus aureus* (NDCM-2257)	*Bacillus substilis* (NICM-2477)	*Candida albicans* (MTCC-1637)	*Aspergillus niger* (NCIM-1005)
Ligand (H_2L)	18	17	11	10	18	16
Cr(III) complex	21	15	14	12	22	15
Fe(III) complex	20	16	13	12	24	14
Mn(II) complex	24	14	14	13	15	16
Co(II) complex	15	14	11	15	12	30
Ni(II) complex	22	15	10	14	13	20
Cu(II) complex	18	17	14	13	14	21
Ofloxacin*	30	30	–	–	–	–
Azithromycin*	–	–	15	20	–	–
Fluconazole*	–	–	–	–	28	30
DMSO negative control	–	–	–	–	–	–

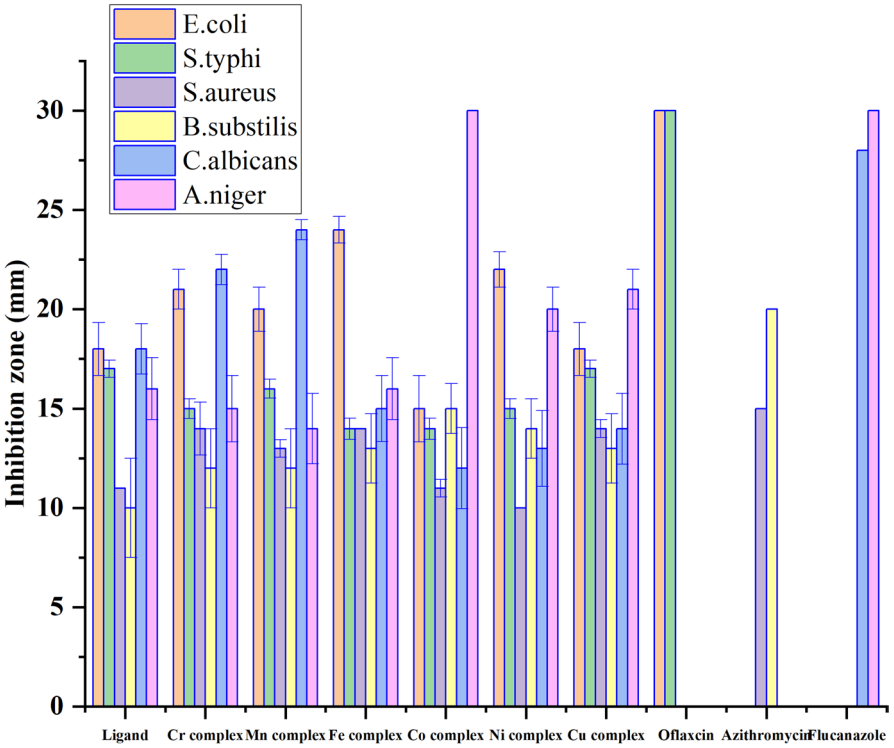

Fig. 10 Inhibition zone growth of microorganism: comparison ligand with metal complexes and standard drugs

azithromycin and fluconazole were used as a (+ ve control) for the comparison of inhibition zone growth [63]. The better activity of compounds was found and this may be due to the presence of an exchangeable proton in (HC=N–) of azomethine group, O-atom in (>C=O) group, delocalized π-electrons of (naphthalene-1-yl) ring, and extra supportive of piperidone moiety. The inhibition zone results are presented in Table 11 and their bar graph (Fig. 10). The results showed that the microbial activity of the ligand also considerably compared to coordinated metal (II/III) complexes. The inhibition zone data indicate gram −ve bacteria, i.e. *E. coli*, and *S. typhi* are more potentially active than gram + ve bacteria, i.e. *S. aureus* and *B. substillis* which is supported by simulation molecular docking analysis. Such group specificity may be due to increase in lipophilicity caused by chelation. The coordination of metal ion with ligand the increases bioactivity, this can be described on the basis of the *Tweedy's chelation theory* (TCT) [64, 65]. On chelation, the polarity of the metal ion is reduced due to the overlap of ligand's orbital and sharing of the positive charge of metal ion with donor atoms. Further, it increases the delocalization of electrons of the chelate ring, the respiration process of cells and blocks the synthesis of proteins which further restricts the growth of organisms. Moreover, the extra benzenoid ring in the structure of

the ligand and its metal complexes reveals the more potential activities against bacterial and fungal growth resistance. Within the fungi, the C. *albicans* is more moderately active than the *A. niger* strain and this may be due to the presence of the *ONO* donor atoms of hydrazone ligand. In azomethine (>C=N) group, an exchangeable proton towards the metal complexes intensify the destroying ability of the human pathogenic microorganisms. The in vitro antimicrobial activities was performed by using a minimum inhibitory concentration (1 mg/ml) of tested with ligand, metal complex and std. drugs. The biological potency of compounds is governed by some factors: (i) The geometrical structure, (ii) ONO donor atoms, (iii) total charge on the metal complex ion, (iv) size of microorganisms, its medium and tolerance factors [66]. The ligand and metal complexes were active against two strains of viz., *E. coli* having an inhibitory zone range of (15–24 mm) than *S. typhi* (14–17 mm) shows a broad spectrum activities in the order of metal complexes of Mn(II) > Ni(II) > Cr(III) > Fe(III) > Cu(II) > H_2L ligand. This may be due to the smaller size (2.0 µm) of *E. coli*, which displayed better sensitivity than the facultative anaerobic S. Typhi size of (5 µm) which has a motile flagella. The compounds in the order of Cr(III) ≈ Mn(II) ≈ Cu(II) > Fe(III) > H_2L ligand showed good antimicrobial activity when treated with B. subtilis and S. aureus inhibitory zone of (10–14 mm) and (10–15 mm) respectively [67]. Moderate activities against *S. auresus* are observed in the complexes of Co(II) > Ni(II). Due to its protective endospores and tolerance in extreme environments, B. subtilis bacteria exhibits less performance than S. aureus. All the compounds treated of *A. niger's* fungal species resulted in good activity of Co(II) > Ni(II) > Cu(II) complexes. All inhibitory zone data reveal that the metal (II/III) complexes show the moderate to good antimicrobial activities than the free ligand. The Co(II) complex is superior among all compounds showing inhibitory zone of 30 mm when compared to std. drug of fluconazole and hence treated good antifungal candidate. The antimicrobial potency result are compatible with targeted *E. coli* protein of peptide deformylase, adenylate kinase, and fungal protein of DNA polymerase with tridentate hydrazone ligand [68, 69].

Conclusions

Herein, we have presented two types of metal complexes in the form of [M(L)$Cl(H_2O)_2$]; [M = Cr(III) and Fe(III)] and [M(HL)$Cl(H_2O)_2$]; [M = Mn(II),Co(II),Ni(II),Cu(II)] with (*E*)-*N*′-((2-hydroxynaphthalen-1-yl)methylene)-4-oxopiperidine-1-carbohydrazide (H_2L) ligand and characterized them by various physicochemical and spectral techniques. The experimental and theoretical studies are quite compatible with each other for the proposed octahedral geometry of metal complexes. The synthetic studies showed the importance of tridentate moiety, *N*-heterocycle in piperidone nucleus present in the ligand. The elemental analysis showed 1:1 ligand-to-metal stoichiometry ratio in addition to the non-electrolytic behavior of metal complexes. All compounds were displayed their superb absorption and fluorescence emission properties. The ESR tensor component features of $A_{\parallel}$ (168 cm^{-1}) > $A_{\perp}$ (55.54 cm^{-1}) in which no metal–metal interaction showed distorted octahedral

geometry of Cu(II) complex. The surface morphology of ligand was distinct from the complex proved by an imaging by SEM analysis. The powder XRD diffraction data inferred showed their nanocrystalline nature. TG analysis of metal complexes indicated the presence of two coordinated-H_2O and one Cl^- ion metal complex. The kinetic parameters of (Ea, Z, ΔS, ΔH, ΔG) indicate a good thermal stability, endothermicity and non-spontaneity due to 'structural order' of metal complexes. The small energy band gap of (HOMO → LUMO) in ligand and metal complexes was sufficient to charge transfer effect. Molecular docking revealed the better binding affinity of the hydrazone ligands with the receptors of Adenylate kinase, DNA polymerase and peptide deformylase. The coordination of ligand with metal ions have enhanced potential antibacterial and antifungal activity against selected pathogenic species. More general, this investigation contributes to structural dynamics in fluorescence, antimicrobial and pharmacological applications.

Supplementary Information The online version contains supplementary material available at https://doi.org/10.1007/s11164-023-05169-2.

Acknowledgements The authors are greatly acknowledged to the authorities of Sant Gadge Baba Amravati University, Amravati for furnished necessary research facilities viz., Bruker-IR instrument, UV-Vis., and Perkin Elmer-TG analyser. The authors are grateful thanks to SAIF-Punjab University, Chandigarh for elemental, NMR (^1H and ^{13}C), HR-Mass spectra and SEM analysis. The authors are also grateful to the sophisticated analytical Instrumental facility of Indian Institute of Technology (IIT)-Mumbai for recording the ESR spectrum and the Principal, Central instrumentation facility, Shri Shivaji Science College, Amravati (M.S.) for powder X-ray diffraction analysis.

Authors' contribution GD have been written original draft; utilized software along with the conceptualization; performed formal analysis and investigation. AS contributed in methodology; writing—review and editing; resources as well as in supervision of research work.

Funding No funding was received from any agencies for this research work.

Availability of data and materials All the spectral data are provided supplementary information.

Declarations

Conflict of interest The authors declares that they have no conflict of interest.

Ethical approval No animal/ human studies were carried out in the present work.

References

1. S. Kumar, J. Devi, A. Dubey, D. Kumar, D.K. Jindal, S. Asija, A. Sharma, Res. Chem. Intermed. **49**, 939 (2023)
2. A. Erdmann, Y. Menon, C. Gros, V. Masson, Y. Aussagues, F. Ausseil, N. Novosad, P. Schambel, M. Baltas, P.B. Arimondo, Future Med. Chem. **8**, 373 (2016)
3. W. Khalid, A. Badshah, A. UllahKhan, H. Nadeem, S. Ahmed, Chem. Cent. J. **12**, 1 (2018)
4. U. Salgin-Goksen, G. Telli, A. Erikci, E. Dedecengiz, B.C. Tel, F.B. Kaynak, K. Yelekci, G. Ucar, N. Gokhan-Kelekci, J. Med. Chem. **64**, 1989 (2021)
5. M. Gaber, A.M. Khedr, M. Elsharkawy, Appl. Organomet. Chem. **31**, 1 (2017)
6. A. Alka, S. Gautam, R. Kumar, P. Singh, N. Gandhi, P. Jain, Results Chem. **5**, 100849 (2023)

7. T.R.F. de Melo, R.C. Chelucci, M.E.L. Pires, L.A. Dutra, K.P. Barbieri, P.L. Bosquesi, G.H.G. Trossini, M.C. Chung, J.L. dos Santos, Int. J. Mol. Sci. **15**, 5821 (2014)
8. W.B. Júnior, M.S. Alexandre-Moreira, M.A. Alves, A. Perez-Rebolledo, G.L. Parrilha, E.E. Castellano, O.E. Piro, E.J. Barreiro, L.M. Lima, H. Beraldo, Molecules **16**, 6902 (2011)
9. X. Yu, L. Shi, S. Ke, Bioorg. Med. Chem. Lett. **25**, 5772 (2015)
10. O.A. El-Gammal, G.M.A. El-Reash, R.A. Bedier, Appl. Organomet. Chem. **33**, 1 (2019)
11. A.A. Mohamed, F.M. Ahmed, W.A. Zordok, W.H. El-Shwiniy, S.A. Sadeek, H.S. Elshafie, Inorganics **10**, 1 (2022)
12. M.S. El-Attar, F.M. Ahmed, S.A. Sadeek, S.F. Mohamed, W.A. Zordok, W.H. El-Shwiniy, Appl. Organomet. Chem. **36**, 10 (2022)
13. H.S. Seleem, G.A. El-Inany, B.A. El-Shetary, M.A. Mousa, F.I. Hanafy, Chem. Cent. J. **5**, 1 (2011)
14. H.H. Repich, S.I. Orysyk, V.V. Orysyk, Y.L. Zborovskii, A.K. Melnyk, V.V. Trachevskyi, V.I. Pekhnyo, M.V. Vovk, J. Mol. Struct. **1146**, 222 (2017)
15. J. Bureš, H. Jansová, J. Stariat, T. Filipský, P. Mladěnka, T. Šimůnek, R. Kučera, J. Klimeš, Q. Wang, K.J. Franz, P. Kovaříková, J. Pharma Biomed. Anal. **105**, 55 (2015)
16. K.D. Praliev, N.A. Belikova, Zh.I. Isin, D.V. Sokolov, Pharm. Chem. J. **21**, 854 (1987)
17. S.N. Mali, B.R. Thorat, D.R. Gupta, A. Pandey, MDPI Engn. Proc. **11**, 1 (2021)
18. H.S. Seleem, Chem. Cent. J. **5**, 1 (2011)
19. W. Cao, Y. Liu, T. Zhang, J. Jia, Polyhedron **147**, 62 (2018)
20. R. Fouad, I.A. Shaaban, T.E. Ali, M.A. Assiri, S.S. Shenouda, RSC Adv. **11**, 37726 (2021)
21. M. Gaber, S.K. Fathalla, H.A. El-Ghamry, Appl. Organo. Chem. **33**, 1 (2019)
22. P. Jyothi, S. Koppu, V. Sumalatha, B. Ushaiah, C. Gyana Kumari, Inorg. Chem. Commun. **110**, 107590 (2019)
23. M. Gaber, N. El-Wakiel, O.M. Hemeda, J. Mol. Struct. **1180**, 318 (2019)
24. Y. Li, C. Qian, Y. Li, Y. Yang, D. Lin, X. Liu, C. Chen, J. Inorg. Biochem. **218**, 111405 (2021)
25. F.K. Ommenya, E.A. Nyawade, D.M. Andala, J. Kinyua, J. Chem. **2020**, ID1745236 (2020).
26. V.P. Singh, A. Katiyar, J. Coord. Chem. **61**, 3200 (2008)
27. A. Pahonţu, C. Paraschivescu, D.C. Ilieş, D. Poirier, C. Oprean, V.P. Ăunescu, A. Gulea, T. Roşu, O. Bratu, Molecules **21**, 1 (2016)
28. L. Tabrizi, D.Q. Dao, T.A. Vu, RSC Adv. **9**, 3320 (2019)
29. V.P. Singh, A. Katiyar, S. Singh, Biometals **21**, 491 (2008)
30. G.M. Dongare, A.S. Aswar, Euro. J. Chem. **13**, 4 (2022)
31. M. Shakir, S. Hanif, M.A. Sherwani, O. Mohammad, S.I. Al-Resayes, J. Mol. Struct. **1092**, 143 (2015)
32. A.S. Alturiqi, A.N.M.A. Alaghaz, R.A. Ammar, M.E. Zayed, J. Chem. **2018**, 8987 (2018)
33. A.K. Sarangi, B.B. Mahapatra, R.K. Mohapatra, S.K. Sethy, D. Das, L. Pintilie, M. Kudrat-E-Zahan, M. Azam, H. Meher, App. Organomet. Chem. **34**, 1 (2020)
34. O.V. Konnik, M.A. Kiskin, D.S. Balaev, V.F. Shulgin, A.N. Gusev, J. Struct. Chem. **64**, 1361–1368 (2023)
35. L.V. Ababei, A. Kriza, A.M. Musuc, C. Andronescu, E.A. Rogozea, J. Therm. Anal. Calorim. **101**, 987 (2010)
36. S. Shit, J. Chakraborty, B. Samanta, A.M.Z. Slawin, V. Gramlich, S. Mitra, Struct. Chem. **20**, 633 (2009)
37. O.M.I. Adly, Spectrochem. Acta Part A Mol. Biomol. Spectrosc. **79**, 1295 (2011)
38. D. Meng, F. Liu, Y. Li, Z. Yang, G. Li, D. Guo, Luminescence **31**, 507 (2016)
39. Y. Li, Z.Y. Yang, M.F. Wang, J. Fluorine **20**, 891 (2010)
40. N. De Acha, C. Elosúa, J.M. Corres, F.J. Arregui, Sensors **19**, 599 (2019)
41. R. Konakanchi, J. Haribabu, J. Prashanth, V.B. Nishtala, R. Mallela, S. Manchala, D. Gandamalla, R. Karvembu, B.V. Reddy, N.R. Yellu, L.R. Kotha, Appl. Organomet. Chem. **32**, 1 (2018)
42. G. Tamasi, L. Chiasserini, L. Savini, A. Sega, R. Cini, J. Inorg. Biochem. **99**, 1347 (2005)
43. K. Karrouchi, S. Fettach, A. El Hassane, I. Bayach, H. Albalwi, S. Arshad, N.K. Sebbar, H. Tachalait, K. Bougrin, F. My El Abbes, B. Himmi, Polycycl. Arom. Compd. **43**, 2 (2023)
44. M. Bashir, A. A. Dar, and I. Yousuf, ACS Omega **8**, (2023).
45. G.M. Dongare, A.S. Aswar, J. Saudi Chem. Soc. **25**, 101325 (2021)
46. L.R. Domingo, M. Ríos-Gutiérrez, P. Pérez, Molecules **21**, 748 (2016)
47. T.L. Yusuf, S.D. Oladipo, S. Zamisa, H.M. Kumalo, I.A. Lawal, M.M. Lawal, N. Mabuba, ACS Omega **6**, 145 (2021)
48. R.G. Parr, C. Hill, N. Carolina, J. Am. Chem. Soc. **121**, 1922 (1999)

49. G. Badhin, N.V. Likhanova, M.A. Domınguez-Aguilar, R. Martınez-Palou, V. Alberto, J.L. Gazquez, J. Phys. Chem. B **110**, 8928 (2006)
50. F. Soleymani-Bonoti, M.A. Kamyabi, N. Arshadi, Comput. Theor. Chem. **1092**, 47 (2016)
51. J.C. Guo, H.G. Lu, S.D. Li, Comput. Theor. Chem. **1018**, 95 (2013)
52. A. Tabbiche, A. Bouchama, N. Chafai, F. Zaidi, C. Chiter, M. Yahiaoui, A. Abiza, J. Mol. Struct. **1261**, 132865 (2022)
53. N.M. El-Barasi, M.M. Miloud, M.M. El-ajaily, R.K. Mohapatra, A.K. Sarangi, D. Das, A. Mahal, P.K. Parhi, L. Pintilie, S.R. Barik, M.N. AminBitu, M. Kudrat-E-Zahan, Z. Tabassum, S.I. Al-Resayes, M. Azam, J. Saudi Chem. Soc. **24**, 492 (2020)
54. M. Sarkar, A. Nath, A. Kumer, C. Mallik, F. Akter, M. Moniruzzaman, M. Ali, J. Mol. Struct. **1244**, 130953 (2021)
55. F. Cheng, W. Li, Y. Zhou, J. Shen, Z. Wu, G. Liu, P.W. Lee, Y. Tang, J. Chem. Inform. Mod. **52**, 3099 (2012)
56. T. Khan, S. Dixit, R. Ahmad, S. Raza, I. Azad, S. Joshi, A.R. Khan, J. Chem. Bio. **10**, 91 (2017)
57. C.A. Lipinski, F. Lombardo, B.W. Dominy, P.J. Feeney, Adv. Drug Deliv. Rev. **64**, 4 (2012)
58. M. Aarjane, A. Aouidate, S. Slassi, A. Amine, Arab. J. Chem. **13**, 6236 (2020)
59. A.C. Ekennia, E.C. Ibezim, O.C. Okpareke, C.U. Ibeji, C.J.O. Anarado, I. Babahan, B. Coban, B. Abulhasanov, F. Cömert, O.T. Ujam, Appl. Organ. Chem. **33**, 1 (2019)
60. A. Misra, S. Sharma, D. Sharma, S. Dubey, A. Mishra, D. Kishore, J. Dwivedi, J. Chem. Sci. **130**, 31 (2018)
61. F. Marandi, K. Moeini, A. Arkak, Z. Mardani, H. Krautscheid, J. Coord. Chem. **71**, 23 (2018)
62. S. Alyar, Ş Adem, Spectrochem. Acta Part A Mol. Biomol. Spectrosc. **131**, 294 (2014)
63. G.M. Dongare, A.S. Aswar, J. Mol. Struct. **1281**, 135107 (2023)
64. A.A. El-Sherif, M.M. Shoukry, M.M.A. Abd-Elgawad, Spectrochem. Acta Part A Mol. Biomol. Spectrosc. **98**, 307 (2012)
65. R.N. Patel, S.P. Rawat, M. Choudhary, V.P. Sondhiya, D.K. Patel, K.K. Shukla, D.K. Patel, Y. Singh, R. Pandey, Inorg. Chim. Acta **392**, 283 (2012)
66. R.R. Zaky, A.Y. Al-dawood, SILICON **12**, 1259 (2020)
67. Y. Deswal, S. Asija, D. Kumar, D.K. Jindal, G. Chandan, V. Panwar, S. Saroya, N. Kumar, Res. Chem. Intermed. **48**, 703 (2022)
68. A.A. Osowole, A.C. Ekennia, O.O. Olubiyi, M. Olagunju, Res. Chem. Intermed. **43**, 2565 (2017)
69. H. Yakan, T.K. Bakır, M.S. Çavuş, H. Muğlu, Res. Chem. Intermed. **46**, 5417 (2020)

Publisher's Note Springer Nature remains neutral with regard to jurisdictional claims in published maps and institutional affiliations.

Springer Nature or its licensor (e.g. a society or other partner) holds exclusive rights to this article under a publishing agreement with the author(s) or other rightsholder(s); author self-archiving of the accepted manuscript version of this article is solely governed by the terms of such publishing agreement and applicable law.

ISSN 2319 - 359X

AN INTERNATIONAL MULTIDISCIPLINARY
HALF YEARLY RESEARCH JOURNAL

IDEAL

Volume - XII Issue - II March - August - 2024

ENGLISH PART - VI

Peer Reviewed Referred and
UGC Listed Journal No. 47026

Single Blind Review/Double Blind Review

ज्ञान-विज्ञान विमुक्तये

IMPACT FACTOR / INDEXING
2023 - 7.537
www.sjifactor.com

❖ EDITOR ❖

Assit. Prof. Vinay Shankarrao Hatole
M.Sc (Math's), M.B.A. (Mkt), M.B.A (H.R),
M.Drama (Acting), M.Drama (Prod & Dirt), M.Ed.

❖ PUBLISHED BY ❖

Ajanta Prakashan
Aurangabad. (M.S.)

The information and views expressed and the research content published in this journal, the sole responsibility lies entirely with the author(s) and does not reflect the official opinion of the Editorial Board, Advisory Committee and the Editor in Chief of the Journal **"IDEAL"**. Owner, printer & publisher Vinay S. Hatole has printed this journal at Ajanta Computer and Printers, Jaisingpura, University Gate, Aurangabad, also Published the same at Aurangabad.

Printed by

Ajanta Computer, Near University Gate, Jaisingpura, Aurangabad. (M.S.)

Published by

Ajanta Prakashan, Near University Gate, Jaisingpura, Aurangabad. (M.S.)

Cell No. : 9579260877, 9822620877

E-mail : ajanta2023@gmail.com, www.ajantaprakashan.in

IDEAL - ISSN 2319 - 359X - Impact Factor - 7.537 (www.sjifactor.com)

EDITORIAL BOARD

Mehryar Adibpour
Faculty of Computing London
Metropolitan University,
Holloway Road, London.

Dr. Ashaf Fetoh Eata
College of Art's and Science,
Salmau Bin Adbul Aziz University. KAS

Dr. Altaf Husain Pandi
Dept. of Chemistry University
of Kashmir, Kashmir, India.

Dr. Ramdas S. Wanare
Associate Professor & Head Accounts & Applied Stat,
Vivekanand Art's Sardar Dalip Sing Commerce
& Science College Samarth Nagar, Aurangabad (M.S.)

Dr Harish Kumar
Assistant Professor Department of History,
Mangalayatan University, Extended,
Ncr 33rd Milestone, Mathura - Beswan
Aligarh (U.P.) 202146.

Dr. P. A. Koli
Professor & Head (Retd),
Dept. of Economics, Shivaji University,
Kolhapur - (M.S.) India.

Dr. Rana Pratap Singh
Professor & Dean School for Environment Science,
Dr. Babasaheb Bhimrao Ambedkar University
of Raebareily, Lucknow- India.

Dr. Joyanta Barbora
Head Dept. of Sociology University of
Dibrugarh- India.

Dr. Jagdish R. Baheti
H.O.D., SNJB College of Pharmacy,
Neminagar, Chandwad, Nashik (M.S.) - India.

Prof. P. N. Gajjar
Head, Dept. of Physics,
University of School of Sciences,
Gujarad University, Ahmedabad- India.

Dr. Binoy Musahary
Department of Political Science,
Nalbari College, Nalbari Assam, P. O. Bidyapur.

Dr. Prashant M. Dolia
Dept. of Computer Science and Applications,
Bhavnagar University, India.

Dr. S. Jeyakumar
Assistant Professor, PG & Research Department of
Commerce, P. M. T. College, Melaneelithanallur,
Sankarankovil Tirunelveli, Tamil Nadu.

Dr. P. S. Buvaneswari
Asst. Professor of Commerce,
University of Madras Chepauk, Chennai-05.

Dr. (CA) Subrahmanya Bhat K. M.
Principal, Department of Commerce,
Swami Vivekananda College, Borim Ponda, Goa.

Dr. G. B. Lamb
Associate Professor & Head,
Department of Mathematics
Baliram Patil College, Kinwat, Dist.Nanded. (M.S.)

EDITORIAL BOARD

Dr. Priyanka A. Masatkar
Assistant Professor, Dept. of Botany,
Ghulam Nabi Azad Arts Commerce and
Science College, Barshitakli, Akola, Maharashtra.

Dr. Dhirajkumar S. Kotme
Head, Department of Marathi,
Jaikranti Airts & Com. Sr. College,
Latur. (Maharashtra)

Dr. Manish Ahir
Head Dept. of Microbiology,
Ghulam Nabi Azad Arts, Commerce &
Science College, Barshitakli, Dist.- Akola. (M.S.)

Dr. Amit Vairale
Head Dept. of Zoology,
Ghulam Nabi Azad Arts, Commerce &
Science College, Barshitakli, Dist.- Akola. (M.S.)

Dr. Nilima Kankale
Dept. of Zoology,
Ghulam Nabi Azad Arts, Commerce &
Science College, Barshitakli, Dist.- Akola. (M.S.)

Dr. Vinod Undal
Dept. of Botany,
Ghulam Nabi Azad Arts, Commerce &
Science College, Barshitakli, Dist.- Akola. (M.S.)

Dr. Siddharth Waghmare
Dept. of Chemistry,
Ghulam Nabi Azad Arts, Commerce &
Science College, Barshitakli, Dist.- Akola. (M.S.)

Dr. Santosh Suradkar
Head Dept. of Botany,
Ghulam Nabi Azad Arts, Commerce &
Science College, Barshitakli, Dist.- Akola. (M.S.)

Dr. Sharad Idhole
Head Dept. of Chemistry,
Ghulam Nabi Azad Arts, Commerce &
Science College, Barshitakli, Dist.- Akola. (M.S.)

Dr. Kailash R. Kale
Dept. of Statistics,
Ghulam Nabi Azad Arts, Commerce &
Science College, Barshitakli, Dist.- Akola. (M.S.)

Dr. Sanjay Deshmukh
Head Dept. of Geology,
Ghulam Nabi Azad Arts, Commerce &
Science College, Barshitakli, Dist.- Akola. (M.S.)

Asst. Prof. Ajit Patil
Head Dept. of Biochemistry,
Ghulam Nabi Azad Arts, Commerce &
Science College, Barshitakli, Dist.- Akola. (M.S.)

Dr. S. B. Khobragade
Head Dept. of Mathematics,
Ghulam Nabi Azad Arts, Commerce &
Science College, Barshitakli, Dist.- Akola. (M.S.)

Dr. Deepika N. Jain
Dept. of Microbiology,
Ghulam Nabi Azad Arts, Commerce &
Science College, Barshitakli, Dist.- Akola. (M.S.)

Dr. Tejas Patil
Dept. of Geology,
Ghulam Nabi Azad Arts, Commerce &
Science College, Barshitakli, Dist.- Akola. (M.S.)

Asst. Prof. Yuvraj Kale
Dept. of Biochemistry,
Ghulam Nabi Azad Arts, Commerce &
Science College, Barshitakli, Dist.- Akola. (M.S.)

EDITORIAL BOARD

Dr. Anant Kute
Dept. of Physics,
Ghulam Nabi Azad Arts Commerce and
Science College, Barshitakli, Akola, Maharashtra.

Astt. Prof. Pramod Tasre
Head Dept. of Statistics,
Jaikranti Airts & Com. Sr. College,
Latur. (Maharashtra)

Asst. Prof. Bhausaheb Gayakwad
Head Dept. of Physics,
Ghulam Nabi Azad Arts, Commerce &
Science College, Barshitakli, Dist.- Akola. (M.S.)

Dr. Amol Shrirao
Dept. of Chemistry,
Ghulam Nabi Azad Arts, Commerce &
Science College, Barshitakli, Dist.- Akola. (M.S.)

Dr. Bhimrao Jaiwal
Dept. of Biochemistry,
Ghulam Nabi Azad Arts, Commerce &
Science College, Barshitakli, Dist.- Akola. (M.S.)

PUBLISHED BY

Ajanta Prakashan
Aurangabad. (M.S.)

CONTENTS OF ENGLISH PART - VI

S. No.	Title & Author	Page No.
1	Morpho Taxonomic Studies of Diversity of Genus Eragrostis Wolf of Family Poaceae of Amravati District, Maharashtra **Dr. Priyanka A. Masatkar**	1-7
2	Rapid study of House Sparrows (Passer Domesticus) From Mahan Dist Akola **Priyanka D. Joshi** **Prof. Nilima Kankale**	8-13
3	MATLAB simulator and Neural Network Classifiers for Iris Detection **Dr. R. D. Chaudhari**	14-20
4	To Study the Different Life Stage of Silkworm Bombyx Mori from Patur Region (Shirla) **Anuradha Datta Karale** **Nilima B. Kankale**	21-29
5	Isolation and Identification of Cellulose Degrading Bacteria from Different Environmental Samples **Miss. Janhavi Surendra Choubey** **Dr. Vijay D. Nanoty**	30-37
6	Study of Spider Diversity at Kapshi Lake, Akola **Kajal N. Wagh** **Prof. Amit Vairale**	38-44
7	Evaluation of Molecular Interaction of 1, 6-Dihydropyrimidine in Acetone and DMSO Solvent **M. M. Mhasal** **P.J. Thakare**	45-53
8	Synthesis, Characterization and Biological Activity of Nitrogen Containing Pyrazolone and its Derivatives **R. N. Gaikwad** **B. N. Chate**	54-60
9	The Poincare Half-Plane Model and Geo Gebra: Powerful Tools for Understanding Hyperbolic Triangles **Rajesh Balkrishna Raut**	61-64

CONTENTS OF ENGLISH PART - VI

S. No.	Title & Author	Page No.
10	Biodiversity Informatics Provides Sound Iformation for Better Management - By Using Computing Tools **Ranjan B. Kalbande**	65-68
11	Comprehensive Study on Catla Fish (Catla Catla): Biology, Ecology, and Socioeconomic Significance **Reena P. Dhote**	69-73
12	Diversity of Butterfly from Kapshi Lake, Akola **Roshani P. Ingle** **Prof. Nilima Kankale**	74-80
13	Reflects the Revitalizing and Renewing Effects of the Cranberry and Yogurt Extract Formulation on the Human Skin **Rupali R. Hatolkar** **Dipika V. Muley** **Shraddha Jaiswal** **Mrs. Quddusa Kamil Farooqui**	81-88
14	Synthesis, Spectral Characterization and Antimicrobial Potent Study of Some Novel 7-[(2-Substitutedimino-4-Phenylimino) Amino-1,3, 5-Dithiazino)] Along with Coumarin Nucleus **S. A. Waghmarea** **K. U. Dongareb** **S. B. Sarkatec** **R. N. Ingoled**	89-96
15	Synthesis, Characterization and Biological Evaluation of Chromene -2-Carbonitrile and Their Derivatives **S. G. Badne** **G. W. Belsare**	97-101
16	Acoustic Parameters of 0.001M Aqueous Solution of Hydroxichloroquine at Different Temperatures **S. H. Shrirame** **A. B. Dhote**	102-107

CONTENTS OF ENGLISH PART - VI

S. No.	Title & Author	Page No.
17	Studies and Assessment of Water Quality Parameters of Akola District Region (Maharashtra) **S. J. Patil**	108-112
18	Recent Trends in Internet of Things: Issue Challenges and Applications **S. M. Dhakulkar** **A. P. Fulari**	113-119
19	Study the Acoustic Parameters of Li, Na, K ion Salts in Aqueous of Different Concentration at 303K **S. P. Burad** **A. B. Dhote**	120-124
20	GIS Based Morphometric Analysis of Pili Watershed in part of Sapan River, Amravati District, Maharashtra, India **S. R. Warghat** **S. V. Kulkarni** **A. A. Gawande** **Y. K. Mawale** **P. S. Tidke**	125-140
21	A Study of Lineaments or Fracture Zones Regime of Ground Water Potential in Katepurna River Basin, Akola District, Maharashtra, India **Dr. S. S Deshmukh** **Dr. Tejas R. Patil** **Dr. G. D. Gaikwad** **P. P. Pali**	141-146
22	Viscometric Studies of 1-Phenyl-3-[4-(3-Allylimino-1,2,4-Dithiazolo) Aminophenyl]-Prop-2-Ene-1-One At Various Molar Concentrations and At 250c in 70 % Ethanol–Water Mixture **S. S. Padhena** **S. A. Waghmareb**	147-150

1. Morpho Taxonomic Studies of Diversity of Genus Eragrostis Wolf of Family Poaceae of Amravati District, Maharashtra

Dr. Priyanka A. Masatkar
Assistant Professor, Department of Botany Ghulam Nabi Azad Arts Commerce and Science College, Barshitakli, Akola, (Maharashtra)

Abstract

Amravati is one of the 11 districts of vidarbha. It includes 14 talukas. Flora of Amravati district has been already studied by Dhore (2002) reported 84 species of grasses, during last 16 years no survey was conducted of the area. Survey of grasses conducted during 2014-2018 revealed 117 species belonging to 60 genera. Eragrostis Wolf is a largest genus of study area, it has 13 species which belong to subfamily Pooideae. The aim of our investigation is to study morphotaxonomic revision of family poaceae. It focuses on details of macro and micro morphology of some important grasses.

Key words - Amravati, Flora, Survey, morphology.

Introduction

Grasses are most beautiful group of monocotyledonous plants. They occur on every soil, in all kind of situations and under all climatic conditions. As grasses do not like shade, they are not usually abundant within the forest. But in open places they grow very well and some times whole tracts become grasslands.

Grasses are important for entire ecosystem. Tiger is the king of forest ecosystem. If we want to save tiger, we have to save the grasses because tigers are indirectly dependant on grasses for their food. Robinson writes “Grass is king” it rules and governs the world, without it the earth would be a barren waste.

In the early days when the population was much limited and when limited land was under cultivation much of it was covered with plenty of green grasses. So the farmers paid no attention to the grasses. But now population has increased, open land is decreased very much and cattles have increased in number hence farmers have to pay more attentation to grasses. The present destruction of grasses is mainly due to overgrazing, increasing agricultural practices, over use of

herbicides, formation of big dams, road widening, clean agricultural practices and trampling by men and cattles. Grazing needs to be inhibited in certain areas and also reduce the use of herbicides. Tender shoots of Bamboo are used as vegetables and also as pickle by locals. The grains of grasses certainly provide a staple food supply for the human beings Oryza sativa, Triticum aestivum, Zea mays, Avena sativa, Setaria italica, Eleusine coracana, Echinochloa colonum, Sorghum speciesand rice feeds more human beings than any other plant product. Sugarcane is main source of sugar. A high proportion of the most fertile and productive soil were developed under a vegetative covers of grasses. Root, rhizome and other part of grasses are good soil builders and effective soil stabilizers. Most of the birds and animals depend upon grassland habitat for food, shelter and normal completion of their life cycles Gould (1968).

Despite utmost importance of grasses to human beings, the study on grasses continues to be a neglected subject. This is mainly because of the feeling that it is a difficult group for identification, the leaves and branches of grasses are very much similar, Small floral organs, special terminology and variation in the structure of spikelet and inflorescence. "Grasses of Burma, Ceylon, India and Pakistan" studied by Bor (1960) is the main standard reference work on Indian grasses.

Study Area

Amravati district is located in the state of Maharashtra-India. It is at $20^0$55' and 20.93 North latitude $77^0$45' and 77.75 East longitudes. It has an average elevation of 343 meters (1125 feet). Total area of the district is 12210 sq. km. Amravati district has tropical wet and dry climate with hot, dry summer from April to June. The annual average rainfall in the district is 852.1 mm and the temperature has recorded between 18^0C to 46^0C (Falling rain Genomics, inc. 2010).

Apart from this, Amravati is one of the largest district of Maharashtra states. It includes fourteen (14) taluka namely Amravati, Achalpur, Warud, Chandurbazar, Dharni, Morshi, Daryapur, Anjangaon Surji, Chandur Railway, Dhamangaon Railway, Teosa, Nandgaon-Khandeshwar, Bhatkuli, and Chikhaldara. Chikhaldara is the largest talukas of Amravati district and Bhatkuli is the smallest one.

Review of Earlier Work

Though botanical exploration of India has long history, Vidarbha and Marathwada regions remained somewhat neglected. A thorough exploration of Marathwada has been done by

Naik and his students for nearly 30 years. Outcome of this work is "Flora of Marathwada" by Naik (1998) which a wonderful survey and reference flora.

The monumental work of Bor. (1953) on "Grasses of Burma, Ceylon, India and Pakistan"(excluding Bambusiae) published about 50 years ago has changed this scenario and created interest on the study of grasses. This resulted in publication of several books on grasses and the latest addition is "Flora of Tamil Nadu-Grasses" by Altaf and Nair (2009) that deals with 447 species (excluding Bamboos).

Patunkar (1980) studied "Grasses of Marathwada" region has also published a book "Grasses of Marathwada".

Recently, Potdar (2012) has published "Grasses of Maharashtra", the book is an outcome of exploration and detailed studies conducted on documents of grass diversity of Maharashtra for last 20 years. During this period 415 species belonging to 125 genera have been described. There are above 10,000-11,000 species belonging to 700 genera in the world (Clayton and Renvoize, 1989 and Watson and Dallwitz, 1992) in India there are more than 1200 species belonging to 268 genera (Karthikeyan et al., 1989, and Moulk 1997). Kamble and Pradhan (1988) reported 87 species belonging to 49 genera from Akola district. Acharya (1985) reported 100 species belonging to 57 genera from Wardha district. Deore (2010) reported 65 species of grasses from Washim district. Karthikeyan (1993) reported 81 species from Yavatmal district and Diwakar (2000) reported 60 species from Buldhana district.

Floristic surveys of different area of Maharashtra have been compiled and published by Botanical Survey of India such as" Flora of Maharashtra state, Monocotyledon", Sharma et al., (1996), "Flora of Maharashtra state, Dicotyledon"vol. I Singh et al., (2000), vol.II Singh et al., (2001).

Material and Methods

Plan of Work

1. Study of Habitat

In every season the selected areas were explored systematically. Grass covered sites were targeted for study. Grasses were collected from different habitats like irrigated fields, unirrigated fields, open grasslands, forest, bunds of field, bank of rivers, wastelands, rice fields and rocky places.

2. Sample collection and preservation

During excursion specimens of grasses were collected and field number is given to each specimen. Field observations were noted down in field diary. After collection the samples are critically studied in laboratory. Then it is dried properly, poisoned by using 2% Mercury Chloride and mounted using conventional methods. For critical cases BSI (Pune) was consulted to match the specimens.

3. Identification

The identification was confirmed by using floras like flora of British India(Hooker 1872-1897), Flora of Bombay Presidency (Cook 1958), Flora of Marathwada (Naik 1998), Flora of Maharashtra(Almeida,1990), Grasses of Maharashtra (Potdar, Salunkhe and Yadav, 2012) Grasses of Marathawada (Patunkar,1980). Specimens were observed under Sterioscopic binocular microscope.

Artificial keys were provided for genera and species. Population variations are critically studied. Latest nomenclature are given in detail for proper taxonomic level. Each grass specimen description was supported by a note on distribution and herbarium specimen number. Genera and species are arranged alphabetically. Floristic analysis was done to get clear picture of grass biodiversity. Grass species are arranged according to N.L. Bor. All the specimens were deposited in the herbarium of S.S.S.K.R.Innani Mahavidyalaya, Karanja (Lad), Dist-Washim.(M.S.)

4. Observations

Species of Eragrostis and habitat.

Sr. No.	Specimen No.	Name of Species	Habitat
1	PAM 110	Eragrostis aspera (Jacq) Nees.	Unirrigated fields
2	PAM 114	Eragrostis atrovirens (Desf.) Trin.ex Steud.	Cultivated fields
3	PAM 28	Eragrostis cilianensis (All.) Vignolo ex Jaunch.	Open grasslands
4	PAM 82	Eragrostis ciliaris (L.) R.	Wastelands
5	PAM 60	Eragrostis coarctata Stapf.	Sandy soil
6	PAM 81	Eragrostis gangetica (Roxb.) Steud.	Stream banks
7	PAM 30	Eragrostis japonica (Thunb.) Trin.	Cultivated fields
8	PAM 98	Eragrostis multicaulis Steud.	Wastelands
9	PAM 62	Eragrostis nutans (Retz.) Nees ex. Steud.	Wet places
10	PAM 80	Eragrostis pilosa (L.) P.Beauv.	Margin of ponds
11	PAM 31	Eragrostis tef (Zuccagni) Trotter	Waste lands
12	PAM 61	Eragrostis unioloides (Retz.) Nees ex.Steud.	Rice fields
13	PAM 64	Eragrostis viscosa (Retz.) Trin.	Sandy soil

Key for the species of Eragrostis

1a -	Spikelets not breaking up at maturity	E. tef
1b -	Spikelets breaking up at maturity	2
2a -	Spikelets breaking up from above downwards rhachis fragile`	3
2b -	Spikelets breaking up from above upwards rhachis tough	7
3a -	Keels of paleasscabrid or smooth, not ciliate	4
3b -	Keels of paleas more or less ciliate	5
4a -	Panicles lax, open thysiform more than 15 cm wide	E. aspera
4b -	Panicles effuse or contracted not thyrsiform less than 15 cm wide	E. japonica
5a -	Panicles effuse, clums and leaves viscous	E. Viscosa
5b -	Panicles spiciform or compact and dense	6
6a -	Annuals lemmas ciliate on keels	E. ciliaris
6b -	Perennials, lammas not ciliate on keels	E. Coaractata
7a -	Perennials	8
7b -	Annuals	9
8a -	Spikelets 1 to 1.2 mm wide, paleras persistent	E. nutans
8b -	Spikelets 2 to 2.5 cm wide, paleas deciduous	E atrouirens
9a -	Plants glandular	11
9b -	Plants eglandular	10
10a -	Tip of lemma acute or obtuse culme 20-40 cm tall	E. ganetica
10b -	Tips of lemma acute, dwarf plant upto 12 cm tall	E. multicaulis
11a -	Plant glandular spikelets 2-4 mm wide, crowded of loose leaves almost always with raised glands on kells and margines	E. cilianecsis
11b -	Plants devoid of glands	12
12a -	Spikelets 2mm or more wide	E. unioloides
12b	Spikelets narrow, less than 1.5 mm wide	E. Pilosa

Conclusion

Present study is the outcome of exploration tours conducted to document the grass diversity of study area from 2014-2018 and visited different areas of Amravati district in different seasons. During this period over 600 specimens were collected from the study area. During the study 117 species belonging to 60 genera were collected.

Out of 60 genera Eragrostis is the largest genus belonging to sub-family pooideae. The 35 species collected from study area were found to be monotypic. In Amravati district pure patches of Aristada, Ischaemum, Themeda, Andropogon, Heteropogon, Dicanthium, Cynodon and Saccharum were observed.

Though grasses are herbaceous in nature, but are tough in texture so it is easy to prepare herbarium speciman. Some of the beautiful grasses are Thelepogon elegans, Mnesithea granularis, Chrysopogon fulvus, Ischaemum rugosum and Dichanthium species.

Some dominant genera are Apluda, Aristada, Dicanthium, Cynodon, Dinebra, Eragrostis, Ischaemum, Rottboellia, Heteropogon, Ophiuros, Setaria.Some grasses have underground rhizomes i.e. Ischaemum pilosum, Cynodon dactylon, Saccharum spontaneum whichcan not be eradicated hence the productivity of crops decreases. Cynodon is the first class fodder grass present throughout study area. It is palatable and resistant to grazing and trampling because of underground rhizomes. Dactyloctenium aegyptium, Chrysopogon fulvus are other palatable species of grasses. Cymbopogon martini, Vetiveria zizanioides, Saccharum spontaneum and Cynodon dactylon are the medicinal grasses. Hollow internodes of Arundo donax are used formaking pens and musical pipes by locals. The forest areas of Melghat (Chikhaldara and Dharni) are of mixed dry deciduous type with teak as dominant species.

Saccharum spontaneum, Vetiveria zizanioides, Arundo donax present along the sides of rivers and stream which reduce the pressure of flood. The dominant tribes of Melghat are Gond, Korku and Gawali. Gond, and Gawali are the tribal residents of Melghat forest range are the consumers as they feed their livestock mainly by grazing of grasses. Efforts are required to prevent free grazing as once vegetation is lost, it is very difficult to restore.

References

- Acharya, R.M. 1985. Flora of Wardha district. Ph.D. Thesis unpublished, Nagpur University, Nagpur.
- Altaf K. and V.J.Nair, 2009. Flora of Tamil Nadu- Grasses, Botanical Survey of India. Calcutta.Deore A.N. 2010.Floristic Survey of Washim District, Ph.D. Thesis unpublished, Amravati University, Amravati.
- Dhore M.A. 2002.Flora of Amravati District with Special Reference to the Distribution of Tree Species, Amravati University, Amravati.
- Diwakar, P.G. and B.D. Sharma. 2000. Flora of Buldhana District, Maharashtra State. Botanical Survey of India, Calcutta.
- Gould, F.W.1968.Grass systematic.McGraw-Hill.New York.
- Kahalkar, V.I. 2009. Floristic studies on Gondia district of Maharashtra state, Ph.D thesis Nagpur University, Nagpur.
- Kambale, S.Y. and S.G.Pradhan.1988.Flora of Akola District, Maharashtra.Botanical Survey of India, Calcutta.
- Karthikeyan K.S. and Anand Kumar.1993.Flora of Yavatmal District.Botanical Survey of India, Calcutta.
- Naik, V.N.1998. Flora of Marathwada, Vol.I and II.Amrut Prakashan, Aurangabad.
- Patil, B. M.1991. Floristic and palynological investigations in the Monocot flora of Chandrapur and Gadchiroli district, of Vidarbha region, of Maharashtra State. Ph.D thesis, Nagpur University Nagpur.
- Patunkar, B.W.1980. Grasses of Marathwada. Scientific Publisher, Jodhpur.
- Potdar, G.G., Salunkhe C.B., and S.R. Yadav, 2012. Grasses of Maharashtra, Shivaji University, Kolhapur.
- Purekar, P.N. 1885. Grasses of Nagpur District-Taxonomy and Palynology. Ph.D thesis Nagpur University, Nagpur.
- Sharma, B.D. S.Karthikeyan, and N.P. Singh, 1996. Flora of Maharashtra state, Monocotyledones. Botanical Survey of India. Calcutta.
- Yadav, S.R. and M.M. Sardesai, 2002. Flora of Kolhapur District Shivaji University, Kolhapur.

2. Rapid study of House Sparrows (Passer Domesticus) From Mahan Dist Akola

Priyanka D. Joshi
Department of Zoology, Ghulam Nabi Azad College of Arts, Commerce and Science, Barshitakli Dist. Akola.
Prof. Nilima Kankale
Guided by Department of Zoology, Ghulam Nabi Azad College of Arts, Commerce and Science, Barshitakli Dist. Akola.

Abstrct

This study aims to comprehensively document on the sparrows across different area of Mahan. Field surveys were conducted in various habitats, including urban, rural, and forested areas, to assess the presence and abundance of different sparrow species. House sparrow (passer domesticus) belongs to family passeridae. the family Passer contains around 28 species.

Keywords: House Sparrows (Passeridae), Mahan region

1. Introduction

The house sparrow (Passer domesticus) is found in many pieces of the world. It has a place with the family Passeridae and variety passer. The word passer originates from Latin which implies sparrow and this term alludes to speed or easy. Sparrow is generally adorable, little and innocuous social feathered creature. House sparrows are started in the Middle East and get acquainted with most pieces of the world.

Kingdom: Animalia

Phylum: Chordata

Class: Aves

Order: Passeriformes

Family: Passeridae

Genus: Passer

Species: domesticus

It is a little feathered creature that has a regular length of 16 cm (6.3 in) and a mass of 24–39.5 g (0.85– 1.39 oz). The house sparrow is emphatically connected with a human area and can live in urban or country settings. The House Sparrow has a verifiable commensal connection with man and has followed his movement of the standard of the earth. Most Passer species are dull-hued flying creatures with short, square tails and squat, conelike mouths, somewhere in the

range of 11 and 18 cm (4.3 and 7.1 in) long. In the Handbook of the Birds of the World, the family Passer contains around 26 species. House sparrows have an inclination to form homes in little gaps in structures, covered rooftops, and even road lights. The genders are dimorphic with the male being intensely designed. Guys and females can be separated particularly - the male has dark throat white cheeks and dark Bib. It has dark cheeks and dims underparts with dark round the eyes. While the female has earthy colored shading with eyes stripe and thick mouth, two wing bars, and a plain throat and bosom. The bill gets darker during the reproducing season and a couple of flying creatures have a totally dark bill. They are short-legged.

Sparrows, small, chirpy birds with a penchant for seeds, are not only a familiar sight in backyards and cityscapes, but also vital components of our ecosystems. India, with its diverse landscapes – from the snow-capped Himalayas to the sun-drenched coasts – provides a haven for a surprising number of these fascinating birds. However, the widespread decline in sparrow populations globally has raised concerns about their conservation status. In India, the decline of sparrows has been particularly noticeable, with various factors such as habitat loss, pesticide use, and changes in urban landscapes contributing to their dwindling numbers.

2. Habitat /Habit

House Sparrows persevere through just in the momentary region of individuals. House Sparrows are firmly connected with individuals and their structures. They are intrigued by structures for perching and haven. They have worn to build their home in cover rooftops, sun conceals, any corner or break, lofts, kitchens, exhaust openings, hanging bins, unused shafts with end tops, garden trees, bushes and so on to give bug food to the youthful.

House Sparrows jump to a limited degree than a stroll on the ground. They are common, taking care of in jam-stuffed rushes and quarreling about pieces or seeds on the ground. House Sparrows can be seen for winged animal feeders; you may likewise observe them swim in roadside puddles or residue washing on open ground, unsettling their otherwise calm disposition and flicking water or residue over themselves. House sparrows are social artists when the winged animals gather in shrubs and assemble. Living in a cozy relationship with people. Guys with bigger measures of dark on the throat tend to command over guys with less dark. At when guys show to an imminent mate, they lighten up their chest, hold their wings incompletely open, fan the tail, and bounce firmly before the female, spinning sideways and here and there bowing all over. Now and then, different guys who spot such a presentation in progress will fly in and start showing also. In herds, guys will in general command over females in fall and winter, yet females stand up for themselves in spring and summer. Typical life expectancy is as long as 12 years.

3. Nesting

House Sparrows home in gaps of structures and different structures, for example, streetlights, service station rooftops, signs, and the overhanging installations that hold traffic lights. They sporadically assemble homes in vines climbing the dividers of structures. House Sparrows are solid contenders for home boxes, as well, now and again uprooting the species the home box was proposed for, for example, bluebirds and Tree Swallows. House Sparrows home in gaps in trees to some degree less regularly. House Sparrow homes are made of coarse dried vegetation, regularly stuffed into the gap until it's about filled. The flying creatures at that point utilize better material, including plumes, string, and paper, for the coating. House Sparrows in some cases fabricate settles close to one another, and these nearby homes can part dividers. House Sparrows routinely reuse their homes. House Sparrows utilize a wide scope of materials for the home structure including fine hair, grass inflorescences, stalks, and underlying foundations of plants, bark, strings, string, and even bits of paper and fleece. Inside home boxes, the home might be essentially a cup of vegetation at the base of the crate or developed with the goal that the home material covers the sides just as the head of the compartment. The most regular tallness while investigating the area of metropolitan sparrow homes was somewhere in the range of three and four meters high. House Sparrows settling in ensured locales, for example, home boxes and gaps in structures will in general beginning reproducing prior and are increasingly fruitful, then those settling among tree limbs.

4. Diversity of House Sparrow

The work on morphology and biology of the house sparrow was initiated around 1900 [1]. Aggressive flocks of sparrows discourage other species of birds from foraging in the same area. Abundance and congregation of house sparrow in a particular area depends on the availability of food sources for both adults and nestlings and essential nest sites around those food sources. Occurrence and abundance of a species in a particular area is determined by biotic factors and different habitat variables such as food sources, habitat covers and relative abundance of other bird species. The following explanatory variables were supposed to affect the abundance of house sparrow Population in a particular area: The food sources are mostly categorized in to three categories.

1. **Leftover food:** This category includes all types of leftover food which are thrown out from the houses and grocery shops and the left over rice grains present in the rice twigs of thatched roof. The left over foods also constituted the rice, wheat, green gram and black gram grains.

2. **Plant buds:** Guava, Citrus, Drum stick trees, and Papayas are the major sources of buds throughout the years. Birds were observed feeding while roosting in the above mentioned trees.
3. **Arthropods:** Arthropods form the major constituent of the nestling diet. There is significant contributions in the field of diversity and conservation of sparrows [2-7]. House Sparrow looking for food in mahan threatened species. the house sparrow population has been declining above 10% in the last three decades in several parts of the world. For this reason the house sparrow has evaluated as Least Concern

5. Importance of House Sparrow

Fossil evidence from a cave in Bethlehem dating back 4, 00,000 years suggests that the house sparrow shared its space with early humans. It simply cannot live without humans and is never found where we are not. Sparrow is a very important member of various urban and natural food chains and food webs and plays a crucial role in ecological balance. The house sparrow is commensal with humans and is considered to be one of the most highly adapted species to urban conditions. Female house sparrow in daytime at Sikar Rajasthan It feeds on grains and also on larva of insects especially mosquitoes which breeds in the water and this mechanism is a natural pest control process It has proven well suited for studies in evolutionary mechanisms, temperature regulation and pest control. It also feeds on larva of mosquitoes which breeds in the water stagnated in the in accessible area of house. The sparrows go in search of larva and feeds on them. This mechanism is a natural pest control process in which human being also favored without any expenses. Sparrow visits many flowers in a day and at the time of visit they carry pollen and. thus is important for pollination.

5.1 Ecological Roles

Each sparrow species exhibits distinct preferences for its habitat. House Sparrows thrive in human settlements, readily utilizing man-made structures for nesting and foraging.

Beyond their charming presence, all these sparrows play crucial ecological roles. They act as seed dispersers, helping in plant regeneration and maintaining the health of various ecosystems. Additionally, they are natural insect predators, keeping insect populations in check and contributing to the ecological balance

Photographs Taken By Different Area of Mahan

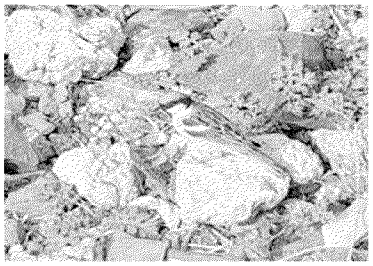

House sparrow form field area of Mahan

House sparrow from urban area of Mahan

House sparrow from household area

Conclusion

In conclusion, this study provides valuable insights of sparrows in Mahan. It can be concluded that the sparrow's population is decreasing without specifications of the cause. For sparrow conservation it is the time to take fruitful efforts to conserve the tiny social bird from becoming rare in future. The sparrow act as seed dispersers, helping in plant regeneration and maintaining the health of various ecosystems. Additionally, they are natural insect predators, keeping insect populations in check and contributing to the ecological balance.

References

1. www.ijcrt.org © 2021 IJCRT | Volume 9, Issue 1 January 2021 | ISSN: 2320-2882 IJCRT2101326 International Journal of Creative Research Thoughts (IJCRT) www.ijcrt.org 2647
2. Ali, S., & Ripley, S. D. (1980). Handbook of the birds of India and Pakistan: Together with those of Bangladesh, Nepal, Bhutan, and Sri Lanka. Oxford University Press.
3. Chakravarthy, A. K., & Sridhar, S. (2013). On the possible role of urbanization in the decline of the House Sparrow Passer domesticus in Bangalore, India. In Avian ecology and conservation in an urbanizing world (pp. 115-128). Springer.

4. Gangoso, L., Agudo, R., Anadón, J. D., de la Riva, M., Suleyman, A. S., Porter, R., & Donázar, J. A. (2013). Reinventing mutualism between humans and wild fauna: insights from vultures as ecosystem services providers. Conservation Letters, 6(3), 172-179.
5. Raman, T. R. S. (2007). Birds of south Asia: The Ripley guide. Smithsonian Institution & Lynx Edicions.
6. Sharma, H. P., & Sathyakumar, S. (2008). Distribution, relative abundance, and conservation status of House Sparrow (Passer domesticus) in Uttarakhand, India. Zoos' Print Journal, 23(12), 5-10
7. Ali, S. The Book of Indian Bird, 1 st edition, Oxford University Press, New Delhi, 1996.
8. Daniels RJR. Can we save the sparrow. Current Science, 2008; 9(5):1527-1528.
9. Hussain A, Dasgupta S, Bargali SH. Case of House Sparrow (Passer domesticus) Population Decline: Role of Semi-Nomadic Pastoralist Community (Van Gujjars) In Their Conservation. International Journal of Conservation Science. 2014; 5(4):493-502.
10. Kamath V, Mathew AO, Lewlyn L, Rodrigues R. Indian sparrows on the brink of extinction: population dynamics combined. International Journal of Renewable Energy and Environmental Engineering. 2014; 02(01):17-22.
11. Kumar A. Status, Distribution, Demography, Threats and Response of House Sparrow (Passer domesticus) to Artificial Nests and Feeds in and around Lucknow, Uttar Pradesh, India. PhD T. Singh R, Kour DN, Ahmed F, Sahi DN. The causes of decline of house sparrow (Passer domesticus) in urban and suburban areas of Jammu Region,. Munis Entomology & Zoology. 2013; 8(2):803-811.
12. Beauregard Erika, François Brischoux, Pierre, Yves Henry, Charline Parenteau, Colette Trouve et al. urbanization cause stress in wild birds during development? Insights from feather corticosterone levels in juvenile house sparrows (Passer domesticus) Ecology and Evolution. 2019; 9(1):640-652
13. Meillere A, Dupoue A, Lourdais O, Angelier F. Traffic noise decreases nestlings' metabolic rates in an urban exploiter. Journa

3. MATLAB simulator and Neural Network Classifiers for Iris Detection

Dr. R. D. Chaudhari
Associate Professor, Shri. R.L.T. College of Science, Akola.

Abstract

Our main aim is to develop a secure biometric recognition system to identify individual person both Irises other than physical or behavioral characteristics. One such method is iris recognition which is one of the most secure and unique features of any person. God has created every individual with an exclusive iris pattern on this earth. The iris recognition technique consists of iris localization, normalization, feature extraction and matching. Their unique feature was extracted and given to the neural network using MATLAB Simulation for detecting the Iris. The match results shows that the individual is identified accurately both the iris of a same Person.

Keywords - Iris recognition, localization, normalization, neural network, person identification, MATLAB

Introduction

Identity verification and identification is becoming increasingly popular. Biometric measures [1] such as recognizing one's fingerprints, face, iris and voice greatly help in person identification authentication, and authorization. Pair of iris recognition has the high potential and non-invasive personal verification. Advances in the field have expanded the options to include biometrics such as iris and retina. Among the large set of options, it has been shown that the iris is the most accurate biometric. The iris is the elastic, pigmented, connective tissue that controls the pupil. Doughman [2] proposed an iris recognition system representing an iris as a mathematical function. Mayank Vatsa proposed a support-vector-machine-based learning algorithm selects locally enhanced regions from each globally enhanced image and combines these good-quality regions to create a single high-quality iris image.[3] proposes algorithms for iris segmentation, quality enhancement, match score fusion, and indexing to improve both the accuracy and the speed of iris recognition Further, Tests on another set of 801 images resulted in false accept and false reject rates of 0.0005% and 0.187% respectively, providing the reliability

and accuracy of the biometric technology[5]. Leila FallahAraghi used Iris Recognition based on covariance of discrete wavelet using Competitive Neural Network (LVQ). A set of Edge of Iris profiles are used to build a covariance matrix by discrete wavelet transform using Neural Network.[4]. Today with the development of Artificial Intelligence algorithm, Iris recognition system may gain speed, hardware simplicity, accuracy and learning ability. The experimental results have shown the effectiveness of the proposed system in comparison with other previous Iris recognition system.

Proposed Work Flow Chart

The complete iris recognition system consists of 4 stages, they are image acquisition, Pre-processing, Feature extraction and Matching. Figure 3.1 shows the flow diagram of Iris recognition system.

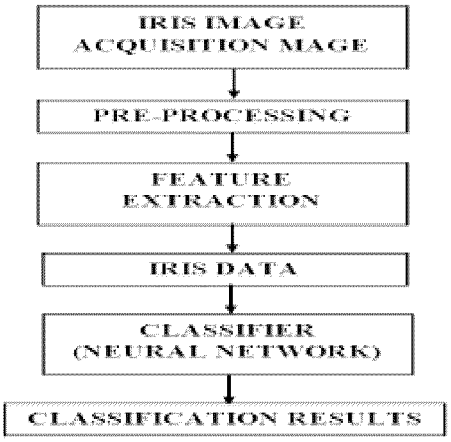

Flow Diagram of Iris Recognition Systems

Image Acquisition

This is very first step of the entire process. When a person wishes to be identified by iris recognition system, his/her eye is first photographed. The camera can be positioned between three and a half inches and one meter to capture the image. Today's commercial iris camera typically used infrared light to illuminate iris without causing harm or discomfort to the subject. In the manual procedure, the user needs to adjust the camera to get the iris in focus and needs to be within six to twelve inches of the camera. This process is much more manually intensive and requires proper user training to be successful. We must consider that the occlusion, lighting, number of pixels on the iris are factors that affect the imagequality. Figure 1.2 shows the sample iris images.

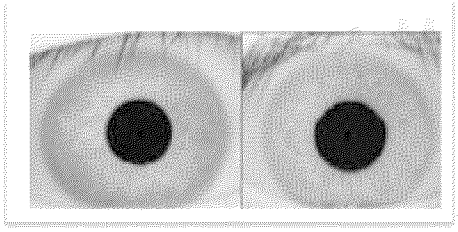

Fig. 1.2 Sample Iris Image

Pre-Processing

The acquired iris image has to be pre- processed to detect the iris, which is an annular portion between the pupil (inner boundary) and the sclera (out boundary). The first step in iris localization is to detect pupil which is the black circular part surrounded by iris tissues. The centre of pupil can be used to detect the outer radius of iris patterns. The important steps involved are :

1. Pupil detection
2. Outer iris localization

The Hough Transform is used for a quick guess of the pupil center and then the Integro-Differential Operator is used to accurately locate pupil and limbus using a smaller search space.

Canny Edge Detection can be used for detecting edges in the entire eye image and Circular Hough Transform for detecting outer boundary of iris by using pupil center and inner boundary of iris. Figure 3.1.2 shows the localized iris image.

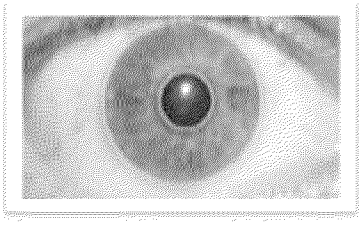

Fig. .1.3 Localized Iris Image.

Normalization

For the purpose of accurate texture analysis, it is necessary to compensate this deformation, since both the inner and outer boundaries of the iris have been detected so it is easy to map the iris ring to a rectangular block of texture of a fixed size. The Cartesian to polar reference transform suggested by Doughman authorizes equivalent rectangular representation of the zone of interest as shown in figure 1.3.

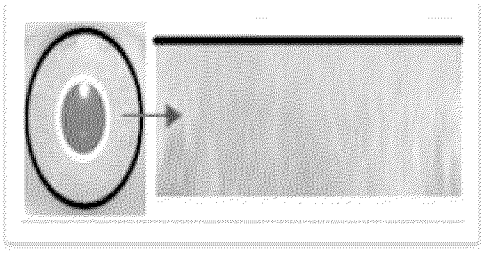

Fig. 1.3 : Iris Rectangular Representation

Pre-processing is a step, which is performed to obtain iris from the eye image. But here we have used standard iris database (i.e. UBIRIS database) so we have extracted features directly using the images.

In order to provide an accurate recognition of an individuals, the most discriminating information present in an iris pattern has been extracted. Only the significant features of the iris have been encoded so that comparison between templates is done. Below figure 1.4 shows the feature extractionstages.

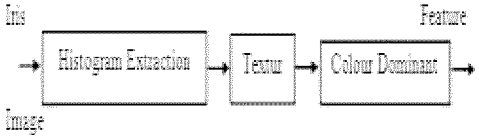

Fig. 1.4: Feature Extraction Stage

Feed forward Network

Feed forward networks consist of a series of layers. The first layer has a connection from the network input. Each subsequent layer has a connection from the previous layer. The final layer produces the network's output.

Feedforward networks can be used for any kind of input to output mapping. A feedforward network with one hidden layer and enough neurons in the hidden layers, can fit any finite input – output mapping problem.

Trainlm is a network training function that updates weight and bias values according to Levenberg – Marquardt optimization as shown in figure 1.5

Trainlm is often the fastest backpropagation algorithm in the toolbox, and is highly recommended as a first – choice supervised algorithm, although it does require extra memory than other algorithms.

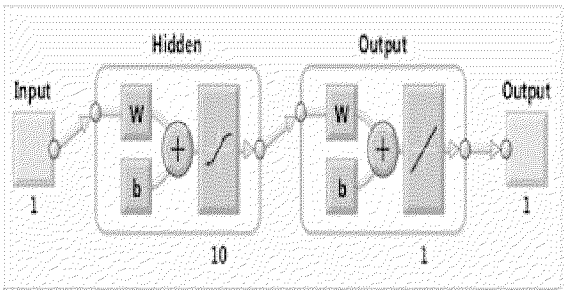

Fig. 1.5 Feedforward Network

Training of Neural Network for Left Iris

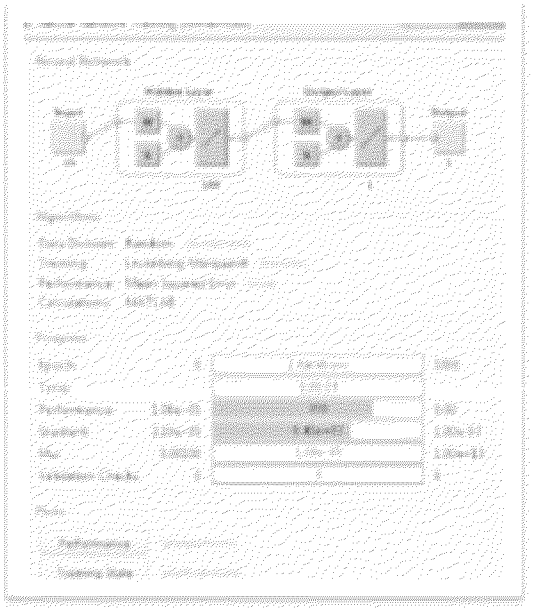

Fig. 1.6 Results of training Network for Right Iris

If the train button is pressed on the menu the neural network training (nntraintool) would be activated from the neural network toolbox. The result of train network is show in fig. 1.6.

In this figure the neural network algorithm would be displayed with 25 input two layers with weight and bias. Hidden layer is 100 and one output layer. According to the present result of training system the epoch is 2 iterations for 100 epochs. Running time is 0.004 hours. The performance is 858 for 1.08e + 05 target. The gradient is 8.41e + 03 for1.00 e – 07 and validationcheck is 0 for 6 must be displayed on to command window. According to the fig. 1.6 the neural network training system has been accomplished and known by the user neural network toolbox is very useful to simulation of this right iris recognition.

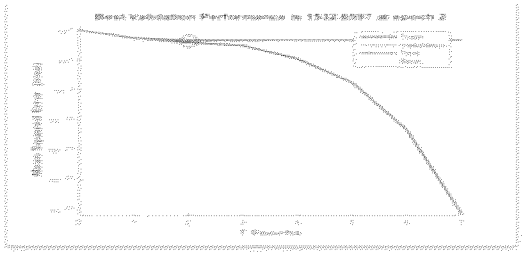

Fig. 1.7 Mean square error of Feedforward NeuralNetwork

The results are found by the algorithm and we can get the number of epochs used and which epoch gives the best result as shown in figure 1.7. As shown in fig. a plot of epoch MSE has been plotted. The epochs get the best validation performance at epoch no. 2. The MSEW is the lowest at this point and hereafter no significant changes take place and no further decrease takes place. Hence this is the best validation performance is 1532.6597 at epoch 2. As shown in fig. 1.8. The training data are shown in the blue colour, validation is shown in blue colour, test data is shown in red colour and zero error is shown from the histogram.

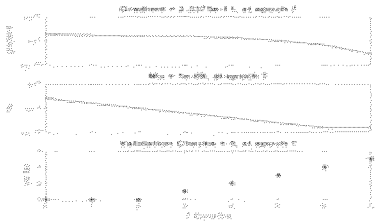

Fig. 1.8Feedforward Neural Network Gradient versus Epoch

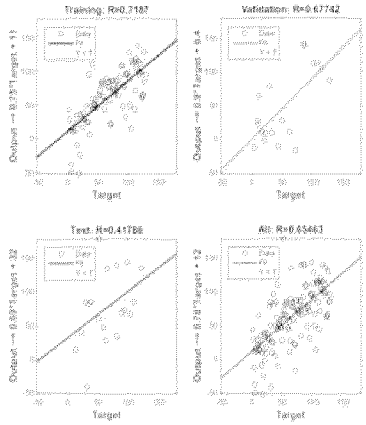

Fig. 1.9 Regression plots for training, testing and validation of ANN

The four plots represent the training, validation, and testing data. The dashed line in each plot represents the perfect result – outputs = targets. The solid line represents the best fit linear regression line between outputs and targets. The R value is an indication of the relationship

between the outputs and targets. If R = 1, this indicates that there is an exact linear relationship between outputs and targets. If R is close to zero, then there is no linear relationship between outputs and targets. For this example, the training data indicates a good fit. The validation and test results also show R values that greater than 0.9. The scatter plot is helpful in showing that certain data points have poor fits. As shown in figure.1.9.

Conclusion

The proposed methodology uses Levenberg – Marquardt feedforward network. Trainlm is often the fastest backpropagation algorithm in the toolbox. According to the fig. 1.6 the neural network training system has beenaccomplished and known by the user neural network toolbox is very useful to simulation of this right iris recognition The results are found by the algorithm and we can get the number of epochs used and which epoch gives the best result as shown in figure 1.7. In this paper gives the training of neural network for detection of right iris from the used database.

References

1. Delac, K., &Grgic.M. "A survey of biometric recognition methods." In 46th international symposium electronics in marine, ELMAR –2004, zadalcroatia. [1] J. Daugman, "New Methods in Iris Recognition" IEEE Trans. Systems, Man, and Cybernetics, Part B, vol. 37, no.5, 2007, pp. 1167-1175.
2. M. Vatsa, R. Singh, A. Noore (2008),"Improving Iris Recognition Performance Using Segmentation, Quality Enhancement, Match Score Fusion, and Indexing," IEEE Transactions on Systems, Man and Cybernetics. Part B. Cybernetics Vol. 38, N° 4,pp. 1021-1035,2008.
3. Leila FallahAraghi, "IRIS Recognition Using Neural Network,"Proceedings of International Multi Conference of engineers and Computer Scientist Vol I, 2010
4. Bhawna chouhan,"Iris Recognition System using canny edge detection for Biometric Identification" International Journal of Engineering Science and Technology (IJEST) Vol. 3 No. 1 Jan 2011.
5. Prof,.S. R. Ganorkar"Person Identification using Iris Recognition" International Journalof Engineering and Technology Vol.3 No.1 February 2011.

4. To Study the Different Life Stage of Silkworm Bombyx Mori from Patur Region (Shirla)

Anuradha Datta Karale
Department of Zoology, Ghulam Nabi Azad Arts, Commerce and Science College, Barshitakli.
Nilima B. Kankale
Department of Zoology, Ghulam Nabi Azad Arts, Commerce and Science College, Barshitakli.

Abstract

Silkworms are crucial in the sericulture industry, providing the silk obtained from their cocoons. Silkworms are the larvae or caterpillars of the domesticated silk moth, known as Bombyx mori. A silkworm has four stages in its life: eggs, caterpillar, pupa, and adult. This takes about 6-8 weeks, depending on the weather. It starts when a female silk moth lays eggs, and they hatch into silkworms. Silkworms eat mulberry leaves. They go through five growing stages, then turn into pupae. In the pupa stage, they make a protective net around themselves using a protein. This net helps them create a cocoon. The silk for the cocoon comes from a thin yarn-like structure made by the silkworm.

Keywords :- Silkworm, Bombyx mori, Sericulture

Introduction

Insects, which make up about 80% of Earth's animal species and 99% of invertebrates, hold great potential for valuable compounds in modern medicine. We share a significant amount of genetic material with all life, even the simplest worms. Among these insects, the Silkworm (Bombyx mori) stands out as a well-known and beneficial lepidopteron insect, particularly valued for producing smooth and luxurious silk fibers. Bombyx mori, it was the first organism in the order lepidoptera for which a draft of the genomic sequence (Xia et al., 2004, Mita et al., 2004) were completed with the haploid nuclear genome of size 530 mb which is broken into 28 chromosomes (Wang et al., 2005).

Sericulture or silk farming is rearing of silkworms for the production of raw silk. Sericulture has become one of the most important cottage industries in number of countries like China, Japan, India, Korea, Brazil, Russia, Italy and France. Today,

China and India are the two main silk producers, together manufacturing more than 60% of the world production each year. Silk is discovered in China about 2700 BC. Silk production

today is a blend of ancient techniques and modern innovations. India is the second largest producer of raw silk after China and the biggest consumer of raw silk and silk fabrics. In India, sericulture is not only a tradition but also a living culture. It is a farm- based, labour intensive and commercially attractive economic activity falling under the cottage and small-scale sector. India is a home to vast variety of silk secreting fauna which also includes an amazing diversity of silk moths to achieve the unique distinction of being a producer of all the five commercially traded varieties of natural silks namely, Mulberry, Tropical Tasar, Oak Tasar, Eri and Muga (Giridhar et al., 2010).

Silk from the Silkworm is proteinaceous in nature and considered as the queen of fibers. The bulk of commercial silk produced in the world is mulberry silk that comes from the domesticated silkworm, Bombyx mori which is a monophagous and voracious eater of the leaves of mulberry plant. Silkworm are lepidopteran insects and their caterpillars spin a cocoon of silk at the end of the larval stage by silk glands. The production of silk depends upon several factors of which the effect of the environmental factors such as biotic andabiotic factors is of vital importance.

Scientific classification

Kingdom Phylum Sub- Phylum	:- :-	Animalia Arthropoda Mandibulata
Class Sub- Class Division Order	:- :-	Insecta Pterygota Endopterygota Lepidoptera
Family Genus Species Binominal Name	:- :-	Bombycidae Bombyx mori *Bombyx mori*

Life cycle

The Mulberry silkworm, Bombyx mori, is a fully domesticated insect with separate sexes, a condition known as dioecious. Internal fertilization occurs following copulation. Its developmental process involves a complex complete metamorphosis, comprising four stages: egg, larva (5 instars), pupa, and adult. The entire life cycle takes around 6-8 weeks. Distribution of life cycle is as follows.

Eggs: - After fertilization, every female moth typically lays around 300 to 400 eggs. These eggs are arranged in clusters on the leaves of a mulberry tree.

Larva :- The larva of silkworm moth is called caterpillar larva. The newly hatched larva is about 4 to 6 mm in length. It has a rough, wrinkled, hairless and yellowish white or greyish worm-like body.

First Instar Larva :- The initial stage of the larva, known as the first instar, typically has a dark brown or black color and is covered with hair-like structures on each body segment. It appears like the ants and hence also called as "ant" or first instar.

Second Instar Larva :- In the second instar stages, the larvae exhibit a light brown body with a shiny milky white head region. They are covered in hair. The mouth is set on the third day of the second instar, and the larvae transition to the third instar on the fourth day.

Third Instar Larva :- When the larva grows and sheds its skin (moult), it enters the third stage, having a new pale yellow or whitish body with a slightly brown head. At this point, it eats entire leaves and small branches of mulberry.

Fourth Instar Larva :- Fourth instar larva: After the third moult the fourth instar resumes and gets the greenish white coloured body with the same-coloured head part. The larvae at this stage feeds on complete leave and small branches of mulberry. The period of fourth instar is 5-6 days. The larvae at this stage feed continuously 24 hours and gains weight 1000 times larger, than before or at first instar stage. The larvae become paint whitish or greenish coloured with spiracles each segment.

Fifth Instar Larva :- after the four moults, silkworm reaches the fifth and final instar and its maximum weight of about 1000 times its own weight at the time of hatching which take place within just a span of 20-25 days. It measures about 6 gms, in weight. In this stage the larvae feeds for 6-8 days and become green yellow in colour and a pair of spiracles present in each segment.

Spinning the silk :- The silk threads are produced by the protein secreted by the silk gland and come out by minute opening to form the cocoon. These spinning larvae make the cocoon around itself.

Pupa :- The thread becomes wrapped around the body of the caterpillar larva forming a complete covering or pupal case called the cocoon. The cocoon- formation takes about 3-4 days.

Imago or Adult :- The mature moth emerges from the cocoon within a span of 2 to 3 weeks, provided it is allowed to complete its life cycle.

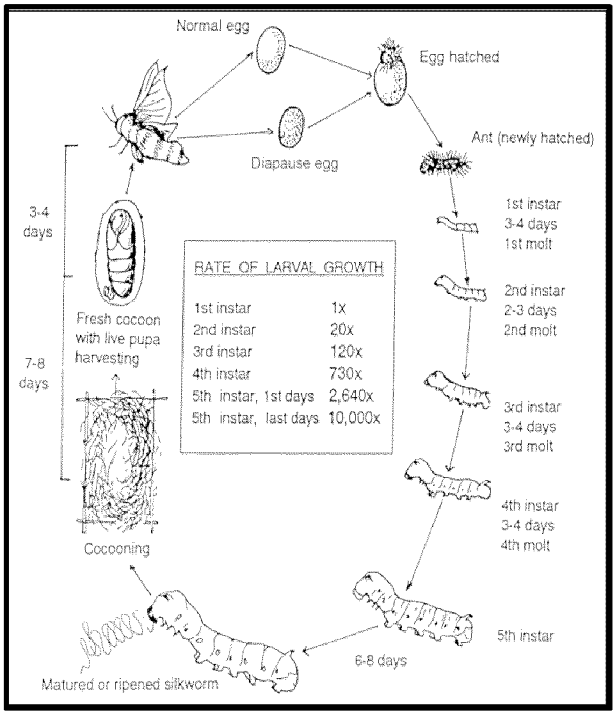

Figure: - Life Cycle of Mulberry silkworm

Material and Methods

Study Area

Akola is the district present in Maharashtra. There are seven district present in Akola, which is: - Akot, Akola, Balapur, Barshitakli, Murtizapur, Patur and Telhara respectively. The present study was carried out in Patur Taluka Village Shirla. Patur is a city and Tehsil in Akola district in the Indian state of Maharashtra. Total number of villages in this Taluka is 90. Distributed in 20.46 North latitudes and 76.94 East

Longitude. Total population of Patur is about 28,531. It belongs to Vidharbha region and Amravati Division. It is located 28 KM towards South from District head quarters Akola. 12 KM from Patur. Shirla Pin code is 444501 and postal head office is Patur. Patur is the Nearest Town to Shirla. Patur is 5 km from Shirla. Road connectivity is there from Patur to Shirla. It is a taluka head quarter. (As of 31 March 2011. Government of Maharashtra). Total population of Patur region in 2024 is about 1,57,631.

Survey and collection of Mulberry Silkworm

With the help of office of the Tehsil sericulture and the permission of local farmers in the tehsil a survey for the active silkworm collection was carried out during the month of 5th of

November 2023 January 2024. During the visit of Shirla from time to time collection of the silkworm is done by actual observation and collection and photographic method.

The method used for the production of mulberry silkworm or mulberry silk the sericulture process follows three primary steps: -

1. Moriculture:- Moriculture refers to the cultivation of mulberry plants, whose leaves are used as silkworm feed. This plant can be grown three different methods.

- Cultivation from seeds
- Root-grafting
- Stem grafting

The stem grafting method is the most commonly used method for mulberry plantation. Here, cuttings.

- Leaf picking: The removal of individual leaves by hand
- Branch Cutting: Removal of the entire branch
- Top shoot harvesting: removal of the mulberry shoot tops.

It is interesting to note that 1 kilogram of mulberry leaves can feed approximately 50 silkworms (from the egg stage to the cocoon stage).

2. Silkworm Rearing :- In sericulture, the silkworm rearing process begins with the laying of eggs by the female silk moth. Typically, 300-500 eggs are obtained from one female silk moth. These eggs are then disinfect with the help of 2% formalin solution. A feeding bed is prepared on a rearing tray by sprinkling chopped mulberry leaves onto it. The hatched larvae are transferred on to this tray via a process known as brushing. In order to maintain humidity, foam strips are soaked in water and place on the tray. The silkworm larvae initially have a good appetite, as they grow, their appetite slowly diminishes until their active stage. At this stage, the silkworm eats enthusiastically until its final feeding stage.Once the silkworms grow up, they look for a good place to make their homes. At this point, their bodies get smaller and see-through. These grown-up silkworms make a protective covering by producing spit from glands on their heads. When this spit touches the air, it turns into silk. Normally, it takes 2-3 days for them to make this covering, but some types of silkworms might take up to 4 days.

3. Silk Reeling:- After the silkworms change into pupae inside the cocoons, the final step of making silk begins. The pupae are killed by boiling the cocoons with steam and dry heat, a process called stifling. After that, the silk threads are taken out from the dead cocoons through a

process called reeling. The cocoons are boiled in water for about 15 minutes, making it easier to separate the silk threads. These threads are twisted into a thread using guides and pulleys. Finally, the silk is boiled again to make it shiny.

Each silk thread has about 50 smaller silk strands. Surprisingly, a single cocoon can give over 900 meters of this silk thread. So, after getting this raw silk from the silkworm, the whole process of sericulture is completed. The natural silk business starts with growing mulberry trees (moriculture) and raising silkworms (sericulture). India is important in this business and produces three types of natural silk: Tasar Silk, Eri, and Muga Silk. Tasar, Eri, and Muga Silks are wild and known as Vanya silks. Eri silk, also called endi or errandi, comes from silkworms that eat Castor plants. The term "eri" comes from the Sanskrit word "eranda," which means castor plant.Tasar silk comes from tasar silkworms, and India is the second-biggest producer. These silkworms eat leaves from trees like Asan, Arjun, and Oak. Muga silk, with its shiny golden color, is made by muga silkworms that feed on Som and Sualu. It's a special silk that makes India proud.

Results and Discussion

The Silkworm (Bombyx mori) life cycle consists of four stages: eggs, larva (caterpillar), pupa (cocoon), and adult moth. After hatching, the silkworm larva feeds on mulberry leaves, spins a silk cocoon during the pupa stage, and transforms into an adult moth. The cycle repeats when the adult lays eggs.The result we got when studying this stages are as follows: -

Stages	**Days/Duration**	**Colour**
Eggs	10-14 days	Pale yellow
Larval stages		
First instar larva	3-4 days	Dark brown & black coloured
Second instar larva	1-3 days	Light brown coloured with skinny milky white head.
Third instar larva	3-4 days	Pale yellow or whitish coloured and slightly brown head.
Fourth instar larva	5-6 days	Greenish white coloured body with slightly brown head.
Fifth instar larva	6-8 days	Greenish yellow colour.
Pupa	10-11 days	At first it shows light colour then converted into dark brown.
Adult(the moth)	3-10 days	Creamy & white coloured moth.

Conclusion

Silkworms are crucial in the sericulture industry, providing the silk obtained from their cocoons. Silkworms are the larvae or caterpillars of the domesticated silk moth, known as Bombyx mori. A silkworm has four stages in its life: eggs, caterpillar, pupa, and adult. This takes about 6-8 weeks, depending on the weather. It starts when a female silk moth lays eggs, and they hatch into silkworms. Silkworms eat mulberry leaves. They go through five growing stages, then turn into pupae. In the pupa stage, they make a protective net around themselves using a protein. This net helps them create a cocoon. The silk for the cocoon comes from a thin yarn-like structure made by the silkworm.

- Growing silkworms can provide jobs for many people and make rural areas better off economically. It's like a tool for creating more money and opportunities in those places.
- Silk farming is a pocket-friendly job for small farmers, giving good returns. Since rich people mostly use silk, it helps money move from the rich to the poor.
- Sericulture provides self-employment opportunities for educated unemployed youth in various sectors. Additionally, several by-products can be produced through sericulture activities.
- People with fewer resources, like those with small plots of land, can consider sericulture as a good job. Raising silkworms on their land can provide enough support for a family of three without needing to hire extra help.
- Silkworms are valuable for genetic and biotechnological research. They produce medicinal products that can be used in medicines. Since all sericulture activities are centered in villages, it helps prevent people from moving from rural to urban areas in search of jobs.
- Sericulture is a women-friendly occupation, playing a crucial role in empowering rural women. In India, 60% of the workforce in sericulture consists of women

References

- Ayandokun, A., Ete, J., Babayemi, I., & Aina-Oduntan, O. (2017). Assessment of two disinfectants in the rearing of Bombyx mori and their effects on larval performance and cocoon yield. African Journal of Agriculture Technology and Environment Vol, 6(1), 45-52.

- Baci, G. M., Cucu, A. A., Moise, A. R., & Dezmirean, D. S. (2021). Applicability of Honey on Silkworms (Bombyx mori) and Quality Improvement of Its Biomaterials. Applied Sciences, 11(10), 4613.
- Banno, Y., Shimada, T., Kajiura, Z., & Sezutsu, H. (2010). The silkworm—an attractive bioresource supplied by Japan. Experimental animals, 59(2), 139- 146.
- Dee Tan, I. Y., & Bautista, M. A. M. (2022). Bacterial Survey in the Guts of Domestic Silkworms, Bombyx mori L. Insects, 13(1), 100.
- Dewangan, S. K. (2017). Employment Generation and Socio-Economic Change through Sericulture in Raigarh District, Chhattisgarh, India. Annals of Natural Sciences, 3(2), 32-42.
- Gupta S.K. and Gaur K.P. (2019). Influence of temperature fecundity, incubation period and fertility of multivoltine mulberry silkworm (Bombyx mori LINN). Eggs.
- Hailu, A. (2016). Assessment of growth and performance of silk worms (Bombyx mori L.) on mulberry leaves at Jimma, South West Ethiopia. Journal of Biology, Agriculture & Healthcare, 6(9).
- Krishnaswami S, Narasimhanna MN, Suryanarayan SK, Kumararaj S (1973) Manual of Sericulture. Vol. 2. Silkworm Rearing. FAO, Rome.
- Pathare, M., Shinde, H. R., & Bagade, A. S. (2021). Economic analysis of silk cocoon production in Maharashtra. Pharma Innovation Journal, 10(11), 534-538.
- Ramya, M. N., & Jagadeesh Kumar, T. S. (2018). The Silkworm, Bombyx mori: A promising model organism to study the longevity-A review. International Journal of Current Microbiology and Applied Sciences (IJCMAS), 7(11), 3433-3442.
- Sarkhel, S., Shrivastava, S., & Pouranik, M. (2017). The effective influence of temperature on the varied characteristic of silkworm: A Review. Asian J. Exp. Sci, 31(2), 31-37.
- Shahd Mehmood. Beneficial importance of insects specifically silkworm (Bombyx mori) as its role in entomological industries.
- Singh, K. P., & Jayasomu, R. S. (2002). Bombyx mori–A Review of its Potential as a Medicinal Insect. Pharmaceutical biology, 40(1), 28-32.

- Soumya, M., Reddy, H., Nageswari, G., & Venkatappa, B. (2017). Silkworm (Bombyx mori) and its constituents: A fascinating insect in science and research. J. Entomol. Zool. Stud, 5, 1701-1705.

- Soumya, M., Reddy, H., Nageswari, G., & Venkatappa, B. (2017). Silkworm (Bombyx mori) and its constituents: A fascinating insect in science and research. J. Entomol. Zool. Stud, 5, 1701-1705.

- Vasantharaj David, V.V. Ramamurthy, 2015, Elements of Economic Entomology, 8th edition, Brillion Publishing, New Delhi.
- Yang, Y., Tang, H., Zhang, Y., Zhu, F., Lü, P., Yao, Q., & Chen, K. (2018). Research progress on the immune mechanism of the silkworm Bombyx mori. Physiological Entomology, 43(3), 159-168.

5. Isolation and Identification of Cellulose Degrading Bacteria from Different Environmental Samples

Miss. Janhavi Surendra Choubey
Shri R. L. T. College of Science, Akola.
Dr. Vijay D. Nanoty
Under the guidance of Principal, Shri R. L. T. College of Science, Akola.

Introduction

One of the delicate protein molecules are enzymes which are necessary for life. Cellulose is the most copious biomass on the planet (Venkata et al., 2013). Plant biomass contains cellulose as the major component of the cell wall as well as algae and oomycetes.

Cellulose accounts for 50% of the dry weight of plant biomass and approximately 50% of the dry weight of secondary sources of biomass such as agricultural wastes.

It is the presiding waste material from agricultural industry in the form of stalks, stems and husk, there has been enormous engrossment in availing cellulose as vitality asset and feed.

Cellulose is a strong fibrous, crystalline polysaccharide, resistant to hydrolysis and is water insoluble it consists of repeating units of D-glucose. Cellulases reasons hydrolysis of the character cellulose fibres to break it into smaller sugars devices and sooner or later generating glucose molecules. It is one of the most versatile organic compounds present on the Earth, it mainly occurs in plants but can be produced by exhausting certain fungal as well as bacterial strains.

According to several research there are only two types of hydrogen bonds in cellulose molecules.

Cellulase enzyme accommodates three classes of soluble extracellular enzymes: 1,4-β-endoglucanase, 1,4-β-exoglucanase, and β-glucosidase (β-D- glucoside glucohydrolase or cellobiase). Endoglucanase is chargeable for random cleavage of β- 1, 4-glycosidic bonds along a cellulose chain.

Exoglucanase is important for cleavage of the nonreducing of a cellulose chain and splitting of the essential fibrils from the crystalline cellulose, and β-1, 4-glucosidase hydrolyses cellobiose and water-soluble cellodextrin to glucose.

Review of Literature

- Verma et al. (2012) conducted a series of examination in which soil samples were obtained (10gm) from Hardoi district, Uttar Pradesh, India. Bacterial colonies were grown over CMC Agar medium. Maximal cellulase production was obtained after 48hrs of incubation at 45oC in medium containing 1.5 % carboxymethyl cellulose (CMC) as substrate. The optimum pH for the isolated enzyme was found to be ranging between 6.5 and 7.5. Their bacteriological studies reported that Bacillus subtilis to be the most frequent cellulolytic bacteria to be found in the agricultural fields.
- Behera et al. (2014) conducted a study that aimed to isolate cellulose degrading bacteria from mangrove soil. According to their results total 15 cellulose degrading bacteria were isolated based on their halo zone formation on Congo red agar medium. The maximum carboxymethylcellulose hydrolysis capacities were ranged from 1.18 to 2.5 cm. A Carboxy-methyl-cellulase test of these fifteen isolates showed that their enzyme activity ranged from 2.471 to 98. 253 U/ml/min. They studied the morphological and biochemical characteristics of the isolates. The isolates that were identified by them were reported as Micrococcus spp., Bacillus spp., Pseudomonas spp., Xanthomonas spp. and Brucella spp.
- Prabhakar et al. (2019) conducted a study which focused on the isolation, identification, and screening of bacteria with high cellulase activity from soil samples. CDB were isolated from soil sample using serial dilution and pour plate method. The isolated bacteria were further identified by the morphological and biochemical tests.

Aims and Objectives

1. To select the site for sample collection.
2. To collect and transport the samples from selected site to the Laboratory.
3. To isolate Cellulose degrading bacteria (CDB) from the given sample.
4. To perform the screening of various CDB's for further work.
5. To study the morphological and biochemical characteristics for identification of selected isolates of CDB.
6. To formulate the medium's composition (carbon source) for the optimum cellulase activity by the isolates.
7. To study the effect of pH and incubation period on the selected CDB isolates.

Materials and Methods

1. Selection of the sites for sample collection

The present study was performed in the Microbiology laboratory at Shri R. L. T. College of Science, Akola.

2. Sample collection and transport from selected site to the Laboratory

The samples were collected from distinct spots during January to April 2023. Soil samples were collected from Vermicompost Shri R. L. T. College of Science Akola, soil from Tilak Park Akola, soil near sugarcane juice shop Durga chowk Akola, Spent Biogas Slurry Shri R. L.T College of Science Akola

The soil samples were collected at different depths. The depths were 10 cm, 9 cm, and 0 cm respectively. About 20 g of soil was collected using a sterile spatula and placed into a sterile bottle.

The Spent Biogas slurry was collected directly from the biogas tank. Pre- sterilized bottles were used for the purpose of collection, and these were brought to lab for isolation of cellulose degrading bacteria. The samples were further stored at 4°C for further use.

3. Processing of Sample

The samples were diluted using ten-fold dilution, where 1ml of sample is transferred to 9 ml of diluent. After first tube, each tube is dilution of the previous dilution tube. Processed samples were poured in the plate after filtration by sieve.

Preparation of CMC media

Measure all the components. Pour the media in conical flask, seal it with cotton plug and sterilize the media in autoclave for 15-20 minutes at 121°C temperature and 15 lbs pressure. Now pour the media in the sterilized petri plates, let the plates cool down and now inoculate or pour the sample in the plates. For preparation of Nutrient broth there is no need to add agar powder.

Methodology

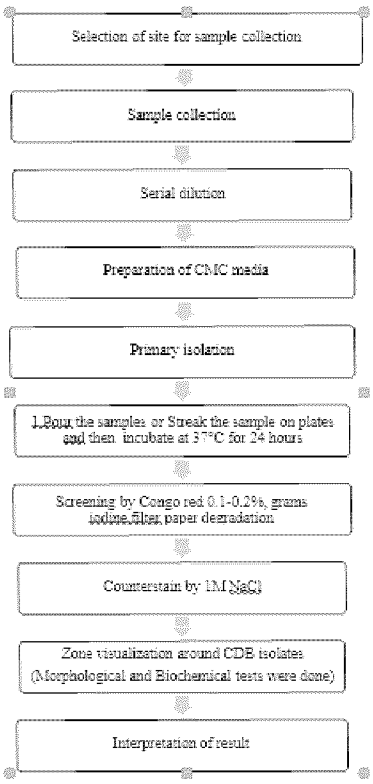

Results and Discussions

Isolation and screening of cellulolytic bacteria

In the present study, fourteen isolates were isolated and screened from soil and Spent Biogas slurry. The isolates obtained were initially identified They were initially identified to produce cellulose degrading enzymes on CMC agar plates. The isolates were selected on the basis of hollow zones producing around the colonies on the CMC agar plates when flooded with Congo red and grams iodine. Among the total isolates obtained, the isolates CDB4 and CDB8 with high zone of clearance i.e., 14.5 and 16 respectively.

After completion of the isolation total 14 isolates were grown on CMC medium and after screening by Congo red and gram's iodine two isolates where further subjected to subculturing and obtaining the pure culture of the bacteria on the basis of formation of zone of clearance (halazones).

Metal ions were added in order to increase the production of Cellulase enzyme in the medium. Calcium chloride, magnesium sulphate, CaCO3 and FeSO4.

In a set of experiment, we have added CaCO3 as a micronutrient in order to enhance the growth of bacteria.

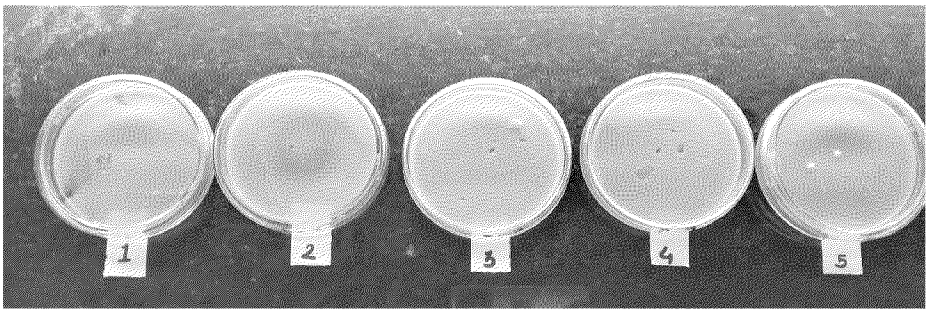

Figure : CMC plates with Calcium carbonate as a nutrient source

The sole source of carbon in the medium i.e., cellulose can be substituted by some other components to visualize the optimum growth of the selected isolates. Microscopic examination of CDB4 isolate was shown gram negative and short rod- shaped bacteria in the same manner colonies of CDB8 was reported to be gram negative and rod-shaped bacteria. According to Muhammad et al. (2012) Bacillus spp. Has shown a remarkable ability of cellulose hydrolysis in terms of Congo red assay by giving a zone, had found various anaerobic hydrolytic and methanogenic bacteria active in cattle dung biogas plants including Syntrophobacte wolinii a propionate degrading bacterium in co-culture with hydrogen utilizing methanogen viz., Mthethanobacterium.

Results indicated that optimum temperature for growth is 37°C, pH 8-9 (indicating alkaline cellulase production in medium) and salt concentration 0.4 % recorded for both the isolates namely CDB4 and CDB8, while the optimum incubation period was 96 hours. Dubey et al. (2014) investigated that optimal pH was 7.0, temperature 26°C for the on the basis of the growth curve.

After the addition of Congo red dye, clear zone of hydrolysis were observed likewise, in another case i.e., of Gram's iodine addition to the CMC plates, zones were observed hence it can be denoted that it is positive for amylase. The highest halozones were similar in case of Congo red and Gram's iodine which was observed for the isolates CDB4 and CDB8.

Sr No.	Biochemical Characteristics	Cdb4	Cdb8
1	Indole		
2	MR		
3	VP	+	+
4	Citrate	+	+
5	Catalase	+	+
6	Oxidase		
7	Motility	+	+
8	Glucose	+ AG	+AG
9	Lactose	+AG	+AG
10	Mannitol	+A	+A

Table 4.3: Biochemical characteristics of isolates.

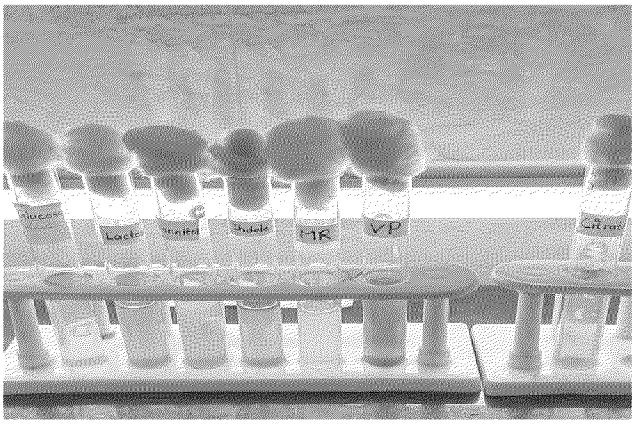

Fig : Biochemical characteristics of isolates.

According to microscopic and biochemical results obtained the CDB4 and CDB8 might be belonging to the Bacillus species.

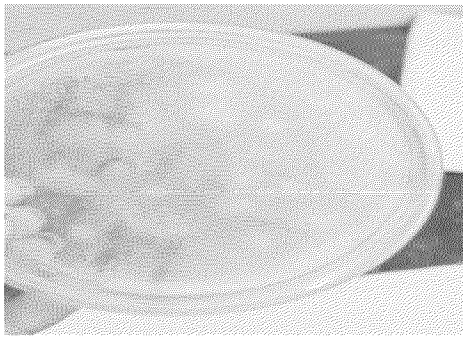

Fig :- Plate after incubation of 96hours.

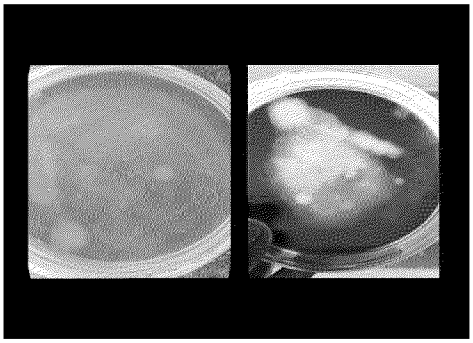

Fig:- After Addition of Congo Red.

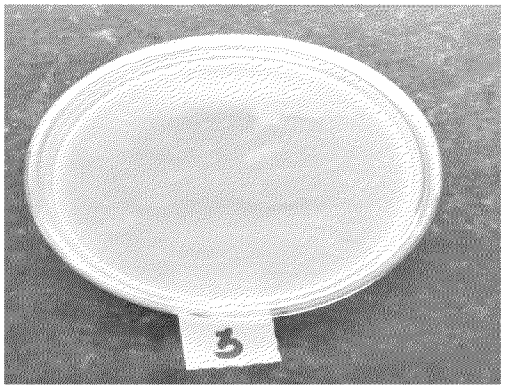

Fig: Pointed colonies on CMC Plates with Calcium carbonate

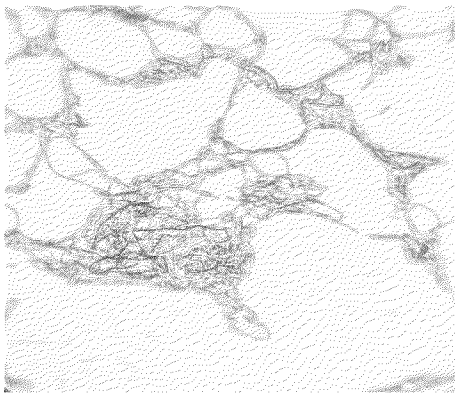

Fig : Showing Morphology of isolate CDB4

Conclusion

From the present study, 14 cellulolytic bacterial isolates were obtained successfully from soil and Spent Biogas slurry. The Gram-negative isolate i.e., CDB4 & CDB8, selected for further studies shown to bear high cellulolytic activities. From the functional tests carried to determine the optimal conditions for cellulolytic activity, the isolate's enzyme activity was found to be high over a range of temperatures i.e., from 37°C to 45°C with the optimum temperature being 37°C. Similarly, enzyme activity was found to be high at the range of pH 7 to pH 9 with an optimum of pH 8, suggesting that the isolate bears alkaline cellulases. The optimum incubation period was of 96 hours which has given highest zone forming isolates. The present study which concludes the isolate to be of Bacillus species gives Indole test negative, Methyl red test negative, Voges-Proskauer test positive, Citrate positive test, Catalase positive and Oxidase negative test, sugar fermentation test's result are as follows glucose acid and gas positive with lactose been acid gas positive with mannitol been showing formation of only acid and no gas.

Application of these two isolates in industries may have several advantages such as high growth rate and ability to secrete proteins extracellularly; these are some features of the Bacillus species. From the present study, it can be concluded that all the two CDB isolates from spent slurry has the capacity to produce cellulase enzyme efficiently in the medium which can probably be helpful for taxonomists and enzymologists, and even some industrialists in their own researches. The use of these CDB's as bio-inoculants can be incorporated to increase soil fertility and to minimize the application of fertilizer. More studies are however needed before industrial application of these isolates.

Future Prospectus

- The isolated organism can be further identified by 16S rRNA sequencing and by PCR amplification of the bacterial DNA.
- Genetic diversity analysis can be performed by Rbac (Universal primer for bacteria) RAPD based markers.
- Research can be done on formulation and optimization of the medium for optimum growth and cellulase production.
- Work can be done for determination of optimal environmental conditions for the isolates.
- Further studies can be progressed in the purification and application of cellulase in different commercial fields. The purified cellulase from the microbial sources can be used in several industries.
- The CDBs can be used for biostoning of denim fabric was also evident, hence there is scope of introducing some more species of bacteria with high efficiency of cellulase production.

References

1. Bai, S., et al. (2012). Cellulase production by Bacillus subtilis isolated from cow dung. Arch Appl Sci Res, 4(1), 269-279.
2. Kuhad, R. C., Gupta, R., & Singh, A. (2011). Microbial cellulases and their industrial applications. Enzyme Research 2011, 1–10.
3. Kuila, A., et al. (2011). Production of ethanol from lignocellulosics: an enzymatic venture. EXCLI journal, 10, 85.
4. Islam, F., & Roy, N. (2018). Screening, purification and characterization of cellulase from cellulase producing bacteria in molasses. BMC research notes, 11(1), 1-6.
5. Karmakar, M., & Ray, R. R. (2011). Current trends in research and application of microbial cellulases. Research Journal of Microbiology, 6(1), 41.

6. Study of Spider Diversity at Kapshi Lake, Akola

Kajal N. Wagh
Department of Zoology, Ghulam Nabi Azad College of Arts, Commerce and Science, Barshitalki, Dist. Akola.
Prof. Amit Vairale
Guided by Department of Zoology, Ghulam Nabi Azad College of Arts, Commerce and Science, Barshitalki, Dist. Akola.

Abstract

The study was conducted at Kapshi Lake Tahasil Barshitakli of Akola District Maharashtra India to study the diversity of Spiders (Class Insecta, phylum Arthopoda). Variety of spiders found in the region shows their relationship in respect of nature and natural habitat. High density of spiders in the lake region as compared to the civilized area is attributed to the high density of varied fauna and flora found in the lake region.

The research shows how the population of spiders responds to change in climate, region and how their morphology changes according to the habitat in which they are dwelling. Spider is one of the important communities in the ecosystem and its study is of as much importance for understanding the ecosystem as a whole.

Keywords: Kapshi, Spider, Population, Diversity.

Introduction

Spiders are one of the most widely recognized groups of Arthropod. Spider populations can be found all over the world and have occupied almost all ecological habitats, except open air and the open sea. They can be traced right from the cold to hot regions of the world. Spiders belong to order Araneae, class Arachnida which are members of phylum Arthropoda. The largest assemblage of animals with jointed legs and hard exoskeleton (A.B.Vairale & G.A.Wagh).

Spiders belonging to the order Araneae, the seventh largest order of the animal kingdom, these are small invertebrate animals distributed throughout the world. Insects constitute the principal portion of the spiders' prey, but certain other arthropods are often consumed. Spiders exhibit stunning morphological diversity and colouration. The exclusive predatory behavior of spiders have a notable impact on the ecosystem (Wise, 1993) and thereby regulate insect populations.

As of November 2023, 51,673 spider species in 136 families have been recorded by taxonomists. Spiders play an important role in regulating insect pests in the agricultural ecosystem. There are currently 1947 spider species in India (Caleb and Sankaran 2023).They are unique among all organisms in their modes of silk production and usage and of reproduction. Spiders from one of the most diverse groups of organisms existing in India but very little documentation has been done on spiders.

Classification

Kingdom - Animalia
Subkingdom - Bilateria
Phylum - Arthropoda
Subphylum - Chelicerata
Class - Arachnida
Order - Araneae

Spiders are predominantly carnivorous invertebrates that feed on a variety of prey, which makes them universal. Their feed mostly consists of insects and other arthropods like collembolans, dipterans, homopterans and also other spiders.

Spiders are abundant and their continued impact on the natural food chain can have numerous effects on insect densities (Foelix, 1996). All spiders produce at least one kind of silk. Orb-weaving spiders are unique in the sense that they can even produce seven different types of silk fibers with unique functional and mechanical properties (Foelix 2011). Spider silk is a one of a kind natural material with a rare combination of high tensile strength and elasticity.Another important and unique characteristics of Spiders is their web which is considered as one of the important feature for the success of spider's ecology.

Spider web is a unique example of high performance natural material design and pattern. In particular, to survive in different environments, spiders have specially optimized and adapted their web architecture by providing housing, protection, and an efficient tool for catching prey. The egg sac of a spider contains eggs in it. In some species the egg sac consists of few silk threads that protects eggs (Huber and Wunderlich 2006) while in some species it has very sophisticated egg sac construction, with a base plate and a cover plate, all of which are coated by numerous layers of silk (Ramirez et al. 2010).

Families

A. Araneidae - These are typically orb weaving spiders, they are distributed all over the world. In general they prefer to live in moist habitats and very rarely found in arid regions. The orb-weaving spider family Araneidae is composed of approximately 3,200 species in 169

genera, making it the third most speciose spider family after Salticidae (jumping spiders) and Linyphiidae (sheet-weavers) (World Spider Catalog, 2023).

Male araneids are much smaller than females and are not commonly seen in the web unlike females. They built spiral wheel shaped webs. Some major genus found in this family are Nephila (Leach), Herennia (Thorell), Argiope.

B. Oxyopidae - The members of the Oxyopidae family have spiny legs through which they are capable of running very fast and jumping on their prey. Hence, they have got the name lynx spiders. Which help them in hunting. Eight eyes that are arranged in a hexagonal shape with a wide clypeus. Spines on the legs are the features of this family. Large number of species are found under this family, some are mentioned here - Oxyopes Latreille, Peucetia Thorell .

C. Salticidae - Spiders of this family can be easily distinguished from other spiders by their four big eyes on the face and four smaller eyes on top of the head. There are more than 5000 species of jumping spiders in the world. These are small to large araneomorph spiders: two tarsal claws: ecribellate: rntelegyne: eight eyes: carapace square fronted with four, forwardly directed eyes of which the anterior median eyes are very large (Coddington, 1991). Some of the species found in this family are Carrhotus viduus, Plexippus paykulli, Plexippus petersi, Stenaelurillus albus, Asemonea Tenuipes, Telamonia dimidiata, Aelurillus sp. Brettus. sp. (World spider Catalog)

D. Lycosidae - Lycosidae or wolf spiders are a clearly delimited and well defined spider family both on somatic and behavioral characteristics. They have a unique eye pattern and a typical egg sac and spider-lings carrying behaviour. 2024). Lycosa, pardosa, Hogna, Hippasa, Arctosa are some of the commonly found genus of this family.

Material and Methods

Study Area and Sampling Site

Kapshi (20 34'43"N) and longitude (7657'18") The Kapshi Lake of Akola is located in Akola tehsil of Akola district in Maharashtra INDIA, it is situated 20 km. away from sub District headquarter Akola. As per 2009 status, Kapshi Lake is the gram panchayat of kapshi Lake village. Kapshi lake 'is the only preliminary study done to list the species and species of spider families, the study is still ongoing. More zoological surveys are planned to study the spider diversity in detail in the near future

The spider creatures were collected from different bits in the Kapashi lake. The spiders were collected from different parts of Kapsh' lake with the help of different methods. This study was conducted during October 2023 to Feb 2024. different methods used for spider collection.

Collection of Spiders - While collecting the spiders we found the majority of them on trees, their foliage and flowers, under the caves of rocks, in the cervices of walls, grass and on the ground. For collection of spiders a number of methods were applied, such as hand collection, sweep netting, beating method, pitfall trap, aerial hand collection, collection by sweep net, Inverted umbrella method, hand-kerchief method.

Result and Discussion

In Barshitakli 127 species of spider belonging to the 12 families were found. In this study I observed that the Araneidae family is the dominant family, in this region I found the 22 species of Araneidae family. I also found other family in this region such as lycosidae, Salticidae, Oxyopidae, Theridiidae and sicariidae. In this region I found 10 species of lycosidae, 16 species of Salticidae, 11 species of Pholcidae, 10 species of Hersiliidae and 12 species of Pisauridae. I rarely found the uloboridae, Theridiidae, Thomisidae, Oxyopidae, Cheracanthiidae, and sicariidae family species in that area. The atmosphere of this region is suitable for the Araneidae family species like cyclosa and Neoscona.

Table 1:- Spider and Their Species.

Family	Species
Araneidae	Araneus Argiope keyserlingi Argiope ameula Cyclosa insulana Gasteracantha Argiope keyserlingi (female)
Salticidae	Myrmarachne Menemerus semilimbatus
Lycosidae	Wolf spider
Thomisidae	Xysticus croceus
Oxyopidae	Oxyopes jananus

Table 2:- Count of Spider Species from Different Habitats of Barshitakli

Family	Total No. of species	Percentage of species
Araneidae	22	18%
Salticidae	16	13%
Lycosidae	10	8%
Thomisidae	8	6%
Oxyopidae	8	6%
Theridiidae	9	7%

Sicariidae	7	5%
Uloboridae	6	5%
Pisauridae	12	10%
Cheracanthiidae	7	5%
Hersiliidae	10	8%
Pholcidae	11	9%

Graph 1:- Chart Showing Distribution Percentage of Spider Family in Study Area.

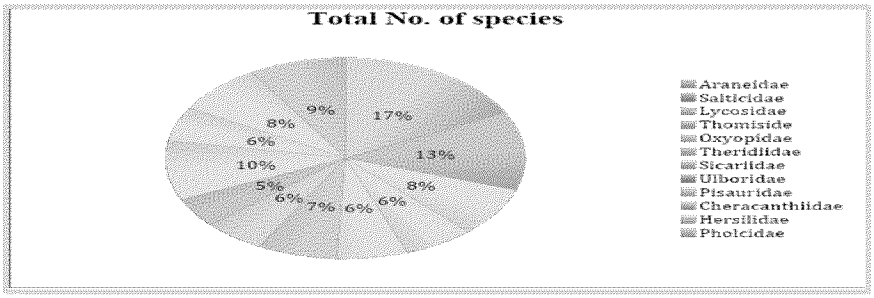

The above result showed that 18% of Araneidae, 13% of Salticidae, 8% of lycosidae and 6% of Oxopidae families are present. I also observed that the uloboridae. Theridiidae and sicariidae in the same percentage.

Photoplate

Araneus (Family Araneidae)	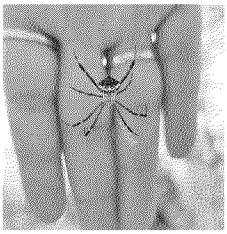 Argiope keyserlingi (Family Araneidae)	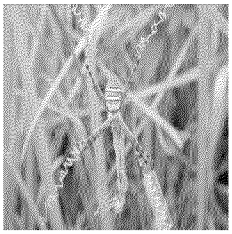 Argiope aemula (Family raneidae)	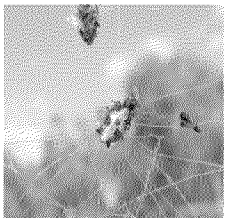 Cyclosa insulana (Family Araneidae)
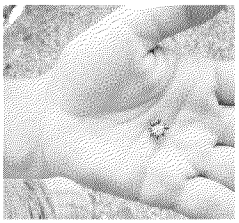 Gasteracantha (Family Araneidae)	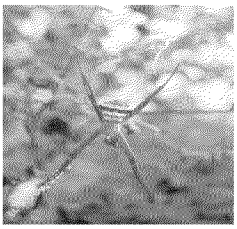 Argiope keyserlingi (Family Araneidae)	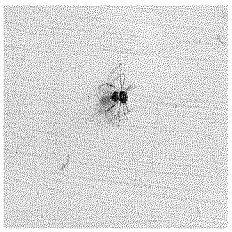 Myrmarachne (Family Salticidae)	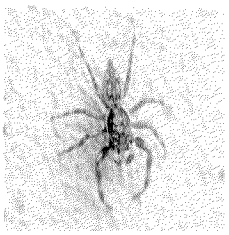 Menemerus semilimbatus (Family Salticidae)

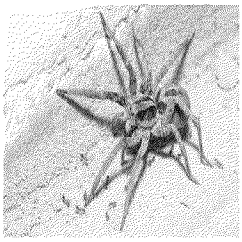 Wolf spide (Family Lycosidae)	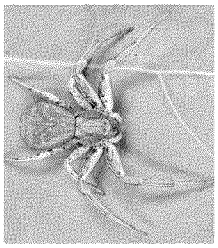 Xysticus croceus (Family thomisidae)	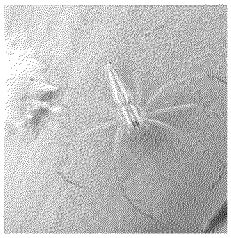 Oxyopes jananus. (Family Oxyopidae)	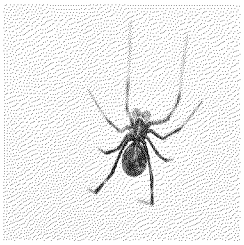 Tepidariorum spider (Family Theridiidae)
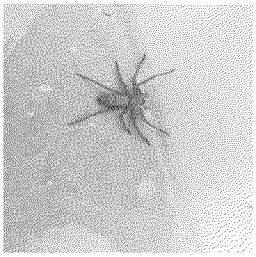 Huntsman spider (Family Sicariidae)	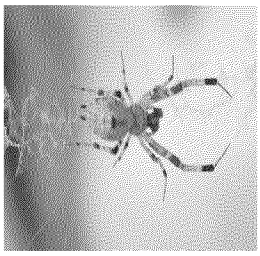 Uloborus plumipes (Family Ulboridae)	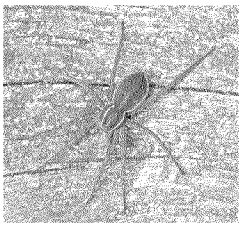 Six-Spotted fishing spider (Family Pisauridae)	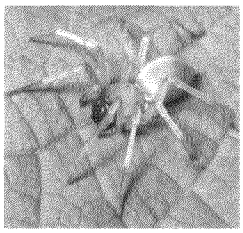 Cheiracanthium (Family Cheracanthiidae)
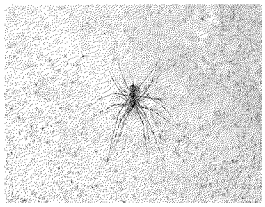 Tree Trunk spider (Family Hersiliidae)		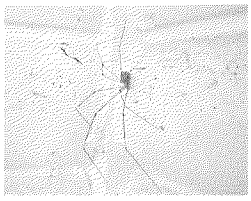 Pholcus phalangioides (Family Pholcidae)	

Conclusion

This study shows the information related to the spider and their species distribution in a particular habitat with response to environment, disturbance and availability of food. The spider such as argiope and Neoscona are the dominant species of spider in the study area kapshi. Various spiders in the kapshilake were found. Most of the spiders found in the Araneidae family and some rarely found were Uloboridae, Theridiidae, Thomiside, Oxyopidae, Cheracanthiidae, and sicariidae family species in that area.

Reference

- Miguel Angel Pinkus Rendo´n1,4, Guillermo Ibarra-Nu´n˜ez2, Victor Parra-Tabla3, Jose Alvaro Garcı´a-Ballinas2 and Yann He´naut2: SPIDER DIVERSITY IN COFFEE

PLANTATIONS WITH DIFFERENT MANAGEMENT IN SOUTHEAST MEXICO 2006. The Journal of Arachnology 34:104–112

- Achal Kumari Pandit. Diversity of common garden and house spider in Tinsukia district Journal of Entomology and Zoology Studies 2019; 7(4): 1432-1439
- Spider diversity and abundance in different habitats of Upper-Northern Rajasthan. International Journal for Environmental Rehabilitation and Conservation ISSN: 0975 — 6272 X (1): 1— 14
- N Priyadarshini1*, R Kumari1, R N Pathak1, A K Pandey2. Biodiversity and Community structure of spiders in Saran, part of Indo-Gangetic Plain, India. Asian Journal of Conservation Biology, December 2015.
- M. Devika, Mohamed Ibrahim N., Julffia Begum A. and Goldin Quadros. Diversity and Feeding Habits of Spiders Across Habitats in Coimbatore District. Indian Journal of Ecology (2022) 49(1): 216-220
- Tanmaya R. Sethy and Janak Ahi. Spider Silk and the Silk of Egg Sacs with its Astonishing Concealed Attributes: A Review. JOURNAL OF NATURAL FIBERS
- U. A. Gajbe. Studies on Some Spiders of The Family Araneidae (Araneae: Arachnida) From Madhya Pradesh, India. zool. Surv. India: 105 (Part 1-2) : 45-60, 2005
- Kandampully Baji Amulya 1,3, Honey Sebastian 2,4 & Ambalaparambil Vasu Sudhikumar 1. A new species of Oxyopes Latreille, 1804 (Araneae: Oxyopidae) from Calicut University Campus, Kerala, India. Serket (2022) vol. 18(3): 299-304.
- B. K. Tikader. Studies on Some Ant-Like Spiders From India (Family: Salticidae).
- Shirbhate Milind V. and Shirbhate Amrita M. Spiders of Katepurna sanctuary from the family Salticidae (Blackwall, 1841). Environment Conservation Jul 20 (18216306 2019.-
- Markus J. Buehler. Imaging and analysis of a threedimensional spider web architecture.
- Amit B Vairale, Gajanan A Wagh. Diversity of spiders in microhabitats of a tropical reserve forest of Amravati, Maharashtra, India. Bioscience Biotechnology Research Communications 14 (1), 446-452, 2021
- Animesh Dey, Susmita Debnath, Biplab Debbarma, PS Chaudhuri. A preliminary study on spider diversity from a house hold garden (artificial mixed plantation) in West Tripura, India. Journal of Research in biology 3 (5), 1009-1017, 2013

7. Evaluation of Molecular Interaction of 1, 6-Dihydropyrimidine in Acetone and DMSO Solvent

M. M. Mhasal
Shri. Shivaji College of Arts, Commerce, Science, Akola.
P.J. Thakare
Shri. Shivaji College of Arts, Commerce, Science, Akola.

Abstract

The main purpose of this study to investigate the impact of binary mixture 1,6 dihydropyrimidine in Acetone and DMSO solvent used to determine the molar refraction and polarizability constant. Molar refractivity (RM) of solution was calculated from density, refractive index data and polarizability (□) was calculated from molar refractivity data.

Keywords: Refractive indices, Molar refraction, Polarizability constant Molecular interaction.

Introduction

One of a unique and important property of liquid is refractive index. Refractometry allows the quantification of concentration changes by means of an associated refractive-index change leading to frequency shifts of optical resonances. The practical application of refractometry, mainly involves the measurement of concentration of one substance dissolved in another. Refractive indices can be measured easily with a high degree of accuracy. The value depends upon the temperature as well as the wavelength of light used. Generally, the D-line of sodium is used for standard measurements. Refractometric measurements directly gave information regarding solute-solvent, solvent-solvent interactions. A.N. Sonar1 and N.S. Pawar have studied the molar refraction and polarizability constant of substituted heterocyclic compounds in different media from refractive indices. Burghate et.al2 have studied the molar refraction and polarizability constant of substituted chalcones in different percentage of acetone-water mixture.

J.D. Pandey et.al3 have studied the refractometric and dielectric studies of binary liquid mixtures at different temperature. J. Padova4 have studied the ion-solvent interaction in mixed solvent using ethanol and acetone medium. The properties of liquid such as viscosity, refractive index and ultrasonic speed of binary mixtures are studied by many workers5. Oswal et al6 have

studied dielectric constants and refractive indices of binary mixtures. Mahajan7 have studied molar refraction and polarizability constant of 2-amino-5-chlorobenzene sulphonic acid in different percentage of dioxane-water mixture. Study of refractive indices in mixed solvents is done by Burghate et al8. Refractometric study on molecular interaction between some bromoalkane and non-polar hydrocarbon is studied by Yadav9. Dadhichi et.al.10 have investigated the measurement of viscosity, refractivity index and metal ligand stability constant of substituted benzofurones in different solvents. The density, viscosity, refractive index and speed of sound in aqueous mixtures of N, N-Dimethylformamide, Dimethyl sulfoxide, N, N-Dimethylacetamide, acetonitrile, ethylene glycol, diethylene glycol, 1,4-Dioxane, tetrahydrofuran, 2-Methoxyethanol and 2- Ethoxyethanol at 298.15K are studied11. Effect of temperature on the partial molar volumes of some bivalent transition metal nitrates and magnesium nitrate in DMF-Water mixtures are studied12. Zhi Zhou have been studied novel fiber optic refractometric method for liquid and gaseous media13. A. M. Kshirsagar et.al. have been studied effect of dioxane on N-(4-hydroxy-6- methyl-1,3,5-triazin-2-yl)-N'-phenylthiocarbamide at 250C in 60% dioxane-water system at various concentrations14.W. B. Shirsath have studied Physiochemical Properties of Binary Mixture of Methanol and Dimethyl sulfoxide (DMSO) and Methanol and Dimethylformamide (DMF)15.Yasmine Chabouni and Fauzia Amireche have been studied physicochemical properties of binary mixtures of glycerol with butanol isomers in the temperature range 293.15–318.15 k and ambient pressure16. D.S.Hedaoo, M. M. Kalaskar and M. P. Wadekar studied Refractometric study of substituted 2,3-dihydroquinazolin-4(1H)-ones in different binary mixture17.A.S. Chandami, P.P.Choudhari and M.P.Wadekar studied molecular interactions in the solution18.Insight into the the solute - solvent interactions by physicochemical and excess properties in binary systems of the ether and allyl-based functionalized ionic liquid with acetonitrile are studied19. Nimbarte, Gaurav Ramesh investigated refractometric study of substituted dihydropyrimidin 2(1H) one in different solvents20.Manoj R Gaware studies of molar refraction and polarizability constant of 6-(4-chlorophenyl)-1,2,3,4-tetrahydro-2,4- dioxopyrimidine-5-carbonitrile in 60% DMSO in the temperature range 298 to 313 K21.To understand intermolecular interaction, molar refraction and polarizability constant studied by Yaseen SA et.al22. Structural arrangement of an atom in molecule responsible for interactions in solvent medium23.

Experimental

Above all substituted heterocyclic compounds have most important life saving drugs. 1,6-dihydropyrimidine is used as anti-diabetic. It is also used in heart diseases, strokes, kidney diseases, blood circulation problem, and blindness and as antipsychotic. It is effective in liver diseases. The solution of above compound is prepared in DMSO solvent by dissolving an appropriate amount by weight. For density measurement all the weight of solution took on Contech balance (0.001gm). The refractive index of solutions is measured of different concentration (0.625x10-3 to 10x10-3) by Abbe refractometer having accuracy with ± 0.01 unit. The constant temperature of the prism box is maintained by circulating water from thermostat. Refractometer was calibrated by using glass test piece of known refractive index supplied with the instrument.

In the present investigation following ligands are used.

(LA) = 2-Amino [4-(3-nitro phenyl) -6-phenyl-1,6-dihydro] -1,3- pyrimidine,

(LB) = 2-Amino [4,6-diphenyl-1,6-dihydro] -1,3- pyrimidine,

(LC) = 2-Amino [4-(4-hydroxy phenyl) -6-phenyl-1,6-dihydro] -1,3-pyrimidine,

(LD) = 2-Amino [4-(2-hydroxy phenyl) -6-phenyl-1,6-dihydro] -1,3-pyrimidine

The molar refraction of solvent and solution are determined by using Lorentz- Lorentz equation.

The molar refraction of solvent, solvent-water mixtures are determined from-

RDMF-W = X1R1 + X2R2 ……(1) where,

R1 and R2 are molar refractions of solvent and water respectively.

The molar refraction of solutions of ligand in solvent -water mixtures are determined from-

$RMix = (n2-1)\,(n2+2) + [X1M1 + X2M2 + 3M3]\,d\,\}$ …… (2)

where, n is the refractive index of solution, X1 is mole fraction of solvent, X2 is mole fraction of water and X3 is mole fraction of solute, M1, M2 and M3 are molecular weights of solvent, water and solute respectively. 'd' is the density of solution.

The molar refraction of ligand is calculated as –

Rlig = Rmix - RDMF – w …… (3)

The polarizability constant (□) of ligand is calculated from following relation- Rlig = 4/3 □No□ …… (4)

where, No is Avogadro's number.

Result and Discussion

The values of refractive index (n), density (d), molar refraction (Rm) and polarizability constant (α) at 300K

Conc.in %	Constant ligand concentration system (0.01M) with change in DMSO			
	Refractive index (n)	**Density (d) gm/cm^3**	**Rm x10^3 cm^3/mol**	**α x10^{-23} cm^3**
Ligand L_A				
20	1.363	0.9976	53.7781	2.1326
40	1.395	1.0041	64.3623	2.5524
60	1.413	0.9944	70.3808	2.7910
80	1.445	1.0032	76.0290	3.0150
100	1.478	1.0012	82.0658	3.2544
Ligand L_B				
20	1.371	0.9993	46.4766	1.8431
40	1.394	1.0005	54.6358	2.1666
60	1.413	0.9857	60.1607	2.3857
80	1.449	0.9979	65.2527	2.5877
100	1.47	0.9997	68.6089	2.7208
Ligand L_C				
20	1.375	1.0029	49.7148	1.9715
40	1.395	1.0040	58.0503	2.3021
60	1.414	0.9957	63.5075	2.5185
80	1.449	1.0038	69.0285	2.7374
100	1.467	1.0016	72.4822	2.8744
Ligand L_D				
20	1.376	1.0062	49.6688	1.9697
40	1.390	0.9947	57.9369	2.2976
60	1.414	0.9932	63.6663	2.5248
80	1.443	0.9920	69.0440	2.7380
100	1.473	0.9988	73.48268	2.9141

Graphical representation of Molar refraction (Rm) verses changes in DMSO solvent percentage at constant (0.01M) ligand concentration

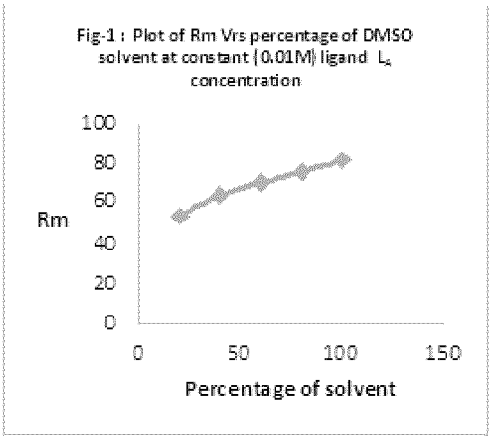

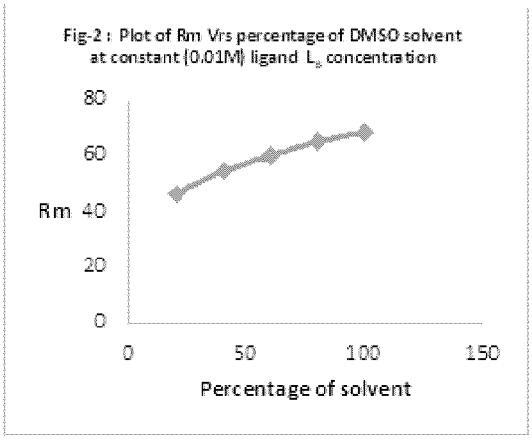

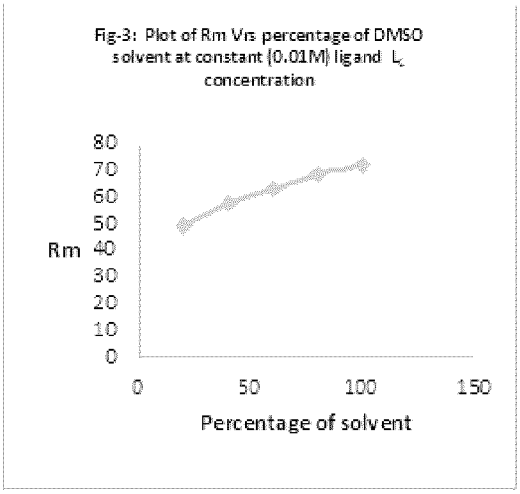

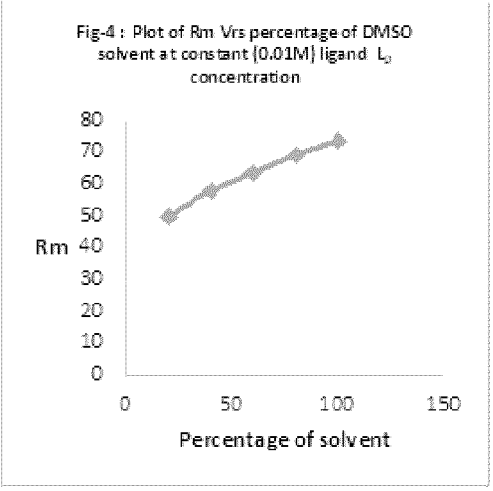

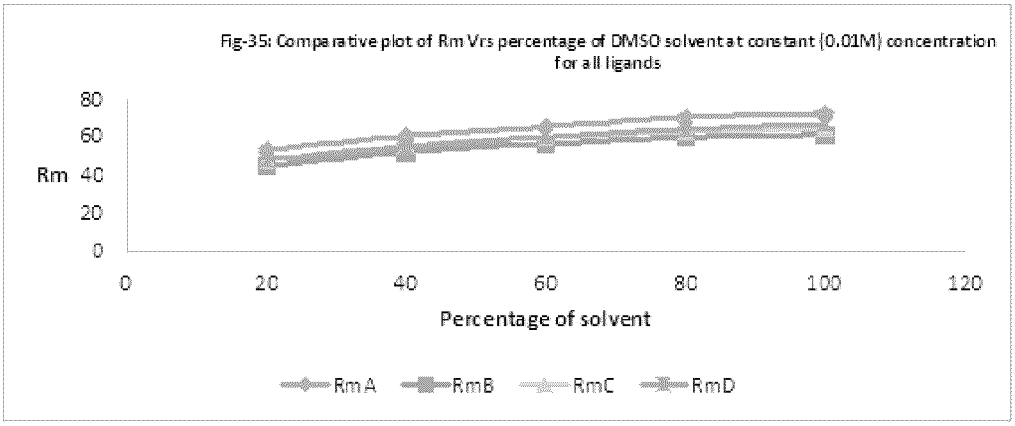

Graphical representation of Molar refraction (Rm) versus change in Acetone solvent percentage at constant (0.01M) ligand concentration

Conc.in %	Constant ligand concentration system (0.01M) with change in Acetone			
	Refractive index (n)	**Density (d) gm/cm^3**	**Rm x10^3 cm^3/mol**	**α x10^{-23} cm^3**
Ligand L_A				
20	1.351	1.0045	51.5776	2.0452
40	1.354	1.0021	58.0016	2.3002
60	1.355	1.0104	60.1695	2.3870
80	1.365	1.0095	62.7370	2.4876
100	1.4	1.1001	63.4008	2.5143
Ligand L_B				
20	1.346	1.0038	42.9098	1.7020
40	1.351	1.0025	48.0155	1.9045
60	1.355	1.0170	50.3987	1.9991
80	1.415	1.0727	56.2931	2.2325
100	1.42	1.0069	61.2389	2.4284
Ligand L_C				
20	1.353	1.0024	46.6540	1.8502
40	1.354	1.0034	52.1190	2.0669
60	1.357	1.0135	54.2340	2.1516
80	1.363	1.0136	56.0443	2.2226
100	1.364	1.0044	57.5689	2.2830
Ligand L_D				
20	1.347	0.9939	46.4519	1.8422
40	1.348	1.0121	51.1423	2.0283
60	1.350	1.0107	53.5564	2.1240
80	1.364	1.0091	56.4311	2.2379
100	1.366	0.9983	58.0446	2.3019

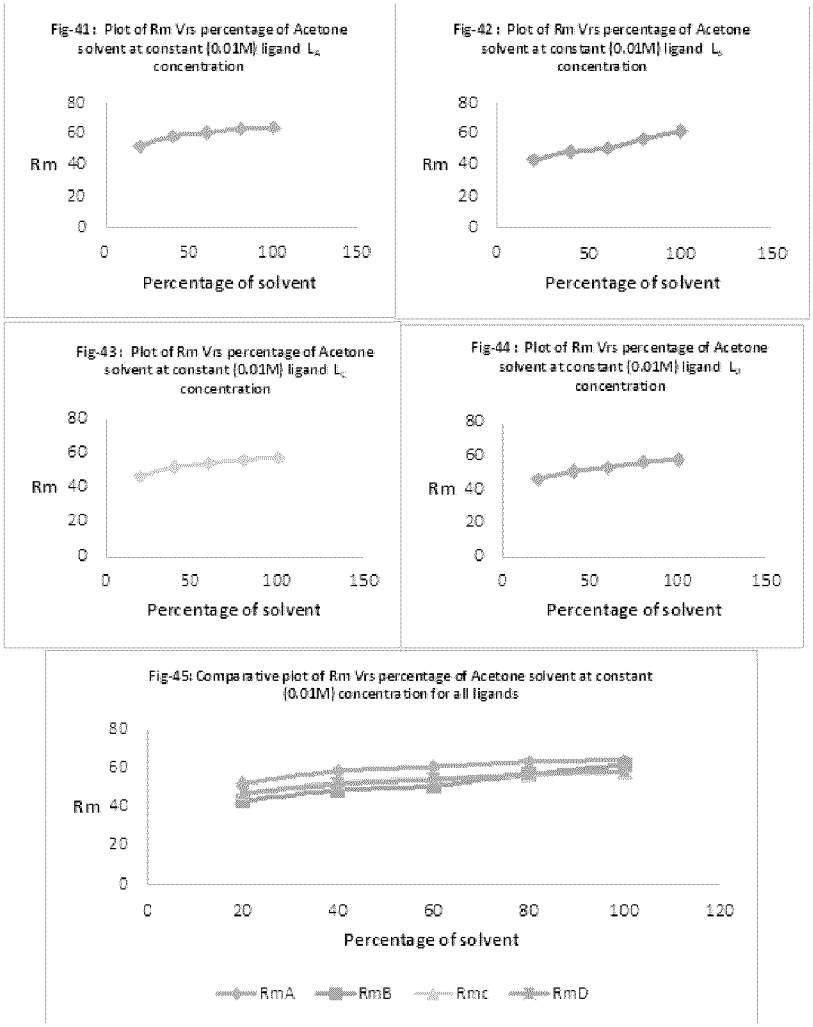

Conclusion

In conclusion, we have demonstrated the values of molar refraction and polarizability constant of 1, 6-dihydropyrimidine with solvent-water mixture. It shows the values of molar refraction and polarizability constant at different concentration of 1,6-dihydropyrimidine in 20%, 40%, 60%, 80% and 100% different solvent water mixture. It was observed form the tables that the molar refraction and polarizability constant of 1,6-dihydropyrimidine decreases in the concentration of 1,6-dihydropyrimidine. From the data it can be predicted that, when the percentage of solvent increases, molar refractivity (true molar volume) continuously increases. At the same time polarizability constant of a substituted aminopyrimidine increases. This may be attributed that with the increase in percentage of solvent it causes decreases in dielectric constant of medium and also considerable dipole association (intermolecular attraction) take place which

can be accompanied by decrease in polarizability. From this study it is clear that when the percentage of solvent increases the solute solvent interactions i.e., interaction of 1,6-dihydropyrimidine and solvent increases which may stabilize the drug activity of higher percentage of solvent.

References

1 A.N. Sonar, N.S. Pawar, Rasayan J. Chem. 2010, 3(2), 250-254.

2 A.S.Burghate, P.B.Agrawal, M. L. Narwade, Asian J. of chem., 2001, 13(4), 1652-1654.

3 J.D. Pandey, Jyotsna Chhabra, N.K. Soni, R.K. Mishtra, Ind. J.of chem., 2006,45 A,653- 656.

4 J. Pandova, Can. J.l of chem.., 1965, 43,458-462.

5 AS Burghate; PB Agrawal; SW Quazi & ML Narwade. Asian J. Chem., 2001, 13(4), 1652.

6 SL Oswal & MV Rathnam. Ind. J. Chem., 1987, 26, 29.

7 DT Mahajan. Ph.D. Thesis in Chemistry Submitted to Amravati University, Amravati,

1. 1997.

8 AS Burghate; PB Agrawal; SW Quazi & ML Narwade. Asian J. Chem., 2001, 13(4), 1652.

9 SS Yadav; Anirudh Yadav; Neetu Kushwaha & Neetu Yadav. Indian J. Chem., 2009,

10 V. S. Jamode, J. C. Dadhichi, D. D. Malkhede, M. L. Narwade, J. Indian Coun. Chemist,

2. (2005), 22(2), 35.

11 T. M. Aminabhavi, B. Gopalakrishna, J. Chem. Eng. Data, (1995), 40(4), 856.

12 M. L. Parmar, D. S. Banyal, Indian J. Chem. Sect A, (2005), 44(8), 1582.

13 Y. N. Kulchin, O. B. Vitrik , A. V. Dyshlyuk, Zhi Zhou, Pacif. Sci. Rev.,(2012),4(1), 23.

14 D. T. Tayade, A. M. Kshirsagar, the Open Phys. Chem. J., (2014), 6, 1.

15 W. B. Shirsath, Journal of Scientific Research (2021), 65, (7),49.

16 Yasmine Chabouni and Fauzia Amireche J. Chem. Eng. Data, (2020), 65, 4, 1679.

17 D. S. Hedaoo, M. M. Kalaskar and M. P. Wadekar, Der Chemica Sinica, (2015), 6(6):7, 14.

18 A. S. Chandami, P. P. Choudhari and M. P. Wadekar, Advances in Applied Science Research, (2016), 7(3):120-126.

19 Dawei Fang,Li Li,jialin Miao,Peizhen Gao,Yuxin Zhang Mei Hong, Journal of the Taiwan Institute of Chemical Engineers (2022),104275.

20 Nimbarte, Gaurav Ramesh, Journal of Advanced Scientific Research, (2021), 12,201-208.

21 Manoj R Gaware, Indian Journal of Science and Technology, (2021), 14(2):113–118.

22 Yaseen SA, Alameen AS, Saif FA, Undre SB, Undre PB. Study of Volumetric and Optical Properties of Cerium Oxide Nano-Fluid. Journal of Physics: Conference Series. 2020; 1644.

23 R Sawale, Kalyankar T, George R, Deosarkar S. Journal of Applied Pharmaceutical Science. (2016), 6(3), 120–124.

8. Synthesis, Characterization and Biological Activity of Nitrogen Containing Pyrazolone and its Derivatives

R. N. Gaikwad
Assistant Professor, Vitthal Rukmini Mahavidyalaya, Sawana, Tq. Mahagaon, Dist. Yavatmal.
B. N. Chate
Associate Professor, Sanjivani Mahavidyalaya, Tq. Chapoli, Dist. Latur.

Abstract

The synthesis of pyrazolone and its derivatives is achieved by a clean, one-pot, multi-component condensation reaction combining ethyl acetoacetate, hydrazine hydrate, aromatic aldehyde in catalytic amount of MSA. This approach has numerous benefits, including a quick reaction time and an easy work-up process. Compounds were identified via mass spectral analysis, NMR, IR, and chemical transformation. The antibacterial activity of the synthesized compounds was assessed against a specific strain of S. aurous and E. coli.

Keywords: aryl aldehyde, ethyl acetoacetate, hydrazine hydrate, MSA, pyrazolone etc.

Introduction

Pyrazolone are a class of organic compounds that feature a five-membered ring containing three carbon atoms and two nitrogen atoms. The molecular formula of pyrazolone is $C_3H_3N_2$. This heterocyclic ring structure imparts unique chemical and pharmacological properties to pyrazolone, making them significant in various fields such as chemistry and medicine. Pyrazolone aromatic nature, stability, and adaptable reactivity are among their essential qualities. They can change chemically in a variety of ways, which makes it possible to create different derivatives with unique characteristics. Pyrazolone have been used extensively in the manufacturing of materials, agrochemicals, and pharmaceuticals. Pyrazolone synthesis is achieved using a variety of techniques, such as condensation and cyclization reactions. These techniques increase the variety of compounds that can be produced by incorporating various functional groups onto the pyrazolone ring. In medicinal chemistry, pyrazolone have been recognized for their biological activities and are frequently used as scaffolds for designing drug candidates. Compounds containing the pyrazolone moiety have been investigated for their anti-inflammatory, antiviral, anticancer, and antifungal properties, among others. Pyrazolone also exhibit interesting coordination chemistry, forming complexes with various metal ions. This property makes them relevant in coordination chemistry and catalysis.

The pyrazolone ring represent a fascinating class of organic compounds with a broad range of applications, from their roles in synthetic chemistry to their significance in drug discovery and materials science. The diverse properties and reactivity of pyrazolone contribute to their continued exploration and utilization in various scientific and industrial fields. Pyrazolone derivatives, which are created with pyrazolone as the primary core, have garnered more and more interest over time. A five-membered heterocyclic organic molecule with two neighboring nitrogen atoms can be found in the center core. The chemical, pharmaceutical, and agrochemical industries are very interested in pyrazolone derivatives[1,2]. Considered an active scaffold with pharmacological importance, pyrazolone and its derivatives exhibit nearly all pharmacological activity. The pyrazolone moiety's pharmacological potential has been demonstrated by the nucleus's presence in pharmacological agents belonging to various therapeutic categories, including rimonabant, difenamizole, an analgesic; fezolamide, an antidepressant; and celecoxib, a potent anti-inflammatory and antipsychotic.[3] Because of their many characteristics and uses, pyrazolones are a class of chemicals that have been studied. These include pyrazol-3-ol and pyrazolin-5-one. Sulfamazone, propyphenazone, and nifenazone[4] are a few of the exploratory small compounds containing pyrazolone that have been considered as potential therapeutic possibilities. Derivatives of pyrazolone are a significant class of heterocyclic chemicals found in numerous medications and synthetic goods. Based on a review of the literature, pyrazolone derivatives exhibit a range of pharmacological actions, including, anti-tubercular[5], anti-fungal,[6,7] anti-bacterial,[8] anti-inflammatory,[9] anti-timor,[10] anti-microbial.[11]

In this study, we have created a sophisticated, effective, simple, and straightforward method for the synthesis of pyrazolone and its derivatives. We do this by employing ethanol as a solvent together with hydrazine hydrate, ethyl acetoacetate, and substituted aryl aldehydes in a catalytic quantity of MSA. In terms of environmentally friendly procedures, the combination of the green technique and the catalyst results in an outstanding product yield. This approach offers many important benefits, including reduced reaction time, solvent-free conditions, atom economy, using a green catalyst, and a more pleasant workup process.

The antibacterial activity of a recently synthesized molecule is the subject of the current antimicrobial study. Using the agar-cup diffusion method, this compound's antibacterial activity was investigated. Both gram positive and gram negative types of bacteria are employed.

1. Gram positive : S.aureus 2. Gram negative : E.coli

Experimental

General

The digital melting point device (Veego-VMD) was used to record the uncorrected melting point of the produced chemical. A.R. Grade chemicals were used. Every chemical employed was of A.R. Grade, and it wasn't purified further. Microwave irradiation was carried out in a Microwave Oven, Model No. MS2079 DB DB1QILN (2450 MHz, 1050 W) equipped with Erlenmeyer flask. The compound's melting point was measured in an open capillary tube and might not be accurate. Using an FT-IR spectrophotometer made by Perkin-Elimer, IR spectra were recorded. KBR Pellet. Using chloroform as a solvent, the 1H NMR spectra and mass were recorded using a Perkin-Elimer spectrophotometer. The chemical shift value was reported in parts per million (ppm) with respect to TMS, which served as an internal standard. Antimicrobial activity assessed by means of the Kirby-Bauer technique. Hi-media Laboratories Pvt. Ltd. in India produced nutritional agar for the development of all strains of S. aureus and E. coli, which was the medium utilized for the investigation of the newly synthesized compound's antibacterial effectiveness.

General Procedure for the synthesis of Pyrazolone and its Derivatives

The combination of **1** ethyl acetoacetate (0.01mmol), **2** hydrazine hydrate (0.01mmol), and **3** aryl aldehyde (0.01mmol) in catalytic amount of Methane sulphonic acid (MSA) in an Erlenmeyer flask and irradiated until completion of the reaction in microwave oven. The reaction mixture was poured in crushed ice and filtered, washed with ethyl acetate, the product was recognized as 3-methyl-4-arylidene pyrazolone (4a-d). The crude product was collected and recrystallized in ethanol and dried. The entire product was characterized by physical constant and spectroscopic techniques and compared with the standard method.

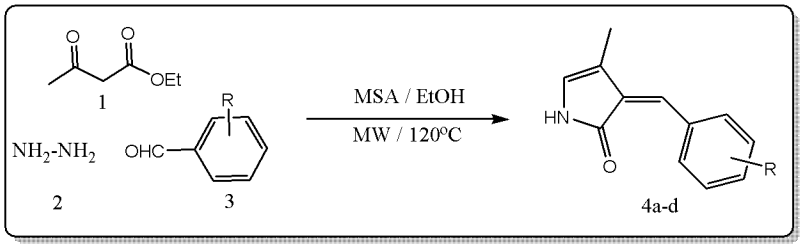

Scheme 1

Result and Discussion

As indicated in the scheme 1, we reported a direct method for the synthesis of pyrazolone and its derivatives by one pot condensation of aromatic aldehyde, hydrazine hydrate, and ethyl-acetoacetate. The yield was really high. In order to assess the extent and constraints of the

methodology, the reactions were conducted in the absence of a catalyst, and the structures of all newly synthesized pyrazolone derivatives were established using chemical transformation, NMR, IR, and mass analysis.

Table1: Synthesis of pyrazolone & its derivatives catalyzed by MSA under M.W. 120oC/300 W)

Product	Name of compound	% yield	Melting Point in ^{O}C
4a	(Z)-3-benzylidene-4-methyl-1,3-dihydro-2H-pyrrol-2-one	94 %	122^{0}C
4b	(Z)-3-(4-chlorobenzylidene)-4-methyl-1,3-dihydro-2H-pyrrol-2-one	89%	215^{0}C
4c	(Z)-4-methyl-3-(3-nitrobenzylidene)-1,3-dihydro-2H-pyrrol-2-one	87 %	195^{0}C
4d	(Z)-3-(4-hydroxybenzylidene)-4-methyl-1,3-dihydro-2H-pyrrol-2-one	92 %	197 ^{0}C

Table 2. Optimization of catalyst concentration of (4b) under M.W. Irradiation

Entry	Catalyst mol %	Time, min	Yields %
1	No catalyst	9	-
2	1	8	76
3	2	7	89
4	**3**	**3**	**95**
5	4	5	85
6	5	8	70

Initially, the mixture of Ethyl acetoacetate, Hydrazine hydrate and substituted aryl aldehydes, (0.01 mol each) was taken in an 50 mL vessel and subjected to microwave irradiation under neat conditions in the absence of catalyst and solvent, and the reaction was failed to get the product under this condition. The reaction was repeated in the presence of catalyst in the range 1-5 mol %. We have optimized the amount of catalyst for the synthesis of (**4b**, Table 1) under microwave irradiation and excellent yield was obtained in only 3 minutes when 3 mol % catalysts are introduced (**Table 2,** entry 4).

A number of approaches have been put forth and modified for the measuring of antibacterial activity. The cup diffusion method[12-14] was used in the current investigation to screen freshly synthesized compounds for antibacterial activity. There are both gram positive and gram negative bacteria among the species, such as S. aureus and E. coli. Agar medium, subcultures, and nutrient broth were prepared in accordance with normal protocol. Sensitivity plates were seeded with 1× 106 CIU ml-1 bacterial in oculims, and each well (diameter of 8 mm)

was filled with 0.1 ml of 1000µgml-1 test compound solution in chloroform, resulting in a concentration of 100µgml-1 for each test compound. Using an antibiotic zone scale, the zone of inhibition was measured following a 24-hour incubation period at 370C. The compounds' inhibition zone records made it abundantly evident that compounds (15) and (18) were quite effective against S. aureus and E. coli. Table 3 summarizes the test compound's antimicrobial activity and its ability to suppress the growth of different bacterial species.

Table 3: Antimicrobial Activity

Compounds	**Inhibition zone recorded in mm**	
Microorganisms	**S. aureus**	**E.Coli**
4a	11mm	14mm
4b	16mm	13mm
4c	13mm	15mm
4d	12mm	17mm

Composition of Nutrient Agar medium:

Peptone : 5.0gm
Yeast extract : 1.5gm
Beef extract : 1.5gm
Sodium chloride : 5.0gm
Agar-agar : 15.0gm
Distilled water : 1000ml
pH : 6.9-7.1

Fig 1: Antimicrobial activity against some selected microorganism.

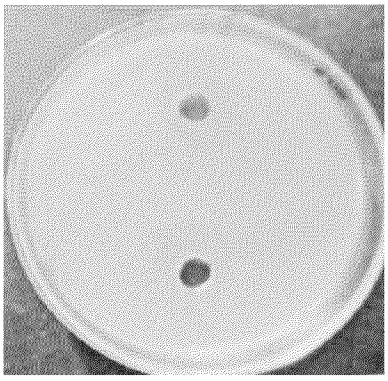

S.aureus

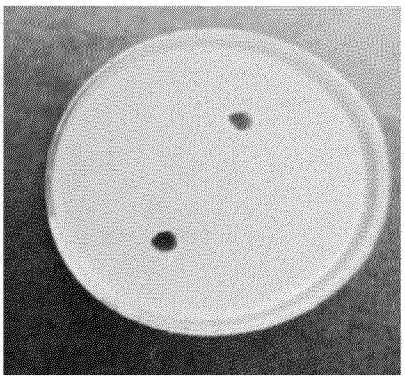

E.Coli

The quality of media that was employed was bacteriostatic. 28 grams of materials were dissolved in one liter of distilled water to create the nutrient agar medium. It was then autoclaved at 121°C for 20 minutes, 15 pounds at a time. After cooling to roughly 50°C, the medium was added to sterile petriplates and allowed to harden. To obtain grass culture, the test bacterial

organisms were then planted onto the media plates with 24-hour-old, fresh, active nutrient broth cultures. Using standard quality cork boarers, agar medium was scooped out of a petridish to create the typical 8.0mm diameter cups. Operations are performed in an ultra-clean laminar flow system under aseptic conditions. The test chemicals were dissolved in chloroform while maintaining the solution's initial 1000µg/ml concentration. As a control, chloroform solvent was utilized. These plates were placed in an incubator and incubated for 24 hours at 37ºC. Following incubation, test drug inhibitory effect was monitored on the plates by looking for a clean zone surrounding the cups. By comparing the plate to the antibiotic zone scale, the diameter of the zone of inhibition was determined.

Spectroscopic characterization.

4c) (Z)-4-methyl-3-(3-nitrobenzylidene)-1,3-dihydro-2H-pyrrol-2-one

Solid: - Melting point = 195ºC

IR (KBr, Cm^{-1}) : 1354, 1260, 1500, 1607, 670.

^{1}HNMR (400 MHz, DMSO-d6): δ 7.2(1H,s), 1.18 (1 H, s), 6.93 (1 H, s), 8.10-8.12 (4H, m).

4d) (Z)-3-(4-hydroxybenzylidene)-4-methyl-1,3-dihydro-2H-pyrrol-2-one

Solid: - Melting point = 197ºC

IR (KBr, Cm^{-1}) : 1354, 1260, 1500, 1607, 670.

^{1}HNMR (400 MHz, DMSO-d6): δ 7.45(1H, s), 6.89 (1 H, s), 9.81 (1 H, s), 5.0(1H,s), 6.93 (4H, m).

Conclusion

We have been able to offer an effective method for the synthesis of pyrazolone derivatives in the presence of MSA in our current study. All of the recently synthesized compounds' structures were determined via mass spectral analysis, NMR, IR, and chemical transformations.

Condensation-enhanced pyrazolone synthesis and its derivatives provide high yields of pyrazolone in good quality and purity at a low cost. It is discovered that compound 4d has greater potency against E. Coli while compound 4b has greater potency against S. Aureus. This approach has the noteworthy advantages of being catalyst-free and having an easy workup procedure. The synthesis process used to create these molecules is very easy to use, clean, economical, green, and environmentally friendly.

References

1. S. Mert, R. Kashmogullari, Postdoc, 2, 450, 2014.
2. G.Mariappan, B.Saha, Journal of pharmacy research, 3, 2856, 2010.
3. P. Gupta, K.Halve, International journal of pharmaceutical sciences and research, 4, 2291, 2015.
4. Z. Zhao, X. Dai, Eurj.Med.Chem, 186, 1118, 93, 2020.
5. K. Karrouchi, S. Radii, Y. Ramli, Molecule, 23, 45, 2018.
6. M.Radii, V. Bernardo, B. Bechi, D. Castagnoio, Tetrahedron letters, 50, 6572, 2009.
7. P. Mitra, A.Mitra, Indian Chem. Soc., 58, 695, 1981.
8. B.Singh, Indian Chem. Soc., 68, 165, 1991.
9. M. Ruoqun, J. Zhu, J. Liu, L.Chem, X. Shen, H. Jiang, Molecule, 15, 3593, 2010.
10. R. Prajuli, J.Banerjee, H. Khanal, Oriental journal of chem., 31, 540, 2015.
11. M. Nashwa El- Metwaly, G. Marwa, A. Thoraya, M. Abelaua, Biogenetic chemistry and applications, 3, 654, 2018.
12. British Pharmacopici Vol. 2, Her Mejestis Stationary Office, London, 12, (1980) British Pharmacopeia's Pharmaceutical press London, (1953)796.
13. Bary A.I., The antimicrobial susceptibility test, Principle and Practices Illusiea and Febiger, Philadelphia, PA, USA, 180.
14. Cavangh F., Analytical Microbiology Academic Press New York, (1963) 126.

9. The Poincare Half-Plane Model and Geo Gebra: Powerful Tools for Understanding Hyperbolic Triangles

Rajesh Balkrishna Raut
R. D. & S. H. National College and S. W. A. Science College, Linking Road, Bandra.

Abstract

The aim of this paper is to illustrate the construction of geodesics and triangles in the hyperbolic half-plane using GeoGebra software. It further demonstrates the bisection of a geodesic segment and the concurrency of medians for a hyperbolic triangle. Also constructing the incircle for hyperbolic triangle and angle bisectors is explained.

Key Words: Poincaré half-plane model, geodesic, midpoint, incircle

Mathematics Subject Classification: 2000. 51M10

1. Introduction

In the Euclidean plane $\mathbb{R}^2$, the three medians of any triangle are concurrent. Similarly, the three angle bisectors of any triangle are also concurrent. The construction of triangles, the midpoint of its side, and the angle bisector for an angle at its vertex can be accomplished by following certain steps. GeoGebra software, which is freely available to all, facilitates the explanation of these constructions in an easy and effective manner. One can practice the above constructions and further verify the concurrency of medians and angle bisectors by selecting appropriate points for constructing a triangle in the GeoGebra graphic view. GeoGebra software is an excellent tool for teachers to demonstrate these topics and assign enjoyable exercises. It also allows users to create new tools. This paper explains some of the above constructions in the Poincaré half-plane model using GeoGebra.

2. Preliminaries

The hyperbolic plane is set $\mathbb{H}^2 := \{x + iy : x, y \in R \text{ and } y > 0\}$ with distance function $\cosh\big(d(x_1 + i\,y_1, x_2 + iy_2)\big) = 1 + \frac{(x_1-x_2)^2+(y_1-y_2)^2}{2y_1y_2}$. In the Poincaré half-plane model, $z = x + iy \in \mathbb{H}^2$ is identified by the point $(x, y) \in \mathbb{R}^2$. Then a geodesic in $\mathbb{H}^2$ is represented by

either semicircle with centre on x-axis or part of a line parallel to the y-axis, both contained in the upper half-plane $\{(x,y) \in \mathbb{R}^2 : y > 0\}$.

3. Some notations

For $z_1 = x_1 + i\,y_1,\ z_2 = x_2 + iy_2$ the geodesic segment is denoted by $[z_1, z_2]$. The mid-point of $[z_1, z_2]$ is the point $m_{12} \in [z_1, z_2]$ equidistant from z_1 and z_2 with respect to the hyperbolic distance. Further for $z_1, z_2, z_3 \in \mathbb{H}^2$ and not on same geodesic, denote by $[z_1, z_2, z_3]$ the triangle formed by geodesic segments $[z_1, z_2], [z_2, z_3]$ and $[z_3, z_1]$. The angle of this triangle at vertex z_1 is defined as the Euclidean angle between the tangents to circular arcs corresponding to geodesic segments, $[z_1, z_2]$ and $[z_3, z_1]$ at vertex z_1. Further the angle bisector at vertex z_1 is the geodesic segment passing vertex z_1 by making equal angle with geodesic segments, $[z_1, z_2]$ and $[z_3, z_1]$ at vertex z_1.

The procedure in the GeoGebra software to create new tools for constructing geodesic segment and its midpoint are illustrated below. Then using these two new tools, construction of medians, incircle and angle bisectors for hyperbolic triangle are illustrated.

4. Construction of Geodesic segments and triangles in $\mathbb{H}^2$

If $x_1 = x_2$ then the geodesic segment $[z_1, z_2]$ is identified by the vertical line segment joining points $(x_1, y_1), (x_2, y_2)$ and when $x_1 \neq x_2$ it is identified by the circular arc. GeoGebra is interactive software. One way to construct this circular arc with centre $c_{12} = (x_{12}, 0)$ is: select points $(x_1, y_1), (x_2, y_2), (x_{12}, 0)$ using point tool, then use command CircularArc to obtained arc and finally move point c_{12} on the x-axis to obtain required circular arc.

Another way of constructing geodesic segment works in both cases. Following theorem is useful in calculations.

Theorem The circle S in $\mathbb{R}^2$ passing through three points $(x_1, y_1), (x_2, y_2)$ and (x_3, y_3) has equation $\text{determinant}\begin{bmatrix} x^2+y^2 & x & y & 1 \\ x_1^2+y_1^2 & x_1 & y_1 & 1 \\ x_2^2+y_2^2 & x_2 & y_2 & 1 \\ x_3^2+y_3^2 & x_3 & y_3 & 1 \end{bmatrix} = 0.$

Further if (x_{12}, y_{12}) is the centre an r is the radius of circle S, then we have relation

$$\begin{bmatrix} 2x_1 & 2y_1 & 1 \\ 2x_2 & 2y_2 & 1 \\ 2x_3 & 2y_3 & 1 \end{bmatrix} \begin{bmatrix} x_{12} \\ y_{12} \\ c \end{bmatrix} = \begin{bmatrix} -(x_1^2+y_1^2) \\ -(x_2^2+y_2^2) \\ -(x_3^2+y_3^2) \end{bmatrix} \text{ where } r = \sqrt{x_{12}^2 + y_{12}^2 - c^2}.$$

Applying above theorem we get a point $w = \left(0.5(x_1 + x_2), 0.5\sqrt{2(y_1^2 + y_2^2) + (x_1 - x_2)^2}\right)$ on $[z_1, z_2]$. Now GeoGebra Command a: CircumcircularArc(z_1, w, z_2) give required arc where order of points z_1, w, z_2 in command CircumcircularArc is important. One can create new tool 'Geodesic' in GeoGebra by taking output object as a, input objects as z_1 and z_2. Now constructing triangle $[z_1, z_2, z_3]$ (see Figure 1) is easy by using this new tool 'Geodesic'.

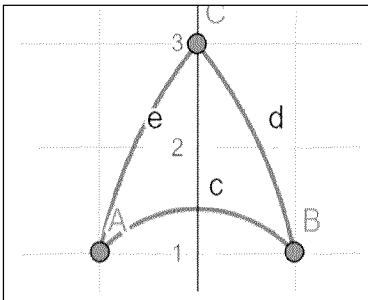

Figure 1 hyperbolic triangle

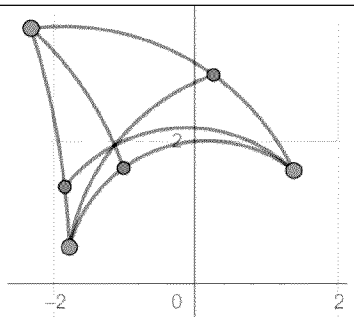

Figure 2 Medians of triangle

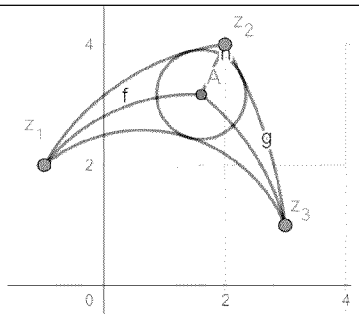

Figure 3 Incircle for triangle

5. Bisecting geodesic segment in $\mathbb{H}^2$

The midpoint of geodesic segment $[z_1, z_2]$ is identified by the point (see 4.4 Lemma in [4]) $m = \left(\frac{x_1y_2 + y_1x_2}{y_1 + y_2}, \sqrt{y_1y_2}\frac{\sqrt{(y_1+y_2)^2 + (x_1 - x_2)^2}}{y_1 + y_2}\right) \in \mathbb{R}^2$. Create new tool 'Hmidpoint' to get point m in GeoGebra. Now using tools 'Hmidpoint' and 'Geodesic' it is easy to get midpoints for sides of triangle $[z_1, z_2, z_3]$ and joining these points to opposite vertices concurrency of medians is verified (see Figure 2).

6. Construction of the incircle and angle bisectors for triangle in $\mathbb{H}^2$

The incircle of a triangle is largest circle contained in it. Every hyperbolic triangle has the incircle, whose centre lies on all three angle bisectors of the triangle. One way to construct the incircle of a hyperbolic triangle is to place one point on each side of the triangle, draw a circle through these three points, and move the points on the sides to adjust the circle's radius and centre, thereby creating the incircle. The other way is by writing equations and solving. The incircle C for triangle $[z_1 = -1 + 2i, z_2 = 2 + 4i, z_3 = 3 + 1i]$ is constructed using steps:

1. 1. Circle C and the geodesic g_1 containing $[z_1, z_2]$ are orthogonal, and C lies inside of g_1. Suppose $p = t + is$ is the centre and r is the radius of C. In this case $x_{12} = (2.5,0)$ is the centre and $r_{12} = 0.5\sqrt{65}$ is the radius for g_1. The Euclidean distance between p, x_{12} give equation $(t-2.5)^2 + s^2 = \left(0.5\sqrt{65} - r\right)^2$. Similarly we get equation from C and the geodesic g_2 containing $[z_2, z_3]$ $(t+5)^2 + s^2 = \left(\sqrt{65} - r\right)^2$.
2. The circle C and geodesic g_3 containing $[z_3, z_1]$ are orthogonal, and C lies outside of g_1. Suppose $p = t + is$ the centre and r is the radius of C. Also $x_{31} = (0.625,0)$ is the centre and $r_{31} = 0.625\sqrt{17}$ is the radius for g_1. The Euclidean distance between p, x_{12} give equation $(t-0.625)^2 + s^2 = \left(0.625\sqrt{17} + r\right)^2$.
3. 3. Solve the three equations obtained in steps 1 and 2 for unknowns t, s, r to get values: $(t, s) = (1.6030192534648684,\ 3.1680011113600326),\ r = 0.7385910230026669$

Now drawing geodesic segments from each vertex of tringle to centre p of incircle C, angle bisectors can be obtained.

Acknowledgement

I thank my Guide Professor A. R. Aithal. Under his guidance I worked on the isoperimetric problem in $\mathbb{H}^2$ for my M.Phil. dissertation.

References

1. Chorwadwala Anisa M. H., "The isoperimetric Problem", Dissertation submitted to the University of Mumbai for the degree of Master of Philosophy in Mathematics in 2003.
2. I. Todhunter, Spherical Trigonometry, Macmillan and Co. Ltd., London (1949).
3. Rajesh Balkrishna Raut, Isoperimetric Problem in $\mathbb{H}2$, Dissertation submitted to the University of Mumbai for the degree of Master of Philosophy in Mathematics in 2005.
4. Riku Klen and Matti Vuorinen Apollonian circles and hyperbolic geometry, Article in The Journal of Analysis · October 2010
5. S. Kesavan, From the Triangle Inequality to the Isoperimetric Inequality, RESONANCE (February 2014).

10. Biodiversity Informatics Provides Sound Iformation for Better Management - By Using Computing Tools

Ranjan B. Kalbande
Department of Botany, Shri. Dr. R. G. Rathod Arts & Science College,
Murtizapur, Dist. Akola, (M.S.) India.

Abstract

Biodiversity provides the assurance of food, countless raw materials such as fiber for clothing, materials for shelter, fertilizer, fuel, medicines and other necessities. The technology of bioinformatics is both versatile and is able to be applied wherever research is being done on genetics, proteins and cells for herbicide-resistant products for crops in agriculture. Biodiversity Informatics is to provide a sound information management infrastructure for biodiversity and Global Change research. In this present research work biodiversity was studied by using computing tools. Biodiversity-Informatics provides sound information for better management by using computing tools

Keywords: Information, Management, Morphology, Biodiversity, Species, Identification etc.

Introduction

The wellbeing and prosperity of earth's ecological balance as well as human society directly depend on the extent and status of biological diversity. In Agriculture, biodiversity provides us with a varied food supply which is needed for balanced human nutrition. A species may be defined as a group of organisms which are able to interbreed freely under natural conditions to produce viable offsprings. Species diversity refers to variety of living species within a geographic area (Glowka, 1994). Genetic diversity refers to the differences in genetic make-up between distinct species as well as the genetic variations within a single species. It encompasses the broad differences between ecosystem types, and the diversity of habitats and ecosystem processes within each ecosystem type. Ecosystem diversity deals with species distribution and community patterns, the role and function of key species, and combines species functions and interactions. Biodiversity informatics is an emerging discipline applying information science, ecology and biodiversity to the understanding and solutions of environmental problems by using computing tools.

Review of Literature

Wattenberg and Breckle (1995) studied tree species diversity of a premontane rain forest in the Cordillera De Tilaran, Costa Rica. The study plot consisted of 25 squares of 20×20 m, located at an altitude of about 1000 m. Dominance and abundance of tree species was critically discussed. Valencia et al., (2004) mapped and studied tree species distributions and local habitat variation in the Amazon. The largest number of species was mid –sized canopy trees with maximum height 10-20m and understrorey treelets with maximum height of 5-10m. Hedge et al., (1998) studied variation in bark thickness in a tropical forest community of Western Ghats in India. They examined the relation between bark thickness and girth in a large sample of trees from evergreen and semi-evergreen rain forest.

Materials and Methods

During study period to acquaint with the forest area, often visits were arranged of the place by taking help of forest guards, foresters, ranger, and collected firsthand information of natural habitat Different sizes of the trees i.e. small, middle and large were also recorded. Photographs of complete tree, flowering twig, bark, fruit and herbarium sheets were taken and samples were preserved. Bioinformatics is more of tools than a discipline. Information technology makes usage of software, hardware and internet based communication systems for the analysis of Biological Data.

Observations and Results

Tree Code	LOCAL NAME	FAMILY	GENERA	BOTANICAL NAME
1	Charoli	Anacardiaceae Lindl.	BUCHANANIA Spreng.	Buchanania Ianzan Spreng. J.
2	Moyen	Anacardiaceae Lindl.	LANNEA A. Rich.	Lannea coromandelica (Houtt.) Merr.
3	Amba	Anacardiaceae Lindl.	MANGIFERA L.	Mangifera indica L. Sp. Pl.
4	Biba	Anacardiaceae Lindl.	SEMECARPUS L.f.	Semecarpus anacardium L. f.
5	Sitaphal	Annonaceae Juss.	ANNONA L.	Annona sqamosa L. Sp. Pl.
6	Dudhi	Apocynaceae Juss.	WRIGHTIA R. Br.	Wrightia tinctoria R. Br. Var rothii (G. Don) Hook.
7	Katesawar	Bombacaceae Kunth	BOMBAX L.	Bombax ceiba L. Sp. Pl.
8	Salai	Burseraceae Kunth	BOSWELLIA Roxb.	Boswellia serrata Roxb. ex. Coleb.
9	Bhosa	Caesalpiniaceae R. Br.	BAUHINIA L.	Bauhinia racemosa Lamk.
10	Kachnar	Caesalpiniaceae R. Br.	BAUHINIA L.	Bauhinia variegata L. Sp. Pl.
11	Amaltas	Caesalpiniaceae R. Br.	CASSIA L.	Cassia fistula L. Sp. Pl.
12	Chinch	Caesalpiniaceae R. Br.	TAMARINDUS L.	Tamarindus indica L. Sp. PI.
13	Dhawada	Combretaceae R. Br.	ANOGEISSUS (DC.) Guill. & Perr.	Anogeissus latifolia (Roxb. ex DC.) Wall.

14	Ain	Combretaceae R. Br.	TERMINALIA L.	Terminalia alata Heyne ex Roth,
15	Arjun	Combretaceae R. Br.	TERMINALIA L.	Terminalia arjuna (Roxb.) Wt. & Arn. Prodr.
16	Behada	Combretaceae R. Br.	TERMINALIA L.	Terminalia bellirica (Gaertn.) Roxb. PI Cor.
17	Tendu	Ebenaceae Gurke	DIOSPYROS L.	Diospyros melanoxylon Roxb. PI. Cor.
18	Aola	Euphorbiaceae Juss.	PHYLLANTHUS L.	Phyllanthus emblica L.s Sp. Pl.
19	Palas	Fabaceae Lindl.	BUTEA Roxb.ex Willd.	Butea monosperma (Lamk.)Taub.
20	Tiwas	Fabaceae Lindl.	DESMODIUM Desv.	Desmodium oojeinensis (Roxb.) Ohashi in Ginkgoana
21	Karanj	Fabaceae Lindl.	PONGAMIA Vent.	Pongamia pinnata (L.) Pierre.
22	Kumbhi	Lecythidaceae - Poit	CAREYA Roxb.	Careya arborea Roxb. PI. Cor.
23	Lendia	Lythraceae J. St. Hil.	LAGERSTROEMIA L.	Lagerstroemia parviflora Roxb. PI. Cor.
24	Rohan	Meliaceae Juss.	SOYMIDA A. Juss.	Soymida febrifuga (Roxb.) A. Juss.
25	Umber	Moraceae Link.	FICUS L.	Ficus racemosa L. Sp. PI.

Table !.

Collection of all the required information available with respect to morphodiversity was done related to the species, specimen samples collections, photographs, plant descriptions, illustrations, height and girth recorded and bark morphology was studied. This study provided a base line information to understand the diversity of the species in the tropical dry deciduous forest

Within widely distributed dry deciduous leafless trees during summer there were a few evergreen trees, the most prominent being Terminalia sp., Madhuca sp., Buchanania sp., Diospyros sp., Lagerstroemia sp., Butea sp. and Ixora sp**.** Out of 456 plant population the highest representation was of Tectona grandis (273); though smaller in number Bridelia airy-shawii P.T.Li, Phyt. Sin. (41) and Wrightia tinctoria R. Br. Var rothii (G. Don) Hook. (40) represented second and third respectively.

Digital bark library of the 40 trees species exhibited diverse surface patterns e.g. smooth, scaly, furrowed, warty and shaggy types.

The computer assisted monitoring of vegetation was done by using World Wide Web to illustrate the out line idea of a new vegetation monitoring methodology through aerial digital satellite maps by using software's to visualize captured data and to zoom it many more times by which wealth of the area was known accurately thereby one could describe relationship in between real world and its computer representation. Mapping of the forest digitally assisted in understanding the complexity of the forest which could not possible even by using any other technical device.

Conclusions

The main intension of using this digital image processing system was to provide current status of forest with its potentially important data for monitoring, planning, conservation and management of the forest.

References

- Blum SD. 2000. An overview of Biodiversity Informatics. From http://research.calacademy.org/research/informatics/sblum/pub/biodivinformatics .html 1-14.
- Brij B. 2008. Bioinformatics: Definition of this New Type of intelligent Technology. From http://www.brightthub.com /science/medical/articles/2282. aspx.
- Hedge V, Chandran MDS, Gadgil M. 1998. Variation in Bark Thickness in a Tropical Forest Community of Western Ghats in India. Functional Ecology 12: 313-318.
- Jain SK. 1998. Some Aspect of Biodiversity and Indian Traditions. Indian Journal of History of Science 33(1):51-62.
- Muthuchelian K, Kannaiyan S, Gopalam A. 2008. Forest Biodiversity. From http://www.vedamsbook.com/no57281.htm 1:1-3.
- Pamayanan: News and Views from Pinoy Environmentalists and Advocates Genetic, Species and Ecosystems Diversity From http://www.bwf.org/bk/ pamayanan/r-genetic.html
- Valencia R, Foster RB, Villa G, Condit R, Svenning JC, Hernandez C, Romoleroux K, Losos E, Magards E, Balslev H. 2004. Tree Species Distributions and Local Habitat Variation in the Amazon: Large Forest Plot in Eastern Ecuador. Journal of Ecology 92: 214-229.
- Wattenberg I, Breckle SW. 1995. Tree Species Diversity of a Premontane Rain Forest in the Cordillera De Tilaran, Costa Rica. Ecotropica 1: 21-30.
- Wilson EO. 2000. A Global Biodiversity Map. Science 29 September 2000. 289, 5488, 2279. ewilson@oeb.harvard.edu.
- Yunus M, Yunus D, Eqbal M. 1990. Systematic Bark Morphology of Some Tropical Trees. Wiley InterScience Botanical Journal of the Linnnean Society 1-2.

11. Comprehensive Study on Catla Fish (Catla Catla): Biology, Ecology, and Socioeconomic Significance

Reena P. Dhote
Ghulam Nabi Azad College of Science Arts and Commerce, Barshitakli, Akola.

Abstract

This paper presents an in-depth analysis of Catla fish (Catla catla), encompassing its taxonomy, morphology, habitat, distribution, biology, ecology, aquaculture practices, economic importance, conservation status, and cultural significance. Drawing from a wide range of scholarly sources and empirical data, this research provides valuable insights into the multifaceted aspects of Catla fish, offering implications for its management, conservation, and sustainable utilization. "Age, Growth and Harvestable size of Catla catla (Ham.) from Lake Pichhola, Udaipur, Rajasthan" is the topic of the current study. The results of this study show that all 20 fish species, belonging to seven families, have been identified in the fish fauna of Lake Pichhola. Of which, Indian Major Carp accounted for 85% of the total landings from the lake, dominating the catch. Furthermore, the percentages of Indian Major carps, Minor carps, and Catfishes were reported to be 8.5%, 6.5%, and 6.3%, respectively.

Introduction

Catla fish (Catla catla), commonly known as Indian carp, is a freshwater species indigenous to the Indian subcontinent. It holds significant socioeconomic importance as a vital source of food and livelihood for millions of people across South Asia. Despite its ecological and cultural significance, comprehensive studies addressing various aspects of Catla fish are limited. This paper aims to fill this gap by providing a comprehensive examination of the biology, ecology, and socioeconomic significance of Catla fish. Researchers and fish fans alike have taken an interest in the Catla catla fish, also referred to as the Indian Carp or Catla [1]. Originating in South Asia, this freshwater fish exhibits a remarkable variety of forms and dimensions, rendering it an intriguing object of study. We will examine the many forms and traits of Catla catla in this piece, illuminating its fascinating diversity and formal importance [2]. Within the family Cyprinidae, which is related to carps, the Catla catla species is distinguished from other fish by its unique appearance. These herbivorous animals are distinguished by their big, flipped mouths, which aid in filter feeding and allow them to efficiently eat plankton and algae [3]. Their sleek, streamlined bodies, marked by a silver hue, reflect their ability to swiftly

navigate through freshwater ecosystems. One of the most intriguing aspects of Catla catla is its diverse range of shapes. The species exhibits variations in body proportions, head size, and fin structure [4]. While some individuals may have elongated bodies with a more pronounced head, others possess a deeper body and a comparatively smaller head. These shape variations not only contribute to the fish's aesthetic appeal but also serve functional purposes, such as adaptation to different aquatic habitats. Catla catla showcases considerable variations in size, allowing for distinct size classifications [5]. On average, these fish can grow up to 1 meter in length and weigh around 40 kilograms. However, larger individuals have been recorded, reaching lengths of up to 2 meters and weighing more than 50 kilograms. Conversely, smaller Catla catla specimens, usually found in ponds and small rivers, measure around 30 centimeters in length [6]. The varying sizes of Catla catla cater to the diverse needs of their habitats and contribute to the overall ecological balance of freshwater ecosystems.

Taxonomy and Morphology

Catla fish belongs to the family Cyprinidae and is classified under the genus Catla. Morphologically, it is characterized by a deep body, a slightly arched head, and a terminal mouth with prominent lips. The body coloration varies from silver to greyish-green, with a conspicuous black spot at the base of the tail fin.

Habitat and Distribution

Catla fish predominantly inhabit freshwater ecosystems, including rivers, lakes, reservoirs, and ponds. They prefer habitats with abundant vegetation and moderate water flow.

Indigenous to the Indian subcontinent, Catla fish are distributed across the river systems of India, Bangladesh, Nepal, and Pakistan. Based on material provided by Dr. E. Woynarovich (Hungary) and Dr. V.R.P. Sinha (FAO Senior Aquaculturist, NACA, Bangkok, Thailand) the Indian carp do not breed naturally in ponds or other confined waters. They are all river spawners, having semifloating, nonadhesive eggs. The eggs have a large perivitelline space, and during swelling they increase their size by about 10 times Swollen, water- hardened eggs are rather delicate, and do not tolerate physical shocks well. This sensitivity to mechanical damage is a very important consideration when Indian carp eggs are to be incubated artificially.

Biology and Life Cycle of Catla (Catla catla)

Catla (Catla catla) is a significant freshwater fish species indigenous to the Indian subcontinent, renowned for its ecological role and socioeconomic importance. This research paper presents a detailed examination of the biology and life cycle of Catla fish, encompassing its morphological characteristics, reproductive biology, growth patterns, and ontogenetic development. Catla fish exhibit distinctive morphological features, including a deep, laterally

compressed body, a slightly arched head, and a terminal mouth with prominent lips. The body coloration ranges from silver to greyish-green, with a conspicuous black spot at the base of the caudal fin. These morphological adaptations are associated with their feeding ecology, habitat preferences, and swimming behavior.

Ecology and Behavior

Catla fish are omnivorous, feeding on a diverse diet comprising plankton, aquatic vegetation, insects, and detritus. They are highly adaptable and exhibit migratory behavior in response to seasonal fluctuations in water levels and temperature. Catla fish play a crucial role in nutrient cycling and trophic dynamics within freshwater ecosystems, serving as both predator and prey to a wide range of species.

Aquaculture Practices

Catla fish farming has gained prominence as a lucrative venture in aquaculture, particularly in South Asia. Aquaculture techniques involve pond culture, cage culture, and integrated farming systems. Key considerations in Catla fish farming include stocking density, nutrition management, water quality maintenance, and disease control. Sustainable aquaculture practices are essential to mitigate environmental impacts and ensure the long-term viability of Catla fish farming.

Economic Significance

Catla fish constitute a significant proportion of freshwater fish production in South Asia, contributing to food security, employment generation, and rural livelihoods. They are highly prized for their high nutritional value, delicious taste, and culinary versatility. The commercial value of Catla fish extends beyond domestic markets, with growing demand in international seafood trade.

Conservation Status Despite their socioeconomic importance, Catla fish face various threats, including habitat degradation, overexploitation, pollution, and invasive species. Conservation efforts are crucial to safeguard Catla fish populations and their habitats. Initiatives focusing on habitat restoration, sustainable fisheries management, and community-based conservation are imperative to ensure the long-term sustainability of Catla fish populations. A multifaceted strategy is required for effective conservation efforts for Catla fish, including policy interventions, community-based conservation programs, pollution control measures, habitat restoration, and sustainable fisheries management. Mitigating anthropogenic impacts and maintaining Catla fish populations require integrated watershed management, protected area creation, enforcement of fishing laws, and promotion of sustainable aquaculture methods.

Discussion

Production Culture based fisheries was a common practice to enhance fish yields, particularly in small water bodies and was widely practiced in Asia and in other developing countries for fish food production (Welcomme and Bartley, 1998; De Silva, 2001) under first level management. It involved regular stocking of suitable species and recaptured at a marketable size. This type of culture was practiced in water bodies such as reservoirs (Phan and De Silva, 2000) and lake (Middendorp et al., 1999) and was considered to have the potential to contribute significantly and increasingly to fish production and food security in developing countries (Lorenzen et al., 1998; Welcomme and Bartley, 1998; Quiros and Mari, 1999). In order to compare the growth and production of stunted and normal (non-stunted) fingerlings of selected major carps, the present study was conducted under second level management. This management enhances the endogenous food production and reduces the utilization of artificial feeds. Only about 15-30% of the nutrients present in supplementary feeds are trapped into harvestable products and the remainings are lost in the surrounding environments (Gross et al., 2000). Therefore, cheaper and efficient means of management practice are essential to increase the fish production through second level management.

Conclusion

In conclusion, Catla fish represent a valuable component of freshwater biodiversity in South Asia, contributing to ecosystem stability, food security, and livelihoods of local communities. However, their conservation status is increasingly threatened by human-induced pressures and environmental degradation. Urgent action is required to address these challenges and implement effective conservation measures to ensure the long-term survival of Catla fish populations and the ecological integrity of their habitats. the biology and life cycle of Catla fish are characterized by a series of interconnected stages, each playing a vital role in the fish's ecological and socioeconomic significance. By elucidating key aspects of Catla fish biology, this research paper contributes to our understanding of their reproductive biology, growth patterns, and ontogenetic development. Future research should focus on addressing knowledge gaps and advancing sustainable management practices for Catla fish populations.

Reference

1. Harikrishnan R, Balasundaram C, Heo MS. Fish health aspects in grouper aquaculture. Aquaculture. 2011; 320(1):1-21. [Crossref] [Google Scholar]
2. Dadar M, Dhama K, Vakharia VN, Hoseinifar SH, Karthik K, Tiwari R, et al. Advances in aquaculture vaccines against fish pathogens: Global status and current trends. Rev Fish Sci Aquac. 2017; 25(3):184-217. [Crossref] [Google Scholar]

3. Gudding R, Van Muiswinkel WB. A history of fish vaccination: Science-based disease prevention in aquaculture. Fish Shellfish Immunol. 2013; 35(6):1683-8. [Crossref] [Google Scholar]
4. Pridgeon JW, Klesius PH. Major bacterial diseases in aquaculture and their vaccine development. Anim Sci Rev. 2012; 7:1-6. [Google Scholar]
5. Aly SM, Albutti A. Antimicrobials use in aquaculture and their public health impact. J Aquac Res Dev. 2014; 5(4):1. [Google Scholar]
6. Balment RJ, Lu W, Weybourne E, Warne JM. Arginine vasotocin a key hormone in fish physiology and behavior: A review with insights from mammalian models. Gen Compar Endocr. 2006; 147(1):9-16. [Cross Ref] [Google Scholar]
7. A study on Age, Growth and Harvestable Size of Catla catla (Ham.) Fish Determination of Fish Age and Growth Measurement (Bhatt A Nakul and Bhanu Kumar Sharma)
8. Ayyappan, S. and J.K. Jena (2003). Grow-out production of carps in India. J. Appl. Aquacult. 13(3/4): 251-282. DOI:10.1300/J028v13n03_04
9. Banerjee, S.M. (1967). Water quality and soil condition of fish ponds in some states of India in relation to fish production. Indian J. Fish., 14: 115-144.
10. Begum, M., M.Y. Hossain, M. A. Wahab and H.M. Kohinoor (2003). Effects of isophosphorus fertilizers on water quality and biological productivity in fish pond. J.Aquacult. Trop., 18(1): 1-12.
11. Bombeo-Tuburan, I. (1988). The effect of stunting on growth, survival, and net production of milkfish (Chanos chanos Forsskaal). Aquaculture, 75(1-2): 97-103. https://doi.org/10.1016/0044-8486(88)90024-5
12. Chakrabarti, N.M. (1998). Biology, Culture and Production of Indian Major Carp: A Review. Narendra Publishing House, Delhi, India, 175 pp. ISBN 13: 9788185375519

12. Diversity of Butterfly from Kapshi Lake, Akola

Roshani P. Ingle
Department of Zoology, Ghulam Nabi Azad College of Arts,
Commerce and Science, Barshitalki, Dist. Akola.
Prof. Nilima Kankale
Guided By Department of Zoology, Ghulam Nabi Azad College of Arts,
Commerce and Science, Barshitalki, Dist. Akola.

Abstract

The present study was evaluating butterflies in the study area like Kapshi lake Region, Maharashtra, India. The results accumulated so far clearly indicate that the overall diversity of Butterflies is richer in the surrounding area of Kapshi Lake, Barshitakli. City lesser in the urbanized area of Barshitakli city. Our Study reflects previous findings that the transformations of forests and natural habitat to urbanization had serve impact not only on single animal population but also on communication as a whole. In particular, species richness and animal biomass are most significantly affected.

Keywords:- Diversity, Kapshi Lake, Butterfly

Introduction

Butterfly fossils date to the Paleocene, about 56 million years ago. Systematic studies on butterfly have been made in different part of world since the turn of 18th century. Heppner 1998 has documented 19238 butterfly species throw out the world. Butterflies makes up a large group of insects known as the order Lepidoptera in phylum Arthropod. There are about 200,000 known species of Lepidoptera of which about 10% are butterflies.

Among the insects' butterflies depends on many host and nectar plants in their lifetime for growth and development. Therefore, host or nectar plants availability and their regeneration status study are essential in understanding the Butterflies population in depth. They help to monitor climate change and environment degradation and are studied as living ecological components of wide importance. They play an important role in the food chain and act as valuable pollinations in the local environment

Butterflies are sensitive s biota, and are several y affected by environmental variations and changes in habital structure.

Classification is done considering butterfly species and families scientifically, but they can also be divided based on their habitual. Although standard classification is listed as

kingdom, phylum, class, order, family, genus and species, there is also in between categories. All butterflies are in the same order, but there is separate.

Families of butterflies, each with its own collection of genera containing one or more species. Some species are pests because in their larval stages they can damage domestic crops or trees; other species are agents of pollination of some plants. Larvae of a few butterflies (eg, harvester) eat harmful insect, and a few are predators of ants, while others live as mutualists in association with ants. Culturally, butterflies are a popular motif in the visual and literary arts. Heppner (1998) has documented 19, 238 butterfly species throughout the world. Over the past century, many researchers have significantly contributed to the field of butterfly ecology within the various ecosystem in India (Bingham, 1905, 1907; Wiliams, 1930; Evan, 1932; Talbot, 1938, Wynter- Blyth, 1947; Kunte, 2000, 2001).

Sharma (2009), Raut and Pendharkar (2010), Kunte et al., (2010), Tewari and Rawat (2013), Sharma and Sharma (2013), and Quraeshi et al., (2014) have reported on the butterfly fauna in a few protected areas of central, northern and north-eastern parts of India.

Classification

Kingdom	-	Animalia are also metazoa
Phylum	-	Arthropoda
Sub Phylum	-	Hexapoda
Class	-	Insecta
Family	-	Total 126 families
Species	-	12000 to 20000.

Butterflies are the most provoking and striking creatures, among the insect group, they are an often regarded as flagship species. The butterfly diversity is high in the tropics compared the world. Their habitat ranges from Arctic to the great desert of the world. The butterflies are divided into two super families viz. Papilionoidea constitutes 11,100 species and Hesperidia constitutes 3,650 species in the world. Others than their aesthetic value, butterflies have important roles in the functioning of forest ecosystem. Because of their diversity, wide distribution specificity to vegetation type, rapid response to perturbation, taxonomic tractability, statistically significant abundance, and ease of sampling, they have been considered useful organisms to monitor environmental changes.

Life Cycle

The life cycle of butterflies can be discussed in four stages, in detail all butterflies have complete metamorphosis. Winged adults lay eggs on the food plant on which their larvae, known as caterpillars, will feed. The caterpillar grows, sometimes very rapidly, and when fully

developed, pupate in a chrysalis. Every stage has different goals to achieve like caterpillar need to eat a lot and adults need to reproduce. The life cycle of butterfly may depend on the type of butterfly, it might take from a month to a whole year. When metamorphosis is complete, the pupil skin splits, the adult insect climbs our, and after its wings have expanded and dried, it flies off. Some butterflies, especially in the tropics, have several generations in a year, while others have a single generation and a few in cold location may take several years to pass through their entire life cycle.

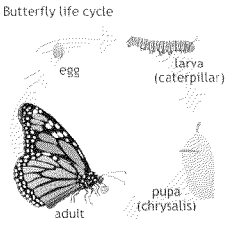

1. Egg
2. Larva (caterpillar)
3. Pupa (chrysalis)
4. Adults (Imago).

Biodiversity is the total variety of life on the earth. The abundance and diversity of butterflies mainly depend upon various factors such as availability of host and Larval food plants, foliage, humid climate, and various other features etc. As butterflies are mainly dependent on these factors, interruption in any of the above will Directly affect their standing in ecosystem. India is one of the 17 "mega diverse" countries of the world. But deforestation and increased human approach in forest and other Ecosystems have resulted into loss of habitat for most of the local species' diversity (Gupta, 2018). Heppner (1998) reported 19238 species of butterflies in the world. Study by Abreau (1931) reported about 177 species of butterflies in Central Provinces. A total of 92species of butterflies were Reported in Gore Wada International Bio Park situated in central India (Patil and Shende, 2014)

Material and Methods

Study Area and Sampling Site

Kapshi (20 34'43"N) and longitude (7657'18") The Kapshi Lake of Akola is located in Barshitakli Tahshil of Akola District in Maharashtra INDIA; it is situated 20 km away from sub District headquarter Akola. As per 2009 status, Kapshi Lake is the gram panchayat of kapshi Lake village. These Butterflies are recorded from different selected habitats which includes riparian habitats, grassland, dry deciduous forest, mixed forest, mixed forest with tall trees and shrubs. Survey was also carried out for grounds butterflies, Butterflies decaying barks of trees, debris, and crevices of rocks.

Survey Method

The field surveys on butterflies were carried out in the study area three times a week for the period of four months from October 2022 to Feb 2023 Butterflies were accessed in the study area from 8am to 10 am in the morning by random observations during walking through the

three selected sites based on habitats present in the study area. In the field, photographs of the butterflies were taken with the aid of camera for the identification. The Photographs taken in the field were later identified and studied with the help of available keys, reference books, and publications.

Identification the Species of Butterflies

The photographs of butterflies were used for the identification of the species of butterfly and helping of guidance. Color pattern, sizes, and shapes as well as their designs were considered in identification of the species of butterfly with the help entomology expert and relevant available literature as well as photography.

Sampling Techniques

The butterflies were observed and recorded directly in the field and photographs were taken and preserved for further identification. In critical conditions, they were captured by hand net following Tiple (2012) and were identified using suitable keys (Evans1932; Wynter-Blyth 1957; Haribal 1992; Kunte 2000; Kehimkar2008) and released in the same habitat from where they were captured with least disturbance. Appropriate precautions were undertaken to guarantee that the scales present on the wings of the butterflies were minimally affected.

Results and Discussion

A total of 8 Butterflies Species were collected from the study area Among the collected species of butterflies Nymphalidae 4, Pieridae 2, Papilionidae 1, and Hesperidae 1.

Plain tigers are commonly observed in various picnic spot on various small tress nearby Kapshi Lake, Tq. Barshitakli, Akola district some are observed on near road surrounding Katepurna Dam Region Because of suitable diverse ecosystem this family members found in very large number.

Table - Count of butterflies' species from different habits in Kapshi region.

Sr No	Species	Family	No of collection from natural habitat	% of species
1	Euploea Mulciber (Euploeacore)	Nymphalidae	8	12 %
2	Lime Swallowtail (Papiliodemoleus)	Papilionidae	10	16%
3	Plain Tiger(Danaus chrysippus)	Nymphalidae	25	39 %
4	Catopsilia florella (Catopsilia florella)	Pieridae	6	9%
5	tiger (Tirumal hamata)	Nymphalidae	5	8%
6	Bush brown (Mycalesis perseus)	Nymphalidae	4	6%
7	Calis alfaceriensis (Calis alfacarirnsis)	Pieridae	3	5%
8	Zabulon Blue skipper (Lon Zabulon)	Hesperidae	3	5%

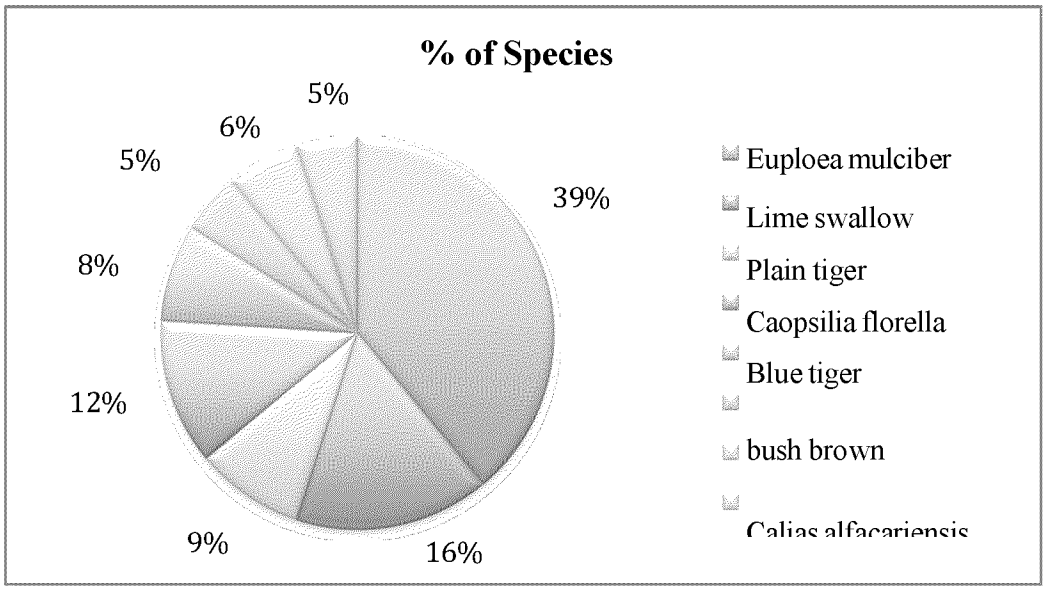

Photoplate

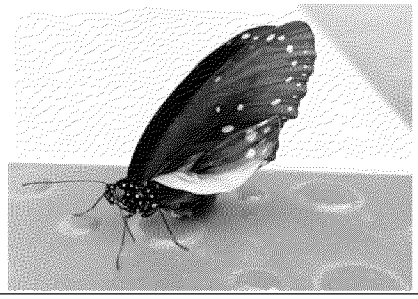	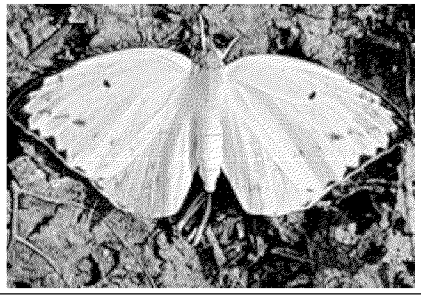
Euploea Mulciber (Euploeacore)	Catopsilia florella (Catopsilia florella)
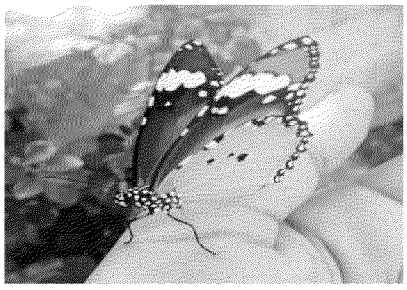	
Plain Tiger (Danaus chrysippus)	Lime Swallowtail (Papilio demoleus)

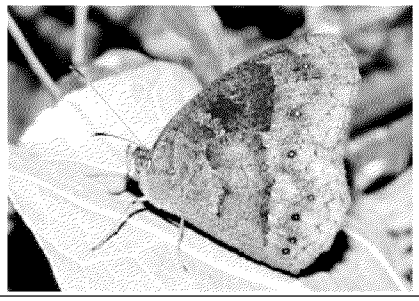	
Bush brown (Mycalesis perseus)	Calis alfaceriensis (Calis alfacarirnsis)
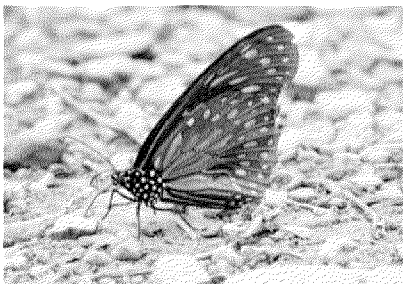	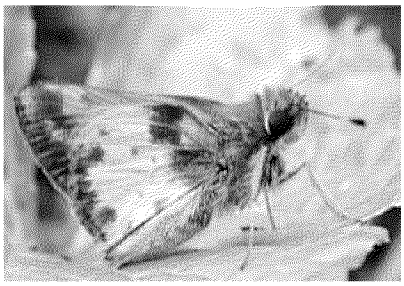
Blue tiger (Tirumal hamata)	Zabulon skipper (Lon zabulol)

Plain tigers are commonly observed in various picnic spot on various small tress nearby Dhagadevi Temple and some are observed on near roadside surrounding katepurna Region. Because of suitable diverse ecosystem this family members found in very large number.

Butterflies are food source for birds, spiders, lizards, mice, and other animals. Caterpillars are also eaten by bats, birds, and other animals. If butterfly population diminish, the impact will be felt higher up and can affect the entire ecosystem.

In above results we observed Euploeamulciber (Euploeacore) 8%, Lime swallowtail (Papiliodemoleus) 16%, Plain tiger (Danaus chrysippus) 39%,Catopsiliaflorella (Catopsilia florella) 9%, Blue tiger (Tirumalhamata) 8%, Bush brown (Mycalesis Perseus)6%, Caliasalfacariensis (Caliasalfacariensis) 5%, Zabulon slippers (Lon Zabulon) 5%.

Conclusion

The present study for the first aim at evaluating butterflies in the study area like Kapshi lake Region, Maharashtra, India. The results accumulated so far clearly indicate that the overall diversity of Butterflies is richer in the surrounding area of Murtizapur city lesser in the urbanized area of Murtizapur city. Our Study reflects previous findings that the transformations of forests and natural habitat to urbanization had serve impact not only on single animal population but also on communication as a whole. In particular species richness and animal biomass are most significantly affected.

Reference

- Arora G.S. (1994). Lepidoptera: Butterflies In: fauna of Rajaji National park, fauna of conservation Areas. Zoological Survey of India, Calcutta, 5, pp.245- 300.
- Arora, G.S. (1995). Lepidoptera: Rophalocera. In: fauna of Nanda Devi Biosphere Reserve Ecosystem series, Zoological survey of India, Calcutta, 1, pp. 61-73.
- Patil P. S. (2022). Butterfly species Diversity from Akola district of Maharashtra, India. www.ijert.org
- Basavarajappa S., Gopi Krishna V., and S. Santhosh (2018). Department of Zoology Kuvempu University Shankaraghatta- 577 451, Karnataka, India.
- Bhavana S. Janwe and Dr. Ramdas R. Kamdi (2002). Review of Distributionand Diversity of Butterflies in Maharashtra.
- Paresh Patel, Priya Uttarwar, Dnyaneshwar Kaymakam (2022). Diversity of Butterflies in Wani, District Yavatmal (M.S).
- Jayant S. Walatkar and M.V. Shirbhate (2004). Diversity of Butterflies from
- Amravati University campus, Maharashtra. Journal of Threatened Texa, 3 (1): 1469-1477
- A.1. Raja and Hemant P. Sapkal (2011). Chromosomal diversity in some common butterflies of family Hesperidae, from Akola district of Maharashtra.
- SprihHarsh (2014). Butterfly Diversity of India Institute of forest Management, Bhopal, Madhya Pradesh, India. Hindavi Publication Corporation Journal of Insect, 2024: 1-4.
- Nimbalkar R.K. (2018). Diversity of Butterflies from Ajanta caves area of Aurangabad District (MS) Int. Res. Journal of Science and Engineering 2018;
- species Issue A6: 20-25.
- John Bhutta and Bishnu K Sharma (2020). Diversity of butterfly in South District of Sikkim. Corresponding authors E-mail: fernofsikkim@gamil.com
- Patil P.S. Butterfly Species Diversity from Akola Dist. of Maharashtra, India. Department of Zoology, R.A. Arts, Shri
- M.K.Commerce and Shri S.R.Rathi Science College, Washim. volume 10, issue z repruary 2022 | 100%: 2020-200K

13. Reflects the Revitalizing and Renewing Effects of the Cranberry and Yogurt Extract Formulation on the Human Skin

Rupali R. Hatolkar
Department of Zoology Smt. Maherbanu College of science and Commerce Akola.
Dipika V. Muley
Department of Zoology Smt. Maherbanu College of science and Commerce Akola.
Shraddha Jaiswal
Department of Zoology Smt. Maherbanu College of science and Commerce Akola.
Mrs. Quddusa Kamil Farooqui
Department of Zoology Smt. Maherbanu College of science and Commerce Akola.

Abstract

The present work is focused on Reflects the revitalizing and renewing effects of the cranberry and yogurt extract of a body in order to respond to the current demands of consumers, offering an innovative product within the organic cosmetic market. The experimental conditions and ingredients required to develop a product able to hydrate and moisturize, at the same time, secondly, the developed laboratory-scale process was scaled up to commercial scale, highlighting the differences between the two. Among the product quality tests, microbiological analysis and dry weigh determination were performed to calculate the content of water and volatiles present in the yogurt and whether microbial contamination was present.

Keyword- Cranberry oil, yogurt extract, water.

Introduction

I. Anatomy of the Skin

The skin is the largest organ, and it's one of the most complicated. it contains many specialized cells and structures. The skin's primary function is to serve as a protective barrier. It helps regulate body temperature, gathers sensory information from the surrounding environment, and plays an active role in the immune system to protect the body from disease. The structure of skin having mainly three layers of skin: the epidermis, dermis, and subcutaneous tissue.

1. The epidermis

- The epidermis is the outermost layer of the three layers of skin. There are five layers of the epidermis:
- Stratum basale – This is bottom layer, which is also known as the basal cell layer, has column shaped basal cells that divide and push older cells towards the surface of the skin.
- Stratum spinosum – This layer, which is also known as the squamous cell layer, is the thickest layer of epidermis.
- Stratum granulosum – This layer contains more keratinocytes moving towards the surface.
- Stratum lucidum – This layer exists only on the palms of the hands and soles of the feet.
- Stratum corneum – This is the outermost or top layer of the epidermis. It's made of dead, flat keratinocytes that shed approximately every two weeks.

2. The dermis

- The dermis is the middle layer of the three layers of skin. It's located between the epidermis and the subcutaneous tissue. It contains connective tissue, blood capillaries, oil and sweat glands, nerve ending, and hair follicles.
- The dermis is splits into two parts- the papillary dermis, which is the thin, upper layer, and the reticular dermis, which is the thick, lower layer 5.

3. The hypodermis

- The hypodermis contains the cells known as fibroblasts, adipose tissue, connective tissue, larger nerves and blood vessels, and macrophages, cells which are part of the immune system and help keep your body free of intruders. The thickness of the hypodermis varies in different.

II. Skin Flora

The term skin flora refers to the microorganisms which reside on the skin. Many of them are bacteria of which there are around 1,000 species upon human skin from nineteen phyla. Most are found in the superficial layers of the epidermis and the upper parts of hair follicles.

Skin flora is usually non-pathogenic, and either commensal or mutualistic. The benefits bacteria can offer include preventing transient pathogenic organisms from colonizing the skin

surface, either by 12 competing for nutrients, secreting chemicals against them, or stimulating the skin's immune system.

III. Body Yogurt

Women today are more aware of skincare and the first step in that is realizing that skin isn't just about the face! We've now learned to pay attention to the rest of our bodies – after all, who doesn't love feeling smooth and supple all over?

To this end, there are many specific products targeted for the body. Skincare products for the face are different from those for the rest of the body for the simple reason that the skin is different on the face and the rest of the body. Facial skin is a lot thinner and more sensitive and needs different ingredients for its care.

When it comes to our hands and feet, we have hand creams and foot creams. For the rest of the body, however, there are a plethora of options that can be quite confusing. The latest buzzword in this area seems to be 'body yogurt.' Since body yogurts are absorbed quickly, they are a boon for busy women who don't have too much time to get ready in the morning. The best way to get the benefits of a body yogurt is to apply it all over freshly washed, slightly damp skin. The yogurt is absorbed in under half a minute, and you can quickly get dressed without having to worry about any greasy, slimy feeling that richer creams, oils or lotions.

Material and methods

List of materials used

Sr. no.	Name of the Ingredients	Exporter
1.	Distilled water	Purenso Global, MP
2.	Glycerin	Purenso Global, MP
3.	Soft Xanthan gum	Purenso Global, MP
4.	Fractionated Coconut oil	Purenso Global, MP
5.	Jojoba oil	Purenso Global, MP
6.	Vegetative emulsifying wax	Purenso Global, MP
7.	Optiphen (preservative)	Purenso Global, MP
8.	Vitamin E oil (antioxidant)	Purenso Global, MP
9.	Cranberry oil	Purenso Global, MP
10.	Yogurt extract	Purenso Global, MP

Table – Lists of Material used

List of Equipment –

- Precision balance : Smt. Maherbanu college Akola
- Mechanical stirrer : Smt. Maherbanu college Akola

- pH meter : Smt. Maherbanu college Akola
- beaker : Smt. Maherbanu college Akola
- measuring cylinder : Smt. Maherbanu college Akola

1. Formulation and evaluation of cranberry body yogurt with yogurt extract.
2. To prepared a highly moisturizing body yogurt.
3. To prepared non sticky, non greasy and non oily body yogurt that lives the skin soft and smooth for longer period of time.
4. To provide all properties such as moisturizing, nourishing, hydrating and soothing property in a single product.

Objectives

1. The basic objective of the formulation is to formulate a product that is easily absorbed bt the skin and is suitable for all skin type and also offer moisturizing benefits that last for up to 48 hours.
2. The body yogurt helps hydrate your skin and leaves it in smooth throughout the day.

The cranberry fragrance is reported to enhance health and well being by improving mood, reducing anxiety and stress.

Active and Excipients profile

Active

1. Cranberry oil

Cranberries include an acid that acts as exfoliate, while vitamin A and C with collagen synthesis. Cranberries also protect your skin from free radicals that cause wrinkles and keep it moisturized. Cranberries have been prized for their medicinal, antioxidant, and anti-aging effects for generations. It boosts cell vitality and protects your skin from environmental harm to high levels of antioxidants like vitamin C, B and B-5. Cranberry is one of the winter remedies to preserve your skin.

2. Yogurt extract

Yogurt is obtained by spiking milk with the use of the so-called “good” bacteria. Its composition is also supplemented by calcium, proteins, beneficial-for-your-health vitamins and minerals which along with the generous dose of the “good” bacteria help your cells regenerate faster.

Excipients

1. Purified water

Water is used in the formulation of virtually every type of cosmetic and personal care product. Water is widely used in chemical reactions as a solvent as a solute or catalyst in inorganic reactions, water is a common solvent, dissolving many ionic compounds, as well as other polar compounds such as ammonia.

2. Gycerin

Uses in cosmetics- Glycerin is a well-known humectants that prevents the premature loss of moisture from cosmetics and personal care products so they don't dry out. Glycerin is used in cosmetics and personal care product mainly to improve skin's smoothness and moisture content.

3. Vitamin E Oil

Vitamin E is a fat- soluble antioxidant which may help protect cell membranes from reactive oxygen species. Various ear diseases and infections are treated with eardrops containing tri ethanol amine polypeptides oleate - condensate

4. Fractionated coconut oil

It is ideal for increasing the topical distribution of essential oil. One of its o=primary benefits is that is non-greasy and is easily absorbed into the skin.

5. Xanthan gum

It is a gum obtained by microbial fermentation from the xanthomonas campestris organism.

6. Jojoba oil

It has a variety of healing properties that may make it effective in treating skin conditions like acne, eczema, and paoriasis.

7. Emulsifying wax

It is used in lotions and creams as athickener and emulsifier.

8. Methyl paraben

Parabens are a family of related chemicals that are commonly used as preservatives in products.

Observation

Incorporation of cranberry extract and yogurt extract at different concentration in base formulation

Sr. No.	Ingredient	F3.1 For 100%	F3.2 For 100%
1	Distilled water	75.5	74
2	Glycerin	2	2
3	Xanthan gum	0.5	1.5
4	Fractionated coconut oil	10	10
5	Jojoba oil	2	2
6	Emulsifying wax	5	5
7	Vitamin E oil	1	2
8	Yogurt extract	2	1.5
9	Perfume and preservative	Q.S	Q.S

Incorporation of actives at different concentration in base formulation

Evaluation and Results

Evaluation test

The evaluation of the product was carried out as per Indian standard (IS) for finished products. The various steps carried out for evaluation of cream in order to prove safety and stability of product.

In – Vitro Evaluation

1. Determination of physical parameters
2. Determination of pH
3. Determination of viscosity
4. Determination of spread ability time
5. Microbial examination
6. Stability studies
7. Comparative study between formulated product and marketed products.
8. In – Vivo Evaluation
9. Patch test
10. Photographic evaluation
11. In Vitro studies:

1. Determination of physical parameters

Sr.No.	parameter	F3.1	F3.2
1	Appearance	+++	+++
2	Colour	++	+++
3	Spreadability	+++	+++
4	consistency	++	+++

Determination of physical parameters

Here,

+ Good, ++ Very Good, +++ satisfied

2. Determination of pH

Determination of pH of body yogurt incorporated with cranberry extract and yogurt extract.

Time interval	F3.1	F3.2
1st Day	4.4	4.5
15th Day	4.5	4.5
30th Day	4.6	4.6

Determination of pH. Of body yogurt incorporated with

Cranberry and yogurt extract

3. Determination of spreadability

Sr. No.	Days of Interval	Initial area	Weight	Time
1	Initial Day	6 cm	15 gm	2.1 sec
2	15th Day	6.3 cm	15 gm	2.1 sec
3	30th Day	6.6 cm	15 gm	2.1 sec

Determination of spreadability

Conclusion

Today Women are more aware of skincare and the first step in that is realizing that skin isn't just about the face! There are many specific products targeted for the body. Skincare products for the face are different from those for the rest of the body for the simple reason that the skin is different on the face and the rest of the body. A body yogurt is essentially a moisturizer that is quickly absorbed into the skin. It contains emulsifiers that form an emollient shield around the skin, keeping a sheet of emollient molecules close to the surface for a long time.

Cranberry is a healthy fruit from an evergreen shrub and multiple nutritional benefits. Cranberry seed oil, due to its favorable physicochemical characteristic, good oxidative stability and the pleasant flavor is valued as edible oil.

References

1. Human physiology-volume 2, by Dr. C.C.Chatterjee.
2. Essentials of medical physiology 8th edition, by K Sembulingam Prema Sembulingam.
3. Research paper:- study of the preventive role of cranberry extract on some physiological parameters in male rate induced by sodium fluoride, Shatha Galal Azez

Naseer Marza Hamza Azez & Hamza (2020): Role of cranberry extract January 2020 Vol. 23(I) : Annals of tropical Medicine & Public Health S407

4. Article product Development studies of cranberry seed oil Nanoemulsion Wael A. Mahdi, Prawez Alam, Abdullah Alshetaili, Sultan Alshehri, Mohammed M. Ghoneim and Faiyaz Shekel.
5. Enhancing yogurt product's ingredients:preservation strategies, processing condition, analytical detection methods, and therapeutic diversity – an overview September 2022 by Rahul Mehra, Harish Kumar, Shafiya Rafique and Naveen Kumar.
6. https:timesofindia.indiatimes.com/beauty/heres-how-using-body-yogurt-can-benefit-your-skin-in-numerous-ways/articleshow/94537224.cms
7. https:/mamaearth.in/blog/everything-you-need-to-know-about-body-yogurt.
8. Saeedi, Masoumeh Eslamifar, Khadijeh Khezei, Kojic acid applications in cosmetic and pharmaceutical preparations, Biomedicine & pharmacotherapy, volume 110, 2019, pages 582-593, ISSN 0753-3322.
9. Briasco, B; Capra, P; Cozzi, A.C; Mannucci, B; Perugini, P. packaging Evaluation Approach to improve cosmetic product safety. Cosmetics 2016,3,32

14. Synthesis, Spectral Characterization and Antimicrobial Potent Study of Some Novel 7-[(2-Substitutedimino-4-Phenylimino) Amino-1,3,5-Dithiazino)] Along with Coumarin Nucleus

S. A. Waghmarea
Department of Chemistry, Ghulam Nabi Azad Arts, Commerce and Science College Barshitakli Dist. Akola. (M.S.), India.
K. U. Dongareb
Department of Chemistry, Ghulam Nabi Azad Arts, Commerce and Science College Barshitakli Dist. Akola. (M.S.), India.
S. B. Sarkatec
Department of Chemistry, Ghulam Nabi Azad Arts, Commerce and Science College Barshitakli Dist. Akola. (M.S.), India.
R. N. Ingoled
Department of Chemistry, Shri Vitthal Rukhmini College,
Sawana, Mahagaon, Dist.Yavatmal, (M.S.) India

ABSTRACT

In a laboratory novel series of 7-[(2-substitutedimino-4-phenylimino)amino-1,3,5-dithiazino)]-4-methyl-2H-chromen-2-one (IIIa-e) ware synthesized by refluxing 7-(5-substituted-2,4-dithiobiureto)-4-methyl-2H-chromen-2-one (Ia-e) with alkyl/aryl isocyanodichlorides (IIa-e) in acetone medium in 1:1 molar proportion. The structures of all the synthesized compounds were justified on the basis of chemical characteristics, elemental analysis and spectral studies and their antimicrobial screening against the gram positive and gram-negative bacteria such as S. typhi, E. coli, S. aureus, A. Aerogenes, B. Subtilis and B. Megatherium etc.

Introduction

Because they are more convenient in a variety of applications, heterocycles incorporating organic molecules are more fascinating. A wide range of applications are covered by the heterocycles' sizes and the heteroatom variety they include. Five members1-2 that are sulphur and nitrogen-containing six participants,3-4 Six members5-8 fused heterocycles and five

members fused heterocycles containing aromatic rings. Particularly, heterocycles that contain both nitrogen and sulphur in one ring are well-known for their many industrial and biological uses. One of the six member heterocycles, 1,3,5-dithiazine, has one nitrogen atom and two sulphur atoms. Additionally, a review of the literature revealed that the 1,3,5-dithiazino nucleus and its derivatives have beneficial biological and medicinal qualities9-10. It is a powerful medication used in the domains of industry, agriculture and medicine.11-13

Various compounds of 1,3,5-dithiazino moieties were reported by Tayade13 to improve industrial, pharmaceutical, medical and agricultural operations. In addition, 1,3,5-dithiazino compounds were synthesized by Raut14 for their fungicidal characteristics. The 1,3,5-dithiazines were previously created in a lab setting using substituted isocyanodichlorides. Shendge15 research group produced a variety of heterocycles with the primary nucleus being 1,3,5-dithiazines. The uses of each 1,3,5-dithiazino moiety vary depending on the substituent affixed to the 1,3,5-dithiazine's basic nucleus. Additionally, a review of the literature revealed that the 1,3,5-dithiazino nucleus and its derivatives have beneficial biological and medicinal qualities. The synthesis of 1,3,5-dithiazines can be done more quickly, cheaply, easily and with less effort with this approach. A new series of 1,3,5-dithiazine was to be synthesized.

Material and Method

Material

All the chemical used were of loba chemie (AR grade).

Method

In the present experiment for the synthesis of different substituted 1,3,5-dithiazino coumarin is conventional refluxing under electronic water bath for different hours for different experiment.

Experimental

All the chemicals used for the synthesis were purified. After refluxing the purity of the compounds were checked by TLC (aluminium TLC) with thin layer thickness of 200 um. The melting points of all synthesize compounds will be recorded using hot paraffin bath. The carbon and hydrogen analysis were carried out on Carlo-Ebra-1106 analyser Nitrogen estimation were carried out with colmon-N-analyzer-29. IR spectra were recorded with Bruker spectrometer in the range 4000-400 cm-1. PMR spectra were recorded on VARIAN 400 MHz spectrometer with TMS as internal standard using CDCL3 and DMSO Solvent.

General Procedure

A reaction of 7-[(5-phenyl)-2,4-dithiobiureto]-4-methyl-2H-chromen-2-one (Ia) and N-phenyl isocyanodichloride (IIa) in 1:1 molar ratio refluxed on water bath in acetone medium for 2 hours. The evolution of the hydrochloride gas was clearly observed during refluxtion. After distillation of excess solvent shining yellow product isolated which on basification with dilute ammonium hydroxide yellow crystalline products afforded.

Similar, procedure was adopted for the synthesis of all the derivatives in the series.

The tentative reaction for the formation of product is depicted below,

Reaction

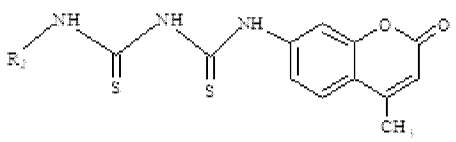

7-[(5-phenyl)-2,4-dithiobiureto]-4-methyl-2*H*-chromen-2-one

(Ia-e)

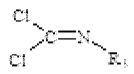

Substituted isocynodichloride

(IIa-e)

Acetone | Refluxed 2 hrs.

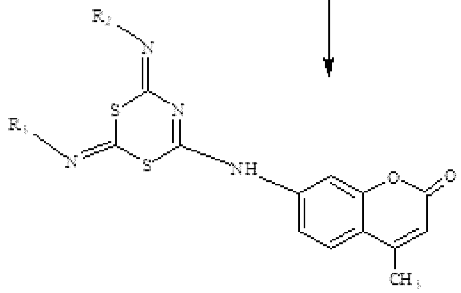

7-[(2-Substituedimino-4-phenylimino)amino-1,3,5-dithiazino]-4-methyl-2*H*-chromen-2-one

(IIIa-e)

where R_2= -phenyl

where R_1= -phenyl,-4-chlorophenyl, -4-methylphenyl, -ethyl, -*tert*-butyl

Similarly, 7-[(5-phenyl)-2,4-dithiobiureto]-4-methyl-2H-chromen-2-one (Ia) was interacted with N-ethyl isocyanodichloride (IIa), N-phenyl isocyanodichloride (IIb), N-tert-butyl isocyanodichloride (IIc), N-4-methylphenyl isocyanodichloride (IId) and N-4-chlorophenyl isocyanodichloride (IIe) by above mentioned method to isolate 7-{[2-(ethylimino)-4-(phenylimino)-1,3,5-dithiazin-6-yl]amino}-4-methyl-2H-chromen-2-one(IIIa), 7-{[2,4-

di(phenylimino)-1,3,5-dithiazin-6-yl]amino}-4-methyl-2H-chromen-2-one (IIIb), 7{[2-(tert-butylimino)-4-(phenylimino)-1,3,5-dithiazin-6-yl]amino}4-methyl-2H-chromen-2-one (IIIc), 7-{2-[(4-methylphenyl)imino]-4-[(phenylimino)-1,3,5-dithiazin-6-yl]amino}-4-methyl-2H-chromen-2-one (IIId) and 7-{2-[(4-chlorophenyl)imino]-4-[(phenylimino)-1,3,5-dithiazin-6-yl]amino}-4-methyl-2H-chromen-2-one (IIIe).

Result and Discussion

Spectral characterization results for all the synthesized compounds are given below

Spectral Characterization

1. 7-{[2-(Ethylimino)-4-(phenylimino)-1,3,5-dithiazin-6-yl]amino}-4-methyl-2H-chromen-2-one(IIIa)

   Colour- Brown red crystalline solid, Molecular formula- C21H18N4O2S2, yield 83%, M.P. 160 0C. FTIR (Kbr) υ cm-1 3443.22 N-H stretching, 3057.52 (C-H Ar Stretching), 1977.07 (C-H Ar Bending,), 1615.05 (N-H bending), 1735.35 (C=O stretching), 1631.13 (C=N stretching); 1H NMR (400 MHz CDCL3 δ ppm)- 3 protons of -CH3 gives singlet at δ 2.33 ppm due to attachment with aromatic ring, 2 protons of two -CH2 gives quartet at δ 3.7 ppm, aromatic protons of -CH= of two aromatic ring gives doublet at δ 7.75, 7.3 7.2, 7.3 and 7.74 ppm, 1 proton of -CH= of conjugated lactone gives singlet at δ 5.60 ppm, proton -NH attached between thionyl group and phenyl ring also desheilded due to thioamide position and gives signal at δ 3.73 ppm. Mol. Wt.: 422.52

2. 7-{[2,4-Di(phenylimino)-1,3,5-dithiazin-6-yl]amino}-4-methyl-2H-chromen-2-one (IIIb)

   Colour- Brown red crystalline solid, Molecular formula- C24H17N4O2S2, yield 86 %, M.P. 147 0C. FTIR (Kbr) υ cm-1 3370.70 N-H stretching, 3030.12 (C-H Ar Stretching), 1570.80 (N-H bending), 1738.45 (C=O stretching), 1607.19 (C=N stretching); 1H NMR (400 MHz CDCL3 δ ppm)- 3 protons of -CH3 gives singlet at δ 2.41 ppm due to attachment with aromatic ring, aromatic protons of -CH= of aromatic ring gives doublet at δ 7.32, 7.4, 7.42 and 7.40 ppm, aromatic protons of -CH= of aromatic ring gives triplet at δ 7.26 and 7.18 ppm, 1 proton of -CH= of conjugated lactone gives singlet at δ 5.84 ppm, proton -NH attached between thionyl group and

phenyl ring also desheilded due to thioamide position and gives signal at δ 3.4 ppm. Mol. Wt.: 470.56

3. 7{[2-(tert-butylimino)-4-(phenylimino)-1,3,5-dithiazin-6-yl]amino}4-methyl-2H-chromen-2-one (IIIc)

   Colour- Brown red crystalline solid, Molecular formula- C23H22N4O2S2, yield 88 %, M.P. 137 0C. FTIR (Kbr) υ cm-1 3370.63 N-H stretching, 3033.23 (C-H Ar Stretching), 1572.23 (N-H bending), 1739.36 (C=O stretching), 1609.96 (C=N stretching); 1H NMR (400 MHz CDCL3 δ ppm)- 3 protons of -CH3 gives singlet at δ 2.25 ppm due to attachment with aromatic ring, 9 protons of three -CH3 gives singlet at δ 1.38 ppm due to attachment with aromatic ring, aromatic protons of -CH= of two aromatic ring gives doublet at δ 7.7, 7.33 and 7.63 ppm, 1 proton of -CH= of conjugated lactone gives singlet at δ 5.56 ppm and proton -NH attached between thionyl group and phenyl ring also desheilded due to thioamide position and gives signal at δ 3.69 ppm. Mol. Wt.: 450.52

4. 7-{2-[(4-Methylphenyl)imino]-4-[(phenylimino)-1,3,5-dithiazin-6-yl]amino}-4-methyl-2H-chromen-2-one (IIId)

   Colour- Brown red crystalline solid, Molecular formula- C26H20N4O2S2, yield 87 %, M.P. 122 0C. FTIR (Kbr) υ cm-1 3372.62 N-H stretching, 3090.55 (C-H Ar Stretching), 1955.59 (C-H Ar Bending,), 1657.30 (N-H bending), 1735.87 (C=O stretching), 1642.57 (C=N stretching); 1H NMR (400 MHz CDCL3 δ ppm)- 6 protons of two -CH3 gives singlet at δ 2.33 and 2.14 ppm due to attachment with aromatic ring, aromatic protons of -CH= of two aromatic ring gives doublet at δ 7.55, 7.63 7.22, 7.36 and 7.76 ppm, 1 proton of -CH= of conjugated lactone gives singlet at δ 5.56 ppm, proton -NH attached between thionyl group and phenyl ring also desheilded due to thioamide position and gives signal at δ 3.56 ppm. Mol. Wt.: 484.59

5. 7-{2-[(4-Chlorophenyl)imino]-4-[(phenylimino)-1,3,5-dithiazin-6-yl]amino}-4-methyl-2H-chromen-2-one (IIIe)

   Colour- Brown red crystalline solid, Molecular formula- C25H17N4O2S2 Cl, yield 88 %, M.P. 157 0C. FTIR (Kbr) υ cm-1 3375.82 N-H stretching, 3092.40 (C-H Ar Stretching), 1940.39 (C-H Ar Bending,), 1655.35 (N-H bending), 1737.32 (C=O stretching), 1634.87 (C=N stretching); 1H NMR (400 MHz CDCL3 δ ppm)- 3 protons

of -CH3 gives singlet at δ 2.85 ppm due to attachment with aromatic ring, aromatic protons of -CH= of two aromatic ring gives doublet at δ 7.69, 7.86 7.25, 7.39 and 7.69 ppm, 1 proton of -CH= of conjugated lactone gives singlet at δ 5.49 ppm, proton -NH attached between thionyl group and phenyl ring also desheilded due to thioamide position and gives signal at δ 3.96 ppm. Mol. Wt.: 505.01

Conclusion

In the present work is cheaper and less time-consuming method for synthesis of organic compound (IIIa-e). All the synthesized compound excellent anti-bacterial results in compare with the ciprofloxacin as a standard drug. After studying zone of inhibition these compounds may be act as finest drugs for the living beings.

Antimicrobial activity

All the synthesized compounds (III-a) to (III-e) were screened for antibacterial activity against S. typhi, E. coli, S. aureus, A. Aerogenes, B. Subtilis and B. Megatherium by disc diffusion method was performed using Mueller Hinton agar as well as nutrient agar medium. Each and every compound was tested at conc. 50 µg/ml in ethanol. The zone of inhibition of all the synthesized compounds were measured after 24-hour incubation at 37 0C. Standard drug used for comparison the activity was Ciprofloxacin.

Table No. 1: Synthesized compound IIIa-e activity against gram-negative and gram-positive bacteria.

Table No. 1. Antibacterial activity of synthesized compound against bacteria (Zone of inhibition in mm after 24 hrs at 37 ^{0}C temp.)

SR No.	Compd.	Gram positive			Gram negative		
		S. aureus	*B. subtilis*	*B. megatherium*	*S. typhi*	*E. coli*	*A. aerogenes*
1	**KUD-IIIa**	11	11	14	12	00	00
2	**KUD-IIIb**	14	00	12	11	00	00
3	**KUD-IIIc**	16	11	00	12	00	11
4	**KUD-IIId**	00	00	11	12	12	00
5	**KUD-IIIe**	14	12	11	14	12	14
6	**Std Ciprofloxacin**	18	16	20	18	20	14

Table No. 1. Antibacterial activity of synthesized compound against bacteria

Referance

1. Sayed, M. T., Elsharabasy, S. A., & Abdel-Aziem, A. (2023). Synthesis and antimicrobial activity of new series of thiazoles, pyridines and pyrazoles based on coumarin moiety. Scientific Reports, 13(1), 9912, 1-9.
2. Gujjar, K., N., & Narasimha S M. (2023). A Review: Important applications of Heterocyclic Compounds, Eur. Chem. Bull., 12(12), 625-630.
3. Sharma, P. K., Amin, A., & Kumar, M. (2020). A review: Medicinally important nitrogen sulphur containing heterocycles. The Open Medicinal Chemistry Journal, 14(1), 49-64.
4. Amin, A., Qadir, T., Sharma, P. K., Jeelani, I., & Abe, H. (2022). A Review on The Medicinal and Industrial Applications of N-Containing Heterocycles. The Open Medicinal Chemistry Journal, 16(1), 1-27.
5. Matin, M. M., Matin, P., Rahman, M. R., Ben Hadda, T., Almalki, F. A., Mahmud, S. & Alshehri, S. (2022). Triazoles and their derivatives: Chemistry, synthesis, and therapeutic applications. Frontiers in molecular biosciences, 9, 864286, 1-8.
6. Bhadoriya, U., & Jain, D. K. (2016). Fused heterocycles as a potent biological agent; recent advancement. International Journal of Pharmaceutical Sciences and Research, 7(5), 1874-1880.
7. El-Sawy, E. R., Abdelwahab, A. B., & Kirsch, G. (2021). Synthetic Routes to Coumarin (Benzopyrone)-Fused Five-Membered Aromatic Heterocycles Built on the α-Pyrone Moiety. Part 1: Five-Membered Aromatic Rings with One Heteroatom. Molecules, 26(2), 483, 1-21.
8. Abu-Hashem, A. A., Hussein, H. A., Aly, A. S., & Gouda, M. A. (2014). Reactivity of benzofuran derivatives. Synthetic Communications, 44(20), 2899-2920.
9. Rakhimova, E. B., Vasil'eva, I. V., Khalilov, L. M., Ibragimov, A. G., & Dzhemilev, U. M. (2011). Effective synthesis of N-substituted 1, 3, 5-dithiazinanes by reactions of N-methyl-1, 3, 5-dithiazinane and 1, 3, 5-trithiane with aromatic amines. Russian Journal of Organic Chemistry, 47, 1300-1304.
10. Tayade, D, T. & Waghmare, S. A. (2016) Synthesis and Spectral Characterization of Some 1,3,5-Dithazines with Chalcone Backbone, Journal of Chemical and Pharmaceutical Research, 4(6), 233–235.

11. Heravi, M. M., Zadsirjan, V., Hamidi, H., & Amiri, P. H. T. (2017). Total synthesis of natural products containing benzofuran rings. RSC advances, 7(39), 24470-24521.
12. Yan, J., Si, W., Hu, H., Zhao, X., Chen, M., & Wang, X. (2019). Design, synthesis and antimicrobial activities of novel 1, 3, 5-thiadiazine-2-thione derivatives containing a 1, 3, 4-thiadiazole group. PeerJ, 7, 7581, 1-18.
13. Tayade, D., T. (2016). Synthesis and Spectral Characterization of Some 1,3,5-Dithazines with Chalcone Backbone, International Journal of Chemistry and Pharmaceutical Sciences, 4(6), 333-335.
14. Raut, P. V., Waghmare, S. A., & Tayade, D. T. (2017). Synthesis of 6-{4-Amino-N-[2-(Diethylamino) Ethyl]-O-Anisamido-5-Yl}- Amino-2-Thio-3-Substitutedamino,4-Substitutedimino-1,3,5-Thiadizines, International Journal of Medical Science and Clinical Invention, 4(12), 3355-3357
15. Shendge, A., S. & Tayade, D., T. (2018). Synthesis and Characterization of 2-(3-Substituted thioamidoformamidino-4- isobutoxyphenyl)-4-methyl-5-carboxy-1,3-thiazoles., Asian Journal of Organic & Medicinal Chemistry, 3(4), 187-189.

15. Synthesis, Characterization and Biological Evaluation of Chromene -2- Carbonitrile and Their Derivatives

S. G. Badne
Department of Chemistry, Shri Shivaji college of Arts, Commerce and Science, Akola.
G. W. Belsare
Department of Chemistry, Shri Shivaji college of Arts, Commerce and Science, Akola.

Abstract

In the present study, an attempt has been made to synthesize and characterize some chromene -2- carbonitrile derivatives, and to evaluate them for their anti-microbial activity. The physicochemical characteristic like melting point, percentage yield, Rf value were evaluated. The synthesized compounds were characterized by IR, NMR and Mass spectroscopy. Compounds exhibited good antimicrobial activity when compared with standard. Further, there is a large scope for the development of other derivatives and their pharmacological screening. Since, the synthesized scheme is simple and now well established it would be easy to synthesize other derivatives by incorporating various substitutions and screenings them for other pharmacological activities like Antibacterial, antiviral, anti- tumor, anti-hyperglycemic, analgesic, anti-inflammatory, for specific target. 2-(-2-cyano-1-phenyl-1H- benzo chromene -3yl)-5-(methylthio)-3-oxo-1 phenyl-2,3-dihydro-1H-pyrazole-4-carbonitrile by using 1- phenyl-3-(-2- phenylhydrazinyl)-4a,10b-dihydro-1H benzo chromene -2- carbonitrile with ethyl 2-cyano-3,3- bis (methylthio) acrylate using K2CO3 as catalyst and DMF solvent. Here 3-hydrazynyl -1- phenyl-4a,10b-dihydro-1H-benzo chromene -2- carbonitrile was prepared by the reaction3- amino -1- phenyl-1H benzo chromene -2- carbonitrile with hydrazine hydrate and 3-amino-1-phenyl-1H benzo chromene -2-carbonitrile was prepared from the mannich base of β-napthol,benzaldehyde and dimethylamine which was reacted with malononitrile.

Keywords – Chromene, Methyl thio, Carbonitrile etc.

Introduction

Chromene is one the privileged medicinal pharmacophore which appear as an important structural component in natural compound and generate great attention because of their interesting biological activity. It is a heterocyclic ring, chromene constitute the basic backbone of various type of polyphenol and widely found in natural alkaloid tocopherol flavonoid and

anthocyanin. Cancer constitutes the second main mortality cause in the word chromene derivative are an attractive template for the identification of potential anticancer agent. In recent year there has been much interest in the class of compound and their potential utility as anti-cancer, many of the natural and synthetic compound contain chromene moiety have been reported with anticancer activity, fused chromene are interesting due to their significant antibacterial and novel biological activity.

Studies on the synthesis of fused amino chromenes are stimulated by diverse biological activity of these compounds. In particular, they exhibit antioxidant properties, while substituted 2-amino-4-H- benzochromenes were proposed as medicine treatment of immune disorders and diabetes complication. Some 3-amino -1H-benzo chromene-2- carbonitriles were reported to possess anti-cancer and anti- bacterial activity. Furthermore,3- amino-1H-benzo chromene-2-carbonitrile may be regarded as heterocyclic β-enamino nitriles that are promising as building blocks for the synthesis of fused chromenes.

Several procedures for the synthesis of 3-amino -1H-benzo chromene-2- carbonitriles have been reported. Among these, the most commonly used in three component condensation of malononitrile with an aldehyde, primarily aromatic one, and naphthalene-2-ol. This reaction is generally carried out in ethanol, acetonitrile, or water in the presence of the base. 3-amino -1H-benzo chromene- 2- carbonitriles having no substituent on C1 was synthesized from 2-hydroxynapthalene-1- carbaldehyde, malononitrile, and the Hantzsch ester in the presence of InCl3. Enantioselective synthesis of 3-amino -1H-benzo chromene-2- carbonitriles from benzylidene malononitriles was also reported.

In our, synthesis of parent compound; we used the ethyl 2 cyano-3,3-bis methylthio acrylate reagent was prepared by the reaction of ethyl cyano acetate, carbon disulphide and dimethyl sulfate in the presence of a base. The thiomethyl group (best leaving group) on C2 position makes it very useful reagent for the preparation of heterocyclic compounds. Moreover, ethyl -2- cyano,3,3- bis methylthio acrylate can also be prepared efficiently using sodium ethoxide as a base.

Material and Methods

General Procedure

In continuation with this we have to synthesize 2-(-2- cyano-1- phenyl- 1-H benzo chromene- 3-yl)-5- (methylthio)-3- oxo-1- phenyl-2,3-dihydro-1H-pyrazole-4- carbonitriles, by using 1-phenyl-3- (-2- phenyl hydrazinyl)-4a,10b-dihydro-1H-benzo chromene-2-carbonitriles with ethyl2-cyano-3,3- bismethylthio acrylates using K2CO3 as catalyst and DMF as a solvent.Here 3-hydrazinyl-1-phenyl- 4a,10b-dihydro-1H-benzochromene-2-carbonitrile was

prepared by the reaction of 3-amino-1-phenyl- 1H-benzochromene-2-carbonitrile with hydrazine hydrate and the 3-amino-1-phenyl-1H-benzo chromene-2-carbonitrile was prepared from the mannich base of β-naphthol, benzaldehyde and dimethylamine was reacted with malononitrile.

β-naphthol is dissolved in minimum quantity of ethanol then benzaldehyde and dimethyl amine are added now the content is reflux for 2 hrs. and kept for 24 hrs.

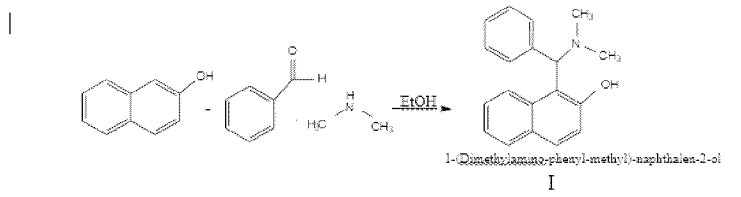

1-(Dimethylamino-phenyl-methyl)-naphthalen-2-ol

I

Mannich base and malononitrile are refluxed for 2 hrs. in presence of DMF as a solvent.

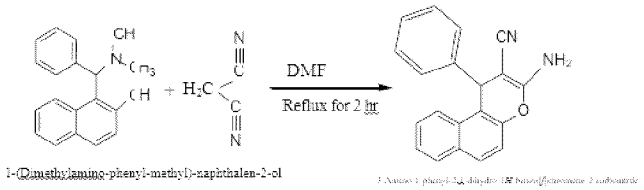

1-(Dimethylamino-phenyl-methyl)-naphthalen-2-ol

I

II

3-amino-1-phenyl-1H-benzo chromene-2-carbonitrile and phenyl hydrazine are refluxed for 2 hours using DMF as a solvent.

2-(- cyano-1- phenyl-1H-benzo chromene-3-yl)-5-methylthio-3- oxo-1- phenyl-2,3-dihydro-1H-Pyrazole-4- carbonitrile by reaction of 1-phenyl-3-(-2-phenylhydrazinyl)-4a. 10b-dihydro-1H-benzo chromene 2-carbonitrile with ethyl-2-cyano-3,3-bis methyl thio acrylate in the presence of potassium carbonate and DMF. The mixture was refluxed for 2-3 hrs.

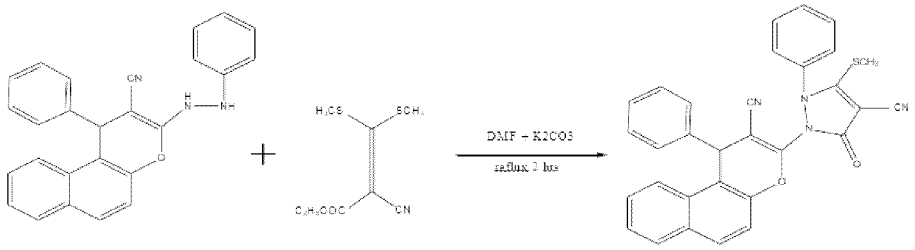

Antibacterial Study of Synthesized Compounds

An antimicrobial is an agent that kills microorganisms (microbicide) or stops their growth (bacteriostatic agents). Antimicrobial medicines can be grouped according to the microorganisms they act primarily against. Chemical agents not only provide the structural basis and energy supply to leaving organism, but also regulate their functional activities. The interaction between potent chemical and leaving system contribute in understanding the life processes and provide effective method for treatment, prevention, and diagnosis of many diseases.

Chemical compound used for these purpose is called as drugs and their action on leaving system called as drug effect. Any chemical substance inhibiting the growth causing death of microorganisms is known as antibacterial agent although a wide range of chemicals have these properties. It is possible to sub divided antimicrobial agent into various group according to the action and purpose for which they are employed. Sub division can be based upon the group of microorganism affected. Thus agents acting on the bacteria are called bacteriostatic or bactericidal, thus acting on fungi static or fungicidal.

Test Procedure

The medium was prepared by dissolving weighed ingredients and was sterilised at 121oC temperature and 15 lbs/ inch pressure for 15 minutes. After sterilization it was cooled down about 50oC and poured at sterilized petri-plates and allow solidifying.

The media plates were seeded with 24hrs old active nutrient both culture of the test organism in order to obtain low culture. A stainless steel crock borer of 6mm diameter was used to bore those cavities. The compounds where taken at a concentration of 1gm/mm using dimethyl sulfoxide DMF as a Solvent. In to the well were added 0.1 ml portion of test compounds in Solvent. The plate was incubating at 37oC for 24hrs.for antimicrobial activity. The zone of inhibition observed around the well after respective incubation was measured in mm by using antibiotic zone order.

The compound was screen for antibacterial activity against Staphylococcus aureus, Kocuria rosea species and Pseudomonas aeruginosa species by using Nutrient agar broth medium.

Result and Discussion

We describe the result of 6-(8-methoxy-2-oxo-2H-chromen-3yl)-4methyl sulfanyl -2H pyran- 2,3dicarbonitrile, which show antibacterial activities. This suggest that compound having potent biological activity.

The salicylaldehyde reacted with ethyl acetoacetate without using Solvent that is Solvent free in 100oC and to formed 3-acetyl coumarine. The reaction condition for 4-methyl sulfanyl-2-oxo-6-(2oxo-2H- chromen-3yl)-2H pyran-2,3dicarbonitrile is formed and use the reactant compound 3-acetyl coumarine and ethyl 2-cyno-3,3biethyl thio acrylate in the presence of pottasium hydroxide and pottasium thiocynide.

In the continuation with this work the compound obtained 6-(8-methoxy-2-oxo2H-chromen-3yl)4- methyl. sulfanyl-2H-pyran-2,3-dicarbonitrile which show antimicrobial activity against S.aureus and K.roses.

The 6- (8-methoxy-2-oxo-2H-chromen-3yl) -4methyl sulfanyl-2H-pyran-2,3-dicarbonitrile was synthesized and characterised for their structure elucidation with their antibacterial study. Various chemical and spectral data supported the structure, it is efficient, inexpensive and is useful in synthesizing pharmacologically important molecule.

References

1. Cintas P. Activated metals in organic synthesis. CRC Press; 2020 Jan 29.;7-10
2. Bhat BA, Dhar KL, Puri SC, Saxena AK, Shanmugavel M, Qazi GN. Synthesis and biological evaluation of chalcones and their derived pyrazoles as potential cytotoxic agents. Bioorganic & medicinal chemistry letters. 2005 Jun 15;15(12):3177-80.
3. Monica Kachroo, Synthesis of some new chalcone derivatives and evaluation of their anticancer activity. Int. J. Drug Dev. and Res, (2013); 5(3):309-315.
4. Mokle SS. Sayeed MA. Kothawar and Chopde. Int. J. Chem. So 2004;2(1):96-100
5. Cheng JH, Hung CF, Yang SC, Wang JP, Won SI, Lin CN. Synthesis and eytotoxic, anti- inflammatory, and anti-oxidant activities of 2, 5% dialkoxyfchalcones as cancer chemo preventive agents. Hioorganic & medicinal chemistry. 2008 Ang 1:16(15):7270-6
6. Seema 1. Habib et al. Chemical and biological potential of chalcone as a source of Drug: A review. LIPPR, (2018); 11(02):104-118.
7. Rajendra Prasad Yejella et al. Synthesis, antimicrobial, and computational evaluation of novel Isobutyl chalcones as antimicrobial agents, UMC, (2017), 1- 14.
8. Sunny Jalhan et al. Various Biological activities of coumarin and Oxadiazole derivatives. Asian J. Pharm Clin Res, (2017); 10(7):38-43)
9. Chapter 5 Synthesis of 7-hydroxy-4-methyl coumarin over Zapo-5 and Lewis acid metal ion-exchanged Zapo-5 molecular sieves 79.90.
10. Antimicrobial Merriam-Webster online dictionary. Archived from the original on (2009).
11. Alivelu Samala et al. Synthesis, characterization of some novel coumarin derivatives and evaluation of their Pharmacological activities. Der Pharma chemical, (2016), 8(12):19-24.
12. Kubba et al. Synthesis and characterization of new coumarin derivatives containing various moieties with antibacterial activities. Int. J. Pharm, Pharm sci, (2015); 7(8):70-74

16. Acoustic Parameters of 0.001M Aqueous Solution of Hydroxichloroquine at Different Temperatures

S. H. Shrirame
Nilkanthrao Shinde Science & Arts College, Bhadrawati Dist.-Chandrapur.
A. B. Dhote
Nilkanthrao Shinde Science & Arts College, Bhadrawati Dist.-Chandrapur.

Abstract

Nowadays ultrasonic velocity plays an majar role in understanding strength and molecular interactions in solutions. Medicines are compounds that are used to dingoes diseases. Hydroxychloroquine is an anti-malarial and antibiotic drug. The ultrasonic velocity, density and viscosity of aqueous solution of hydroxychloroquine was measured at different temperatures. Thermodynamic parameters i.e Relative associations, Specific relaxation time, Rao's Constant, Wada Constant were calculated from the experimentally observed values. It is help to study molecular interactions between hydroxychloroquine and water.

Key Words: antimalarial, Hydroxichoroquine, ultrasonic, molecular interaction.

Introduction

In present era ultrasonic velocity, density, viscosity and acoustic parameters play a very important role because of which it is possible to know the molecular interaction in a solution it has application in various fields like medical field, food processing, oceanography[1-3] etc. There is some considerable interest to aware the intermolecular interaction in liquid mixtures. The main usage of organic mixtures have been used for processing and further formulations of product. Physico-chemical properties of pure and mixtures of organic liquids are having great importance in the field of science and industrial engineering. The thermodynamic properties like Relative associations, Rao's Constant and Wada Constant are used to classify the various intermolecular interactions between solute and solvent in solution.[4-5]

Medication is a very important part in today's modern life, it is used for treatment of human and animal diseases. A drugs is substance that can diagnose various diseases in the human body when it consumed drugs are typically distinguished from food and substances that provide nutritional support.[6-9] Anti-malarial drugs such as Hydroxichloroquine are used to treat malarial infection. This research paper studies the temperature at which 0.001M concentration of Hydroxichloroquine has maximum molecular interactions with water.

In the present research paper ultrasonic velocity, density and viscosities of 0.001M aqueous solution of Hydroxychloroquine at different temperature was measured. This data is useful to calculate thermodynamic parameters such as Relative associations, Specific relaxation time, Rao's Constant and Wada Constant. From these reactivity and molecular interaction of the drug is predicted.

The structure of Hydroxychloroquine is

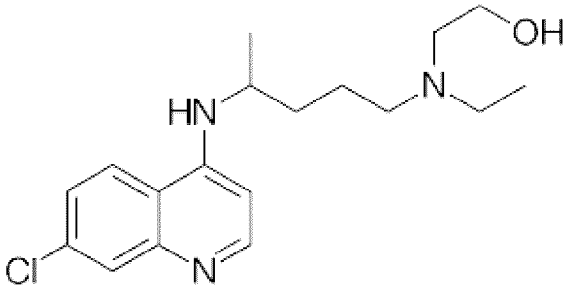

Experimental

Ultrasonic velocities (U) in liquid mixtures prepared with pure AR grade samples were measured using an ultrasonic interferometer (Mittal type, model F-81) operating at 2MHz frequency and temperature 298.15K,303.15K and 308.15K. The accuracy of the speed of sound was ±0.1 ms-1. An electronically digitally controlled constant temperature water bath is used to circulate water through a steel double-walled measurement chamber containing the experimental solution at the desired temperature[10-11]. Density of pure liquid and liquid mixtures was determined using density bottle by relative measurement method with an accuracy of ±0.1Kgm-3.

Ultrasonic velocity

Ultrasonic velocity in liquid and liquid mixtures can be directly measured by ultrasonic interferometer. From the knowledge of wavelength (λ), the velocity of ultrasonic waves in liquid can be calculated by relation,

$$V = \lambda . f \qquad \ldots\ldots\ldots\ldots\ldots\ldots\ldots (1)$$

Where,

λ is the wave length of ultrasonic wave to excite the crystal.

f is the frequency of generator.

Relative associations

Relative association is the measure of extent of association of components in the medium. It is used to assess the association in any solution relative to the association existing in water at 0°C. It is a property of understanding the molecular interaction in liquid mixtures and solutions. The relative association depends on either of breaking up of the solvent molecules on addition of

solute to it or the salvation of ions that are present.[12] It is a function of ultrasonic velocity and is calculated by equation

$$RA = \frac{d_s}{d_o}\left[\frac{v_0}{v_s}\right]^{1/3} \quad \ldots\ldots\ldots\ldots\ldots\ldots\ldots(2)$$

Where,

v_0 is the ultrasonic velocity in solvent.

vs is the ultrasonic velocity in solution.

Specific relaxation time

Specific relaxation time is the time taken for the excitation energy to appear as translational energy. It is absorption of sound wave, the result of a time lag between the passing the ultrasonic wave and return of the molecules to their original position. It is the time constant of an exponential return of a system to equilibrium after a disturbance. It depends on temperature and on impurities. The dispersion of the ultrasonic velocity in solutions and liquid mixtures reveals information about the characteristic time of relaxation process that cause dispersion. It can be calculated from the relation.

$$\tau = 4/3\beta.\eta \quad \ldots\ldots\ldots\ldots\ldots\ldots\ldots (3)$$

Rao's Constant

Molar sound velocity is also called Rao's constant. It is calculated by using the equation

$$R = [Meff/ds]v^{1/3} \quad \ldots\ldots\ldots\ldots\ldots\ldots\ldots (4)$$

Where,

Meff is the effective molar volume.

ds is a density.

v is the ultrasonic velocity.

Wada Constant

Molar compressibility is also known as Wada's constant.

$$W = [M_{eff}/ds]\ ß^{-1/7} \quad \ldots\ldots\ldots\ldots\ldots\ldots\ldots (5)$$

Where,

M_{eff} is the effective molar volume.

ß is the adiabatic compressibility.

ds is density

Result & Discussion

Table 1: Ultrasonic velocity, densities, viscosities Relative associations, Specific relaxation time, Rao's Constant, Wada Constant of aqueous solution of Hydroxichoroquine at 0.001M concentrations and different Temperature

Sr. No	Temperature (K)	Ultrasonic Velocity (m/s)	Density (Kg)	Viscosity (N/m^2)	Relative associations	Specific relaxation time (S)	Rao's Constant	Wada Constant
1	298.15	1325.2	1049.2	0.094	1.096	6.8021	0.1884	0.3615
2	303.15	1331.92	1047.2	0.080	1.095	5.7416	0.1891	0.3626
3	308.15	1380.56	1045.2	0.070	1.084	4.685	0.1918	0.3670

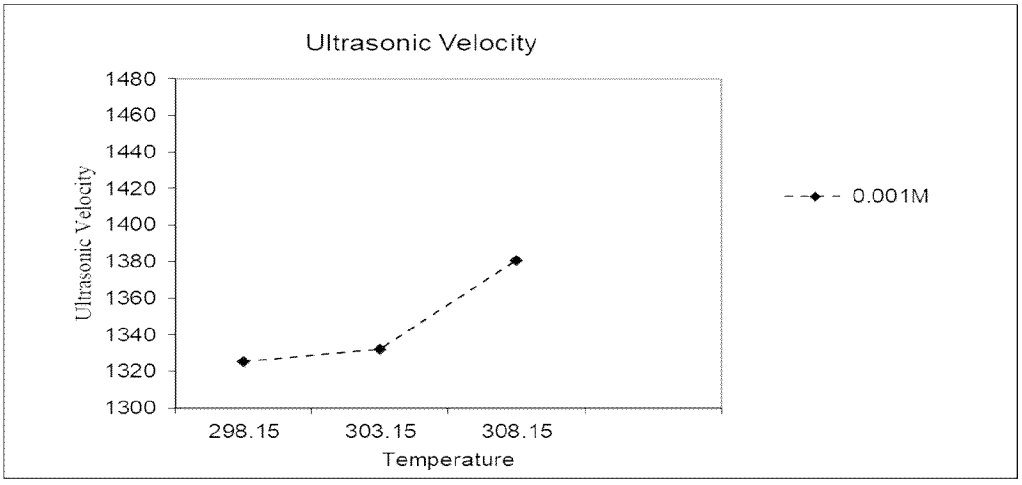

Fig. 1: Variation of ultrasonic velocity with temperature

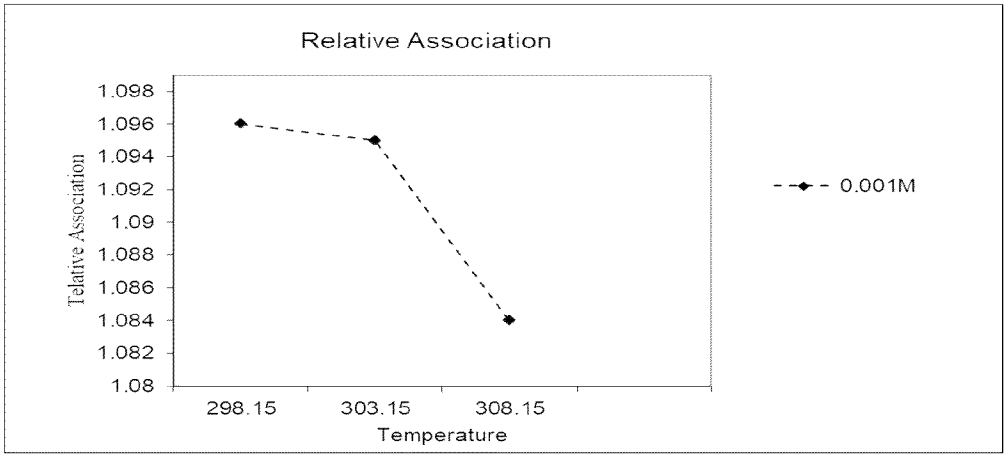

Fig. 2: Variation of relative association with temperature

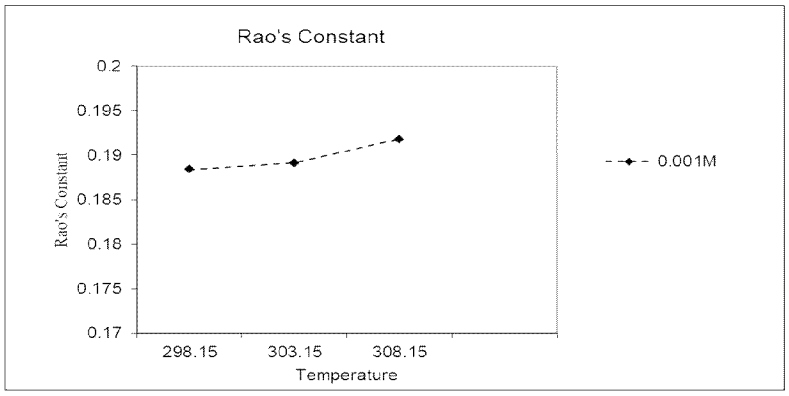

Fig. 3: Variation of Rao's constant with temperature

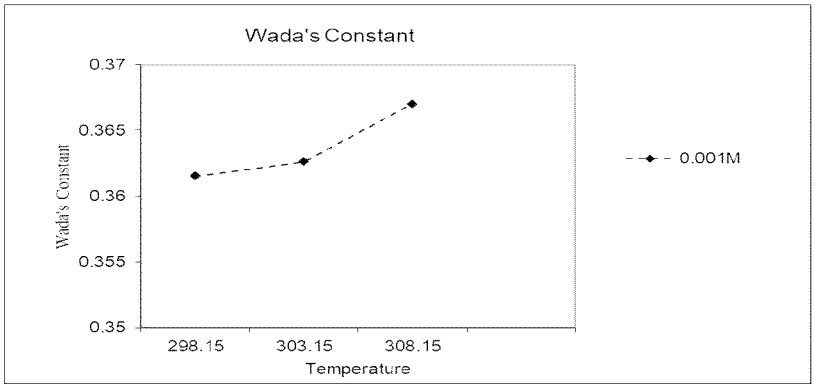

Fig. 4: Variation of Wada's constant with temperature

From table number 1 and figure number 1 we can see that ultrasonic velocity increases with temperature and density and viscosity decrease with temperature, which suggests that the Strong molecular interaction.

From table number 1 and figure 2 we understood that the relative association decreases with temperature which means that this solvent is showing a breaking structure.

From table number 1 figure 3 and 4 we understood that Rao's constant and Wada's constant increase with temperature which means that strong molecular interaction is taking place.

Conclusion

From the above table and figures it is cleared that 0.001M Hydroxichoroquine at different temperatures value of ultrasonic velocity, Rao's constat, Wada's constat increases it suggest that the strong molecular interaction at 308.15 K temperature and Relative Association value decreases it suggest that solvent breaking structure.

Reference

1. G. Thomas, Chemistry for Pharmacy and the Life Sciences, Prentice Hall, London, uk, 1996.

2. A. M. Ababneh, C. C. Large, and S. Georghiou, "Solvation of nucleosides in aqueous mixtures of organic solvents: relevance to DNA open basepairs," Biophysical Journal, vol. 85, no. 2, pp. 1111–1127, 2003.
3. T. B. Thoe, D. K. Aspinwall, and M. L. H. Wise, "Review on ultrasonic machining," International Journal of Machine Tools and Manufacture, vol. 38, no. 4, pp. 239 –255, 1998.
4. Dhote AB , Study of Acoustic Parameters of Rabeprazole Sodium in Different Solvents at 298.15K, Int. Res. J. of Science & Engineering, 2020; Special Issue A7: 860 -863 ISSN: 2322-0015
5. Drug". Dictionary.com Unabridged. v 1.1. Random House. 20 September 2007. Archived from the original on 14 Sep. 2007
6. A. B. Dhote, G. R. Bedare, K. P. Jumde Ultrasonic Velocity and Jones-Dole Equation B Coefficients for Aqueous Solution of Piperacillin and Tazobactam at Different Temperatures, hInternational Journal of Scientific Research in Science and Technology 9 (6) Print ISSN: 2395-6011 | Online ISSN : 2395-602X, 1104 -1106
7. Doxycycline for Malaria Chemoprophylaxis and Treatment: Report from the CDC Expert Meeting on Malaria Chemoprophylaxis Kathrine R. Tan,* Alan J. Magill, Monica E. Parise, and Paul M. Arguin, Am J Trop Med Hyg. 2011 Apr 5; 84(4): 517 – 531.doi: 10.4269/ajtmh.2011.10 -0285
8. U. G. Pathak, J. V. Patel, and P. H. Parsania, "Ultrasonic speed and thermodynamic parameters of novel epoxy resin solutions based on cardo symmetric double Schiff bases at 308.15 K," Journal of Solution Chemistry, vol. 41, no. 5, pp. 755 –765, 2012.
9. "Drug Definition". Stedman's Medical Dictionary. Archived from the original on 2014-05-02. Retrieved 2014 -05-01
10. C. Senthamil Selvi, K. Venkataramanan, V. Kannappan, C.Thenmozhi and S. Ravichandran, Asian Journal of Chemistry, 26 (8), 2471 (2014).
11. J. F. Kincaid and H. Eyring, "Free volumes and free angle ratios of molecules in liquids," The Journal of Chemical Physics, vol. 6, no.620, 1938.
12. Study of Relative Association, Apparent Molar Compressibility and Free Length of Entacapone API in alcohols at different Frequencies Sachin Deorao Zade, Padma Sachin Zade, Pravin J. Ganjre, Sunanda Shashikant Aswale and Shashikant Rajeshwar Aswale Indian Journal of Pharmaceutical Education and Research | Vol 50 | Issue 4 | Oct-Dec, 2016

17. Studies and Assessment of Water Quality Parameters of Akola District Region (Maharashtra)

S. J. Patil
Department of Chemistry Balapur (M.S.) India.

Abstract

Water is essential for all living being. Human need water in many daily activities like farming, drinking, cooking, etc. Quality of water is directly related to the life of human being. If the quality of water is not good then it affects the human life. During 10/07/2023 to 23/10/2023 surface water samples and open well water samples were collected from different sampling point in the range of 30km of Akola district region. Twenty water samples were analysed in the laboratory for their physical and chemical properties. Tests were performed in the laboratory for analysis of pH, EC, ORP, BOD, Hardness, Chlorides, TDS, DO etc. All the results were compared to the results against drinking water quality standard WHO (World Health Organization) and ISI Standard. The usefulness as well as un-usefulness, and importance of these parameters were discussed in predicting surface water and open well water quality characteristics.

Key Words; Drinking Water, BOD, COD, Physico-chemical study.

Introduction

Generally water is available in the form of ground water, surface water, springs, and atmospheric water. The quality of the water vary widely depending on the location and environmental factors.Water is absolutely essential not only for survival of human beings but also for animals, plants and all other living things. Water is transparent, tasteless, colourless, odourless inorganic chemical substance.In developing countries many water resources are not good for human being because they contain harmful biological, chemical and physical agent . Polluted water decreases the quality of water. i.e it is not potable for human being.For good health water should be safe. The river carries and assimilates industrial waste, festival waste and runoff from agricultural land. The water in that region becomes unhealthy for human being. The season wise variation always occurs in water quality. To control the variation (spatial or temporary) regular monitoring is essential.

Experimental

During 10/07/2023 to 23/10/2023 twenty water samples were collected of Akol district region. All samples collected in glass bottles as per standard. Presentation and transportation of water samples to the laboratory were as per standard methods. The bottles marked for the study of ground water and surface water stability for drinking and other domestic purpose. Water temperature was measured on the site by using mercury thermometer. Oxidation-reduction potential measured by potentiometer. Conductance measured by conductometer. pH measured by pH meter. Distilled water and A.R. grade samples were used. Parameters and method used to analyse samples are given below in the tables 1 & 2.

Hardness was varied in various regions. It was 82.6 ppm to 388 ppm. Hardness is due to presence of magnesium carbonate, calcium carbonate and bicarbonates. When decomposition rate and evaporating rate increases the concentration of magnesium and calcium increases.

Dissolved solids or total dissolved solids (TDS) due to the various types of, natural sources, minerals, sewage, urban runoff and industrial waste present in the water in dissolve form. The range of TDS was varied in various region. The range of TDS was 412.1 mg/L to 550 mg/L. Chloride is very important parameter for assessing the water quality. Higher concentration of chloride shows higher degree of organic pollution Percentage of chloride was varied in different region. In high evaporation the sodium and chloride ions attract each other and form salt crystal or it may be due to natural processes such as the passage of water through natural salt formation in the earth or it may be pollution from industrial waste. High chloride content may lead to laxative effects

Results and Discussion

The results of physical and chemical parameters are given in the table. All samples were odourless and colourless.The ph is important parameter of water which determine the suitability of water for human being for various purpose like drinking, cooking, bathing and agricultural purpose.The ph value of pure and neutral water is 7. The pH values of the water samples recorded in the range 7.21 to 7.42. Most of the water samples were alkaline in nature. The D.O. concentration of water samples varied from 6.55mg/L to 8.35 mg/L. The magnesium concentration and calcium concentration in the water samples ranges from 63.3mg/L to 161 mg/L and 17.3 to 161mg/L

Table 1

Parameters	Method	Standard values (WHO 1993)	ISI 1991
Colour	colorimeter		-
Odour	By smelling		-
Temperature	Thermometer	100°C	-
pH	pH meter	7.5 to 8.5	6.5 to 8.5
D.O.	Winkler method	< 5.0 mg/L	< 5.0
Alkalinity	Titrimetric	-	-
Chlorides	Titrimetric	250 mg/L	250
TDS	-	500 mg/L	500
Total hardness (as $CaCO_3$)	Titrimetric	100 mg/L	300
Total magnesium	Titrimetric	150 mg/L	30
Total Calcium	Titrimetric	100 mg/L	75 mg/L
BOD	Titrimetric	Not more than 8 mg	-
COD	Titrimetric	Not more than 250 mg/L	-
ORP	Potentiometer	-	-

Sr. No	**Location**	**pH**	**Conductance(ʊ)**	**ORP (mv)**	**TDS (mg/L)**	**DO (mg/L)**	**Chlorides (mg/L)**	**TH (ppm)**	**Mg (mg/L)**	**Ca (mg/L)**	**BOD (mg/L)**	**COD (mg/L)**
1	Bordi river,Bodkha	7.4	375	47.4	425	7.18	31.4	361	151	108	1.80	16.2
2	Bordi river,Chinchkhed	7.3	377	58.6	475	7.29	21.61	388	159	161	2.59	14.2
3	Bordi river,Patur	7.39	311.5	49.6	436.1	7.42	24.6	371	161	141	1.68	17.3
4	Bordi river,Shirla	7.40	390.1	51.3	492	7.39	28.6	362	126	148	1.74	16.1
5	Bordi river,Tandali	7.3	429.6	51.8	495	7.65	27.9	277	136	128	2.11	15.9

6	Morna river,Astool	7.38	430	63.5	462.5	7.79	29.1	226	91	69	1.73	20.1
7	Morna river,Pardi	7.39	420	57.5	475	7.2	28.6	235	96	56	2.55	16.1
8	Morna river,Agikhed	7.28	441.6	54.2	462.1	7.15	26.7	285	101	56	2.35	18.3
9	Morna river,Khamkhed	7.31	416.4	54	537	7.6	27.6	211	111.3	49	2.52	18.8
10	Morna river,Warkhed	7.34	430.1	52.2	412.1	7.25	30.1	235	116	55	2.23	17.1
11	Nakashi	7.26	466.6	56	420	7.93	115.5	85.3	97.8	17.3	2.01	21.83
12	Mazod	7.32	448.6	54.6	451	7.35	67	171.5	110.1	76.3	1.88	21.46
13	Indira nagar	7.39	451	56	506	7.10	42.9	211.3	88	58.6	2.01	21.53
14	Wadegaon	7.26	423.1	59.3	511	8.35	82.9	242	76.6	121	2.11	22.1
15	Channi phata	7.31	437	57.2	526	6.15	65.4	269.3	74	101	1.89	22.23
16	Chikhalgaon	7.36	514	55.6	293.1	7.85	54.1	118	85	62	1.77	23.3
17	Patur	7.40	543.6	57.8	473.3	7.52	61	98.6	63.3	44.3	1.98	23.3
18	Pardi	7.42	474	51.6	550	8.01	51.5	82.6	88	24.6	2.01	22.16
19	Khanapur	7.29	521.6	52.2	501.6	7.83	49	111.3	85	38.3	2.03	22.11
20	Tapalpatur	7.21	567	60	479	8.11	82.6	115.3	81	29.3	2.10	21

Conclusion

According to the various parameters studied, it is concluded that the TDS in some region is high. High value of TDS may cause gastrointestinal troubles. There are few treatment options

to reduce TDS in water, such as reverse osmosis system, Water filters and softners. Both water sources are useful for human consumption.

Acknowledgement

Authors are thankful to Principal of Shri Shivaji College, Akot for encouragement and providing necessary facilities

References

1. S.S.Castaneda, R.J.Sucgang, R.V.Almoneda, N.D.S.Mendoza and C.P.C.David, "Environmental Isotopes and measure ions for tracing leachate contamination from a municipal landfill in metro Manila, Philippines" Gernal of Environmental Radioactivity 110(2012), pp.30-37
2. Mane T.T. and Hingane Hemlata N, "Existing situation of solid waste management in pune city, India" Research journal of recent sciences, Volume-1, 2012, pp.348-351
3. Mona A, Hagras Assistant Professor, Irrigation and Hydraulics Departament, Faculty of Engineering, Ain Shams University, Cairo-Egypt
4. Jayant chutia, Mrudal Buragohain & Siba Prasad sharma Chem. Sci. 7(2) 1143-1152 (2009)
5. S.D. Dara, "Environmental Chemistry and Pollution Control", S.Chand and Company Publication
6. L.K. Gupta, D.P.Upadhyay, int. J.Chem. 9(4).2011
7. NEERI (1986) manual on water and waste water analysis Nagpur
8. Rajdeep Kumar and R.V.Singh int J chem, sci 7(4) 2534(2009)
9. Jadhavar, V.R. Ghorade, I.B and Patil S.S. ,(2010), Assessment of groubd water quality in and around Nagothane Region Dist Raigadh, Maharashtra, J.Aqua.Biol.,25(2);91-99

18. Recent Trends in Internet of Things: Issue Challenges and Applications

S. M. Dhakulkar
Assistant Professor, Department of Computer Science, G. S. Tompe Arts, Commerse and Science College, Chandur Bazar.
A. P. Fulari
Assistant Professor, Department of Computer Science, G. S. Tompe Arts, Commerse and Science College, Chandur Bazar.

Abstract

The world is undergoing towards modern technology, while specialized companies are existing a terrible rush in the information technology towards the so-called Internet of things IoT or Internet of objects, which is the integration of things with the world of Internet, by adding hardware and software. To be smart and able to communicate with each other and participate effectively in all aspects of daily life, new forms of communication between people and things, and between things themselves is required. Which will change the traditional life into a high style of living. In this review paper various application, challenges and issues of IoT were discussed.

Keywords: Internet of things (IoT), Smart Communication, Smart city, Network interface

1. Introduction

In Today's Day to day life Internet of Things is an emerging topic of technical, social and economic importance. IoT is everywhere, although we know that a device is part of it. For consumers, new IoT goods like Internet-enabled devices, home automation components and power management devices take initiative toward seeing "Smart home", which provides us more security and energy efficiency.

The IoT technology improved levels of independence quality of life at reasonable cost [1]. Internet of things systems such as networked vehicles, smart traffic systems, and sensors embedded in roads and bridges bring us closer to the idea of "smart cities", which reduce congestion and energy consumption. IoT technology offers the potential to transform agriculture, industry, and energy production and distribution is increasing availability of information along

the production value chain using networked sensors. A number of companies and research organizations have a wide range of expectations about the potential impact on Internet of Things over the next decade. [2].

2. Issues and Challenges of IoT

In all aspects of human lives, the sharing of IoT based systems and the various technologies involved in transferring data between embedded devices made it complex and directed to many problems and challenges.

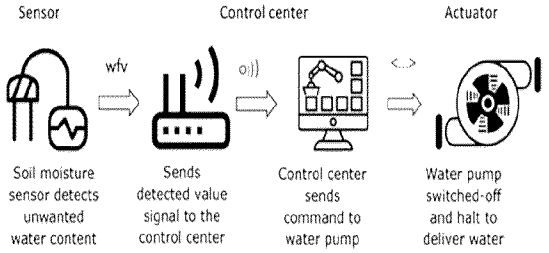

Figure 14. Example of an actuator (pump water).

2.1 Security

While security aspect is older in the IT context, The features of many IoT applications present new and unique security challenges. Poorly secured IoT devices and services can act as potential entry points for a cyber attacker and expose user data to theft by leaving data flow inadequately protected [6]. Every poorly secured device connected to the Internet has the potential to affect Internet security. The ability of some devices to automatically connect to others, and the potential for deploying these devices in insecure environments [7].

2.2 Privacy

The data flows and user confidentiality that IoT devices provide can open up unbelievable and exceptional value for IoT users, but concerns about privacy and potential harms may hinder the full adoption of IoT. This means that privacy rights and respect for user privacy expectations are integral to ensuring user confidence in the Internet, connected devices, and related services [8].

2.3 Interoperability and Standards

The ability to exchange information between various IoT devices and systems is called interoperability. This exchange of information is not dependent on published software and hardware. The four levels of interoperability are technical, semantic, syntactic, and organizational [9]. Interoperability as an important issue, so researchers have several solutions

such as adaptive, gateway based, virtual network and service-based architecture. [10]. There are still some challenges that remain with the possibility of interoperability which could be major area for future studies [11].

2.4 Legal, Regulatory, and Rights

Many real-life problems have been solved with the development of the Internet of Things but have also given rise to critical and legal challenges such as data security, privacy protection, trust, security, and data usability [12]. It has observed that the main IoT users support privacy, safety government rules and regulations regarding data protection due to mistrust of IoT devices.

2.5 Emerging Economies and Development

The Internet of Things holds great promise to deliver social and economic benefits to emerging and developing economies areas such as sustainable agriculture, water quality and use, health care, manufacturing, and environmental management, among others. [13].

3. Application of IoT

IoT applications promise to make our lives easier and bring enormous value with new wireless networks, high sensors, and superior capabilities. IoT applications uses several important areas. The following application areas are the top for 2020 analysis [14].

3.1 Manufacturing/Industrial

The IoT manufacturing application area covers a widespread range connection from objects to objects, projects from inside and outside. For the inside, many IoT-based factory automation and control projects include comprehensive smart factory solutions with many elements such as production floor monitoring, wearable devices and augmented reality in the shop floor, remote PLC or automated quality control systems.

Autonomous vehicles with the convergence of technologies like robotics, sensors, 3D cameras, 5G connectivity, software and artificial intelligence, autonomous vehicles having found their way safely onto factory floors as a means of increasing the speed and accuracy of routine operation [15].

Machine utilisation IoT architecture has emerged as a popular and powerful way to monitor machine usage. They can also be used to compare the performance of devices across one or more sites [16].

3.2 Transportation/Mobility

Maintaining vehicle health relies on the use of Internet of Things (IoT) communication tools that collect data about the performance of different parts, transfer that data to the cloud in real time and assess the risk of a possible malfunction of the vehicle's hardware or software. [17].

According to a recent study by Tony and James [18], car ownership will decrease by 80% by 2030. You can see that actually happen. City dwellers sell or never buy cars. They choose to use ride-sharing like Uber, DiDi and Alibaba bikes, in addition to relying on steadily improving public transportation services.

3.3 Energy

With energy consumption worldwide expected to grow by 40% over the next 25 years, the need for a smarter energy solution has reached an all-time high. Fortunately, there are some major shifts towards more efficient energy management from smart light bulbs to fully autonomous offshore oil platforms. Overall, IoT is transforming nearly every part of the energy industry from generation to transmission to distribution and changing how energy companies and customers interact. Safety drones [19] that can be used as part of a risk management system to reduce employee risks at nuclear plants or on mining sites.

3.4 Retail

More retailers are realized that, they can improve their cost efficiency and customer experience through use of IoT. Retail now accounts for 9% of selected projects, up from 5%. [20].

3.5 Smart Cities

A study shows that using existing smart city applications, cities improve quality of life indicators (such as crime, traffic, and pollution) by between 10% and 30%. Internet of Things in our day to day life as part of your home, transportation, or city, relate to a more efficient and enjoyable life experience [21].

3.6 Healthcare

For specific IoT health applications such as telehealth consulting, digital diagnostics, remote monitoring, and robotic assistance demand is increasing. IoT Healthcare apps help to decrease waiting time for the emergency room, tracking the patients, employees, and inventory;

Strengthening drug management. IoT has also introduced several wearables and devices which has made lives of patients and doctors comfortable [22].

3.7 Supply Chain

Internet of Things devices are an operative way to track and authenticate products and shipments using GPS and other technologies in the supply chain. Also, they can monitor product storage conditions which enhance quality management throughout the supply chain.

3.8 Agriculture

The current population of the world is 7.8 billion in 2020 and it is expected to reach 8.6 billion in 2030, 10 billion in 2050 and 11.2 billion in 2100 [24]. So, to satisfy feed of this huge population required to marry agriculture to technology and obtain good results.

One of many possibilities that exist for solving this problem is a smart greenhouse. Which is a revolution in agriculture, creating a self-regulating microclimate suitable for plant growth through the use of sensors, motors, and monitoring and control systems that and automate the growth process improve growing conditions [25].

3.9 Buildings

Smart building technology can achieve higher levels of integration between existing building systems. However, smart building technology will go beyond those concepts have an amazing ability to connect people with technology. [26].

4. Conclusion

The Internet of Things holds an important promise to provide social and economic benefits to the emerging and developing economy. Areas such as sustainable agriculture, water quality and use, health care, manufacturing and environmental management, needs to be addressed also the issues and challenges associated with IoT must be considered.

References

1. Domingo, M.C., "An Overview of the Internet of Things for People with Disabilities." Journal of Network and Computer Applications, 35, 584-596. 2012
2. Manyika, et al. (2015) The Internet of Things: Mapping the Value Beyond the Hype. Mckinsey Global Institute, San Francisco.
3. Global Connectivity Index. Huawei Technologies Co., Ltd., 2015.
4. IEEE Communication Society—IEEE Communication Magazine.

5. Bradbury, D. (2015) How Can Privacy Survive in the Era of the Internet of Things? The Guardian, April 7, Sec. Technology.
6. Gatsis, K. and Pappas, G.J. (2017) Wireless Control for the IoT: Power Spectrum and Security Challenges. 2017 IEEE/ACM Second International Conference on Internet-of-Things Design and Implementation (IoTDI), Pittsburgh, 18-21 April 2017, 341-342.
7. Babovic, Z.B., Protic, V. and Milutinovic, V. (2016) Web Performance Evaluation for Internet of Things Applications. IEEE Access, 4, 6974-6992.
8. Wilton, R. (2014) CREDS 2014-Position Paper: Four Ethical Issues in Online Trust. Issue Brief No. CREDS-PP-2.0. Internet Society.
9. Van-der-Veer, H. and Wiles, A. (2008) Achieving Technical, Interoperability-The ETSI Approach.
10. Noura, M., Atiquazzaman, M. and Gaedke, M. (2017) Interoperability in Internet of Things Infrastructure: Classification, Challenges and Future Work. Third International Conference, IoTaaS 2017, Taichung, 20-22 September 2017, 11-18.
11. Noura, M., Atiquazzaman, M. and Gaedke, M. (2019) Interoperability in Internet of Things: Taxonomies and Open Challenges. Mobile Networks and Applications, 24, 796-809.
12. Tzafestad, S.G. (2018) Ethics and Law in the Internet of Things World. Smart Cities,
13. The Internet Governance Forum Dynamic Coalition on the Internet of Things (DC IoT) Has Been Particularly Active in Considering the Impact and Challenges of IoT in Emerging and Developing Economies. http://www.iot-dynamic-coalition.org
14. IOT Analytics: Market Insight for IOT; Top 10 IoT Applications in 2020. https://iot-analytics.com/top-10-iot-applications-in-2020
15. Automotive Systems Manufacturer Faurecia (ASMF). https://www.mobile-industrial-robots.com/en/about-mir/news/mobile-industrial-robots-announces-strategic collaboration-with-faurecia-to-optimize-its-internal-logistics-globally
16. IoT in Manufacturing. https://www.scnsoft.com/blog/iot-in-manufacturing
17. The Next Level of Predictive Maintenance. https://connectitude.com/sv/the-next-level-of-predictive-maintenance

18. Tony Seba and James Arbib; Rethinking Transportation 2020-2030. https://static1.squarespace.com/static/585c3439be65942f022bbf9b/t/591a2e4be6f2e1c13df930c5/1494888038959/RethinkX+Report_051517.pdf
19. Public Safety Drones Use: Policy and Legal Challenges.https://medium.com/homeland-security/public-safety-drone-use-policy-legal-challenges-491a504a1b3c
20. The Internet of Things (IoT) in the Retail Industry—Evolutions and Use Cases. https://www.i-scoop.eu/internet-of-things-guide/internet-things-retail-industry
21. Durán-Sánchez, A., et al. (2017) Sustainability and Quality of Life in Smart Cities: Analysis of Scientific Production. In: Sustainable Smart Cities. Creating Spaces for Technological, Social and Business Development, Springer, Berlin, 159-181.
22. https://econsultancy.com/internet-of-things-healthcare
23. The Internet of Things Changing the Future of Supply Chain.https://cerasis.com/future-of-the-supply-chain
24. Projections of Population Growth. https://en.wikipedia.org/wiki/Projections_of_population_growth
25. Smart Greenhouse Remote Monitoring Systems.https://www.postscapes.com/smart-greenhouses
26. What Is Smart Home Technology?https://www.pcmag.com/news/the-best-smart-home-devices.

19. Study the Acoustic Parameters of Li, Na, K ion Salts in Aqueous of Different Concentration at 303K

S. P. Burad
Nilkanthrao Shinde Science & Arts College, Bhadrawati.
A. B. Dhote
Nilkanthrao Shinde Science & Arts College, Bhadrawati.

Abstract

The use of Ultrasonic Velocity study is well recognized approach for the study of molecular interaction in fluids. Thermodynamic properties are convenient parameter for interpreting solute-solvent and solute-solute interaction in solution phase. The density, velocity and viscosity of Lithium ,Sodium and Potassium salt in water of different concentration are calculated at 303K .Acoustic parameter were calculated from experimental data which help to predict molecular association.

KeyWords: Aqueous Lithium solution, AqueousSodium solution, Aqueous Potassium solution, Ultrasonic, Molecular interaction, acoustic parameter.

Introduction

Ultrasonic waves sound waves too high pitched for human ears to detect. Their frequencies range from 20,000 Hertz to about 10 trillion Hertz. Ultrasonic waveswork on the principle that sound is reflected at different speed by tissues or substances ofdifferent densities. The use of Ultrasound is one of the important tool for study of molecular interaction in different binary mixture of solution. In industry ultrasonic waves have been used in the testing of machinery and machine part. In medical, analyticaland different field ultrasonic investigations are very useful.

The ultrasonic waves helps the study of molecular interaction in liquids provide valuable information regarding internal structure, internal pressure, molecular association,complex formation etc.The ultrasonic techniquesalso reveal weak interaction due to its useful wave length range. Moreover ultrasonic parametersare directly related to a large number of molecule or thermodynamic parameter. Since various liquid state theories are based upon thermodynamic consideration, ultrasonic absorption, coefficients and velocities provide means to study them.

The Ultrasonic study of binary liquid mixture is important in understanding the nature of molecular interaction. The nature and degree of molecular interaction of different salt in the solution depend upon the nature of ions and nature of solvent. Ultrasonic velocity and derived acoustic parameter provide valuable information about the molecular interaction. This has been studied for various binary mixtures with respect to variation in concentration of liquid. The acoustic thermodynamic parameter have been used to study different kinds of association , molecular motion and various types of interaction and their strength influenced by the size of different ions and the solvent

Inpresentinvestigation Ultrasonicvelocityandrelatedacousticparametersof LiCl, NaCl and KCl with water havebeencalculatedat303Kfor differentmolefraction (0.06 to 0.09) concentration.

Materialand Experimental Method

Inthepresentexperimental work the different molefractionof LiCl, NaCl and KCl inwater has been prepared. All the salt and solvent used are of AR Grade sample. All thesolutions werepreparedindeionizedanddistilledwater. Following parameterswerecalculated

Velocitymeasurement

The ultra sonicve locity of binary mixture for Li Cl in water, Na Cl in water and KCl in water has been measured using an ultrasonic inter ferometer (Mittal type, Model F-81) working at 2MHz fre quency and attemperature 303K.The accuracy of sound velo city was+0.1ms-1. An electronically digital operated constanttem perature water bathhas beenused to circulate water through the double walled measuring cell made up of steel containing the experimental solution at the desiredtemperature.

Density Measurement

The densities was measuredusinga 25 mlspe cificdensity bottle by measuremen twithanac curacy of + 0. 01 Ns-1m- 2 relative specific gravityof 0.01Kg. The weigh tof the sample was measure dusingan electronic digital balance withana ccuracyof+0.1mg

Viscosity Measurement

Ostwald Viscometer was used for measuring viscosity of flowing time with the accuracy of +0.1 by usingdigitalstopwatch.

The parameters such as adiabatic compressibility (β), inter molecular free length (Lf), andacousticimpedance (Z), arecalculatedbyusingthefollowing

Relation (1- 3).

$\beta=(U2\rho)-1$ .....(1)

$Lf=KT\beta a½$ ……(2)

$Z=U\rho$ …… (3)

Result and Discussion

The experimentally measured values of ultrasonic velocity density and viscosity of the solution and calculated values of acoustic parameter such as adiabatic compressibility, acoustic impendence intermolecular free length for LiCl in water are reported in TableI NaCl in water are reported in Table IIand KCl in water are reported in Table III for different molar concentration (0.06 to 0.09 Mole fraction) at temperature 303K.

Table I,II and III and fig 1 shows that ultrasonic velocity increases with increase in concentration of aqueous solution of LiCl, NaCl , and KCl shows that as concentration increases there is strong molecular association between solute and solvent. Hence strong molecular interactions exist in aqueous solution of LiCl as compared to NaCl and KCl.

The variation of ultrasonic velocity in mixture depends upon the increase or decrease in intermolecular free length as there is gradual decrease it also indicate strong molecular interaction in the solution with increase in concentration. The increase in viscosity with increase inconcentration also indicate the good molecular forces between the solute and solvent molecule.

From Table I,II and III it is observed that Acoustic impendence increases with increase in concentration of aqueous solution of LiCl, NaCl and KCl respectively .Acoustic impendence have opposite behavior of that adiabatic compressibility and intermolecular free length.

As the calculated values of adiabatic compressibility and intermolecular free length are continuously decreases in table I,II and III it shows greater molecular interaction ions and solvent .The values of above acoustic parameter for Li is less as than Na and K ion hence the Li ion salt interact more as compared Na and K ions salts

According to coulombs law, the smaller an ions the greater molecular interaction it will have the larger is ion the weaker is the attraction. By using the charges on ions and its size we can determine which ion will have the strongest and weakest ion-dipole interaction force .Due to smaller in size of Li+ ion it has more intermolecular interaction with polar solvent water as compared to Na+ ion and K+ ion.

Table I:Measured values of ultrasonic velocity (U), Density (ρ), Viscosity (η), Adiabaticcompressibility (β), Acoustic Impendence (z), Mean Free length (Lf) of aqueous solution LiCl at 303K

LiCl in H_2O at 303K						
Mole Fraction	Veocity	Density	Viscocity	Adiabatic compressibility	Acoustic Impendence	Free Length
0.06	1586.32	1026.14	1.1204	3.872681521	1.62778640	0.41214198
0.07	1592.32	1031.21	1.1485	3.824654278	1.64201631	0.40957841
0.08	1596.14	1035.06	1.1531	3.792211158	1.65210067	0.40783756
0.09	1601.02	1037.41	1.1841	3.760590596	1.66091416	0.40613367

TableII: Measuredvaluesofultrasonicvelocity (U), Density (ρ), Viscosity (η), Adiabatic Compressibility (β), AcousticImpendence (z), Mean Freelength (Lf) of aqueous solution of NaClat303K

NaCl in Water at 303K						
Mole Fraction	Veocity	Density	Viscocity	Adiabatic compressibility	Acoustic Impendence	Free Length
0.06	1550.31	1037.61	1.1201	4.009855796	1.608617159	0.41937771
0.07	1554.12	1039.26	1.1445	3.983884042	1.615134751	0.41801735
0.08	1560.71	1042.18	1.1532	3.939243611	1.626540748	0.41566876
0.09	1565.32	1045.32	1.171	3.904311606	1.636260302	0.41382164

TableIII: Measuredvaluesofultrasonicvelocity (U), Density (ρ), Viscosity (η), Adiabatic Compressibility (β), AcousticImpendence (z), MeanFreelength (Lf) of) of aqueous solution KCl at303K

KCl in Water at 303K						
Mole Fraction	Veocity	Density	Viscocity	Adiabatic compressibility	Acoustic Impendence	Free Length
0.06	1534.61	1047.23	1.0658	4.054729412	1.60708963	0.42171777
0.07	1542.81	1049.32	1.0981	4.003751912	1.618901389	0.41905840
0.08	1551.16	1051.32	1.1189	3.953228154	1.630765531	0.41640593
0.09	1557.2	1053.26	1.1256	3.915395332	1.640136472	0.41440862

Conclusion

In present investigation the various acoustic parameters such as adiabatic compressibility, Intermolecular free length, Acoustic impendence have been evaluated from Ultrasonic velocity, Density and viscosity for aqueous solution of LiCl, NaCl and KCl at 303K. From the study it is concluded that Values of ultrasonic velocity, viscosity and acoustic impendence are gradually

increases with increase in concentration of aqueous solution of Li, Na and K and decrease ofIntermolecular free length, Adiabatic compressibility which indicate strong molecular interaction between solute and solvent in of each salt aqueous solution y increase in mole fraction concentration at constant temperature.

The study of all the acoustic parameter concludes that Salt of Li ions interact more with solvent has strong intermolecular interaction as compared to salt of Na ion and K ion due to smaller in ion size.

References

1. J.Blitz, FundamentalsofUltrasonic, Butterworth&Co.Ltd. London, (1963).
2. M.K.S.Suslick, Ultrasound: It's Chemical, Physicaland BiologicalEffects, VCH, Weinheim, (1988).
3. T.J.Mason; Ed., Sonochemistry. Theuseofultrasoundinchemistry, Roy. Soc. Chem., (1990).
4. N., Kulkarni, B. Moudgil, M. Bhardwaj, Am. Cer. Soc., Cer. Bull73, 6 (1994).
5. M.C., Bhardwaj, Proc. Am. CeSoc89 (1998)
6. S. Acharya, R. Palikray., G. C. Mohanty, Ind. J.PureandAppl. Phys.,41,855–857
7. Sunanda S. Aswale, Shashikant R. Aswale Aparna B. Dhote, International Journal of Science and Research (IJSR), ISSN (Online): 2319-7064,464-467
8. Sunanda S. Aswale, Shashikant R. Aswale Aparna B. Dhote 0971-9563) Vol 14 (2), December 2014, pp. 251-254
9. Ubagaramary D, Muthu Vijayan Enoch IV, Mullainathan S, Kesavaswamy,

20. GIS Based Morphometric Analysis of Pili Watershed in part of Sapan River, Amravati District, Maharashtra, India

S. R. Warghat
Department of Geology, Bharatiya Mahavidyalaya, Amravati.
S. V. Kulkarni
Department of Geology, Bharatiya Mahavidyalaya, Amravati.
A. A. Gawande
Department of Geography (Geoinformatics), Savitribai Phule Pune University, Pune.
Y. K. Mawale
Department of Geology, Sant Gadge Baba Amravati University, Amravati.
P. S. Tidke
Department of Geology, Sant Gadge Baba Amravati University, Amravati.

Abstract

The present paper deal with the morphometric analysis of the Pili watershed, it is tributary of Sapan River, Achalpur Taluka, Amravati District, Maharashtra, India. The study area is situated in the Survey of India Toposheet nos. 55G/7, 55G/11, and 55G/10 lie between latitude 21°24'0" N, 21°12'0" N longitude 77°30'0" E, and 77°39'0" E. The main purpose of the work is to determine the complete stream properties from the measurement of various stream attributes. The quantitative drainage analysis is done aspects wise such as linear aspects, aerial aspects and relief. The linear aspects include stream order, stream number, stream length, bifurcation ratio, mean length of stream orders, stream length ratio, mean stream length ratio, and form factor. The areal aspects involve drainage density, stream frequency, and texture ratio, as well as the constant channel maintenance and length of overland flow. The relief aspects include relief ratio, relative relief, ruggedness number and melton ruggedness number. Morphometric analysis is carried out using ArcGIS software, an advanced tool for measuring the drainage basin, the earth's surface dimensions of landform, and shape within a short time. The direction of the basin is from North to South. Based on the above results, it is inferred that in the study area, groundwater prospects are good.

Key Words: Morphometric Analysis, Remote Sensing, G.I.S., Pili River, Achalpur

Introduction

Morphometry is the measurement and mathematical analysis of the configuration of the Earth's surface and the shape dimensions of its landforms. Morphometric analysis is a significant tool to understand channel networks, ground slopes, structural control, geologic and geomorphic history of a drainage basin (Strahler, 1957, 1964). Pioneering work in the field of Morphometric characteristics has been carried out by Horton (1932 and 1945). He has carried out a revolutionary study for evaluating the morphometric setup. Schumm (1956) investigated the evolution of the drainage system as per the slope. Melton (1958) studied the geomorphic properties of the matured drainage system. Strahler (1952, 1956). Miller (1953) and others are based on the premise that for the given conditions of lithology, climate, rainfall, and other relevant. Morphometric analysis of a watershed provides a quantitative description of the drainage system which is an important aspect of the characterization of watersheds (Strahaler, 1952, 1957, 1964).

The morphometric analysis is performed successfully through the measurement of linear, aerial, relief aspects (Pareta and Pareta, 2012; Magesh et al., 2011; Prakash et.al., 2016). The basin morphometric parameters are strongly associated with basin hydrologic processes (Altaf et al. 2013; Pophare and Balpande, 2014; Prakash et al. 2017; Kaushik and Ghosh, 2018). Remote sensing (RS) and GIS technology have been playing an effective role in the morphometric analysis and it has great potential as it gives cost-effective results (Pankaj and Kumar, 2009; Sangita and Nagarajan, 2010; Samal and Nagarajan, 2015). Digital elevation model (DEM) is the dataset used for making the stream network, creating slope map and also for various studies (Jensen 1991; Pareta and Pareta, 2011, Forkuor and Maathuis, 2012; Kaushik and Ghosh 2015; Patel et al. 2016;). Using GIS software exact representation and quantitative measurements with more accurate results are possible in less time. Morphometric analysis using remote sensing and GIS techniques have been well demonstrate recently by some of the researchers (Sarmah and Tiwari 2012; Vandana, 2013; Singh and Kanhaiya, 2015; Chandrashekar et. Al., 2015; Sahu et.al., 2016; Moharir et.al 2017; Kumar 2018; Prakash et al 2019; Gautam et. al., 2020; Bhatt et.al., 2021; Shelar et.al., 2022)

Study Area

The Pili River rises in the Satpura range in Madhya Pradesh at an elevation of about 340 m to 750 m. The study area is located in Achalpur and Chandur Bazar talukas of Amravati

district, Maharashtra. It is sub tributary of the Sapan River, with a basin area covering a total of 250.89 sq.km area. The study area comes under Survey of India Topographic sheets Nos. 55G/7, 55G/10, 55G/11. It falls between latitude 21°24'0" N, 21°12'0" N longitude 77°30'0" E and 77°39'0" E.

Aim and Objective of the study

Aim – GIS based morphometric analysis Pili watershed part of Sapan River, Amravati district Maharashtra.

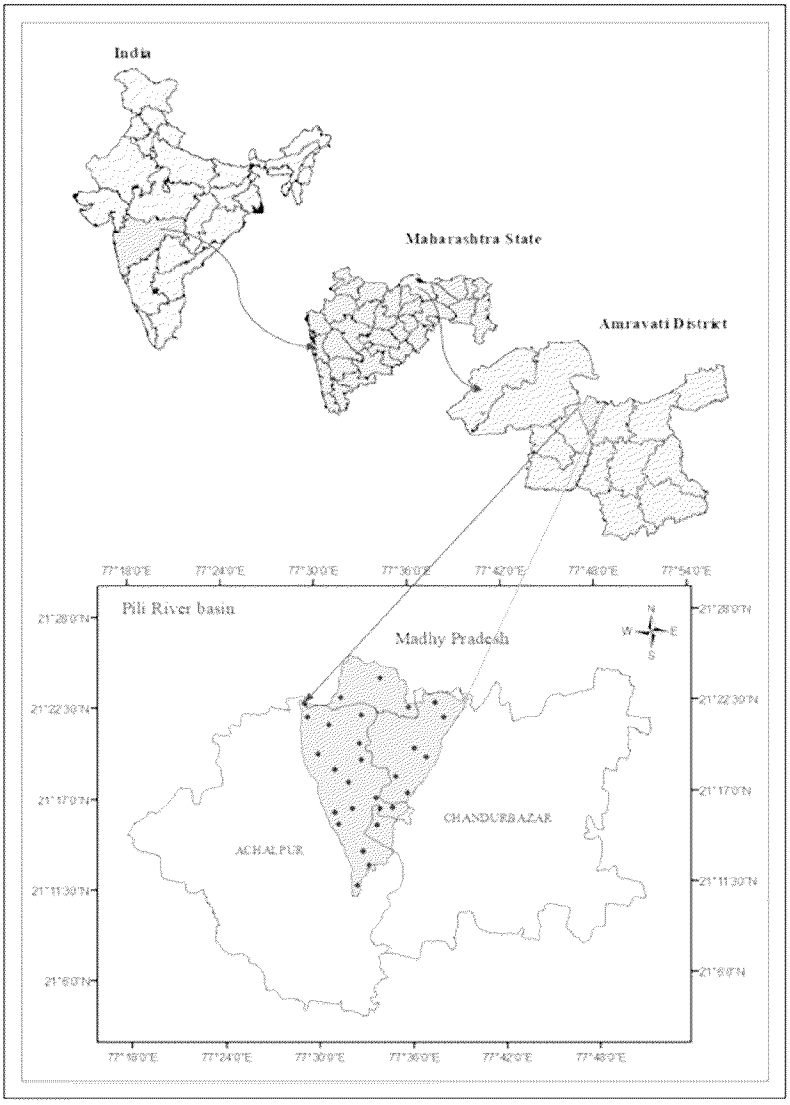

Figure 1: Study area Location map

Objectives

- To study morphometric analysis of the Pili River basin.
- To assess the hydrodynamic condition of surface and groundwater reserves of the study area.
- To understand the water scarcity in the study area.
- Synthesize and compilation of all the data for the management of hydrogeological resources and sustainable development of the study area.

Materials and Methods

The following material and methodology will be adopted to achieve the various objectives of the proposed research.

Data and Software Used

- Topographical Map: Survey of India (1:50,000) 55G/11, 55G/10, 55G/7.
- ASTER (DEM) with 30m spatial resolution.
- LISS-IV Mx satellite imagery with30m spatial resolution
- ArcGIS 10.3 software

Methodology

The morphometric parameter such as linear, aerial, and relief aspects of the study area were determined and computed using the GIS approach. The methodology adopted for the morphometric analysis is described as follows;

- The entire study area is delineated from the rectified mosaic survey of India topographic maps 55H/7, 55H/13 on a scale of 1:50000 with help of ArcGIS environment assigning using projection UTM, WGS 1984, 43 N Zone.
- Digitization of drainage in the study area from the geo-reference survey of India toposheet.
- Various Morphometric parameters such as linear, aerial, and relief aspects for the study area were computed as per the methodology suggested by Horton, Strahler, etc.

Firstly, from the satellite image, the drainage characteristics have been extracted and a drainage map has been prepared. This was used to confirm the morphometric characteristics from the survey of India toposheet. The linear, aerial, and relief aspect of the taluka has been determined on a grid basis.

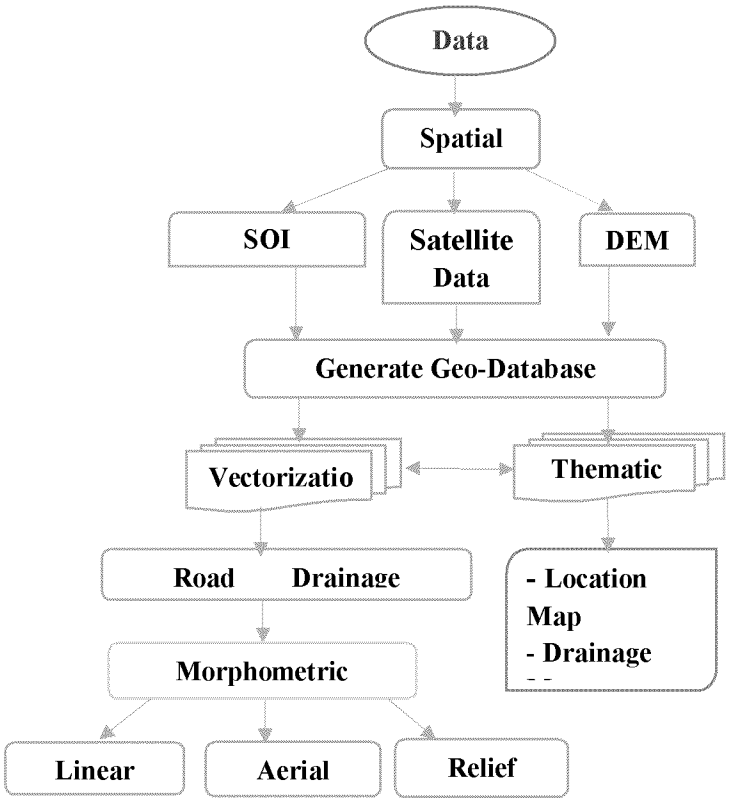

Figure 2: Flow chart of the Morphological analysis.

Results and Discussion

The present study integrated the use of the GIS technique and the results of morphometric parameters that have been determined are discussed and briefly described. Results of morphometric parameters such as linear, aerial, and relief aspects for the study area are shown in Table 2, Table 3, and Table 4. The study of the Pili river is the 6^{th} order basin. The total drainage basin area of the Pili River basin is 250.89km. Morphometric parameters such as linear, areal, and relief for the basin area were calculated based on the formula suggested by Horton (1945), Strahler (1964), Schumn (1956), and Miller (1953). In the present study, the morphometric analysis is carried out using mathematical formulae given in Table 1.

Table 1: The different parameters executed for morphometric analysis

Sr. No	Morphometric Parameters	Methodology	References
1.	Area (A)	Calculate in GIS	-
2.	Perimeter (P)	Calculate in GIS	-
3.	Basin length (Lb) (km)	Lb= 1.312*A	Nookaratnam et.al (2005)
4.	Stream order (Nu)	Hierarchical rank	Strahler (1957)
5.	Stream length (Lu) (km)	Length of the stream	Horton (1945)
6	Mean stream length	Lsm = Lu/Nu	Strahler (1957)
7	Bifurcation ratio (Rb	Rb=Nu/N(u+1)	Horton (1945)
8.	Stream length ratio (Rl)	RL = Lu/Lu-1	Horton (1945)
10.	Drainage density (Dd)	Dd=∑Lt/A,	Horton (1945)
11	Stream frequency (Fs)	Fs=N /A	Horton (1945)
12.	Drainage texture (Rt)	Rt = Nu/P	Horton (1945)
13.	Length of Overland Flow (Lo):	Lo = 1/D*2	Horton (1945)
14.	Constant Channel Maintenance (C)	C=1/Dd	Horton (1945)
15.	Form factor (Ff)	Rf = A/Lb2	Horton (1945)
16.	Circulatory ratio (Rc)	Rc = 4*Pi*A/p2	Strahler (1964)
17.	Elongation ratio (Re)	Re = (2/Lb) *(A/pi)0.5	Schuman (1956)
18.	Shape index (Sw):	Sw=1/Ff	Horton (1932)
19.	Texture ratio (T):	T= Nu/P	Horton (1945)
20.	Compactness Coefficient (Cc):	$Cc = Pc/Pu$	
21.	Height of basin mouth (z):	The lowest elevated point of the basin	Schumm (1956)
22.	Height of highest point of the basin (Z):	The heights elevated point of the basin	Schumm (1956)
23.	Basin relief (R):	R= H-h	Schumm (1956)
24.	Relief ratio (Rh):	Rr= R/Lb	Schumm (1956)
26.	Ruggedness number (RD):	HD= H×Dd	Strahler (1964)
27.	Coarse ratio (Cr):	R*Dd/1000	Choreley (1986
28.	Melton Ruggedness Number (MRn):	MRn=H-h/A0.5	Melton (1965)

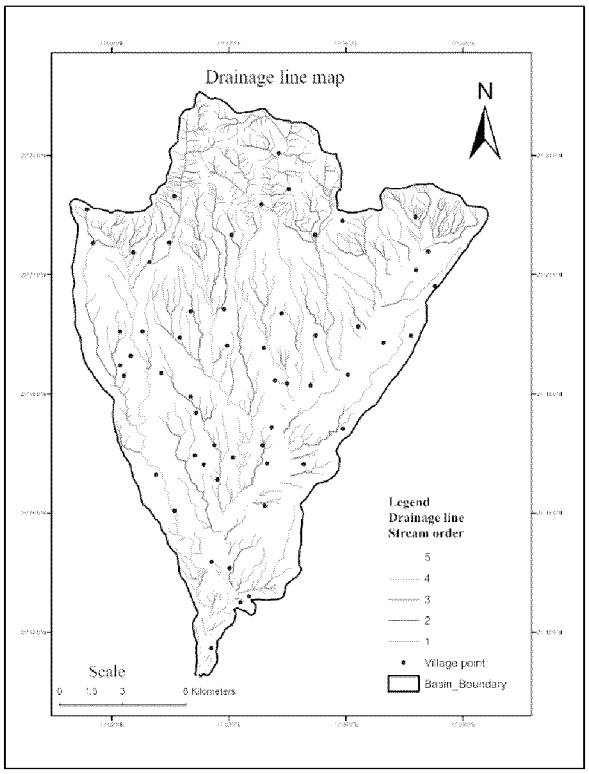

Figure 3. Drainage map of Pili River Basin

Morphometric Analysis

1. Linear Aspect

Stream ordering (Nu)

Stream order is the first step of quantitative morphometric analysis. It is observed that as the stream order increases, the number of segments. The number of streams of any certain order will be fewer than for the next lower order but it is more numerous for the next higher order. In the present study, the order-wise stream numbers estimated are given in Table 2.

Stream length (Lu)

Stream length (Lu) is defined as the total length of all streams of each order in the drainage basin. The length of each stream was calculated by the law proposed by Horton (1945). The stream length of the basins was measured with the help of GIS software. Generally, the total length of stream segments in first-order streams is maximum and decreases as the stream order increases. The maximum length of the Pili River basin is 604.98 km. Where the length of the I order is 339.06 Km, the II order stream is119.64 Km, the III order stream is 51.80 Km, the IV order stream is 64.68 Km, V order stream is 29.80 Km.

Mean stream length (Lsm)

The mean stream length is calculated by dividing the total stream length of order 'u' and the number of streams of the segment of order 'u'. In the study area, it is needed that Lsm varies from 0.6820 to 29.802 km.

Stream length ratio (RL)

The stream length ratio (RL), is the ratio of the mean length of the stream of a given order (Lu) to the mean length of the stream of the next lower order (Lu-1). The stream length ratios between the streams of different orders of the study area show a change in the basin. This change might be attributed to a variation in slope and topography, indicating the late youth stage geomorphic development in the stream of the study area. The stream length ratio for orders II/I is 00.23, and for III/II, IV/III, and V/IV are 0.24, 0.20, and 0.16 respectively.

Bifurcation ratio (Rb)

The bifurcation ratio is the ratio between the number of streams in the previous order and the next. The bifurcation ratio of a large basin is generally is average of the bifurcation ratio of the order of the streams within it. The higher value of the bifurcation ratio indicates a strong structural control in the drainage pattern whereas the lower value indicates less affected drainage by structure disturbances (Strahler1964). In the present study area, the ratio varies from 4 to 6 in the basin area.

Mean Bifurcation ratio (Rb)

The mean bifurcation ratio is the arithmetic mean of bifurcation ratios. In the present study, the mean bifurcation ratio of the Pili basin is 4.77.

Table 2: Linear aspect of the morphometric parameter of the study area

Parameter	**Results**				
Stream order (U)	I	II	III	IV	V
Stream number (Nu)	497	119	29	6	1
Stream length (Lu) in km.	339.06	119.64	51.80	64.68	29.80
Mean stream length (Lu)	0.682	1.005	1.786	10.786	29.802
Bifurcation ratio (Rb)	I/II	II/III	III/IV	IV/V	V
	4.18	4.10	4.8	6	-
Mean Bifurcation ratio (Rb)	4.77				
Stream length ratio (Rl)	II/I	III/II	IV/III	V/IV	-
	0.23	0.24	0.20	0.16	
Área (A)	250.89 sq. km				
Perímeter (P)	81.45m.				

2. Aerial aspect

Drainage density (Dd)

Drainage density is defined as the ratio of the total length of the streams of all orders of the basin to the area of the basin. The drainage density is a quantitative measure of the average length of stream channel for the whole basin. Low drainage density generally results in areas highly resistant to permeable subsoil material, dense vegetation, low relief, and coarse drainage texture. High drainage density is resultant of weak or impermeable subsurface material, thin vegetation, hilly relief, and fine drainage texture. The drainage density of the present study is 2.41 indicating low drainage density.

Stream frequency (Fs)

Stream frequency is the number of streams per unit area of the basin (Horton, 1945).It mainly depends upon the lithology of the basin and reflects the texture of the drainage network. The stream frequency of the study area is 2.60. An increase in stream frequency concerning an increase in drainage density has been noticed in all sub-study areas.

Drainage texture (Rt)

Horton (1954) defines drainage texture as the total number of segments all the order to perimeter of the area. The drainage texture of the pili river basin has a value of 6.17, falls under the moderate coarse drainage texture category. In present study shows the density is variable and suggests moderate coarse drainage texture.

Length of Overland Flow (Lo)

The length of overland flow is approximately equal to half of the average distance between the channels and reciprocal of the drainage density (Horton, 1945). The higher value of Lo is indicative of true relief, whereas the low value of Lo is indicative of high relief. The value of overland flow is found to be 0.82 indicating low relief.

Constant channel maintenance (C)

Channel maintenance constant is inversely proportional to drainage density. The constant of channel maintenance (C) depends on the slope of the basin, the nature of the rocks, and the duration of erosional activity. The C value of the study area is 0.41. Areas with a low value of constant channel maintenance are categorized as regions with close dissection and somewhat influenced by structural constraints. The large value of C signifies a higher infiltration rate and maturity to an old stage of the river.

Form factor (Ff)

Rf is the ratio of basin area to the square of the basin length and is a quantitative expression of drainage basin outline (Horton 1932). During the present study, the value of the form factor in the study area is 0.36 which indicates that the area is nearly circular.

Circulatory ratio (Rc)

It is influenced more by the length, frequency, and gradient of streams than the slope and drainage pattern of the basin (Strahler, 1957). It is a ratio, which indicates the stage of dissection in the study region. If, the Rc values approach 1, which indicates that, the basin shapes are circular with uniform infiltration for the present study the value of the circulatory ratio is found 0.47 and it indicates that, the basin is nearly circular.

Elongation ratio (Re)

Schumm (1956) defined elongation ratio as the ratio of the diameter of a circle of the same area as the drainage basin and the maximum length of the basin. The Re values generally range between 3.4 which shows the study area basin is elongated in shape.

Shape index (Sw)

The shape index of the area is 2.77. The shape index refers to the elongated basin with high peak discharge.

Texture ratio

The texture ratio is one of the most important factors in the drainage morphometric analysis, which depends on the underlying lithology infiltration capacity, and the relief aspect of the terrain. The texture ratio of the study area is 6.17.

Table: 3. Aerial aspect of the morphometric parameter of the study area

Parameters	Results
Drainage density (Dd)	2.41
Stream frequency (Fs)	2.60
Drainage texture (Rt)	6.17
Length of Overland Flow (Lo)	0.82 sq. km
Constant Channel Maintenance (C)	0.41
Form factor (Ff)	0.36
Circulatory ratio (Rc)	0.47
Elongation ratio (Re)	3.03
Shape index (Sw)	2.77
Texture ratio (T)	6.17
Compactness Coefficient (Cc)	0.04

3. Relief aspects

The relief aspect of drainage basins relates to the three-dimensional characteristics of the basin, including landform area, volume, and altitude, and involves the use of morphometric methods to determine the terrain characteristics of the basin. With the help of slope and DEM maps, we are able to calculate relief factors.

Basin relief (R)

Basin relief is a parameter that determines the stream gradient and influences, the flood pattern, and the volume of transported sediment (Hadley and Schumm, 1961). Basin relief understanding the denudational characteristics of the basin. The pili basin relief value is 295 m.

Relief ratio (Rh)

According to Schumm (1954) noted relief ratios can be calculated by multiplying the maximum basin length (Lb) by the basin relief 'H', resulting in a dimensionless ratio equal to the tangent of the angle formed by the intersection of two planes at the basin's mouth. An indicator of erosion intensity on a drainage basin's slope is the relief ratio, which measures the overall steepness of the drainage basin. The relief ratio for the exciting study is 11.19.

Relative relief (Rhp)

This term was given by Melton (1957) and in the present study, it is noted that the Pili basin area has maximum relative relief of 2.13.

Ruggedness number (RD)

It is the product of maximum basin relief (H) and drainage density (D) (Strahler, 1958). ruggedness number values are high which indicates the slope issteep and long as well. In the present study, the value of the ruggedness number is 0.79, which indicates a gentle slope of the area.

Melton Ruggedness Number (MRn)

According to Melton (1965), the MRn is calculated by using the total basin relief divided by the total basin area of the watershed in which the basin is located. The Melton Ruggedness Number of Pili Basin is 0.68.

DEM (Digital Elevation Model) Map

In the study area, a DEM map was prepared based on the 30-meter resolution of ASTER DEM data. DEM map shows the elevation of the study area, the highest point is 640 m on elevation and the lowest point is 340 m on elevation. The DEM map is shown in fig. 4.

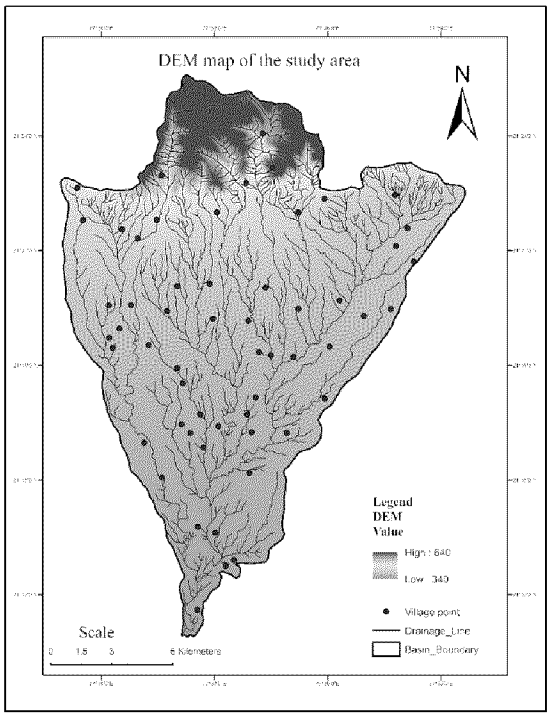

Figure 4: DEM map of the study area

Table 4: Relief parameters of the Pili basin

Parameters	Results
Height of basin mouth (z)	340 m
Height of highest point of the basin (Z)	635 m
Basin relief (R)	295 m
Relief ratio (Rh)	11.19
Relative relief (Rhp)	2.13
Ruggedness number (RD)	0.79
Melton Ruggedness Number (MRn)	0.68

Conclusion

The present study demonstrates that remote sensing techniques and GIS play a vital role in the study of Morphometric analysis of the Pili River Sub-tributary of Sapan River. The morphometric analysis studies are helpful for the occurrences of the porous and permeable zone in the rock formation and morphometric studies direct control of groundwater movement and occurrences. The result of the analysis shows that the Pili River has a dendritic drainage pattern

and 6th order basin. It Indicates homogenous lithology and variations in the values of Rb among the study area attributed to the difference in topography and geometric development. In all areas of the study, the Fs values demonstrate a positive correlation with the Dd values, indicating an increase in the stream population, which is related to an increase in drainage density. On the other hand, the values of Dd indicate that the region has highly permeable subsoil, dense vegetation, and low relief, indicating a highly permeable subsoil. Drainage texture varies from very coarse to fine and shape parameters of the study area viz; Re, Rc, and Rf values indicate that the Pili River basin is more or less elongated. Relief aspects and visual interpretation of the DEM of the study area indicate gentle to moderate slope, low runoff, and high infiltrations.

References

1. Altaf F, Meraj G, Romshoo AS (2013). Morphometric analysis to infer the hydrological behaviour of Lidder Watershed, Western Himalaya, India. Geography J 2013:1–14
2. Bhatt S.C., Rubal Singh, Rahul Singh, Mohd Saif, and M. M. Singh (2021). GIS-based Approach for Morphometric Analysis of Jamini Basin and Its Sub watersheds: Implication for Conservation of Soil and Water Resources. Geological and Geo-Environmental Processes on Earth pp 243–257, Springer Natural Hazards, https://doi.org/10.1007/978-981-16-4122-0_16
3. Chandrashekar H, Lokesh VK, Sameena M, Roopa J, Ranganna G (2015). GIS based morphometric analysis of two reservoir catchments of Arkavati River, Ramanagaram District, Karnataka. International Conference on water resources, Coastal and Ocean Engineering (ICWCOE2015). Aquat Procedia 4:1345–1353
4. Forkuor, J. and Maathuis, B. (2012). Comparison of SRTM and ASTER Derived Digital Elevation Models over Two Regions in Ghana—Implications for Hydrological and Environmental Modeling. In: Piacentini, T. and Miccadei, E., Eds., Studies on Environmental and Applied Geomorphology, In Tech, London, Chapter 9, 219-240.
5. Gautam, P.K., Singh, D.S., Kumar, D., Singh A.K. (2020). A GIS-based Approach in Drainage Morphometric Analysis of Sai River Basin, Uttar Pradesh, India. J Geol Soc India 95, 366–376. https://doi.org/10.1007/s12594-020-1445-9
6. Horton, R.E. (1932). Drainage basin characteristics Trans. Am. Geophys. Union, v. 13, pp. 350-361.

7. Horton, R.E. (1945). Erosional development of streams and heir drainage basins. Bulletin of the Geological Society of America, 56, 275-370
8. Jensen SK (1991). Applications of hydrologic information automatically extracted from digital elevation models. Hydrol Process 5(1):31–44
10. Kaushik P and Ghosh P (2015). 3D DEM delineation of Chambal river basin from SRTM data using remote sensing and GIS technology. Int J Remote Sens Geosci 4(4):1–6
11. Kaushik P and Ghosh P (2018). Morphometric analysis of Shipra River sub-basin, India, remote sensing and GIS approach. Int J Creat Res Thoughts 6(1):1536–1546
12. Kumar, Bijendra & Tripathi, Anshuman. (2018). A GIS-based approach in drainage morphometric analysis of Rihand River Basin, Central India. Sustain. Water Resour. Manag.. 4. 10.1007/s40899-017-0118-3.
13. Magesh N.S., Chandrasekar N. and Soundranayagam J.P. (2011). Morphometric evaluation of Papanasam and Manimuthar watersheds, parts of Western Ghats, Tirunelveli district, Tamil Nadu, India: a GIS approach. Environ Earth Sci 64(2): 373-381
14. Melton, M.A. (1958). Correlating the structure of morphometric properties of the drainage system and their controlling agents.Jour. Geol., v. 66, pp. 442-460.
15. Miller, V.C. (1953). A quantitative geomorphic study of drainage basin characteristics in the Clinch Mountain area, Virginia and Tennessee, Proj. NR 389-402, Tech Rep 3, Columbia University, Department of Geology, ONR, New York.
16. Moharir, Dr. Kanak & Pande, Dr. Chaitanya & Varade, Abhay & Pande, Rajeshwari. (2017). Morphometric analysis in Koldari watershed of Buldhana district (MS), India using geoinformatics techniques. Journal of Geomatics. 11 (1).
17. Pankaj A, Kumar P (2009). GIS-based Morphometric Analysis of five major-watersheds of Song river, Dehradun District, Uttarakhand with special reference to landslide incidences. J Indian Soc Remote Sens 37:157–166
18. Pareta K, Pareta U (2011). Quantitative morphometric analysis of watershed of Yamuna basin, India using ASTER (DEM) data and GIS. Indian Journal Geomatics Geosciences 2(1):248–269

19. Pareta K, Pareta U (2012). Quantitative geomorphological analysis of watershed of Ravi River basin, HP India. Int J Remote Sensing GIS 1:47–62
20. Patel A, Katiyar KS, Prasad V (2016). Performances evaluation of different open source DEM using differential global positioning system (DGPS). Egypt J Remote Sens Space Sci 19(1):7–16
21. Pophare AM, Balpande US (2014). Morphometric analysis of Suketi river basin, Himachal Himalaya, India. J Earth Syst Sci 123:1501–1515
22. Prakash K, Mohanty T, Singh S, Chaubey K, Prakash P (2016) Drainage morphometry of the Dhasan river basin, Bundelkhand craton, central India using remote sensing and GIS techniques. Journal of Geomatica 10:21–132
23. Prakash K, Rawat D, Singh S et al (2019). Morphometric analysis using SRTM and GIS in synergy with depiction: a case study of the Karmanasa River basin. North Central India Apply Water Sci 9 (1):13. https://doi.org/10.1007/s13201-018-0887-3
24. Prakash K, Singh S, Mohanty T, Chaubey K, Singh CK (2017) Morphometric assessment of Gomati river basin, middle Ganga plain, Uttar Pradesh, North India. Spat Inf Res 25:449–458
25. Sahu N, Reddy O, Kumar N et al (2016). Morphometric analysis in basaltic terrain of central India using GIS techniques: A case study. Appl Water Sci. https://doi.org/10.1007/s13201-0160442-z
26. Samal DR, Gedam SS, Nagarajan R (2015). GIS based drainage morphometry and its influence on hydrology in parts of Western Ghats region, Maharashtra. India. Geoc Int 30(7):755–778
27. Sangita Mishra.S. and Nagarajan, R., (2010). Morphometric analysis and priotization of sub- watersheds using GIS and Remote Sensing techniques: a case study of odisha, India, International Journal of Geomatics and Geosciences Vol 1, No3. pp501-510.
28. Sarmah K, Jha LK, Tiwari BK (2012) Morphometric analysis of a highland micro watershed in East Khasi Hills District of Meghalaya, India: using remote sensing and geographic information system (GIS) techniques. J Geol Reg Plan 5:142–150
29. Schumm SA (1956) Evolution of drainage systems and slopes in Badlands, at Perth Amboy, New Jersey. Geol Soc Am Bull 67:597–646

30. Shelar RS, Shinde SP, Pande CB, Moharir Kanak N, Orimoloye Israel R, Mishra Arun P, Varade Abhay M (2022). Sub-watershed prioritization of Koyna river basin in India using multi criteria analytical hierarchical process, remote sensing and GIS techniques. Physics and Chemistry of the Earth, Parts A/B/C. Elsevier, Volume 128, December 2022, 103219. https://doi.org/10.1016/j.pce.2022.103219
31. Singh S, Kanhaiya S (2015) Morphometry of the Barakar river basin, India: a remote sensing and GIS approach. Int J Curr Res 7(7):17948–17955
32. Strahler A. N (1957) Quantitative analysis of watershed geomorphology. Trans Am Geophys Union 38:913–920
33. Strahler AN (1952) Hypsometric Analysis of Erosional Topography. Bulletin of the Geological Society of America 63:1117–1142
34. Strahler AN (1956) Quantitative Slope Analysis. Bulletin of the Geological Society of America 67:571–596
35. Strahler, A.N., (1964).Quantitative geomorphology of drainage basins and channel networks In. Handbook of Applied Hydrology:39–76, McGraw Hill Book Company, New York, Section 4-II, (9).
36. Vandana M (2013) Morphometric analysis and watershed prioritization: a case study of Kabani river basin, Wayanad district, Kerala, India. Indian J Geo-Mar Sci 42:211–222

21. A Study of Lineaments or Fracture Zones Regime of Ground Water Potential in Katepurna River Basin, Akola District, Maharashtra, India

Dr. S. S Deshmukh
Ghulam Nabi Azad Arts, Commerce and Science College, Barshitakli, Dist. Akola.
Dr. Tejas R. Patil
Ghulam Nabi Azad Arts, Commerce and Science College, Barshitakli, Dist. Akola.
Dr. G. D. Gaikwad
Shri Shivaji Arts, Commerce and Science College, Akola.
P. P. Pali
Shri Shivaji Arts, Commerce and Science College, Akola.

Abstract

This investigation determines the ground water potential zone of in Katepurna River Basin, Akola district in Maharashtra were individually demarcated and their area computed, with the aided by using remote sensing & GIS mapping. Satellite imagery and landsat image of the study area shown that small lineaments 20-22 and big lineaments 15-18 which have S-N and E-W trend which appear to have been emplaced in fracture zones. Length of these lineaments ranges from varies lengths with width. Bore wells constructed on and near the lineaments show that vertical extension depth ranges from 30m to 60m bgl. Similarly number of high yielding borewell and dug well fall on straight line which is actually the lineaments of fracture zone trend in study area. It is also commonly seen that the fracture zones generally have dance vegetation cover, irrigation, etc. than other areas. Thus their cumulative ground water capacity or ground water potential is very high in this study area along the lineaments or fracture zone. Our secondary objective is to cement a link between the fracture zone and the infiltration zones of deep aquifers, to establish its impotence in the hydrodynamic functioning of hydrogeological system. Samples collected from various bore wells that were used for drinking purposes.

Keywords: DEM data, GIS, LANDSAT 8, lineaments, infiltration.

Introduction

Water plays a vital role in the development of any activity in the area. Thus the availability of surface and ground water governs the process of planning and development. The surface water resources are inadequate to fulfill the water demand. Productivity through

groundwater is quite high as compared to surface water, but groundwater resources have not yet been properly developed through exploration. Keeping this in view, the present study attempts to select suitable locations for groundwater exploration in hard rock areas using an integrated approach through field investigations, geomorphological, petrographic, geochemical, stratigraphic, remote sensing, geoelectrical soundings and GIS techniques. Lineaments typically refer to the prominent features or characteristics of something, wuch as the distinguishing features of a face or the main elements of a system. Watershed management is the process of creating and implementing plans, programs, and projects to sustain and enhance watershed function that affect the plant, animal, and human communities within a watershed boundary. Features of a watershed that agencies seek to manage include water supply, water quality, drainage, storm water runoff, water rights and the overall planning and utilization of watersheds. Landowners, land use agencies, storm water management experts, environmental specialists, water use surveyors and communities all play an integral part in the management of a watershed. Ground water has and would continue to pay a crucial role for food and fodder production, drinking water supply, drought mitigation and economic development of the country. The ground water being relating to subterranean resource, it needs to be explored through sub surface techniques of ground water exploration.

Study Area

The study area, Katepurna River basin is located within the Akola district of Maharashtra covered under the Survey of India toposheet nos.55H/2, H/3, H/5 and H/6 and bounded by latitude 20° 25" - 20°47" 50’ and longitude 77° - 77° 25”. The Akola district falls in the Western part of Vidarbha region and it is bounded by Amravati in the East, Washim in the South and Buldana in the West (Fig 1.1).

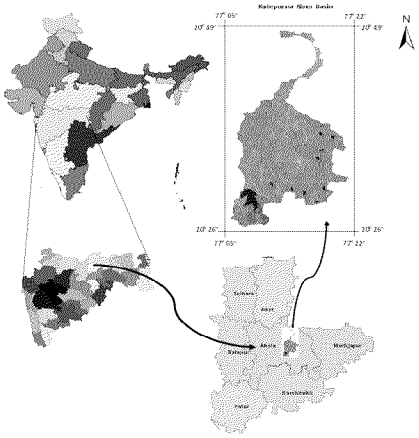

Fig. 1 Location Map of Study Area

Results and discussion

Delineating lineaments is the initial step in defining the intricate groundwater potential in the crystalline terrain of the basaltic region. Remote sensing data provides spectral and spatial coverage of the study area, offering cost-effective information on the various factors that govern groundwater movement and occurrence.

Geomorphologic studies have demonstrated the presence of five distinct landforms namely shallow dissected plateau, moderately dissected plateau, highly dissected plateau, undulations and valley fills. The shallow dissected plateau is characterized by the presence of thick weathered mantle ranging from 4 to 8 mtr with less dissection, and intersecting lineaments indicating a potential storage zone. The depth to water level ranges from 5- 10 m bgl during post monsoon and 12 – 18 m bgl. In pre monsoon. The safe yield in the open dug wells various from 45 – 70 m/d with sustained discharge of over 3-5 hours indicating pheratic and confined to semi confined aquifer conditions. The moderately dissected plateau occurs along the fringes of steep scarps indicating moderate thickness of the weathered horizons showing 3-5m. The bed rock is shallow and depth to water level various from 3-8 m bgl with moderate water bearing horizons depending upon the placement of interflow zone suggesting the recharge nature and higher hydraulic potential. The highly dissected plateau is characterized by the presence of compact and massive lava flows showing intricate network of dissection. The availability of groundwater is scare due to negligible weathered mantle except where the top portion is either altered or due to the presence of vesicular horizon, which may retain some groundwater.

The lineaments gives the results as presented in Fig. 2. This concerns the study area to better illustrate the automatically extracted lineaments. The obtained results from the satellite image interpretation are discussed to reveal the applicability of remote sensing in the mapping and analysis of lineament with a view to delineating zones that are suitable for groundwater development in the study area. The lineament map generated from the study area was used as a confirmatory tool on the possible reasons for general low groundwater yield in the area. The map provides necessary information, for a better understanding of how the interrelationship could be a major contributing factor to the groundwater prospect of the area. The lineaments are oriented in the SN and EW direction, especially for the macro structures which account for about 2 to 4% of the structures. These macro structures occur mainly at the SN end to the EW part of the study area with length varies meter to km. On the basis of above finding, a bore well and dug well highly potential along lineaments or fracture zones. This lineaments may act as a good aquifer which could be tapped through bore well and dug well.

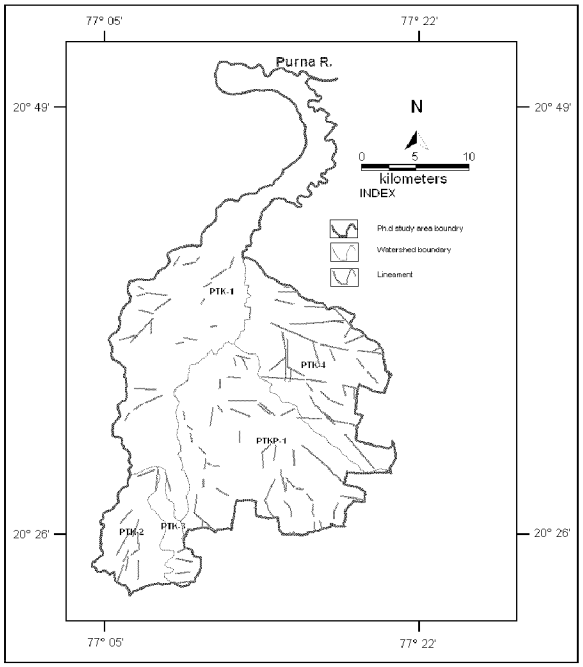

Fig. 2 Lineament Map of the Study area

Conclusion

The use of GIS and remote sensing in the research of productive aquifers in the study area, allowed us to make some observations on the optimization of the positioning of water drillings in this region. The results show that this area has been affected by intense tectonic activity. The structural lineaments of the region are mostly "North- south and East -west" direction. Many additional details can be extracted from radar interferometry images such as SRTM. We mean the topography, lineaments and watersheds that will play an important role in the choice of the high flow water-drilling site. We got good results that can serve as a guide or decision-making tools for future field investigations in the study area. The results obtained after satellite image processing are reliable and are close to the reality of the field. That is why satellite images are therefore a privileged tool for acquiring information capable of assisting decision-makers. It is concluded that the lineament and drainage pattern play a significant role in the groundwater development of this study location and may be responsible for the generally low groundwater prospect in the study area. The lineaments intersection results and the drainage pattern orientation explained the cause of failure/low yield of the wells/borehole in the area. This phenomenon is due to huge disagreement between the lineament and surface water flow direction. Most of the lineaments are in north-south and eastern-western direction while the drainage orientation is in east west direction, arising from this, large number of the available structures do not interact effectively with the surface water and therefore liable to dry up in the

dry season. In other words, the area with ineffective interaction between the lineament and drainage system showed low groundwater potential while area with reasonable interaction displayed moderate to high groundwater potential. North-western part, central part and some part of the southern region of the study area are characterized with high groundwater potential while the remaining part are characterized with moderate groundwater potential except small portion to the south-western part which is of low groundwater potential.

References

- Adyalkar P.G. 1984. "Hard rock hydrogeology in Indian Scenario, Presidential address, section of Geology of Geography, 71st session, Ind. Sci. Cong., Ranchi; pp. 52.
- Adyalkar, P.G., Ayyangar, R.S., Tikekar, S.S. and Khare, Y.D. (1996). Groundwater potential of Deccan Flood Basalt of Nagpur District in Maharashtra: An imprint derived from satellite imagery In Deccan basalt, Gondwana Geol. Soc. Sp. Vol. 2, pp. 485-492.
- Alexander, P. 0., 1981. Age and duration ofDeccan Volcanism: K - Ar evidence. Mem. Geo. Soc. India, Vol. 3, pp. 244-258
- Alexander, P.O., 1981. Age and duration of Deccan Volcanism : K-Arevidence. Mem. Geal. Sac. India, Val. 3, pp. 244-258.
- Aliden, J, B, 1949. Dyke in Western India - A discussion of their relationship with the Deccan Traps. Trans. Nat. Inst. Sci. Ind., Vol :3, pp. 123-157.
- Allegre C.J. M. Trevor, J.F. Minster, B. Minister and F. Albarede 1977, Systematic use of trace elements in igneous processes. Contrib. Mineral Petrol. Vol : 60 pp. 55-75.
- Baker, B.H., Goles, G.C., Leeman, W.T. and Lindstorm, M.M., (1977). Geochemistry and petrogenesis of a basalt-Bemoreite Trachyte suit from the southern part of the Gregory Rift. Keneya. Contrib. Mineral. Petrol., Vol:64, pp.303302.
- Baker, B.H., Goles, G.C., Leeman, W.T. and Lindstrom, M.M., 1977. Geochemistry and Petrogenesis of a Basalt-Benmoreite Trachyte Suite from the southern part of the Gregory Rift, Kenya. Contrib. Mineral. Petrol., Vol: 64, pp.303-332.
- Balasubramanium, A., Thiruganana Sambandan, R., Chellaswamy, R. and Sastry, J. C. V. 1989. Digital modelling of the hydrogeochemical facies of groundwater of Tamilnadu, India. Int. Nat. Workshop on Appropriate Methodologies of GWRM. Hyderabad, Vol. II. pp. 761-767.

- Cain D., Helsel, D.R. and Regone, S. E. (1989). Preliminary evaluation of regional groundwater quality in relation to land use. Groundwater, v.27, pp.230-244.
- Cambell, I.H., 1977. A studyofMacro-rythmic layering and cumulate process in the Jimberlana intrusion, Western Australia: The upper layered series Petrol. Vol.l8, pp. 183-215.
- Canter A.D,, Palmer R.C. and Monkhous R.A., 1987. Mapping the vulnerability of groundwater to pollution from agriculture practice, particularly with respect to nitrate. In: Vulnerability of sol and groundwater to pollutants (W.van Duijvendooden and II.G. Van Waegcningh. cd.s.). TNO committee on hydrogeological research. The Hague, nroceeding and inlomialion No. 3H, pp. 333-342.
- Chandra, S., Anand Rao, V. and Singh, V. S., A combined approach of Schlumberger and axial pole–dipole configurations for groundwater exploration in hard-rock areas. Curr. Sci., 2004, 86, 1437–1443.
- Ihekoronye, A. I., & Ngoddy, P. O. (1985). Integrated food science and technology for the tropics. Macmillan.
- Mahanta, C., Enmark, G., Nordborg, D., Sracek, O., Nath, B., Nickson, R. T., & Bhattacharya, P. (2015). Hydrogeochemical controls on mobilization of arsenic in groundwater of a part of Brahmaputra river floodplain, India. Journal of Hydrology: Regional Studies, 4, 154-171.
- Oladipo, I. C., & Adeboye, O. A. (2015). Physico-chemical and bacteriological analysis of well water used for drinking and domestic purposes in Ogbomosho, Nigeria. International Journal of Current Microbiology and Applied Sciences, 4(9), 136-145.
- Pandey, V. P., Chapagain, S. K., & Kazama, F. (2010). Evaluation of groundwater environment of Kathmandu Valley. Environmental Earth Sciences, 60, 1329-1342
- Rao, S. M., & Mamatha, P. (2004). Water quality in sustainable water management. Current science, 942-947.
- Tebutt, T. H. Y. (1983). Principles of quality control. Pergalmon, England, 235.

22. Viscometric Studies of 1-Phenyl-3-[4-(3-Allylimino-1,2,4-Dithiazolo) Aminophenyl]-Prop-2-Ene-1-One At Various Molar Concentrations and At 250c in 70 % Ethanol–Water Mixture

S. S. Padhena
Department of Chemistry, Rajarshee Shahu Science College,
Chandur Railway, Dist. Amravati.
S. A. Waghmareb
Department of Chemistry, Ghulam Nabi Azad Arts, Commerce & Science College,
Barshitakli, Dist. Akola.

Abstract

Present research comprises the viscometric study of 1-phenyl-3-[4-(3-allylimino-1,2,4-dithiazolo)aminophenyl]-prop-2-ene-1-one, at different molar concentrations (0.1M, 0.05M, 0.025M and 0.012M) by keeping constant temperature (250C) in 70 % ethanol-water system. This viscometric investigations help to study the solute–solute, solute-solvent interactions of solute with solvent and effect of dilution of solvent. This investigation directly gave the information regarding to the pharmacodynamic of this drug.

Keywords: 1,2,4-dithiazolo, ethanol-water mixture, viscometric measurements.

Introduction

The viscosity of a fluid is a measure of its resistance to gradual deformation by shear stress or tensile stress. The technique of viscosity measurements plays a vital role in pharmaceutical, industrial, medicinal, agricultural, biochemical and drug sciences. The viscosity measurement of solution provides brief information regarding molecular weight of the solute, solute-solute, solute-solvent and solvent-solvent interactions. Hence, Viscosity measurement is very essential to know the constituents and arrangement of any molecule. The number of in vivo activities of the drug like absorption, transmission and its effect will directly relate to viscosity measurements and solvent interactions in the human anatomy. Study of the viscosity measurements is user-friendly, sensitive and precise.

The major role of viscosity measurement is in the study of various interactions between solute and solvent. Polar solute readily dissolves in water resulting strong interaction between solute and solvent, hence cause structuredness. While, non-polar solute does not dissolves in

water readily. Determination of viscosity of an electrolyte in a solution is a smart way to obtain data on solute-solute and solute-solvent interactions. We know that, drug's activity and viscosity is concerning with drug-receptor interactions. The electrolytic interactions in liquid binary mixtures explained in terms of β-coefficient of viscosity

Several numbers of properties provide information about the nature of liquid. Viscosity is one of the important physical properties of liquids and solutions. Aqueous and non aqueous solutions are the bulk phenomena. Bulk Phenomena involves various types of interactive forces. It also provides brief information about aqueous and non aqueous solute-solute and solute-solvent interactions and information regarding the transport property of the drugs and ion-solvent interactions.

1-phenyl-3-[4-(3-allylimino-1,2,4-dithiazolo)aminophenyl]-prop-2-ene-1-one nucleus containing drug create their own identity and importance in drug and pharmaceutical chemistry. Accounting all these things it became very interesting to carry out the viscometric measurements of 1-phenyl-3-[4-(3-allylimino-1,2,4-dithiazolo)aminophenyl]-prop-2-ene-1-one at various concentrations (0.1M, 0.05M,0.025M and 0.012 M) by keeping constant temperature(25^0C) in 70% ethanol-water system. This investigation helps to examine the pharmacodynamic and pharmacokinetic of the drug.

Materials and Methods

Experimental

All chemicals used in investigation are AR grade. Solutions prepared fresh at each experiment. In this work, all solutions are prepared by using double distilled water. Mechaniki Zaktady Precyzyjnej Gdansk balance (Poland make [±0.001gm]) is used for taking weights and density is measured by Bicapillary method (Internal diameter of bicapillary is of 1 mm). Viscosity measurements are carried out by Ostwald's viscometer. Elite themostatics water bath is used for temperature maintenance. Ample time was allowed to attain thermal equilibrium in between viscometer and water bath.

Present research work is carried out for the viscometric measurements of 1-phenyl-3-[4-(3-allylimino-1,2,4-dithiazolo)aminophenyl]-prop-2-ene-1-one, at different molar concentrations (0.1M, 0.05M, 0.025M and 0.012M)by keeping constant temperature (25^0C) in 70 % ethanol-water system .The viscometric readings were taken as described in literature.

Observations and Calculations

The molecular interactions values in terms of β-coefficient of drugs obtained by viscometric investigation data, which is tabulated in following manner. The result obtained was

mentioned in **Table No. 1**. According to Jone's-Dole equation, $(\eta r-1)/\Gamma C = A+\beta\Gamma C$ at different concentration and different percentage. A and β-coefficient values calculated and are enlisted in **Table No.2.**

Table No.1

Viscosity Measurements At Different Concentrations And Determination Of Relative And Specific Viscosities At Different Concentrations At 25^0c

Medium - 70% Ethanol-Water

Temp T(°C)	Conc. C (M)	√C	Time t (sec.)	Density ρx10^{-3} (kg.cm $^{-3}$)	ή$_r$	ή$_{sp}$=ή$_r$-1	(ή$_r$-1)/√C (pa-s)
25	0.100	0.3178	472	2.05442	2.4235	1.4812	3.65855
	0.050	0.2476	356	2.05120	2.5214	1.2014	3.40125
	0.025	0.2225	342	2.65205	2.2014	1.0915	3.28952
	0.012	0.2104	482	2.42512	2.1214	1.1252	3.09452

A and β Co-Efficient Values from Graphs for 70%

TABLE NO.2 - FOR [1-phenyl-3-[4-(3-allylimino-1,2,4-dithiazolo)aminophenyl]-prop-2-ene-1-one]

W-E Mixture(%)	Temp° C	Mean "A"	β (Slope "m")
70	25	3.3849	-3.1524

Graphical Representation

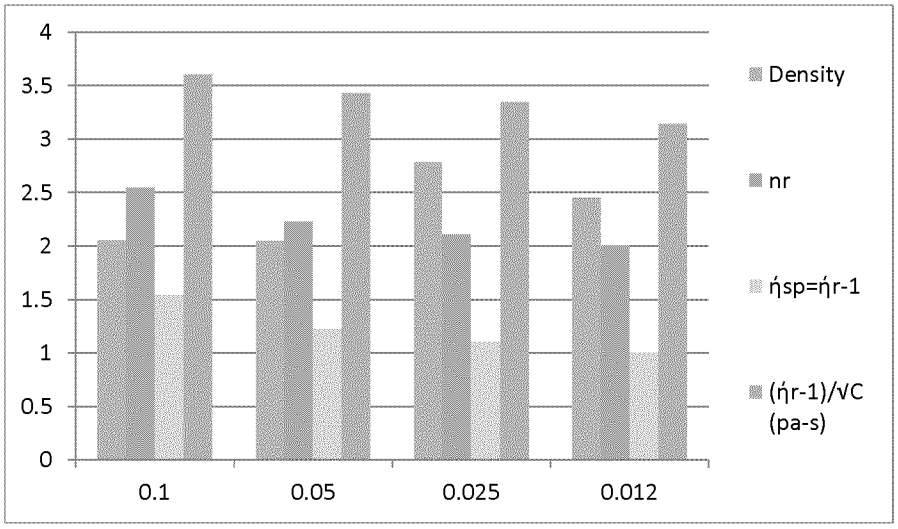

Result and Discussion

The relative viscosity was determined by using following formula

η_r = Ds x ts / Dw x tw

And the relative viscosities have been analyzed by Jone's-Doles equation as ,

$(\eta r-1)/\Gamma C = A+\beta\Gamma C$

The graphs are plotted between $(\eta r-1)/\Gamma C$ versus ΓC. The graph for each system gave linear straight line gave value of β-coefficient.

Conclusion

In present investigation it is concluded that at constant temperature the density and relative viscosity of drugs decreases along with decreasing concentration as (0.1M, 0.05M, 0.025M and 0.012 M).When concentration decreases the number of solute molecules in solution decreases simultaneously increases percentage of solvent molecule as a result solvation effect increases . From this investigation we can examine the pharmacodynamic of drug. The potency of these drug can be increased by substituting different substituent on the parent drug.

References

1. D.M.Tigellar, A.E.Palker, C.M.Jackson, K.M.Anderson, J.W. Ight and R.F. Savinell, Macromolecules, 2009, 42(06), 1888.
2. A. Pal and S. Kumar, J. Indian Chem. See., 2004, 81, 1019.
3. F Saleem. Eur. Pot., CHAPPL, 2008, 87, 19.
4. M. Imran, T. Kokab, S. Latif, M. Liviu and Z.Mahmood. J.Chem.Soc.Pak. 2010, 32(2), 223-228.
5. W.A.L. Izonfuo and C.C. Obunwa, Ind.J.Chem. 1999, 38A, 939.
6. A.H.F. Abd El-Waheb, A.H. Bedair, F.A.Eid, A.F.El-Haddad, A.M.Adawy El-deeb, Journal of Serbian Chemical Society, 2006, 71(5), 471-481.
7. U.N.Dash and S.Supkar, Proc.Ind.Acad.Sci.Chem.Soc. 1995, 107,541.
8. E.A.Gonna and B.M, Al-Jahadalli, Am.J.Condenced Matter Physics, 2012, 2(1), 16-21.
9. J. Singh, T. Kaur, V. Ali and D.S. Gill, J. Chem. Soc, Faraday Tram., 1994, 90(4), 579.
10. B.B. Baldaniya and P.K. Patel, E-Journal of Chemistry, 2009, 6(3), 673-680.
11. H.K. Semwal, S.C. Bhatt and B.S. Semwal, J. Pure Appl. Ultrason., 2003, 25, 6.
12. G. Jones and M. Doles, Journal of American Chemical Society, 1929, 51, 2950.
13. M.N. Roy, D.Nandi and D.K. Hazra, J.Ind.Chem.Soc. 1993, 70,121.
14. Parajuli R. and Medhi C., Journal of Chemical Sciences, 2004, 116(4), 235-241.
15. Solanki and I. Thakur, Indian Journal of Chemistry, 2007, 45B, 517.

International Journal of Scientific Research in Science and Technology
Available online at : www.ijsrst.com
OPEN ACCESS
Print ISSN: 2395-6011 | Online ISSN: 2395-602X
doi : https://doi.org/10.32628/IJSRST173876

$MnFe_2O_4$ Nanoparticle as a New and Magnetically Separable Nanocatalyst for Solvent-Free Synthesis of dihydropyrano[2,3-c] Pyrazole Derivatives

Santosh B. Gaikwad [1,2] and Kishore Puri [2*]

[1, 2]Department of Chemistry, Late Pundalikrao Gawali Arts and Science College, Shirpur (Jain), Washim – 444 504 (Maharashtra), India

[*2]Department of Chemistry, Shri Shivaji College of Arts, Commerce and Science, Akola – 444 003 (Maharashtra), India

*Corresponding Author: knpuri333@rediffmail.com

ARTICLEINFO

Article History:
Accepted: 22 Jan 2024
Published : 29 Jan 2024

Publication Issue :
Volume 11, Issue 1
January-February-2024
Page Number :
318-326

ABSTRACT

This study focused on synthesising $MnFe_2O_4$ (Manganese Ferrite) nanoparticles using the sol-gel method. We then applied these nanoparticles as a catalyst for synthesising dihydropyrano[2,3-c]pyrazole derivatives at a specific temperature. The significant advantage of this process is that it requires only short reaction times and no solvents. Additionally, the crude pyranopyrazole derivatives can be purified through a simple recrystallization process. The catalyst is reusable, magnetically separable and maintains its activity even after five uses. The chemical integrity of the catalyst was confirmed through FT-IR, ^{1}H NMR, and ^{13}C NMR techniques.

Keywords: Solvent-free synthesis, Magnetically separable, Manganese Ferrite, Pyranopyrazole, Nanocatalyst

I. INTRODUCTION

Multicomponent reactions (MCRs) are considered one of the best ways to synthesize heterocyclic compounds using simple and easily available materials. MCRs are highly efficient as they reduce the number of synthesis steps required to form complex compounds, which makes them time-saving and environmentally friendly. Therefore, there is a growing interest in designing new MCRs that follow the principles of green chemistry [1, 2]. Pyranopyrazole, which could be synthesized through a four-component reaction, is one of the most important types of oxygen–nitrogen heterocyclic compounds with lots of biological, pharmaceutical, and agrochemical applications. For instance, antimicrobial, antiplatelet, anti-inflammatory, antitumor, antibacterial, insecticidal, fungicidal, antitubercular agent, herbicidal, and inhibitor of human chk1 kinase, as well as UV absorber are some of the important activities of pyranopyrazole and its derivatives (Fig. 1). Because of the great importance and numerous utilizations of

Copyright © 2023 The Author(s): This is an open-access article distributed under the terms of the Creative Commons Attribution **4.0 International License (CC BY-NC 4.0)** which permits unrestricted use, distribution, and reproduction in any medium for non-commercial use provided the original author and source are credited.

pyranopyrazole and its derivatives, modifying the procedure for its synthesis are at the top of scientific research [3, 4]. Using heterogeneous nanocatalysts to synthesize pyranopyrazole has attracted great importance among previous methods on account of high efficiency.

Manganese and ferric oxide are commonly used metal oxides due to their practical advantages such as being readily available, low cost, less toxic, and easy to synthesize. In recent times, binary metal oxide photocatalysts have gained significant attention for their efficient catalytic activity and stability in removing organic pollutants from the air and sewage [5-6]. Spinel structures with the formula AB_2O_4 are well-known materials for their ability to incorporate various ions into their crystal structure. In the $MnFe_2O_4$ structure, Mn^{2+} and Fe^{3+} are distributed in tetrahedral and octahedral sites respectively, which is a typical spinel structure. The corresponding general formula is written as $A_{tet}B_{2oct}O_4$ [7]. The high activity of this spinel compound is due to the high amounts of Fe^{3+} species and compositional homogeneity. Magnetic nanoparticles possess unique physicochemical properties and have attracted the attention of various researchers [8-10]. Spinel ferrite compounds show great potential as green heterogeneous catalysts in various organic functional group transformations and as catalytic supports [11-14].

Pyrano[2,3-c]pyrazoles are a type of heterocycles that have great potential for use in the pharmaceutical field. They exhibit a wide range of biological activities such as anti-inflammatory [15], anticancer [16, 17], inhibition of human Chk1 kinase [18], antimicrobial [19], and also as biodegradable agrochemicals [20]. It has been reported that pyrazoles play a vital role as essential synthetic intermediates [21]. One of the methods used for their production involves the base-catalyzed cyclization of 4-aryliden-5-pyrazolone [22]. However, new approaches have been developed for the synthesis of pyrazoles, including processes based on β-cyclodextrin[23], cinchona alkaloid derivatives[24], $Sc(OTf)_3$ [25], triethylamine [26], water or ethanol media [27, 28], imidazole [29], CuO/ZrO_2 [30] and triethyl benzyl ammonium chloride [31].

As part of our ongoing research into the development and use of nanoparticles and their application [32-35], we have decided to use these nanomaterials as a nanocatalyst in organic transformation. Hence, We used one of the new nanocatalysts for the synthesis of dihydropyrano[2,3-c]pyrazole derivatives under solvent-free conditions at specific temperature conditions. (**Scheme-1**).

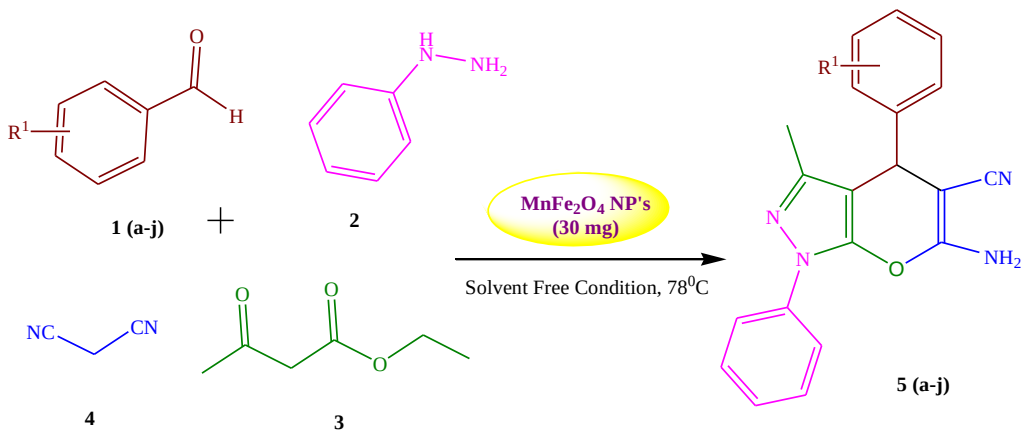

Scheme-1: Schematic representation of Manganese ferrite catalysed synthesis of dihydropyrano[2,3-c]pyrazole derivatives

II. METHODS AND MATERIAL

A) Materials:

All chemicals were purchased from Sigma-Aldrich and SD-Fine Chemical in Mumbai, India, and used without purification. All the aqueous solutions were prepared in distilled water.

B) Characterisation Methods:

Fourier transform infrared (FT-IR) spectra of dihydropyrano[2,3-c]pyrazole derivatives were recorded on the Shimadzu IR spectrophotometer. ^{1}H and ^{13}C NMR spectroscopy performed by Bruker Advance Neo 500 MHz NMR Spectrophotometer, SAIF, Chandigarh.

C) Synthesis of magnetic separable $MnFe_2O_4$ nanocatalyst:

The sol-gel method was employed to synthesize nanoparticles of manganese ferric oxide ($MnFe_2O_4$). The procedure involved dissolving 0.25 M of manganese chloride and 0.25 M of ferric chloride separately in 100 ml of distilled water. The solubility of manganese chloride and ferric chloride in water was improved by adding 0.1 N hydrochloric acid. Two solutions were mixed together with constant stirring. After the solutions were mixed, 1 gram of citric acid solution was added as a surfactant. The pH of the solution was then adjusted to be 8-8.5 (basic) using 3-3.5 ml of NH_4OH solution. The mixture formed a precipitate which was stirred constantly for an hour at room temperature. The mixture was then filtered using Whatman filter paper No. 42 and washed with deionized water 2-3 times. Finally, the obtained product was dried in an oven at 100°C for 2 hours. After drying, the material was calcinated for 3 hours at 500°C. The final product was a black precipitate, which was used as a magnificent for the synthesis of dihydropyrano[2,3-c]pyrazole derivatives.

D) Synthesis of dihydropyrano[2,3-c]pyrazole derivatives:

Magnetic separable $MnFe_2O_4$ nanocatalyst as catalyst (30 mg) was added and mixed to a mixture of aromatic aldehyde (1 mmol), malononitrile (1 mmol), ethyl acetoacetate (1 mmol) and phenylhydrazine (1 mmol) under solvent-free conditions at 78°C temperature for the suitable time. After completion of the reaction, which was identified by TLC (n-hexane/ethyl acetate: 8:2), the magnetically separable nanocatalyst was separated by external magnetic material and washed with aqueous ethanol. After confirmation of product formation, recrystallised from ethanol which resulted in precipitation of the desired dihydropyrano[2,3-c]pyrazole derivatives. All of the obtained product(s) are known and were identified by comparison of their physical data with those reported in the literature (see Table 1). Some of the synthesized compounds were characterized by IR and NMR data. Given below are spectral data for some selected pyranopyrazole derivatives.

E) Spectral data analysis for compounds:

6-Amino-3-methyl-4-(4-nitrophenyl)-1-phenyl-1,4 dihydropyrano[2,3-c]pyrazole-5-carbonitrile ***(5c)****:*

^{1}H NMR (500 MHz, DMSO-d6): δ = 8.21 (d, J = 8.8 Hz, 2H), 7.72 (d, J = 8.4 Hz, 2H), 7.51 (d, J = 8.8 Hz, 2H), 7.43 (t, J = 7.6 Hz, 2H), 7.21 (s, NH2), 7.16 (t, J = 6.4, 1H), 4.91 (s, 1H), 2.35 (s, 3H) ppm. **^{13}C NMR (500 MHz, DMSO-d6):** δ = 168.85, 159.62, 150.28, 145.80, 144.33, 142.49, 133.49, 128.80, 125.87, 123.91, 120.49, 97.43, 67.69, 33.13, 13.90 ppm. **FT-IR (KBr):** $\bar{\nu}$ = 3227, 2921, 2193, 1685, 1566, 1506, 1415, 1347, 1267, 1105, 847 cm^{-1}.

III.RESULTS AND DISCUSSION

The study investigated the impact of $MnFe_2O_4$ magnetic nanoparticle catalyst with different concentrations (10-30 mg) on the one pot four-component reaction of substituted benzaldehyde, phenylhydrazine with Malononitrile and ethyl acetoacetate under various conditions (**Table 1**). The

results clearly indicate that the best yield of 6-amino-3-methyl-1, 4-diphenyl-1, 4-dihydropyrano[2,3-c]pyrazole-5-carbonitrile (5a) was achieved by carrying out the reaction in the presence of 10 mol% of $MnFe_2O_4$ magnetic nanoparticle without solvent. (**Table 1, run no. 8**). The yield increased as the catalyst load was raised from 10 to 30 mg, while with the use of larger amounts of the catalyst (35 mol %), the yield of the product remained the same.

Table 1:

Synthesis of dihydropyrano[2,3-c]pyrazole (**5a**) using different conditions with different concentrations of Manganese ferrite nanocatalyst at 78°C temperature.

Sr. No.	Solvents	Catalyst (mg)	Time (min)	Yield (5a)
1.	DCM	10	68	58
2.	CH_3CN	10	74	64
3.	THF	10	46	67
4.	H_2O	10	49	70
5.	EtOH	10	40	74
6.	Solvent-free	10	37	80
7.	Solvent-free	20	30	90
8.	Solvent-free	30	22	98
9.	Solvent-free	40	21	98

After optimizing the reaction conditions, we aimed to investigate the efficiency and scope of a procedure that resulted in the production of numerous dihydropyrano[2,3-c]pyrazole derivatives. This was achieved through a one-pot four-component condensation reaction involving substituted benzaldehyde, phenylhydrazine, Malononitrile, and ethyl acetoacetate. The reaction was catalysed by a small amount of $MnFe_2O_4$ magnetic nanoparticle catalyst and carried out under solvent-free conditions. The results are displayed in **Table 2**. The impact of substituents on the aromatic ring was evaluated in terms of yields under these reaction conditions. Both types of aromatic aldehydes, including those with electron-releasing and electron-withdrawing substituents on their aromatic ring, produced the desired products in high to excellent yields in a short reaction time. The reaction time of aromatic aldehydes with electron-withdrawing groups was faster than those with electron-donating groups. Moreover, the recyclability and reusability of the catalyst were also considered in the condensation of benzaldehyde, phenylhydrazine, Malononitrile, and ethyl acetoacetate. Similarly, the magnetic nanoparticle catalyst was separated and reused for an alternative reaction.

TABLE 2:

Synthesis of numerous dihydropyrano[2,3-c]pyrazole derivatives using 30 mg of manganese ferrite nanocatalyst with solvent-free reaction conditions at 78°c temperature.

Sr. No.	Aldehyde	Product (5a-5h)	Time (min)	Yield (%)	Melting Points (°C)	
					Found	Reported
1.	Benzaldehyde	5a	21	98	170-173	(169-171) [36]
2.	4-Methoxybenzaldehyde	5b	23	91	173-175	(174-176) [37]
3.	4-Nitrobenzaldehyde	5c	14	95	196-198	(197-198) [38]
4.	2-Chlorobenzaldehyde	5d	12	98	138-140	(140-142) [36]
5.	4-Chlorobenzaldehyde	5e	17	95	173-176	(175-178) [36]
6.	4-Hydroxybenzaldehyde	5f	28	89	211-214	(213-215) [39]
7.	4-Methylbenzaldehyde	5g	39	85	168-170	(170-171) [38]
8.	4-Bromobenzaldehyde	5h	18	93	181-185	182–184 [40]

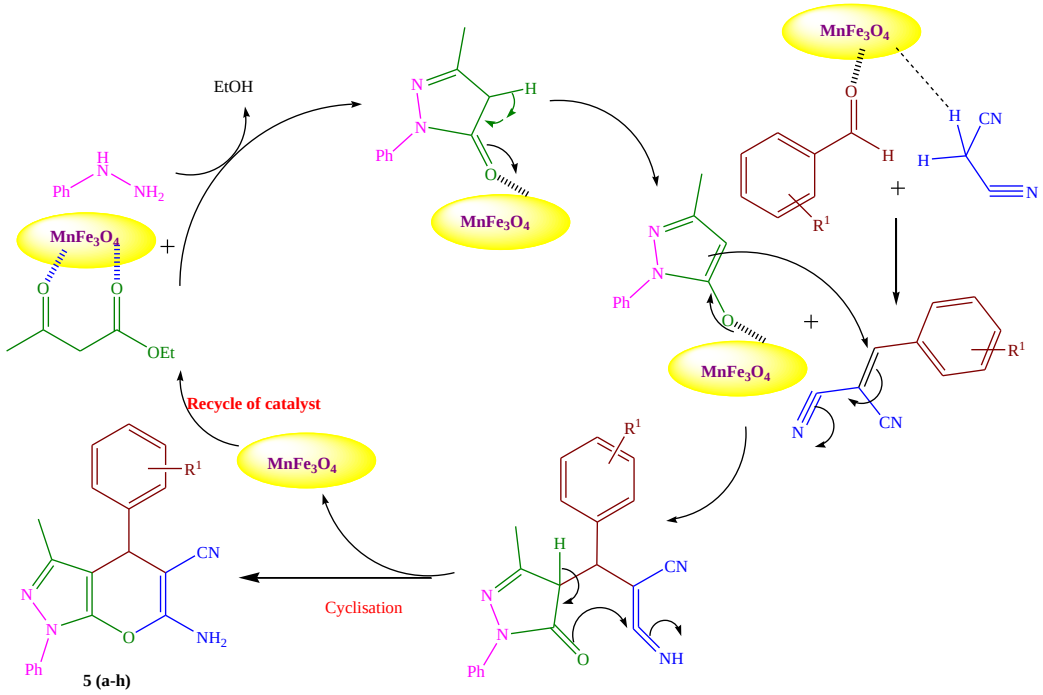

Scheme 2: The probable mechanism for the synthesis of dihydropyrano-[2,3-c]-pyrazole derivatives using the magnetically separable $MnFe_2O_4$ catalyst

In addition to performing a one-pot four-component reaction of substituted benzaldehyde, phenylhydrazine with Malononitrile and ethyl acetoacetate, we isolated the magnetic nanoparticle catalyst using magnetic separating material upon completion of the reaction and studied the feasibility of reusing and recycling the catalyst for several runs. The results, illustrated in **Table 3**, demonstrate that the magnetically separable $MnFe_2O_4$ catalyst could be recycled and reused for up to five runs without significant loss of its catalytic activity. The results are summarized in **Table 3**.

TABLE 3:

Reusability of the magnetically separable $MnFe_2O_4$ catalyst for the Synthesis of dihydropyrano[2,3-c]pyrazole derivatives

Run of typical reaction **(5a)**	1	2	3	4	5
Isolated % of yields (%)	98	97	97	95	94

IV. CONCLUSION

In conclusion, firstly, we have synthesised $MnFe_2O_4$ magnetic nanoparticles using the sol-gel method via the eco-friendly method. A new and efficient protocol for the solvent-free one-pot four-component synthesis of dihydropyrano[2,3-c]pyrazole derivatives at 78°C in the presence of the magnetically separable $MnFe_2O_4$ catalyst. Its catalytic investigation was done in the organic transformation of the synthesis of one-pot four-component dihydropyrano[2,3-c]pyrazole derivatives under solvent-free conditions at 78°C. One of the noteworthy advantages of this study is the easy product isolation, cleaner reaction profile, eco-friendliness, high yield, short reaction time, and recycling and reusability of the $MnFe_2O_4$ magnetic nanocatalyst.

V. ACKNOWLEDGEMENT

We thank the Principal, Shri Shivaji College of Arts, Commerce and Science, Akola, for providing the Research Laboratory facility and the Sophisticated

Analytical Instrumentation Facility (SAIF) and CIL, Chandigarh, for their characterisation facility.

VI. CONFLICTS OF INTEREST

The authors declare no conflict of interest.

VII. REFERENCES

[1] R. Afshari, and A. Shaabani, Materials functionalisation with multicomponent reactions: State of the art. ACS Comb. Sci. 20, 499–528 (2018).

[2] A. Dömling, W. Wang, and K. Wang, Chemistry and biology of multicomponent reactions. Chem. Rev. 112, 3083–3135 (2012).

[3] M. Mamaghani, and R. Hossein Nia, A review on the recent multicomponent synthesis of pyranopyrazoles. Polycycl. Aromat. Compd. 41, 223–291 (2019).

[4] M. Koohshari, M. Dabiri, and P. Salehi, Catalyst-free domino reaction in water/ethanol: An efficient, regio- and chemoselective one-pot multicomponent synthesis of pyranopyrazole derivatives. RSC Adv. 4, 10669 (2014).

[5] A. Mary Jacintha, A. Manikandan, K. Chinnaraj, S. Arul Antony, P. Neeraja, Comparative studies of spinel MnFe2O4 nanostructures: structural, morphological, optical, magnetic and catalytic properties. Journal of nanoscience and nanotechnology 15 (12), 9732-9740 (2015)

[6] L. Zhang, Y. Wu, Sol-gel synthesised magnetic MnFe2O4 spinel ferrite nanoparticles as a novel catalyst for oxidative degradation of methyl orange. Journal of Nanomaterials 2013, 2-2 (2013).

[7] Y. Zhang, J. Wang, Z. Su, M. Lu, S. Liu, F. Gu, J. Liu, Y. Tu, T. Jiang, Spinel MnFe2O4 nanoparticles (MFO-NPs) for CO2 cyclic decomposition prepared from ferromanganese ores. Ceramics International 46 (9), 14206-14216 (2020).

[8] A. Maleki, Z. Hajizadeh, and P. Salehi, Mesoporous halloysite nanotubes modified by CuFe2O4 spinel ferrite nanoparticles and study of its application as a novel and efficient heterogeneous catalyst in the synthesis of pyrazolopyridine derivatives. Sci. Rep. 9, 1 (2019).

[9] A. Maleki, and R. Firouzi-Haji, L-Proline functionalised magnetic nanoparticles: A novel magnetically reusable nanocatalyst for one-pot synthesis of 2, 4, 6-triarylpyridines. Sci. Rep. 8, 1 (2018).

[10] Z. Hajizadeh, F. Radinekiyan, R. Eivazzadeh-keihan, and A. Maleki, Development of novel and green NiFe2O4/ geopolymer nanocatalyst based on bentonite for synthesis of imidazole heterocycles by ultrasonic irradiations. Sci. Rep. 10, 1 (2020).

[11] F. Xiao-Jun, H. Xiao, L. Lu, L. Qingye, C. Li, W. Juan, Polydopamine-anchored polyether on Fe3O4 as magnetic recyclable nanoparticle-demulsifiers, Colloids and Surfaces A: Physicochemical and Engineering Aspects 617 126142 (2021).

[12] S.A. Nining, P.T. Anggito, E. Agung, A. Muhammad, A.S. Eko, B.K.P. Witha, G. Masno, S. Perdamean, Syntheses of ferrofluids using polyethylene glycol (PEG) coated magnetite (Fe3O4), citric acid, and water as the working liquid in a cylindrical heat pipe, Nano-Structures & Nano-Objects 25, 100654 (2021).

[13] P. N. Anantharamaiah, H. M. Shashanka, R. Kumar, J. A. Chelvane, and B. Sahoo, Chemically enabling CoFe2O4 for magnetostrictive strain sensing applications at lower magnetic fields: Effect of Zn substitution. Mater. Sci. Eng. B Solid State Mater. Adv. Technol. 266, 115080 (2021).

[14] B. N. Sahu, S. C. Sahoo, N. Venkataramani, S. Prasad, & R. Krishnan, Observation of

extraordinarily large magnetisation in CoFe2O4/ ZnFe2O4 bilayers. J. Magn. Magn. Mater. 523, 167629 (2021).

[15] F. Nicolas, M.F. Lisa, H. Rob, P. Andrew, G.S.R. Alan, E.S. Allan, Identification of chemically diverse Chk1 inhibitors by receptor-based virtual screening, Bioorganic & Medicinal Chemistry 14 4792-4802 (2006).

[16] M.E.A. Zaki, E.M. Morsy, F.M. Abdel-Motti, F.M.E. Abdel-Megeid, The Behaviour of Ethyl 1-acetyl-4-aryl-5-cyano-3-methyI-1,4-dihydropyrano 2,3-c pyrazol-6-ylimidoformate Towards Nucleophiles, Heterocyclic Communications 10, 97-102 (2004).

[17] J.L. Wang, D. Liu, Z.J. Zheng, S. Shan, X. Han, S.M. Srinivasula, C.M. Croce, E.S. Alnemri, Z. Huang, Structure-based discovery of an organic compound that binds Bcl-2 protein and induces apoptosis of tumor cellsProc. Natl. Acad. Sci. U.S.A. 97(13), 7124-7129 (2000).

[18] (a) E.A.Z. Magdy, A.S. Hanan, A.H. Ola, E.R. Aymn, Pyrazolopyranopyrimidines as a Class of Anti-Inflammatory Agents, Zeitschrift für Naturforschung C, 61, 1-5 (2006); (b) C.K. Sheng, J.H. Li, N. Hideo, Studies on heterocyclic compounds. 6. Synthesis and analgesic and antiinflammatory activities of 3,4-dimethylpyrano[2,3-c]pyrazol-6-one derivatives, J. Med. Chem. 27(4), 539-544 (1984).

[19] (a) W.P. Smith, L.S. Sollis, D.P. Howes, C.P. Cherry, D.I. Starkey, N.K. Cobley, Dihydropyrancarboxamides Related to Zanamivir: A New Series of Inhibitors of Influenza Virus Sialidases. 1. Discovery, Synthesis, Biological Activity, and Structure–Activity Relationships of 4-Guanidino- and 4-Amino-4H-pyran-6-carboxamides, J. Med. Chem. 41(6), 787-797 (1998); (b) K. Mazaahir, S. Shilpi, R.K. Khalilur, S.T. Sharanjit, Aqua mediated synthesis of substituted 2-amino-4H-chromenes and in vitro study as antibacterial agents, Bioorg. Med. Chem. Lett. 15(19), 4295-4298, (2005).

[20] (a) H. Junek, H. Aigner, Syntheses with Nitriles, XXXV. Reactions of Tetracyanoethylene with Heterocyclic Compounds, Chem. Ber. 106(3), 914-921 (1973); (b) H. Wamhoff, E. Kroth, K. Strauch, Dihalogentriphenylphosphorane in der Heterocyclensynthese; 271: Heterokondensierte 1,2,4-Triazolo[1,5-c]pyrimidine aus Enaminonitrilen via O-Ethylformimide, Synthesis, 1993(11), 1129-1132 (1993).

[21] A.V. Stachulski, N.G. Berry, A.C.L. Low, S.L. Moores, E. Row, D.C. Warhurst, I.S. Adagu, J.F. Rossignol, Identification of isoflavone derivatives as effective anticryptosporidial agents in vitro and in vivo, J. Med. Chem. 49 (2006) 1450-1454.

[22] H.H. Otto, Synthesis of Some 4H-Pyrano[2.3-c]pyrazoles, Arch. Pharm. 307 (1974) 444-447.

[23] G. Vasuki, K. Kumaravel, Rapid four-component reactions in water: synthesis of pyranopyrazoles, Tetrahedron Lett. 49 (2008) 5636-5638.

[24] G. Sanjib, Z. Cong-Gui, Organocatalysed enantioselective synthesis of 6-amino-5-cyanodihydropyrano 2,3-c pyrazoles, Tetrahedron Letters 50 (2009) 2252-2255.

[25] K. Kumari, D.S. Raghuvanshi, V. Jouikov, K.N. Singh, Sc(OTf)3-catalyzed, solvent-free domino synthesis of functionalized pyrazoles under controlled microwave irradiation, Tetrahedron Lett. 53(9), (2012) 1130-1133.

[26] A.M. Shestopalov, Y.M. Emeliyanova, A.A. Shestopalov, L.A. Rodinovskaya, Z.I. Niazimbetova, D.H. Evans, Cross-condensation of derivatives of cyanoacetic acid and carbonyl compounds. Part 1: Single-stage synthesis of 1′-substituted 6-amino-spiro-4-(piperidine-4′)-2H, 4H-pyrano[2,3-c]pyrazole-5-carbonitriles, Tetrahedron. 59(38) (2003) 7491-7496.

[27] Y. Peng, G. Song, R. Dou, Surface cleaning under combined microwave and ultrasound

irradiation: flash synthesis of 4H-pyrano[2,3-c]pyrazoles in aqueous media, Green Chem. 8 (2006) 573-575.

[28] A.M. Shestopalov, Y.M. Emeliyanova, A.A. Shestopalov, L.A. Rodinovskaya, Z.I. Niazimbetova, D.H. Evans, One-Step Synthesis of Substituted 6-Amino-5-cyanospiro-4-(piperidine-4‘)- 2H,4H-dihydropyrazolo[3,4-b]pyrans, Org. Lett. 4(3), (2002) 423-425.

[29] A. Siddekha, A. Nizam, M.A. Pasha, An efficient and simple approach for the synthesis of pyranopyrazoles using imidazole (catalytic) in aqueous medium, and the vibrational spectroscopic studies on 6-amino-4-(4′-methoxyphenyl)-5-cyano-3-methyl-1-phenyl-1,4-dihydropyrano[2,3-c]pyrazole using density functional theory, Spectrochem. Acta. A.: Molecular and Biomolecular Spectroscopy, 81(1), (2011) 431-440.

[30] S. Maddila, S. Rana, R. Pagadala, Sh. Kankala, S. Maddila, S.B. Jonnalagadda, Synthesis of pyrazole-4-carbonitrile derivatives in aqueous media with CuO/ZrO2 as recyclable catalyst, Catal. Commun. 61 (2015) 26-30.

[31] D. Shi, J. Mou, Q. Zhuang, L. Niu, N. Wu, X. Wang, Three-Component One-Pot Synthesis of 1,4-Dihydropyrano[2,3-c]pyrazole Derivatives in Aqueous Media, Synth. Commun. 34 (2004) 4557-4563.

[32] J. S. Godse, S. B. Gaikwad, V. B. Bhise, S. T. Gaikwad, R. P. Pawar, S. B. Ubale, synthesis and comparative study of nano zinc oxide structures with and without cetyltrimethylammonium bromide using sol-gel method, Heterocyclic Letters, 9(4) (2019) 455-460.

[33] J. S. Godse, S. B. Gaikwad, V. B. Bhise, R. P. Pawar and S. B. Ubale, Synthesis of Co3O4 Nanomaterial with Cetyltrimethylammonium Bromide Using Sol–Gel Method in Environmentally Benevolent Aqueous Media, Advanced Science, Engineering and Medicine, 12(6) (2020) 719-722.

[34] J. S. Godse, S. B. Gaikwad, V. B. Bhise, R. Suryawanshi, S. B. Ubale and R. P. Pawar, Synthesis of Binary Manganese Cobalt Oxide (MnCo2O4) Nanomaterial in Environmentally Benign Aqueous Media, Letters in Applied NanoBioScience, 12(4) (2023) 157.

[35] J. S. Godse, S. V. Pawar, S. B. Gaikwad, V. B. Bhise, S. S. Dhotre, S. B. Ubale and R. P. Pawar, Citric Acid Mediated Synthesis of Spinel Binary Copper Manganese Oxide (CuMn2O4) Nanomaterial using Sol-Gel Method, Letters in Applied NanoBioScience, 12(4) 2023 180.

[36] D. Azarifar, S.M. Khatami, M.A. Zolfigol, R. Nejat-Yami, Nano-titania sulfuric acid-promoted synthesis of tetrahydrobenzo [b] pyran and 1, 4-dihydropyrano [2, 3-c] pyrazole derivatives under ultrasound irradiation, J. Iran. Chem. Soc. 11 (2014) 1223-1230;

[37] K. Eskandari, B. Karami, S. Khodabakhshi, Novel silica sodium carbonate (SSC): Preparation, characterization and its first catalytic application to the synthesis of new dihydropyrano[2,3-c]pyrazoles, Catal. Commun. 54 (2014) 124-130

[38] D. Azarifar, S.M. Khatami, R. Nejat-Yami, Nano-titania-supported Preyssler-type heteropolyacid: An efficient and reusable catalyst in ultrasound-promoted synthesis of 4H-chromenes and 4H-pyrano[2,3-c]pyrazoles, J. Chem. Sci. 126 (2014) 95-101

[39] A. Hasaninejad, M. Shekouhy, N. Golzar, A. Zare, M.M. Doroodmand, Silica bonded n-propyl-4-aza-1-azoniabicyclo[2.2.2]octane chloride (SB-DABCO): A highly efficient, reusable and new heterogeneous catalyst for the synthesis of 4H-benzo[b]pyran derivatives, Appl. Catal. A. Gen. 402 (2011) 11-22.

[40] F. Karc, Synthesis of some novel pyrazolo[51-c][1,2,4]triazine derivatives and investigation of

their absorption spectra, Dyes Pigm. 76 (2008) 97–103.

Cite this article as :

Santosh B. Gaikwad, Kishore Puri, "MnFe2O4 nanoparticle as a new and magnetically separable nanocatalyst for solvent-free synthesis of dihydropyrano [2,3-c]pyrazole derivatives", International Journal of Scientific Research in Science and Technology (IJSRST), Online ISSN : 2395-602X, Print ISSN : 2395-6011, Volume 11 Issue 1, pp. 318-326, January-February 2024. Available at doi : https://doi.org/10.32628/IJSRST173876

Journal URL : https://ijsrst.com/IJSRST173876